

Lecture Notes in Electrical Engineering 1065

Sunil Kumar Goyal
Dheeraj Kumar Palwalia
Rajiv Tiwari
Yeshpal Gupta *Editors*

Flexible Electronics for Electric Vehicles

Proceedings of the 3rd International
Conference, FlexEV 2022

 Springer

Lecture Notes in Electrical Engineering

Volume 1065

Series Editors

Leopoldo Angrisani, Department of Electrical and Information Technologies Engineering, University of Napoli Federico II, Napoli, Italy
Marco Arteaga, Departamento de Control y Robótica, Universidad Nacional Autónoma de México, Coyoacán, Mexico
Samarjit Chakraborty, Fakultät für Elektrotechnik und Informationstechnik, TU München, München, Germany
Jiming Chen, Zhejiang University, Hangzhou, Zhejiang, China
Shanben Chen, School of Materials Science and Engineering, Shanghai Jiao Tong University, Shanghai, China
Tan Kay Chen, Department of Electrical and Computer Engineering, National University of Singapore, Singapore, Singapore
Rüdiger Dillmann, University of Karlsruhe (TH) IAIM, Karlsruhe, Baden-Württemberg, Germany
Haibin Duan, Beijing University of Aeronautics and Astronautics, Beijing, China
Gianluigi Ferrari, Dipartimento di Ingegneria dell'Informazione, Sede Scientifica Università degli Studi di Parma, Parma, Italy
Manuel Ferre, Centre for Automation and Robotics CAR (UPM-CSIC), Universidad Politécnica de Madrid, Madrid, Spain
Faryar Jabbari, Department of Mechanical and Aerospace Engineering, University of California, Irvine, CA, USA
Limin Jia, State Key Laboratory of Rail Traffic Control and Safety, Beijing Jiaotong University, Beijing, China
Janusz Kacprzyk, Intelligent Systems Laboratory, Systems Research Institute, Polish Academy of Sciences, Warsaw, Poland
Alaa Khamis, Department of Mechatronics Engineering, German University in Egypt El Tagamoa El Khames, New Cairo City, Egypt
Torsten Kroeger, Intrinsic Innovation, Mountain View, CA, USA
Yong Li, College of Electrical and Information Engineering, Hunan University, Changsha, Hunan, China
Qilian Liang, Department of Electrical Engineering, University of Texas at Arlington, Arlington, TX, USA
Ferran Martín, Departament d'Enginyeria Electrònica, Universitat Autònoma de Barcelona, Bellaterra, Barcelona, Spain
Tan Cher Ming, College of Engineering, Nanyang Technological University, Singapore, Singapore
Wolfgang Minker, Institute of Information Technology, University of Ulm, Ulm, Germany
Pradeep Misra, Department of Electrical Engineering, Wright State University, Dayton, OH, USA
Subhas Mukhopadhyay, School of Engineering, Macquarie University, NSW, Australia
Cun-Zheng Ning, Department of Electrical Engineering, Arizona State University, Tempe, AZ, USA
Toyoaki Nishida, Department of Intelligence Science and Technology, Kyoto University, Kyoto, Japan
Luca Oneto, Department of Informatics, Bioengineering, Robotics and Systems Engineering, University of Genova, Genova, Genova, Italy
Bijaya Ketan Panigrahi, Department of Electrical Engineering, Indian Institute of Technology Delhi, New Delhi, Delhi, India
Federica Pascucci, Dipartimento di Ingegneria, Università degli Studi Roma Tre, Roma, Italy
Yong Qin, State Key Laboratory of Rail Traffic Control and Safety, Beijing Jiaotong University, Beijing, China
Gan Won Seng, School of Electrical and Electronic Engineering, Nanyang Technological University, Singapore, Singapore
Joachim Speidel, Institute of Telecommunications, University of Stuttgart, Stuttgart, Germany
Germano Veiga, FEUP Campus, INESC Porto, Porto, Portugal
Haitao Wu, Academy of Opto-electronics, Chinese Academy of Sciences, Haidian District Beijing, China
Walter Zamboni, Department of Computer Engineering, Electrical Engineering and Applied Mathematics, DIEM—Università degli studi di Salerno, Fisciano, Salerno, Italy
Junjie James Zhang, Charlotte, NC, USA
Kay Chen Tan, Department of Computing, Hong Kong Polytechnic University, Kowloon Tong, Hong Kong

The book series *Lecture Notes in Electrical Engineering* (LNEE) publishes the latest developments in Electrical Engineering—quickly, informally and in high quality. While original research reported in proceedings and monographs has traditionally formed the core of LNEE, we also encourage authors to submit books devoted to supporting student education and professional training in the various fields and applications areas of electrical engineering. The series cover classical and emerging topics concerning:

- Communication Engineering, Information Theory and Networks
- Electronics Engineering and Microelectronics
- Signal, Image and Speech Processing
- Wireless and Mobile Communication
- Circuits and Systems
- Energy Systems, Power Electronics and Electrical Machines
- Electro-optical Engineering
- Instrumentation Engineering
- Avionics Engineering
- Control Systems
- Internet-of-Things and Cybersecurity
- Biomedical Devices, MEMS and NEMS

For general information about this book series, comments or suggestions, please contact leontina.dicecco@springer.com.

To submit a proposal or request further information, please contact the Publishing Editor in your country:

China

Jasmine Dou, Editor (jasmine.dou@springer.com)

India, Japan, Rest of Asia

Swati Meherishi, Editorial Director (Swati.Meherishi@springer.com)

Southeast Asia, Australia, New Zealand

Ramesh Nath Premnath, Editor (ramesh.premnath@springernature.com)

USA, Canada

Michael Luby, Senior Editor (michael.luby@springer.com)

All other Countries

Leontina Di Cecco, Senior Editor (leontina.dicecco@springer.com)

**** This series is indexed by EI Compendex and Scopus databases. ****

Sunil Kumar Goyal · Dheeraj Kumar Palwalia ·
Rajiv Tiwari · Yeshpal Gupta
Editors

Flexible Electronics for Electric Vehicles

Proceedings of the 3rd International
Conference, FlexEV 2022

 Springer

Editors

Sunil Kumar Goyal
Manipal University Jaipur
Jaipur, India

Dheeraj Kumar Palwalia
Rajasthan Technical University (RTU)
Kota, India

Rajiv Tiwari
Malaviya National Institute of Technology
Jaipur, India

Yeshpal Gupta
Lincus Inc. Arizona—USA
Arizona, AZ, USA

ISSN 1876-1100

ISSN 1876-1119 (electronic)

Lecture Notes in Electrical Engineering

ISBN 978-981-99-4794-2

ISBN 978-981-99-4795-9 (eBook)

<https://doi.org/10.1007/978-981-99-4795-9>

© The Editor(s) (if applicable) and The Author(s), under exclusive license to Springer Nature Singapore Pte Ltd. 2024

This work is subject to copyright. All rights are solely and exclusively licensed by the Publisher, whether the whole or part of the material is concerned, specifically the rights of translation, reprinting, reuse of illustrations, recitation, broadcasting, reproduction on microfilms or in any other physical way, and transmission or information storage and retrieval, electronic adaptation, computer software, or by similar or dissimilar methodology now known or hereafter developed.

The use of general descriptive names, registered names, trademarks, service marks, etc. in this publication does not imply, even in the absence of a specific statement, that such names are exempt from the relevant protective laws and regulations and therefore free for general use.

The publisher, the authors, and the editors are safe to assume that the advice and information in this book are believed to be true and accurate at the date of publication. Neither the publisher nor the authors or the editors give a warranty, expressed or implied, with respect to the material contained herein or for any errors or omissions that may have been made. The publisher remains neutral with regard to jurisdictional claims in published maps and institutional affiliations.

This Springer imprint is published by the registered company Springer Nature Singapore Pte Ltd. The registered company address is: 152 Beach Road, #21-01/04 Gateway East, Singapore 189721, Singapore

Paper in this product is recyclable.

Preface

In recent years, the world has witnessed a significant shift toward sustainable transportation solutions, with Electric Vehicles (EVs) emerging as a key component of this transformation. As the demand for EVs continues to rise, so does the need for advanced technologies that can efficiently manage and control the flow of electrical energy. This book, titled “Flexible Electronics for Electric Vehicles,” explores the crucial role of flexible electronics in the successful integration and operation of EVs. The transition from conventional internal combustion engine vehicles to EVs requires more than just replacing the power source. It demands a comprehensive reimagining of the entire vehicle architecture, including the powertrain, energy storage systems, and charging infrastructure.

The book entitled “Flexible Electronics for Electric Vehicles” contains a collection of best selected research papers on flexible electronics technologies and their applications in the context of EVs presented during the 3rd International Conference on Flexible Electronics for Electrical Vehicle (FlexEV 2022), held at Manipal University, Jaipur, Rajasthan, India during July 28–29, 2022. The FlexEV 2022 is having four tracks, viz, Flexible Electronics & Applications, Electric Vehicle Technology & Infrastructures, Materials & Device, Battery Management & Intelligent Systems. A total of 175 manuscripts have been submitted by authors of different countries through Easy Chair Conference Management System. After thorough peer double review process, totally 56 papers were accepted for presentation in the conference and final publication. The high-quality content with broad range of the topics is thoroughly peer-reviewed and published on suitable recommendations. The book aims to provide a comprehensive understanding of the fundamental principles, design considerations, and emerging trends in this rapidly evolving field.

Throughout this book, a wide range of topics have been given which present the latest state-of-the-art research and development in the field of EVs. Flexibility enables the integration of various power sources, including battery packs, supercapacitors, and fuel cells, while adapting to different charging standards and power grid requirements. We explore the challenges and opportunities presented by flexible electronics and discuss innovative solutions to address them. Moreover, this book aims to bridge the gap between theoretical knowledge and practical application. It

provides numerous real-world examples, case studies, and design considerations to assist engineers, researchers, and students in developing effective solutions for EVs. We also highlight the latest advancements in the field, including wide-bandgap semiconductor devices, advanced control techniques, and thermal management strategies. It is important to note that this book is an effort to present the material in a clear and accessible manner, ensuring that even readers new to the field can grasp the key concepts.

Jaipur, India
Kota, India
Jaipur, India
Arizona, USA

Sunil Kumar Goyal
Dheeraj Kumar Palwalia
Rajiv Tiwari
Yeshpal Gupta

Acknowledgements

We would like to express our gratitude to the numerous experts, researchers, and industry professionals who have contributed to the development of this book through their valuable insights and knowledge. Their collective expertise has been instrumental in creating a comprehensive resource that addresses the challenges and opportunities of power electronics for electric vehicles.

We would like to sincerely thank the keynote speakers **Dr. Jaume Anguera** from Romon Llull University, Barcelona, Spain; **Dr. Luciano Oliveira** from Salvador, Brazil; **Dr. Shantanu Bhattacharya** from IIT, Kanpur; and **Dr. Mathew Dyson** from IDTechEx., United Kingdom for their informative lecture. It helped to magnify the theme of the conference and inspired many of us as well as participants.

We would also like to extend our gratitude to Technical Committee consisting numerous researchers, experts, and reviewers for their constant and rigorous efforts for the desired review process of all the papers to ensure the quality of publication.

We would also be thankful to the management, faculty members, and supporting staff of Manipal University Jaipur for their constant encouragement and support for successful conduction of this International Conference.

Finally, we hope that “Flexible Electronics for Electric Vehicles” will serve as a valuable guide and reference for anyone interested in exploring the exciting world of electric vehicles. We believe that through a deeper understanding of this technology, we can accelerate the transition toward a cleaner, more sustainable future of transportation.

FlexEV 2022

Sunil Kumar Goyal
Dheeraj Kumar Palwalia
Rajiv Tiwari
Yeshpal Gupta

Contents

Detection and Classification of Power Quality Disturbances Using Variational Mode Decomposition and Deep Learning Networks	1
P. Vijaya Bhargava Phani Dutt and Harish Balaga	
Performance Evaluation of Brushless Direct Current Motor for an Electric Vehicle with Various PWM-Based Controllers	13
Rinki Roy Chowdhury and G. Koperundevi	
Comparison of Different Topologies of Multilevel Inverter	25
G. Shilpa, Divyansh Singh, Sayan Ghosh, and S. Mohneesh	
Design and Analysis of Off-Grid Solar Photovoltaic System for a Residential Building in Omaxe City, Jaipur	35
Peeyush Garg, Mahipal Bukya, and Panoram Kumar	
Behaviour of Constant Speed Wind Power System Under Different Operating Conditions	41
Ganesh P. Prajapat, Vikas Sharma, D. K. Yadav, Surender Singh Tanwar, and K. G. Sharma	
A Review of Architecture and Topologies Used for Electric Vehicle Charging Stations	51
Aayushi Priyadarshini, Shekhar Yadav, Nitesh Tiwari, and Utkarsh Shukla	
Trends and Developments of Electric Vehicles: Current State and Future Perspectives	63
Dođan ÇELİK	
Performance Estimation of Multilayer-Stack-Channel IGZO-Based Thin-Film Transistor in Double-Gate Mode	75
Shashi Kant Dargar, Abha Dargar, Shilpi Birla, and V. Hima Deepthi	

Towards Space Sensor Network and Internet of Things: Merging CubeSats with IoT	85
Charalampos Koulouris, Piromalis Dimitrios, Izzat Al-Darraj, Georgios Tsaramirsis, Alaa Omar Khadidos, Adil Omar Khadidos, and Panagiotis Papageorgas	
Advancement in Electric Vehicles and Battery Technology and Their Impact on the Global and Indian Market	101
Anavi Malhotra, Nikhil Vivek Shrivastava, and Gauri Gangwar	
Quaternary Multiplier with Modified Carry Using Carbon Nanotube FETs	113
G. V. S. Ajay and Sarada Musala	
Design and Verification of 3D Network-on-Chip Router	123
Gurleen Kaur and Deepika Bansal	
A Framework for Evaluating the Ergonomics of Mechanical Designs of Gaming Controllers	135
Fatimah Albargi and Nura Albuhairee	
Triggering an Email Alert Based on Price Comparison by Web Scraping Using Python	145
Shikha Singh, Garima Srivastava, Vandana Dubey, and G. R. Mishra	
Enhanced Hyperledger Fabric Network Set-Up for Remittance and Settlement Process	157
Parveen Mor, Rajesh Kumar Tyagi, Charu Jain, and Deepak Kumar Verma	
Distribution System Operation with Minimum Topological Variations	169
Praveen Agrawal, Neeraj Kanwar, Nikhil Gupta, K. R. Niazi, and Anil Swarnkar	
A Combined DG Integration-Network Reconfiguration-Based Method for Network Loss Minimization and Voltage Profile Improvement	179
Deepak Porwal, Manoj Fozdar (SMIEEE), and Rajive Tiwari	
Thermal Sensing Behavior of SiC Schottky Diode in 200–600 K	189
Jaya, Bhavya Sinhar, V. K. Dasaraju, and Suman	
Design and Performance of a Circularly Polarized Planar Microstrip Antenna with Improved Gain	197
Shipra Tiwari, Pramod Sharma, and Shoyab Ali	

Cost–Benefit Analysis on Electrical Vehicle Charging Station Using the Vehicle-To-Grid Technology from Python Language 205
 Naresh Kumar Golla, Suresh Kumar Sudabattula, Sai Nithika Yakkali, and Yerolla Harshith

Performance Analysis of a 3.2-kW Solar PV Electric Vehicle Charging Station Under Variable Climatic Conditions 219
 Bhuwan Pratap Singh, Sunil Kumar Goyal, and Shahbaz Ahmed Siddiqui

Application of SEPIC Converter to Developed Electric Vehicle Charging Station Based on PV Source 233
 Ram Niwash Mahia and Rajat Kumar

Regenerative Braking Integrated with Anti-lock Braking Mechanism in Electric Vehicle 247
 Gagneet Kour and Surbhi Gupta

Investigating Opto-Electronic Performance of RbSiBr₃ Multi-junction Solar PV Material: A Path Toward Sustainable Development 259
 Hansraj Karwasara, Karina Khan, Mamta Soni, Amit Soni, and Jagrati Sahariya

An Overview of Distributed Generation Integration Techniques, Present Trends and Future Scope 269
 Deepak Porwal, Manoj Fozdar (SMIEEE), and Rajive Tiwari

Design and Control of Battery Management System for Electric Vehicle 277
 Bharat Singh, Deepanshu Rawat, Pulkesh Parwani, Rhydham Gupta, and Tisha Kapoor

Current Conduction in Nichrome/p-Si Schottky Diode 285
 Ekta Sharma, Ankit Panchal, Reena Rathi, Vamshi Krishna Dasaraju, and Suman

III & V Group Elements and Heterostructures for Optoelectronics: A Survey 293
 Jayesh Jain, Amit Rathi, and Priya Chaudhary

Load Shedding Technique for Maintaining Voltage Stability 305
 Prashant Kumar Sharma, Akash Sharma, and Rajive Tiwari

Implementation of Renewable Sources for Designing EV Charging Station with Hybrid Storage Device as Reserve Source 315
 K. N. D. V. Sai Eswar and M. Arun Noyal Doss

A Cost-Efficient Energy Management of EV Integrated Community Microgrid	329
Divya Mathur, Neeraj Kanwar, and Sunil Kumar Goyal	
Automatic Target Recognition from ISAR Images: A Review	341
Hari Kishan Kondaveeti, Rakesh Kancharla, K. Raja Sravan Kumar, and Valli Kumari Vatsavayi	
A Survey Study and Comparison of Drones Communication Systems	351
Charalampos Koulouris, Piromalis Dimitrios, Izzat Al-Darraj, Georgios Tsaramirsis, Alaa Omar Khadidos, Adil Omar Khadidos, and Panagiotis Papageorgas	
Studying the Optoelectronic Properties of NaSnCl₃ Solar PV Material: A Step Towards Sustainable Development	363
Shikha Sharma, Hansraj Karwasara, Karina Khan, Mamta Soni, Amit Soni, and Jagrati Sahariya	
Overview of India's Battery-Swapping and Charging Infrastructure for Electric Vehicles	371
Devjani Bhattacharya and Kumud Kumar Sharma	
Real-Time Network Traffic Analysis for Threat Detection	381
Yogesh Gupta, Amit Saraswat, and Sunil Kumar Goyal	
Machine Learning-Based DC Microgrid Control for Electric Vehicle Charging Stations	395
Anirudh Pratap, D. K. Palwalia, Mohit Tepan, Nikhil Jain, Anjali Kumari, and Anil Mina	
Tree Shaped Nature-Inspired Ultra-Wideband Antenna for Wireless Body Area Networks Applications	405
Laxmi Narayan Balai	
Machine Learning-Based Model for Predicting Failure of Physical Machines in Cloud Computing	413
Priti Kumari, Vandana Dubey, Meenal Jain, and G. R. Mishra	
Solar Inverter Equipped with a Battery Management System	423
Babu Naik Gugulothu, Moinuddin Pasha, P. Deepa, K. Y. Kusuma, and Ponnamm Naga Roopa	
Optimal Power Sharing in a Meshed MTDC Grid Through Robust Current Flow Controllers	435
Lokesh Garg and Sheetla Prasad	
Design of EV Charging Station with Integrated Renewable Energy Sources	449
Devarakonda Ashwin Kumar and Natarajan Karupiah	

Impact on Solar Energy Generation with Dual-Axis Solar Tracking System Including Different Weather Conditions 465
 Rajendra Singh and Neeraj Tiwari

Semantic Normal Form for Performance-Critical Databases 473
 Adil Khadidos, Alaa Khadidos, Yasser Ades, and Mohammad Yamin

Wireless Charging for Electric Vehicles: A Review 485
 Tushar Mehndiratta and Rakesh Kumar

Optimal Reactive Power Dispatch Problem Using Novel Wild Horse-Based Optimizer 495
 Gaurav Gangil, Sunil Kumar Goyal, Amit Saraswat, and Yeshpal Gupta

An Insight into Algorithms and Self Repair Mechanism for Embedded Memories Testing 505
 Vinita Mathur, Aditya Kumar Pundir, Sudhanshu Singh, and Sanjay Kumar Singh

Rapid Protection System Using Single-End Current Data for Capacitive Compensated Power Transmission Network 519
 Shoyab Ali, Annapurna Bhargava, and Akash Saxena

Enhancement of Breakdown Voltage Using Trench Edge Termination Technique in SiC-Based Power Device 531
 Ankit Panchal, Ekta Sharma, Vamshi Krishna Dasaraju, and Suman

A Brief Review on the Barriers of Electric Vehicle Adoption and Present Scenario in India 539
 Satyaki Biswas, Sadasiva Behera, and Nalin B. Dev Choudhury

Simulation of Battery Management System for Protection in Electric Vehicle Against the Battery Failures 551
 Sachin Paliwal, Amandeep Gill, and Manjeet Singh

A Comparative Study of Deep Learning Methods for Short-Term Solar Radiation Forecasting 565
 Praveen Kumar Singh, Amit Saraswat, Yogesh Gupta, Sunil Kumar Goyal, and Yeshpal Gupta

Electric Two-Wheeler BLDC Hub Motor Design, Modeling, and Performance in Real-Time Use 577
 Manikanta Akella, Sanjay Patil, and Kiran Wani

A Comprehensive Review of Wireless Electric Vehicle Charger 589
 Sandesh Patel, Shekhar Yadav, and Nitesh Tiwari

Investigation of Control Algorithm for PMSM-Based Electric Vehicle Using Vehicle Dynamics 599
 Bharat Singh, Ankur Chowdhury, Vishal Mishra, and Ankur Jain

About the Editors

Dr. Sunil Kumar Goyal comes with rich and diversified experience of more than 22 years in various fields including teaching, research, and administration as well. He has a strong flair for writing and research and has authored a number of research articles in international journals/conferences of high repute. He is a regular reviewer of research articles for many high-impact journals including IET GTD, Electric Power Applications, Renewable Power Generation, etc. He has delivered many expert lectures on different platforms. He is instrumental in organizing several events in various capacities and has chaired/co-chaired sessions at a number of national/international conferences. He is currently working as an Associate Professor in the Department of Electrical Engineering, at Manipal University Jaipur since August 2014. He has more than 22 years of teaching and research experience. His area of research includes induction generators for renewable energy generation in standalone and grid-connected modes, economic operation of power systems, and different optimization techniques. He is also a senior member of the IEEE Power & Energy Society.

Prof. Dheeraj Kumar Palwalia received his B. Tech. and M. Tech. in 1996 and 1999 respectively from Malviya National Institute of Technology, Jaipur. He received his Ph.D. from the Indian Institute of Technology Roorkee in the year 2010. He is serving as a Professor at the Department of Electrical Engineering, Rajasthan Technical University, Kota. His research interests include power electronics and drives, induction generators, renewable energy, active power filter, fuel cell and digital controller design.

Dr. Rajiv Tiwari is working as a professor and Head of the Department of Electrical Engineering at MNIT Jaipur. During the last 26 years of his long service at the MNIT Jaipur, his teaching, research, and development interests have been in the areas of AI Applications to Power Systems, Power System Operation and Control, Smart Grid, Power System Dynamics and Voltage Stability Studies, FACTS Devices, Renewable Integration in Power Systems. He has supervised many Doctoral and Master's theses in the above areas. He has published many papers in reputed international journals and conferences and also published two books on electronic devices and circuits.

He has organized several short-term courses and trained railway engineers. He has invented a new FACTS device (Amalgam power flow controller, i.e. APFC), which is recognized worldwide and published in IEEE Transactions on power systems. This device helps to maintain stability in power transmission systems. Dr. Tiwari is a recipient of the president award in scouting.

Dr. Yeshpal Gupta is working as Vice President of Engineering at Lincus Inc., Arizona—USA. He has over fifteen years of experience in energy engineering, renewable energy, and GHG verifications. Dr. Gupta specializes in reviewing utility rebate EE and RCx applications, integrated energy audits, evaluating new and renewable energy technologies, and conducting GHG verification and validation audits. He is highly proficient in energy and demand savings calculation for custom installations in large commercial and industrial facilities. Dr. Gupta has reviewed more than 750 custom applications from a wide variety of market sectors and end-uses. Additionally, Dr. Gupta is experienced in evaluating greenhouse gas emissions from industrial and commercial sites. Dr. Gupta received his Ph.D. in Mechanical Engineering from Arizona State University. Dr. Gupta has also published articles in various International Journals and presented in several such as ASHRAE, ACEEE, and Solar Energy. He is associated with California Technical Forum, the American Solar Energy Society and California ARB Lead Verifier.

Detection and Classification of Power Quality Disturbances Using Variational Mode Decomposition and Deep Learning Networks



P. Vijaya Bhargava Phani Dutt  and Harish Balaga 

Abstract Nowadays, electronic gadgets become part of everyone's life, and as a drawback, it injects power quality disturbance (PQD) into the power system, which results in maloperation of the device, affects system stability, and reduces the life of the machine. It is somewhat difficult to detect and identify what type of power quality disturbance is occurred in the power system network. Due to the data complexity, it's highly difficult to separate PQDs data from other data like normal system data and data during faults. In this paper, power quality disturbance data is generated as per IEEE standards and this data is processed by the variational mode decomposition (VMD) to extract hidden features from the PQD signals. These features are transformed into 3D image vectors, which are used to train the convolutional neural network (CNN). In this work, the study is made on VMD parted with various pre-trained CNNs and compared their results with developed CNN models, to find the optimum classifier.

Keywords Power quality disturbance (PQDs) · Variational mode decomposition (VMD) · Convolutional neural network (CNN)

1 Introduction

Maintaining a reliable power supply to customers with power quality is important. But the increase in usage of electronic devices leads to lessening the power quality, affecting the performance of the appliance of customer and affecting system stability. To reduce these effects proper PQ measures should be implemented, choosing proper PQ measures is possible by detecting PQ disturbance. Detection and classification of PQD is a challenging task due to the similarities and complexity of PQ signals. So main task is to choose the proper technique that presents features from the signal and

P. V. B. P. Dutt (✉) · H. Balaga
Vardhaman College of Engineering, Hyderabad, India
e-mail: phanidutt047@gmail.com

classify the PQ event accurately. The work involves two steps: 1. features extraction from PQ signal and 2. detection and classification of PQ events.

Nowadays, there are several techniques available for feature extraction of any signal. This technique has its advantages and disadvantages which depend on the applications and with which partner classification algorithm is used. So far, the feature extraction techniques that are used in many works are short-time (STFT) Fourier transform [1], Fourier transform (FT) [2], Discrete Fourier transform (DFT) [3], Kalman filters (KF), Hilbert–Huang transform (HHT), Continuous Wavelet Transform (CWT), Discrete Wavelet Transform (DWT), Empirical mode decomposition (EMD), Gabor transform (GT), Wigner-Ville distribution (WVD) [4], etc. Once the extraction is done, data-driven approaches are used to identify PQD due to their ability to uncover relevant information hidden within the collected features. Data-driven approaches like Probabilistic neural network (PNN), Decision tree (DT), Artificial Neural Network (ANN), Convolutional Neural Networks (CNN), Recurrent Neural Networks (RNN) [5], Support Vector Machine (SVM) [6], etc. are used to detect and classify PQ events.

Various types of neural network-based methods are available like CNN, LSTM (long short-term memory) [7], RNN, Gated Recurrent Unit (GRU) [8], and hybrid models [9]. Compared to LSTM and CNN, the CNN-LSTM hybrid model gives more accurate results in the classification of PQ events. However, this deep learning network gives results based on the probability of output classification, which means if for certain input PQD signal output neurons may get equal values that affect the accuracy. To improve the accuracy, hybrid models are coming into existence, for example, discrete wavelet transform-based ANN, where feature extraction of PQ signal is done by wavelet transform. These extracted samples get normalized and fed as training input to ANN for the classification of PQD. Wavelet transform-based CNN where features of voltage/current are extracted and developed images are given to CNN to classify PQD [10]. But in real-time environment, current/voltage signals are disrupted by noise, with such a signal classification of PQ disturbance by the traditional method leads to an inaccurate result. To overcome this noise effect, a hybrid CWT-CNN model is used to detect the PQ events. But CWT requires more memory and time as its sampling is continuous. So discrete wavelet transform (DWT) comes into existence as its function is similar to CWT and requires less memory and time. DWT-ANN [11] hybrid model can work well, but wavelet transform has a disadvantage, the signal aliasing effect, which affects complex signal detection and leads to poor accuracy. A new feature extraction technique called VMD can be used, where aliasing shows no effect on its operation. Any data-driven method along with VMD can be the best choice for PQ event detection. In this work, different data-driven methods are parted with VMD to obtain the optimum method.

2 Mathematical Model of PQDs

2.1 Generation of PQ Disturbance

Simple power quality disturbances are sag, swell, harmonics, transients, interruption, and flicker. However, a real-time system may undergo complex PQ disturbances, where two or more PQ disturbances overlap. In real time for any system, the availability of a large set of PQD data for the different conditions is difficult. So, by knowing system ratings and previously stored log data of any system, one can obtain min and max limits of simple PQDs. With the help of mathematical formulae and MATLAB, synthetic signals based on the mathematical representation of the disturbances are produced and presented in Table 1.

For each kind of power quality disturbance, up to 2000 samples are generated in a MATLAB environment. Sample data for each type of PQD is shown in Fig. 1.

3 Variational Mode Decomposition (VMD)

VMD is a tool to extract features from a given input signal. The input signal is decomposed into numerous sub-signals using VMD [13] and every sub-signal is generated based on Intrinsic Mode Function (IMF) which is amplitude modulated and frequency modulated (AM-FM).

$$\text{IM function is - } G_n(t) = K_n(t) * \cos(\varphi(t)) \tag{1}$$

where $\varphi(t)$ —non-decaying function, $K_n(t)$ —always positive value, and n represents n^{th} mode.

Decomposition aims to discover the smallest sum of n-variational modes of their bandwidth.

$$\min_{\{G_n\}, \{w_n\}} \left\{ \sum_n \left\| \partial_t \left[\left(\delta(t) + \frac{j}{\pi t} \right) * G_n(t) \right] e^{-jw_n t} \right\|_2^2 \right\} \tag{2}$$

where $\{G_n\} = \{G_1, G_2, \dots, G_n\}$ and $\{w_n\} = \{w_1, w_2, \dots, w_n\}$.

Equation (2) constraints are

$$\sum_n G_n = S_x \tag{3}$$

where S_x represents original signal, $\sum_n = \sum_{n=1}^n$.

This constraint is dealt by Quadratic penalty + Lagrangian (L) methods, so resulted augmented L is

Table 1 Mathematical expression of six PQDs [12]

PQD-Classes	Mathematical formula	Ranges of parameters
Sag	$C(1 - r\{u(t - t_1) - u(t - t_2)\}) \sin(\omega t - \theta)$	$T \leq t_2 - t_1 \leq 9T,$ $0.1 \leq r \leq 0.9$
Swell	$C(1 + r\{u(t - t_1) - u(t - t_2)\}) \sin(\omega t - \theta)$	$T \leq t_2 - t_1 \leq 9T,$ $0.1 \leq r \leq 0.8$
Harmonics	$C \left\{ \sin(\omega t - \theta) + \sum_{n=3}^7 s_n \sin(n\omega t - \phi_n) \right\}$	$0.05 \leq s_3, s_5, s_7 \leq 0.15,$ $-\Pi \leq \phi_3, \phi_5, \phi_7 \leq \Pi$
Flickers	$C \{1 + q \sin(\omega_f t)\} \sin(\omega t - \theta)$	$0.05 \leq q \leq 0.1,$ $10 \leq f_f \leq 20 \text{ Hz},$ $\omega_f = 2f_f$
Transients	$C \{ \sin(\omega t - \theta) + \alpha e^{\lambda((t - t_1) - \tau)} \sin(\omega_n(t - t_1) - v)(u(t - t_1) - u(t - t_2)) \}$	$0.5T \leq t_2 - t_1 \leq 3T, 0.1 \leq \tau \leq 0.9,$ $-\Pi \leq v \leq \Pi$ $300 \leq f_n \leq 900 \text{ Hz},$ $\omega_n = 2f_n$
Interruption	$C \{1 - r\{u(t - t_1) - u(t - t_2)\} \sin(\omega t - \theta)\}$	$T \leq t_2 - t_1 \leq 9T,$ $0.9 \leq r \leq 1.0$

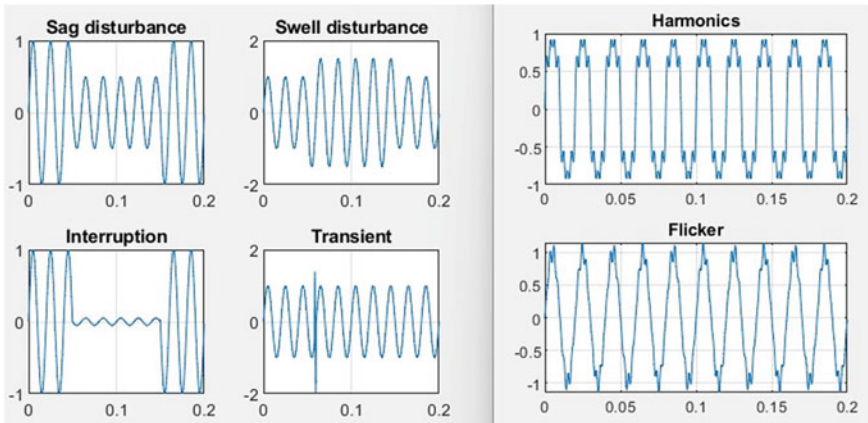


Fig. 1 Six classes of generated PQDs as per Table 1

$$L(\{G_n\}, \{w_n\}, q) = \alpha \sum_n \left\| \partial_t \left(\left(\delta(t) + \frac{j}{\pi t} \right) * G_n(t) \right) e^{-j\omega t} \right\|_2^2 + \left\| S_x(t) - \sum_n G_n(t) \right\|_2^2 + \left(q(t), S_x(t) - \sum_n G_n(t) \right) \quad (4)$$

By solving above variational problem, G_n , w_n , and q updated until the below given equation holds good:

$$\sum_n \|G_n^{N+1} - G_n^N\|_2^2 / \|G_n^N\|_2^2 < \epsilon r \quad [11]$$

as Eqs. (5–7) are

$$G_n^{N+1} = \operatorname{argmin}_{G_n} L(\{G_{i < n}^{N+1}\}, \{G_{n \leq i}^{N+1}\}, \{w_i^N\}, q^N) \quad (5)$$

$$w_n^{N+1} = \operatorname{argmin}_{w_n} L(\{G_i^{N+1}\}, \{w_{i \leq n}^{N+1}\}, \{w_{n \leq i}^N\}, q^N) \quad (6)$$

$$q^{N+1} = q^N + \tau \left(S_x - \sum_n G_n^{N+1} \right) \quad (7)$$

$F = \text{vmd}(S_x)$ performs VMD on S_x signal. By default, it generates five IMFs and stores them in variable F .

4 CNN—Convolutional Neural Networks

CNN is coming under the deep learning method, where input is given in terms of images to classify different classes. It has at least one convolutional layer along with RELU, pooling, fully connected layer, SoftMax layer, and classification layer. Here the input image which is fed to the convolutional layer is processed by filters and activation function in a convolutional layer. Based on the chosen size of filter, the output size of a convolutional layer is decided. Pooling layer down samples the input which can reduce the number of samples at the output without losing features of a signal. The number of classes at the output is decided by a fully connected layer, where the number of filters is equal to the number of classes at the output. The convolutional layer is the first step to processing the image data.

For a given input D -data, the result from the convolutional layer is obtained by the following equation:

$$L_r^v = \sigma \left(\sum_{b=1}^k F_k^v D_{r+k-1}^v + z^v \right) \quad (8)$$

where L —output value, F^v — v th filter kernel of convolutional layer, z is bias, σ —activation function.

The output element from polling is represented by

$$P_r^v = \max(L_{r+s}^v) \quad (9)$$

where s denotes filter size.

5 Proposed Method

In this work a hybrid model, VMD along with CNN, is implemented with MATLAB, where the datasets of different PQDs are generated as per IEEE standard. These data are processed by VMD to decompose the input data signal at a frequency of 1 kHz into five different IMFs, and the retrieved feature data is converted into 3D images. The acquired 3D images are processed by CNN to detect and classify the output class of PQD events. The scheme of workflow is shown by Fig. 2 in detail.

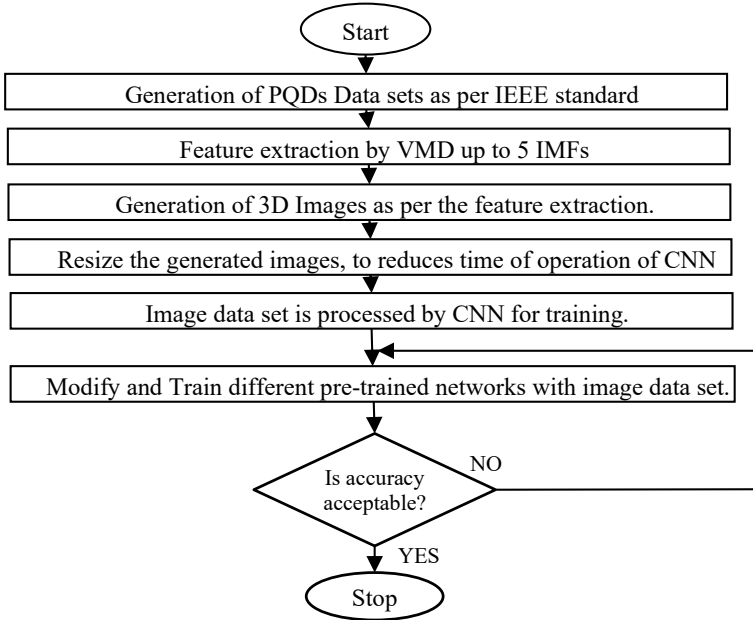


Fig. 2 Represents the workflow of this project

6 Output of VMD

VMD output called IMFs for interruption and flicker events are shown in Fig. 3. These IMFs are transformed into 3D images, which are used as input vectors for CNN as shown in Fig. 4.

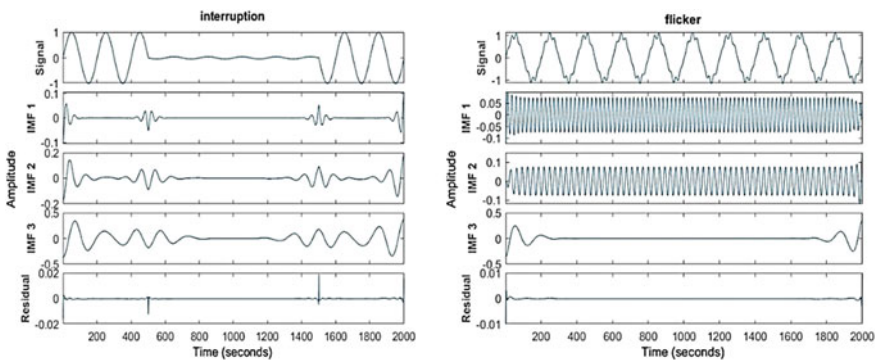


Fig. 3 VMD output-IMFs for interruption and flicker-PQD

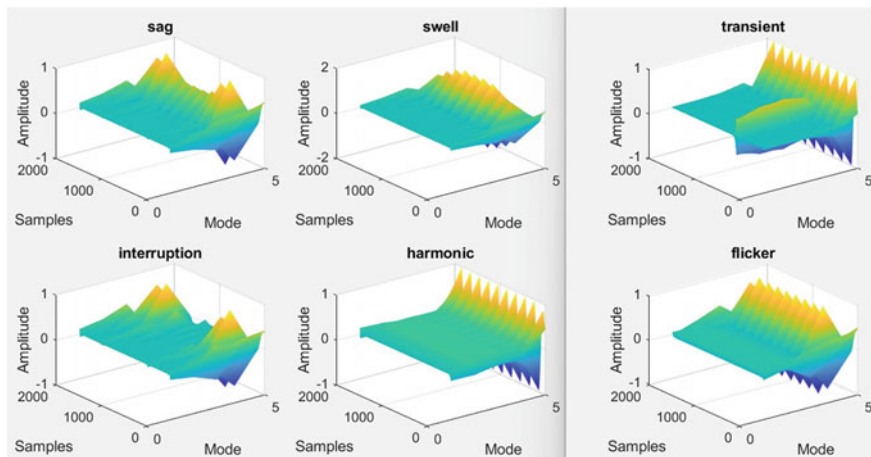


Fig. 4 Generated 3D images from IMFs results of VMD for six PQDs

7 Training of CNN

The proposed CNN models are trained with input as 3D vectors. Pre-trained CNNs such as Resnet50, Resnet18, AlexNet, and Teachable machine neural networks are trained with this data. And Resnet50, Resnet18, and AlexNet are modified and trained with data of 3D vectors. The authors observed that a normal pre-trained network is high time-consuming for training and testing, whereas modified Resnet18 and modified Resnet50 take less time for training and give results in no time. However, in this work, identification of PQDs by VMD-CNN, results are compared with other PQDs identification methods such as Modular NN, DWT-ANN, VMD-SVM, VMD-KNN, and WVD-CNN. The modified CNN of Resnet18 is shown in Fig. 5.

After completion of data generation, this data is divided into a 70:30 ratio, 70% of data for training and 30% for testing. The total number of datasets generated is $6 \times 2000 = 12,000$ image datasets. Each batch consists of 66 image data used to train CNN with a maximum of 30 epochs.

8 Results

In this work, the generated data is processed with different pre-trained CNNs and with modified versions of Resnet18 (MRN18), AlexNet (MAN), Resnet50 (MRN50), and Teachable machine (TM). And their results are compared to choose an optimum model for this proposed method. While training CNN in MATLAB with different

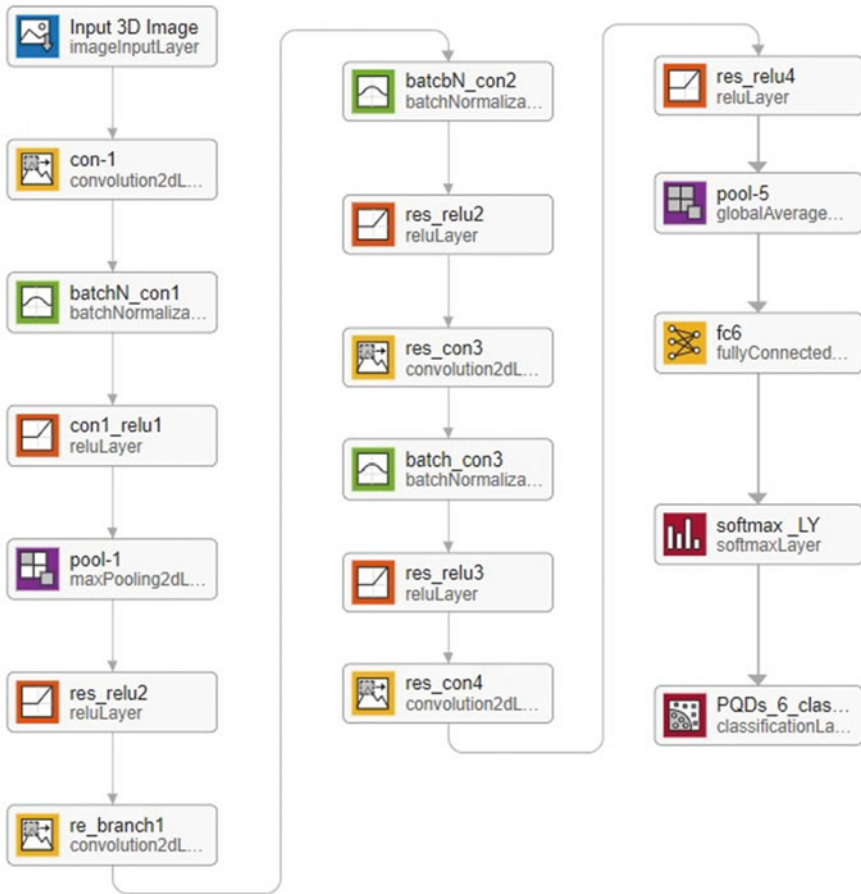


Fig. 5 The architecture of Modified-Resnet18 model (proposed model)

optimizers, it was observed that Adam optimizer gave more accuracy than sgd and rmsprop optimizers. Figure 6 displays the validation and loss plots for the improved CNN, whereas Fig. 7 displays the accuracy and loss plot for the VMD-TM. Results of proposed model are compared with other model results and tabulated in Table 2.

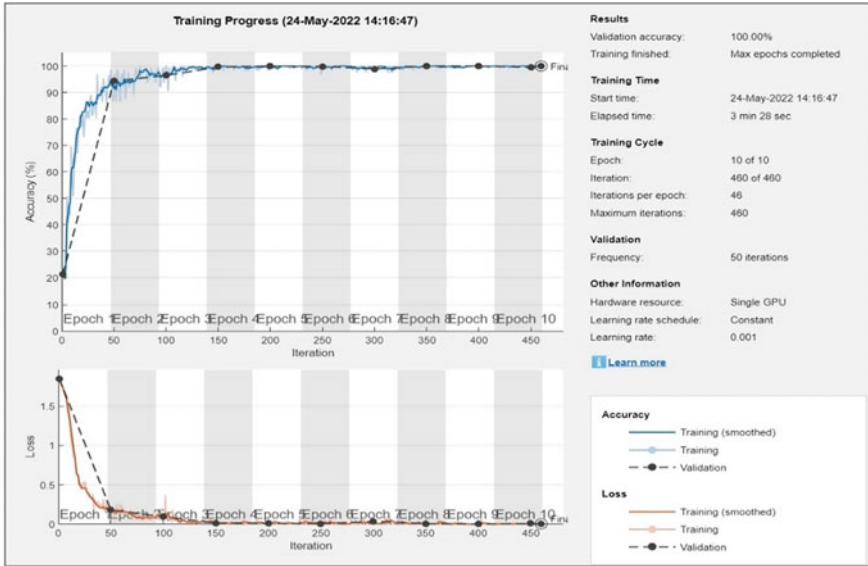


Fig. 6 Accuracy and loss plot for modified Resnet18 (proposed model) trained by Adam optimizer

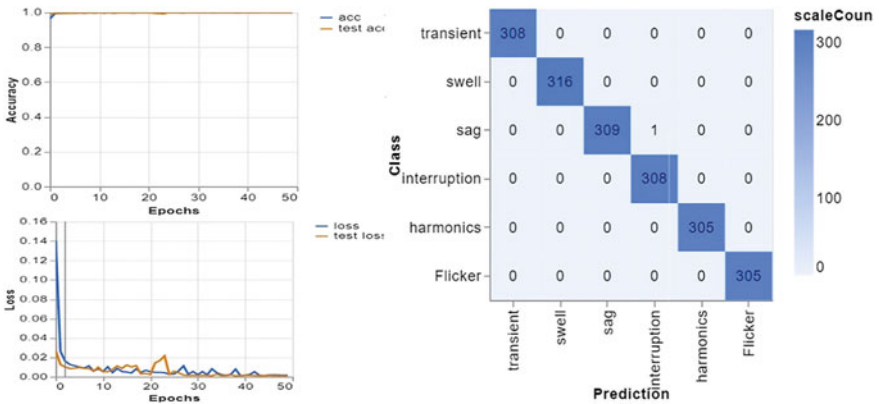


Fig. 7 Confusion matrix and accuracy, loss plots of VMD-Google Teachable machine

Table 2 Comparison results of different data-driven classifiers with the proposed model

Data-driven classifier		Accuracy (%)
DWT-ANN [14]		90
Modular NN [15]		89.7
LSTM [16]		96.7
RNN [16]		91.5
GRU[16]		96.4
CNN-LSTM[16]		98.4
WVD-CNN [4]		99.67
VMD-SVM [17]		98.7
VMD-ANN [17]		98.33
Proposed models	VMD-MRN18	100
	VMD-MAN	99.21
	VMD-MRN50	97.66
	VMD-TM	100

9 Conclusion

This work looks at the usefulness of several deep learning architectures for detecting and classifying Power Quality Disturbances. In this, VMD technique is used to retrieve the hidden features in PQDs signal and used different classifiers of CNN such as modified Resnet18, modified Resnet50, modified AlexNet, modified VVG16, and Google Teachable machine. Here VMD with normal Resnet50 gave an accuracy of 93.76% and VMD with AlexNet gave an accuracy of 95.31% but here normal Resnet50, Resnet18, and AlexNet network have more complexity and are time-consuming for training and validation. Models developed in this work took less time for training and validation and gave accurate results. Proposed modified Resnet18 parted with VMD trained by Adam optimizer gave validation accuracy of 100%.

References

1. Jamali S, Farsa AR, Ghaffarzadeh N (2018) Identification of optimal features for fast and accurate classification of power quality disturbances. *Meas. J. Int. Meas. Confed* 116(November 2016):565–574. <https://doi.org/10.1016/j.measurement.2017.10.034>
2. Heydt GT, Fjeld PS, Liu CC, Pierce D, Tu L, Hensley G (1999) Applications of the windowed FFT to electric power quality assessment. *IEEE Trans Power Deliv* 14(4):1411–1416. <https://doi.org/10.1109/61.796235>
3. Masoum MAS, Jamali S, Ghaffarzadeh N (2010) Detection and classification of power quality disturbances using discrete wavelet transform and wavelet networks. *IET Sci Meas Technol* 4(4):193–205. <https://doi.org/10.1049/iet-smt.2009.0006>
4. Cai K, Cao W, Aarniovuori L, Pang H, Lin Y, Li G (2019) Classification of power quality disturbances using Wigner-Ville distribution and deep convolutional neural networks. *IEEE Access* 7:119099–119109. <https://doi.org/10.1109/ACCESS.2019.2937193>

5. Senthil Vadivu U, Keshavan BK (2017) Power quality enhancement of UPQC connected WECS using FFA with RNN. In: Conference proceedings-2017 17th IEEE international conference on environment and electrical engineering and 2017 1st IEEE industrial and commercial power systems Europe, EEEIC/1 and CPS Europe 2 2017, no 1. <https://doi.org/10.1109/EEEIC.2017.7977566>
6. Abdullah, Khan MU, Aziz S, Usman A, Jalil T (2021) Soft computing approach for classification of complex power quality events. In: 2021 international conference on artificial intelligence. ICAI 2021, pp 223–228. <https://doi.org/10.1109/ICAI52203.2021.9445264>
7. Aksoy A, Ertürk YE, Erdoğan S, Eydurani E, Tariq MM (2018) Estimation of honey production in beekeeping enterprises from eastern part of Turkey through some data mining algorithms. *Pak J Zool* 50(6):2199–2207. <https://doi.org/10.17582/journal.pjz/2018.50.6.2199.2207>
8. Chung J, Gulcehre C, Cho K, Bengio Y (2014) Empirical evaluation of gated recurrent neural networks on sequence modeling, pp 1–9. <http://arxiv.org/abs/1412.3555>
9. Garcia CI, Grasso F, Luchetta A, Piccirilli MC, Paolucci L, Talluri G (2020) A comparison of power quality disturbance detection and classification methods using CNN, LSTM and CNN-LSTM. *Appl Sci* 10(19):1–22. <https://doi.org/10.3390/app10196755>
10. Dai S, Wu X (2021) A CNN-based power quality disturbance decomposition and classification system using wavelet transform. In: ACM international conference proceeding series, pp 1–5. <https://doi.org/10.1145/3469213.3470284>
11. Ijaz M, Shafiullah M, Abido MA (2015) Classification of power quality disturbances using Wavelet Transform and Optimized ANN. In: 2015 18th international conference on intelligent system application to power systems, ISAP 2015, vol 4, no 05, pp 1423–1427. <https://doi.org/10.1109/ISAP.2015.7325522>
12. Igual R, Medrano C, Arcega FJ, Mantescu G (2018) Integral mathematical model of power quality disturbances. In: Proceedings of the international conference on harmonics and quality of power, ICHQP, vol 2018-May, pp 1–6. <https://doi.org/10.1109/ICHQP.2018.8378902>
13. Dragomiretskiy K, Zosso D (2014) Variational mode decomposition. *IEEE Trans Signal Process* 62(3):531–544. <https://doi.org/10.1109/TSP.2013.2288675>
14. Alshahrani S, Abbod M, Alamri B, Taylor G (2015) Evaluation and classification of power quality disturbances based on discrete Wavelet transform and artificial neural networks. In: Proceedings of the universities power engineering conference, vol 2015-Novem, no Upec. <https://doi.org/10.1109/UPEC.2015.7339928>
15. Bhende CN, Mishra S, Panigrahi BK (2008) Detection and classification of power quality disturbances using S-transform and modular neural network. *Electr Power Syst Res* 78(1):122–128. <https://doi.org/10.1016/j.epsr.2006.12.011>
16. Mohan N, Soman KP, Vinayakumar R (2018) Deep power: deep learning architectures for power quality disturbances classification. In: Proceedings of 2017 IEEE international conference on technological advancements in power and energy: exploring energy solutions for an intelligent power grid, TAP energy 2017, pp 1–6. <https://doi.org/10.1109/TAPENERGY.2017.8397249>
17. Abdoos AA, Khorshidian Mianaei P, Rayatpanah Ghadikolaei M (2016) Combined VMD-SVM based feature selection method for classification of power quality events. *Appl Soft Comput J* 38:637–646. <https://doi.org/10.1016/j.asoc.2015.10.038>

Performance Evaluation of Brushless Direct Current Motor for an Electric Vehicle with Various PWM-Based Controllers



Rinki Roy Chowdhury  and G. Koperundeivi 

Abstract Electric vehicles will replace combustible automobiles to enhance driving performance and cut emissions, all of which will contribute to sustainable development. The potential to lengthen an electric vehicle's range is necessary for proper EV operation. BLDC motor drives are the most viable for electric vehicles as they have a simple structure, less weight, a broader speed range, noiseless operation, strong starting torque, accurate and precise control, and high dynamic responsiveness as compared to a DC motor. But torque oscillations cause increased noise, vibrations, and inefficiencies. The most popular controllers are direct torque control (DTC) and field-oriented control (FOC). But DTC has disadvantages, including problems with control at low speeds with huge current and torque pulsation formation. Hence, a field-oriented control (FOC) of a BLDC motor utilizing sinusoidal pulse width modulation (SPWM), space vector pulse width modulation (SVPWM), a fuzzy/PID logic control scheme (FLC/PID), and finally a bio-intuitive spider web-based algorithm control scheme has been compared. The torque pulsation values, the controller expense for each case, as well as the settling time and peak overshoot for the speed obtained are explored to evaluate the effectualness of the techniques for electric vehicle implementation. The system assessment is performed using the MATLAB/Simulink platform.

Keywords SPWM · SVPWM · Fuzzy/PID controller · Spider web-based controller

1 Introduction

The performance of an electric traction drive is defined by the electric motor, which is a vital part. In contrast to an AC motor, a DC motor requires a commutator and brushes, which are subject to wear and tear and need frequent maintenance. Some

R. R. Chowdhury · G. Koperundeivi (✉)
Department of EEE, National Institute of Technology Puducherry, Karaikal 609609, India
e-mail: koperundeivi@nitpy.ac.in

of the most popular AC motor drives for electric vehicle applications alongside their pros and cons are presented in [1]. Because of the benefits of BLDC motors, such as higher torque-to-weight ratio and compact size, they are a viable option for lighter electric vehicles [2].

Harmonics triggered by back-EMF and flux linkage are both non-existent in a BLDC motor's stator since it is coreless. Mutual torque generates only an effectual ripple [3]. Torque ripple is the fundamental issue of BLDC motors used in industrial applications. In the literature, multiple control methods to reduce torque ripples for a BLDC motor-fed electric vehicle have been reported. The most popular controllers are direct torque control (DTC) and field-oriented control (FOC). The FOC is also known as vector control, which is a type of current vector control created for variable frequency motor drives and voltages, resulting in electromagnetic field control [4]. Unlike the FOC, the DTC does not necessitate the use of a current regulator, a complicated coordinate transformation, or a large number of parameters. But DTC has disadvantages, including problems with control at low speeds with huge current and torque pulsation formation [5]. Contemporary DTC utilizes torque and flux hysteresis controls, resulting in higher torque and flux fluctuations [6, 7]. PI controllers have major deficiencies, notably in response to a change in load conditions. Hence, using a blend of fuzzy and PID methodologies, a controller has been designed to supervise the BLDC motor's speed and torque ripple control [8]. In industrial applications, there are several different pulse width modulation techniques available. Out of this, the SVPWM outperforms SPWM in terms of DC bus utilization harmonic distortion, reducing BLDC torque ripple and enhancing BLDC speed regulation effectiveness [9]. The DC-link capacitor for the drive is large and hefty, and the working temperature reduces its endurance. The cost and size of the driver can be reduced with greater torque ripples by avoiding the use of a DC-link capacitor. A sophisticated control method using a combination filter, which is a regulated capacitor, with a spider web-based controller is proposed [10, 11].

In this work, field-oriented control of a BLDC motor employing conventional sinusoidal pulse width modulation (SPWM), space vector pulse width modulation (SVPWM), fuzzy/PID logic regulator, and ultimately a bio-intuitive spider web algorithm controller has been assessed to check the torque pulsation values, the controller price for each case, as well as the settling time and peak overshoot for speed to test the accuracy of the methodologies.

2 System Description

The system shown in Fig. 1 incorporates the dynamics of a BLDC motor with an AC input to feed a full-bridge diode rectifier, which in turn feeds an inverter to a BLDC motor drive-fed electric vehicle with a large DC-link capacitor for the cases analyzed with PWM controllers like SPWM, SVPWM, and fuzzy/PID controller. When using a spider web-based controller, torque ripples are minimized by coupling a tiny capacitor and a switch. A load torque value of T_m is applied to the drive, to

calculate the torque and speed of the motor under various loading conditions. When the BLDC motor is connected to the rectifier-fed inverter arrangement, one switch is always ON during any phase of the motor’s operation, while the other switch alternates between being ON and OFF based on the outputs from the Hall sensor. This is known as the buck converter operation of the BLDC motor [11].

Depending on whether the phase current is kept at the reference current or not, the rectified voltage level for a particular reference current is divided into zones 1 and 2. Zone 2 features a non-linear and unexpected phase current. Since torque and phase current are connected, it is clear from (1) that electromagnetic torque T_e becomes unmanageable in zone 2 [11]. Here ω will be the angular velocity (rads^{-1}) and t is the time in seconds.

$$T_e = \frac{1}{\omega(t)} e(t) i_m(t) \tag{1}$$

The selected BLDC motor drive’s transfer function can be illustrated in (2).

$$G_i(s) = \frac{\omega_m(s)}{V_d(s)} = \frac{\frac{1}{k_e}}{\tau_e \tau_m s^2 + \tau_m s + 1} \tag{2}$$

where ω_m is the speed of the motor, V_d is the DC-link voltage, τ_m is the mechanical time constant, τ_e is the electrical time constant, and k_e is the back-EMF co-efficient. The converter transfer function is given in (3). Gain K_c is used to tune the controller utilizing the Ziegler–Nichols tuning approach.

$$G_c(s) = \frac{d(s)}{V_d(s)} = \frac{K_c}{\tau_c s + 1} \tag{3}$$

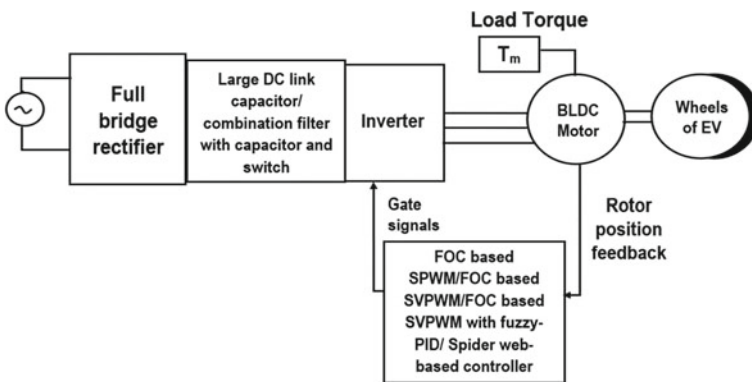


Fig. 1 BLDC motor drive-fed electric vehicle with various PWM controllers

2.1 *Sinusoidal Pulse Width Modulation (SPWM) and Space Vector Pulse Width Modulation (SVPWM)*

To generate SPWM signals for an inverter, the triple sinusoidal outputs are probed with a high-frequency carrier triangle signal. The sinusoidal frequency is 50 Hz and the carrier wave frequency is 5 kHz. Gate pulses are generated by the comparator and used to activate the inverter switches. The more advanced PWM variant known as SVPWM is perfect for use with variable frequency drives. There are only eight possible layouts for a voltage source inverter. Only two of the eight have zero switching states, while the other two have zero output voltages, making them non-switching states. Only six of the eight have non-zero output voltages [4].

2.2 *Fuzzy/PID Controller with SVPWM*

The suggested methodology [11] utilizes Mamdani-type fuzzy set theory, with the integration of common PID controllers [12]. Modifications in fault factors are transferred into linguistic terms with a single output of torque constraint, and membership functions for speed error and deviation in speed have been chosen. The reason for choosing the speed to generate the torque limit is that i_q and i_d will be generated using speed and change in speed errors E and C_e , respectively, for an FOC-controlled system. The i_q generated will be proportional to the torque produced. Computational simplicity exists because the triangular membership functions are chosen for both input and output. The output value is the torque limit, as shown in Fig. 2b, which has a clear linear variation with the degree of membership function, whose value ranges from 0 to 1. The input values are speed error and change in speed error, as shown in Fig. 2. Three distinct labeling linguistics have been established, namely, NE—negative error, ZE—zero errors, and PE—positive error, with the corresponding H—high, M—medium, and L—low as listed in Table 1. The defuzzification method chosen will be the centroid method to be processed into a crisp value [13].

2.3 *Spider Web-Based Controller*

To produce the pulse, an open-loop control approach with two main stages is used. The back emf generated by the BLDC motor is evaluated first, and then the spider jumps between two positions by either making a new web or eating the old web. The pulses given to the inverter are based on the angle switch in the mode of operation of a BLDC motor. In the second step, the spider compares the back-emf value with the input voltage of the inverter, and whenever the value of the back emf falls below the input voltage, the capacitor has to discharge. Hence, a pulse is generated and fed to the switch placed along with a capacitor [14].

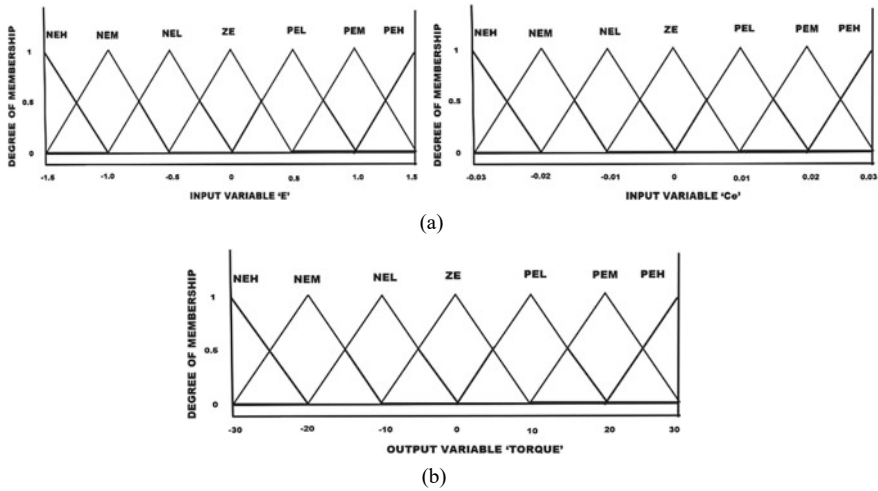


Fig. 2 **a** Speed of the motor and error deviation in the speed of the motor error and **b** torque limit of the motor

Table 1 Fuzzy rule-based controls [13]

E/C_e	NEH	NEM	NEL	ZE	PEL	PEM	PEH
NEH	NEH	NEH	NEM	NEM	NEL	NEL	ZE
NEM	NEM	NEM	NEL	NEL	ZE	PEL	PEL
NEL	NEH	NEM	NEM	NEL	NEL	ZE	NEH
ZE	NEM	NEL	NEL	ZE	PEL	PEL	PEM
PEL	NEL	NEL	ZE	PEL	PEL	PEM	PEM
PEM	NEL	ZE	PEL	PEL	PEM	PEM	PEH
PEH	ZE	PEL	PEL	PEM	PEM	PEH	PEH

3 Simulation Results and Discussion

The BLDC motor specifications chosen are given in Table 2. With an input voltage of 310 V, the rectifier is connected with the large DC-link capacitor, which can be calculated using (4), wherein V is the peak V_{dc} , frequency is denoted by f , and C is the capacitance of the big DC-link capacitor [14].

$$C = \frac{\text{Power}}{2\pi f V^2} = \frac{6000}{2\pi * 50 * 310^2} = 198 \mu\text{F} \tag{4}$$

The pulse is then successively supplied to inverter switches using fuzzy/PID-based SVPWM, space vector pulse width modulation, and sinusoidal pulse width modulation. The controller has two control loops: an inner current control loop and

Table 2 Specifications of the BLDC motor chosen

Characteristics	Values (unit)
Stator inductance per phase	2.01 m H
Stator resistance per phase	0.56 Ω
Moment of inertia	0.0725 kgm ²
Friction coefficient	0.055 Nm s rad ⁻¹
Rated speed	1500 rpm
Rated power	1.2KW
Back-emf constant	0.53 V/rads ⁻¹

an outer speed control loop. As a result, a 220 μ F capacitor is selected since it offers the best value on the market. We reduce the cost of the motor drive using a spider web-based strategy by swapping out a large DC-link capacitance for a switch and a small capacitor. The value of small capacitor C_s for the spider web-based controller is given as in (6) where I_{avg} is the average current taken to the motor from the DC bus which can preserve $i_m(t)$ at I_{ref} [14]. The switch is simple to operate, no additional materials are required to make sure rapid switching. The switching loss of extra switches is not significant due to the lower switching frequency and current connected with the inverter's MOSFETs.

$$t = \frac{1}{2\pi f} \sin^{-1}\left(\frac{E}{V_m}\right) = \frac{1}{2\pi * 50} \sin^{-1}\left(\frac{95}{305}\right) = 0.0577 \text{ s} \quad (5)$$

$$C_s = \frac{2t I_{avg}}{V_m - E} = \frac{2 * 0.0577 * 0.02}{305 - 95} = 10 \mu\text{F} \quad (6)$$

As illustrated in Fig. 3a, a load torque of 10 Nm is initially applied, followed by a load torque of 20 Nm at 6 s, which causes the torque to develop and the speed to fall below their respective rated values at that time. Additionally, utilizing SVPWM and SPWM approaches, Fig. 3b, c displays the corresponding electromagnetic torque generated by the motor. For SVPWM and SPWM, the torque ripples generated are provided by (7) and (8), respectively.

$$T_{\text{ripple}} = \frac{T_{\text{max}} - T_{\text{min}}}{T_{\text{avg}}} * 100\% = \frac{20.3819 - 18.15}{19} * 100\% = 13.15\% \quad (7)$$

$$T_{\text{ripple}} = \frac{21 - 17.5}{19} * 100\% = 18.42\% \quad (8)$$

While Fig. 4a, b shows the torque fluctuations produced by the spider web-based controller and the fuzzy/PID controller, respectively, their pulsation values can be calculated using (7) as 14.63% and 7.89%. According to [15, 16], the settling time (T_s), defined as the amount of time needed for the response curve to reach 5% or 2% of the final value, and the overshooting, defined as the maximum peak value of the response curve measured from the desired response of the system, are the two

main parameters that should be minimized. The trial-and-error technique is used to determine the PID controller parameters for the scheme. The optimal option for the gains was established by testing with various iterations. As an outcome, we picked 0.6 as the proportional gain, 6 as the integral gain, and 0.002 as the derivative gain. That can all be incorporated straight into the motor controller. The torque pulsations in Figs. 3b, c and 4b show a lower overshoot value of starting torque due to the presence of PID controllers in these techniques compared to the spider web-based controller approach in Fig. 4a, which helps them to reduce or eliminate steady-state error. As the steady-state error is high in the spider web-based controller approach, the settling time of torque after the application of load torque is increased compared to other techniques.

The speed regulation achieved by PWM controllers is shown in Fig. 5a, b, with fuzzy/PID controllers providing the best speed regulation. The calculated values of percentage overshoot and settling time from the corresponding speed responses are given in Table 3, along with a comparison of cost and torque ripples. The ripples are highest for the SPWM method with 18.42%, with an increased settling time of 3.22 s and a speed overshoot of 2.1%. This method is also costly as a large DC capacitor is employed in it. The SPWM, when compared with SVPWM, draws more current with higher pulsations in the torque profile and has lower maximum voltage values. In the spider web-based controller, although it has higher torque ripples of 14.63%, a longer settling time of 2.26 s, and increased overshoot percentages of 2% compared to the SVPWM method, it utilizes only a small capacitor with switch combination, making it an affordable and durable method. A blend of PID and the fuzzy controller has the least torque ripples of only 7.89% with a decreased settling time of 1.98 s and the least speed overshoot of 0.5% with a large capacitor employed in them. In general, they offer better stability to the system by reducing its steady-state error.

4 Conclusion

A field-oriented control (FOC) of a BLDC motor utilizing sinusoidal pulse width modulation (SPWM), space vector pulse width modulation (SVPWM), fuzzy/PID logic control scheme (FLC/PID), and finally a bio-intuitive spider web-based algorithm control scheme has been compared. For choosing the technique best fit for application to an electric vehicle, we may opt for the fuzzy/PID controller-based technique as it has lessened torque ripples and better speed response with improved overshoot percentage and settling time in its speed response than other techniques and provides a stable operation of the system. The spider web-based controller is the cheapest technique as it uses a small capacitor and switch combination, a contrast to the other techniques where the large capacitor is used but the stability of the system is not guaranteed.

As a future scope of this analysis, the cost of fuzzy/PID controller which is high due to the presence of a large capacitor can be considered to be replaced by smaller rated capacitors. This will make the controller affordable and efficient.

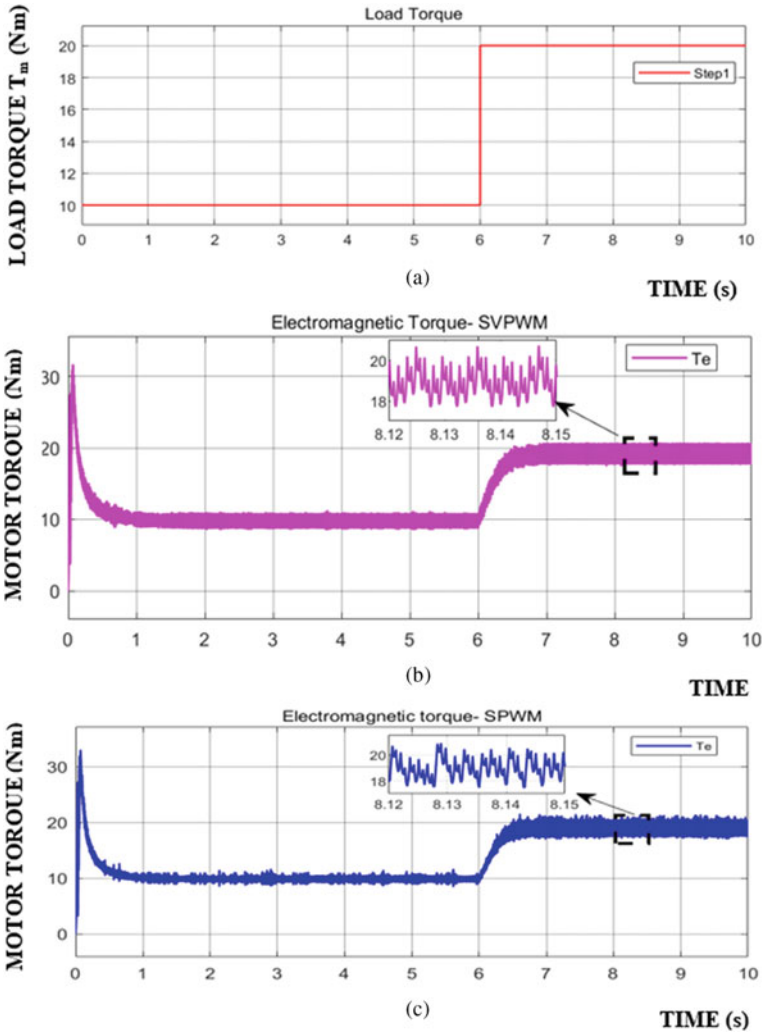


Fig. 3 a Load torque applied to BLDC motor drive in Nm, b Motor torque produced by SVPWM controller in Nm, c Motor torque produced by SPWM controller in Nm

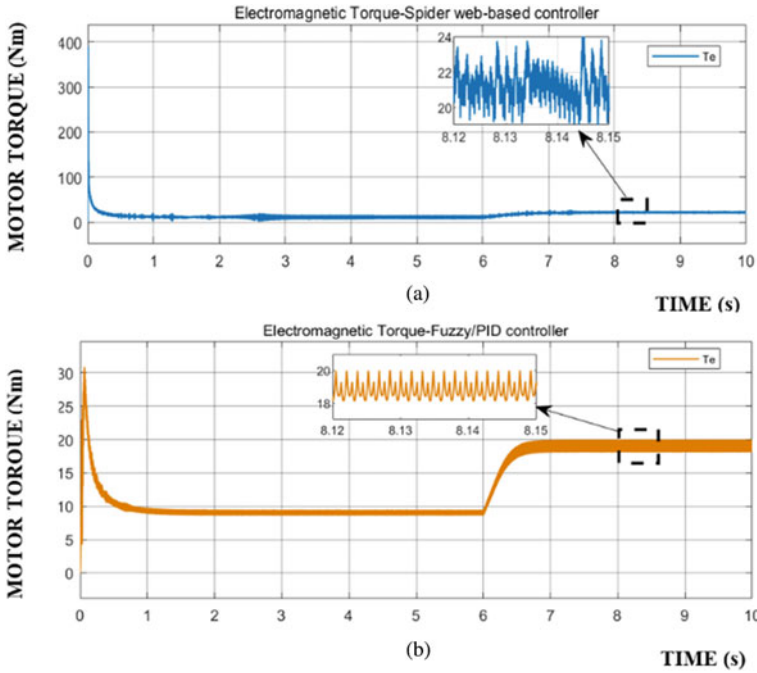


Fig. 4 a Motor torque produced by spider web-based controller in Nm, b Motor torque produced by fuzzy/PID controller in Nm

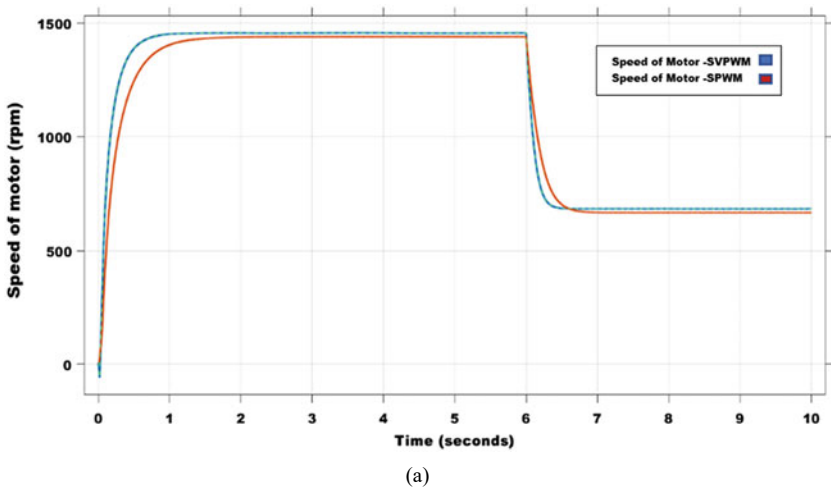
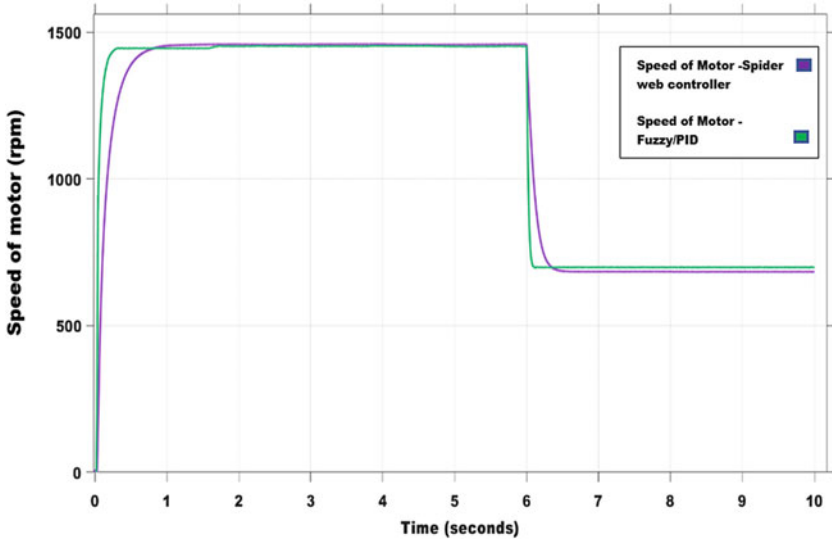


Fig. 5 a Speed produced by a motor using SPWM and SVPWM, b Speed produced by a motor using fuzzy/PID controller and spider web-based controller



(b)

Fig. 5 (continued)

Table 3 Comparison of all cases

Cases	Torque ripple (%)	Cost	Settling time (s)	Speed overshoot (%)
SPWM	18.42	High	3.22	2.1
SVPWM	13.15	High	2.34	1.3
Fuzzy/PID	7.89	High	1.98	0.5
Spider web-based controller	14.63	Low	2.26	2.0

References

1. Kumar M, Moulik B (2021) Dynamic modeling and analysis of control techniques of an induction motor drive for application in an electric vehicle. In: Proceedings–international conference on computing, communication, and intelligent systems 2021, ICCICIS, pp 1037–1042
2. Gadewar SV, Jain AM (2017) Modelling and simulation of three phase BLDC motor for electric braking using MATLAB/simulink. Int J Electr Electron Data Commun 5(7):48–53
3. Maharajan MP, Xavier SAE (2019) Design of speed control and reduction of torque ripple factor in BLDC motor using spider based controller. IEEE Trans Power Electron 34(8):7826–7837
4. Gujjar MN, Kumar P (2017) Comparative analysis of field-oriented control of BLDC motor using SPWM and SVPWM techniques. In: Proceedings–2nd IEEE international conference on recent trends in electronics, information & communication technology 2017, RTEICT, pp 924–929
5. Korkmaz F, Topaloğlu İ, Çakır MF, Gürbüz R (2013) Comparative performance evaluation of FOC and DTC controlled PMSM drives. In: Proceedings-4th international conference on power engineering, energy and electrical drives 2013, POWERENG, pp 705–708

6. Patil MS, Medhane R, Dhamal SS (2020) Comparative analysis of various DTC control techniques on BLDC motor for electric vehicle. In: Proceedings-7th international conference on smart structures and systems 2020, ICSSS, pp 1–6
7. Kumar KVP, Kumar TV (2016) Direct torque control of brush less DC motor drive with modified switching algorithm. In: Proceedings–IEEE international conference on power electronics, drives and energy systems 2016, PEDES, pp 1–5
8. Apribowo CHB, Musyaffa' A, Maghfiroh H (2021) Fuzzy logic controller and its application in brushless DC motor (BLDC) in electric vehicle-a review. *J Electr Electron Inf Commun Technol* 3(1):35–43
9. Li B, Wang C (2016) Comparative analysis on PMSM control system based on SPWM and SVPWM. In: Proceedings-Chinese control and decision conference 2016, CCDC, pp 5071–5075
10. Fathima A, Vijayasree G (2021) Design of BLDC motor with torque ripple reduction using spider-based controller for both sensed and sensorless approach. *Arab J Sci Eng* 47(3):2965–2975
11. Samitha Ransara HK, Madawala UK (2015) A torque ripple compensation technique for a low-cost brushless DC motor drive. *IEEE Trans Ind Electron* 62(10):6171–6182
12. Nanda B (2015) Fuzzy logic based field oriented control of permanent magnet synchronous motor. *Int J Electr Electron Data Commun* 3(8):27–33
13. Dhamodharan RV, Kowsalya M, Priyadharshini G (2015) SVPWM based performance analysis of BLDC motor. *Int J Adv Res Electr, Electron Instrum Eng* 4(3):1570–1576
14. Veni KSK, Kumar NS, Gnanavadivel J (2017) Low-cost fuzzy logic-based speed control of BLDC motor drives. In: Proceedings-2017 international conference on advances in electrical technology for green energy 2017, ICAETGT, pp 7–12
15. Chowdhury R (2020) Cob-web building controller for reduced torque ripples in BLDC motor drive. *Int J Res Appl Sci Eng Technol* 8:725–732
16. Sharma PK, Sindekar AS (2016) Performance analysis and comparison of BLDC motor drive using PI and FOC. In: Proceedings-international conference on global trends in signal processing, information computing and communication 2016, ICGTSPICC, pp 485–492
17. Ahmed AM & Ali-Eldin A, Elksasy M, Areed F (2015) Brushless DC motor speed control using both PI controller and fuzzy PI controller. *Int J Comput Appl* 109:29–35

Comparison of Different Topologies of Multilevel Inverter



G. Shilpa, Divyansh Singh, Sayan Ghosh, and S. Mohneesh

Abstract Multilevel inverters are being used in the production/industrial sector for quite some time. They are generally used to achieve high power output from medium-level voltage sources. They reduce the harmonic distortion (also known as total harmonic distortion or THD) present in the output voltage generated by these multilevel inverters. This paper tries to compare the different topologies of multilevel inverters which are cascaded h-bridge multilevel inverter, modular multilevel converter, and diode clamped multilevel inverter. The topologies have been simulated in MATLAB SIMULINK software and the final results are tabulated.

Keywords Multilevel inverter (MLI) · Diode clamped MLI · Cascaded H-bridge MLI (CHB) · Modular multilevel converter (MMC) · Pulse width modulation (PWM) · Phase disposition pulse width modulation (PD-PWM) · Phase opposition disposition (POD-PWM) · Total harmonic distortion (THD)

1 Introduction

Multilevel inverters have played an important role by enabling us to achieve a waveform close to sinusoidal waveform from DC supply [1–3]. The more the sinusoidal a waveform is, lower the harmonic distortions present in it. Multilevel inverters were introduced which made the generation of more than two levels in the output voltage possible [4–7].

The three topologies used for comparison here are diode clamped, cascaded H-bridge multilevel inverter and modular multilevel converter. These circuits were simulated on the MATLAB (SIMULINK) software and the output voltage waveforms were obtained from the same. The modulation techniques which are used are level-shifted pulse width modulation (PWM), namely, Phase Opposition Disposition PWM (POD-PWM) and Phase Disposition PWM (PD-PWM) [8–12]. The circuits

G. Shilpa · D. Singh (✉) · S. Ghosh · S. Mohneesh
Department of Electrical and Electronics Engineering Bangalore, BMS Institute of Technology and Management, Bangalore, India
e-mail: divyanshsingh2405@gmail.com

simulated produces five levels of voltage in the output. The comparison between them is drawn on the basis Total Harmonic Distortion (THD), the total number of switches required, etc.

2 Different Topologies of MLI

In this paper, three topologies considered and simulated are diode clamped MLI, cascaded H-bridge MLI, and modular multilevel converter.

2.1 Diode Clamped MLI

The diode clamped MLI is also known as neutral point clamped MLI (NPC-MLI) and is quite popular in low-level inverters. In the case of a five-level diode clamped MLI we have voltage levels as $-V_{dc}/2$, $-V_{dc}/4$, 0 , $V_{dc}/4$, and $V_{dc}/2$. By controlling the switching pattern of all the switches, it is possible to obtain a stepped output waveform. For an N-level diode clamped inverter, we need $2(N - 1)$ switches. In this topology, more number of diodes is required. Hence this topology is not suitable for higher voltage levels (such as 9-level or 15-level MLI) (see Fig. 1).

2.2 Cascaded H-Bridge MLI (CHB-MLI)

This topology uses H-bridges (an electronic circuit that resembles the shape of the letter “H”) connected to each other in a cascade connection. To obtain higher voltage levels in the output, more h-bridges can be connected together to achieve the said objective. The number of bridges required depends upon the number of output levels needed in the output. The relation between the number of bridges and the number of levels is as follows: for $(2n + 1)$ levels in the output waveform, we have to use n h-bridges in the circuit. Hence, in order to obtain five levels in the output waveform, we will need $2n + 1 = 5$, i.e., $n = 2$ bridges. The five voltage levels that will be obtained in the output waveform are $-2V_{dc}$, $-V_{dc}$, 0 , $+V_{dc}$, and $+2V_{dc}$. Here V_{dc} is the voltage rating of the DC voltage source connected in each half of the circuit. This topology uses less number of components than the other two topologies considered. Every bridge added to the existing network will increase the number of levels in the output waveform by 2. Since it requires lesser components than the other two topologies, it is also cheaper to build and it is easier to increase the number of levels in this topology (see Fig. 2).

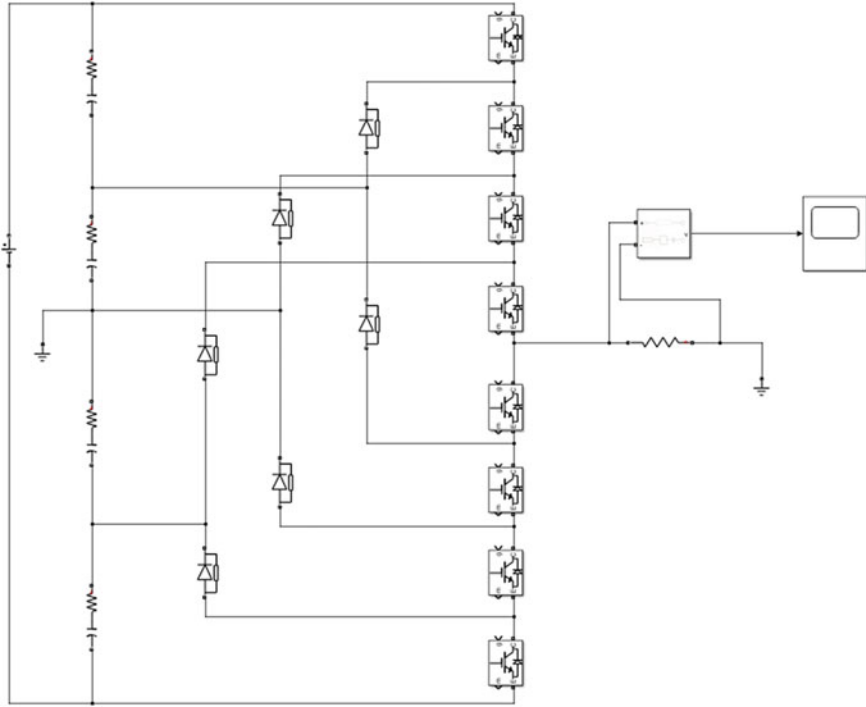


Fig. 1 5 Level diode clamped MLI

2.3 Modular Multilevel Converter (MMC)

It is a comparatively newer voltage source converter used for high-voltage applications. The output voltage levels produced by this converter are $-V_{dc}$, $-V_{dc}/2$, 0 , $+V_{dc}/2$, and $+V_{dc}$ where V_{dc} is the DC voltage source applied to each half of the converter. Each leg has two arms known as upper and lower legs. Each arm has sub-modules that are identical to each other and depending upon the switching pattern, the voltage sources get connected together to produce the net output voltage across the measuring terminals. The limitations of this circuit can be listed as follows: bigger circuits, complicated control strategies, etc. (see Fig. 3).

3 Modulation Techniques

In this paper, we have made use of two pulse width modulation (PWM) techniques for the three topologies. They are Phase Disposition PWM (PD-PWM) and Phase Opposition Disposition PWM (POD-PWM).

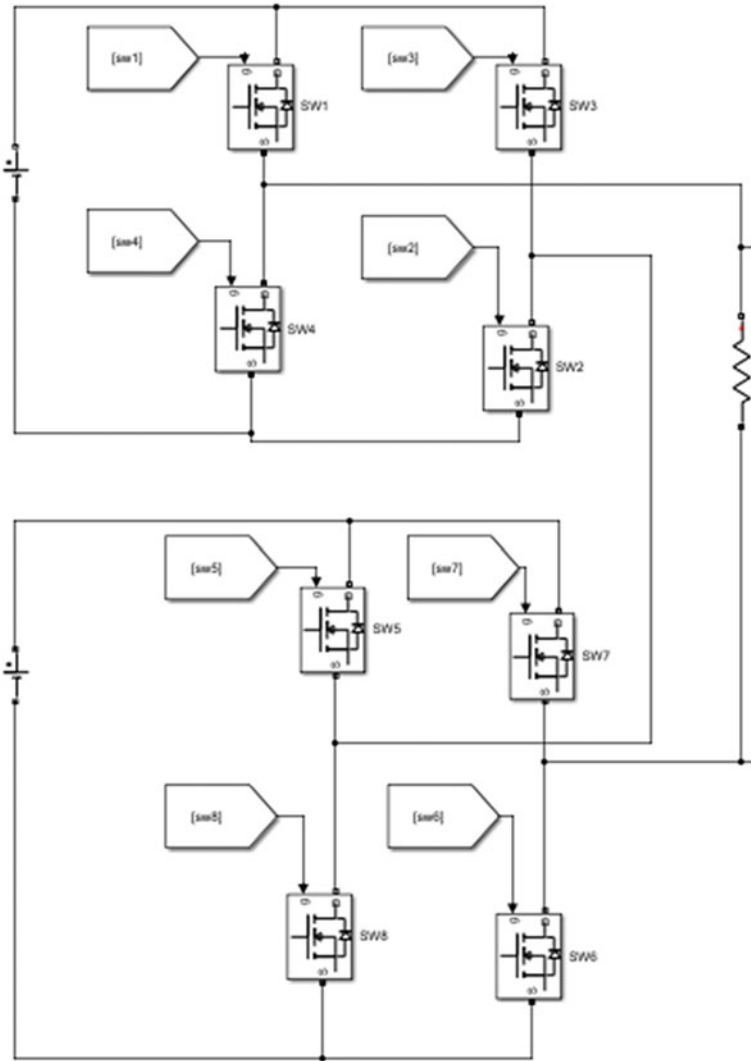


Fig. 2 5 Level cascaded H-bridge MLI

3.1 Phase Disposition Pulse Width Modulation (PD-PWM)

In the mentioned technique, the triangular waves (carrier waves) are in phase with respect to each other and are arranged in a manner as shown in Fig. 4. The carrier waves are compared with the reference wave (sinusoidal wave) to obtain the pulses required for triggering the switches.

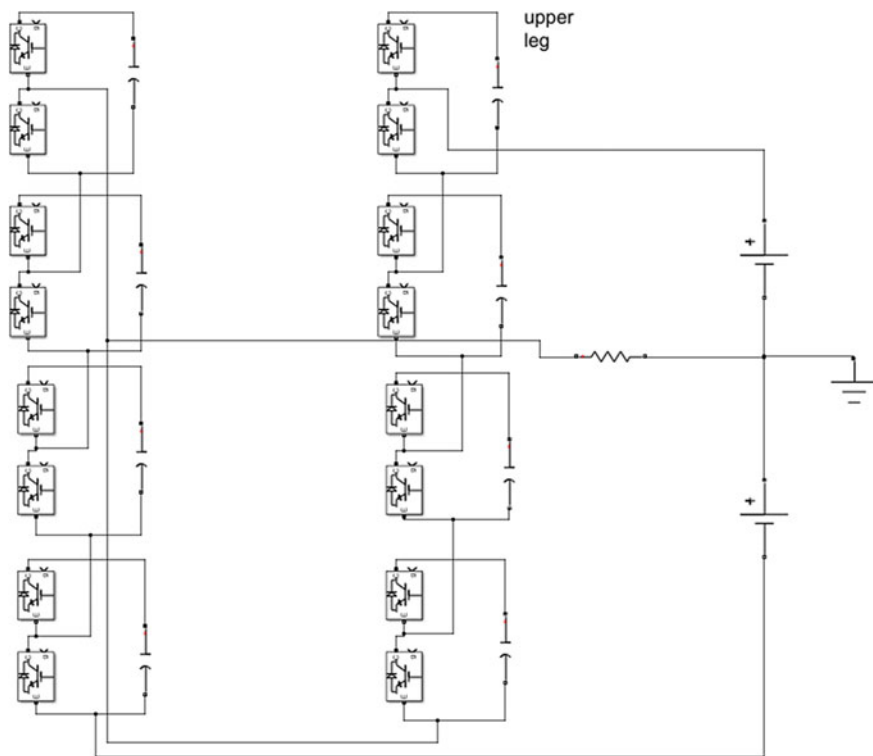


Fig. 3 Five-level modular multilevel converter

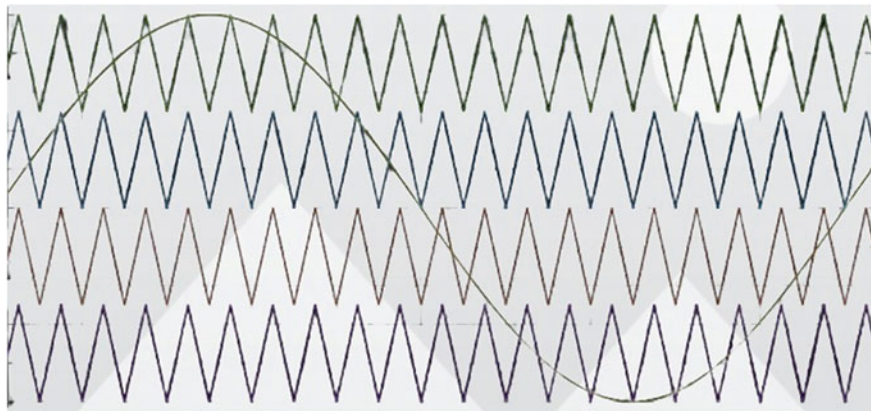


Fig. 4 PD-PWM, four triangular (carrier) waves and one reference sinusoidal wave

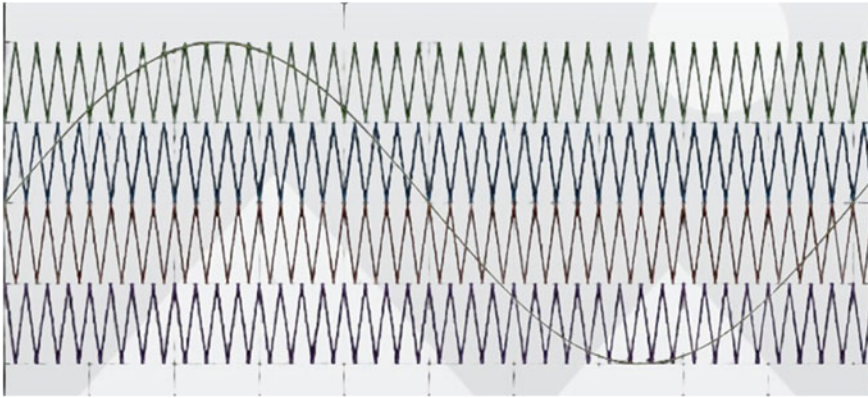


Fig. 5 POD-PWM, four triangular(carrier) waves and one reference sinusoidal wave

3.2 Phase Opposition Disposition Pulse Width Modulation (POD-PWM)

In this technique, the triangular waves (carrier waves) are in phase above the reference line and out of phase by 180° with the triangular waves below the reference line. The generated waveform is shown in Fig. 5.

4 Results

The three topologies of multilevel inverters with two types of modulation techniques were simulated in MATLAB SIMULINK. The results obtained for five-level multilevel inverters are as shown below.

4.1 Diode Clamped

See Figs. 6 and 7.

4.2 Cascaded H-Bridge (CHB)

See Figs. 8 and 9.

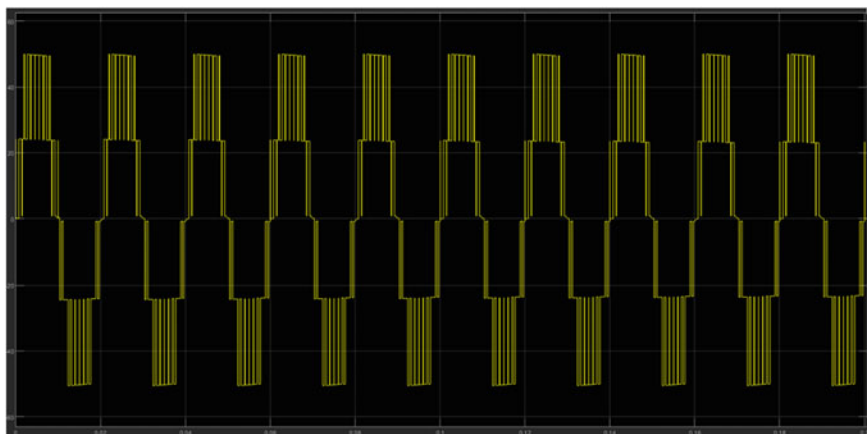


Fig. 6 Output voltage waveform obtained in diode clamped topology with PD-PWM technique

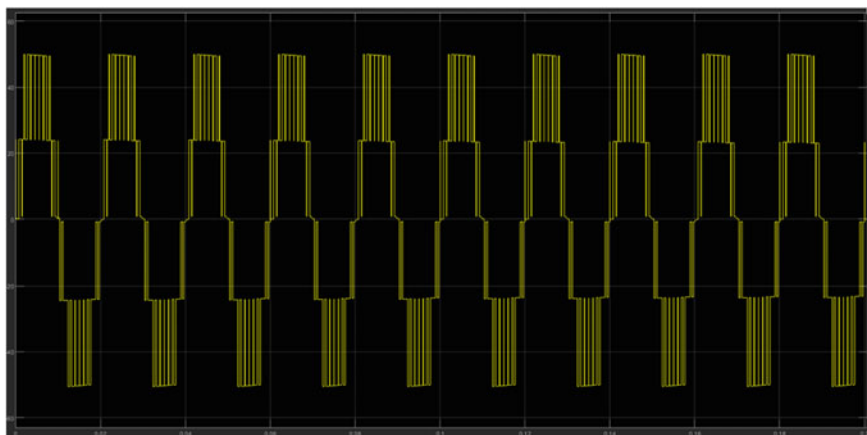


Fig. 7 Output voltage waveform obtained in diode clamped topology with POD-PWM technique

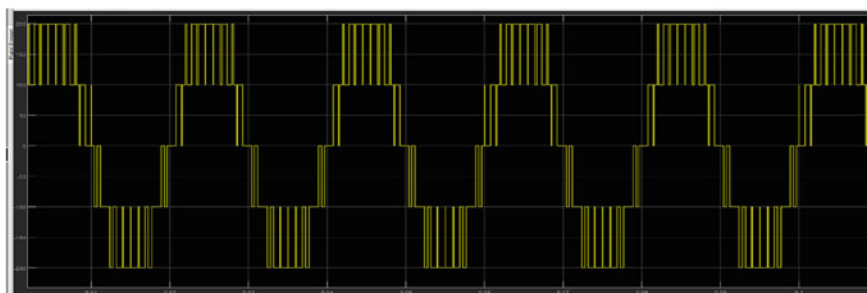


Fig. 8 Output voltage waveform obtained in CHB topology with PD-PWM technique

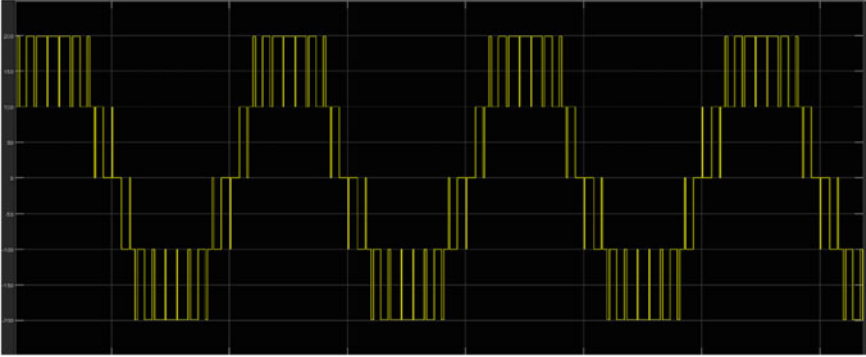


Fig. 9 Output voltage waveform obtained in CHB topology with POD-PWM technique

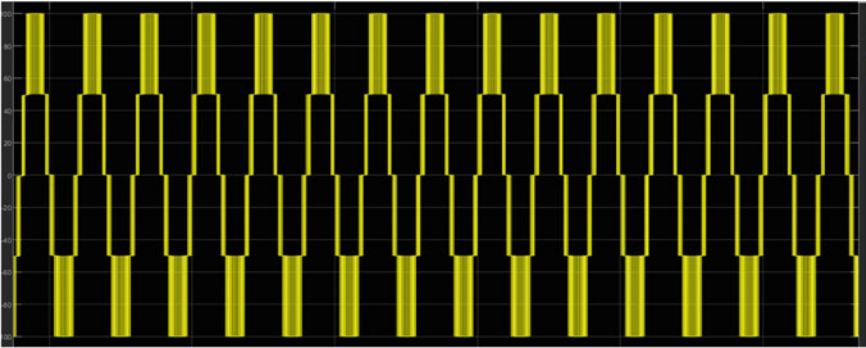


Fig. 10 Output voltage waveform obtained in MMC topology with PD-PWM technique

4.3 *Modular Multilevel Converter (MMC)*

See Figs. 10 and 11.

The total harmonic distortions (THDs) of the three topologies for the two modulation techniques are tabulated below (see Table 1).

The other parameters that are compared are as follows (see Table 2).

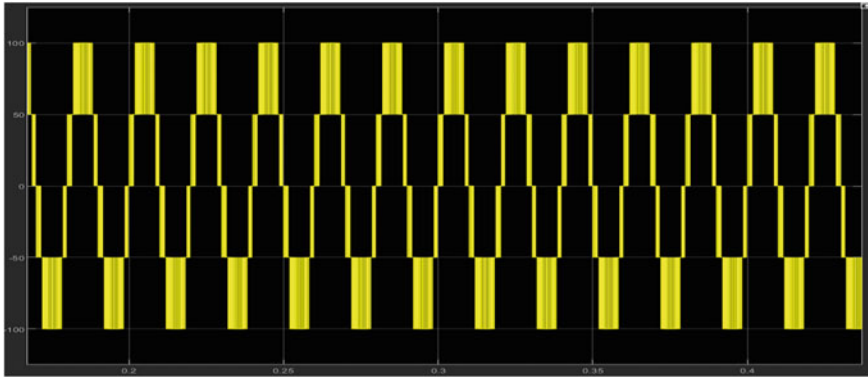


Fig. 11 Output voltage waveform obtained in MMC topology with POD-PWM technique

Table 1 Comparison of THD observed in the output voltage waveform of all the circuits

Topology/switching technique	Total harmonic distortions (THDs)	
	PD-PWM	POD-PWM
Diode clamped	29.76	29.37
Cascaded H-bridge	26.90	26.93
Modular multilevel converter	37.15	37.89

Table 2 Comparison of other parameters of the circuits simulated

Parameters	Diode clamped	CHB	MMC
Complexity	Medium-level complexity	Increases at higher level	Low
No. of switches	8	8	16
No. of capacitors	4	0	8
No. of diodes	14	8	16
No. of DC battery	1	2	2
THD	Medium	Lowest	Highest

5 Conclusion

From the simulation results, we can conclude that cascaded h-bridge topology of MLI is the best among the three topologies. The total harmonic distortion observed in the output voltage is the least compared to other two topologies, viz, diode clamped MLI and modular multilevel converter. The other advantage of cascaded h-bridge is that higher levels in the output waveform can be easily obtained by cascading required number of h-bridges to the circuit.

References

1. Lai JS, Peng FZ (1996) Multilevel converters—a new breed of power converters. *IEEE Trans Ind Appl* 32:509–517
2. Rodriguez J, Lai S, Peng FZ (Aug 2002) Multilevel inverters: survey of topologies, controls, and applications. *IEEE Trans Ind Appl* 49(4):724–738
3. Anjali Krishna R, Padma Suresh L (2016) A brief review on multi level inverter topologies. In: 2016 international conference on circuit, power and computing technologies [ICCPCT]
4. Patil PH, Rajeev M (2015) Comparison of three different topologies of a fivelevel multilevel inverter. *IJERT*. Conference proceedings. ISSN: 2278-0181, ICNTE-2015
5. Nanda L, Dasgupta A, Rout UK (2017) A comparative study of different topologies of multi-level inverter with SIMULINK. *Inventive Systems and control (ICISC)*, 2017 international conference on IEEE
6. Sharma V (Nov 2017) Diode clamped multilevel inverter switching topology. *IJERT* 4(11). ISSN: 2347-6982, 2349–204X
7. Chandragupta Mauryan KS (Jan 2020) Design of five-level cascaded H-bridge multilevel inverter. https://doi.org/10.1007/978-981-15-2256-7_7
8. Gupta KK, Jain S (2012) Topology for multilevel inverters to attain maximum number of levels from given DC sources. *IET Power Electron* 15(4):435–446
9. Holmes G, Lipo TA (2003) Pulse width modulation for power converters
10. Kang DW, Hyun S (2005) Simple harmonic analysis method for multi-carrier PWM techniques using output phase voltage in multi-level inverter. *IEEE Proc Electron Power Appl* 152(2)
11. Rathore S, Kirar MK, Bhardwaj SK (Sep 2015) Simulation of cascaded H-bridge multilevel inverter using PD, POD, APOD techniques. *Int J (ECIJ)* 4(3)
12. Kang DW, Rodríguez J (2004) Direct torque control with imposed switching frequency in an 11-level cascaded inverter
13. Beig AR, Dekka A (2012) Experimental verification of multilevel inverter-based standalone power supply for low-voltage and low-power applications. *IET Power Electron* 5(6):635–643

Design and Analysis of Off-Grid Solar Photovoltaic System for a Residential Building in Omaxe City, Jaipur



Peeyush Garg , Mahipal Bukya, and Pancham Kumar

Abstract The solar energy is a prominent alternative source of energy for wide range of utilities including industrial and domestic requirements. The electricity has been irreplaceable requirement to run the household equipment's, which is generally supplied by government body. The electricity charges and regularity of uninterrupted supply are always prime concern at many places in India. So, the solar photovoltaic sustainable modules are one of the better options of existing electricity supply. This article discussed the design and evaluation of a small off-grid solar PV plant for fulfilling the energy needs of a residential house, situated at Omaxe City, Jaipur. The average monthly and annually consumption of 172 m² area villa are around 350 units and 4200 units, respectively. A 2 KW off-grid solar photovoltaic system was installed and investigated to meet the energy requirement. The presented analysis has also discussed its financial implication, economic benefits, and the reduction of the traditional energy reservoirs.

Keywords Solar energy · Photovoltaic system · Electricity consumption · Economic benefits

1 Introduction

The solar energy is a green energy and suitable alternative of convectional energy [1]. Convectional fossil energy has many adverse side effects like climate change, pollution, disturb the bio-diversities, and especially adverse effects on human health

P. Garg

Department of Electrical Engineering, Manipal University Jaipur, Dahmi Kalan, India

M. Bukya (✉)

Manipal Institute of Technology Bengaluru, Manipal Academy of Higher Education, Manipal, India

e-mail: mahipalbukya@gmail.com

P. Kumar

Department of Electrical Engineering, Bhartiya Skill Development University, Jaipur, India

[2, 3]. The scarcity of fossil fuels is one of the main reasons to find appropriate substitute of clean energy sources [4, 5].

The utilization of renewable energy technologies for energy generation is increasing at a quicker rate in the modern period [6, 7]. In addition to the fact that solar energy systems have a poor efficiency, an energy payback period study must be performed to evaluate the most cost-effective conditions.

Ample daylight and solar radiation level makes Rajasthan a perfect place to use solar energy to convert into electric energy throughout the year. This geological location generally depicts solar radiation of 6–7 kWh/m²/day with approximately 300 sunny days per year [8–10].

This article discusses the design and evaluation of a solar PV plant for fulfilling the energy needs of a residential house of two BHK with a land area of 172 m², located in Omaxe City, Jaipur. Omaxe City Jaipur is a town in the Indian state of Rajasthan which is located at 26.84-degree latitude and 75.63-degree longitude. The average daily electrical unit usage in the residence is roughly 12 units, and the average monthly consumption is approximately 350 units.

An efficient solar PV system with a capacity of 2 kWp has been identified, built and an economic analysis of the system has been conducted. In this case, a cost–benefit analysis has also been performed to determine the amount of time during which the planned solar PV system will provide free energy.

2 Electrical Load Estimation

A solar PV system is designed from the ground up, starting with an assessment of electrical load at the proposed location, and then proceeding to the sizing and selection of inverters, the sizing and selection of batteries, then the size and selection of solar PV modules. Construction of a solar PV system necessitates the collection of geographic and weather information about the site [10–14]. Table 1 indicates the electrical load estimation of domestic Villa.

3 Designing of PV System

The designed system mainly comprises inverter, battery bank, and PV cell. The complete layout of designed system is represented in Fig. 1 and has shown the energy flow in the system. The solar panel converted the solar energy into electrical energy, which was further provided to charge controller unit. The charge controller unit is not only regulating the solar panel performance also handling the charging of battery unit. Then the off-grid inverter is used to convert the dc-to-ac signal, for further utilization by AC domestic load. Many control strategies and home automation system are available and implemented to optimize the power requirement and provide better control of household utilities and domestic load [15–17].

Table 1 Electrical load estimation of Omaxe City Villa for a day

Type of load	Power rating (Watt)	Hours of use (Hrs.)	No. of load	Total power (Watt)	Total energy (Wh)
Bulb	15	10	5	90	450
Tub light	40	10	2	80	800
Fan	60	16	3	180	2760
Cooler/heater	150	15	1	150	2250
TV	80	7	1	80	560
Computer/laptop	120	5	1	120	600
Refrigerator	150	24	1	150	3600
Electric iron	1000	1	1	1000	1000
Total				1550	12,020

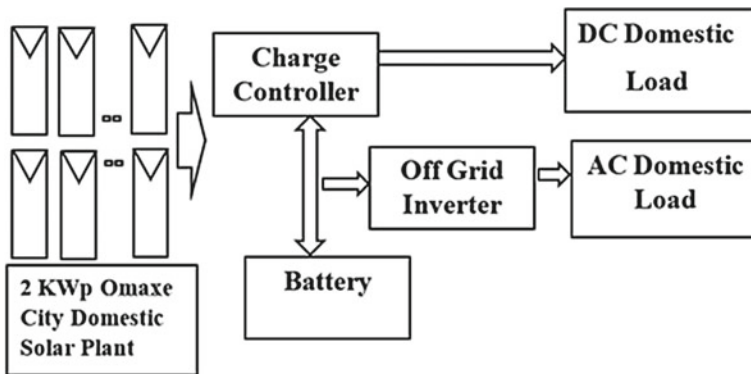


Fig. 1 Layout of Omaxe City domestic solar power plant schematic diagram

The present work is described about the selection of proper inverter, battery bank, and PV cell for the required load estimated for a building. The estimated maximum power requirement for a villa is 1500 W and total energy required is 12,020 Wh for a day. In the process of designing, the sizing and selection of off-grid inverter is calculated, considering the power efficiency of the inverter is 80–85%. The inverter voltage is 24 V, and the required real power is 1550 W, as depicted in Table 1. The efficiency is ratio of output power to input power. So, the input of inverter system must be $1500/0.85 = 1824$ W. As a result, a 2KVA, 24 V off-grid converter is required to power a solar PV system with an approximate power rating of 2000 Wp.

Also, the total energy required in a day is 12,020 W-Hour (Wh). Considering 85% efficiency, the required energy per day is 14,141 Wh per day. Next is the selection and sizing of battery for store energy and backup. As per previous analysis, the total required energy is 14,141 W-h or Volt-Ampere-hr (VAh). As we know system voltage is of 24 V, battery capacity must be 589.2 Ah. Now, the battery bank size selection

depends on battery capacity in Ampere-hour (Ah), depth of discharge (DOD) of battery, and efficiency of the Battery, which are 589.2 Ah, 80% and 85%, respectively. So, the real capacity of battery bank is 866.5 Ah, which is essentially used to decide the battery bank size.

The required battery bank size is same as the calculated real power. Lithium cell (Li-Cell) of 250 Ah/12 V is most common battery used in market nowadays. There are many series–parallel arrangement of cells which can be constructed to battery bank. As the required system voltage is 24 V, total two Li-cell need to be connected in series to achieve the desired system voltage. After that, total four such series arrangements need to be connected in parallel to develop a battery bank of desired current capacity requirement (866.5 Ah). So, the resultant arrangement of cells in battery pack can be nomenclated as 4S2P. Overall, eight cells are required to prepare the battery bank of the developed system.

The battery bank is supplied by solar-powered PV module. The selection of solar power module depends on power rating of the module and the specification of battery bank. As a thumb rule, 1 KWp solar plant generates 4 kWh energy per day. Consider that the available solar power module has rating of 320 W/30 V. The number of PV module required can be estimated by dividing the required total power generation to specified power by one module. Here, the number of PV modules required is 11 for the designed system.

4 Cost Analysis of Developed PV System

A solar PV system for any purpose, small or big, residential, or commercial, may be designed using the technique indicated in previous section. It's also important to remember that the following approach and assumptions were chosen for their simplicity and that they are sufficient for a first estimate.

This is very necessary to estimate the development cost of designed PV system and compare with alternatives available in market. The developed solar photovoltaic system is established with mainly three particulars, including solar panel, solar battery pack, and solar inverter. The selection of these particulars is explicated in previous section. The current cost calculation of developed solar photovoltaic system is mentioned in Table 2, which is approximately Rs. 3.15 lakhs.

The advancement in solar panel and batteries has been tending toward more efficiency, better performance, and lower cost, so it will be best suited for domestic buildings compared to conventional distribution systems. So, the approximate cost estimation of 2 KW solar PV system is in the range of 3–3.5 lakhs in present. There are many alternatives packages available in market with same estimated cost. UTL Off-Grid Solar System specifications have been considered for analysis and are mentioned in Table 3.

The energy payback time (EPBT) of design system is ratio of total cost of solar power plant to yearly unit cost generation by solar plant, which is around 11.5 years.

Table 2 Cost calculation of developed solar photovoltaic system

Particulars	Description	Qty	Unit price	Price (Rs)
Solar panel	Make: Adani 320 Wp/30 V	11	10,500	1,15,500
Solar battery	Make: Luminous 200 Ah/12 V	8	20,000	1,60,000
Solar inverter	Make: UTL Gamma, Capacity = 2KVA, Max PV Voltage = 45 V–90 V, Max PV Current = 80 A	1	26,000	26,000
Installation cost	2 KW	–	7,000	14,000
	Total price (in Rs.)			3,15,500

Table 3 2 KW UTL make off-grid solar PV system specification

Particulars	Description
Solar system capacity	2 kW
Solar panel quantity	6 nos
Solar inverter	2.5 kVA solar inverter
Solar battery	4 nos
Accessories	Fasteners, cable tie, crimping tool, earthing kit, lightning arrestor
System warranty	25 years
MC4 connector	2 pair
DC wire and AC Wires	30 and 20 m
Space required	18.5 m ²
Average generation	8 units per day

The life cycle of plant is around 25 years. The proposed system will produce free electricity for around 13.5 years after 11.5 years.

5 Conclusion

With the use of real-time market pricing and associated criteria, this study attempts to evaluate the financial viability of a solar PV system for a residential property in Omaxe City, Jaipur and determine its financial viability.

The 2 kWp solar PV system has been created, and it requires 11 solar PV modules with a capacity of 320 Wp, eight batteries with a capacity of 200 Ah/12 V, and one 2KVA inverter. The plant's economic payback time (EPBT) is 11.5 years, compared to the cost of installing a solar PV system, which is Rs. 3,15,000. During the system's lifetime, the planned system would generate free power worth Rs 3.68 lakhs, which can be utilized for other purpose and produce additional income to the user.

References

1. Kannan N, Vakeesan D (2016) Solar energy for future world: A review. *Renew Sustain Energy Rev* 62:1092–1105
2. Perera F, Nadeau K (2022) Climate change, fossil-fuel pollution, and children's health. *N Engl J Med* 386(24):2303–2314
3. Mohtasham J (2015) Renewable energies. *Energy Procedia* 74:1289–1297
4. Wang H, Wang G, Qi J, Schandl H, Li Y, Feng C, Liang S (2020) Scarcity-weighted fossil fuel footprint of China at the provincial level. *Appl Energy* 258:114081
5. De Cian E, Sferra F, Tavoni M (2016) The influence of economic growth, population, and fossil fuel scarcity on energy investments. *Clim Change* 136(1):39–55
6. Basha JS, Jafary T, Vasudevan R, Bahadur JK, Ajmi MA, Neyadi AA, Fattah IR (2021) Potential of utilization of renewable energy technologies in gulf countries. *Sustainability* 13(18):10261
7. Lin B, Li Z (2022) Towards world's low carbon development: the role of clean energy. *Appl Energy* 307:118160
8. Bhukya MN, Kumar M, Kant A (2021 Apr) Renewable energy: potential, status, targets and challenges in Rajasthan. In: *Journal of physics: conference series*, vol 1854, no 1. IOP Publishing, p 012004
9. Mahaver VK, Rao KVS (2018 Nov) Solar energy potential of the state of Rajasthan in India. In: *2018 3rd international innovative applications of computational intelligence on power, energy and controls with their impact on humanity (CIPECH)*. IEEE, pp 56–61
10. Kumar BS, Sudhakar K (2015) Performance evaluation of 10 MW grid connected solar photovoltaic power plant in India. *Energy Rep* 1:184–192
11. Adaramola MS (2014) Viability of grid-connected solar PV energy system in Jos, Nigeria. *Int J Electr Power Energy Syst* 61:64–69
12. Sheoran M, Kumar P, Sharma S, Bukya M (2022) Current situation analysis of solar PV waste management in India. *Mater Today Proc* 58:773–782
13. Anonymous 2017 press information Breau, ministry of new and renewable energy, government of India. <http://pib.nic.in/newsite/pmreleases.aspx?mincode=28>. Accessed 13 Aug 2017
14. Ayompe LM, Dufy A, McCormack SJ, Conlon M (2011) Measured performance of a 1.72 kW rooftop grid connected photovoltaic system in Ireland. *Energy Convers Manag* 52(2):816–825
15. Bukya M, Bajaj A, Garg P, Saraswat A (2020) Design and implementation of Arduino based control system for power management of household utilities. In: Kalam A, Niazi K, Soni A, Siddiqui S, Mundra A (eds) *Intelligent computing techniques for smart energy systems*. Lecture notes in electrical engineering, vol 607. Springer, Singapore
16. Shankar A, Garg P, Bansal D (2022 Mar) Smart lighting system for commercial buildings using digital camera. In: *2022 8th international conference on advanced computing and communication systems (ICACCS)*, vol 1. IEEE, pp 890–894
17. Garg P, Agrawal S, Yiyang W, Saraswat A (2018) Design and implementation of interactive home automation system using LabVIEW. In: *Proceedings of first international conference on smart system, innovations and computing*. Springer, Singapore, pp 371–381

Behaviour of Constant Speed Wind Power System Under Different Operating Conditions



Ganesh P. Prajapat, Vikas Sharma, D. K. Yadav, Surender Singh Tanwar, and K. G. Sharma

Abstract The use of renewable energy technologies has risen highly in the recent past due to the modern policies of reducing the carbon emission. Wind power is also one of such a system which has highest share after solar power. Thus, this paper concentrates on the behaviour of a fixed speed wind power system running under different operating conditions. Although the wind turbine system operating on variable speed with maximum power extraction feature is quite popular but such a generator has complexity in its control and not robust. While the fixed speed wind generators are robust and quite simple in structure and thus needs attention of the operator and researchers for its investigation. The mathematical modelling of the constant-speed wind turbine system connected to the grid has been presented in this paper and further has been examined under the variable wind conditions and disturbances in the grid in terms of voltage sag and voltage swell. The results found are useful for the academicians, new researchers as well as operators to know the behaviour of such a system under different disturbance scenarios and take the appropriate decisions.

Keywords Fixed speed wind power generation systems · Open-loop control · Two-mass model · Generator model

G. P. Prajapat (✉) · V. Sharma
Engineering College, Bikaner, Rajasthan 334004, India
e-mail: ganeshprajapat@alumni.iitd.ac.in

D. K. Yadav
UD, Rajasthan Technical University, Kota, Rajasthan 324010, India
e-mail: dkyadav@rtu.ac.in

S. S. Tanwar · K. G. Sharma
Engineering College, Ajmer, Rajasthan 305001, India
e-mail: sst269@gmail.com; stanwar@ah.iitr.ac.in

K. G. Sharma
e-mail: kgsharma@ecajmer.ac.in

1 Introduction

Since the previous decade, there has been a considerable increase in the renewable energy conversion technologies into the current power grid. This is because of the reduction in the conventional power generation from fossil fuel, environment concerns and accordingly the policies of the governments. Different kind of subsidies and other support provided by the various public and private agencies are also encouraging. This inspires the researchers to evaluate the impact of the renewable power systems on the grid. Wind power is one of such a renewable power being added into the grid significantly after solar power, and as a result the control and operation of wind turbine systems are a top focus for researchers in this field. The generation of power through wind is being done by the different type of generators [1–3]. Induction generators are popular choice for the generation from wind. Squirrel-cage induction generators for fixed wind speed and doubly-sided-fed-induction generators (DFIG) for variable wind speeds are frequently employed with the wind power systems [4–6]. The wind power generation through squirrel-cage induction generator is a robust scheme and being used extensively. Although there is good controllability with the doubly-fed induction generators with its popular maximum energy extraction control, there is quite complexity in it [7]. Also DFIGs are not suitable for the constant average wind speeds operating with the modern high inertia wind turbines [8–10]. However, permanent magnet synchronous generators (PMSG) are also used in many of the wind power systems but these are suitable for the low-power applications only [11, 12]. Thus, this paper focuses on the wind power system with the squirrel-cage induction operating under constant average wind speed and its behaviour under various kind of disturbances.

The following is how the paper flows: the mathematical modelling of the system of induction generator-based wind power generation system with all its components are presented in II. Further, Part IV details the simulation findings and discussion for various disturbance scenarios, followed by conclusion in Section V.

2 Studied System Dynamics

The study's fixed speed wind turbine system's schematic diagram is depicted in Fig. 1. As indicated in figure, through a gear train, the wind turbine is driving the generator. The generator is furthermore electrically linked through a transmission line to the electrical grid. The gear train's goal is to raise the generator's rotational speed to match the grid's frequency. Although the induction generator operates on the grid frequency, the speed of the generator needs to be the higher than the synchronous speed so that it has the ability to inject electricity into the grid.

As the wind blows, the turbine rotates which further runs the generator. The generator is designed in such a way that it should operate above the synchronous speed. The power generated by the induction generator will be delivered to the

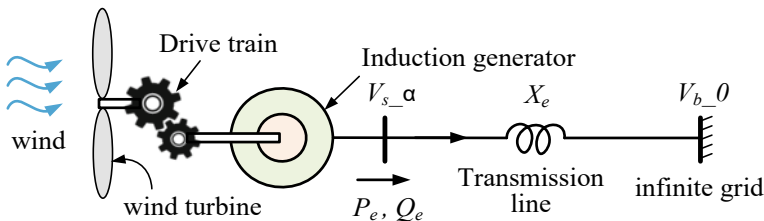


Fig. 1 Schematic diagram of induction generator powered by the wind

grid at grid frequency. The mathematical modelling of the complete studied system includes the model equations of the turbine, gear train, induction generator and grid connections. The turbine power can be expressed as follows:

$$P_t = \frac{1}{2} \rho A C_p(\lambda, \beta) v_{\text{wind}}^3 \quad (1)$$

where v_{wind} is the wind speed, A is the area covered by the wind turbine blades, ρ is the wind air density, C_p is the turbine power coefficient which depends on the pitch angle, β and tip speed ratio, λ . It can further be expressed in p.u. as follows:

$$P_{t_{pu}} = k_{\text{opt}} C_{p_{pu}} v_{\text{wind}_{pu}}^3 \quad (2)$$

$$k_{\text{opt}} = \frac{1}{2S_b} \rho A C_{p_{\text{MAX}}} v_{\text{wind}_{pu}}^3 \quad (3)$$

The gear train can be modelled considering separate masses of the generator and turbine since there is a wide difference in the inertia of both of the entities. Thus, the power balance equations for the turbine-generator using the two-mass model are as follows:

$$\dot{\omega}_t = \frac{T_t - T_s}{2H_t} \quad (4)$$

$$\dot{\omega}_r = \frac{T_s - T_e}{2H_g} \quad (5)$$

$$\dot{\theta}_{tw} = \omega_B(\omega_t - \omega_r) \quad (6)$$

$$T_t = \frac{P_{t_{pu}}}{\omega_t}, T_s = k_s \theta_{tw} + c_d \frac{d\theta_{tw}}{dt} \quad (7)$$

$$T_e = \frac{1}{\omega_s} (E'_q I_{qs} + E'_d I_{ds}) \quad (8)$$

where T_t , T_s and T_e are torques associated with the turbine, shaft and electrical, respectively, H_t and H_g are the respective inertia and ω are the speeds for respective cases. θ_{tw} is the shaft twist while k_s and c_d are the shaft parameters. Further, the generator can be modelled by the following set of equations and readily available with the author's earlier work [13–15] and reproduced here for the completeness of the paper:

$$k_1 \dot{I}_{qs} = -R_1 I_{qs} + L'_s I_{ds} + \omega_r E'_q - \frac{E'_d}{T_r} - V_{qs} + k_m V_{qr} \quad (9)$$

$$k_1 \dot{I}_{ds} = -R_1 I_{ds} - L'_s I_{qs} + \omega_r E'_d + \frac{E'_q}{T_r} - V_{ds} + k_m V_{dr} \quad (10)$$

$$\frac{1}{\omega_B} \dot{E}'_q = R_2 I_{ds} - \frac{E'_q}{T_r} + (1 - \omega_r) E'_d - k_m V_{dr} \quad (11)$$

$$\frac{1}{\omega_B} \dot{E}'_d = -R_2 I_{qs} - \frac{E'_d}{T_r} - (1 - \omega_r) E'_q + k_m V_{qr} \quad (12)$$

where R and L are the system electrical parameters wherein subscript “s” stands for stator and “r” stands for the rotor of the generator. E' and I are the generator's internal voltage and current, respectively, with the concerned subscript.

If the generator voltage is $V_s \angle \alpha$ and the infinite bus voltage is $V_b \angle 0^\circ$, then the stator voltage and current can be expressed by the following set of equations using Ohm's law:

$$\mathbf{I}_s = I_{qs} + j I_{ds} \quad (13)$$

$$V_{qs} = \text{real}\{V_b + j \mathbf{I}_s X_e\} \quad (14)$$

$$V_{ds} = \text{imag}\{V_b + j \mathbf{I}_s X_e\} \quad (15)$$

The power pumped into the grid by the generator can expressed as follows:

$$P_e = \frac{V_s V_b \sin(\alpha)}{X_e} \quad (16)$$

$$Q_e = \frac{V_s^2 - V_s V_b \cos(\alpha)}{X_e} \quad (17)$$

Ultimately, the complete studied system can be modelled by the set of differential and algebraic equations where (4)–(6) and (9)–(12) are the differential equations and (13)–(17) are the algebraic equations which further can be used during the simulations.

3 Results and Discussions

The simulation of a constant-speed wind turbine system was carried out in MATLAB using *ode15s* solver using the differential and algebraic equations mentioned in the section above. The system was examined under the different disturbances wherein initial steady-state conditions were obtained using *fsolve*.

3.1 Behaviour During Step Wind Change

The system's behaviour under step wind speed has been studied and the responses drawn are shown in Figs. 2, 3 and 4.

The results show that as the wind speed changes from the base wind speed, 12 m/s to 11.5 m/s at $t = 10$ s and 11.5 m/s to 12.5 m/s at $t = 30$ s, respectively, the generator oscillates for a small amount of time and then settled to a new steady state. The generator speed exhibits the oscillations along with the stator voltage and active power in Figs. 2 and 3 but the deviations are not significant since the induction generator tries to operate on the constant speed.

Additionally, Fig. 4 shows that the generator is running on maximum power point tracking (MPPT) when it is running on the base wind speed, 12 m/s but somewhat out of MPPT when operating other than base wind speed.

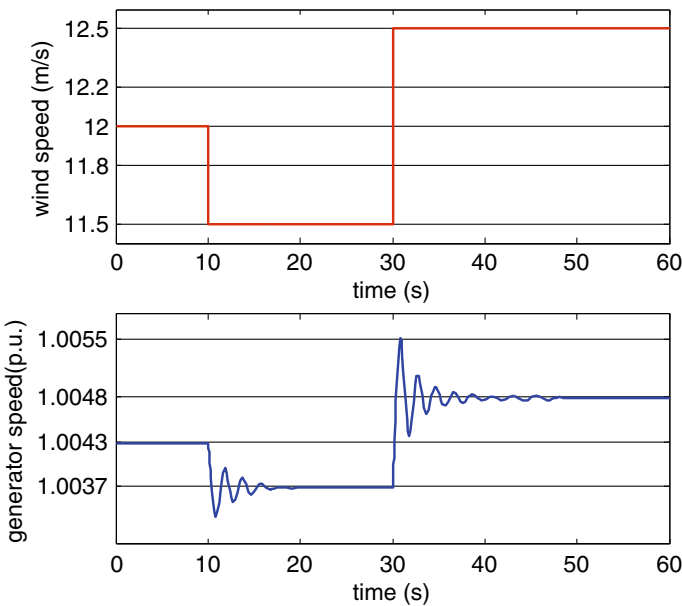


Fig. 2 Wind speed change and generator speed

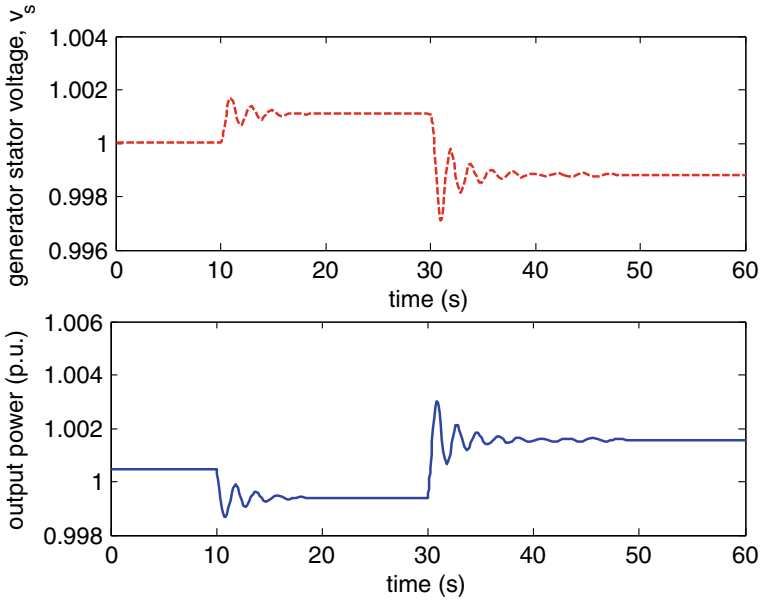


Fig. 3 Generator voltage and during step wind speed disturbance

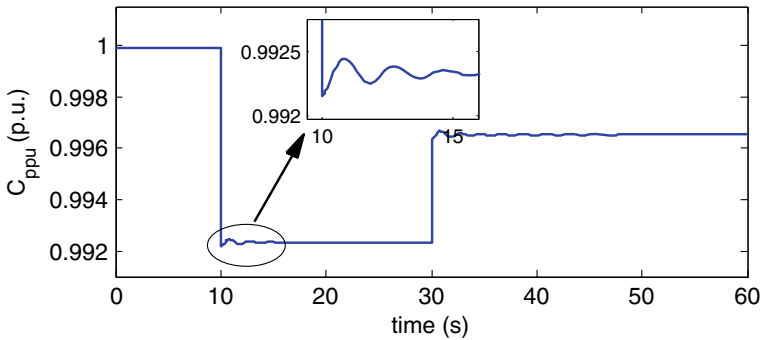


Fig. 4 Turbine power coefficient $C_{p_{pu}}$

3.2 Effect of Voltage Sag and Swell on Infinite Bus

It is quite often that there is the change in the voltage level of the grid and hence such a disturbance has also been taken into consideration during analysis. The system responses during the voltage sag and swell are shown in Figs 5 and 6. It can be seen from Fig. 5 that due to the voltage sag in the infinite bus from 1.0 p.u. to 0.9 p.u. at $t = 10$ s and voltage swell from 0.9 p.u. to 1.1 p.u. at $t = 30$ s, the generator voltage also changes accordingly with some oscillations in it. Further, the fluctuation in the

generator speed has some different frequency. It is interesting that the generator is oscillating at lower frequency during the grid disturbance while it was observed that these oscillations are of higher frequency during wind speed change as observed in Fig. 2. The output of the wind power system also changes in a similar pattern as the generator speed, as shown in Fig. 6.

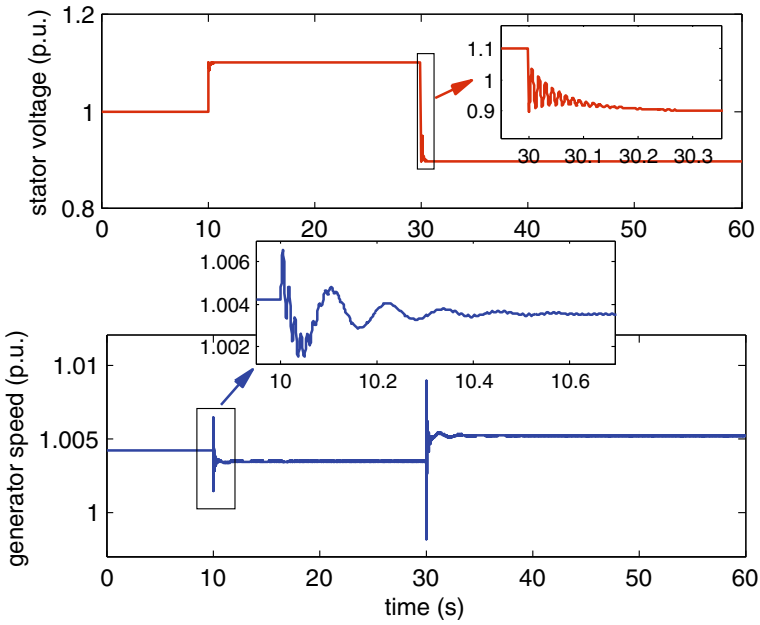


Fig. 5 System responses during voltage sag and voltage swell near infinite bus

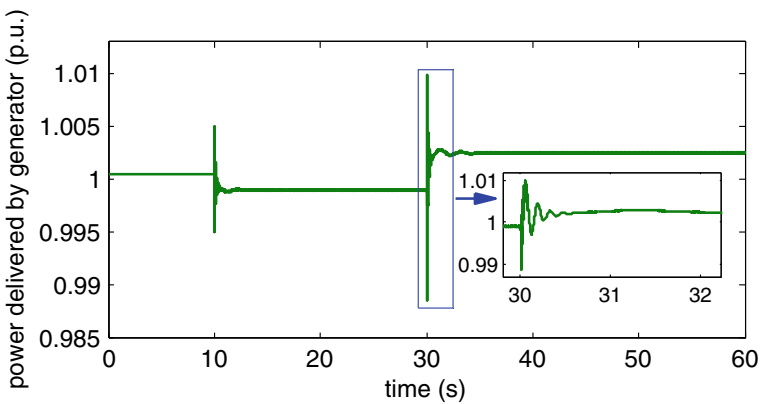


Fig. 6 Power output during voltage sag and voltage swell in infinite bus

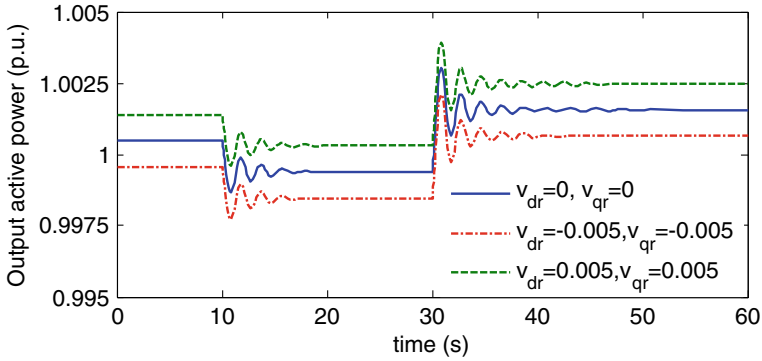


Fig. 7 Operation during different rotor-injected voltages

3.3 Responses Under Different Rotor-Injected Voltages

This sub-section elaborates the possibility of control of the induction generator. Although the studied system in this paper consists of an induction generator and there is the unavailability of the rotor connections in such a generator, the effect of the rotor voltage onto the operation of the generator gives the deep insight about the behaviour of the generator if rotor connections are available. Further, this'll also help to design a controller in future.

Thus, the studied wind turbine system with the induction generator has also been examined with rotor voltage change and the responses recorded are shown in Fig. 7. It was found that the injected rotor voltage alters the generator's operating point, which results in the generator's speed varying at various rotor voltage levels. This'll also change the turbine power coefficient definitely and hence the need of MPPT comes into the picture which can be achieved by using DFIG. However, the pattern of responses due to the disturbances remains same.

4 Conclusion

This paper investigates the wind power generation system based on constant-speed induction generator. The behaviour of such a system was examined in this paper with the different kind of disturbances. It was observed from the responses that the generator oscillates in different frequencies in the different type of disturbances. The oscillations are of lower frequencies when wind speed disturbance occurs while higher frequencies when subjected to the grid disturbance. The results found are useful for the operators and engineers to know the behaviour of such a system and take the appropriate decisions when subjected to the disturbances. The system was also examined under the different level of the rotor voltage which ultimately helps to the look into the possibilities of various controls of the generator.

References

1. Ackermann T (2005 Feb) Wind power in power systems. Wiley, New York
2. Prajapat GP, Senroy N, Kar IN (2016) Small signal stability improvement of a grid connected DFIG through quadratic regulator. In: 2016 IEEE 6th international conference on power systems, ICPS 2016
3. Heier S (2014) Grid integration of wind energy: onshore and offshore conversion systems, 3rd ed. Wiley, Chichester, West Sussex, United Kingdom
4. Yenduri K, Sensarma P (2016) Maximum power point tracking of variable speed wind turbines with flexible shaft. *IEEE Trans Sustain Energy* 7(3):956–965
5. Prajapat GP, Senroy N, Kar IN (2016) Eigenvalue sensitivity analysis based optimized control of wind energy conversion systems. In: 2016 IEEE innovative smart grid technologies-Asia (ISGT-Asia)
6. Miao L, Wen J, Xie H, Yue C, Lee WJ (2015) Coordinated control strategy of wind turbine generator and energy storage equipment for frequency support. *IEEE Trans Ind Appl* 51(4)
7. Prajapat GP, Bhui P, Kumar P, Varma S (2019) Estimation based maximum power point control of DFIG based wind turbine systems. In: 2019 IEEE PES GTD grand international conference and exposition Asia, GTD Asia 2019
8. Chen Z, Yin M, Zou Y, Meng K, Dong ZY (2017) Maximum wind energy extraction for variable speed wind turbines with slow dynamic behaviour. *IEEE Trans Power Syst* 32(4):3321–3322
9. Prajapat GP, Senroy N, Kar IN (2018) Modified control of DFIG-WT for the smooth generator speed response under turbulent wind. In: 2017 14th IEEE India council international conference, INDICON 2017
10. Ghosh S, Senroy N (2015) Electromechanical dynamics of controlled variable-speed wind turbines. *IEEE Syst J* 9(2):639–646
11. Li Y, Xu Z, Wong KP (2017) Advanced control strategies of PMSG-based wind turbines for system inertia support. *IEEE Trans Power Syst* 32(4)
12. Wang Y, Meng J, Zhang X, Xu L (2015) Control of PMSG-based wind turbines for system inertial response and power oscillation damping. *IEEE Trans Sustain Energy*
13. Prajapat GP, Senroy N, Kar IN (2021) Estimation based enhanced maximum energy extraction scheme for DFIG-wind turbine systems. *Sustain Energy Grids Netw* 26
14. Prajapat GP, Senroy N, Kar IN (2018) Stability enhancement of DFIG-based wind turbine system through linear quadratic regulator. *IET Gener Transm Distrib* 12(6)
15. Anaya-Lara O, Jenkins N, Ekanayake J, Cartwright P, Hughes M (2009) Wind energy generation: modelling and control, vol 54, no 2. Wiley, England

A Review of Architecture and Topologies Used for Electric Vehicle Charging Stations



Aayushi Priyadarshini , Shekhar Yadav , Nitesh Tiwari ,
and Utkarsh Shukla 

Abstract Electric vehicles (EVs) have been increasingly popular in recent years due to their high efficiency, decreased reliance on fossil fuels, and low maintenance requirements. Because of its high power transformation efficiency, dependability, and simple interface with a renewable energy source, DC bus-connected EVs are preferable to AC ones. Transformer-based charger installation is too expensive and heavy. At a reduced load, it is unable to offer more efficiency. Transformerless charging stations are used to avoid these kinds of problems. It works with high voltage levels and provides higher energy efficiency. An extremely fast-charging station, which is similar to a gasoline car and can allow refueling, uses a solid-state transformer. The article is firstly reviewing the various renewable energy source connected to charging station infrastructures. Secondly, the transformerless charging station is used to enhance the power density. After that, reviewed on solid-state transformer replacing the low-frequency transformer. In the end, charging station levels and standards are also discussed.

Keywords Electric vehicle (EV) · Renewable energy sources (RES) · Charging station · Energy storage unit (ESU) · Solid-state transformer (SST)

A. Priyadarshini (✉) · S. Yadav · N. Tiwari · U. Shukla
Department of Electrical Engineering, Madan Mohan Malaviya University of Technology,
Gorakhpur, UP, India
e-mail: aayushipriyadarshini@gmail.com

S. Yadav
e-mail: syee@mmmut.ac.in

N. Tiwari
e-mail: niteshwr1994@gmail.com

U. Shukla
e-mail: shuklautkarsh475@gmail.com

1 Introduction

Electric vehicles are most popular in transportations sectors because the other vehicles are depending on fossil fuels like petrol and diesel. EVs are independent of fossil fuels and have few emissions [1]. Distribution networks use renewable energy sources (RES) to provide the electricity to charging station grid, and also reduce emissions. For huge capacity perforation of EV charger points increasing the charging demand, this is the reason for enhancing the utility grid demand [2]. To attenuate the power demand problem, the power achieved from RES is combined with the power converter methodology. EV charging station uses RES for lossless power conversion, reduces the cost of the stations, less emission, and enhances the connection of the utility grid [3]. Photovoltaic (PV) and fuel cells are connected to RES through DC or AC buses [4]. Control of steady-state voltage and transient voltage, etc. is difficult in multipoint charging stations [5]. PV cells have been installed on the rooftop of workplaces for charging, reducing the land requirement and investment cost [6]. Various types of multipoint EV charging stations are connected with RES and have their control strategies [7]. The recommended EV control strategy for the new current loop control methodology would increase the EVs maximum rate of charging capacity only in those circumstances where generation outpaces load demand. [8]. The AC microgrid has been the most popular format; however, DC-based microgrid achieved popularity because of the advantages they offer over their counterpart [9]. The transformerless charging station is used to rise the power density [10]. It means charging stations are working without a line frequency (LF) transformer. Two way of neglecting the LF transformer, first low-voltage grid is used, and the second used current amplitude for charging [11]. Fast charging of EV can be achieved by transformerless charging station [12]. DSTATCOM (distribution static compensator) and APF (active pass filter) are used in this type of EV charging for increasing performance and efficiency [13]. EV cells charge through an isolated DC/DC converter which is parallel connected and give more current and galvanic isolation [14]. For buffering the power used battery storage device in form of a non-segregated split sub-module [15]. A solid-state transformer (SST) is used for extremely fast charging (XFC) in a traction system, it has a medium-to-low voltage (LV) transformer [16]. SST is small in size and has low-cost maintenance than LF transformer [17]. SST is amenable to future modular structures [18]. This appears in the smart grid context, where the normal transformer is removed by SST to enhance the power control capability [19]. EV has two types of charger named as on-board and off-board chargers. For low-power applications, on-board chargers are beneficial to use, on-board charging is possible at any location, and its battery management system is simple but a late-charging process, power transfer is slow at the time of charging and added the vehicle weight. When high power and quick charging are necessary, the off-board charger is employed, adding no further weight to the vehicle [20]. But difficult to place at any location, also indicating battery heating problem and charging cost is high. A fast-charging station for EV is very important for making EV more appealing and charging the EV within an hour, it has low cost and less

impact on the grid [21]. So for XFC, SST is used to get the best design standards for high power utilization [22]. The EV uses a battery and a super-capacitor (SC) as an energy storage device to acquire a complicated power under various operating conditions. To manage this kind of complicated power, many DC–DC converters are employed [23].

2 Multipoint Charging System

The multipoint charging station is a combination of energy sources and an energy storage unit in place of distributed loads, showing the potential of processing in an attached grid. Charging the EV without any losses in power conversion is provided with the help of a charging station with RES. Various kinds of RES are connected to DC buses such as wind, PV, super-capacitors, and fuel cells. Some problem arises in multipoint charging station like the steady-state voltage, transient voltage, and limiting of frequency. Also, additional problems are rising with short circuits and protection during islanding quality of power and system fault conditions. Renewable energy is the main source of PV in DC bus systems powered by RES with local load and EVs have various arrangements to supply power. The various types of multipoint EV charging stations with RES are shown in Fig. 1.

2.1 DC Isolated EV Charging

Whether they use non-renewable or renewable energy sources, DC isolated EVs require charging. Common DC buses are utilized for both these sort of charging supplied by RES and charging for sufficient integrated storage. Integration of DC charged station with a source of energy frequency and synchronized phase not required like AC grid. Lots of greenhouse gases have been discharged by diesel power plant and this power plant only transports on a remote location and faces leakage and posing issues on the island, and for handling such challenges RES is using lots of area of the world. So many uncertainties and changes have been founded in the generation of RES which leads to instability in the system. DC isolation has only a stabilization problem that is required by DC bus voltage. This type of EV charging station is supply load power. It means electricity is generated on the other

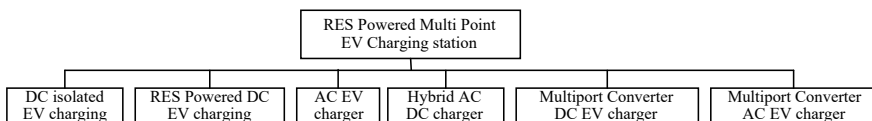
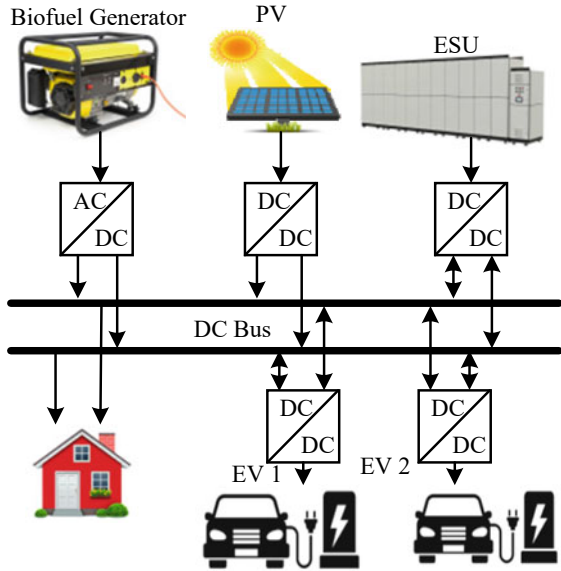


Fig. 1 Different types of multipoint EV charging stations

Fig. 2 Isolated DC EV charging station



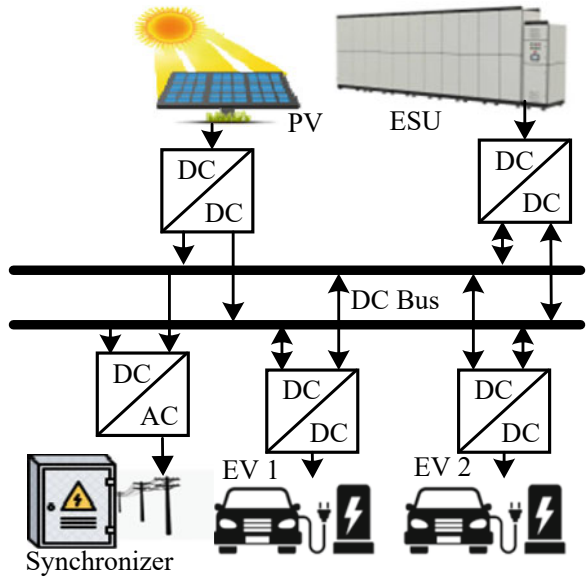
side. The architecture of the DC isolated EV charging station is shown in Fig. 2. The DC isolated EV charging has a control strategy based on consumption of load and climatic conditions. An optimization-based control strategy is most followed by DC isolated charging systems, optimization is based on dividing output which is satisfied by constraints. Control energy storage and biofuel generators carry out power balancing, generation, and load consumption using a control method based on the DC bus voltage.

2.2 Renewable Energy-Powered DC EV Charging

RESs are energized by DC EV charging stations and they have a common DC bus in the middle of the load and source and permit them to work in parallel to battery storage and PV cell (see Fig. 3). Most EVs are charged by RES like PV and ESU and they decide according to power management. ESU is attached to a bidirectional DC converter and PV is attached to a boost converter through a DC bus. They have energy storage capability to feed the loads that are connected to households and the grid. The disadvantage of this infrastructure is DC-to-AC conversion for a combination of the grid. This type of charging station works on different modes and they are situated according to the power available on the station. These types of charging stations charge the EV cell by DC supply.

The power required by charging stations has been decided by the State of Charge (SOC) of the EV, charging mode, and plugging time. This control strategy is used

Fig. 3 Renewable energy source-energized DC EV charging station



for preventing circulating current to produce optimal operation. For maintaining DC bus voltage drop control strategy is required. Fuzzy command, hierarchical control, and multi-agent-based control are advanced control strategies used to control the fluctuation of voltage levels. An energy storage system to keep limited capacity is important to minimize a DC bus voltage fluctuation and control power balance.

2.3 AC EV Charging

AC EV charging station is the same RES-energized DC EV charging station. The only difference is using a common AC bus to connect the load. ESU is connecting to the AC bus via bidirectional DC-to-AC converters. This type of charging provides a sufficient selection for sizing all parts. The connection between load and grid provides affability to the EV charging in form of battery charge and discharge and management of maximum time. Common AC bus-coupled charging has well-defined standards that are used as a home-based charger. Solar DC bus-based charging system is more suitable for a low amount of conversion losses. AC bus EV charging station requires the common coupling for compensation of power to calculate the active power at that point.

AC EV charging stations have a charging and discharging control strategy. If ESU power is greater than zero then it shows discharge state otherwise charge state. For the linked load to receive higher quality power, frequency- and SOC-based controls are needed. The various energy forms can be managed using supervisor-based control.

2.4 Hybrid AC and DC Charging

Hybrid charging is beneficial for both AC and DC charging (see Fig. 4). PV cells and fuel cells are combined with a common DC bus with a DC-to-DC converter. DC loads like EV are attached to a common DC bus by a DC-to-DC buck converter. AC grid is connected to wind turbine and diesel generator and grid system. AC load like AC motor connected through AC grid and AC grid voltage is about 230 V or 400 V. A hybrid charging system generally required the AC supply or attached to RES. They have many benefits like regulation of bus voltage and frequency and provide a better condition of the island. For system-wide control, the AC and DC buses both require a bidirectional control system. To coordinate the inputs such that they do not overlap, a three-layer coordinated control technique for the hybrid AC–DC microgrid was created. All DC charging stations receive a synchronized supply from the first layer, which also regulates the DC grid voltage. A frequency from a three-phase AC grid is maintained and the AC bus voltage regulation is managed by the second layer. The third layer acts as a link between AC and DC microgrids through an interlinking converter. Various power flow processes, including those from a vehicle to grid (V2G) and from a PV system to an ESU, are made possible by its control.

Fig. 4 Hybrid AC and DC charging

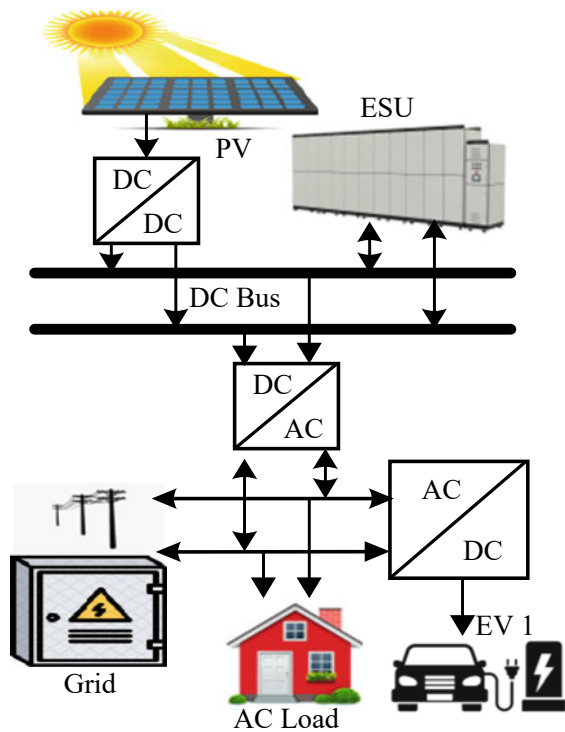
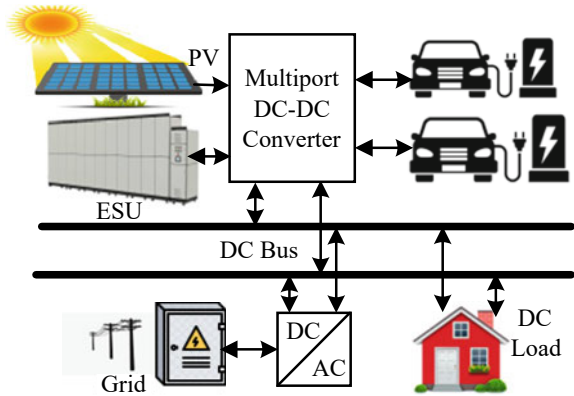


Fig. 5 Multiport DC converter EV charger



2.5 Multiport DC Converter for EV Charger

The multiport DC converter-based EV charger connection is depicted in Fig. 5. The EV charger is based on direction and contains bidirectional/unidirectional converters depending on connecting points and demands. This type of charging mode works for various loads and sources. When generating more PV power, extra power by using the same multiport converter is provided to the grid. In a multiport converter, various ratings of batteries and sources are attached. Multiport converter with DC source connection gives the direct DC power from DC source to charging station. DC-to-DC boost converter on power side can be controlled by MPPT (maximum power point tracking) control technique. With converter control, it is achieving the fast-charging operation with available direct DC power. Based on the requirement converter uses interface EV load and it may be bidirectional or unidirectional. In bidirectional charging, it can work in Buck mode and Boost mode. The charging current limit is increased when the converter is functioning like a buck converter. Multiport DC converter EV charging with RES is used for an uninterrupted supply of power to store the energy by using a hybrid source in EV or without storage.

2.6 Multiport AC Converter-Based EV Charger

A multiport AC converter charger is the same as a multiport DC charger and the only difference is a multiport AC converter used a common AC bus connection. Multiport converters with the integration of various sources and loads reduce numbers of components and enhance the density. The main source of power for a multiport AC converter-based charging station is the grid. One drawback of this charging station is that when different types of multiport converters are linked to a shared AC bus, AC-to-DC conversion is required. The control strategy for multiport AC converter-based EV charger is similar to the control of DC bus-based charger, but there have

differences in the numbers of multiport converters that are attached to the AC grid. This type of multiport converter has a direct connection with the communication-based control strategy. A link of different RES with load or grid storage elements in a multiport converter gets the attention of the research field.

3 Transformerless Charging Stations

Transformerless charging stations mean removing the LF transformer from stations to enhance the power density. Basically, for removing the LF transformer, the voltage level should be stepped down, there is the connection of the front-end converter, so we have two ways. The first way is a low-voltage grid used for supplying to the charging station. High conduction loss is caused by high current stress. The second way is charging current amplitude, it has decreased by applying a medium-voltage grid to the charging station. In some research papers [10, 11], the use of a medium-voltage grid cascaded multi-level inverter will be the second method (see Fig. 6). In this figure, charging stations are connected to a multi-level converter made up of all phases of an AC/DC/DC converter with the 4.8 kV medium-voltage (MV) distribution network. On the DC side, battery storage is necessary in the place of a capacitor.

In a research paper [10], battery bank in megawatt is required for filling the gap between the charging and also grid power is present. By using this method, we can achieve fast EV charging and active power filtering, and the battery bank is charged without processing the EV charger. On the battery bank side, multiple charging and discharging effects are not found, and power increasing and decreasing of the charging station by LF transformer is removed, and adding the various multi-level converters and battery banks, this is not reviewed in the paper [10]. In paper [11], DSTATCOM and APF function by using the same topology for the station is

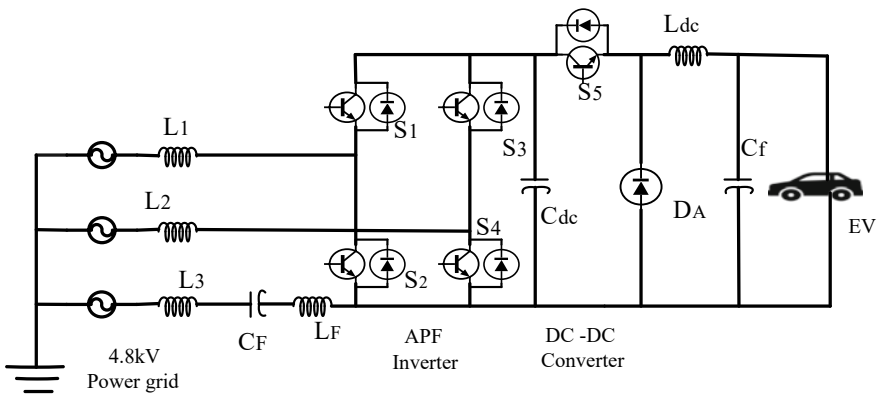


Fig. 6 Cascaded multi-level converter charging station

provided. Modeling of this topology is shown in [12, 13], which uses simulation model to find out the stability and performance. This includes a greater number of power electronic components and efficiency. Reliability and cost of stations are not discussed. Moreover, it needs a distribution network at 4.8 kV, this voltage level is not common for the present infrastructure.

4 Solid-State Transformer for Extremely Fast Charging

SST for XFC is used in railway traction distribution system. This topology is removing the grid frequency and the need for a MV-to-LV transformer, which can associate directly through the medium-voltage grid. For the function of a step-down, it gives reactive power control, voltage regulation, galvanic isolation, a better quality of power operation, and easy incorporation of renewable energy source systems. Moreover, SST cost and size are less than LFT. SST provides the power flow either bidirectional or unidirectional which can regulate better active and reactive power and offers V2G function. Therefore, protection functions like limiting and isolating the fault current with power factor control (PFC) are performed by SST. EV charging stations through SST have a common link of DC bus to provide between RES and battery storage system and DC-to-DC converter so that confirms the lesser conversion stage and ensure the efficiency should be high.

A high-frequency transformer (HFT) that provides galvanic isolation is utilized in conjunction with XFC in SST. Compared to an LV line frequency transformer, HFT operates at higher frequencies. To achieve high-frequency performance in SST, the transformer's size must be lowered, which implies space savings. Using SST installment cost of the charging station will be decreased.

The comparison between LFT and SST for XFC is shown in Table 1. With the compact size of MV SST, power losses of MV SST are half, and volume and weight decrease by about one-third of LFT. Multi-module for SST interfaces MV grid directly for achieving specific voltage and power level, and for high power requirement requires the addition of more module of SST. But in the LFT charging station, enhancement of charging ability requires the replacement of transformers. SST-based charging stations are used where high voltage and high power are required to charge the EV. Implementation and design of SST are very challenging, so more effort is required for the fast development of SST in XFC.

5 Charging Station Levels and Standards

The charging station has three voltage levels, level 1, level 2, and level 3. Charging station levels have been chosen according to the power level of the grid. Power levels of EV charging determine the charging time, cost, suitable equipment for an EV

Table 1 Comparison between LFT and SST for XFC

Parameters	LFT for XFC	SST for XFC
Cost	High	Low
Control	Easy, simple	Complex, control
Reliability	More	Less
Flexibility	Less	More
Protection	Straightforward	Complex
Technical ability	High	Low

charging station, and employment of utility of the grid. Table 2 shows the levels of the charging station.

Charging stations have various types of standards and they are formed by the Society of Automotive Engineers (SAE). This standard is placed according to cords and chargers. SAE includes generally two standards that are American standards SAEJ1772 and International Electro-Technical Commission IEC 61,851 that define physical, electrical, communication, and performance requirements for a charging station. SAEJ1772 follows the regulation of constant voltage and rectification of EV and defines connectors for AC. Off-board charger-based charging station for utility used SAWJ2293 standards. Many more standards are followed by EV charging stations and they have different scopes and types of charging.

Table 2 Different types of charging levels in AC and DC

Levels	Type of supply	Voltage rating (V)	Current rating	Power output (kW)	Charging time	Charger type
DC level 1	DC	200–500	<80 A	40	22 min	Off-board
DC level 2	DC	200–500	<200 A	100	10 min	Off-board
DC level 3	DC	200–600	<400 A	240	30 min	Off-board
AC level 1	Single-phase AC	120–240	13–16 A	1.9–3	7 h	On-board
AC level 2	Single/ three-phase AC	208–240	80 A	20	3 h	On-board
AC level 3	Three-phase AC	300–600	400 A max	120–240	30 min	On-board

6 Conclusion

This paper has summarized reviews of the multipoint charging station powered by renewable energy systems with different charging sources like AC, DC, and hybrid. The multipoint charging station has different control strategies for an EV and also provides an idea about selecting the suitable strategy of control for EV charging. This paper includes studies about transformerless charging stations and solid-state transformers based on extremely fast-charging stations. Transformerless charging stations are used in place of LF transformers to improve power density, and SST is used for XFC stations to give better performance of power quality, voltage regulation, and easy interaction with RES. The paper also overviews three types of levels of EV chargers with AC and DC sources and charger standards. Levels and standards are selected according to the requirement of an EV charging station.

References

1. Woodcock J, Edwards P, Tonne C, Armstrong BG, Ashiru O, Banister D, Beevers S, Chalabi Z, Chowdhury Z, Cohen A, Franco OH (2009) Public health benefits of strategies to reduce greenhouse-gas emissions: urban land transport. *Lancet* 374(9705):1930–1943
2. Schroeder A, Traber T (2012) The economics of fast charging infrastructure for electric vehicles. *Energy Policy* 43:136–144
3. He J, Yuan Z, Wang S, Hu J, Chen S, Zeng R (2009) Effective protection distances of low-voltage SPD with different voltage protection levels. *IEEE Trans Power Deliv* 25(1):187–195
4. Mwasilu F, Justo JJ, Kim E-K, Do TD, Jung J-W (2014) Electric vehicles and smart grid interaction: a review on vehicle to grid and renewable energy sources integration. *Renew Sustain Energy Rev* 34:501–516
5. Sharma A, Srinivasan D, Trivedi A (2015) A decentralized multi agent system approach for service restoration using DG islanding. *IEEE Trans Smart Grid* 6(6):2784–2793
6. Gamboa G, Hamilton C, Kerley R, Elmes S, Arias A, Shen J, Batarseh I (2010) Control strategy of a multi-port, grid connected, direct-DC PV charging station for plug-in electric vehicles. In: *IEEE energy conversion congress and exposition*, pp 1173–1177
7. Ma TTH, Yahoui H, Vu HG, Siauue N, Morel H (2017) A control strategy of DC building microgrid connected to the neighborhood and AC power network. *Buildings* 7(2):42
8. Bhargavi KM, Jayalakshmi NS (2019) A new control strategy for plug-in electric vehicle of DC microgrid with PV and wind power integration. *J Electr Eng Technol* 14(1):13–25
9. Unamuno E, Barrena JA (2015) Hybrid ac/dc microgrids Part I: review and classification of topologies. *Renew Sustain Energy Rev* 52:1251–1259
10. Wang S, Crosier R, Chu Y (2012) Investigating the power architectures and circuit topologies for megawatt superfast electric vehicle charging stations with enhanced grid support functionality. In: *IEEE international electric vehicle conference*, pp 1–8
11. Crosier R, Wang S, Jamshidi M (2012) A 4800-V grid-connected electric vehicle charging station that provides STACOM-APF functions with a bi-directional, multi-level, cascaded converter. In: *27th annual IEEE applied power electronics conference and exposition (APEC)*, pp 1508–1515
12. Crosier R, Wang S, Chu Y (2012) Modeling of a grid-connected, multifunctional electric vehicle charging station in active filter mode with DQ theory. In: *IEEE energy conversion conference and exposition (ECCE)*, pp 3395–3402

13. Crosier R, Wang S (2013) DQ-frame modeling of an active power filter integrated with a grid-connected, multifunctional electric vehicle charging station. *IEEE Trans Power Electron* 28(12):5702–5716
14. Vasiladiotis M, Rufer A, Béguin A (2012) Modular converter architecture for medium voltage ultra-fast EV charging stations: global system considerations. In: *IEEE international electric vehicle conference*, pp 1–7
15. Vasiladiotis M, Rufer A (2014) A modular multiport power electronic transformer with integrated split battery energy storage for versatile ultrafast EV charging stations. *IEEE Trans Industr Electron* 62(5):3213–3222
16. Avdeev B, Vyngra A, Chernyi S (2020) Improving the electricity quality by means of a single-phase solid-state transformer. *Designs* 4(3):35
17. Huber JE, Kolar JW (2016) Solid-state transformers: on the origins and evolution of key concepts. *IEEE Ind Electron Mag* 10(3):19–28
18. Abu-Siada A, Budiri J, Abdou AF (2018) Solid-state transformers topologies, controllers, and applications: state-of-the-art literature review. *Electronic* 7(11):298
19. Huber JE, Kolar JW (2014) Volume/weight/cost comparison of a 1MVA 10 kV/400 V solid-state against a conventional low-frequency distribution transformer. In: *IEEE energy conversion congress and exposition (ECCE)*, pp 4545–4552
20. Savio Abraham D, Verma R, Kanagaraj L, Giri Thulasi Raman SR, Rajamanickam N, Chokkalingam B, Sekar KM, Mihet-Popa L (2021) Electric vehicles charging stations' architectures, criteria, power converters, and control strategies in microgrids. *Electronics* 10(16):1895
21. Ahmadi M, Mithulananthan N, Sharma R (2016) A review on topologies for fast charging stations for electric vehicles. In: *IEEE international conference on power system technology (POWERCON)*, pp 1–6
22. Tahir Y, Khan I, Rahman S, Nadeem MF, Iqbal A, Xu Y, Rafi M (2021) A state-of-the-art review on topologies and control techniques of solid-state transformers for electric vehicle extreme fast charging. *IET Power Electron* 14(9):1560–1576
23. Tiwari N, Yadav S, Arya SR (2022) Speed control of battery and super-capacitor powered EV/HEV using PID and fuzzy logic controller. *Int J Innovative Comput Appl* 13(2):97–114

Trends and Developments of Electric Vehicles: Current State and Future Perspectives



Doğan ÇELİK 

Abstract Increasing transport electrification results in more charging stations with outstanding impacts on the electricity networks. Therefore, various charging approaches as well as grid integration strategies are being enhanced to reduce the adverse impacts of EV charging and to promote the profits of EV grid integration. Maximizing the advantages of EVs with smart charging infrastructure, distributed generators, and reliable communication systems is critical to measuring effects on the electrical grid. With the increasing importance given to this area, this paper addresses the current EV status and investigates an extensive overview on significant international EV charging and grid interconnection standards. The characteristics of the EV technologies are investigated and discussed. The main charging techniques, battery technologies, and charging standards are overviewed and discussed. Some results based on registrations of the EVs, battery demand, and electric cars including battery electric vehicles (BEVs), fuel cell electric vehicles (FCEVs), and plug-in hybrid electric vehicles (PHEVs) are analyzed and examined.

Keywords Electric vehicle · Smart charging · EV charging standards · Vehicle to building · Vehicle to home · Vehicle to grid

1 Introduction

Electric vehicles (EVs) are rapidly appearing as an advantageous transportation to reduce environmental pollution worldwide [1, 2]. Recently, the emissions from conventional vehicles (CVs) outstandingly induce to progressively serious environmental problems. The CVs that employ only an internal combustion engine (ICE) exhaust fossil fuels and extract gases such as nitrogen oxides, hydrocarbons, and carbon oxides. However, the EVs are not yet suited to the ICE experience and one of the important aspects in an EV is the safety guarantee [1]. The low energy efficiency of the CVs and the energy crisis provide good advantageous to evolve EVs

D. ÇELİK (✉)

Van Yuzuncu Yıl University, 65080 Van, Turkey

e-mail: dogancelik@yyu.edu.tr

[3]. In this regard, new type of the EVs have substantial benefits for the greenhouse effect, environmental degradation, and reducing the global energy shortage [4, 5]. Direct and indirect transport electrification technologies such as battery electric vehicles (BEV), hybrid electric vehicles (HEV), fuel cell electric vehicles (FCEV), and plug-in HEV (PHEV) provide important prospective to significantly diminish transport sector emission levels. The evolution of FCEV technologies is still in the early improvement stages, and it is anticipated that electrification of the sector will be primarily provided by HEV and BEV in the medium term [6]. Besides reducing CO₂ emissions, EVs also have the capability to integrate with distributed resources, particularly solar PVs in urban areas.

Integrating EVs into electrical grids creates several challenges. The EV charging stations have been increased with the rapid growth of vehicle electrification. Increasing demand for charging power and stochastic patterns of charging behavior are causing electricity shortages and substantial power oscillations in the power system [7]. Regardless of the extent to which smart charging methods are implemented, the mass adoption of electric vehicles will result in a significant increase in electricity demand in contrast to the power systems currently designed to fulfill. On the other hand, the efficiency of the EV and renewable resources integration can be farther increased by various demand-side management methods, ancillary power reserve, and applying smart charging. Also, higher integration level of renewable resources in traditional energy or transportation system will lessen reliance on traditional fossil fuel energy. However, the intermittent and indiscriminate nature of renewable resources can cause unstable power oscillations in the electric networks and even result in grid faults. Besides, companies still have contradictory opinions on the effect of electric vehicle load on electricity demand and whether and to what extent this can be reduced by smart charging behavior or adapting power systems to that load [8–10].

This paper investigates and examines current state and future perspectives of trends and developments of the EVs. Recent status of transport electrification stock and global battery demand according to the modes and regions has been addressed and analyzed. The key benefactions of this paper are detailed discussion of the EVs and related technologies, consisting of

- Electrification of transportation has been discussed and overviewed.
- Different types of EV technologies are studied and analyzed.
- Smart charging technologies have been examined and addressed.
- Charging standards recommended by the IEC and Society of the Automotive Engineers (SAE) have been overviewed and conducted.

2 Electrical Vehicle (EV) Technologies

The main problems in the ICE vehicles are fossil fuel consumption with increasing fuel prices, which result in CO₂ emissions to the environment and energy security. The EVs can be categorized into five categories based on technologies and strategies as shown in Fig. 1.

- The BEVs are operated by 100% electricity. The BEVs include an electric motor, a controller, and an energy storage battery. The electric battery is charged using mains power with a charger that is a vehicle specific or plugged into a charging station [10, 11].
- The HEVs consist of an electric motor and a conventional ICE as two power units. There are series hybrid, power-split hybrid, and parallel hybrid HEVs. The HEVs are not supplied with the main grid, but convert kinetic energy into electrical energy through the energy produced in braking [10, 11].
- The PHEVs include an electric motor and an ICE. The PHEVs run on gasoline and possess a large battery that is loaded through an external plug in the mains. The difference of HEVs is that they are tied to the electrical network [10, 11].
- Fuel cell electric vehicles (FCEVs) employ electric powertrains like BEVs, but they produce electricity using a hydrogen-powered fuel cell. The FCEVs are categorized as zero emission vehicles [10, 11].
- Extended range electric vehicles (EREVs) are composed of supplementary ICE, which provide power for batteries of vehicles. The difference with PHEVs and HEVs, the EREVs' engine is only employed for charging without linking to the wheels [10, 11].

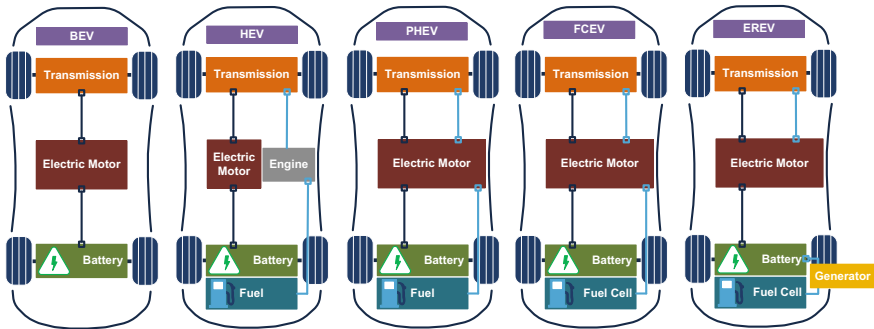


Fig. 1 Categories of the EVs

3 Smart Charging Technologies

Smart charging for the EVs ensures an important role in unleashing the synergy between low-carbon electricity and clean transportation. Smart charging indicates adjusting the charge cycle of EVs to both the requirements of the vehicle users and the situations of the energy system. Batteries in cars are effective in integrating highly renewable energy into the energy system. Smart charging provides a specific level of management over the charging operation. It consists of various technical charging and pricing alternatives. The major forms of smart charging operations are unidirectional controlled charging (V1G), vehicle to home (V2H), vehicle to grid (V2G), and vehicle to building (V2B). Figure 2 describes the connection between smart charging strategies and enables flexibility in energy systems today. Each type of strategies provisions various choices to ensure the flexibility of power systems and promotes the combination of variable renewable energy, predominantly solar and wind [12].

The battery capacity, range, energy consumption, and charging time for various recent EV models are summarized in Table 1 [13, 14]. The charging techniques are mainly conductive charging, battery exchange, and wireless (inductive) charging. The conductive charging is categorized as overnight charging and pantograph (bottom-up and top-down) as depicted in Fig. 3. At the present time, the furthest used type of charging is conductive charging and includes various modes [15, 16].

Various EV charging standards are employed around the world to handle with the infrastructure of the EV charging stations. The U.S. utilizes the SAE and IEEE standards, while Japan and Europe use CHAdEMO standards. Standards Administration of China (SAC) employs GB/T standards, like to the IEC standard. The SAE and ICE charging standards are outlined and given in Table 2. The level of power in IEC is named “Mode” while the level of power in SAE is named “Level”. Charging Mode 1/Level 1 is further employed at offices and homes at night for slow charging. The charging Mode 2/Level 2 and Mode 3/Level 3 are utilized for private and public charging facilities and Mode 4 is operated for fast charging [15, 16].

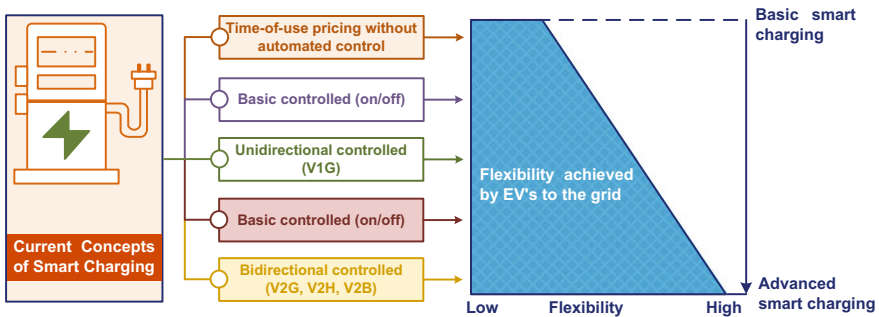


Fig. 2 The connection between smart charging strategies

Table 1 Battery technologies for various EV models

EV model	Drive	EV range	Charging time (h)	Battery (kWh)	Energy consumption [kWh/100 km] (kWh)
Hyundai Kona Electric	FWD	258 mi (415 km)	28	64	14.3
Audi e-tron S/ 55	AWD	208 mi (335 km)	42	95	–
Kia Niro EV (e-Niro)	FWD	239 mi (385 km)	28	64	14.3
Tesla Model Y	AWD	326 mi (525 km)	36	80	20,8
Tesla Model S Plaid	AWD	396 mi (637 km)	45	100	21
Lucid Air Dream Edition	AWD	520 mi (837 km)	–	113	–
Tesla Model X Plaid	AWD	340 mi (547 km)	45	100	21
Tesla Model 3 Standard	RWD	263 mi (423 km)	27	60	–
Volkswagen ID.4 Pro S	AWD	240 mi (386 km)	–	82	–
Kia Niro EV (e-Niro)	FWD	239 mi (385 km)	28	64	14.3
BMW i3, BMW i3s	RWD	153 mi (246 km)	12	42.2	12.9
Volvo C40	AWD	210 mi (338 km)	–	78	–
Nissan LEAF	FWD	149 mi (240 km)	18	40	17
Jaguar I-PACE EV400	AWD	234 mi (377 km)	39,5	90	21.2

AWD: All wheels drive, RWD: Rear wheels drive, FWD: Front wheels drive

Reserve of generation system that considered three scenarios as without V2G, with V2G, and with V2G and a wind farm are shown in Fig. 4 [17]. The reserve potential of the network has increased with the combining of the V2G and a wind farm.

Fig. 3 The main charging techniques

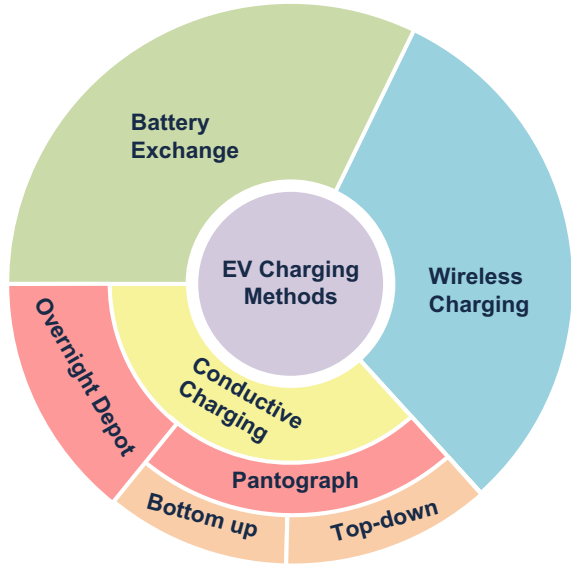


Table 2 EV charging standards

Standards	Phase	Voltage and current range	Level/mode	Source
SAEJ1772	Single	120 V/16 A	Level 1	AC
	Single	240 V/3–80 A	Level 2	AC
	DC	200–450 V/80 A	Level 1	DC
	DC	200–450 V/200 A	Level 2	DC
IEC61851	Single	120 V/16 A	Mode 1	AC
	Single	240 V/80 A	Mode 2	AC
	DC	200–450 V/80 A	Mode 4	DC
IEC62196	Single	120 V/16 A	Mode 1	AC
	Single	240 V/32 A	Mode 2	AC
	Single	250 V/32–250 A	Mode 3	AC
	DC	600 V/400 A	Mode 4	DC

4 Results and Discussions

In this section, registrations of the EVs in various countries, recent status of transport electrification stock, and global battery demand with mode and region have been discussed and examined in detail.

In the net-zero emissions scenario, it is estimated that 25% of heavy trucks, 55% of buses, and 85% of 2/3-wheelers will be electric by 2030 around the world. The registrations of the EVs in various countries are depicted for the PHEVs and BEVs

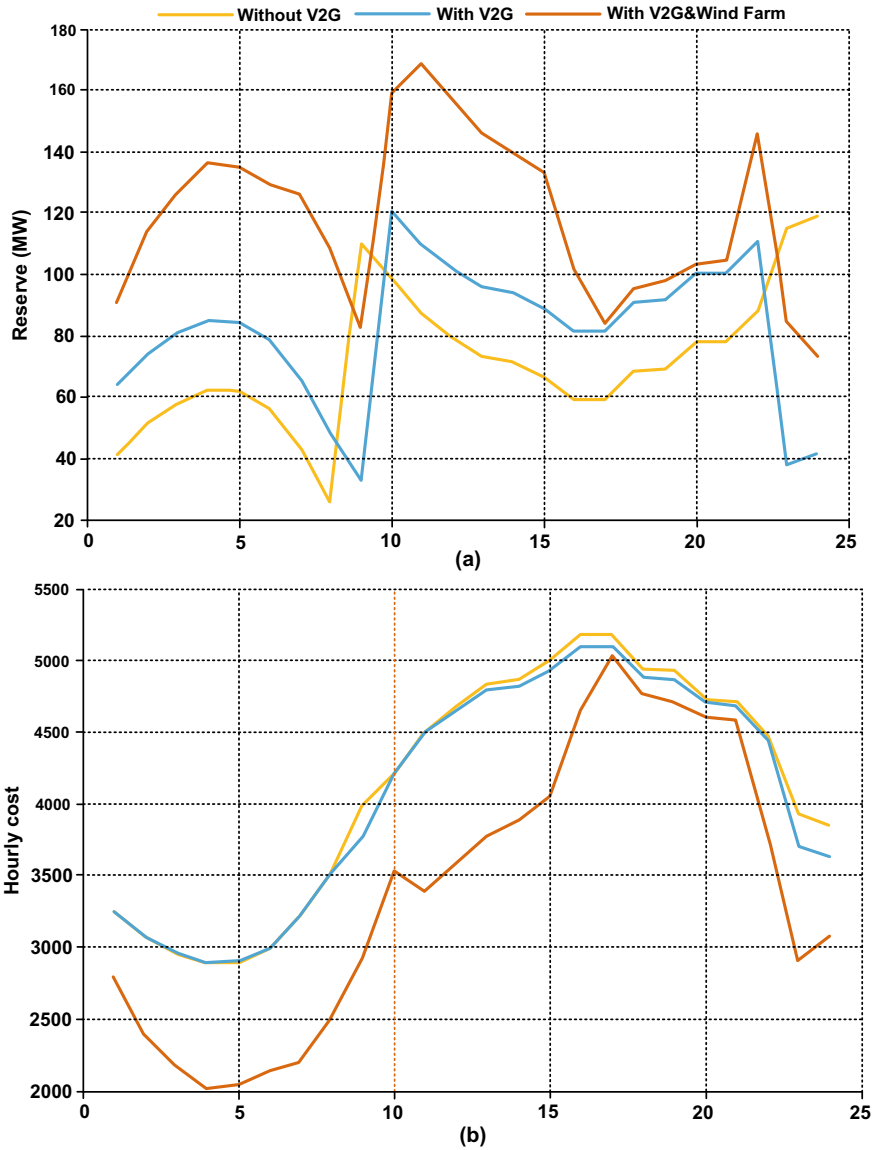


Fig. 4 Reserve of generation system for various scenarios: a) hourly reserve of grid and b) hourly generation cost

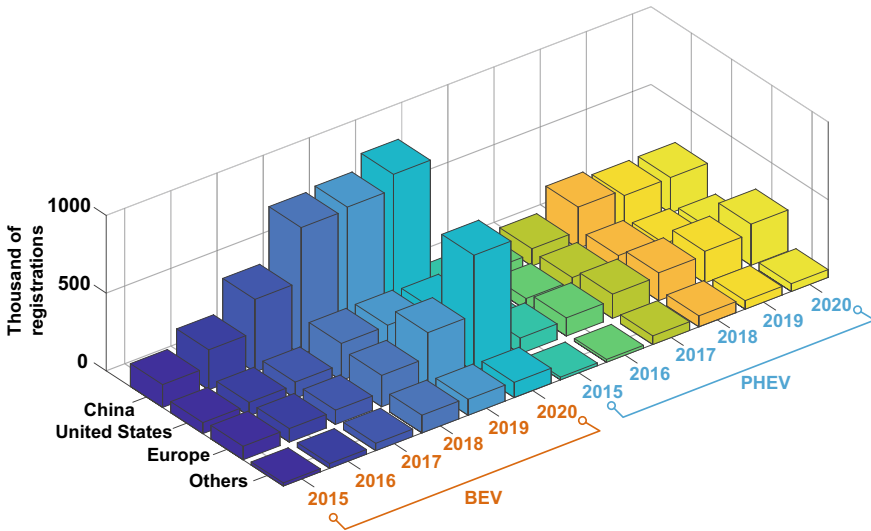


Fig. 5 The registrations of the EVs in various countries

between 2015 and 20,202 in Fig. 5 (source date used in Fig. 5 [16]). 82 000 new electric buses were recorded around the world in 2020, up to 10% from 2019. The registrations of the worldwide electric truck have achieved 7400 units, up to 10% according to 2019.

Electric cars including passenger light-duty BEVs, PHEVs, and FCEVs have achieved 10 million in 2020 around the world while BEVs enumerate two-thirds of the electric car fleet of the world (source date used in Fig. 6 [18]). The largest increment in 2020 with nearly 1.4 million is Europe with a sales share of 10%. China reached 1.2 million registrations with 5.7% sales share and the United States (US) achieved 295,000 registrations with 2% sales share (see Fig. 6) [18–20].

Automotive battery manufacturing achieved 160 GWh in 2020, an increase of 33% compared to 2019 as shown in Fig. 7a. Average battery costs dropped 13% to the average worldwide battery pack price. As depicted in Fig. 7b, China keeps going to possess battery production, with around 70% of cell manufacturing capacity and fabrication more than half of all batteries for light commercial vehicles around the world. China has the greatest share of demand at around 80 GWh, but Europe had the biggest increment with 110% in 2020, reaching 52 GWh (source date used in Fig. 7 [18]).

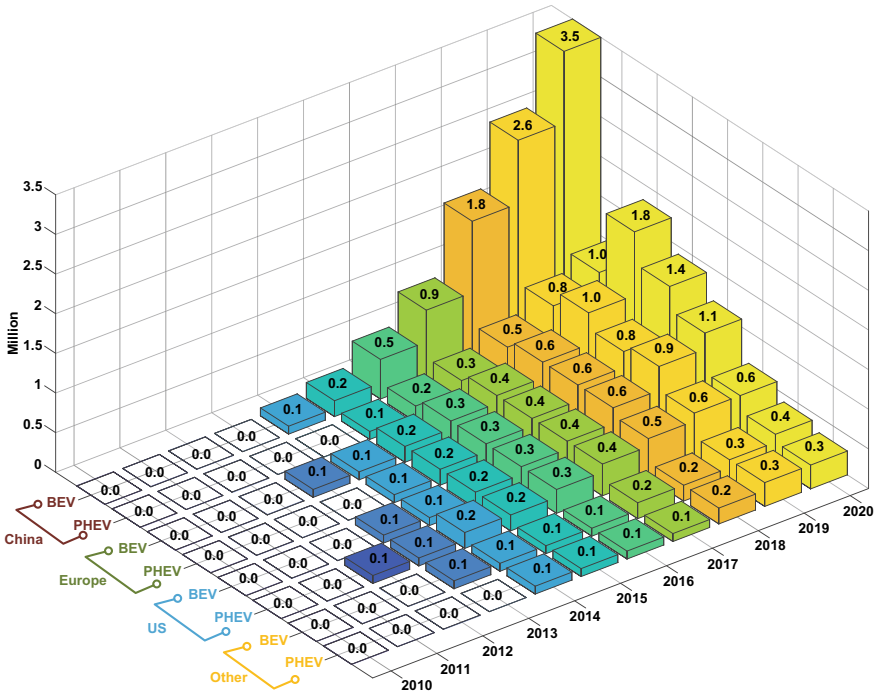


Fig. 6 Transport electrification stock by mode and region around the world

5 Conclusions

The EVs achieve a significant role in low-carbon emission and have prominent impacts on the electricity grid. In this context, this paper presents an in-depth investigation of the latest progresses and challenges for EVs and their charging infrastructure, consisting of the EV technologies, EV charging standards and methods. Besides, this paper focuses on the latest trends in smart charging technology, which can lessen the charging time of the EVs and promote the use of available renewable energies for charging EVs. Important insights of the state of the art of EV technologies, smart charging, and EV standards to the researchers have been provisioned. Some essential data about registrations of the EVs in various countries, transport electrification stock, and global battery demand have been investigated and analyzed in detail.

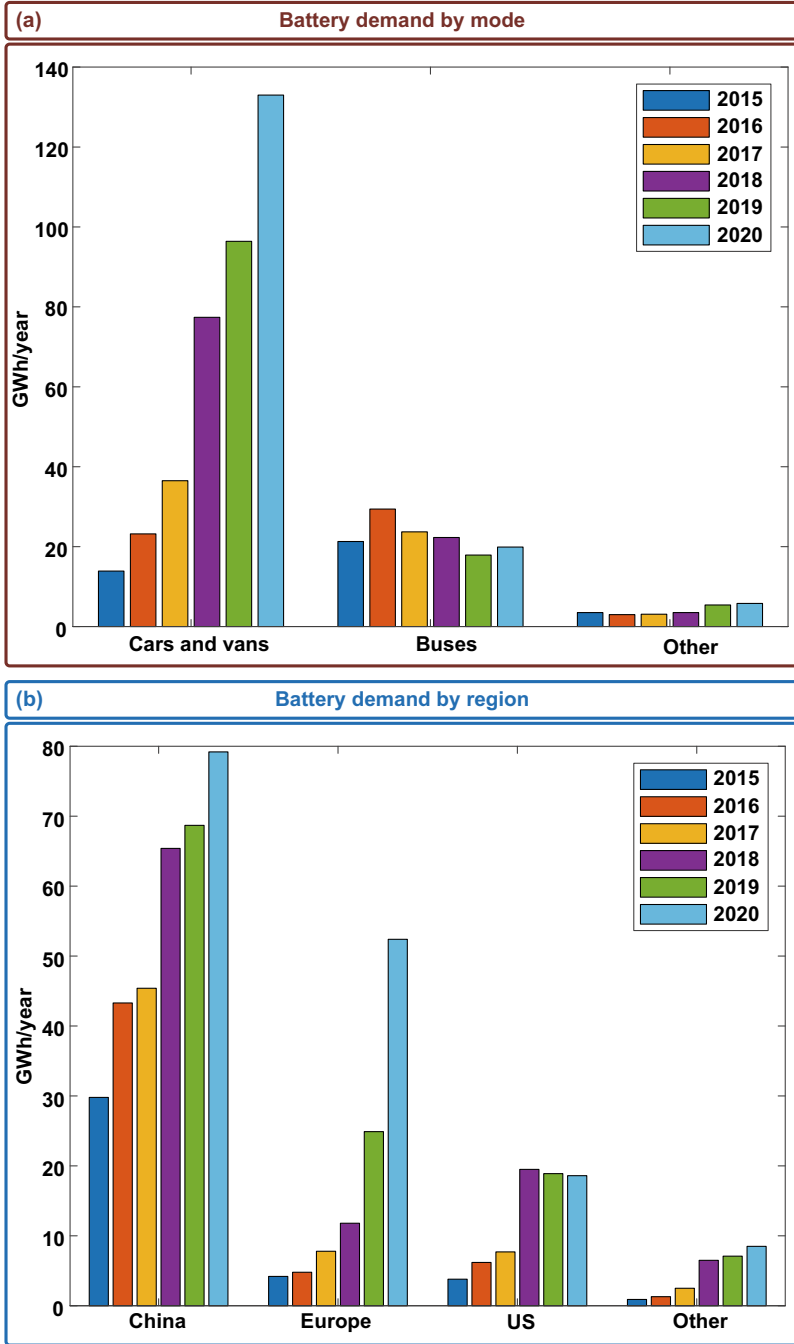


Fig. 7 Global battery demand for **a** mode and **b** region

References

1. Bukya M, Kumar R (2020) Safety consideration and design of high voltage cable for electric vehicle. In: 2020 international conference on power electronics & IoT applications in renewable energy and its control (PARC), pp 485–490
2. Bukya M, Kumar R, Gupta RK (2020) A study on safety issues and analytical evaluation of stresses for HVDC cable in electrical vehicle. In: AIP conference proceedings, vol 2294, no 040001
3. Li Z, Khajepour A, Song J (2019) A comprehensive review of the key technologies for pure electric vehicles. *Energy* 182:824–839
4. Yang X, Zhang Y (2021) A comprehensive review on electric vehicles integrated in virtual power plants. *Sustain Energy Technol Assess* 48:101678
5. Rodrigues AL, Seixas SR (2022) Battery-electric buses and their implementation barriers: analysis and prospects for sustainability. *Sustain Energy Technol Assess* 51:101896
6. Manzolli JA, Trovão JP, Antunes CH (2022) A review of electric bus vehicles research topics—methods and trends. *Renew Sustain Energy Rev* 159:112211
7. Wu Y, Wang Z, Huangfu Y, Ravey A, Chrenko D, Gao F (2022) Hierarchical operation of electric vehicle charging station in smart grid integration applications—an overview. *Int J Electr Power Energy Syst* 139:108005
8. Gönül Ö, Duman AC, Güler Ö (2021) Electric vehicles and charging infrastructure in Turkey: an overview. *Renew Sustain Energy Rev* 143:110913
9. Mangipinto A, Lombardi F, Sanvito FD, Pavičević M, Quoilin S, Colombo E (2022) Impact of mass-scale deployment of electric vehicles and benefits of smart charging across all European countries. *Appl Energy* 312:118676
10. Spencer SI, Fu Z, Apostolaki-Iosifidou E, Lipman TE (2021) Evaluating smart charging strategies using real-world data from optimized plugin electric vehicles. *Transp Res Part D: Transp Environ* 100:1030230
11. Barbosa W, Prado T, Batista C, Câmara JC, Cerqueira R, Coelho R, Guarieiro L (2022) Electric vehicles: bibliometric analysis of the current state of the art and perspectives. *Energies* 15(2):395
12. IRENA (2019) Innovation outlook: smart charging for electric vehicles. International Renewable Energy Agency, Abu Dhabi
13. The mobility house, Charging time summary for EVs, 28-11-2021 2021. https://www.mobilityhouse.com/int_en/knowledge-center/charging-time-summary (2021)
14. Hannan MA, Mollik MS, Al-Shetwi AQ, Rahman SA, Mansor M, Begum et al (2022) Vehicle to grid connected technologies and charging strategies: operation, control, issues and recommendations. *J Clean Prod* 339:130587
15. Arif SM, Lie TT, Seet BC, Ayyadi S, Jensen K (2021) Review of electric vehicle technologies, charging methods, standards and optimization techniques. *Electronics* 10(16):1910
16. Das HS, Rahman MM, Li S, Tan CW (2020) Electric vehicles standards, charging infrastructure, and impact on grid integration: a technological review. *Renew Sustain Energy Rev* 120:109618
17. Imani MH, Yousefpour K, Ghadi MJ, Andani MT (2018) Simultaneous presence of wind farm and V2G in security constrained unit commitment problem considering uncertainty of wind generation. In: 2018 IEEE Texas power and energy conference (TPEC), pp 1–6
18. IEA Electric Vehicles, IEA, Paris <https://www.iea.org/reports/electric-vehicles> (2021)
19. IEA, Energy Storage, IEA, Paris <https://www.iea.org/reports/energy-storage> (2021)
20. IEA, Global EV Outlook 2021, IEA, Paris <https://www.iea.org/reports/global-ev-outlook-2021> (2021)

Performance Estimation of Multilayer-Stack-Channel IGZO-Based Thin-Film Transistor in Double-Gate Mode



Shashi Kant Dargar , Abha Dargar, Shilpi Birla, and V. Hima Deepthi

Abstract Several additional amorphous oxide materials have been employed as promising materials in Thin-Film Transistor (TFT) applications due to their good transparency, resilience, and cost-effectiveness. However, due to low attainable mobility and low turn-on currents, the single-layer channel a-IGZO TFT is insufficient. To improve the switching characteristics of IGZO TFTs, this research suggests a multi-stack channel configuration. In this study, the source of performance enhancement in double-gate TFTs, compared to the Single-Gate (SG) multi-layer stack channel structure, has been described. Low mobility and Subthreshold Swing (SS) degradations occur in SG multi-layer stack channel TFTs. The field-effect mobility (FE) of SG TFTs ($14.70 \text{ cm}^2/\text{V}\cdot\text{s}$) increases to $24.92 \text{ cm}^2/\text{V}\cdot\text{s}$ when the gate voltage ($V_G = 10 \text{ V}$) is increased. From the channel's top to the gate-insulator interface (1.3×10^{18} per cubic cm), the concentration of electrons in SG TFT declines gradually (1.86×10^{18} per cubic cm). The current density in the DG structure of the multi-stack channel drops from 7.5 A per cm^2 to 2.5 A per cm^2 , leading to accumulation in the a-IGZO bulk and a large drain current. When the results from the proposed structure were compared to current results, they were found to be extremely encouraging and promising for future displays.

Keywords Multilayer stack channel · Thin-film transistor · IGZO · Display · Microelectronics · VLSI

S. K. Dargar (✉) · A. Dargar · V. H. Deepthi
Kalasalingam Academy of Research and Education, Virudhunagar 626126, TN, India
e-mail: drshashikant.dargar@ieee.org

S. Birla
Department of Electronic Engineering, Manipal University Jaipur, Dahmi Kalan, Rajasthan, India

1 Introduction

The extensive control of the electrical and optical features, high transparency, and moderate mobility for optoelectronics applications make zinc oxide material a proven superior candidate among the other Transparent Conducting Oxide (TCO). Because of their large mobility, scalability, and low-temperature developments, several attempts have spanned over two decades to create ZnO-based oxide Thin-Film Transistors (TFTs) for next-generation displays, opaque and flexible displays and 3D displays [1]. A TFT is structured by depositing thin films of a semiconductor layer, an insulating layer, and the substrate's metallic contacts. The TFTs fall under a special kind of field-effect device classification, wherein the device current is modified based on similar principles as a Metal–Oxide–Semiconductor (MOS) transistor. However, the TFTs are dissimilar from a MOSFET in insulating substrate/body, operation mechanism due to accumulation, and the undoped channel. Amorphous-indium gallium zinc oxide has clear, uneven atomic connection, opto-electrical capabilities, transmittance, and durability, which has made it suitable for sensors, photovoltaic, large-area electronics, and switching in organic LED, UHD, and LCDs [2–4]. On the other hand, low film density is caused by the single-active layer channel's inherent restriction, which makes α -IGZO materials suitable for transparent electronics in the thrust of high field mobility due to their huge bandgap and irregular bonding features. The α -IGZO materials have a wide bandgap and an amorphous crystalline nature; they offer high field mobility and are most suited in printed transparent devices. However, a single layer of IGZO in the channel suffers low film density. Additionally, several double-layer arrangements have been developed because the active channel layer's structure (i.e., single or multi-stack) affects device performance and the materials used. Besides, ITO, IZO, and amorphous-IZO in the channel layer have also been tried in the past [5, 6]. The authors have proposed a multi-stack channel with three layers in the past, where they have reported the gate control using two gates [7, 8]. In this study, the electrical properties of a multi-layer stack with a tri-active layer device structure that has two different gate control structures, namely, Single-Gate (SG) and Double Gate (DG), are evaluated.

2 Structure Description

Previous research has established that the defect's density, e.g., oxygen vacancies, can be reduced by making robust active layers. However, thin-film transistors are usually affected due to low mobility—accordingly, the TFTs of high mobility and stable electrical characteristics have demanded the future display applications.

The oxide TFTs are comprised of a buried layer and a bi-channel layer accumulated by sputtering, which exists to achieve larger mobility. Figure 1 depicts the sketched layout, including single-gated and double-gated device structures. The

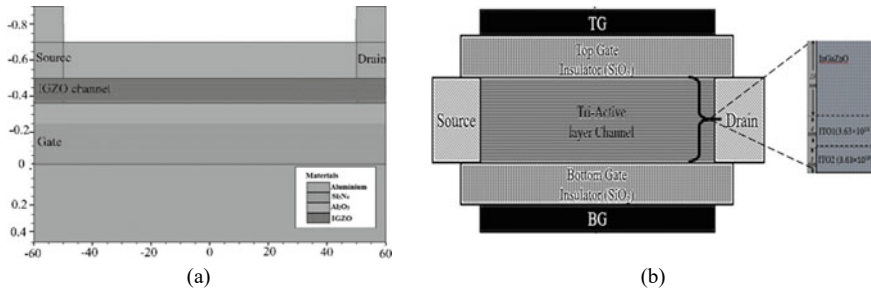


Fig. 1 Schematic of **a** SG TFT **b** DG-multi-stack TFT structure

intended structure consists of a silicon dioxide insulator and three active layer channels. The channel layer is a total of 30 nm *thick*, in which α -IGZO: ITO thickness ratio is 27:3 or 27:1, respectively. The channel is 25 μm long in lateral. For the simulation of the device structures, design parameters have been incorporated from the author's previous work [9].

3 Experimental Details

As it is well known that Gallium (Ga) makes a much higher ionic potential in comparison to Indium (In) or Zinc (Zn), it forms much tighter bonds with oxygen ions. As a result, Ga inclusion destroys the formation of oxygen vacancies, and thereby the g_{td} and g_{gd} drop owing to the rise in Ga concentration. The current I_{off} and subthreshold swings (SS) increase when more mobility rises [10]. On the other hand, increased Ga affects a lower off-current and a sharper SS, but at the cost of declining device mobility. Therefore, double-active layer architectures have been suggested to improve the device's electrical performance and overcome discrepancies. The Electronic Band Mobility (EBM) of the amorphous-IGZO device is indicated to lie between 10 and 20 $\text{cm}^2\text{V}^{-1}\text{s}^{-1}$ in the literature [11–14]. In contrast, mobility of the order of 59 $\text{cm}^2\text{V}^{-1}\text{s}^{-1}$ has been recorded for the amorphous-IZO combination [15]. To facilitate the same, a-IGZO with (In:Ga:Zn) atomic ratio of 1:0:1 and (1:1:1) taking EBM of 50 $\text{cm}^2/\text{V}\cdot\text{s}$ and of 15 $\text{cm}^2/\text{V}\cdot\text{s}$, respectively, were used in the dual active layer in order to attain high mobility channel structure. The electron affinity ($\chi_{\alpha\text{-IGZO}}$) of the device can be determined using linear correlation amid the three constituting composites of the a-IGZO material, as given by

$$\chi_{(\alpha\text{-IGZO})} = X\chi_{(\text{In}_2\text{O}_3)} + Y\chi_{(\text{Ga}_2\text{O}_3)} + Z\chi_{(\text{ZnO})}$$

where X, Y, and Z resemble the molar percentages of In_2O_3 , Ga_2O_3 , and ZnO, which are 4.4 eV, 3.2 eV, and 4.5 eV, correspondingly, adjusted from [16]. Each run of the TFT channel consists of layers with varying sublayer thicknesses for a total thickness

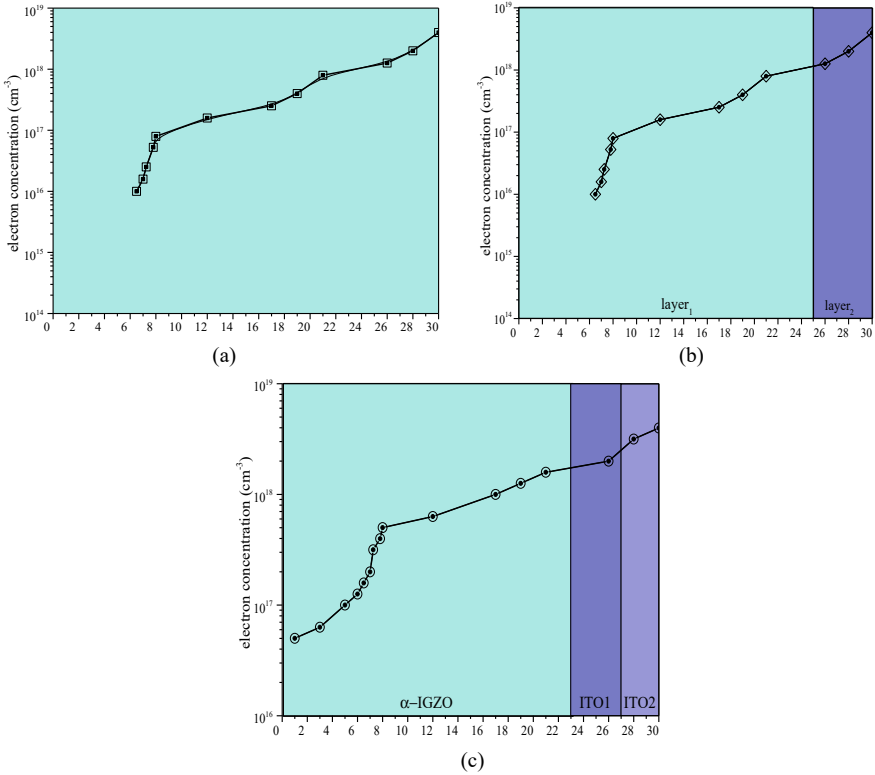


Fig. 2 Carrier distribution along the channel length **a** one layer, **b** two layer with layer1: layer2 = 25:5 in nm, **c** tri-layer with layer1: layer2: layer 3 = 23:7:3 in nm

of 30 nm. The layer interface’s proximity to the conductive channel between layer 1 and 2 may be responsible for the low turn-on voltage. Because of the positive gate bias, numerous carriers already exist in the primary conductive channel. The electrical parameters concerning the different channel distance x are listed with reference to the various channel stacks as shown in Fig. 2 which are shown in Table 1.

4 Result and Discussion

As a result of channel simulation, the current and voltage relation among gate drain, i.e., transfer characteristics, has been obtained from the device simulation and compared with electrical device characteristics. As discussed in the preceding sections, the single-gate and double-gate-type structures of IGZO TFT were simulated using the electronic simulator. The process simulation of the device structure is

Table 1 Amorphous-IGZO TFT electrical parameters alongside channel distance x

At altered x of channel layer1							(Multi-stack channel)
Symbol (Unit)	0 nm	15 nm	23 nm	25 nm	27 nm	30 nm	23 nm/4 nm/3 nm
V_{TH} (V)	1.18	-0.41	-2.62	-1.52	-3.22	1.85	-4.24
I_{ON} ($\mu A/\mu m$)	1.70	2.096	1.167	1.034	0.855	0.285	9.23
I_{OFF} (nA/ μm)	1.3E-2	3.3E-3	8.2E-6	3.9E-7	1E-9	2.1E-7	4.9E-8
SS (mV/Dec.)	0.290	0.275	0.283	0.164	0.190	0.663	0.198

shown in the flowchart depicted in Fig. 3. This section presents the electrical results obtained from the device simulation.

The I_D-V_G of the intended device, which concerns the transfer characteristics, is illustrated in Fig. 4. In the case of DG TFT, the intense set of observational points below the threshold has been noticed that warrants large OFF currents and results in relatively larger (SS). While Fig. 5 exhibits the drain current characteristics of single-gated and double-gated device structures.

The doping dissemination in a single-gate IGZO TFT referring to Fig. 6 exemplifies the origin of drain current in an SG-IGZO TFT. The substantial concentration

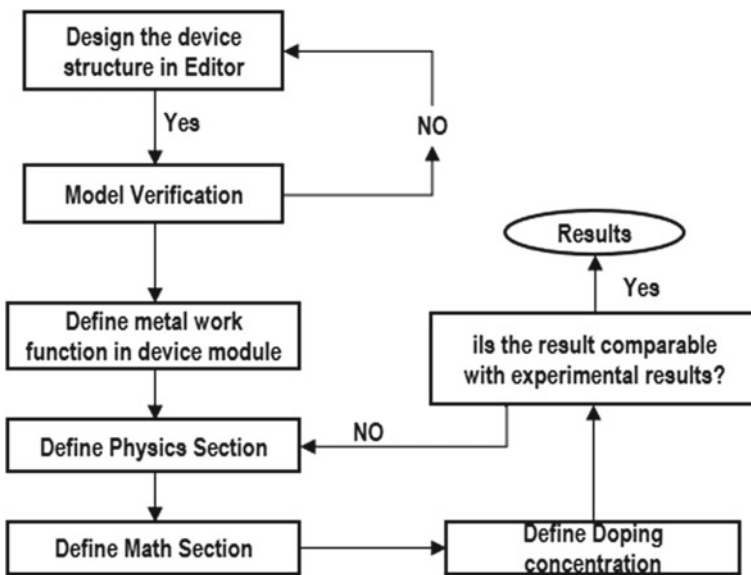


Fig. 3 Process flowchart of the device design

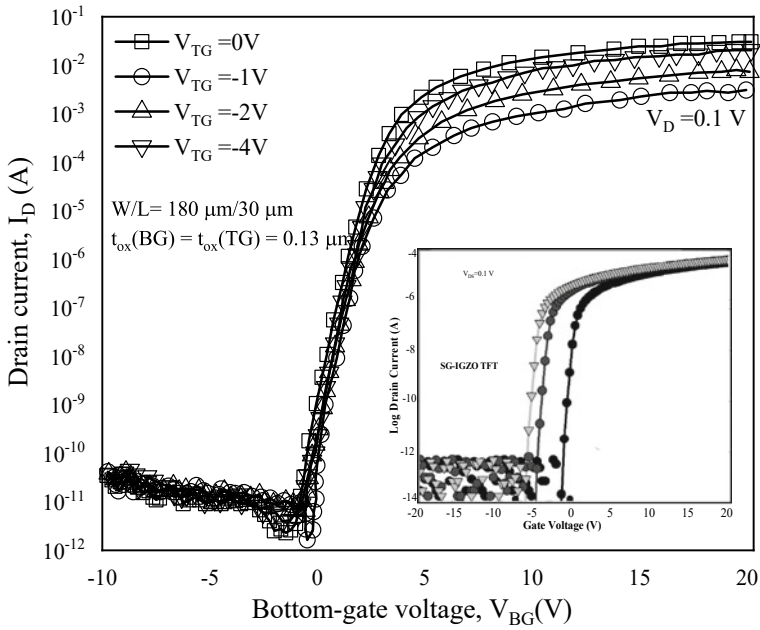


Fig. 4 Transfer characteristics (I_D - V_G) of SG and DG-TFTs

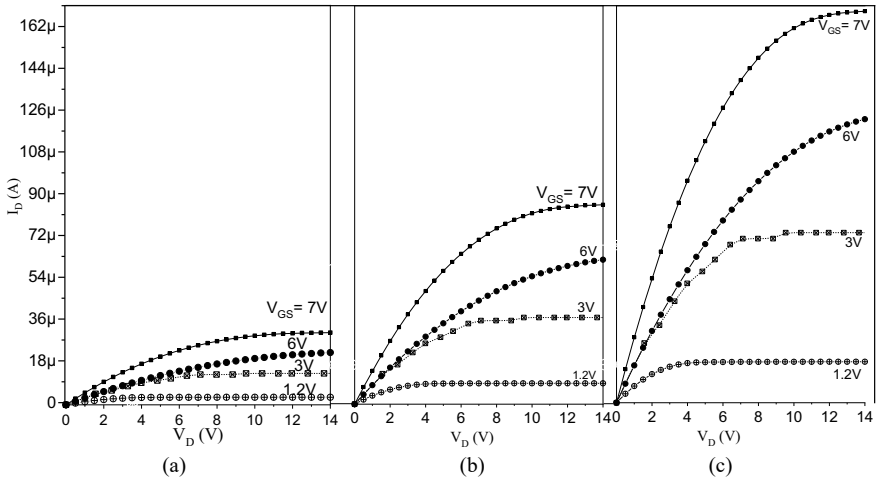


Fig. 5 Drain current comparative with respect to **a** SG-Bottom, **b** SG-Top, and **c** Double-Gate structure

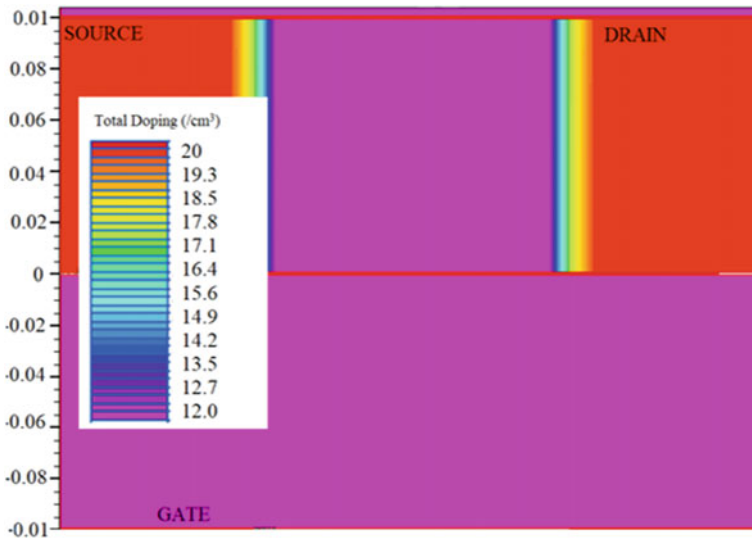


Fig. 6 SG-IGZO TFT doping distribution

is accumulated at the drain interface. Figure 7 demonstrates the electric field distribution in the Double-Gate (DG) Tri-Active Layer channel structure from which it is apparent that the accumulation of complete channel has considerable diminishment when approaching the nearby source from the channel or from the drain-to-channel interfaces. The weakening accumulation causes increased drain current. Using the I–V characteristics as obtained from Figs. 4 and 5, electrical characteristics have been extracted using the standard methods [17–19] and are listed in Table 2. The double-gate IGZO TAL TFT structure increases field-effect mobility, and high I_{ON}/I_{OFF} ($\sim 10^7$) could also be attained. However, the SG structure has a desirably low subthreshold (158 mV/decade).

The comparison to existing coplanar DG TFT results and the presented device structures are shown in Table 2. The enactment of the proposed device is reflected in this update. The electrical parameters expressed in Table 2 display improvements in lower threshold voltage, increased I_{ON}/I_{OFF} , comparable SS, and improved mobility with both overlap and offset structure of the device compared to coplanar DG TFT for one or both gate biasing conditions.

In this design, possibly because the channel stack layer thickness engineered in TALTFT is considerably effective for improving the electron transport or the ITO and a-IGZO thin films show the identical bandgap producing a junction between ITO and a-IGZO which is modeled as a homojunction rather a heterojunction in other combinations. Furthermore, due to high carrier distribution in the ITO compared to a-IGZO, an analogous band bending occurs in the CB of the proposed channel and does not affect the I_{OFF} much, and larger mobility is obtainable [20, 21].

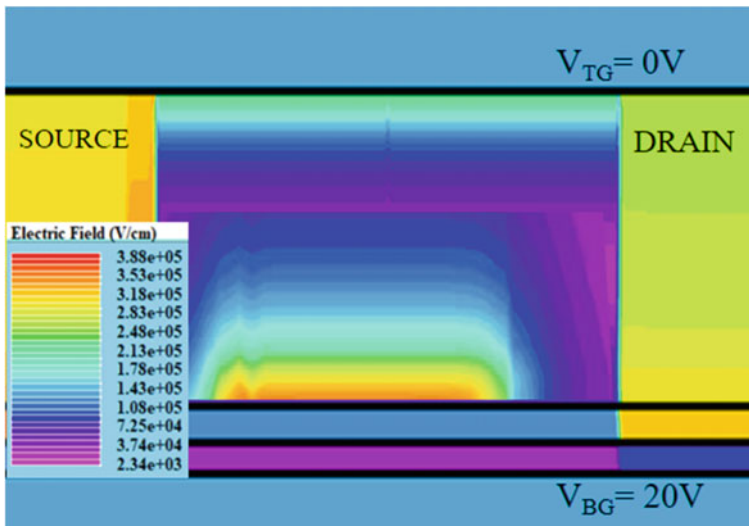


Fig. 7 Electric field distribution in DG-multi-stack IGZO TFT

Table 2 Extracted parameters and comparison between SG and DG IGZO TFT device

Parameters	SG-TAL	SG-TAL	DG-TAL	IGZO coplanar structure [20]		
	SG (bottom-gate)	SG (top-gate)	(Dual-gate bias)	SG (bottom-gate)	SG (top-gate)	(Dual-gate bias)
V_{TH} (V)	-3.3	-1.23	-2.6	0.42	0.54	0.55
I_{ON}/I_{OFF}	$\sim 10^2$	$\sim 10^4$	$\sim 10^7$	$\sim 10^5$	$\sim 10^4$	$\sim 10^7$
μ_{FE} ($\text{cm}^2 \text{V}^{-1} \text{s}^{-1}$)	16.35	14.74	24.92	11.52	12.8	13.08
SS (V/decade)	0.16	0.19	0.22	0.286	0.153	0.100

5 Conclusion and Future Work

The cause of performance enhancement in the double-gate IGZO compared to the single-gate architecture is described in this paper. Mobility and SS degradations have caused anguish in the SG TFTs. The field-effect mobility (FE) of single-gate TFTs is $14.70 \text{ cm}^2/\text{V}\cdot\text{s}$, whereas the FE of double-gate TFTs is $24.92 \text{ cm}^2/\text{V}\cdot\text{s}$. From the channel's top to the gate-insulator contact ($1.3 \times 10^{18} \text{ cm}^{-3}$), the density of electrons in SG TFT decreases steadily ($1.86 \times 10^8 \text{ cm}^{-3}$). The current density of the DG TFT reduces from 7.5 to $2.5 \text{ A}/\text{cm}^2$ for similar scenarios, creating buildup in the a-IGZO bulk and resulting in a greater drain current. The DG IGZO TFT can replace the high mobility of SG TFTs in array circuits such as flexible RFIDs, ultra-HD displays, and wearable electronics. However, improving subthreshold swing (SS) persists in DG and SG, both IGZO TFT architectures and would necessitate more study and structural changes.

References

1. Nomura K, Ohta H, Takagi A, Kamiya T, Hirano M, Hosono H (2004) Room-temperature fabrication of transparent flexible thin-film transistors using amorphous oxide semiconductors. *Nature* 432(7016):488–492
2. Fortunato E, Barquinha P, Martins R (2012) Oxide semiconductor thin-film transistors: a review of recent advances. *Adv Mater* 24(22):2945–2986
3. Kamiya T, Nomura K, Hosono H (2010) Present status of amorphous In–Ga–Zn–O thin-film transistors. *Sci Technol Adv Mater*
4. Sheng J, Han KL, Hong T, Choi WH, Park JS (2018) Review of recent progresses on flexible oxide semiconductor thin film transistors based on atomic layer deposition processes. *J Semicond* 39(1):011008
5. Kim SI, Kim CJ, Park JC, Song I, Kim SW, Yin H, Lee E, Lee JC, Park Y (2008) High performance oxide thin film transistors with double active layers. In: 2008 IEEE international electron devices meeting, pp 1–4
6. Park JS, Maeng WJ, Kim HS, Park JS (2012) Review of recent developments in amorphous oxide semiconductor thin-film transistor devices. *Thin Solid Films* 520(6):1679–1693
7. Dargar SK, Srivastava VM (2019) Design and analysis of novel tri-active layer channel amorphous-IGZO thin-film transistor. *Micro & Nano Letters* 14(13):1293–1297
8. Dargar SK, Srivastava VM (2019) Design and analysis of IGZO thin film transistor for AMOLED pixel circuit using double-gate tri active layer channel. *Heliyon* 5(4):e01452
9. Dargar SK, Srivastava VM (2019) Double-gate tri-active layer channel amorphous-IGZO thin film transistor for AMLCD pixel circuit. In: 2019 photonics & electromagnetics research symposium-spring (PIERS-Spring), pp 2448–2453
10. Li X, Yin S, Xu D (2015) Simulation study on the active layer thickness and the interface of a-IGZO-TFT with double active layers. *Front Optoelectron* 8(4):445–450
11. Bae H, Choi H, Oh S, Kim DH, Bae J, Kim J, Kim YH, Kim DM (2012) Extraction technique for intrinsic Subgap DOS in a-IGZO TFTs by De-embedding the parasitic capacitance through the photonic $C-V$ measurement. *IEEE Electron Device Lett* 34(1):57–59
12. Bae M, Lee KM, Cho ES, Kwon HI, Kim DM, Kim DH (2013) Analytical current and capacitance models for amorphous indium-gallium-zinc-oxide thin-film transistors. *IEEE Trans Electron Devices* 60(10):3465–3473
13. Kim Y, Kim S, Kim W, Bae M, Jeong HK, Kong D, Choi S, Kim DM, Kim DH (2012) Amorphous InGaZnO thin-film transistors—Part II: modeling and simulation of negative bias illumination stress-induced instability. *IEEE Trans Electron Devices* 59(10):2699–2706
14. Bae M, Kim Y, Kong D, Jeong HK, Kim W, Kim J, Hur I, Kim DM, Kim DH (2011) Analytical models for drain current and gate capacitance in amorphous InGaZnO thin-film transistors with effective carrier density. *IEEE Electron Device Lett* 32(11):1546–1548
15. Kim HS, Park JS, Jeong HK, Son KS, Kim TS, Seon JB, Lee E, Chung JG, Kim DH, Ryu M, Lee SY (2012) Density of states-based design of metal oxide thin-film transistors for high mobility and superior photostability. *ACS Appl Mater Interfaces* 4(10):5416–5421
16. Fung TC, Chuang CS, Chen C, Abe K, Cottle R, Townsend M, Kumomi H, Kanicki J (2009) Two-dimensional numerical simulation of radio frequency sputter amorphous In–Ga–Zn–O thin-film transistors. *J Appl Phys* 106(8):084511
17. Chen BW, Eric KY, Chang TC, Kanicki J (2018) Physical origin of the non-linearity in amorphous In–Ga–Zn–O thin-film transistor current-voltage characteristics. *Solid-State Electron* 147:51–57
18. Dargar SK, Srivastava VM (2020) Design of double-gate tri-active layer channel based IGZO thin-film transistor for improved performance of ultra-low-power RFID rectifier. *IEEE Access* 8:194652–194662
19. Rim YS, Chen H, Kou X, Duan HS, Zhou H, Cai M, Kim HJ, Yang Y (2014) Boost up mobility of solution-processed metal oxide thin-film transistors via confining structure on electron pathways. *Adv Mater* 26(25):4273–4278

20. Baek G, Kanicki J (2012) Modeling of current—voltage characteristics for double-gate a-IGZO TFTs and its application to AMLCDs. *J Soc Inform Display* 20(5):237–244
21. Ishida K, Meister T, Shabanpour R, Boroujeni BK, Carta C, Cantarella G, Petti L, Mtozenrieder N, Salvatore GA, Troster G, Ellinger F (2016) Radio frequency electronics in a-IGZO TFT technology. In: 2016 23rd international workshop on active-matrix flatpanel displays and devices (AM-FPD), pp 273–276

Towards Space Sensor Network and Internet of Things: Merging CubeSats with IoT



Charalampos Koulouris, Piromalis Dimitrios, Izzat Al-Darraj, Georgios Tsaramirsis, Alaa Omar Khadidos, Adil Omar Khadidos, and Panagiotis Papageorgas

Abstract The fourth industrial revolution, also known as Industry 4.0, has been impacted by the advancements of various technological areas, including microsatellites. The Internet of Space Things (IoST) and Space Sensor Networks (SSNs) are generally integrated into microsatellites as well as Internet of Things (IoT) devices that have recently been used in modern applications. Compared to the traditional microsatellites and IoT devices, the current IoST and SSN devices have the advantages of collecting IoT data in remote areas where there is no network or Internet, sending data with low power between mobile devices and satellite constellations, ensuring global coverage of data exchange, and so on. Due to the mentioned individual advantages, the IoST and SSNs devices have been widely applied in microsatellites and IoT devices. The IoST devices can be integrated with a satellite constellation and CubeSats or IoT receivers. Beside this, the IoST devices are implemented in other applications as a bigger satellite constellation which have both IoT receivers and space sensors such as satellite dishes and RF devices. This paper

C. Koulouris · P. Dimitrios

Industrial Design and Production Engineering Department, University of West Attica, P. Ralit and Thivon 250, 12244 Egaleo, Greece

I. Al-Darraj

Automated Manufacturing Department, University of Baghdad, Al-Khwarizmi College of Engineering, Baghdad, Iraq

G. Tsaramirsis

Abu Dhabi Womens's College, Higher Colleges of Technology, Abu Dhabi, UAE

A. O. Khadidos

Faculty of Computing and Information Technology, Department of Information Systems, King Abdulaziz University, Jeddah, Saudi Arabia

A. O. Khadidos (✉)

Faculty of Computing and Information Technology, Department of Information Technology, King Abdulaziz University, Jeddah, Saudi Arabia

e-mail: akhadidos@kau.edu.sa

P. Papageorgas

Department of Electrical and Electronics Engineering, University of West Attica, P. Ralit and Thivon 250, 12244 Egaleo, Greece

surveys the current research and technologies of IoST and SSNs within their applications in microsatellites and IoT devices. The impact of IoST on Industry 4.0 is also discussed in this paper.

Keywords Internet of Space Things · Space sensor networks · Satellites · Microsatellites · Industry 4.0

1 Introduction

In space applications, there are numerous satellites in the low earth orbit segment. In the past, older satellites which were usually used by television networks were only relay satellites. Nowadays, satellites are much smaller and equipped with SSNs to receive RF signals, take photos, and process data. This data can be sent through space Internet constellations. Then, it will propagate to the Internet or process to act like an edge computing device. Thus, having a global satellite constellation with IoT SSNs can ensure a truly global data connection of IoT earth and space objects. The IoTs are new smart electronic devices that can be connected to the Internet and used to propagate information about sensors to the cloud. The application of IoT, over 5G and 6G networks, is a major area of interest for modern technologies in the market [1, 2]. For example, a satellite IoT constellation is used by IoT devices in remote areas where there is no other Internet connection or 4G/5G. Such applications can be implemented in specific environments such as out on sea, during a flight [3–5], and other remote areas. However, satellites with IoST devices can ensure a global coverage of data exchange for earth-based objects, airplanes, and possibly other space objects that are equipped with IoT transceivers. Thus, the satellites or microsatellites that receive the rf IoT signal from earth-based objects or airplanes can propagate and process this data to other satellites. Therefore, the satellites are acting as an edge node to process data and communicate with other satellites as well as ground stations on earth. Similarly, the architecture of satellite constellations has been changed and included microsatellites which are specialized in data collection only without any capabilities of direct communication with ground stations on earth. Instead, microsatellites communicate using other satellites that serve as network hubs and these propagate the data to the ground stations. The ground stations process the data and send it to the Internet. This data is then processed again from web servers and computers and presented in the cloud. Hence, companies, people, and computers can then use this data. There are many satellites and microsatellites orbiting the earth. On 1 January 2021, there were 6542 satellites. This number is increasing every week with new rocket launches [6]. The SSN systems for satellites and IoT devices can be categorized into three types: the SSN systems that connect earth objects with the satellites, the SSN systems that connect satellites with each other, and the SSN systems that connect the satellites with the ground station that can be a normal RF signal with a satellite dish or a laser [7]. The restrictions of IoST systems are that RF signals cannot be obtained from a lot of receivers in orbit [8].

Furthermore, in the situation of satellites orbiting at high speed, it is difficult for satellites to cooperate with each other and transfer data between them. Moreover, SSN systems are restricted by sensitivity to receive RF signals, range of distance that can propagate signals, power to transfer data, size, data that they can process on the spot (edge computing), and number of devices that they can connect simultaneously. Consequently, integrating IoST and SSNs devices together propagates the data from IoT objects to the cloud faster, processes the data faster in the edge network and/or the cloud, and presents the information and data faster and accurately to the users [9]. In terms of microsatellite, CubeSats is developed and implemented to be dominant satellite technology with more than 800 satellites launched. CubeSats are used by companies, universities, researchers, and business platforms to gather information from space and connect devices. The integration between the IoT devices and small satellites combination is developed to make a powerful system called the Internet of Space Things (IoST) [10]. Practically, in the market, there are many deployments of satellites which make access to space easier, such as SpaceX [11], Blue Origin [12], One Web [13], Iridium Next [14], and others. Many other companies are designing and deploying cube satellites to gather satellite imagery and connect all the remote areas of the planet to the Internet [15]. The area of IoST is vast and has many opportunities for exploration not only by organizations dealing with microsatellites, but also by companies dealing with the processing and distribution of data. The fourth industrial revolution, usually referred to as Industry 4.0, has been impacted by IoST. Industry 4.0 is a new term to describe the use of computing, robotics, artificial intelligence, and the Internet in manufacturing and industries [16]. IoT devices are used extensively in Industry 4.0, since IoT devices are used extensively to connect objects with centralized computer systems and/or the cloud. An example of an aerospace scenario with IoT and IoST devices is presented in Sect. 5 of this paper.

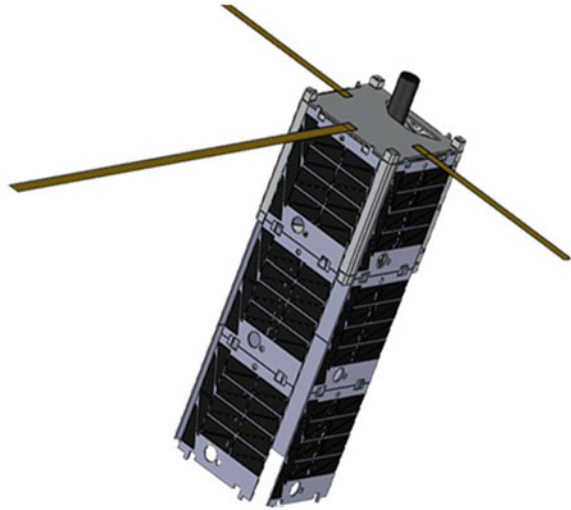
The rest of this paper is structured in the following order: The state of the art of IoST is presented in Sect. 2. Section 3 explains the IoT connectivity. Section 4 explains the latest research done by the various space agencies. Section 5 explains the impact of IoST to Industry 4.0. Finally, Sect. 6 concludes this work.

2 IoST: State of the Art

2.1 Architecture of IoT/IoST Systems

IoST systems are a system of interconnected IoT devices, directly or indirectly connected to the Internet via satellites. The IoT data can be accessed all over the globe from computers, mobiles, embedded systems, and other Internet-connected devices. In three stages, the IoT data generally is forwarded to the cloud as: (1) collecting it from the IoT device through a sensor; (2) forwarding it to a local computer, which can be either an embedded device or a normal computer; (3) and forwarding it through

Fig. 1 A deployed CubeSat rendered image



the Internet protocol to the cloud after making the necessary computations. Satellites have many different sizes and architectures. Microsatellites are in the order of multiples of approximately “u cubic centimetres”, where “u” is in the range of 10–60. Microsatellites are hosting IoT devices, cameras, batteries, solar panels, Attitude Determination and Control System (ADCS), communication transceivers, and antennas. Figure 1 shows a 1u satellite with expendable solar panels [17].

IoT architecture can be characterized as centralized or decentralized. Inside a smart home, there are IoT devices like smart lock, motion sensor, smart speaker, smart thermostat, etc. Hence, they are all connected to a central embedded system, i.e. a centralized IoT architecture approach. On the contrary, in the decentralized IoT architecture, a decentralized system can be the whole global system of interconnected IoT devices in the cloud. In this situation, many different IoT systems and embedded devices are connected to different web servers, computers, and databases. Moreover, there is no central computer to manage all the IoT devices. Generally, IoT device architecture has four layers [18] as shown in Fig. 2. The first layer has the sensors and IoT devices. The second layer is the IoT gateway or aggregation layer. The third layer is in the cloud and is called the event processing layer. The fourth layer is the application layer.

Recently, the use of space objects to provide data services has greatly increased. In turn, a new dimension, called space, is integrated with the Internet and IoT architecture to generate new data services named IoST. Due to the complexity of the interconnected devices in IoT and the Internet, it remains difficult to design a single diagram for the architecture of IoT or IoST. For the last 10 years, CubeSats and small satellites were used extensively to collect data as part of IoST service data systems, as shown in Fig. 3.

Many of the CubeSats specialize only in data collection without any capabilities to directly communicate with ground stations on earth [19]. Instead, they communicate

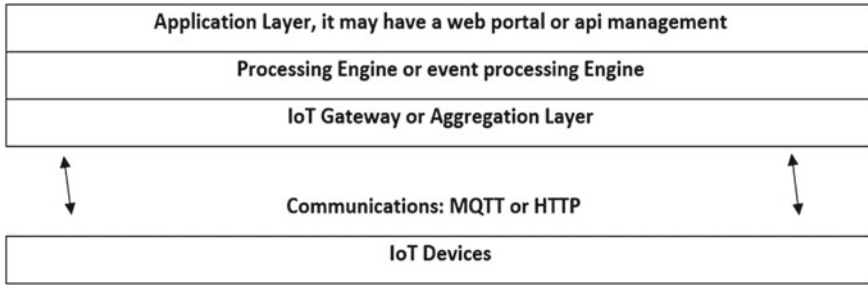


Fig. 2 IoT device architecture

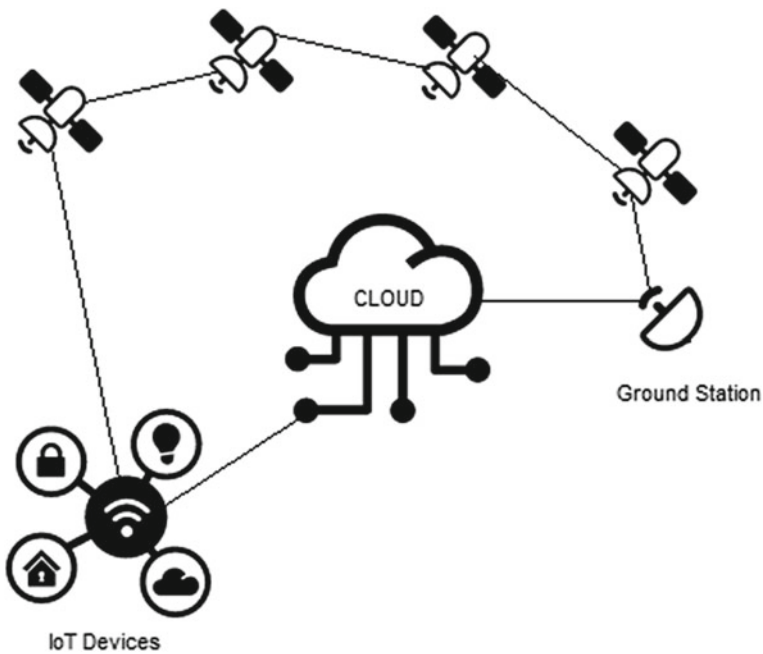


Fig. 3 A combination of cloud computing, IoT devices, and IoT satellites

using other satellites that serve as network hubs. Once the data from the satellite hubs reaches earth, data is stored into the cloud. The IoST has four main parts; (1) the satellites orbiting the earth, which can be CubeSats or big satellites, (2) the IoT sensors in earth that send signals to space, (3) the ground stations that receive all signals from the orbiting satellites, and (4) the cloud computing architecture that stores and processes all the data.

2.2 *IoST-Satellite Technologies*

During the last decade, many technologies have been introduced by various competitive companies to create a global satellite Internet coverage by deploying thousands of satellites in low earth orbit [6]. For instance, SpaceX with project Starlink has developed an affordable global satellite Internet connection service with a low cost to access space (to enter the low earth orbit) by operating reusable rockets. SpaceX with project Starlink deployed their first 60 satellites (from total 12,000 satellites), which created a train of orbiting stars in the night sky. As of February 2021, they had deployed 775 satellites. It is believed that project Starlink will deliver the first affordable and global Internet connection through satellites. Small computers such as Raspberry Pi and Siemens IoT as well as many other devices such as home automation, robotics, cars, warehouses, ships, cameras, and wearables are connected to the Internet. CubeSats technology could not miss the opportunity to connect these IoT devices to the Internet and use the ability of the CubeSats to control remote areas and observe the earth from above. IoT devices have been used inside the CubeSats in orbit to receive rf signals and data. In the last two decades, there was another IoST-satellite technology named iridium satellites, which provided a reliable machine-to-machine (M2M) application through the iridium 9603 transceiver [14]. This type of IoST system provides global coverage with 82 operational satellites [14]. Furthermore, there is a promising project in the future using iridium satellites called iridium cloud connect that will have a cloud application running in Amazon Web Services [14]. The goal of iridium Cloud Connect is to provide an end-to-end connection of all IoT devices, iridium satellites, and the cloud together. However, expanding an IoST-satellite system to be connected with pre-existing satellite constellations is a high-cost endeavour [14]. Hence, there is a need to design more affordable satellite constellations. CubeSat constellations are cheaper to design and deploy due to the small size of the CubeSat. In many countries, a CubeSat constellation is created to connect devices in the ground and create an IoT network. An excellent example of such IoT CubeSat constellations is Fleet [20] and Myriota in Australia. The aim of Fleet and Myriota technologies is to connect remote industries in Australia in situations where there is no 3G, 4G, or Wi-Fi. Fleet technology achieved this connectivity with a LoRaWAN Gateway modem, a real plug-and-play modem. With these modems, 1000 sensors can be connected to the satellite constellation within a range area reaching 15 km [20]. Industries like mining, oil and gas, large agriculture areas, and others are using the Long-Range (LoRa) Gateway [21] to connect to the satellite constellation. LoRa is a widely used technology for the IoT devices and IoST CubeSat constellations [20]. The LoRa which is presented by LoRa alliance is a wireless technology applicable for long-range, low-power, and low-data-rate applications. Thus, IoT devices using a small battery can send signals great distances at a very low data rate. Then, a LoRa gateway is able to collect all the signals from up to 1000 IoT devices [20]. The gateway then is connected to the Internet and uploads the data to the Things network [22]. In case the gateway is in a remote place, it can send the data to the CubeSats constellation every time a CubeSat is available to listen to the LoRa gateway. The

CubeSats constellation then relays the information to the appropriate ground station, which then sends the data to the Things network. The biggest advantage of the Things Network is that it can allow low-power devices to use remote gateways to access the open-source distributed network, thereby exchanging data with applications [22]. This means that even at the most remote areas of the world, a device using a very small battery can relay its data to the Internet. The IoT devices and the LoRaGateway are connected through the LoRaWAN. The most common and appropriate orbit for CubeSats for earth observation is the polar orbit [23]. A polar orbit is very suitable for earth observation satellites because each satellite passes over the equator in a different longitude. A polar orbit has an inclination of 90 degrees to the body's equator [23]. A demonstration of a simulation of a polar orbit in AGI, STK is shown in Fig. 4.

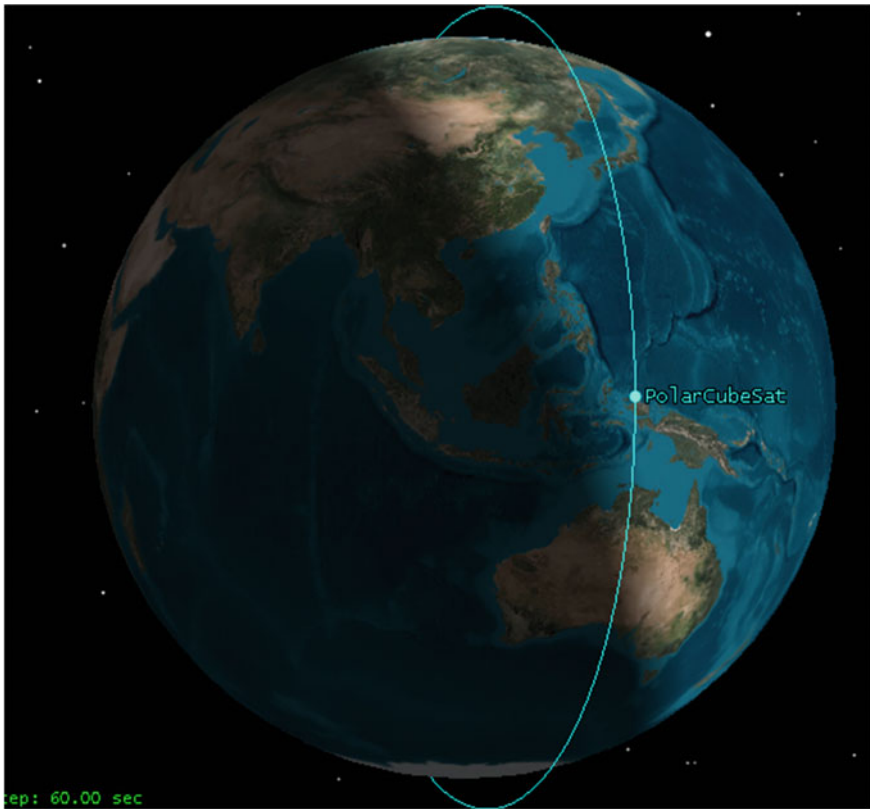


Fig. 4 Polar orbit simulation in AGI STK

3 IoT Connectivity

3.1 Types

There are various ways of communication in the IoT approach. The type of the communication depends on the device and the application. The application can be, for example, a smart wearable device connected to a smart phone, or a temperature meter connected to an embedded device, and so on. However, the wide use of IoT devices and networks has led to the invention of technologies to support these kinds of applications. In these technologies, numerous IoT protocols exist to support the potential applications and satisfy the needs at the terrestrial space as shown in Table 1 [24].

3.2 LoRaWAN/SigFox IoT Technologies

LoRaWAN has a few issues in terms of both the architecture and protocols. Furthermore, LoRaWAN architecture is not integrated with the Long-Term Evolution (LTE) network. Consequently, “LoRaWAN is not a complete network stack in the OSI model. It lacks the common features of network layer, session layer and transport layer” [25]. One of the key aspects of LoRaWAN is the long battery life of its devices. LoRa devices are designed to enter deep sleep mode when not transmitting messages, thereby maximizing battery life. The life cycle of any IoT device in a remote area depends on its battery capacity, so entering sleep mode when the device is not in use will extend its battery life. SigFox [26], which is another French company active in the development of IoT devices and architectures, is one of the two most common IoT producers. The SigFox network has a star-like architecture. Billions of IoT objects transmit their data to the SigFox network when their signal reaches the SigFox stations. Every SigFox station is connected to the SigFox cloud, which sends the messages to many customer services and IT platforms.

SigFox invented a lightweight protocol to process each message. Compared with IPv6, the protocol overhead it uses is much smaller, the protocol frame size is lighter, and less data is sent, so the total energy required to generate sparse messages is also less. Therefore, energy can be saved, so the battery in the IoT device can be used for a longer time. Table 2 compares the two major commercial IoT technologies (SigFox and LoRa).

Table 1 IoT protocol features

Technology	Protocol	Range	Bit rate/frequency	Applications
Bluetooth	BLE (Bluetooth low energy protocol)	10 m	1 Mb/s (2 Mb/s in Bluetooth 5)	IoT, Apps with low energy consumption, smart gadgets, Bluetooth smart sensors connecting to the Internet via 6LoAPAN
Wi-Fi	Wi-Fi standard 802.11	50 m	2.4 GHz band 450–600 Mbps	
5 GHz band 1300 Mbps	IoT, home, office, industry, high bandwidth applications			
ZigBee	ZigBee 3.0	10–20 m	2.4 GHz	Industrial, scientific, medical, and IoT
MQTT IoT	MQTT protocol			IoT, remote locations where bandwidth is limited, obtaining data from so many electrical devices IT communications or infrastructure
CoAP	Internet protocol suite, mostly UDP			Sensor network nodes
DDS	Data distribution service			
Data-centric publish-subscribe			High-performance, expandable and real-time machine-to-machine communication	

Table 2 LoRaWAN and SigFox comparison

	Sigfox	LoRaWAN
Technique	Ultra narrow band	Chirp spread spectrum
Modulation	UL:DBPSK	
DL: GFSK	Frequency	
Chirps		
Channel BW		

4 Applications

Scientific research from researchers in universities and institutions for CubeSats and IoT has been the initial driving force that started the big boom in microsatellites. The CubeSat architecture and deployment was an innovation from Stanford University's SSDL and California Polytechnic State University [27]. Since then, many universities, institutions, NASA, the European Space Agency (ESA), and many companies and individuals are using this innovative platform to conduct scientific experiments for astronomy, telecommunications, earth observation, and, of course, Internet of Things. Internet of Things devices on earth and space, combined with a cube satellite network in low earth orbit, can create a new type of IoT communication applications, the IoST, as pointed out in [10], their innovative new type of IoST technology. The main components of this type are the following layers:

- Infrastructure layer which represents the hardware devices, like CubeSats, servers, and IoT hardware.
- Control and Management Layer, for controlling and managing the hardware.
- Policy layer, which allows external devices to communicate with the IoST system.

Researchers in [28] have proposed a design of CubeSats. It was a new model of communication for the IoST, an innovative design of a CubeSat network, IoT, and multi-band radio frequencies capable of offering a global and unique Internet of Things space coverage. This new CubeSat design can offer an integration of multi-frequency front ends and antennas able to communicate simultaneously in multiple bands ranging from the microwave to the mm-wave and the THz band.

Researchers from Blavatnik School of Computer Science [29] have designed and placed tags in birds. In their innovative design of an animal tag, they had constructed and placed IoT tags to animals. For instance, they placed tags on wild owls and kestrels. They placed IoT tags that track animals all over the world. Animals can be tracked from space and ground level if they are wearing a tag. The tag transmits data about their position, temperature, and any other data the researchers want. As pointed out by [29], the Icarus project is a unique project for tracking animals with IoT tags. The ICARUS system was installed in 2018 [29] on the International Space Station to track animals from space, utilizing the very tiny IoT sensors the animals were carrying. The IoT animal sensor was a 5 g tag with GNSS, accelerometer, magnetometers, temperature sensor, and 500 MB memory. The project also had an innovative design of four nanosatellites to verify InterSatelliteLink (ISL) feasibility. The four nanosatellites were developed by the Technical University of Berlin (TUB) with an S Band transceiver radio as the main payload in a nanosatellite swarm mission called S-NET [29]. The S-NET had a 100kbps crosslink, 1Mbps downlink rates, and its size was small enough to be accommodated in a CubeSat. The InterSatelliteLink links the CubeSat with a radio and propagates data between the CubeSats in forms of IoT data, operational data, relative position data and operation schedule or payload data. Furthermore, they proposed an InterSatelliteLink (ISL) network design for CubeSat based on the Open System Interconnection Model (OSI framework). The

model uses a physical abstract communication layer that represents frequency, bandwidth, channel coding, and modulation, a data link abstract communication layer that represents media access control, and a network layer that represents topology and routing [26]. Small Satellite InterSatelliteLink (ISL) missions for IoT have been conducted in the past by researchers and companies. The first academic ISL mission was the SNAP-1 made in Surrey (UK) in 2002 [30], it offered a one-way UHF communication with a 9.6 kbps data rate. Notable past and future InterSatelliteLink (ISL) missions are SNAP-1, CanX-4 & 5, EDSN, Iridium Next, Diamond, S-Net, CPOD, and PROBA-3. Scientists from the University of Chile have proposed a MAC [28] protocol-like system for IoT systems with CubeSats. According to them, many of the protocols already implemented in space and ground scenarios are not suitable for an IoT CubeSat-like system but “Aloha-based protocols are good candidates for the MAC layer in nanosatellites devoted to IoT connectivity due to their simplicity of implementation and their minimum hardware requirements” [31]. Almonacid and Franck [32] investigated the possibility of a global CubeSat network to provide global coverage of IoT. They concluded that such a global CubeSat network can provide energy-efficient coverage for IoT devices and can be a platform for the development of scientific and university projects.

Google is using Imagery Space [33] to aid the navigation in Google Earth and Google Maps. They once had their One-Earth observation satellites, however they sold the satellite network to Planet Labs, a leading earth imagery space CubeSat Company [33].

5 CubeSat Research by Space Agencies

5.1 *CubeSat Research from NASA and ESA*

NASA has conducted many experiments with CubeSats [34]. It’s worth noting that it is one of the biggest institutional organizations that uses the CubeSat platform extensively for scientific experiments and academic projects [34]. It provides numerous information in CubeSat development and has participated in many academic and scientific projects. One such informational guide is the CubeSat101 [35], which provides very useful information for first time CubeSat developers. NASA also developed the Near-Earth Network CubeSat Communications which has a network of 17 ground stations and is able to provide telecommunication functionalities to CubeSats [35]. The near-earth network features specialized radios to help CubeSat missions reach high data rates; support missions transitioning to X, S, Ka, and X-band links; and ease mission planning, integration, and test scheduling processes. The near-earth network is administered by NASA Goddard space flight centre.

The European Space Agency (ESA) is increasingly utilizing small “CubeSat” nanosatellites [36]. These demonstrations of CubeSats in orbit are used to show

the miniaturized technologies of CubeSat electronics and laser-radio communications, and to support ESA Education activities. Since 2013, ESA has begun many CubeSat missions funded under the In-Orbit Demonstration part of the General Support Technology Programme. Examples of these missions are.

- QARMAN [34].
- RACE (planned 2022) [37], a planned two 6-unit CubeSat mission demonstrating autonomous rendezvous and docking maneuvers. RACE will use new miniaturized technologies including six Degree-of-Freedom micro-propulsion, compact navigation sensors, and micro-docking systems.

6 Industry 4.0

The term Industry 4.0 was invented by the German scientific community in order to advance its industrial capabilities. IoT devices are used extensively in Industry 4.0, since IoT devices are used extensively to connect objects with centralized computer systems and/or the cloud. According to the German federal government's High-Tech Strategy focussing on information and communication technology, "IoT is a key technology to make smart and improved manufacturing. In the industries, the IoT devices are used in robots and security measures, to connect things in a centralized system to control objects" [38].

IoT devices are helping to make the systems smarter in a computing system. Artificial intelligence functions and algorithms use the IoT data to train their neural networks and their AI functions with the IoT datasets. Industry 4.0 is using IoT devices to connect robots, AI, computers, and the Internet all in one system, making industries more efficient and autonomous.

An example scenario is the use of small robots with IoT devices by Rolls Royce [39].

These small robots make a swarm formation, capable of moving inside an aircraft engine to inspect it and send the data through an IoT device (possibly connected through a satellite) to a central computer system on the ground [40]. These swarm robots are released through a snake-like robot inside an aircraft engine during a flight. Then they are deployed and walk inside the engine to find malfunctions, possibly being able to repair parts of the engine and carry cameras to transmit videos back to engineers, who were miles away.

The information exchange between engineers on earth (maybe also a computer on flight) can be done through IoT devices. IoT devices can propagate this information through two possible paths: (1) directly from the aircraft to earth or (2) through a satellite network, with the latter being more practical since aircrafts fly over oceans. In this case, the IoT and telecommunication devices of the aircraft send the information to a satellite, then the satellite propagates this information to a ground station on earth or to another satellite (until the data transmits to a ground station on earth through a satellite able to send the signals to a ground station). This has to be a two-way communication in order to be more efficient.

7 Conclusions and Future Directions

CubeSat constellations and IoT have had enormous new applications in the last 5 years, driven by both the miniaturization of electronic devices, the CubeSat platform, and the new long-range IoT devices. The current stage of technology is the combination of LoRa gateways and CubeSat constellations that collect the data from the LoRa gateways and propagate the data back to the ground station and eventually to the Internet in the cloud. Mega constellations with the goal to provide a global Internet connection are under development, but there is uncertainty if these constellations will offer affordable Internet globally and cover all remote areas of the planet. In addition, these mega constellations will take a decade to be fully deployed.

CubeSats and IoT can have many new applications in remote areas of the planet and especially in the shipping industry and airline industry. In the sea, there is no 3G/4G network, there are no electric grids, and there is always a need to connect to the Internet.

There is still much research to be done from companies and universities to find more reliable long-range IoT devices that will be able to send signals directly to the CubeSats and LoRa/Sigfox receivers in the CubeSats that will be able to receive all these signals from the IoT devices in the ground. That includes more research in edge computing, where satellites must obtain the capability to process data and make complex calculations in their one. Another area for future research is to investigate how CubeSats could connect to each other and exchange data in a swarm. Satellites could also be used to detect fires or areas of high risks for fires, monitor planes, ships, and more.

References

1. Kumar S, Tiwari P, Zymbler M (2019) Internet of Things is a revolutionary approach for future technology enhancement: a review. *J Big Data* 6(1)
2. Gubbi J, Buyya R, Marusic S, Palaniswami M (2013) Internet of Things (IoT): a vision, architectural elements, and future directions. *Future Gener Comput Syst* 29(7):1645–1660
3. Al-Darraj I, Derbali M, Tsaramirsis G (2021) Tilting-rotors quadcopters: a new dynamics modelling and simulation based on the Newton-Euler Method with lead compensator control. In: 2021 8th international conference on computing for sustainable global development (INDIACom), pp 363–369. <https://doi.org/10.1109/INDIACom51348.2021.00063>
4. Al-Darraj I, Piromalis D, Kakei AA, Khan FQ, Stojmenovic M, Tsaramirsis G, Papageorgas PG (2021) Adaptive robust controller design-based RBF neural network for aerial robot arm model. *Electronics* 10:831. <https://doi.org/10.3390/electronics10070831>
5. Al-Darraj I, Derbali M, Jerbi H, Khan FQ, Jan S et al (2021) A technical framework for selection of autonomous uav navigation technologies and sensors. *Comput Mater Contin* 68(2):2771–2790
6. Villela T, Costa CA, Brandão AM, Bueno FT, Leonardi R (2019) Towards the thousandth CubeSat: a statistical overview. *Int J Aerosp Eng* 2019:1–13
7. Bisio I, Marchese M, Portomauro G (2007) Multi attribute based algorithm for reliable satellite-based sensor networks. In: *IEEE GLOBECOM 2007–2007 IEEE global telecommunications conference*

8. Tekbiyik K, Kurt GK, Yanikomeroglu H (2021) Energy-efficient RIS-assisted satellites for IoT networks. *IEEE Internet Things J*, 1
9. Stergiou C, Psannis KE, Kim B-G, Gupta B (2018) Secure integration of IoT and Cloud Computing. *Future Gener Comput Syst* 78:964–975
10. Akyildiz IF, Kak A (2019) The internet of space things/CubeSats: A ubiquitous cyber-physical system for the connected world. *Comput Netw* 150:134–149
11. Starlink.com, Oct-2021. <https://www.starlink.com/>. Accessed Oct 2021
12. Blueorigin.com. <https://www.blueorigin.com/>. Accessed 07 Oct 2021
13. OneWeb, “Homepage,” Oneweb.world. <https://www.oneweb.world/>. Accessed 07 Oct 2021
14. Iridium’s next step. Iridium museum, 2021. <https://www.iridiummuseum.com/exhibits/iridiums-next-step/>. Accessed Oct 2021
15. Planet. Planet.com. <http://www.planet.com>. Accessed 07 Oct 2021
16. Rana AK, Sharma S (2021) Industry 4.0 manufacturing based on IoT, cloud computing, and big data: manufacturing purpose scenario. In: *Lecture notes in electrical engineering*. Springer Singapore, Singapore, pp 1109–1119
17. Lambdasat. Lambdasat.com. <http://www.lambdasat.com>. Accessed 07 Oct 2021
18. Burhan M, Rehman RA, Khan B, Kim B-S (2018) IoT elements, layered architectures and security issues: a comprehensive survey. *Sensors (Basel)* 18(9)
19. Myriota. Myriota.com, 09 Feb 2019. <http://www.myriota.com>. Accessed 07 Oct 2021
20. Fleet.space. <https://www.fleet.space/galaxy>. Accessed 07 Oct 2021
21. Bor M, Vidler JE, Roedig U (2016) LoRa for the Internet of Things. In: *Proceedings of the 2016 international conference on embedded wireless systems and networks*, pp 361–366
22. Gateways. Thethingsnetwork.org. <https://www.thethingsnetwork.org/docs/gateways/>. Accessed 07 Oct 2021
23. Rast M (2002) ESA’s future plans for Earth observation from polar orbit. In: *Proceedings of IGARSS ’94-1994 IEEE international geoscience and remote sensing symposium*
24. Yoon Z, Frese W, Briess K (2019) Design and implementation of a narrow-band intersatellite network with limited onboard resources for IoT. *Sensors (Basel)* 19(19):4212
25. Dow C, Lea P (2019) *Mastering IOT: build modern IoT solutions that secure and monitor your IoT infrastructure*. Packt Publishing, Birmingham, England, p 276. ISBN 9781838645434
26. Vejlggaard B, Lauridsen M, Nguyen H, Kovacs IZ, Mogensen P, Sorensen M (2017) Coverage and capacity analysis of sigfox, LoRa, GPRS, and NB-IoT. In: *2017 IEEE 85th vehicular technology conference (VTC Spring)*
27. Puig-Suari J, Turner C, Ahlgren W (2002) Development of the standard CubeSat deployer and a CubeSat class PicoSatellite. In: *2001 IEEE aerospace conference proceedings (Cat. No.01TH8542)*
28. Akyildiz IF, Jornet JM, Niewa S (2019) A new CubeSat design with reconfigurable multi-band radios for dynamic spectrum satellite communication networks. *Ad Hoc Netw* 86:166–178
29. Toledo S et al (2014) Lightweight low-cost wildlife tracking tags using integrated transceivers. In: *2014 6th European embedded design in education and research conference (EDERC)*
30. Underwood CI, Richardson G, Savignol J (2003) In-orbit results from the SNAP-1 nanosatellite and its future potential. *Philos Trans A Math Phys Eng Sci* 361(1802):199–203
31. Ferrer T, Céspedes S, Becerra A (2019) Review and evaluation of MAC protocols for satellite IoT systems using nanosatellites. *Sensors (Basel)* 19(8):1947
32. Almonacid V, Franck L (2017) Extending the coverage of the internet of things with low-cost nanosatellite networks. *Acta Astronaut* 138:95–101
33. Planet to acquire terra Bella from Google, sign multi-year data contract. Planet.com. <https://www.planet.com/pulse/planet-to-acquire-terra-bella-from-google/>. Accessed 07 Oct 2021
34. Nieto-Peroy C, Emami MR (2019) CubeSat mission: from design to operation. *Appl Sci (Basel)* 9(15):3110
35. NASA CubeSat Launch Initiative (2017) CubeSat101 basic concepts and processes for first-time CubeSat developers
36. Chin A, Coelho R, Nugent R, Munakata R, Puig-Suari J (2008) CubeSat: the pico-satellite standard for research and education. In: *AIAA SPACE 2008 conference & exposition*

37. RACE double CubeSat mission. Esa.int. https://www.esa.int/ESA_Multimedia/Images/2019/06/RACE_double_CubeSat_mission. Accessed 07 Oct 2021
38. Kim JH (2017) A review of cyber-physical system research relevant to the emerging IT trends: Industry 4.0, IoT, big data, and cloud computing. *J Ind IntegrManag* 02(03):1750011
39. SWARM robots. Rolls-royce.com. <https://www.rolls-royce.com/media/our-stories/insights/2018/swarm-robots.aspx>. Accessed 07 Oct 2021
40. How Rolls Royce is applying AI and robotics for smart engine maintenance. Packtpub.com, 20 Jul 2018. <https://hub.packtpub.com/how-rolls-royce-is-applying-ai-and-robotics-for-smart-engine-maintenance>. Accessed 07 Oct 2021

Advancement in Electric Vehicles and Battery Technology and Their Impact on the Global and Indian Market



Anavi Malhotra, Nikhil Vivek Shrivastava , and Gauri Gangwar

Abstract The global rising greenhouse gas emission (GHG) rate and the improving technology for more efficient automobiles have given electric vehicles a significant boost and penetrative scope on international markets. With their battery technology, EVs offer an alternative to conventional IC engine vehicles. This paper has discussed battery technology advancements that have opened new channels for bringing revolutionary changes to respective EV sectors. A brief comparison of multiple battery sources for technological advancements gives us an idea of their future trends, predicting their market share values, reliability, and scope. This provides us with global market share data for the EV boost amendments. While researching reforms, government initiatives, and the highest revenue market share trends in countries, a factual representation of the values of different countries was conveyed. To keep up with the advancing trends, the Indian government has taken several steps to reform the EV sector, including implementing schemes and regulations that affect state markets to ensure future linear growth at the national level. Collaboration between the government and the private sector has also increased to promote and develop consumer awareness.

Keywords Electric vehicles · Plug-in hybrid vehicles · EV batteries · Market share · Impact on Indian market

1 Introduction

The significant advancements in Electric Vehicles (EV) in India and worldwide have given the market a confident boost. The rising greenhouse gas emission (GHG) rate worldwide contributed to the overall rise and development [1].

A. Malhotra · N. V. Shrivastava (✉) · G. Gangwar
Department of Mechatronics Engineering, Manipal University Jaipur, Jaipur, Rajasthan 303007, India
e-mail: nikhilvivek.shrivastava@jaipur.manipal.edu

An increase in transport rate emissions was observed in India due to its growing population and economic development. As a result, it is now necessary to quantify emissions at intervals to assess pollution levels and the impact of government-implemented control strategies. The stories of CO₂ emission are linked to the amount of fuel type and fuel consumed [2]. These emissions of pollutants have led to the degradation of the environment; consequently, the need to move away from fossil fuels and more towards sustainable alternatives is more important than ever.

These emissions of pollutants have led to the degradation of the environment; consequently, the need to move away from fossil fuels and more towards sustainable alternatives is more important than ever. As currently, imports fulfil 82% of India's oil demand, with the automotive sector responsible for 99.6% of total petrol consumption in India. On the other hand, diesel demand accounts for 67% 3. India imports roughly 81.7% of its crude oil, and in power consumption, it ranks third. EVs play an essential role in this shift as they work on non-convenient resources and provide a critical achiever for the goal. Adoption of electrification can help in reducing vehicular emissions. The battery technology used in electric vehicles offers a positive alternative to the growing GHG problems [3]. The technologies that can become a factor for accelerating EV adoption in India can be narrowed down to bidirectional charging, improved battery technology, production tech, infrastructure tech, and innovative technology. The current EV's capital outlay is about 1.5–3 times the Internal Combustion Engine Vehicle (ICEV). For most recent EVs, the concepts of constant weight-saving design, consistent power design, and optimum safety have been implemented to make them more lucrative [4, 5]. Gradual acceptance to EV over last few years has been found worldwide and is presented in Fig. 1 [6].

In view of the development in the battery technology, the current study aims to discuss the various types of advances in EV technology, types of EV's and tried to predict the scope and challenges to EV adaptation worldwide and in India.

2 Types of Electric Vehicles

2.1 *Electric Vehicles*

An electric vehicle, in general terms, is a vehicle that uses one or more electric motors for propulsion. They can be further understood as hybrid vehicles which require 14 different classes, speed, pressure sensors, and temperature. Their complex architectural diagram generally includes current, between 15 and 20, and thermistor temperature sensors which should be between 20 and 30. Electric vehicles are divided into sub-categories depending on their structure and technologies discussed below.

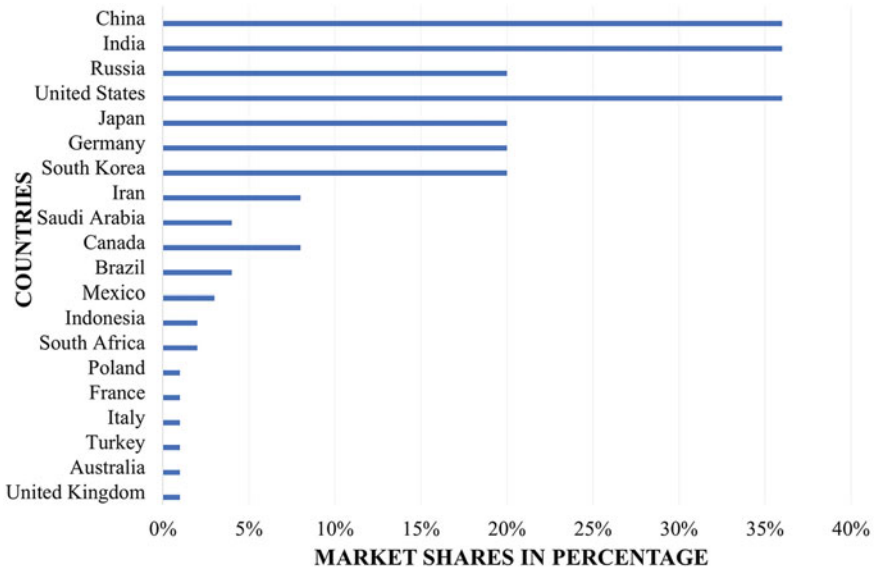


Fig. 1 Global market share of EV in percentage [6]

2.2 Battery Electric Vehicles (BEV)

Battery electric vehicles or pure electric vehicles are automobiles powered via stored electricity with no secondary means or substitute source of power. They use rechargeable high-voltage batteries, electric motors, and controllers, which help manage the power electronics. BEVs have many advantages, including simple design, convenience of operation, and a complete noise cancellation feature. The disadvantage that BEVs face is a lower range per charge. When compared to their alternatives, the ICE engine automobiles lack power density, travel per mile, and running speed [7, 8]. In 2020, the global market for electric vehicle batteries will be worth USD 21.95 billion. From 2021 to 2028, the market is expected to grow at a CAGR of 28.1% (approximately USD 27.30 billion to approximately USD 154.90 billion). BEV has been presented to use grid power to replace fuel use. Most of the electricity is generated from non-petroleum sources, the vast majority of which are domestic [9].

2.3 Hybrid Electric Vehicles (HEV)

The hybrid electric vehicle works on two types of power sources. Combining an internal combustion engine (ICE) and electric motors provides HEV with high fuel efficiency, powerful mechanism, and low emissions [10, 11]. HEV can conserve

energy from different mediums like regenerative braking systems to charge the batteries. The total hybrid vehicle market is estimated to be 4,169 thousand units in 2018 and is projected to grow at a CAGR of 8.94% from 2018 to 2025, to reach 7,593 thousand units by 2025 [12]. Presently, an HEV can operate nearly twice as efficiently as a standard internal combustion engine in India [13].

2.4 Plug-In Hybrid Electric Vehicles (PHEV)

A PHEV is an electric vehicle that is a hybrid that mainly consists of a battery pack that can be charged by connecting it to an external power source through a charging wire. It can still be accessed on an internal combustion engine-powered generator [14, 15].

In all-electric mode, PHEVs generate no tailpipe emissions. The plug-in hybrid electric vehicle would account for nearly 20–25% of the market share for electric cars in 2020. The dual functionality of PHEVs of being able to run on a charged battery, or switch to the combustion engine when the battery is depleted, provides them with the opportunity to have non-stop functioning [16].

The approximate compound annual growth rate in the above EV types is presented in Fig. 2.

3 Advancements in Battery Technologies

As the future resources are advancing and new aspects are being studied and experimented with, the change in the battery technology of the EVs is also increasing at a significant speed. New alternatives are replacing the old conventional materials for more durability and enhanced performance. A comparative study of all the technologies is given in Table 1 to understand their impacts and function better.

4 World Market Scales

Electric vehicle sales had risen in 2019 by 2.1 million globally, bringing to 7.2 million the total stock, breaking previous records. Electric vehicles accounted for 2.6% of vehicle sales worldwide in 2019, and the global car stock is around 1%, reflecting a growth year over a year of approximately 40% [19, 20]. Electric cars are gaining some traction as technology advances in powering two- and three-wheelers, buses and trucks, and the market expands. Recently, ground-breaking policy announcements have made essential advancements in encouraging EVs implementation in significant vehicle markets. Other structural measures include requirements for zero-emission

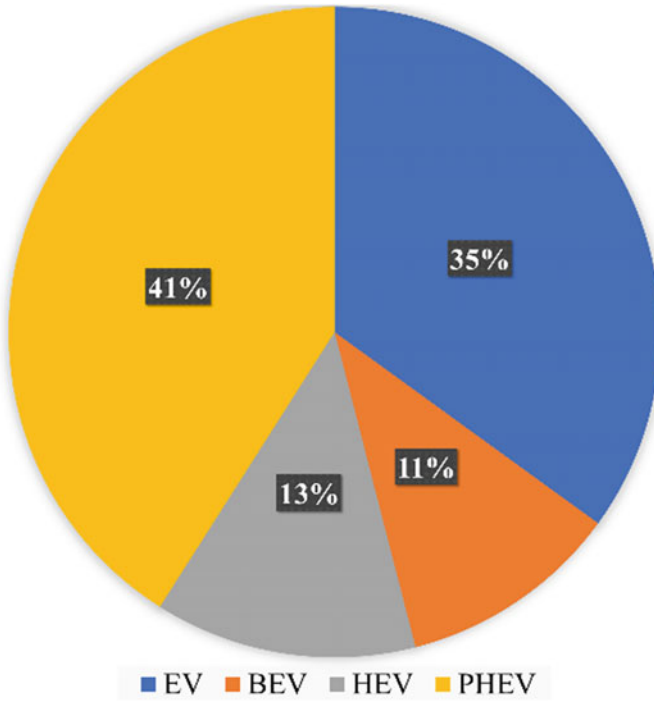


Fig. 2 Percentage of compound annual growth rate for all EVs used in India

vehicles and fuel economy standards. It implies that hybrid vehicles’ future has sent clear long-term signals to manufacturers and consumers.

In 2010, only about 17 000 electric vehicles were on the road nationally 7. The number rose to 7.2 million by 2019, with exports from China accounting for 47% of the total. More than 1,00,000 electric vehicles were on the road in 9 nations, with market shares above 1% in at least 20 countries [21]. China being on top with nearly 1.06 million electric cars sold in the year 2019, which was followed by Europe and US with around 560,000 and 326,000 electric cars sold, respectively, representing nearly 90% of total sales [22]. In Europe, Norway tends to have the highest revenue market share (56%) in 2019, followed by Iceland (23%) and the Netherlands (15%) as shown in Fig. 3 [23].

Most of all two- or three-wheelers worldwide is estimated to be 350 million. This results from the restrictions on two- or three-wheelers with internal combustion engines in many Chinese cities, which affects the world market because of China’s leading industrialization. Chinese investors have invested more than \$1.4 billion in electric vehicle and battery start-ups in the last 3 years.

In 2019, EV incentives for more than 90% of the global vehicle market in terms of revenue (covering more than 50 nations). However, significant markets like China and the United States have begun a gradual phase-out at the national level. Norway

Table 1 A comparison between the different battery technologies used by the industry

Type of battery	The working of the battery	Energy density of the battery	Lifetimes/ cycles	The market share
Lithium-ion battery	In LIB'S, positively charged lithium ions travel between the anode and the cathode in the electrolyte	LIB has a high cyclability but a low energy density	The typical estimated life of a lithium-ion battery is about 2–3 years. We are providing EV with an undisturbed 2-year maintenance span	The global lithium-ion battery market size is projected to grow from USD 41.1 billion in 2021 to USD 116.6 billion by 2030; It is expected to grow at a CAGR of 12.3% from 2021 to 2030 [17, 18]
Solid-state battery	A solid-state battery is a battery technology that uses solid electrodes and a solid electrolyte instead of the liquid or polymer gel electrolytes found in lithium-ion or lithium polymer batteries	Solid-state battery technology is believed to deliver higher energy densities (2.5x), by enabling lithium metal anodes	The solid-state battery technology could increase the lifetime of electric vehicles to that of gasoline cars up to 10–15 years	The global solid-state battery market size was valued at USD 590.9 million in 2020 and is expected to grow at a compound annual growth rate (CAGR) of 36.0% from 2021 to 2028
Aluminium-ion Battery	Aluminium-ion batteries have an aluminium anode	The energy density potential for aluminium-ion batteries is around 1060 Wh/kg in comparison to lithium-ion's 406 Wh/kg limit	An aluminium-ion battery can operate over 10,000 cycles	The aluminium-ion battery market is expected to show a healthy growth between 5.2 and 6.8% during the forecast period of 2021–2028. Demand for aluminium-ion battery due to its advantages is expected to show much higher rise with respect to its competitors in upcoming years

(continued)

Table 1 (continued)

Type of battery	The working of the battery	Energy density of the battery	Lifetimes/ cycles	The market share
Lithium-sulphur battery	Lithium-sulphur batteries (LiS) typically have a lithium anode and a sulphur-carbon cathode	They have low cyclability, caused by expansion and harmful reactions with the electrolyte, they also have a high energy density of 2600 Wh/kg	The lifespan of lithium-sulphur button cells can be up to 1,400 cycles	The global lithium-sulphur battery market is forecasted to grow at a CAGR of 71.06% during the period 2018–2022
Metal-air battery	Metal-air batteries have a pure-metal anode and an ambient air cathode	Mechanically rechargeable zinc (Zn)-, magnesium (Mg)-, and aluminium (Al)-, air batteries have a greater power storage capacity and higher energy density	When not in use, they degrade quickly, as corrosion eats away at their metal electrodes. Their lifetime varies from metal-to-metal present in the composition	The global metal-air battery market size is predicted to \$1,123,100.00 Click or tap here to enter text

continues to lead globally, accounting for 75% of all plug-in electric vehicles, with Iceland, Sweden, and Finland finishing in the top five. Norway has made a significant breakthrough in the field of battery electric vehicles. In March 2019, 76% of all automobile sales in Oslo consisted of electric cars. Along with this, the world’s largest plug-in hybrid ferry with a capacity of 2,000 passengers is bound to start its operations from Norway to Sweden [24]. Germany is also listed as the top European plug-in market, with multiple reforms and technological advancements happening within the country. In the transportation sector, the US has been at the forefront of promoting electrification and sustainable sources. Following China and Europe, the US had more than 570,000 plug-in electric vehicles in December 2016, making it the third-largest market for EV [25].

5 National EV Front

The COVID-19 pandemic has affected businesses of all sizes across all industries globally and nationally. Local businesses were compromised, and the bigger industries shifted their outlook to minimize the effects of the shifting global dynamics. The

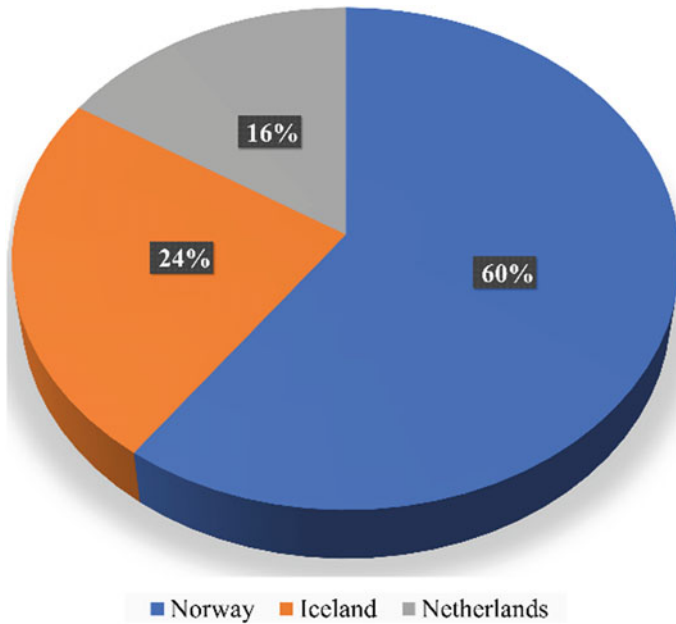


Fig. 3 Approximate market share of EV in Norway, Iceland, and Netherlands

Indian automotive sector experienced some reforms and ease of restrictions in the electric vehicle sector to help and support the nation-wide growth of EVs as a measure to the prevailing state. There has been a growth in the demand for EVs in India, especially in the sector of two-wheelers and three-wheelers. This was observed due to the want of permanent clean resources which were available at affordable amenities. As shown in Fig. 4, the growth and sales are not linear throughout the country and vary from state to state due to the state of maturity of the market, which is influenced by several factors.

To help the markets grow after the pandemic, government has launched multiple initiatives such as the National Electric Mobility Mission Plan (NEMMP) and Faster Adoption and Manufacturing of (Hybrid &) Electric Vehicles in India (FAME1). The Government has also provided tax exemptions and subsidies to EV manufacturers and consumers. The recent hike in fuel prices because of disrupted supply chains due to lockdowns has also increased the popularity of the EVs, as electric scooters and motorbikes are already at par with ICE vehicles in terms of upfront cost [26] and the EV market share may rise to almost 50% till 2026 as shown in Fig. 5.

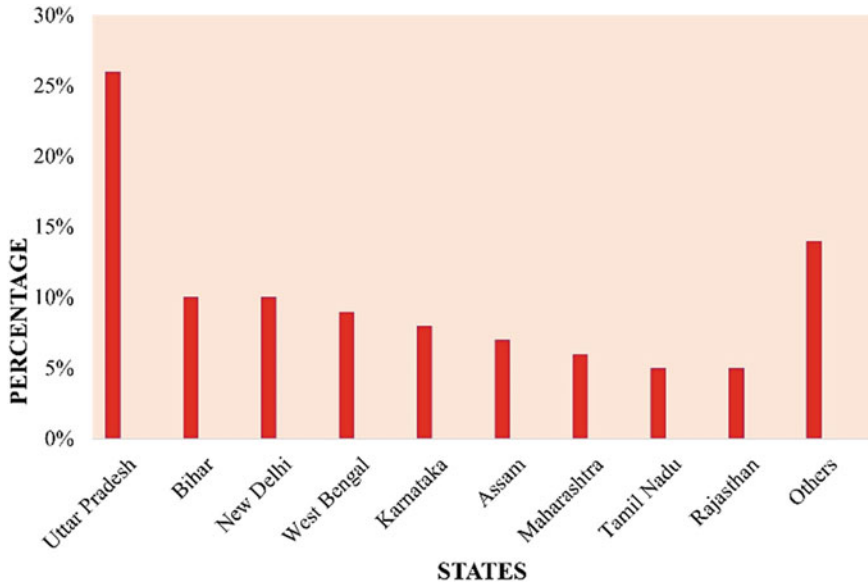


Fig. 4 Regional registered EV in India (2020)

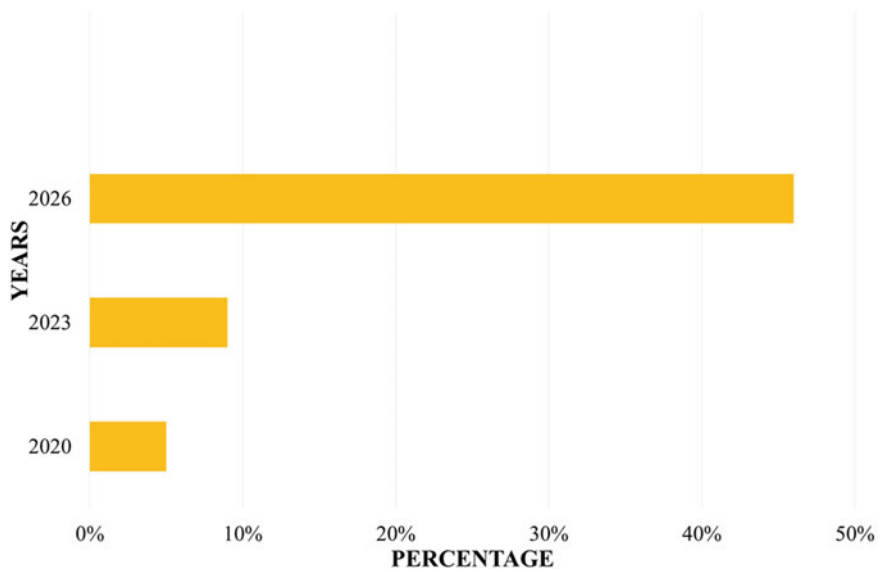


Fig. 5 Prediction of market share of EV till 2026

6 The Government Initiative

The Indian Government took the initiative and established the National Mission for Electric Mobility (NMEM2020). According to the National Mission for Electric Mobility, it has two vital purposes that are interconnected (NMEM):

1. Energy security at the national level.
2. Increased manufacturing capability for the entire range of electric car technology.

In January 2012, the Ministry of Heavy Industries announced its ambitious proposed action plan for Electric Mobility, with an objective of six to seven million vehicles on the road by 2020. To enable XEVs (all sorts of electric vehicles) that are dependable, cost-effective and efficient to meet consumer expectations [27].

Collaboration between the Government and private sector has become more frequent to encourage and develop naturally occurring consumer awareness, manufacturing capabilities, infrastructure and technology. This industrial collaboration will assist India in becoming a global leader in the XEV two-wheeler and four-wheeler market almost by 2020, with total XEV sales of 6–7 million units, enabling the Indian automotive industry to accomplish global XEV manufacturing leadership and bringing about the national fuel security with a target of 400,000 passenger battery electric cars (BEVs) by 2020, rescuing 120 million barrels of oil and four metric tonnes of CO₂ [28].

The Indian Government authorized the National Mission on Electric Mobility in 2011 to speed the manufacturing process and introduce a full range of electric vehicles. In 2013, the Government devised an EV strategy. The National Electric Mobility Mission Plan (NEMMP) 2020 was launched to establish the EV and Hybrid Vehicle (HV) markets while ensuring national fuel security. With an expenditure of INR 8.95 billion in 2015, the Government implemented the Faster Methods of Hybrid and Electric Vehicle Adoption and Manufacturing Act, including subsidies for hybrid buses and electric two- and three-wheelers and electric vehicles. With an expenditure of INR 100 billion, the scaled-up of Faster Methods of Adoption and Manufacturing of Hybrid and EV methods went into effect in April 2019. These methods can be used to support the purchasing of electric vehicles which may cost approximately around INR 85.96 billion and charging infrastructure development costing approximately INR 10 billion [28].

7 Conclusion

This study investigated the technological developments in electric vehicles and batteries for electric vehicles. In the case of EVs, batteries are crucial because they determine the vehicle's autonomy. We have compared various types of batteries based on cycle life, performance, charging and discharging time and their market share and found that there is great scope for research and development of future technologies

which are expected to be a solution that allows for the storage of greater amounts of power and charging in shorter periods of time. The EV could benefit from this type of technology as well, reaching higher ranges, which could aid in its adoption by drivers and users.

Further we have tried to see the global acceptability and impact of EV on Indian market. It can be concluded that since the manufacturing of electric cars is becoming increasingly common, and its market share is likely to increase appreciably. By 2022, India's GDP is expected to expand by 9%. We have conveyed the international and national standing of the EV sector amidst the pandemic and Industrial 4.0 reforms. A clear prediction has been established for an analyst to understand the improving automation of electric vehicles.

References

1. Hacker F, Harthan R, Matthes F, Zimmer W (2009) Environmental impacts and impacts on the electricity market of a large-scale introduction of electric cars in Europe-critical review of literature. In: ETCACC Technical paper, vol 4, pp 56–90
2. Khan M, Kar NC (2009) Hybrid electric vehicles for sustainable transportation: a Canadian perspective. *World Electr Veh J* 3(3):551–562
3. Omer AM (2008) Energy, environment and sustainable development. *Renew Sustain Energy Rev* 12(9):2265–2300
4. Ramalingam K, Indulkar CS (2015) Overview of plug-in electric vehicle technologies. In: Rajakaruna S, Shahniah F, Ghosh A (eds) *Plug in electric vehicles in smart grids: integration techniques*. Springer, Singapore, pp 1–32
5. Niu S, Xu H, Sun Z, Shao ZY, Jian L (2019) The state-of-the-arts of wireless electric vehicle charging via magnetic resonance: principles, standards and core technologies. *Renew Sustain Energy Rev* 114:109302
6. Bunsen T, Cazzola P, Gorner M, Paoli L, Scheffer S, Schuitmaker R, Tattini J, Teter J (2018) *Global EV outlook 2018: towards cross-modal electrification*, p 141
7. Wu D, Ren J, Davies H, Shang J, Haas O (2019) Intelligent hydrogen fuel cell range extender for battery electric vehicles
8. Tie SF, Tan CW (2013) A review of energy sources and energy management system in electric vehicles. *Renew Sustain Energy Rev* 20:82–102
9. Pillot C (2013) Micro hybrid, HEV, P-HEV and EV market 2012–2025 impact on the battery business. In: *World electric vehicle symposium and exhibition (EVS27)*, pp 1–6
10. Sabri M, Danapalasingam KA, Rahmat MF (2016) A review on hybrid electric vehicles architecture and energy management strategies. *Renew Sustain Energy Rev* 53:1433–1442
11. Harshavarthini S, Divya M, Bongarla R, Priya CH, Balaji R (2021) A critical investigation on regenerative braking energy recovering system on HEV based on electric and natural extracted fuel
12. Hemanth G, Suresha B (2021) Hybrid and electric vehicle tribology: a review. *Surf Topogr Metrol Prop* 9(4):043001
13. Wirasingha SG, Schofield N, Emadi A (2008) Plug-in hybrid electric vehicle developments in the US: trends, barriers, and economic feasibility. In: *Vehicle power and propulsion conference*, pp 1–8
14. Kontou E, Yin Y, Ge YE (2017) Cost-effective and ecofriendly plug-in hybrid electric vehicle charging management. *Res Rec* 2628(1):87–98
15. Emadi A, Lee YJ, Rajashekara K (2008) Power electronics and motor drives in electric, hybrid electric, and plug-in hybrid electric vehicles. *IEEE Trans Ind Electron* 55(6):2237–2245

16. Redelbach M, Özdemir ED, Friedrich HE (2014) Optimizing battery sizes of plug-in hybrid and extended range electric vehicles for different user types. *Energy Policy* 73:158–168
17. Raj T et al (2022) Recycling of cathode material from spent lithium-ion batteries: challenges and future perspectives. *J Hazard Mater* 429:128312
18. Neiri N, Kim N, Cho N (2021) Spent graphite from end-of-life lithium-ion batteries (LIBs) as a promising nanoadditive to boost road pavement performance
19. Muneer T, Kolhe M, Doyle A (2017) Electric vehicles: prospects and challenges
20. Aichberger C, Jungmeier G (2020) Environmental life cycle impacts of automotive batteries based on a literature review
21. Xue C, Zhou H, Wu Q, Wu X, Xu X (2021) Impact of incentive policies and other socio-economic factors on electric vehicle market share: a panel data analysis from the 20 countries
22. Hamdi-Cherif M, Li J, Broin EÓ (2021) Leveraging the transport sector to mitigate long-term climate policy costs in China: a behavioural perspective. *Clim Policy* 21(4):475–491
23. Testa G (2017) A comparative, simulation supported study on the diffusion of battery electric vehicles in Norway and Sweden
24. Ajanovic A, Haas R, Schrödl M (2021) On the historical development and future prospects of various types of electric mobility
25. Altenburg T, Bhasin S, Fischer D (2021) Sustainability-oriented innovation in the automobile industry: advancing electromobility in China, France, Germany and India. *Innov Dev* 2(1):67–85
26. Chewprecha U, Prabhu VS, Mukhopadhyay K (2021) Regional impact of automobile policy in India. In: *Economy-wide assessment of regional policies in India*. Palgrave Macmillan, Cham, pp 193–234
27. Brown S, Pyke D, Steenhof P (2010) Electric vehicles: the role and importance of standards in an emerging market. *Energy Policy* 38(7):3797–3806
28. Bhagwat P, Hadush SY, Bhagwat S (2019) Charging up India's electric vehicles: infrastructure deployment and power system integration

Quaternary Multiplier with Modified Carry Using Carbon Nanotube FETs



G. V. S. Ajay and Sarada Musala 

Abstract The paper proposes the use of carbon nanotube FET (CNTFET) to implement a quaternary multiplier with modified carry. To begin with, CNTFET will be used to design the Quaternary multiplier circuit. A quaternary 4:1 multiplexer is used. The designs are simulated using cadence Spectre software with the technology of CNTFET 32 nm. The existing Quaternary multiplier faces a problem in carrying output which is eliminated in the proposed Quaternary multiplier.

Keywords Multi-valued logic (MVL) · CNTFET · Quaternary logic · Quaternary multiplexer

1 Introduction

Technology and science have improved our ability to process information, speed up processing, and store information. As compact integrated circuits have been developed, energy consumption has decreased and system performance has improved. Researchers have successfully adapted nanoscale technologies for solving problems such as leakage currents, higher power consumption, and short channel effects since the development of CMOS transistors. CNTFETs have higher performance speeds due to their high carrier mobility, lower latency, lower power consumption, and small intrinsic capacitors [1]. Multi-value logic and transistors significantly reduce the volume of circuits [2]. MVL circuits overcome the drawbacks of binary circuits such as a large number of connections and high power consumption. Therefore, mathematical functions can be executed more quickly and a greater number of computations can be performed. Multi-valued logic and CNTFETs have been utilized in a variety of circuit designs.

G. V. S. Ajay · S. Musala (✉)

Vignan's Foundation for Science Technology and Research, Vadlamudi, Andhra Pradesh 522213, India

e-mail: sarada.marasu@gmail.com

2 Carbon Nanotube Field Effect Transistors

A CNT is a one-atom-thick graphene tube that has been transformed into a pipe. The rotational axis of the nanotube plates determines whether they are conductive or semi-conductive [3, 4]. As a result of the chirality vector $C = ma_1 + na_2$ for graphite a_1 and a_2 , the CNT is composed of tubular graphite plates, and its chirality (m, n) determines the twisting of the CNT. The metal conductivity is determined by the product of m and n which is a multiple of 3 or both of them being equal. In all other cases, it will exhibit a semi-conductive property. CNTFETs are characterized by a large variation in threshold voltage that is based on carbon tube diameter.

$$V_{th} \cong \frac{Ebg}{2e} = \frac{\sqrt{3}aV\pi}{3eDCNT} \cong \frac{0.436}{DCNT(\text{nm})}$$

where carbon-carbon atom's distance is represented with "a" and $a = 2.49 \text{ \AA}$, $V\pi = 3.033 \text{ eV}$ is the bond strength of carbon π - π bond present between two C (carbon) atoms, DCNT is the diameter of a CNT, and e represents the electron unit charge.

3 Quaternary Inverters

In quaternary logic functions, four values are indicated with the digits 0,1,2, and 3 which correspond to voltage levels 0, 1/3 VDD, 2/3 VDD, and VDD, respectively [5, 6]. In this paper, we used three quaternary inverters to design the multiplier, namely, positive, negative, and intermediate quaternary inverters (PQI, NQI, and IQI) which are widely used to build the quaternary circuits. The difference between the three quaternary inverters is that they differ in the chirality values applied to the PCNFET and NCNFET which produces different outputs for all the three inverters. These inverter's truth table is shown in Table 1 [7] (Figs. 1, 2, and 3).

The circuit diagrams of these inverters are shown below:

In this section, we will discuss the existing quaternary multiplier. The authors had proposed a quaternary multiplier using a 4:1 multiplexer which has 24 transistors. Table 2 shows the quaternary multiplier's truth table [7].

Table 1 Quaternary inverter's truth table

Input	Out		
	NQI	IQI	PQI
0	3	3	3
1	0	3	3
2	0	0	3
3	0	0	0

Fig.1 NQI circuit

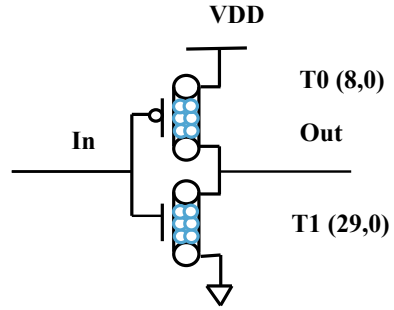


Fig. 2 IQI circuit

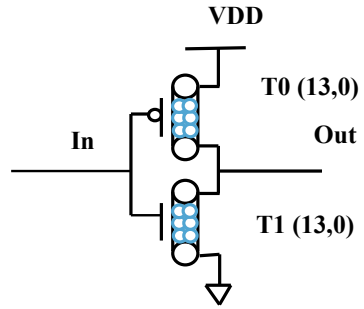
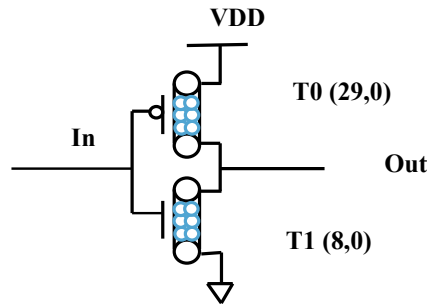


Fig. 3 PQI circuit



4 Existing Quaternary Multiplier

The NQI, IQI, and PQI functions of signal A are represented with the symbols A_N , A_I , and A_P . An output signal is selected based on the selection signal. The product block (Fig. 4a) and carry block (Fig. 5a) form the circuit diagram of a quaternary multiplier [7]. To implement an array quaternary multiplier, quaternary adders should be used to realize it.

For $B = 0/1/2/3$, the data signals $D1/D2/D3/D4$ will be transmitted, respectively, to the output. Figure 4b shows the circuit diagram for the existing 4:1 multiplexer [7]. From Table 2, we can observe that when $B = 0$, both the outputs will be 0 irrespective

Table 2 Truth table of quaternary multiplier

A	Product					Carry			
B	0	1	2	3		0	1	2	3
0	0	0	0	0	0	0	0	0	0
1	0	1	2	3	A	0	0	0	0
2	0	2	0	2	AR	0	0	1	1
3	0	3	2	1	$\overline{A^3}$	0	0	1	2

of A. When $B = 1$, product = 1, carry = 0 for $A = 0/1/2/3$. For $B = 2$, product = 0/2/0/2 and carry = 0/0/1/1 when $A = 0/1/2/3$. For $B = 3$, product = 0/3/2/1 and carry = 0/0/1/2 when $A = 0/1/2/3$.

Proposed Quaternary Multiplier

A problem has been detected in the existing carry circuit (Fig. 5). For $A = 3$ and $B = 2$, the carry output should be logic “1”, but all the PCNFETs present in the circuit are switched on resulting in logic “2” [7]. This problem has been rectified by adding one more PCNFET with B_P as a signal applied to the gate of the PCNFET [8–20]. The modified carry schematic diagram is shown in Fig. 6. This modified carry produces a result of logic “1” for the combination $A = 3$ and $B = 2$.

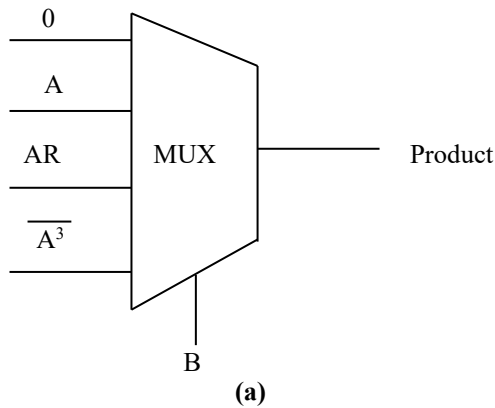


Fig. 4 a Product block of quaternary multiplier [7]. **b** Circuit diagram of 4:1 quaternary multiplexer

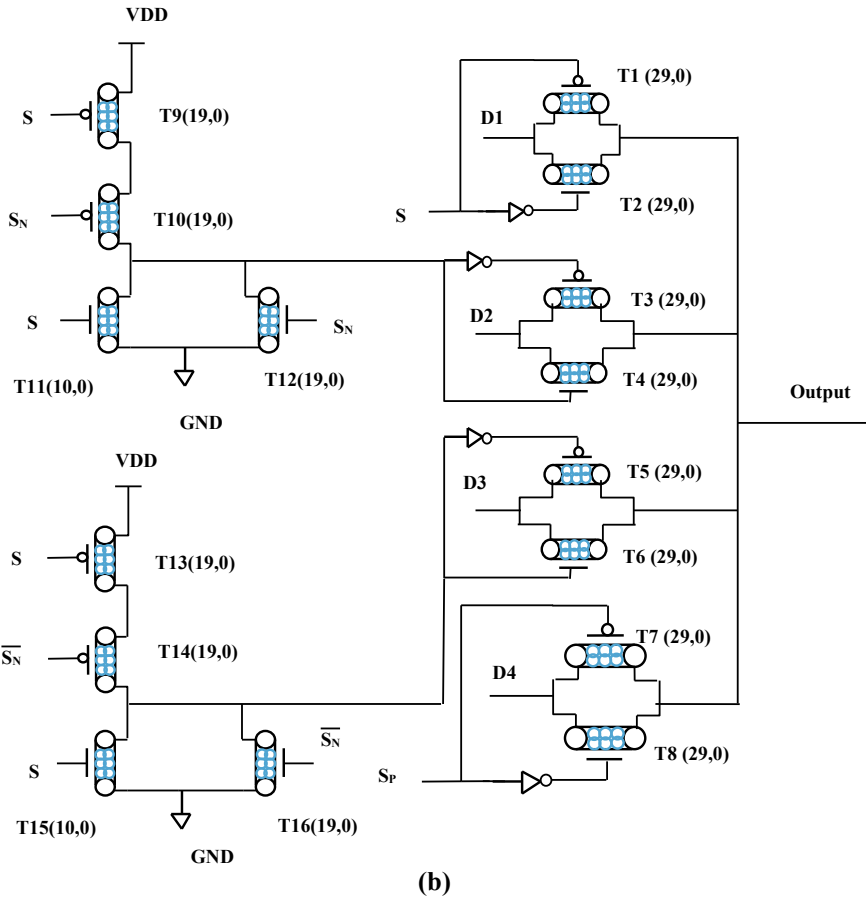


Fig. 4 (continued)

5 Simulation Results

With 32-nm CNTFET technology, Cadence Spectre software is used for simulation. CNTFET models are taken from Stanford University nano-Hub. The transient results are shown in Figs. 7 and 8 at 0.9 V supply voltage. As shown in Fig. 7, an existing quaternary multiplier exhibits a transient response, where we can observe that for the combination “ $A = 3$ and $B = 2$ ” the carry output is logic 2, but it should be logic 1 as per the truth table of the quaternary multiplier. Figure 8 is the simulation result of the quaternary multiplier with a modified carry block. It is evident that for the input combination “ $A = 3$ and $B = 2$ ” the carry output is logic 1 which is the same as the theoretical output. The problem with the existing quaternary multiplier is shown in Fig. 7 and was eliminated in Fig. 8. The power, delay, and PDP values of existing and

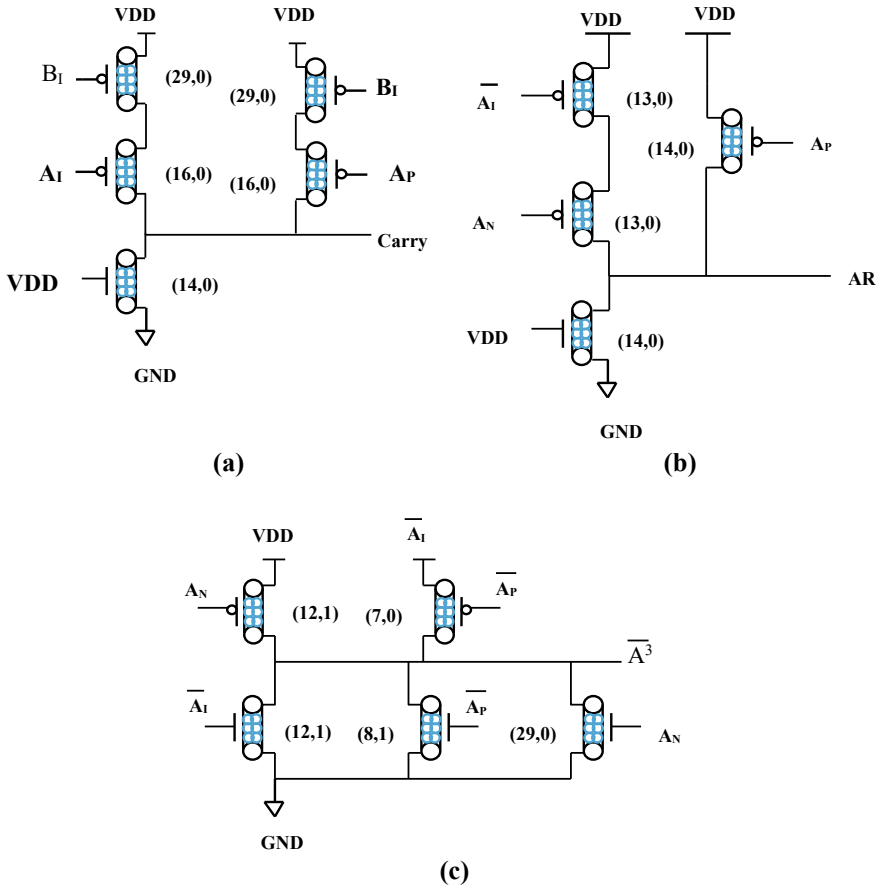


Fig. 5 a Circuit diagram for carry block of quaternary multiplier[7]. b Circuit diagram for AR block of quaternary multiplier[7]. c Circuit diagram for A^3 block of quaternary multiplier[7]

proposed quaternary multiplier circuits at different voltages are shown in Table 3. From Table 3, it can be said that the proposed quaternary multiplier is having less power and PDP.

Fig. 6 Circuit diagram of modified carry block

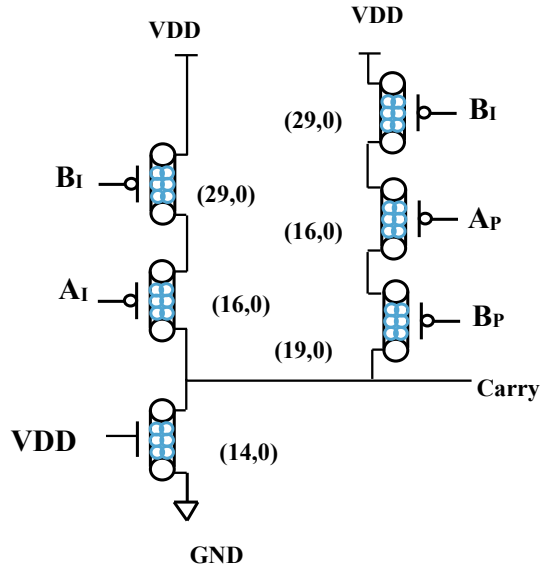


Fig. 7 Transient response of existing quaternary multiplier [7]

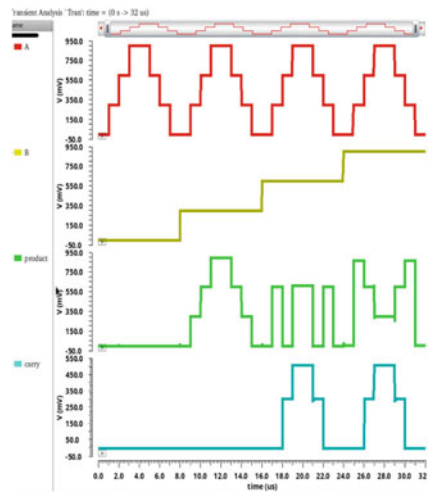


Fig. 8 Proposed quaternary multiplier's transient response

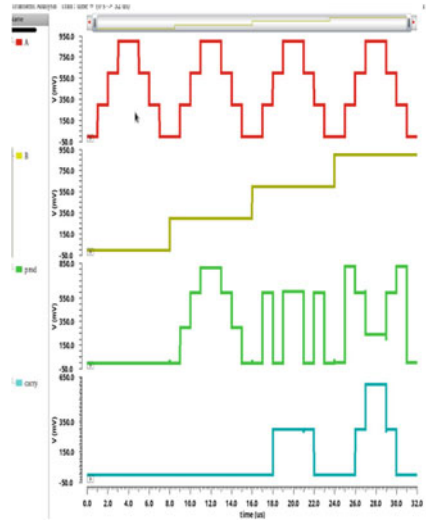


Table 3 Power, delay, and PDP of quaternary multipliers

Circuit	VDD	Power (μ W)	Delay (ns)	PDP (fJ)
Existing multiplier [7]	0.7	2.363	2.044	4.829
Proposed multiplier		2.329	2.038	4.746
Existing multiplier [7]	0.8	4.001	2.019	8.078
Proposed multiplier		3.91	2.019	7.894
Existing multiplier [7]	0.9	6.178	2.015	12.448
Proposed multiplier		6.015	2.014	12.11
Existing multiplier [7]	1.0	9.255	2.012	18.621
Proposed multiplier		9.011	2.012	18.13
Existing multiplier [7]	1.1	13.48	2.012	27.243
Proposed multiplier		13.15	2.010	26.43
Existing multiplier [7]	1.2	18.83	2.010	37.848
Proposed multiplier		18.38	2.010	36.94

6 Conclusion

In this study, a new carry block is modified by making use of CNTFET. The problem in the existing carry block in [7] is rectified by adding another PCNFET in the modified carry block. The simulation results indicate that the modified quaternary multiplier has lower power and PDP at different operating conditions. The proposed quaternary multiplier uses 54 transistors.

References

1. Sinha S, Chaudhury S (2014) Advantage of CNTFET characteristics over MOSFET to reduce leakage power. In: Proceedings of the IEEE international Caracas conference on devices, circuits and systems. <https://doi.org/10.1109/ICDCSyst.2014.6926211>
2. Moore GE (2006) Cramming more components onto integrated circuits. Reprinted from electronics, volume 38, number 8, April 19, 1965, pp 114 ff. In: IEEE solid-state circuits society newsletter, vol 11, no 3. pp 33–35, <https://doi.org/10.1109/N-SSC.2006.4785860>
3. Iijima S (1991) Helical microtubules of graphitic carbon. *Nature* 354.6348:56–58
4. Javey A, Guo J, Wang Q, Lundstrom M, Dai H (2003) Ballistic carbon nanotube field-effect transistors. *Nature* 424(6949):654–657
5. Dubrova E (1999) Multiple-valued logic in VLSI: challenges and opportunities. In: Proceedings of NORCHIP'99
6. Gupte AN, Goel AK (1991) Study of quaternary logic versus binary logic. In: Proceedings first great lakes symposium on VLSI. pp 336–337. <https://doi.org/10.1109/GLSV.1991.143992>
7. Rahmati S, Farshidi E, Ganji J (2021) Low energy and area efficient quaternary multiplier with carbon nanotube field effect transistors. *ETRI J.* 43. <https://doi.org/10.4218/etrij.2020-0045>
8. Musala S, Vasavi PD (2022) A novel quaternary multiplexer using CNTFET. In: 2022 6th international conference on devices, circuits and systems (ICDCS). pp 196–199, <https://doi.org/10.1109/ICDCS54290.2022.9780772>
9. Roosta E, Hosseini S (2019) A novel multiplexer-based quaternary full adder in nanoelectronics. *Circuits, Syst, Signal Process* 38. <https://doi.org/10.1007/s00034-019-01039-8>
10. Gadgil S, Vudadha C (2020) Design of CNTFET-based ternary ALU using 2:1 multiplexer based approach. *IEEE Trans Nanotechnol* 19:661–671. <https://doi.org/10.1109/TNANO.2020.3018867>
11. Moaiyeri MH, Navi K, Hashemipour O (2012) Design and evaluation of CNFET-based quaternary circuits. *Circuits Syst Signal Process* 31:1631–1652. <https://doi.org/10.1007/s00034-012-9413-2>
12. Sharifi F, Moaiyeri MH, Keivan N. A Novel quaternary full adder cell based on nanotechnology. *Int J Mod Educ Comp Sci* 7(3)
13. Vudadha C, Surya A, Agrawal S, Srinivas MB (2018) Synthesis of ternary logic circuits using 2:1 multiplexers. In: IEEE transactions on circuits and systems I: regular papers, vol 65, no 12. pp 4313–4325, <https://doi.org/10.1109/TCSI.2018.2838258>
14. Patel V, Gurumurthy KS (2011) Design of high performance quaternary adders, In: 2011 41st IEEE international symposium on multiple-valued logic, pp 22–26, <https://doi.org/10.1109/ISMVL.2011.65>
15. Patel P, Doddapaneni N, Gadgil S, Vudadha C (2019) Design of area optimised, energy efficient quaternary circuits using CNTFETs. In: IEEE international symposium on smart electronic systems (iSES) (formerly iNiS)
16. Bodapati S, Krishnamurthy S (2016) Carbon nanotube FET-based low-delay and low-power multidigit adder designs. *IET Circuits Devices Syst* 11.<https://doi.org/10.1049/iet-cds.2016.0013>
17. Das D, Banerjee A, Prasad V (2018) Design of ternary logic circuits using CNTFET. In: 2018 international symposium on devices, circuits and systems (ISDCS), pp 1–6. <https://doi.org/10.1109/ISDCS.2018.8379661>
18. Stepchenkov YA, Diachenko YG, Rogdestvenski YV, Diachenko DY, Shikunov YI (2020) Self-timed multiply-add-subtract unit alternates. In: IEEE conference of Russian young researchers in electrical and electronic engineering (EIconRus)
19. Haixia W, Shunan Z, Zhentao S, Xiaonan Q, Yueyang C (2011) Design of low-power quaternary flip-flop based on dynamic source-coupled logic. In: 2011 international conference on electronics, communications and control (ICECC). pp 826–828, <https://doi.org/10.1109/ICECC.2011.6066389>

20. Temel T, Morgul A (2002) Multi-valued logic function implementation with novel current-mode logic gates. In: 2002 IEEE international symposium on circuits and systems. Proceedings (cat. no. 02CH37353), pp I-I. <https://doi.org/10.1109/ISCAS.2002.1009982>

Design and Verification of 3D Network-on-Chip Router



Gurleen Kaur and Deepika Bansal 

Abstract Devices with rapid speed, low power, and minimal space usage are necessary for modern life. An increase in the amount of data transfer from one IP block to another existing on the same chip reduces the operating frequency of the system-on-chip device due to an increase in the number of IP blocks. Network-on-chip router can operate at a higher speed and consume less area, which is a viable solution to the stated problem. Furthermore, the performance of the network on chip router can be significantly improved by adding 3D IC technology, which improves network throughput and provides minimal latency. The 3D NOC router has been designed by reversible logic to prevent loss of information and to reduce heat dissipation, gate counts, and garbage outputs. In the paper, 3D NOC router has been designed and verified using Verilog HDL. An improved reversible logic-based 3D NOC router has been simulated and synthesized. The results indicate low latency, high performance, and improved frequency design.

Keywords 3D NoC router · Verilog HDL · Simulation · Synthesis · Verification · Reversible logic

1 Introduction

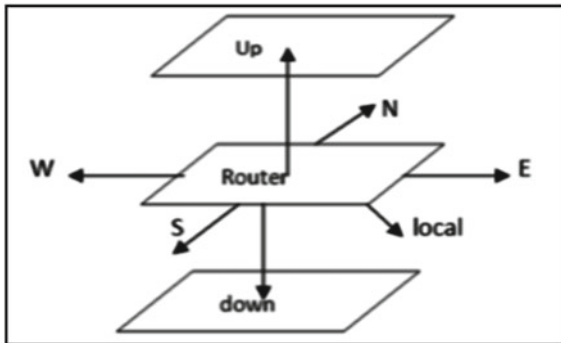
Technology used in portable devices like cameras, smartphones, and other gadgets is known as system on chip (SoC). With a wide range of applications and benefits, SoC has become a crucial component of the electronics industry [1]. With the increase in the complexity of SoC, more and more circuits are needed on a single chip to increase the functionality of a device, which results in a decrease in the operating frequency. Further, damage to a single transistor might require replacement in an entire system as, due to congestion, a single device cannot be replaced [2].

G. Kaur · D. Bansal (✉)

Department of Electronics & Communication Engineering, Manipal University Jaipur, Jaipur, Rajasthan 303007, India

e-mail: deepika.bansal386@gmail.com

Fig. 1 Representation of 3D NoC router



The network is established inside the chip in the NOC rather than connecting all IP blocks, thereby resolving the wire routing congestion problem [3]. The topology of the NoC architecture has a significant impact on both the cost and the performance of the entire network. The NOC architecture’s topology determines the physical arrangement and connections between nodes and channels, so it has a big impact on latency and power usage [4].

The NoC router contains five input and five output ports to enable communication in local, east, west, north, and south directions, in addition to a control unit to send data to the specified port as displayed in Fig. 1. The 3D NoC router adds two ports to the 2D NoC router, allowing communication in both top and down directions [4].

Layers of 2D NoC routers are stacked on top of one another to create a 3D NoC router physically. Though the 3D NoC router increases network throughput and provides minimal latency [5], it also increases area and power dissipation as compared to the 2D NoC router.

Reversible logic reduces heat dissipation, gate counts, and garbage outputs along with preventing loss of information. Reversible logic is one of the techniques used in the EDA industry for the same purpose. For these reasons, 3D NoC routers can improve by adding reversible logic. Reversible logic gates have a one-to-one mapping between inputs and outputs. Some of the key reversible gates used in reversible logic synthesis are Feynman, Fredkin, Toffoli, and Peres gates [6]. Feynman and Fredkin are used in this work, and the block diagram of both gates is shown in Figs. 2 and 3. The truth table of Feynman and Fredkin gates is tabulated in Tables 1 and 2. The Feynman gate is also referred to as the Controlled-Not (CNOT) or copying gate. The Fredkin gate, invented by Edward Fredkin, is referred to as the CSWAP gate, and it is a universal gate.

Fig. 2 Feynman gate

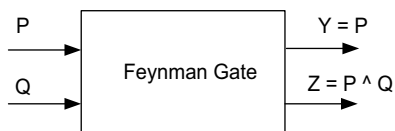


Fig. 3 Fredkin gate

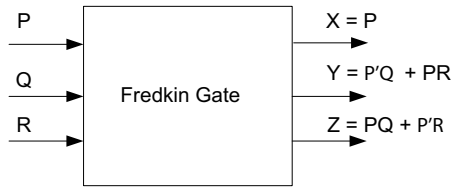


Table 1 Truth table of Feynman gate

P	Q	Y	Z
0	0	0	0
0	1	0	1
1	0	1	1
1	1	1	0

Table 2 Truth table of Fredkin gate

P	Q	R	X	Y	A
0	0	0	0	0	0
0	0	1	0	0	1
0	1	0	0	1	0
0	1	1	0	1	1
1	0	0	1	0	0
1	0	1	1	1	0
1	1	0	1	0	1
1	1	1	1	1	1

2 3D NoC Router Architecture

In a 3D NoC router, data entering from any of the ports will go directly to the control unit, where data will be inserted as an input to all seven multiplexers. The port selects and reset signal of first in first out (FIFO) will be supplied by the user, which acts as an input to the de-multiplexer (de-mux) controller. The de-mux controller will supply a request signal (req) based on the port select and reset signal values, which will be set. If the req signal is set to high, then any one of the valid ports will be selected and the reset signal will be low. Port select will also be connected to seven multiplexers, and based on the value of port select, data for a particular input port will be sent out from the multiplexers. The multiplexer output will be input to the D flipflops.

The req signal (output of the de-mux controller) is connected to the input of the de-multiplexer. Based on the value of port select, req signal will act as an enable for any one of the D flipflops. The output of the D flipflops along with their enable value

will go to their respective FIFO. The enable of the D flipflop will act as req signal for FIFO. Reset and req signals will serve as inputs to the up-counter.

The value of the read pointer is decided by reset, req, and empty logic. The decision logic will generate empty and full signals based on read pointer and write pointer. Then, req, reset, full, and data_in signals will serve as inputs to the SISO shift register. Write pointer and data_out signals will be received from SISO. Data_out, full, and empty signals will be the outputs of each FIFO. In this way, data gets transferred from input to output port in 3D NoC router. Architecture of 3D NoC router consists of three main modules, namely.

A. Top Module

A 3D NoC router can transfer data from seven input ports to seven output ports, namely, local, east, west, north, south, top, and bottom. The top module of the 3D NoC router is designed using structural modeling of Verilog HDL [7, 8]. The top module consists of seven FIFO for seven directions. A control unit is also used in top module to grant requests and transfer data to the specified output port. Various signals present in the top module consist of

- An input signal with a set time and frequency is known as a clock signal.
- Reset signal is another input signal. As a router reset, all data_out ports should be given the number 0.
- Seven data_in and seven data_out signals are used to receive and send the data at a specified location.
- The active high reset signals of all seven FIFO are input. Data can be requested only when reset is low. This helps in ensuring that at a time, only one data (3 bits) is being sent to a particular FIFO, i.e., till the time the current data (3 bits) gets written, no other data can be sent to that FIFO.
- Empty and full signals of seven FIFO are output signals, which are used to determine the status of each FIFO, whether the respective FIFO is empty or full.
- Port select is a 3-bit input signal used to select the port where the data needs to be transferred. Address of the ports is specified below (Table 3):

B. Control Unit

The control unit consists of seven multiplexers, seven D flipflops, one de-multiplexer, and one de-mux controller [1]. The control unit module is also designed using Verilog

Table 3 Output port addresses

Output port	Address
Local	000
East	001
West	010
North	011
South	100
Top	101
Bottom	110

structural modeling. The functionality of the control unit is to send data to the proper port by enabling only one D flipflop at a time and to ensure that one data packet (3 bits) is ever transferred to a given FIFO. Various signals are used in the control unit, such as reset, clock, reset all FIFO, data inputs, data outputs, port select, and enable. Enable signals are control unit outputs that are fed into D flipflops.

C. Fifo

Data synchronization is done using the principle of first in first out. Data loss must be avoided, if the source device's data writing frequency is higher than the destination device's data reading frequency. In this case, FIFO is utilized. The amount of data that must be stored should match the depth of the FIFO.

In this work, FIFO is made up of serial-in serial-out shift register, decision logic, and an up-counter [1]. Data coming as an input to FIFO will be sent serially to SISO, which is comprised of three reversible D flipflops made from Fredkin and Feynman gates using behavioral and structural modeling [3]. Whenever any data goes into SISO, then that data comes out after three cycles. Hence, SISO can store a single data point for three cycles. SISO has write pointer logic. The reset signal of the router, the req signal, and the full signal of the FIFO should be low to increase the write pointer logic.

The next module of FIFO is the 3-bit binary synchronous up-counter, which consists of the read pointer logic. To increase the read pointer, the targeted FIFO should be empty, the req signal would be high, and the reset of the router does not apply. The locations of the read and write pointers are used by decision logic to determine whether a FIFO is full or empty.

3 Simulation Results

This work has been verified using the self-checking Verilog testbench [7, 8]. Testbenches are used to drive stimulus to the design under test (DUT), so that the hardware models can be verified. A self-checking testbench can display messages about the functioning of the signals. If there is any error in the output, the self-checking testbench will display those messages with the time stamp where the error has occurred, and then that error can be fixed. Here, the self-checking testbench will display a message if the reset is not working appropriately or if the port selected is 111, i.e., an invalid port address.

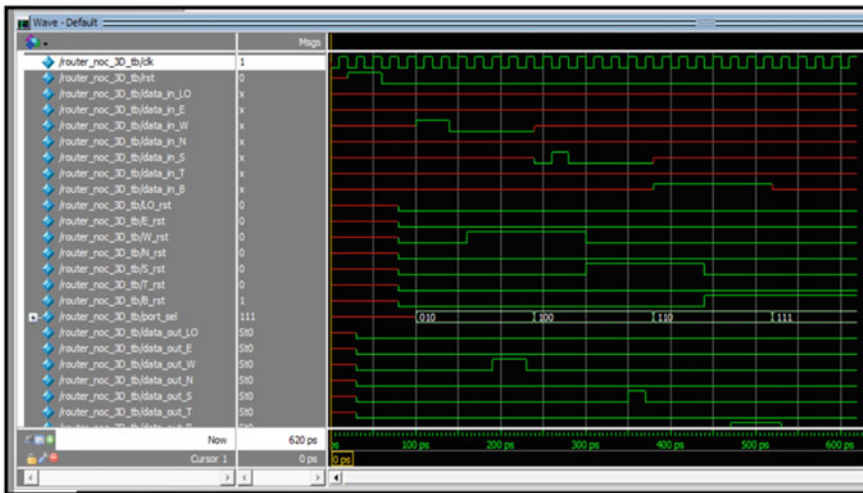


Fig. 4 Simulation result—data, port select, and reset signals

This simulation has been carried out on ModelSim Intel FPGA Starter Edition. From Fig. 4, it can be observed that a clock is applied for a time period of 20 ps. Initially, the reset signal is applied and all the data_out signals, namely, data_out_LO, data_out_E, data_out_W, data_out_N, data_out_S, data_out_T, and data_out_B are set as logic “LOW”. Then data 110 has been sent on FIFO West, and as soon as 3-bit data_in is sent, the reset signal of FIFO West (W_rst) goes high, which indicates a high reset signal. Data cannot be sent to FIFO West. Also, as soon as the first bit of data is sent to FIFO West, the port address of FIFO West—010 is selected, which can be seen on port_sel signal.

Similarly, data 010 is sent to FIFO South, port address 100 gets selected. Then after 3 bits of data, S_rst goes high. When data 111 is sent to FIFO Bottom, port address 110 gets selected so 3 bits of data, B_rst goes high. Also, it can be observed from Fig. 4, that after five cycles of data_in, data_out is correctly received. Data_in should remain stored in FIFO for three cycles, and non-blocking assignment is used in code for the purpose of sequential logic in both data_in and data_out logics. A two-cycle delay should be present.

In Fig. 5, the empty signals of the corresponding FIFOs represent the west, south, and bottom FIFOs when they were picked by port address. The full signals represent the west, south, and bottom FIFOs after 3 bits of data were put into each of them.

Figure 6 displays the output of the transcript window. When reset is applied, all the data_out signals are successfully set to 0 at 40 ps. Figure 6 also indicates that at 520 ps, an invalid port was selected for sending data.

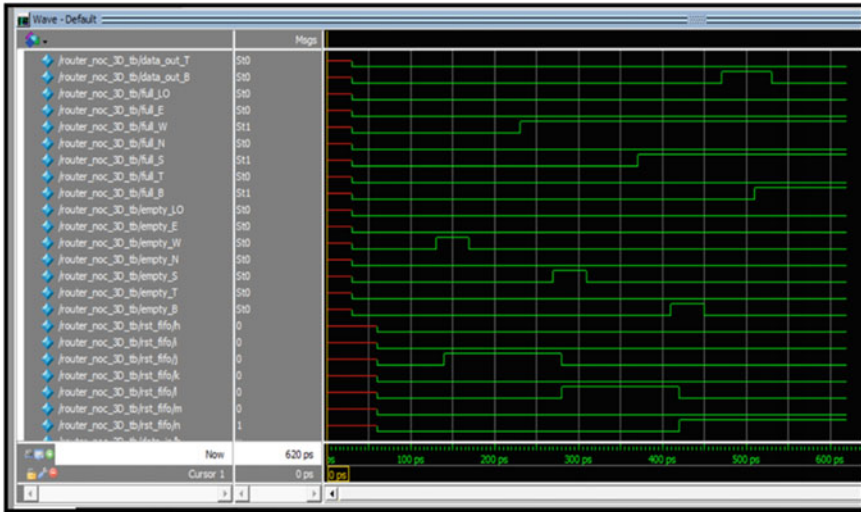


Fig. 5 Simulation result—empty, full, and reset FIFO signals

```
>SIM> run -all
#
# 40 RESET IS WORKING
# 520 INVALID PORT ADDRESS
# ** Note: #finish : C:/Users/mydell/Desktop/Gurleen/VIII Semester/Manipal/Project/3D NoC Router/tb/router_noc_tb_3D.v(83)
# Time: 620 ps Iteration: 0 Instance: /router_noc_3D_tb
# 1
# Break in Module router_noc_3D_tb at C:/Users/mydell/Desktop/Gurleen/VIII Semester/Manipal/Project/3D NoC Router/tb/router_noc_tb_3D.v line 83
```

Fig. 6 Transcript window

4 Synthesis Results

This synthesis has been carried out on the Arria II GX FPGA of Quartus Prime Lite Edition. Figure 7 shows the top module of the work. The top module consists of one control unit and seven FIFOs in local, east, west, north, south, top, and bottom directions. The control unit contains seven multiplexers, seven D flipflops, one de-mux controller, and one de-multiplexer as displayed in Fig. 8. The internal architecture of one FIFO west is shown in Fig. 9. Other FIFOs consist of the same architecture. As expected, this FIFO contains up-count (instance name U1), decision logic (instance name D1), and SISO register (instance name S1).

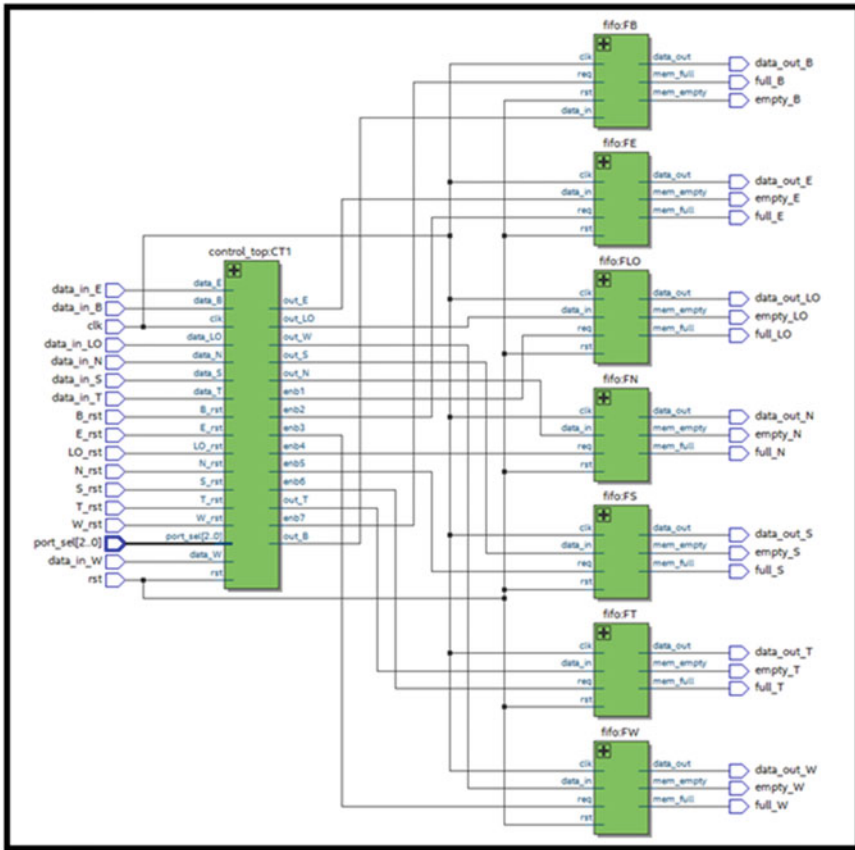


Fig. 7 Top module synthesis

Table 4 shows power reports of the implementation of 3D router on Artix-7 FPGA using Xilinx Vivado. According to Table 4, the total on-chip power needed is 7.427W, of which the device’s dynamic power makes up 98% and static power consumption the remaining 2%. The resource consumption reports for the same goal are shown in Table 5. The quantity of slice LUTs, slice registers, F7 muxes, slice, LUT as Logic, Bonded IOB, and BUFGCTRL accessible on the Artix-7 FPGA and used for the construction of 3D NoC Router Design is shown in Table 5. To implement this design, a total of 88 LUTs, 86 FFs, and 40 IOs are needed. The time report for the target is included in Table 6.

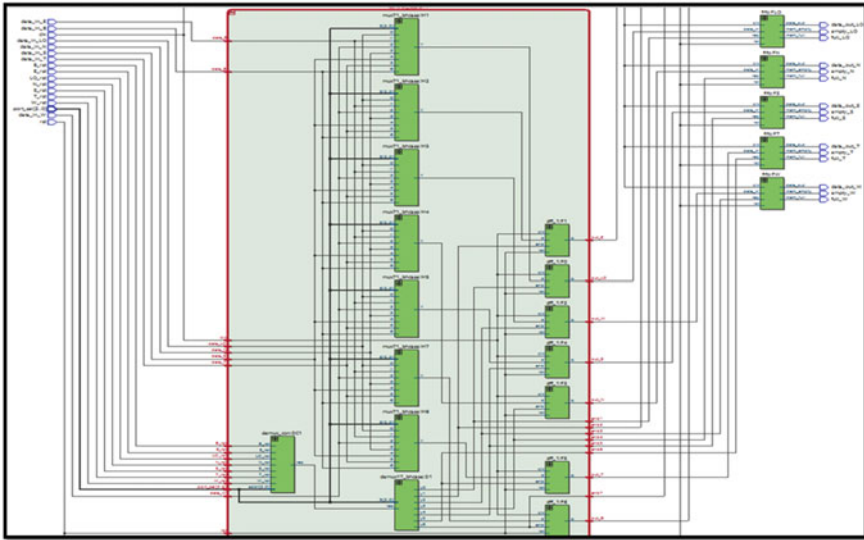


Fig. 8 Internal architecture of control unit

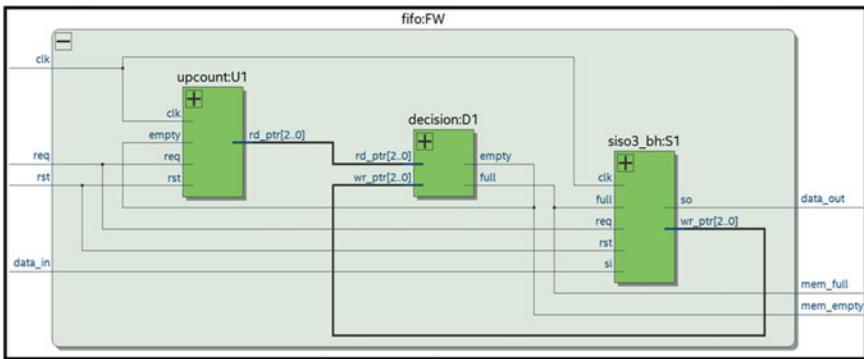


Fig. 9 Internal architecture of FIFO

Table 4 Power report

Dynamic power	Signals	0.445W
	Logic	0.494W
	I/O	6.330W
Static power	0.158W	
Total on-chip power	7.427W	

Table 5 Resource utilization report

Slice LUTs (134600)	88
Slice registers (269200)	86
F7 Muxes (67300)	2
Slice (33650)	35
LUT as logic (134600)	88
Bonded IOBs (400)	40
BUFGCTRL (32)	1

Table 6 Timing report

Maximum frequency	260.01 MHz
Minimum period	3.846 ns

5 Conclusion

The 3D NoC router has seven input and seven output ports. This model can route data in the local, east, west, north, south, top, and bottom directions. This model has been designed using Verilog HDL and verified using a self-checking Verilog testbench. The design consists of one control unit and seven FIFOs. The design has been simulated on ModelSim Intel FPGA Edition and synthesized on Quartus Prime Lite Edition. Power, timing, and resource utilization reports have been generated using Xilinx Vivado. This router can work up to a maximum of 260.01 MHz frequency, utilizes about 88 LUT, 86 FF, and 40 IO, which comprises less than 1% utilization of the Artix-7 FPGA, and consumes 7.247W of total on-chip power. The result indicates better frequency and utilization results. This model can be used to connect multiple devices and route information between them. Additionally, reversible logic is incorporated into the design, which prevents loss of information, reduces heat dissipation, and reduces gate counts and garbage outputs.

References

1. Sobarad SM, Sarkar S (2016) FPGA Implementation of high speed and low area four port network-on-chip (NoC) router. *IOSR J VLSI Signal Process (IOSR-JVSP)* 6(6), Ver. III:52–57
2. Veadesh B, Venkatapragadeesh B (2018) Design and analysis of an efficient 3D – Network on – chip (NoC) router”. *Int Conf Recent InnovElectr, Electron Commun Eng (ICRIEECE)*
3. Sastry Hari SK, Shroff S (2006) Efficient building blocks for reversible sequential circuit design. In: 49th IEEE international Midwest symposium on circuits and systems, vol 2, 6–9 Aug 2006
4. Opoku Agyeman M, Ahmadinia A (2011) Low power heterogeneous 3D networks-on-chip architectures. In: 2011 international conference on high performance computing & simulation, 04–08 July 2011. pp 533–538
5. Bhattacharya S, Sen A (2019) Power and delay analysis of logic circuits using reversible gates. *Int J Latest Technol Engi-Neering, Manag Appl Sci (IJLTEMAS)* VIII(XII):54–63

6. Bhatia IS, Randhawa DKK (2021) Design and implementation of reversible logic gates using silicene-based p - n junction logic devices. J Comput Electron 20:735–744. <https://doi.org/10.1007/s10825-020-01625-z>
7. Palnitkar S (1996) Verilog HDL: a guide to design and synthesis, 2nd edn. SunSoft Press, 9788129700926
8. Navabi Z (1999) Verilog digital system design, 2nd edn. McGraw-Hill, 9780071373043

A Framework for Evaluating the Ergonomics of Mechanical Designs of Gaming Controllers



Fatimah Albargi and Nura Albuhaire

Abstract Human–computer interaction emphasizes bringing people technical solutions that can solve their problems and deliver them functionality with the minimum unpleasant starting from designing the product till delivering it to user. In this paper, we selected an article from the news that talks about a product that is designed for kids. We analyzed the product from the perspective of universal design, user-centered design, and interactive design. We bring on the advantages and the disadvantages of the mentioned design and we suggested a design solution for the issue we found.

Keywords First keyword · Second keyword · Third keyword

1 Introduction

Technology is currently serving humans in almost every aspect of their lives. Technology plays a significant role in our daily life starting from fulfilling various basic living needs, to supporting accomplishing work requirements, and to provide us with entrainment as well. The value of certain technical product can be affected by many factors such as its functionality and how comfortable it was to be used. For filling this need of having functional and comfortable technical product sciences start to concentrate on more human-centered computing that puts humans as end-user in the role starting from designing till implementing and delivering the product.

Designing a product is an early stage of creating a product after understanding the problem and defining the proposed solution. Putting an effort into designing a product plays a significant role in the success of the product. Human-centered design is an important area that concerns designing technologies that can deliver its functionality and bring the user a joyful experience. It involves the perspective of

F. Albargi (✉) · N. Albuhaire

College of Computing in Alqunfudhah, Umm Alqura University, Makkah 201514, Saudi Arabia
e-mail: fmoqurmti@uqu.edu.sa

N. Albuhaire

e-mail: nmbuhiry@uqu.edu.sau.sa

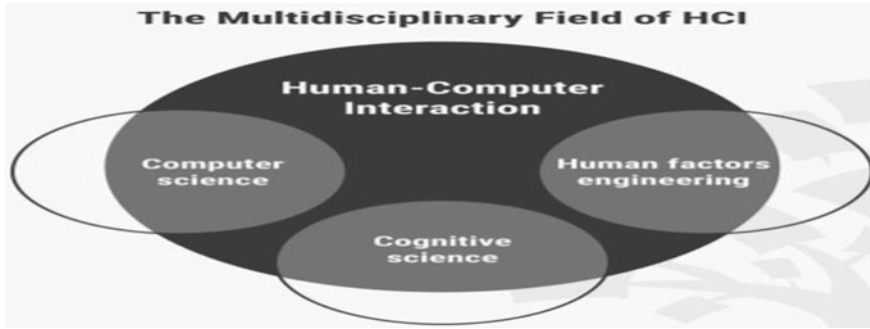


Fig. 1 Multidisciplinary field of Human-Computer-Interaction [1]

humans in the process of designing any technological solutions. We can say in other words it is the area of designing for people. In human-centered design, the creator first asks questions such as whom this product will be for? In what context will be used? And what problem will it solve? and what it is functionality? Such questions will bring an essential understanding of the product at an early stage from the design process. The field recently is mostly known as human-computer interaction HCI because it studies the interactions that happen between the user and the technology and how that affect the users and drives them to practice in a novel way. The areas of computer science and the areas of computer science and cognitive science and the human factor engineering come together to produce meaningful work in the human-computer interaction area, and it brings a different perspective to the domain and that all enhance the quality of the technology we produce when considering the HCI principles and bring users more pleasant experience. Figure 1 shows the multidisciplinary field of Human-Computer-Interaction.

In this paper, we discussed a human-centered design and how it is mentioned in news. We took one of the news that is related to a product design and analyzed the product from the perspective of the human-centered design. We mentioned the strength and weaknesses we think of in the design and proposed a solution for the problem we found. The product we chose is designed for kids and designing for kids is a domain that needs more especially than designing for an adult since kids have their characteristics that depend on different factors such as gender, age, and cognitive skills. Also, when designing for kids the design of the product got affected by the goal of creating the product whether it is educational, entertaining, or some thing that provide health support. The good design will deliver the kid user a comfortable experience of using the device and get the advantage of it. The principles we discussed in this paper, universal design, human-centered design, and human computing interaction are essential to be considered when designing for kids. this paper provides an example of analyzing a product from these perspectives and proved suggested solutions for the found issues. Here are the links that this paper is based on:

- The HCI-related news story, which is about experiencing a prototype for a product called Pip.
- <https://thenextweb.com/dd/2017/11/14/pip-insane-lovechild-nintendo-switch-raspberry-pi-want-one/>
- The product page at Kickstarter, to provide more details about the product (Pip)
- <https://www.kickstarter.com/projects/1464832835/pip-the-playful-handheld-device-you-progr.>

Additionally, for backing up the paper, we have used external references which are listed in the reference section.

2 The News Story Summary

The article “Pip is the insane lovechild of a Nintendo Switch and a Raspberry Pi (and I want one)” is written by the MATTHEW HUGHES on December 14, 2016. Matthew wrote about his experience in trying on going developing product called Pip. In the article, Hughes has introduced the Pip, which is kids target product to teach kids how to code. He introduced Pip capabilities and features as well as his experience feedback for the product.

Pip is a handheld device that aims to enable kids to play with technology, coding, and creation. With Pip it is possible for kids to play games and make their own games. Pip connects to browser-based environment that is setup to enable user to build, execute, and test software in various programming languages. Pip simplifies a way for kids to learn how to program using drag and drop programming. It has also allowed physical computing by playing with the hardware, such as attaching LED's and Motors. Further details on pip hardware are in the next heading.

At the beginning of this month, Hughes got visited by the founders from Curious Chip, to play with prototype unit of Pip. Hughes stated that he got interesting experience with pip. He found the device interactive and responsiveness, bright touchscreen, and colorful device. He added it is obvious that the product is aimed at kids. It has rugged chassis that could probability withstand drop or two. It is suitable starter for someone who is interested in game development.

2.1 *Brief Description of Pip*

The Pip is created by Carious Chip, Group who creates hardware and software for kids, adult, tinker, and educators. Pip is target on kids to provide them learning experience through having fun. Pip enables kids to make fun games, invent their own apps, or take control of objects around them.

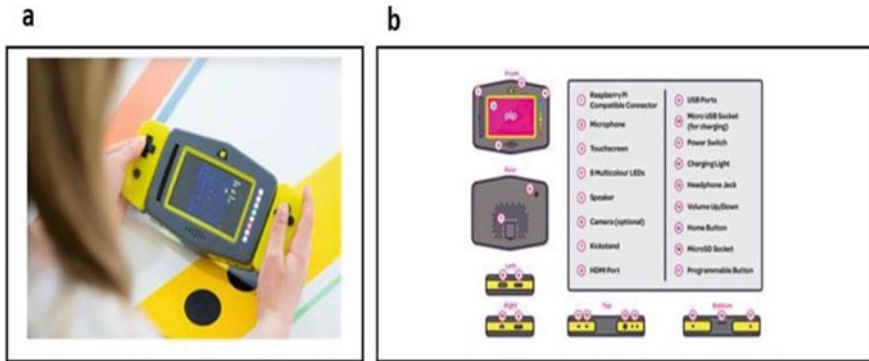


Fig. 2 a Pip in hand; b pip hardware components [2]

Kids can start with drag and drop programming, then go on to play with real code, and tinker with technology. It is designed to suit beginners and those who know more in coding. See Figs. 1 and 2 to have a look about the Pip hardware.

3 How This News is Relevant to Human-Centered Computing

As the human-centered computing concern of understanding the interaction between human and technology systems, and use this to better design, implement, and evaluate the interactive systems [3]. The goal of Pip is to provide programming learning through interaction with pip. So, it is essential to consider human-computer interaction rules in Pip's development. I see this news touch on the human-centered computing from various perspectives:

- Universal Design

The Pip product is aimed to serve wide range of users around the world, with different ages, capabilities, and coding skill levels. The product aimed to kids but could also be used by game-fan adults to gain programming skills. This was supported by the idea of Universal design.

“UD is the process of designing so as many people as possible can benefit in as many situations as possible” [2]. Additionally, Pip is an entrepreneur product in the area of delivering technical skills for young through having fun; therefore, there is a chance for Pip to introduce for new ideas in gaining technical skills for kids, such as Kids Developing Environment, kid's labs, kid's industries, where specialist could get benefit from young creativity and innovations. The product also follows the universal design principle which I will explain in the next section.

- User-centered design

It touches on user-centered design for applying empirical measurement. As mentioned in the news, Pip development team uses prototypes for analyzing the user's reaction to product sample.

Additionally, it touches on user-centered design for applying iterative design. In the second Article, it is shown that Pip went through multiple design iterations. Further explanation is given in the next section.

- Social interaction

Pip users have the advantage of web-community called "Spaceport". In Spaceport, users could share their made ideas and provide feedback on other's products. Spaceport is a "Asynchronous Co-Located based communication where multiple users can communicate at the same web-location but different times" [3].

4 How This News is Relevant to Human-Centered Computing

This news story and Pip as product touch on good user-centered design. The goal of Pip is mainly shaped around the user. The goal is to provide user with a product which provides learning with fun. For applying good user-centered design, Pip development team, Curious Chip, insures to apply the following three main principles:

- Clearly focus on user and tasks:

When Pip was still as an idea, it was cleared that it mainly targets kids as users. This leads to put more focus and studying on kids' cognitive and behavior skills, and kid's attitude. This helped to design for the various kids' characteristics. Also, it helped with deciding on the product capabilities, product styles, and the appropriate content of Pip such as games and programming languages. For insure better result the developing team, involved the children in the design process to have their feedback continuously and improve the design based in their feedback [4, 5].

- Empirical measurements

The Pip development team observes and records user's reaction with prototypes, as mentioned in the news story. The feedback from this analyzing process will be beneficial in understanding current design issues and address it in further design [6, 5].

- Iterative design

Pip went through multiple design iteration. In each cycle, a prototype is tested to identify the issues. Then it gets fixed and prototyped, to check the fixed issue and to explore more new issues. This iterative design process enables the team to come up with better design and functionality for each cycle, see Fig. 3 [6, 5, 7].



Fig. 3 Pip device product, powered by Raspberry Pi [2]

5 Proposing Improvement on Pip

One thing we have noticed is it needs improvement on pip is the input port functionality (buttons, switches, sockets). Pip has multiple buttons to help interact with it. We found an issue in the design that needs to be considered.

The issue is that no indicators exist for the user to know about each button functionality, see Fig. 4. This will create an issue in interaction with Pip for first time. It leads multiple attempts for the user to use Pip input/output ports (Fig. 5) [2].

To address this issue, I have redesigned the 11 to 17 input/output ports to better have an indication about its functionality, see Fig. 4.

- For input 11: I added power icon to indicate it is a power switcher.
- For Input 12: I added the word light.
- For input 13: I added headphone icon to indicate it's a headphone jack.



Fig. 4 Iterative design process for pip, multiple prototypes [2]

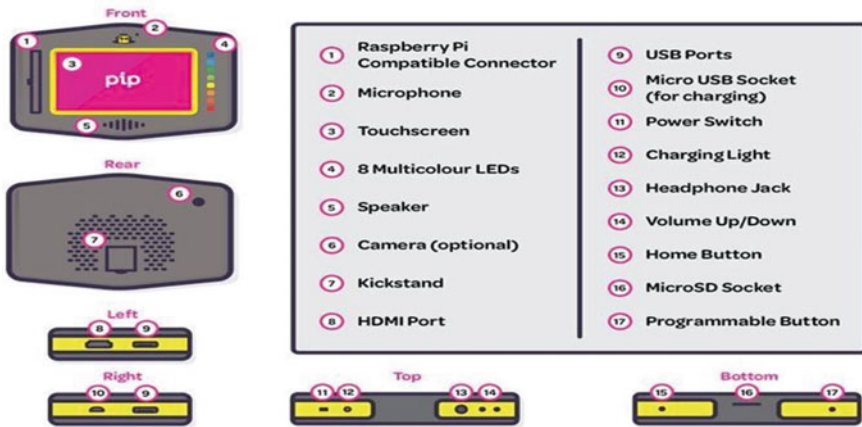


Fig. 5 Lack of functionality identikit in Pip’s input/output ports [2]

- For input 14: I have added a speaker icon with plus and minus icons on the controlling buttons.
- For input 15: I added the word home with a roof simple above it to indicate that this button is a home button.
- For input 16: I added the abbreviation SD, to indicate it is a micro-SD socket.
- For input 17: I added the word programming to indicate that this button is used for Programming.

This design is better than what it was before, because

- It keeps the functionality of each input item visible for the user
- “The more visible functions are, the more likely users will know what to do next” [9].
- It is more usable design. It makes it easier for the user to learn about the in- put/ output functionality. Usability more easier learnability [3].
- The new design creates stronger information scent by using cues (recognizable word, icons) to figure out what are the choices available [8].
- The new design increases the kid confidence about the action he takes to interact with Pip, which will decrease the poor information scent, such as poor confidence and multiple errors [8].
- The new design is more kids-suitable design. It considers kids need to have information that will help them to interact with Pip. The new design puts user’ needs into consideration. It refers to the first principles in user-centered design, which is to understand users and task [10].
- The new design Apply is a better universal design. Because with the improvement made, it would more recognizable and flexible to be used by a wider range of users around the globe.

“Universal Design is the process of designing so as many people as possible can benefit in as many situations as possible” [2].

6 The Reason Behind Getting Interested in Pip’ News

Selecting the paper topic is driven by a personal experience for me Fatimah. I have found the news about Pip interesting for me because it touches on a personal experience, and I found that Knowing about Pip is special. I have an 8-year daughter, Reaman, 3rd Grade. I have seen that she is curious about knowing more about technology. In Fig. 6, Redesign Pip’s input/output ports noticed this from the type of questions she asks for me if she saw me working on any type of code, and from the detailed feedback she brings from her technology class. I realized that in advance basic knowledge in technology will be beneficial for her. So, I kept searching for tools that could provide kids with both computing skills and fun.

I have registered her in How Girls Code courses, where she got basic concepts about computer science and programming. She got learned and interested, but still, it is not that fun for her as it is class-based learning. She also went through the experience of learning coding basic skills through kid’s games’ websites. It is interesting and beneficial, but it has limited in terms of allowing kids to be creative.

When I first read about Pip I found interesting because it gives kids a handheld device that they can physically interact with as a toy and learn from. Also, appreciate that Pip enables kid’s to be creative by creating their own games, connecting Pip to objects around them, and sharing their creativity in post-space community.

After getting this experience with my daughter I become more aware that kids’ need to have accessibility to fun-learning tools that could introduce them to technology via entertainment. Therefore, in future, I plan to use my mobile programming skills (Android programming) to create Apps that carry out the idea of teaching codes via creative games.

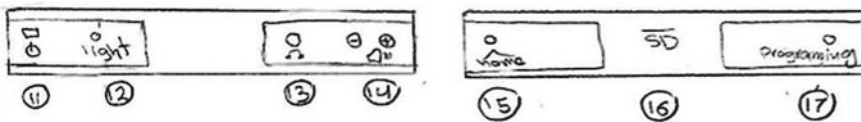


Fig. 6 Redesign Pip’s input/output ports

7 Conclusion

In this paper, we talked about the human–computer interaction domain and the importance of considering the principles of interaction design when designing a technological product. Secondly, we selected an article about designing a new product called “pip” and review the mentioned design from a different perspective and finally we suggested a design improvement that we see is required to improve the functionality and enhance the user experience. We analyzed the design and the prototype from three prospective social interactions, user-centered design, and Universal Design. From the user-centered design perspective, we highlighted the strong design aspect in the product such as the focus on user and tasks, empirical measurements, and iterative design. We also mentioned another design component we see as not good design and need to be improved. We propose an improved design for the issue of missing functionality labeling. The redesign we proposed brings more comfortability to the user when using the product as the functionality of each part of the product becomes clear and visible for the user. Through the reoccurrence design prototype that Pips went through, Pips labeling problem has not been fixed till the time of writing this paper. So the finding in this work is valuable to improve Pip functionally and bring better experience to its users.

References

1. Kozak OS, Analysis of illustration influence on human-computer interaction. Figure 2. Research gate <https://doi.org/10.13140/RG.2.2.24793.95845;2020>.
2. Hughes MW (2017) Pip is the insane lovechild of a Nintendo Switch and a Raspberry Pi (and I want one). The New Web website. Retrieved From: <https://thenextweb.com/dd/2017/11/14/pip-insane-lovechild-nintendo-switch-raspberry-pi-want-one/>
3. University of Maryland, Baltimore County (UMBC) (2017) Department of information systems page, MS in HCC. Retrieved From: <https://informationsystems.umbc.edu/home/graduate-programs/master-of-science-programs/master-of-science-in-human-centered-computing-hcc/>
4. Babich NK (2018) Top 4 principles of human-centered design. Retrieved from: <https://uxplanet.org/top-4-principles-of-human-centered-design-5e02751e65b1>
5. Hamidi FD (2017) Universal usability for inclusion and community engagement. Slide 6. Retrieved from:https://blackboard.umbc.edu/bbcswebdav/pid-2749593-dt-content-rid-14147393_1/courses/HCC629_4116_FA2017/Week12-UniversalUsability-HAMIDI.pdf
6. kickstarter (2017) Pip-digital creationin your pocket.Retrieved from: <https://www.kickstarter.com/>
7. Smith AN (2017) Process of Interaction design lecture, slide 5–9. Retrieved from: https://blackboard.umbc.edu/bbcswebdav/pid-2677159-dt-content-rid-12397510_1/courses/HCC629_4116_FA2017/Week10-InfoDesign.pdf
8. Smith AN (2017) Information design lecture, slide 37, 38. Retrieved from: https://blackboard.umbc.edu/bbcswebdav/pid-2677159-dt-content-rid12397510_1/courses/HCC629_4116_FA2017/Week10-InfoDesign.pdf

9. Smith AN (2017) Design Principles Lecture, slide12. Retrieved from: https://blackboard.umbc.edu/webapps/blackboard/execute/content/file?cmd=view&content_id=_2656957_1&course_id=_34922_1
10. Preece JR, Rogers YE, Shorp HN (2015) Interaction design, beyond human-computer Interaction. Chapter 9:327–328

Triggering an Email Alert Based on Price Comparison by Web Scraping Using Python



Shikha Singh , Garima Srivastava , Vandana Dubey ,
and G. R. Mishra 

Abstract Web scrapping offers a response for the people who want to grab the access to structured information on the web in an electronic plan. Web scrapping, otherwise called web extraction, is a strategy to separate information from the World Wide Web (www) and save it to a record framework or dataset for later recovery or examination. Web scratching utilizes savvy robotization to extricate millions and billions of information from the unlimited information facilitated over the web. Web scrapping has various utilizations like Price Intelligence, Market Research, Real Estate, News and content monitoring, and so on. This paper is about scrapping the prices from different e-commerce websites and then comparing them and finally triggering an email having the link of the website offering a lesser price for the same product. Various websites like trivago, for example, offer least price for specific services after comparing the prices offered by different websites. Authors have attempted to cater this service for a large variety of products and user be getting an email as a result, which will have the link specifying the details of the product along with the website offering least price.

Keywords Web scrapping · Price comparison · SMTPLIB · Request library · BeautifulSoup library · Email trigger

S. Singh · G. Srivastava
Amity University Uttar Pradesh, Lucknow, U.P., India
e-mail: ssingh8@lko.amity.edu

G. Srivastava
e-mail: gsrivastava1@lko.amity.edu

V. Dubey (✉)
C. Byregowda Institute of Technology, Kolar, Karnataka, India
e-mail: vandanashuklaec05@gmail.com

G. R. Mishra
Dr. Ram Manohar, Lohia Avadh University, Faizabad, U.P., India

1 Introduction

Web scrapping is the procedure of gathering the structure web information in a computerized design. It is also known with names like “Data Extraction” or “Data Scrapping”. Some major uses of web scrapping are price intelligence, price monitoring, news monitoring, price comparison, and market research among the list. Generally, this method of web data extraction is mostly used by the owners of organizations and individuals who need to make the utilization of the tremendous amount of the web data available publicly, to make better and smarter decisions. We all have at some point of time copied and pasted some data from the web, and this activity of copying and pasting data from a website hosted over the web is the same activity as performed by a web scraper, just at a manual level. So basically, unlike doing this mind desensitizing manual activity of extracting data, web scrapping uses smart automation to extract millions and billions of data from the endless data hosted over the Internet. Web scrapping works in two parts: a **web crawler** and a **web scraper**. To put it another way, the web crawler is the horse, and the web scraper is the chariot. The scraper is led by the crawler, through the web, from where the requested data is extracted.

The crawler. Generally called as a “spider”, a web crawler, it is basically an artificial intelligence that surfs the web to index and search for data by following links and exploring.

The scraper. A web scraper is a specific tool designed to precisely and rapidly extract information from a website. Web scrapers differ a lot in respect to their design and their complexity, in respect to the project.

Scrapping tool. A web scrapping tool is a software program that is especially designed for extracting (or “scrapping”) important and required data from the websites. A scrapping tool makes HTTP requests to a desired web page and scrapes the data from the page. Generally, it parses information that is freely open and visible to the clients and delivered by the server as HTML.

Figure 1 depicts the basic procedure of web scrapping. For a small project, a general web scrapping process goes like:

1. Identification on the target website.
2. Collection of the URLs owned by the web pages from where the data is to be extracted from.
3. A request to the collected URLs is made to get the HTML of the web page.
4. To find the data in the HTML, locators are used.
5. Data is saved in a JSON or CSV file or some other structured format.

There are a few challenges one needs to face if the data is required at scale. For example, if the layout of the website changes, then also trying to maintain the scraper, proxy management, execution of the JavaScript, or working-around-antibots [1]. All these are extremely technical issues and a result of which a lot of resources can get over. There are a number of open-source web data scrapping tools that can be

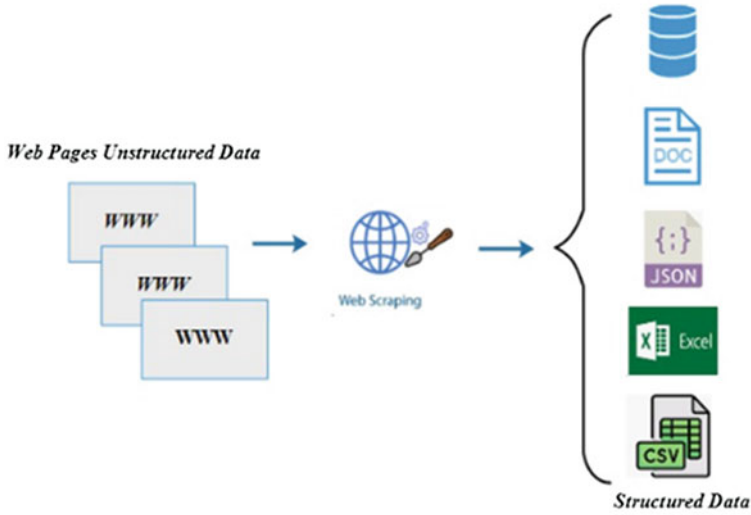


Fig. 1 Web scrapping procedure

used but they all come with their own limitations. So, for the same reason, many businesses opt to outsource their web data projects. This paper is about scrapping the prices from different e-commerce websites and then comparing them and finally triggering an email regarding the link of the website offering a lesser price for the same product. The product title, price, and the product URL have been extracted and then used in comparing the prices and displaying the minimum amount and then triggering an email accordingly. This paper aims to compare the price of a particular product that is requested by the user, from various e-commerce websites and intern firing an email about the same to the user.

The paper starts with the brief introduction of the web scrapping, followed by exhaustive literature survey on the various existing methods of web scrapping and its utilization. Third section takes the methodology of extracting the web data pertaining to various prices of products offered by different sites and make comparison of prices. Finally, triggering an email reflecting link with the least price of the product is shown in the result section. Lastly, the paper is supported by conclusion and future scope of the work.

2 Literature Survey

Web scrapping, also known as web extraction, is a technique to extract data from the World Wide Web (www) and save it to a file system or database for later retrieval or analysis [2]. Web scrapping is eminent for a “Screen Scrapping”. The web scrubber

programming is anticipated thorough for all significant information from various web-based stores and mining, and assortment it into the new site [3]. The scrubber instrument is used to forgot data from the web. Web scrapping is getting progressively valuable as a way to effortlessly gather and sort out the plenty of data accessible on the web [4]. Utilizing a straightforward language like Python, you can creep data out of complex sited utilizing basic programming. Web scratching is prominent for a “Screen Scrapping” [5]. The web scrubber writing computer programs is expected careful for all critical data from different online stores and mining, and combining it into the new webpage. The scrubber instrument for the web is utilized for failure in remembering information from the web. Web data is scrapped utilizing Hypertext Transfer Protocol (HTTP) or through a web browser [6]. This is accomplished either manually by a user or automatically by a bot or web crawler. Due to the fact that an enormous amount of heterogeneous data is constantly generated on the WWW, web scrapping is widely acknowledged as an efficient and powerful technique for collecting big data. Web scrapping is the strategy which means to resolve this issue [7]. Web scratching is utilized to change unstructured information on the web into organized information that can be put away and investigated in a focal nearby dataset or bookkeeping page. There are different web scratching procedures including Traditional duplicate and paste, Text grapping and ordinary articulation coordinating, HTTP programming, HTML parsing, DOM parsing, Web scrapping programming, Vertical accumulation stages, Semantic explanation perceiving, and Computer vision site page analyzers [8]. The proposed framework thinks about the item from various sites and furnishes clients with an outline of the total determinations about the item and their costs on the specific sites. It likewise shows about the progressing bargains and permits the clients to add any ideal item to the list of things to get informed when cost drop happens [9]. The point of correlation shopping is to lay out effective cooperative work system among many shopping sites, and a definitive point is that building a “one-stop” virtual assistance stage between the Internet-based retailer and the general population, and give a fast service channels of data administration, to give productive and high-quality shopping administrations [10]. Information Feeding is the technique which comprises the vendor site entering the underlying data of the items and the index of the offers straightforwardly on the examination site. This technique for providing information basically comprises permitting or empowering online dealers to furnish the information related with the items they offer (the cost or different details like delivery costs, stock levels, limits, and so on) in the particular information design characterized by the CSEs. While permitting them to refresh their data as they see fit [11]. The apparent convenience of advertisements and client assistance experience assumptions are significant empowering agents to price comparison sites use [12]. It is essential for a price comparison website to return the results inclusive of the lowest prices and better deals in accordance to what sort of deal customers/buyers want to actually grab, but the results must be accurate. It is also dependent on the fact that how frequently the database is being updated else the customers/buyers will get confused when the results are compared with from the other already existing websites [13]. The associated showcasing covers with web showcasing techniques somewhat, due to offshoots utilize

normal publicizing strategies. Those techniques utilize successful site improvement (SEO), paid web search tool advertising (PPC—Pay Per Click), content showcasing, email promoting, and in some sense show publicizing. Furthermore, the subsidiary promoting in some cases utilizes moderate procedures of distributing surveys of items or administrations presented by an accomplice. The provider in online business as short for business-to-business in electronic trade, that is, selling items or administrations between organizations through the web by means of an Internet-based deals entryway [14]. Six measures named as the review administration, informal virtual entertainment, excellent web-based plan, security, and trust are fundamental as well as auxiliary administrations that affect shopper devotion. The objective of this study is to figure out which components in movement partner sites can affect change rates. In the vacationer area, customer dedication is significant [15]. Affiliate Marketing is a kind of execution-based progressing in which a business pays in any event helper for each guest or client brought by the part's own showing attempts. It is a kind of online displaying methodology wherein a wholesaler propels a business try through advancement on their site and that prompts business repays the part with the commission each time a visitor, the client makes bargains [16]. Affiliate marketing is a web-based system in which affiliates are compensated for promoting a specific product to other businesses or individuals. This document delves into affiliate marketing fundamentals while also presenting the current situation of the industry in India and other countries. Affiliate marketing is a marketing strategy that connects merchants with independent sellers who are prepared to put in the time and effort to sell a merchant's items.

3 Methodology

As shown in Fig. 2, methodology includes various steps like installation of libraries, fetching data from websites, cleaning the data, storing them in databases for comparison, and finally based on least value generating an email about the same.



Fig. 2 Flowchart of the methodology

3.1 Installation of Libraries

- a. **Installation of “requests” library [3]:** This library helps in getting the permission for accessing an URL and get the data from the particular website.
- b. **Importing BeautifulSoup:** BeautifulSoup helps in extracting data from the website without HTML tags.
- c. **Giving an URL:** Storing the URL of the page in a variable, from which the data is to be scrapped.
- d. **User Agent in headers:** It basically checks from which browser the user is trying to fetch the data. For entering the user agent for your browser, just type in the search engine, “my user agent” and the user agent for the particular browser will be displayed on the screen.
- e. **Requesting the URL:** The URL of the page from which the information is to be scratched is to be mentioned.

3.2 Fetching Data and Cleaning It

A. For Amazon: Storing the URL of the product’s Amazon page in the variable “amazon_product_url”. First step is requesting the url and the headers from the particular webpage and then using “BeautifulSoup” the page’s content is stored in soup. Following this the content of soup is prettified. Now the Amazon page gets opened and by right-clicking on the product title and perform inspect. After clicking on inspect, the screen will be displayed and then the ID used of the product’s title on the web page is found and used in the code. In the HTML source code element with ID “productTitle” contains the title of the particular product. This will print the product title but the data displayed will have HTML tags in it, so the data needs to be cleaned to proceed further. To clean the content, remove the HTML tags and strip the text from it. Similar to how we got the product title, we can get the price tag by clicking on and doing inspect, we will get the following html source code. Here, the ID is “priceblock_ourprice” containing the price tag of the product. So, in order to fetch the price the following code is required (Fig. 3):

Now, the price of the product is stored in the variable “amazon_product_price”. By this same procedure, the price tag of the e-commerce website “Flipkart” will be scrapped.

```
price = soup.find(id = 'priceblock_ourprice')
price = price.get_text() # Will get text from html tags
amazon_product_price = price.strip() # Removing special characters like \n (newline)
print(amazon_product_price )
```

Fig. 3 Scrapping the price of the product

B. For Flipkart: Storing URL of the product’s Flipkart page in the variable “flipkart_product_url” as done for Amazon, then requesting the url and the headers from the webpage and then using BeautifulSoup the page’s content is stored in soup. Following this the content of soup is prettified using the third line of code. Now similar to what we did with the Amazon page, the Flipkart page is opened and then by right-clicking on the product title and inspect. We will get the HTML code after clicking on inspect. The layout here was a bit different than that of the Amazon’s HTML source code. In Flipkart’s case, the price tag has to be fetched from a class element whereas in Amazon’s case, it was the “span id”. So, in order to fetch data from the class element in HTML and store it in a variable.

3.3 Storing Data

The code in Fig. 4 depicts the initializing data to be stored in the database. The code in Fig. 5 depicts that the stored data in the database is being loaded.

```
In [ ]: import pickle
def storeData():
    #initializing data to be stored in db
    amazon = {'key' : 'amazon', 'product_name' : 'Lenovo'}
    flipkart = {'key' : 'flipkart', 'product_name' : 'Lenovo'}

    #database
    db = {}
    db['amazon'] = amazon
    db['flipkart'] = flipkart

    #its important to use binary mode
    dbfile = open('price_data', 'ab')

    #source,destination
    pickle.dump(db, dbfile)
    dbfile.close()
```

Fig. 4 Storing data in a database

```
In [ ]: #Loading Stored Data
def read_data():
    dbfile = open('price_data', 'rb')
    sb_store = pickle.load(dbfile)
    for items in sb_store:
        print(items, ':::', db[items])
    dbfile.close()
```

Fig. 5 Loading the stored data from the database

```
In [ ]: amazon_product_price = float(amazon_product_price[1:])
        flipkart_product_price = float(flipkart_product_price[1:])
```

Fig. 6 Converting the scraped prices to float

```
In [ ]: min_price = min (amazon_product_price, flipkart_product_price)
```

Fig. 7 Finding the minimum price

```
In [ ]: if min_price = amazon_product_price,
        Company = Amazon
        URL = amazon_product_url
        else if min_price = flipkart_product_price,
        Company = Flipkart
        URL = flipkart_product_url
```

Fig. 8 Storing the company name and the URL of the minimum price product

3.4 Comparing Prices

The prices are initially scraped as a string since they have the currency symbol with them. So, in order to remove the currency symbol and use the prices as number so that they can be later compared as amounts, the prices are converted to float from string for comparison.

The code in Fig. 6 shows the code used to convert the price values to float values. Finding the minimum price using the min () function of Python in Fig. 7.

The company offering the minimum price of the product is obtained as output of the min() function and then stored in the variable “Company” and the URL of the same is stored in the variable “URL” (Fig. 8).

3.5 Triggering Email

Using the SMTP, a function is to be written in order to trigger a notification mail to our mail IDs. First of all, the “smtplib” library is to be imported at the start of the code. Then, a function is to be written after the comparison of the prices is done.

The code in Fig. 9 will send a mail from a particular sender’s account to the recipient’s account with a specific Subject and Body of the mail, as to whatever

```
In [77]: from smtplib import SMTPException
def send_mail():
    server=smtplib.SMTP("smtp.gmail.com",587)
    server.ehlo()
    server.starttls()
    server.ehlo()
    server.login('██████████@gmail.com','vllhgtrkiciskv')
    subject = "Price Fell Down "
    if Company == "Flipkart":
        body="https://www.flipkart.com/boat-rockerz-480-bluetooth-headset/p/itmcc05f4bce267p16-ACCE1D9NSG27965kl16-15TACC1E2DF
msgf"Subject:{subject}\n\n{body}"
        server.sendmail('██████████@gmail.com','██████████@gmail.com',msg)
        print("Mail Sent")
        server.quit()
    else:
        body="https://www.amazon.in/dp/B07XLBHFC?pd_rd_i=B07XLBHFC&pd_rd_w=07hzR&pf_rd_p=a75ba368-11d2-4ce4-98f8-b19e803dc!
msgf"Subject:{subject}\n\n{body}"
        server.sendmail('██████████@gmail.com','██████████@gmail.com',msg)
        print("Mail Sent")
        server.quit()
```

Fig. 9 Function to trigger a mail

is mentioned in the function. And as a result of this a mail will be triggered and a confirmation message will be displayed, since it was mentioned in the smtp function.

4 Result

The mail is triggered successfully using the SMTP Library and the mail is received in the recipient's inbox with the subject as "Price Fell Down", the body of the mail is also received as mentioned in the used code as shown in Fig. 10.

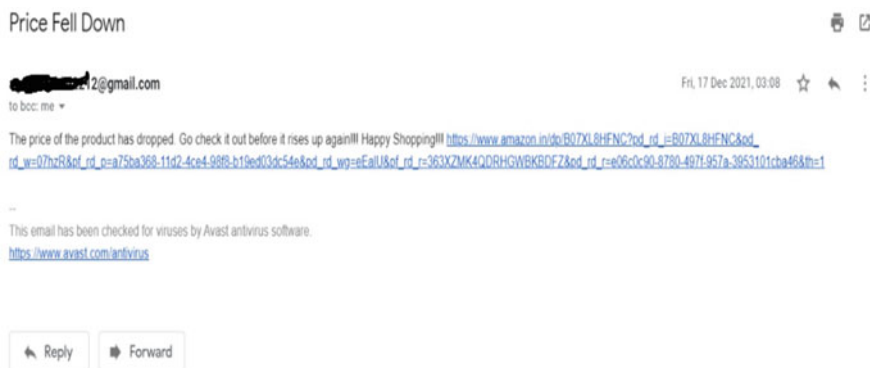


Fig. 10 Body content of the mail

5 Conclusion and Future Scope

Authors have gained an insight of the working of the web scrapping domain. The uses, types, and techniques were important aspects of the domain and have helped in completion of the target. Utilizing Python libraries made it easier in fetching and cleaning of the data, storing, and finally comparing them to achieve the least price target. Further improvements that can be made by adding a proper GUI to the present work and display it in well-structured manner on the screen. So far, the code has been developed to scrape the price of a product, compare it, and then trigger an email with the link of the e-commerce website that is offering a less price than the other e-commerce website. In the coming future, the code can be expanded to accept any product mentioned in a search bar and scrape the price and compare it and then trigger a mail based on the comparison. A GUI can be developed, and the tool can be made more user-friendly.

References

1. Mitchell R (2018) Web scraping with Python: collecting more data from the modern web. O'Reilly Media, Inc
2. Zhao B (2017) Web scraping. In: Schintler L, McNeely C (eds) Encyclopedia of Big Data. Springer, Cham. https://doi.org/10.1007/978-3-319-32001-4_483-1
3. Thomas DM, Sandeep M (2019) Data analysis by web scraping using python. In: 2019 3rd international conference on electronics, communication and aerospace technology (ICECA). IEEE
4. Prof Nandwani U, Mr Mishra R, Mr Patil A, Mr Siddiqui W (2021) Data analysis by web scrapping using python. Int J Res Eng Appl Manag (IJREAM) 7. ISSN: 2454-9150, Special Issue
5. Julian LR, Friska N (2015) The use of web scraping in computer parts and assembly price comparison. In: 2015 3rd international conference on New Media (CONMEDIA). IEEE
6. Thomas DM, Mathur S (2019) Data analysis by web scraping using python. In: 2019 3rd International conference on electronics, communication and aerospace technology (ICECA). pp 450–454. <https://doi.org/10.1109/ICECA.2019.8822022>
7. Sirisuriya DS (2015) A comparative study on web scraping
8. Ambre A, Gaikwad P, Pawar K, Patil V (2019) Web and android application for comparison of e-commerce products. Int J Adv Eng, Manag Sci (IJAEMS)
9. Shevalkar SG, Dr Kawathekar S (2021) Extraction of product's price using binary search algorithm for online shopping. Int J Innov Res Sci, Eng Technol (IJIRSET), e-ISSN: 2319-8753, p-ISSN: 2320-6710
10. Laghmari G, Khali Issa S, Ait Kbir M (2019) Comparison shopping engines. Int J Adv Comput Sci Appl (IJACSA) 10(7)
11. Kwarteng MA, Jibril AB, Botha E, Osakwe CN (2020) The influence of price comparison websites on online switching behavior: a consumer empowerment perspective. In: Hattingh M et al (eds) International federation for information processing 2020 Published by Springer Nature Switzerland AG 2020. I3E 2020, LNCS 12066, pp. 216–227, 2020.
12. Muneeb K, Aamir ZK (2021) A comparative study on affiliate marketing websites. <https://doi.org/10.13140/RG.2.2.34854.45120>.
13. Fahim T, Prof Nasabi A (2020) A study on consumer attitude towards affiliate Marketing for E-Business. Int J Innov Res Eng & Manag (IJIREM) 7(4). ISSN: 2350-0557

14. Prof Ahmad Khan S, Prof Imran Khan Md, Prof Menon B (2020) A Thorough study on affiliate marketing. *Int J Creat Res Thoughts (IJCRT)* 8(5). ISSN: 2320-2882
15. Persson E (2019) Evaluating tools and techniques for web scraping (Dissertation). Retrieved from <http://urn.kb.se/resolve?urn=urn:nbn:se:kth:diva-271206>
16. Dr Mohit V, Asst Prof Sarangdhar PD (2020) A study of affiliate marketing-future and opportunity for aspirant in India. *Dogo Rangsang Res J* 10(6), ISSN: 2347-7180

Enhanced Hyperledger Fabric Network Set-Up for Remittance and Settlement Process



Parveen Mor, Rajesh Kumar Tyagi, Charu Jain, and Deepak Kumar Verma

Abstract Blockchain is a magnificent technology that has the ability to decentralize the storage, sharing, and management of data and information. Hyperledger Fabric, an open-source, permissioned blockchain initially introduced by IBM as Hyperledger Fabric v1.0 and then more recently as Hyperledger Fabric v1.4.4, is one of the most recent blockchain systems to emerge. There is no clear technique for comparing attributes like performance, security, and scalability, despite the fact that there are multiple blockchain platforms. Furthermore, the new Hyperledger Fabric version was never compared to any other blockchain platform. In the study, the evaluation and settlement for Hyperledger Fabric 1.4.4 have been done. A complete set-up is presented in this document. As more Hyperledger Fabric networks go live, serviceability and operational aspects are becoming increasingly critical. With logging enhancements, health checks, and operational analytics, Fabric v1.4 takes a major step ahead. Fabric v1.4.4 is hence the recommended release for production use. Under heavy workload circumstances, however, the performance of the Hyperledger Fabric v1.4.4 platform did not match that of conventional database systems.

Keywords Blockchain · Hyperledger fabric · IPFS (interplanetary file system) · Distributed ledger

P. Mor (✉) · R. K. Tyagi · C. Jain
Amity School of Engineering and Technology Gurgaon, Gurgaon, Haryana, India
e-mail: mor.praveen439@gmail.com

R. K. Tyagi
e-mail: rkyagi@ggn.amity.edu

C. Jain
e-mail: cjain@ggn.amity.edu

D. K. Verma
Greater Noida Institute of Technology Greater Noida, Noida, Uttar Pradesh, India

1 Introduction

Blockchain is a revolutionary technology that alters the way data and transactions are stored and recorded. A blockchain is comparable to a standard database, but the concept behind it is to eliminate the intermediary [1, 13]. When Satoshi Nakamoto created Bitcoin, a digital money, in 2008, blockchain was first revealed [2]. The technology, on the other hand, is currently considered the backbone of the majority of cryptocurrencies in use today. A publicly distributed ledger, which is controlled by no one and copied by every node in the network, lies at the heart of this technology [19]. Non-financial uses for blockchain include public services [1], trust systems [3], security, and the Internet of Things [4, 5]. According to a comprehensive analysis of blockchain research concerns in [6–8], the primary restrictions and difficulties that have not been fully explored are latency and throughput. Because established blockchain frameworks are expected to have a high number of nodes, scalability testing is also required. One of the research gaps in the blockchain sector, according to the report, is that the majority of existing research focuses on the Bitcoin platform rather than alternative blockchain platforms. Hyperledger Fabric [9], an open-source, permissioned blockchain initially published by IBM as Hyperledger Fabric v1.0 and then more recently as Hyperledger Fabric v1.4.4 [8] is one of the most current blockchain systems. This research is one response to this requirement, and it aims to conduct performance tests on two Hyperledger Fabric versions: v1.0 [7] and v1.4.4 [8].

1.1 *Blockchain Technology in Financial Industry*

Modern electronic payment systems rely on multi-party trustworthy third parties to execute payments safely [14]. Banks have begun to welcome demands from one another because of the desire to reduce transaction costs. This innovation made investing easier by allowing traders to deposit notes from other banks straight into their own accounts, eliminating the need to convert paper money into gold for fund transfers [5]. The payee's bank, on the other hand, was in a different situation since it was now known to the payer's bank that the gold settlement would have to be fulfilled by obtaining a letter from another bank. This may be done bilaterally if the note's approval was confined to a small number of banks. Blockchains based on a locked public ledger, in which only authorized employees may join, are preferred by financial institutions because they prioritize reliability, consistency, and performance [3].

Section 2 of this paper explains the blockchain as a technology and role of Hyperledger Fabric in implementing the peer-to-peer networks. Section 3 has details of the research methodology followed to implement the end-to-end solution. It also explains the underlying key components of distributed ledger. Section 4 has the actual implementation details of installation, configuration for setting up the Blockchain

network for remittance and settlement Process. Outcomes and discussions have been mentioned in Sects. 5 and 6 has the conclusion of this implementation.

2 The Distributed Ledger

Blockchain is a peer-to-peer distributed transaction record [9] preserved and maintained in a chain of connected blocks. It is defined as the technology that allows all nodes in a network to share records without maintaining and owning none of them [4]. Client computers or mobile devices are nodes or peers in the network. Since the Internet, this technology has been regarded as one of the most transformative paradigms [6, 7, 12]. In extreme scenarios, such as with distributed cryptocurrencies [15, 16], a trustworthy third source, such as a central bank, is not expected. For a population of approximately 2.5 billion “non-banking,” these new payment and delivery systems enable the introduction of a range of transformative investment products, such as electronic transfers, one end point to another end point lending, or—anti-money facilitating banks, potentially simplifying, and lowering transaction costs, such as cross-border payments [11, 17, 18].

3 Research Methodology

Hyperledger Fabric, an open-source technology appropriate for corporate use, is managed by IBM and the Linux Foundation. Unlike Bitcoin and Ethereum, Hyperledger Fabric lacks a cryptocurrency, and network access is limited to network members only. The network is open to everyone. The PBFT [21] approach is used in Hyperledger Fabric to verify transactions and build blocks. Transactions in Hyperledger Fabric are governed by chain code (smart contract), which is a software that allows you to create and construct network-interacting apps. An isolation method called as channel can be used to ensure the privacy of transactions between network participants. The channel makes certain that the transaction and data are secure. A transaction, according to Hyperledger Fabric’s official documentation [6], for ordering and validation, a peer sends an invoke or instantiate request. The invoke transactions read and write on the ledger, whereas the instantiate request constructs a chain code in a specified channel. The Hyperledger Fabric architecture [22] is made up of peer nodes, ordering nodes, and client applications. The certificate authorities are used to produce the component identities. In a block, the ordering nodes gather and organize transactions from various applications. In this study, we will evaluate the performance of two Hyperledger Fabric versions: version 1.0 and version 1.4.4. The two versions, v1.0 and v1.4.4, have somewhat different architectures. The majority of the differences between the two architectures are due to the new version’s ability to add and defend additional responsibilities. In v1.4.4, there are three categories of peers: endorsing peers, committed peers, and ordering service, whereas in v1.0,

there are only two types of peers: validating peers and no validating peers. In v1.4.4, several fundamental flaws in the design of v1.0, such as performance and scalability [33], were found and fixed [30].

4 How Does the Hyperledger Fabric Network Work?

Since this research is focused on remittance and settlement via blockchain technology, some of the major other sources have been investigated, which are used for payments and are capable of securely and efficiently processing large amounts of data [10], so that we can better understand the properties, applications, and Hyperledger Fabric network settlement to make the Blockchain Technology that we are researching work. A and B have chosen to invest in a Fabric blockchain network as a joint venture. Organization A will supply two peers, one orderer and two client apps that will use the blockchain network's services. Organization B will provide two peers, one orderer and one client app. Organizations A and B have chosen to create a consortium in order to share a different application channel. Each application channel is governed by its own set of rules. As depicted in Fig. 1, each blockchain network member organization is responsible for preparing its peers to join the network. All of these peers must be set up with the necessary cryptographic materials, such as Certificate Authorities and other data. For each network participant, the cryptogen generates network artifacts, identity certificates, and private keys [12].

OrdererOrgs

PeerOrgs

- OrdererOrgs refers to the organizations that maintain and operate our blockchain network's orderer nodes. In the Hyperledger Fabric ecosystem, the orderer is a node that arranges transactions and creates blocks for our channel.
- Organizations that own and administer peer nodes on the blockchain network are referred to as PeerOrgs. Our organizations are bankA and bankB. The peer node has the ability to read and publish transactions to the blockchain ledger, as well as run chaincodes.

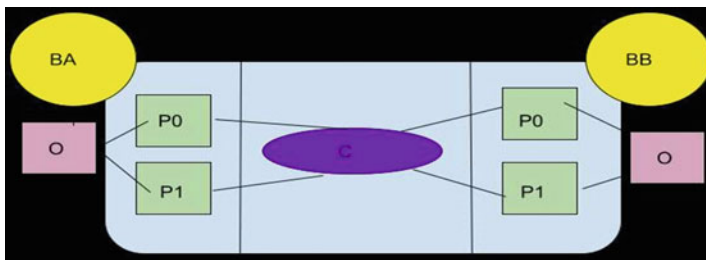


Fig. 1 Hyperledger fabric network

The PeerOrgs tag in the crypto config.yaml file describes the properties of such an organization. [Banka.example.com](#) and [bankb.example.com](#) are two peer organizations. Each organization will be paired with two other organizations.

[Peer0.banka.example.com](#), [peer1.banka.example.com](#), [peer0.bankb.example.com](#), and [peer1.bankb.example.com](#) are the nodes that will be used. Figure 2 explains the various network components.

Steps to bring network online:

1. Use the cryptogen program to generate certificates for all channel participants.
2. Using the configtxgen program create the network artifacts (including the genesis block).
3. Using all of the appropriate yaml files as input, run the docker-compose command to start the containers that house the network components. Run the scripts to build the channel, using the fabric tools available in the cli container, and carry out end-to-end tests, to ensure the network and peers are up and running. Figure 3 contains the output of the step when a new user is getting created to kick off the processing.

Step 1: Create a new USER

Now we need to add our user to the sudo group. Switch to our newly created user:

Step 2: Install Prerequisites, Install Git, CURL, docker, docker-compose, Node.js, NPM, and Python.

Step 3: Install Hyperledger Fabric Binaries, Docker Containers, and Samples. You will find a new folder called fabric-samples inside your home folder.

Step 4: Test the sudo Installation: To ensure that everything is working properly, we'll run a pre-built script called "Build Your First Network or BYFN," which will check to see whether everything is installed properly. When installation test is successful, process will show connection successful message, same output can be seen in Fig. 4. Network execution test step has been captured in Fig. 5.

Check if all the docker containers are running:

Clean the network.

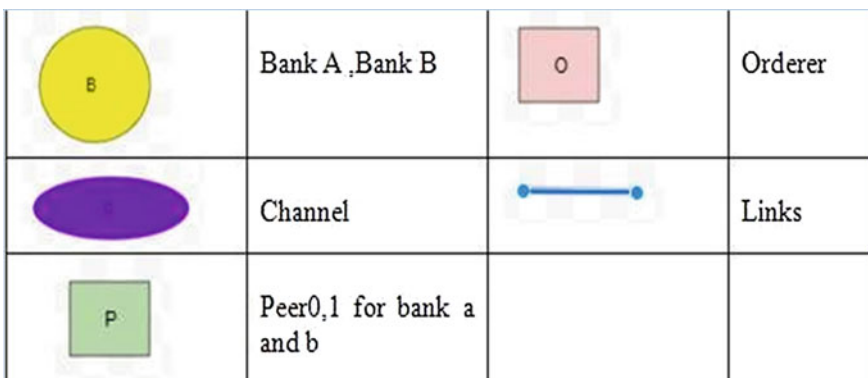


Fig. 2 Network components

```

New password:
Retype new password:
passwd: password updated successfully
Changing the user information for fabric
Enter the new value, or press ENTER for the default
  Full Name []: parveen mor
  Room Number []: 1234
  Work Phone []: 9958507588
  Home Phone []: 9716906800
  Other []: 123456
Is the information correct? [Y/n] y
blockchain@blockchain-VirtualBox:~$

```

Fig. 3 Creating user

```

START
Build your first network (BYFN) end-to-end test

Channel name : mychannel
Creating channel...
+ peer channel create -o orderer.example.com:7050 -c mychannel -f ./channel-art
ifacts/channel.tx --tls true --cafile /opt/gopath/src/github.com/hyperledger/fa
bric/peer/crypto/ordererOrganizations/example.com/orderers/orderer.example.com/
msp/tlscaerts/tlsca.example.com-cert.pem
+ res=0
+ set +x
2021-09-04 18:07:48.054 UTC [channelCmd] InitCmdFactory -> INFO 001 Endorser an
d orderer connections initialized
2021-09-04 18:07:48.313 UTC [cli.common] readBlock -> INFO 002 Received block:
0
===== Channel 'mychannel' created =====
Having all peers join the channel...
+ peer channel join -b mychannel.block
+ res=0
+ set +x
2021-09-04 18:07:48.658 UTC [channelCmd] InitCmdFactory -> INFO 001 Endorser an
d orderer connections initialized
Activate Windows

```

Fig. 4 Network installation test

```

2021-09-04 18:11:39.048 UTC [chaincodeCmd] checkchaincodeCmdParams -> INFO 002
Using default vscc
2021-09-04 18:11:48.239 UTC [chaincodeCmd] install -> INFO 003 Installed remote
ly responder<status:200 payload:"OK" >
===== Chaincode is installed on peer1.org2 =====
Querying chaincode on peer1.org2...
===== Querying on peer1.org2 on channel 'mychannel'... =====
Attempting to Query peer1.org2 ...3 secs
+ peer chaincode query -C mychannel -n mycc -c '{"Args":["query","a"]}'
+ res=0
+ set +x
90
===== Query successful on peer1.org2 on channel 'mychannel' ===
===== All GOOD, BYFN execution completed =====

END

```

Fig. 5 Network execution test completed

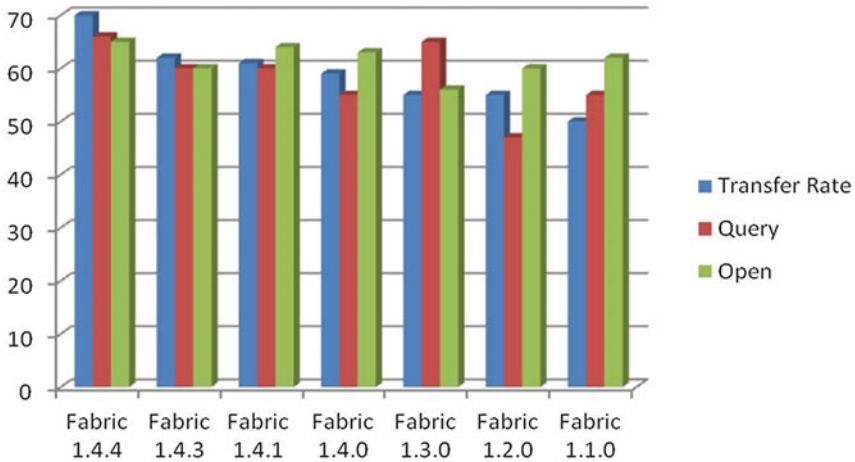


Fig. 6 Success rate of Hyperledger Fabric 1.4

Congratulations! Your machine’s Hyperledger Fabric network has now been successfully configured.

5 Outcomes and Discussions

5.1 Probability of Success

Figure 6 shows the number of successful transactions out of 200 that were initiated by the various functionalities in the smart contract of different Hyperledger Fabric versions. The success rate for the Transfer function in most Hyperledger Fabric SDK versions is less than 62%, with the exception of Fabric 1.4.4, which has a 71% success rate. Fabric 1.1.0, on the other hand, has the lowest success rate, with only 42 completed transactions out of 200. It can be seen that when the version of Hyperledger Fabric grows, the success rate of the Transfer function improves.

5.2 Average Response

Figure 7 depicts the average delay of each Blockchain SDK for e-commerce transactions. The average delay of each Blockchain SDK for executing the Open, Query, and Transfer functionalities is shown in Figure 8. All Blockchain platforms examined had the same average latency of 0.5 second for the Query function. For the Transfer

function, all Hyperledger Fabric SDKs outscored prior versions of fabric by a considerable margin, just as they did for the Open function. Fabric SDKs' average latency reduced from Fabric 1.3.0 to Fabric 1.4.0 and 1.4.1 but increased for Fabric 1.4.3 and 1.4.4.

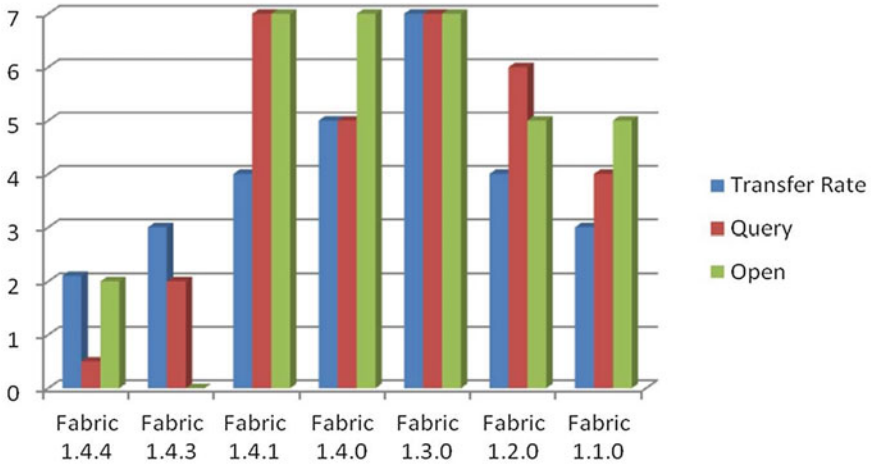


Fig. 7 Average response of all fabric

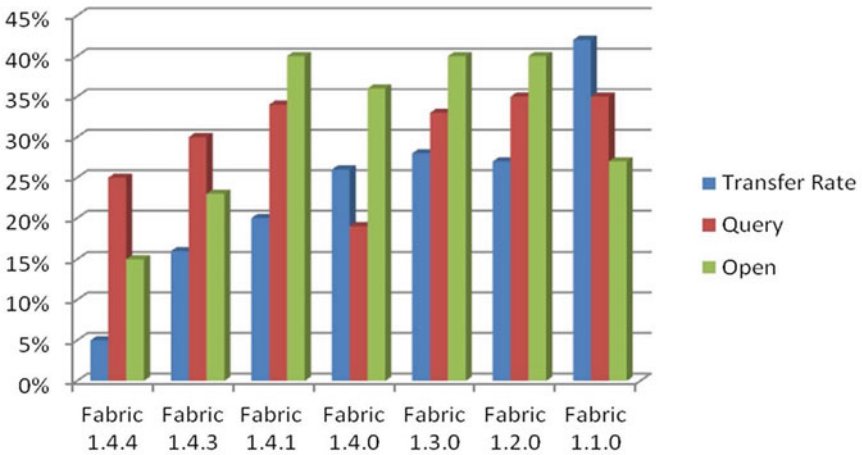


Fig. 8 CPU consumption of all Hyperledger Fabrics

5.3 *Average Latency of Hyperledger Fabric*

See Fig. 7.

5.4 *CPU Usage*

The average CPU consumption in % for each Blockchain platform when performing the Open, Query, and Transfer operations is shown in Fig. 8. Fabric 1.1.0 requires higher CPU processing power than all previous versions of Hyperledger Fabric, similar to the memory utilization findings. Although the difference between Fabric 1.2.0 and Fabric 1.3.0 is not significant in the Open function, Ethereum is found to demand a significant amount of CPU resources in the Query and Transfer functions.

6 Conclusion

The goal of the blockchain is to exchange data among all parties that have access to it via an application. The entry in this ledger can be unfettered (“permissionless”) or restricted (“permissioned”). The Hyperledger Fabric network set-up is necessary, according to the research, and the research proved that the Hyperledger Fabric network can be used to generate smart contracts since both Hyperledger and Ethereum are incredibly versatile, although they shine in different areas. Ethereum is a generic platform for any application because to its robust smart contract engine. It is, however, transparent and requires no clearance, which has an impact on performance scalability and security. Hyperledger uses a permissioned mode of operation with access control to address concerns regarding consistency, scalability, and privacy. The community of Fabric operators has grown since the first v1.0 release of Hyperledger Fabric. The Fabric team collaborated with network operators to provide v1.4.4 with an emphasis on stability and production operations. The following are the paper’s key study:

- (1) The current Hyperledger Fabric version has never been compared to any other blockchain platform.
- (2) Both Fabric v1.0 [7] and Fabric v1.4.4 have flaws and new measurement features have been added to the open-source performance evaluation tool.
- (3) The impact of system factors (e.g., number of transactions, node type) on performance, especially scalability, was investigated first.
- (4) The outcomes of this study will assist the corporate community in selecting the best blockchain platform for their requirements. The programming approach for developing apps has been enhanced as a result of this version.
- (5) The Hyperledger Fabric network’s functioning is also defined here. The work of the Hyperledger Fabric network is evaluated in this study.

In the future, academics can look at how blockchain technology can be used to various use cases and data scenarios in a range of industries, including as banking, health care, retail, and telecommunications. This network arrangement can handle more than 5000 transactions simultaneously. This article compares standard financial sector methodologies against the Hyperledger Fabric network to discover which is better for creating smart contracts in terms of performance and scalability.

References

1. Ensor A, Schefer-Wenzl S, Miladinovic I (2018) Blockchains for IoT payments: a survey. In: 2018 IEEE Globecom workshops (GC Wkshps), 9–13 Dec. 2018
2. Ekbote B, Hire V, Mahajan P, Sisodia J (2017) Blockchain based remittances and mining using CUDA. In: IEEE international conference on smart technology for smart nation
3. Li D, W Eric Wong, Chau M, Pan S, Seng Koh L (2020) A survey of mobile NFC payment: challenges and solution using blockchain cryptocurrencies. In: 7th international conference on dependable systems and their applications (DSA). IEEE
4. Akanfe O, Valecha R, Raghav Rao H (2020) Design of a compliance index for privacy policies: a study of mobile wallet and remittance services. In: IEEE transactions on engineering management, page 1–13, 16 September 2020
5. Dashkevich N (2020) Steve counsel, and Giuseppe Destefa. In: Blockchain application for central banks: a systematic mapping study, July 27, 2020
6. Desai H, Kantarcioglu M, Kagal L (2019) Hybrid blockchain architecture for privacy-enabled and accountable auctions. In: 2019 IEEE international conference on block-chain (Blockchain), 14–17 July 2019
7. Popova NA, Butakova NG (2019) Research of a possibility of using blockchain technology without tokens to protect banking transactions. In: 2019 IEEE conference of Russian Young researchers in electrical and electronic engineering (EIConRus), Jan. 2019
8. Sakho S, Jianbiao Z, Essaf F, Badiss K (2020) Improving banking trans- actions using blockchain technology. In: 2019 IEEE 5th international conference on computer and communications, 13 April 2020
9. Sood A, Simon R (2019) Implementation of blockchain in cross border money transfer. In: 2019 4th international conference on information systems and computer networks (ISCON) GLA University, Mathura, UP, India. Nov 21–22, 2019
10. Ricci P, Mammanco V (2019) RemBit: a blockchain based solution for remit- tances to Ethiopia. In: 2019 IEEE symposium on computers and communications (ISCC), July 2019
11. Norta A, Leiding B, Lane A (2019) Lowering financial inclusion barriers with a blockchain-based capital transfer system. In: IEEE INFOCOM 2019—IEEE conference on computer communications workshops (INFOCOM WKSHPs), September 2019
12. Awan KM, Yamin MM, ur Rehman Z, Shah PA (2017) Implementation of information security techniques on modern android based Kiosk ATM/Remittance Machines. In: 2017 international conference on information and communication technologies (ICICT), Dec. 2017.
13. Ali M et al (2016) Blockstack: a global naming and storage system secured by block-chains. USENIX annual technical conference
14. Mills D, Wang K, Malone B (2016) Distributed ledger technology in payments, clearing, and settlement, Series 2016-095. Washington: Board of Governors of the Federal Reserve System, 2016
15. Jones KL (2019) Blockchain: building consensus and trust across the space sector. In: 35th space symposium, technical Track, Colorado Springs, Colorado, United States of America Presented on April 8, 2019

16. Lindman J, Tuunainen MRVK (2017) Opportunities and risks of blockchain technologies in payments—a research agenda. In: 2017, Hawaii international conference on system sciences
17. Achanta R (2018) Cross-border money transfer using blockchain—enabled by big data. White paper Published by Infosys in 2018.
18. Campbell-Verduyn M (2018) Bitcoin, crypto-coins, and global anti-money laundering governance. Springer
19. Zichichi M et al (2020) A distributed ledger based infrastructure for smart transportation system and social good. In: 2020 IEEE 17th annual consumer communications & networking conference (CCNC)
20. Adulla M (Reddy et al., White paper: hyperledger blockchain performance metrics, V1.01 published October 2018)
21. Castro M, Liskov B (1999) Practical Byzantine fault tolerance. In: Proceedings of the 3rd symposium on operating systems design and implementation (OSDI '99). pp 173–186
22. Cachin C (2016) Architecture of the hyperledger blockchain fabric. IBM Res
23. Androulaki E et al (2017) Cryptography and protocols in hyperledger fabric. In: Real-world cryptography conference

Distribution System Operation with Minimum Topological Variations



Praveen Agrawal, Neeraj Kanwar, Nikhil Gupta, K. R. Niazi,
and Anil Swarnkar

Abstract Distribution network reconfiguration (DNR) is a well-established operational strategy for distribution systems to improve its performance. Also, several social and techno-economic objectives can also be effectively achieved in contemporary distribution systems by optimally placing distributed resources (DRs). However, with integration of DR, distribution system becomes active distribution systems and it has dynamically changing nature of load and generation. Therefore, it is important to reinvestigate the effectiveness of existing NR strategy. In this paper, a new NR strategy is suggested for power loss minimization where the network topology varied only once during a day. An investigation is carried about existing and proposed reconfiguration strategies while considering some realistic scenarios pertaining to contemporary distribution systems. The application results are shown on 33-bus test distribution system.

Keywords Distributed resources · Network reconfiguration · Smart grid

1 Introduction

In the present scenario, the distribution systems are taking new shapes by utilization of diverse distributed resources (DRs), automation in switching and other related control schemes, etc. On the other hand, the system performance is the biggest challenge in present competitive and deregulated environment. However, topological structure regulation of distribution networks can provide better electric power and more benefit to electric power companies [1]. This process is known as network reconfiguration (NR). However, the benefits of NR may be substantially reduced in the presence of optimally placed DRs as they can also effectively manage power

P. Agrawal · N. Gupta · K. R. Niazi · A. Swarnkar
Department of Electrical Engineering, Malaviya National Institute of Technology, Jaipur, India

N. Kanwar (✉)
Department of Electrical Engineering, Manipal University Jaipur, Jaipur, India
e-mail: nk12.mnit@gmail.com

flow among distribution feeders. In this context, distribution network operators (DNOs) may face great relief if distribution network topology is allowed to change for specific operating state(s) using remote controlled switches (RCSs). But the task becomes challenging with variable load demand and uncertain power generation from renewable energy sources (RESs). Nevertheless, distribution networks cannot be reconfigured frequently for each varying system state due to involved switching cost, probable switching transients, etc. This naturally urges to reinvestigate the NR strategy for contemporary distribution systems and to develop suitable reconfiguration strategy that minimizes topological variations yet preserves adequate performance of distribution systems.

NR was first proposed by Merlin and Back [2]. After that enormous research work has been done to solve optimal NR problem of passive distribution systems by addressing a variety of one or more objectives. Later, the widespread integration of DRs makes distribution systems active and this leads to new dimensions while addressing NR problem. Several researchers proposed optimal allocation of distributed generation (DG) units, e.g., while considering NR [3] or solved the optimal NR problem in the presence of DRs [4]. However, variability in load and uncertainty in power generation were not considered.

Optimally placed DRs and NR both manages power flow among distribution feeders in different ways [5], the fixed configuration strategy may be preferred over the conventional network reconfiguration (CNR) strategies. References [6, 7] envisage fixed topology operation for different time spans but remain silent about the amount of loss reduction achieved using proposed strategy. In [8], the hourly reconfiguration was evaluated assuming DGs as the source of constant power, but load variability was not considered. The decentralized approach is suggested in Ref. [9]. Jabr [10] proposed a coordinated approach for fixed configuration with capacitor switching and PV inverter control over a period of 8 h to avoid frequent switching actions. Some interesting real-time NR strategies are suggested in [11, 12].

In day-ahead reconfiguration, DNO decides the best strategy of network before a day whereas in real-time reconfiguration the DNO does this task using RCSs to achieve techno-economic objectives. However, it would be better if the offline reconfiguration is adopted for normal operation and online reconfiguration for emergency operation of active distribution systems. While considering normal system of contemporary distribution systems, the enhancement in energy efficiency and node voltage profile via NR may lose relevance as optimally placed diverse DRs can do this more effectively. With this concern, the distribution system operation with fixed topology throughout a day seems to be an interesting alternative NR strategy. The strategy can greatly relieve DNOs on account of prospective switching transients, cost of switching operations, and the ease in system operation. Such a simplified NR strategy is yet not been explored and investigated to the best of authors' knowledge. Optimal NR problem is characterized as a non-linear with hard complex and combinatorial nature. Population-based heuristic algorithms have great potential to solve such complex problems.

In this paper, a new NR strategy, called fixed network topology (FNT) strategy, is proposed for contemporary distribution systems that is not varied throughout the

day. A more realistic formulation of problem is done with variable load demand. The variability in load demand is assumed to happen due to different categories of customers. Power generation from renewable DGs is also having intermittent nature. Both load and power generation from DRs are modeled using deterministic uncertainty sets [13]. The complex combinatorial NR problem is solved using a new variant of CSO, i.e., ICSO [14]. Simulation results are obtained on a standard test distribution system.

2 Problem Formulation

The distribution networks cannot be repeatedly reconfigured with each varying system states in the view of excessive line switching cost, life span of line switches, prospective switching transients, and dangerous over voltages. The later become crucial in the presence of renewable DGs and shunt capacitors. The conventional hourly reconfiguration causes greatest loss reduction; therefore, a fixed network topology (FNT) may be preferred to avoid the problems of overvoltage transient and frequent switching operations cost. Therefore, FNT is suggested to operate the distribution system in a fixed topology that pertains throughout a day. The strategy may relieve DNOs to great extent as it not only reduces complexity of system operation but also provides minimum switching operations and associated techno-economic benefits. In proposed reconfiguration strategy, the synthetic data are generated for load and renewable generation for the next 24 h and based on which an optimal radial topology is explored for the forthcoming day.

One of the major differences between transmission and distribution systems is that distribution systems usually provide committed feeders to various categories of customers [15]. Each customer possesses its different load profile, also a definite variety in load demand exists among distribution buses. Residential, industrial, and commercial feeders are denoted by r , i , and c , respectively. The objective function for the CNR strategy can be formulated as follows:

$$\begin{aligned} \min . P_{\text{Loss}}^{st} = & \sum_{r=1}^{N_r} R_r \frac{P_{r,st}^2 + Q_{r,st}^2}{|V_{r,st}|^2} + \sum_{i=1}^{N_i} R_i \frac{P_{i,st}^2 + Q_{i,st}^2}{|V_{i,st}|^2} + \\ & \sum_{c=1}^{N_c} R_c \frac{P_{c,st}^2 + Q_{c,st}^2}{|V_{c,st}|^2} \end{aligned} \quad (1)$$

where $P_{r,st}$, $P_{i,st}$, $P_{c,st}$ are active power flow in kW; $Q_{r,st}$, $Q_{i,st}$, $Q_{c,st}$ are reactive power flow in kVAR; and $V_{r,st}$, $V_{i,st}$, $V_{c,st}$ are voltage at different feeders in per unit. N_r , N_i , N_c are sets of nodes and R_r , R_i , R_c are line resistances in ohms.

However, for FNT strategy, considering all the system states of a typical day the objective function is formulated as given by (2).

$$\min . E_{\text{Loss}} = \sum_{st=1}^{\text{ND}} P_{\text{Loss}}^{st} \cdot T^{st} \quad (2)$$

where ND are total system states considered for the typical day. E_{Loss} is energy loss in kW h during the day and P_{Loss}^{st} shows real power loss at st state in kW. T^{st} is load duration for each state st .

Objective functions framed for CNR and FNT are solved while satisfying following network operational constraints besides power flow constraints:

$$V_{\text{mn}} \leq V_{r,st} \leq V_{\text{mx}}; \forall r \in N_r, \forall st \in ND \quad (3)$$

$$I_{n,st} \leq I_n^{\text{max}}; \forall n \in N \quad (4)$$

$$\Phi_{st}(k) = 0 \quad (5)$$

Variable nature of load demand and power generation is dealt with recently developed deterministic polyhedral uncertainty sets [13]. A self-adaptive deterministic uncertainty set is generated in this method. These sets require only historical data of generation and load for a year.

3 Results

The simulation results are obtained on a 33-bus test distribution system [16]. Before simulations, the system is modified by considering load diversity and assuming integrated DRs with system. The distribution system is assumed with dedicated residential (R), industrial (I), and commercial (C) customers being fed through the set of nodes 1–15, 22–29, and 16–21 and 30–33, respectively, as given in [13]. The forecasted load factors for each of the system state prevailing for 1 hour and considered for a typical day. Further, wind turbines (WTs), solar photo-voltaic (SPVs), micro-turbines (MTs), and shunt capacitors (SCs) are assumed to be present in the system. The sizing and siting of these DRs are referred from [17] as shown in Table 1.

Existing and proposed methods of NR are compared by analyzing the following four different cases:

- Case-1: System is reconfigured without diverse load and with renewable DGs.
- Case-2: System is reconfigured without diverse load but considering DGs with fixed capacity.
- Case-3: System is reconfigured with diverse load and renewable DGs.
- Case-4: System is reconfigured with diverse load and DGs with fixed capacity.

In Case-1 and Case-3, distributed storages of adequate capacity and control strategies are assumed to be connected in the distribution system. Therefore, fixed

Table 1 Sizing and siting of DRs considered

		Node 12	Node 14	Node 24	Node 25	Node 30
SPV	Capacity (kWp)	–	280	840	–	560
	Fixed power (kW)	–	110	300	–	200
WT	Capacity (kWp)	–	420	700	–	420
	Fixed power (kW)	–	220	360	–	220
MT (kW)		–	–	800	–	–
SC (kVAr)		300	–	–	300	600

power dispatches (FPDs) can be obtained from renewable DGs. However, the power dispatches from MTs and SCs are considered same as their respective capacities for simplicity. While ignoring load diversity in Case-1 and Case-2, for each bus the load factor is reserved as the average of the load factors for different types of buses considered. This nullifies the impact of load diversity and provides same daily load profiles of the system. This is important to get valid comparison results.

Reconfiguration of distribution network is done for each case to optimize the power losses. CNR and FNT strategies are applied considering a sample day. The system is optimally reconfigured for each individual state in CNR strategy. Whereas all states are simultaneously optimized using proposed FNT strategy. The best result is obtained for these two strategies after 100 independent trials of Improved CSO (ICSO). The results obtained for Case-1 using CNR strategy are presented in Fig. 1 and compared with base case. Topology obtained at each state using CNR strategy is shown in Table 2 for Case-1.

Total losses obtained at base case are 2621.34 kW that have been reduced to 576.37 kW before reconfiguration and 394.33 kW after reconfiguration, respectively. Also total 84 switching operations are required using this strategy. By opening 7, 8, 9, 25, and 16 lines, optimal network topology by FNT is obtained. With this fixed topology, daily energy losses are found to be 426.11 kWh. The switching operations required for this topology are only 4 while compared with the optimal topology of the state 24 of Table 2, i.e., 5, 7, 9, 16, 33, i.e., FNT requires closing of switches 8 and 25 and opening of switches 5 and 33. Proposed NR strategy drastically reduces switching operations for this scenario but at slightly increased power losses.

Similar results are obtained for other cases. The results are briefly described in Tables 3 and 4. The tables show energy loss in kWh (A), reduction in energy loss in kWh (B), percentage reduction in energy loss (C), minimum node voltage in p.u. (D), and total switching operations (E) required for a typical day. The effect of load variety, different type of DG, and the comparison of both strategies upon these parameters now can be inferred. It can be seen from Table 3 that the consideration of intermittency in DG power generation results in more than double switching operations, i.e., from 84 to 40 and 90 to 36. However, the effect of considering load diversity is not so visual. The table also shows that if load diversity is considered, the power losses are reduced, i.e., from 394.33 kW to 351.77 kW and 318.54 kW to 283.26 kW. Similarly, reduced power losses can be achieved using fixed power generation from

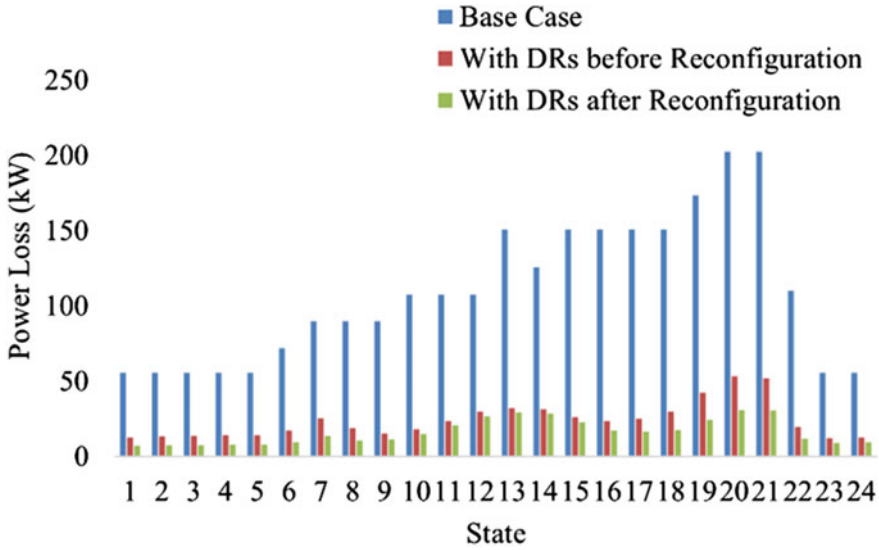


Fig. 1 Results obtained using CNR strategy for Case-1

Table 2 Topology obtained at each state using CNR strategy for Case-1

State	Topology	State	Topology
1	2, 8, 17, 25, 34	13	5, 7, 9, 16, 21
2	8, 17, 25, 33, 34	14	5, 9, 16, 20, 33
3	8, 17, 25, 33, 34	15	7, 9, 21, 25, 29
4	8, 16, 25, 33, 34	16	8, 9, 25, 33, 35
5	8, 17, 25, 33, 34	17	8, 17, 25, 33, 34
6	8, 17, 25, 33, 34	18	7, 8, 17, 27, 34
7	7, 9, 22, 28, 34	19	7, 9, 17, 28, 34
8	8, 17, 25, 33, 34	20	7, 9, 17, 28, 34
9	16, 25, 33, 34, 35	21	7, 9, 17, 28, 34
10	9, 21, 25, 29, 33	22	7, 8, 17, 26, 34
11	5, 9, 16, 21, 33	23	5, 7, 9, 16, 33
12	5, 9, 16, 20, 33	24	5, 7, 9, 16, 33

Switching operations required in total = 84

DGs, i.e., from 394.33 kW to 318.54 kW and 351.77 kW to 283.26 kW. But this loss reduction is more pronounced than the former one. Similar inference can be drawn from Table 4 where FNT strategy is employed except the fact that there is not much variation in the total number of switching operations among all scenarios. However, total switching operations are found to be reduced drastically whereas losses are slightly increased using FNT strategy while compared with Table 3. Similarly, node

voltages not affected much using these two different NR strategies. This is found to be true for all cases.

Finally, Table 5 compares these two strategies over different cases by taking difference of corresponding results from Tables 4 to 3. It can be seen that proposed topology strategy causes insignificant increment in loss reduction without any measurable change in node voltage profile while considering all cases. However, proposed method seems to be very promising while considering switching operations, specifically under uncertain power generation cases, i.e., Case-1 and Case-3.

FNT strategy suggests fixed radial topology of distribution network throughout the day which is very attractive for DNOs as it reduces complexity of system operation, prospective transients, and overvoltages, and offers increased life span of switchgears. Large-scale integration of DGs and SCs or other similar devices in distribution systems may originate overvoltages in secondary distribution systems which would be very serious phenomenon. With these concerns, conventional NR may not be preferred whereas other day-ahead reconfiguration strategies, having multiple topologies during a day, may not remain attractive means for DNOs. In this context, FNT strategy, which suggests fixed topology, seems to be promising on account of safe and simplified operation of distribution systems.

Table 3 Results for CNR strategy for different cases

Particular	Case-1	Case-2	Case-3	Case-4
Load diversity	Not taken	Not taken	Taken	Taken
DG power	Intermittent	Fixed	Intermittent	Fixed
A	394.33	318.54	351.77	283.26
B	182.04	171.54	131.66	127.03
C	31.58	35.00	27.23	30.96
D	0.9744	0.9755	0.9744	0.9755
E	84	40	90	36

Table 4 Results for FNT strategy for different cases

Particular	Case-1	Case-2	Case-3	Case-4
Load diversity	Not taken	Not taken	Taken	Taken
DG power	Intermittent	Fixed	Intermittent	Fixed
A	426.11	332.9	383.74	297.58
B	150.26	157.99	99.69	112.71
C	26.07	32.24	20.62	27.47
D	0.9667	0.9727	0.9701	0.9727
E	2	4	2	4

Table 5 Results for comparison of CNR and FNT strategies

Cases	Daily energy loss (kWh)	Daily energy loss reduction (%)	V_{mn} (p.u.)	Switching operations required daily
Case-1	31.78	-5.51	-0.0077	-82
Case-2	13.55	-2.76	-0.0028	-36
Case-3	31.97	-6.61	-0.0043	-88
Case-4	14.32	-3.49	-0.0028	-32

4 Conclusions

The paper highlights the importance of fixed topology operation of contemporary distribution systems by proposing a new NR strategy, called FNT strategy, considering variability in load demand and uncertain renewable power generation. The complex NR problem is solved for loss minimization using a newly suggested variant of CSO, i.e., ICSO. Detailed simulation results reveal that a noticeable fall in switching operation of line switches may be achieved using FNT strategy but with a trivial increased energy losses and without much affecting node voltage profiles. In this context, proposed NR strategy seems to be a simple, effective, and promising tool for DNOs. The decision must be taken by DNO while selecting fixed topology operation pertaining to other operational complexities of active distribution systems. This may lead to paradigm shift in reconfiguration of contemporary distribution systems that are generally operated under dynamically varying system states.

References

1. Chen S, Hu W, Chen Z (2016) Comprehensive cost minimization in distribution networks using segmented-time feeder reconfiguration and reactive power control of distributed generators. *IEEE Trans Power Syst* 31(2):983–993
2. Merlin A, Back H (1975) Search for a minimum-loss operating spanning tree configuration in an urban power distribution. In: *Proc. 5th power syst. comput. conf.*, Cambridge, UK. pp 1–18
3. Rao RS, Ravindra K, Satish K et al (2013) Power loss minimization in distribution system using network reconfiguration in the presence of distributed generation. *IEEE Trans Power Syst* 28(1):317–325
4. Kanwar N, Gupta N, Niazi KR, et al (2017) Optimal allocation of DGs and reconfiguration of radial distribution systems using an intelligent search based TLBO. *Electr Power Compon Syst*, Taylor & Francis 45(5):476–490
5. Kanwar N, Gupta N, Niazi KR, et al (2015) 'Improved meta-heuristic techniques for simultaneous capacitor and DG allocation in radial distribution networks. *Int J Electr Power Energy Syst* 73:653–664
6. Bueno EA, Lyra C, Cavellucci C (2004) Distribution network reconfiguration for loss reduction with variable demands. In: *Proc. IEEE/PES T&D Latin America*, São Paulo, Brazil. pp 384–389
7. Queiroz LMO, Lyra C (2009) Adaptive hybrid genetic algorithm for technical loss reduction in distribution network under variable demands. *IEEE Trans Power Syst* 24(1):445–453

8. Zidan A, El-Saaddany EF (2012) Network reconfiguration in balanced and unbalanced distribution systems with variable load demand for loss reduction and service restoration. In: Proc. IEEE power and energy soc. gen. meet., San Diego, CA, USA
9. Ding F, Loparo KA (2015) Hierarchical decentralized network reconfiguration for smart distribution systems—Part II: applications to test systems. *IEEE Trans Power Syst* 30(2):744–752
10. Jabr RA (2014) Minimum loss operation of distribution networks with photovoltaic generation. *IET Renew Power Gen* 8(1):33–44
11. Capitanescu F, Ochoa LF, Margossian H et al (2015) Assessing the potential of network reconfiguration to improve distributed generation hosting capacity in active distribution systems. *IEEE Trans Power Syst* 30(1):346–356
12. Alemohammad SH, Mashhour E, Saniei M (2015) A market-based method for reconfiguration of distribution network. *Electr Power Syst Res* 125:15–22
13. Kanwar N, Gupta N, Niazi KR et al (2018) Optimal distributed resource planning for microgrids under uncertain environment. *IET Renew Power Gener* 12(2):244–251
14. Kanwar N, Gupta N, Niazi KR, et al (2015) Improved cat swarm optimization for simultaneous allocation of DSTATCOM and DGs in distribution systems. *J Renew Energy, Hindawi*, 1–10
15. Kanwar N, Gupta N, Niazi KR, et al (2015) Optimal distributed generation allocation in radial distribution systems considering customer-wise dedicated feeders and load patterns. *J Mod Power Clean Energy* 3(4):475–484
16. Baran ME, Wu F (1989) Network reconfiguration in distribution system for loss reduction and load balancing. *IEEE Trans Power Deliv* 4(2):1401–1407
17. Kumar P, Gupta N, Niazi KR et al (2016) Prospectives of day-ahead network reconfiguration for smart distribution systems considering load diversity. *Int J Electr Energy* 4(3):184–188

A Combined DG Integration-Network Reconfiguration-Based Method for Network Loss Minimization and Voltage Profile Improvement



Deepak Porwal , Manoj Fozdar (SMIEEE), and Rajive Tiwari

Abstract Distribution system operators (DSOs) are opting network reconfiguration as a simple and cost-effective way of reducing network losses and avoiding the islanding effect occurring due to line outages. The continuously increasing integration of distributed generators has posed Volt-VAr optimization as major concern. This paper focuses on optimal network losses and bus voltage enhancement by network reconfiguration in DG-embedded system. The voltage stability indices are used to accommodate the DG at appropriate location. This practice is performed in MATLAB and validated on IEEE 33-bus distribution system. The proposed study finds the reduced network losses, improved supply reliability, and better voltage profile.

Keywords Voltage profile improvement · Network loss minimization · Network reconfiguration

1 Introduction

Climate change is being notably experienced by several countries worldwide. Increasing power demand and rising network complexity have put serious challenges for existing power generation as well as transmission systems. These all have collectively led to increased investment and adoption of renewable-based clean and green energy sources. Renewable sources are comparatively low-power, low-voltage devices and can be integrated at distribution or local consumer level. Hence avoids the cost associated with heavy transmission losses which otherwise would have occurred.

With the presence of distributed generators (DGs), energy market is shifting from centralized single entity to decentralized and distributed market enabled with several other ancillary services [1, 2]. DGs provide local reliable power, contribute to reactive

D. Porwal (✉) · M. Fozdar (SMIEEE) · R. Tiwari
Department of Electrical Engineering, Malaviya National Institute of Technology, Jaipur,
Rajasthan 302017, India
e-mail: deepakporwal1512@gmail.com

power compensation, and hence remove the need of spinning reserves and compensating devices. On the other hand, excessive DGs presence have raised over-voltage and power quality issues in distribution system. This has also started slowly reflecting in transmission side [3]. Authors in [4] discussed solar-based DG affecting line losses and voltage profile.

Integrating DGs in the system have high capital and maintenance cost. So, locating suitable site and placing appropriate DGs' size are highly important. Atwa et al. [5–7] proposed various techniques for DGs placement to reduce network losses and maintain its stability. In [8], researchers optimally placed discrete capacity small generators by using Genetic Algorithm. El-Khaltam et al. [9] formulated an objective function for optimal DG sizing and siting considering the financial aspects of it. A multi-DG optimal placement problem was discussed using genetic algorithm in [10].

Optimal Volt-Var control is another major challenge in such systems. Volt-Var optimization in DG-integrated system reduces peak-load intervals and minimizes energy losses. For Volt-Var control, optimal size and location of DGs and FACTS devices are used for losses reduction, cost reduction, and voltage profile enhancement [11–14]. Several different devices like DGs, voltage boosters, and switched shunt are compared for voltage regulation in [15–18]. Schmitt et al. [19–21] discussed Volt-Var optimization by simultaneous implementation of DGs (wind- and solar-powered plants), shunt capacitor, and voltage regulator at appropriate locations. Vita et al. [22] presented a new algorithm for distributed generators' optimum utilization by using decision-making approach. Reddy et al. [23] suggested a new technique of PSO for DG siting and sizing that results in improved reliability and enhanced power quality. Devalalaji et al. [24] used DGs along with D-STATCOMs for overall reduction in losses and maintain network stability. Di Silvestre et al. [25] achieved improved efficiency in an islanded distribution system by energy loss reduction.

Distribution network reconfiguration plays an important role in total loss reduction while keeping the operating and system constraints within limits. Network reconfiguration provides cost-effective and easy-to-implement solution over above techniques. A variety of reconfiguration strategies were proposed for power loss reduction and each method had their respective merits and demerits. Reconfiguration implementation on real-time distribution system was observed by applying a genetic algorithm-based method for loss minimization [26]. The results obtained reduced the computation and convergence time, minimized power losses that were better compared to traditional GA. In [27], a heuristic method utilized optimization technique for distribution network reconfiguration and achieved resistive loss minimization. Ye and Wang [28] presented a Refined Plant Growth Algorithm (PGSA) for reconfiguring the distribution system. Sathish Kumar and Jayabarathi [29] used a bacterial foraging algorithm-based technique for reconfiguring the network to minimize power losses. Authors of [30–32] utilized network reconfiguration technique for improving system performance. Some researchers determined only DG capacity and its positioning for power loss reduction without taking into account the network reconfiguration. While some other focused only on reconfiguration part but ignored DG sizing and siting for power loss optimization. Later, authors of [33–35] used both reconfiguration and

DG optimization technique to determine optimal power losses. But, both parts were handled separately.

A combined reconfiguration and DG unit allocation-based method can help in achieving optimal power losses in the distribution system. The thought was to operate reconfiguration process simultaneously with distributed generation optimization to reduce power losses and finding the optimal location of DG for a fixed penetration level. In [36], the researcher achieved best setting simultaneously for optimal reconfiguration and optimizing DG size to mitigate the distribution problem. But the voltage profile improvement is not discussed while reducing line power losses. This paper uses both DG installation and reconfiguration aiming to achieve optimal power losses and improved voltage profile together. This helps to minimize investment and operation-related costs along with reducing energy losses.

2 System Description

Standard IEEE 33-bus test system employed at distribution level is taken in this paper. It has 33 nodes as buses and 32 lines as branches fed by a main substation at node 1. For base voltage 12.66 kV and for base MVA 100MVA are considered. While total active and reactive load of 3715 kW and 2300kVAR are taken, respectively. Aforesaid system is developed in MATLAB software and depicted in Fig. 1.

Here, dotted lines shown in system are tie-line switches. These are five in number and present between node pairs 18–33, 12–22, 8–21, 25–29, and 9–15. They are Normally Open (NO) type and close their contacts when operated. Radial topology distribution system can be transformed into a meshed network with the help of these switches.

The system data (line and load data) is taken from [36].

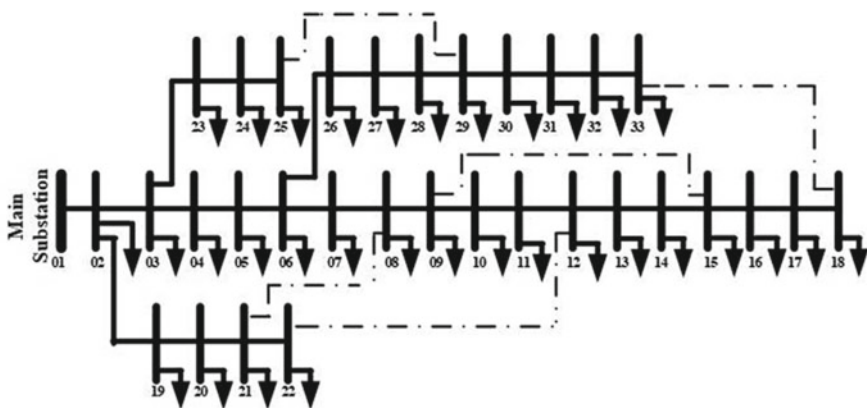


Fig. 1 IEEE 33-bus test distribution system

3 Proposed Methodology

This paper simulates the above-mentioned radial nature distribution system and analyzes the impacts of simultaneous application of DG and network reconfiguration. System is tested first for without DG case. Most critical buses are identified by performing the load flow. The buses are prioritized as per index value of their voltage stability. Then, the DG placement and network reconfiguration procedure is performed as.

1. DGs act as voltage regulation device at point of common coupling by providing local power fulfillment. The total losses (active and reactive both) are recorded, and the voltage at buses aimed to maintain close to $1pu$.

2. Network reconfiguration is attained by operating the tie-line switches. This helps to reduce the islanding effect and increase supply reliability with reduced losses.

3. System radial nature is maintained by opening specific branches which further leads to lower the losses without affecting the feeder loads.

3.1 Voltage Stability Assessment

Voltage stability is important in monitoring stability of entire power system and its security. Sudden load fluctuation, tripping of transmission lines/generators, and malfunction of on-load tap changing transformers lead to voltage instability. Some of the most commonly used methods to counter voltage instability are

- Placing distributed generation units at weak buses.
- Placing switched shunt capacitors at load end nodes.
- Placing FACTS devices in voltage regulation mode at appropriate locations.
- Load shedding of non-essential loads.

The voltage stability indices (VSI) is used in determining the weak lines and buses. This indice is useful in evaluating critical buses, placement of DGs, capacitors, and FACTS devices for voltage enhancement. VSI of a line is calculated as per Eq. 1.

$$VSI_{ij} = \frac{4 \times Z_{ij}^2 \times Q_j}{V_i^2 \times X_{ij}}$$

where X_{ij} , Z_{ij} are the line reactance and impedance, respectively. Q_j and V_i are receiving node reactive load and sending node voltage, respectively.

The VSI_{ij} is calculated for each line in the system. As seen in Eq. 1, it is directly related to the reactive power loading of individual buses. VSI ranges from 0 to 1. The lines with VSI closer to 1 are reaching toward instability. Lines 7–8, 23–24, 24–25, 28–29, 29–30, and 30–31 have higher VSI values as shown in Table 1.

Table 1 Lines with higher voltage stability indices

S. no.	From bus	To bus	VSI
1	7	8	0.824
2	23	24	0.781
3	24	25	0.874
4	28	29	0.403
5	29	30	0.899
6	30	31	0.344

It is clear that end nodes of these lines are susceptible to voltage collapse. So, buses 7, 8, 23, 24, 25, 29, 30, and 31 are candid locations for DG placement. The DG is placed at these buses and voltage profiles are analyzed.

3.2 DG Placement at Candidate Location

DGs are gaining more popularity in terms of controllability with advanced power electronics. DG placement at the most critical buses becomes important for voltage profile improvement. So, the DG is placed at the above candidate locations with fixed penetration and the voltage profiles obtained are depicted in Fig. 2.

Placement of DG at these buses also reduces total losses (active and reactive both). Total line losses for various DG locations are shown in Fig. 3.

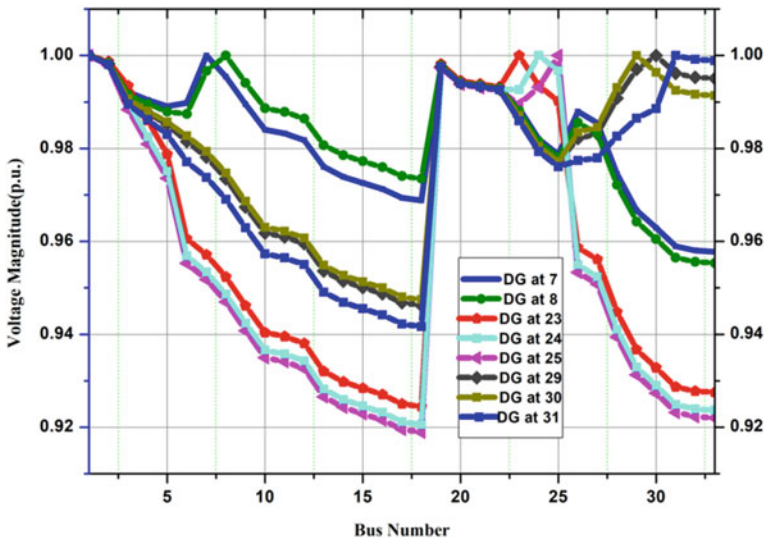


Fig. 2 Bus voltage profiles for DG penetration at various locations

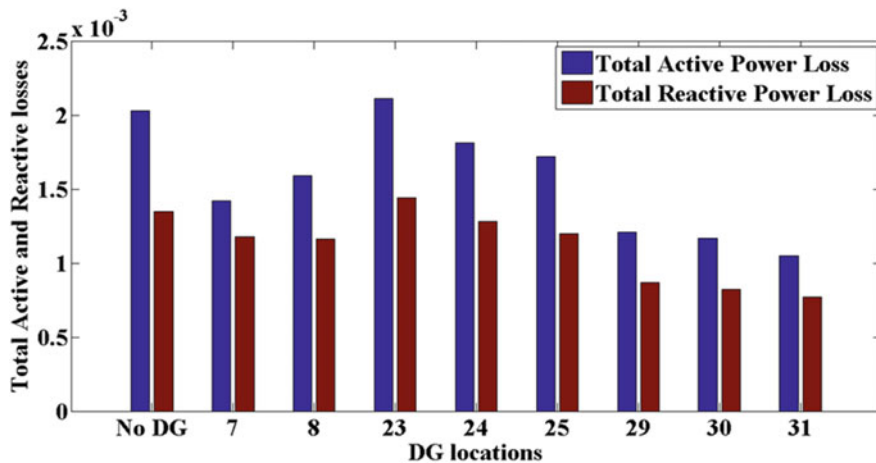


Fig. 3 Total line losses in absence and presence of DG

Figure 3 shows that total losses are less in comparison to without DG case. DG placement helps to fulfill local power demand, and hence reduces the line stress by reducing the line flow. Thus, significant reduction is achieved in total active and reactive line losses. DG placement at buses 29, 30 and 31 gives the minimum line losses. While DG placement at bus 7 or bus 8 gives better voltage profile. So, case with improved voltage profile and optimal line losses is chosen. It is observed that bus 29 is the most suitable location for DG installation. It keeps the bus voltages close to $0.95p.u.$ and overall line losses are less than DG at other buses. DG penetration of 20 percent of overall load demand (MVA) is taken for the case study at bus 29.

3.3 Network Reconfiguration

The network reconfiguration is performed to avoid any service disruption. The opening of any circuit breaker may cause the corresponding line to open. Thus, the tie-line switches are provided to convert the radial system into a meshed one. They can be closed in the event of any line failure to maintain the supply continuity to all network loads.

With DG integrated at bus 29, now the network reconfiguration is applied to check the outage event and total line losses. Firstly, the tie-line switch with their end nodes having maximum voltage difference is identified, the switch is then closed. The voltage differences calculated between tie-line switch end nodes are given in Table 2.

Table 2 clearly shows that voltage difference across tie-line switch 36 is maximum, so it is closed. The total kW (active) and kVAr (reactive) losses obtained are 0.00131 pu and 0.00093 pu. Among the corresponding node pair 18–33, node 18 is at

Table 2 Voltage difference between tie-line switch nodes

Tie-line switch	From bus	To bus	Voltage difference
33	21	8	0.01875
34	9	15	0.01732
35	12	22	0.03204
36	18	33	0.04392
37	25	29	0.02277

minimum voltage 0.94748 pu. So, the adjacent line 17–18 is opened to maintain the network radial. With the opening of line 17–18, kW (active) and kVAr (reactive) losses are obtained as 0.00122 pu and 0.00087 pu, respectively. Further, the line 16–17 is checked for opening, keeping the 17–18 closed. The kW and kVAr losses obtained are 0.00123 pu and 0.00088 pu, respectively. As the losses obtained in opening 17–18 are less compared to 16–17, so the line 17–18 is chosen for opening and maintaining the radial nature. This procedure is repeated for the next consecutive tie-line switches and shown in Table 3.

Table 3 Tie-line switch operation with kW (active) and kVAr (reactive) losses

Line	Active power losses	Reactive power losses
18–33 (Closed)	0.00131	0.00093
17–18 (Opened)	0.00122	0.00087
16–17 (Opened)	0.00123	0.00088
12–22 (Closed)	0.00087	0.00064
11–12 (Opened)	0.00086	0.00064
10–11 (Opened)	0.00085	0.00063
9–10 (Opened)	0.00084	0.00063
8–9 (Opened)	0.00083	0.00063
25–29 (Closed)	0.00103	0.00079
24–25 (Opened)	0.00122	0.00092
23–24 (Opened)	0.00199	0.0015
28–29 (Opened)	0.00086	0.00066
21–8 (Closed)	0.00085	0.00068
7–8 (Opened)	0.00085	0.00067
6–7 (Opened)	0.00089	0.00073
5–6 (Opened)	0.001	0.00085
9–15 (Closed)	0.00084	0.00067
14–15 (Opened)	0.00084	0.00067
13–14 (Opened)	0.00086	0.00068
12–13 (Opened)	0.00088	0.00069

4 Conclusion

A new approach of simultaneous DG placement and network reconfiguration is used in this paper for voltage profile improvement and network loss reduction in distribution system using MATLAB software. Some buses are critical based on their reactive power loading. The technique used voltage stability indices first to detect the most sensitive buses, followed by selecting the most appropriate location for DG placement and then optimal active and reactive power loss reduction by network reconfiguration to ensure the supply reliability. Tie-line switches are closed based on the maximum voltage difference between the corresponding end nodes. The results obtained validate that the DG placement and network reconfiguration together effectively result in voltage profile improvement and active and reactive power loss reduction. The load flow computation time is an important parameter in this aspect. This method not only maintains service reliability but providing alternate path also results in lowering the network losses.

References

1. Pillai R, Ghatikar R, Ahuja A (2017) Integration of multivariate distributed energy resources for demand response: applications in the Indian scenarios. *CIRED-Open Access Proc J* 2017:1849–1852. <https://doi.org/10.1049/oap-cired.2017.0755>
2. Rogers BT, Jason M, Tom Tsay C (2017) Studies on the time and locational value of DER. *CIRED-Open Access Proc J*, 2015–2018. <https://doi.org/10.1049/oap-cired.2017.0403>
3. Yi HH, Mohammad Zhang Y, Chen M, Lin X (2018) Impact of the uncertainty of distributed renewable generation on deregulated electricity supply chain. 1–1. <https://doi.org/10.1109/PESGM.2018.8585836>
4. Balamurugan K, Srinivasan D, Reindl T (2012) Impact of distributed generation on power distribution systems. *Energy Procedia* 25:93–100. <https://doi.org/10.1016/j.egypro.2012.07.013>
5. Atwa YM, El-Saadany EF, Salama MMA et al (2010) Optimal renewable resources mix for distribution system energy loss minimization. *IEEE Trans Power Syst* 25(1):360–370
6. Akorede MF, Hizam H, Aris I, et al (2011) Effective method for optimal allocation of distributed generation units in meshed electric power systems. *IET Gener, Transm Distrib* 5(2):276–287
7. Abu-Mouti FS, El-Hawary ME (2011) Optimal distributed generation allocation and sizing in distribution systems via artificial bee colony algorithm. *IEEE Trans Power Deliv* 26(4):2090–2101
8. Kuri B, Redfern M, Li F (2004) Optimization of rating and positioning of dispersed generation with minimum network disruption. *Proc. IEEE power engineering society general meeting, Denver, USA, June*, pp 2074–2078
9. El-Khaltam W, Bhattacharya K, Hegazy Y et al (2004) Optimal investment planning for distributed generation in a competitive electricity market. *IEEE Trans Power Syst* 19(3):1674–1684
10. Vatani M, Alkaran D, Sanjari M, Gharehpetian G B (2015) Multiple distributed generation units allocation in distribution network for loss reduction based on a combination of analytical and genetic algorithm methods. *IET Gener, Transm Distrib* 10. <https://doi.org/10.1049/iet-gtd.2015.0041>
11. Lee T, Hu S, Chan Y (2013) D-STATCOM With Positive-sequence admittance and negative-sequence conductance to mitigate voltage fluctuations in high-level penetration of distributed-generation systems. *IEEE Trans Industr Electron* 60(4):1417–1428

12. Zeinalzadeh A, Estebarsari A, Bahmanyar A (2019) Simultaneous optimal placement and sizing of DSTATCOM and parallel capacitors in distribution networks using multi-objective PSO. *IEEE Milan Power Tech* 2019:1–6
13. Ranamuka D, Agalgaonkar AP, Muttaqi KM (2019) Innovative Volt/VAR control philosophy for future distribution systems embedded with voltage-regulating devices and distributed renewable energy resources. *IEEE Syst J* 13(3):3153–3164
14. Kamel S, Ramadan A, Ebeed M, Yu J, Xie K, Wu T (2019) Assessment Integration of wind-based DG and DSTATCOM in Egyptian distribution grid considering load demand uncertainty. *IEEE Innov Smart Grid Technol-Asia (ISGT Asia)* 2019:1288–1293. <https://doi.org/10.1109/ISGT-Asia.2019.8881437>
15. Liu Y, Li J, Wu L (2019) Coordinated optimal network reconfiguration and voltage regulator/DER control for unbalanced distribution systems. *IEEE Trans Smart Grid* 10(3):2912–2922
16. Aziz T, Mhaskar UP, Saha TK, Mithulananthan N (2013) An index for STATCOM placement to facilitate grid integration of DER. *IEEE Trans Sustain Energy* 4(2):451–460
17. Muttaqi KM, Le ADT, Negnevitsky M, Ledwich G (2015) A coordinated voltage control approach for coordination of OLTC, voltage regulator, and dg to regulate voltage in a distribution feeder. *IEEE Trans Ind Appl* 51(2):1239–1248
18. Bokhari A et al (2016) Combined effect of CVR and DG penetration in the voltage profile of low-voltage secondary distribution networks. *IEEE Trans Power Delivery* 31(1):286–293
19. Schmitt KEK, Canha LN, Antunes Mda, P. R. Pereira, “A smart local voltage regulator methodology for dynamic integration between volt-var control and distributed energy resources,” 2018 IEEE PES Transmission & Distribution Conference and Exhibition - Latin America (T&D-LA), 2018, pp. 1–5.
20. Kelly N, Dehghanpour K, Nehrir H (2018) Loss Minimization for distributed PV integration using particle swarm optimization with volt-var control. *IEEE Power & Energy Soc Gen Meet (PESGM)* 2018:1–5
21. Singhal A, Ajarapu V, Fuller J, Hansen J (2019) Real-time local volt/var control under external disturbances with high PV penetration. *IEEE Trans Smart Grid* 10(4):3849–3859
22. Vita V (2017) Development of a decision-making algorithm for the optimum size and placement of distributed generation units in distribution networks. *Energies* 10:1433. <https://doi.org/10.3390/en10091433>
23. Reddy SC, Prasad PVN, Laxmi AJ (2012) Power quality and reliability improvement of distribution system by optimal number, location and size of DGs using Particle Swarm Optimization. In: 2012 IEEE 7th international conference on industrial and information systems (ICIS), pp 1–6
24. Devalalaji KR, Ravi K (2015) Optimal size and siting of multiple DG and DSTATCOM in radial distribution system using Bacterial Foraging Optimization Algorithm. *Ain Shams Eng J* 7. <https://doi.org/10.1016/j.asej.2015.07.002>
25. Di Silvestre ML, La Cascia D, Sanseverino E, Zizzo G (2016) Improving the energy efficiency of an islanded distribution network using classical and innovative computation methods. *Util Policy*. <https://doi.org/10.1016/j.jup.2016.04.004>
26. Mendoza J, Lopez R, Morales D, Lopez E, Dessante P, Moraga R (2006) Minimal loss reconfiguration using genetic algorithms with restricted population and addressed operators: real application. *IEEE Trans Power Syst* 21(2):948–954. <https://doi.org/10.1109/TPWRS.2006.873124>
27. Shirmohammadi D, Hong HW (1989) Reconfiguration of electric distribution networks for resistive line losses reduction. *IEEE Trans Power Delivery* 4(2):1492–1498. <https://doi.org/10.1109/61.25637>
28. Ye J, Wang FZ (2009) A refined plant growth simulation algorithm for distribution network reconfiguration. In: 2009 IEEE international conference on intelligent computing and intelligent systems. pp 357–361
29. Sathish Kumar K, Jayabarathi T (2011) Power system reconfiguration and loss minimization for distribution systems using bacterial foraging optimization algorithm. *Electr Power Energy Syst* 36:13–17

30. Zhu IZ (2002) Optimal reconfiguration of electrical distribution networks using the refined genetic algorithm. *Elect Power Syst Res* 62:37–42
31. Huang YC (2002) Enhanced genetic algorithm-based fuzzy multi objective approach to distribution network reconfiguration. *Proc Inst Elect Eng* 149(5):615–620
32. Kim H, Ko Y (1993) Artificial neural network based feeder reconfiguration for loss reduction in distribution systems. *IEEE Trans Power Del* 8(3):1356–1367
33. Zhu Z (2002) Optimal reconfiguration of electrical distribution networks using the refined GA. *Electr Power Syst Res* 62:37–84
34. Yasin ZM, Rahman TKA (2006) Network Reconfiguration in a power distribution system under fault condition with the presence of distributed generation. In: International conference on energy and environment (ICEE), 28–30 Aug 2006
35. Olamie J, Niknam T, Gharehpetian G (2008) Application of particle swarm optimization for distribution feeder reconfiguration considering distributed generators. *Appl Math Comput*:575–586
36. Dahalan WM, Mokhlis H, Bakar A, Halim A, Jamian JJ (2013) The simultaneous application of optimum network reconfiguration and distributed generation sizing using PSO for power loss reduction. *Optymalizacja rekonfiguracji sieci elektroenergetycznej i rozmiarów generatorów rozproszonych w redukcji strat energetycznych - zastosowanie algorytmu PSO*. 89:137–141

Thermal Sensing Behavior of SiC Schottky Diode in 200–600 K



Jaya, Bhavya Sinhmar, V. K. Dasarraju, and Suman

Abstract This work describes a high-temperature probe that may be used in industrial settings as a trustworthy alternative to thermocouples with a short life duration. As legislation aimed at reducing the industrial impact on the environment progresses, precise temperature control and energy efficiency have emerged as critical research areas, exerting ever-increasing criteria from temperature sensors. Silvaco TCAD's ATLAS module is used to design Pt/4H-SiC Schottky diode and its thermal sensitivity is observed in the current range of 1–50 nA and in the temperature range 200–600 K. Sensor is found to be well operational within this temperature range and temperature sensitivity is observed its maximum value at 1 nA which is 3.15 mV/K.

Keywords Temperature sensor · Atlas module · Temperature sensitivity · Schottky diode

1 Introduction

Previous research indicates that organic and inorganic semiconducting materials are suitable for application in temperature sensors. Therefore, temperature sensors and their applications in many industries will be the focus of attention. Some devices can be damaged to a great extent while working with high temperatures and some with low temperatures. There are many semiconductor devices that can be destroyed by temperature extremes. Monitoring temperature levels is very important in achieving the best quality and yield in electronic devices. Real-time temperature monitoring at crucial points in integrated circuits (ICs) aids in the early detection of system

Jaya · B. Sinhmar (✉)
Chaudhary Ranbir Singh University, Jind 126102, India
e-mail: bhavyasinhmar@gmail.com

V. K. Dasarraju
Northern Illinois University, Dekalb, IL 60115, USA

Suman
Department of Physics, Government College for Women, Rohtak 124001, India

breakdown and lowers maintenance costs and system damage. In some devices, fans are also inserted to maintain the temperature requirement or cool down the system. But if the fan fails in doing so, the device may get damaged. Therefore, the industrial sector needs precise and accurate temperature sensors which lead to low-cost and highly efficient electronic devices [1–3].

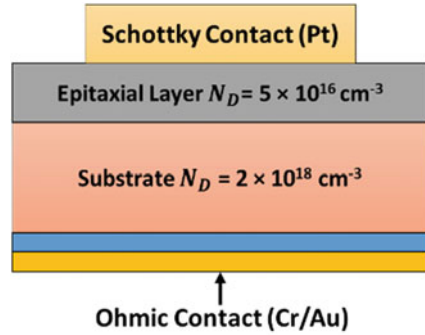
High heat, corrosion, strong vibrations, etc., are some common reasons that decrease the lifespan of thermocouple [4]. Considering the aforementioned requirements, due to the low-cost production procedures that are completely compatible with CMOS technology, silicon (Si)-based temperature sensors are commonly used in the devices [5, 6]. However, silicon's physical characteristics deteriorate when high thermal budgets are present, rendering Si-based devices unsuitable at temperatures higher than $T = 130\text{ }^{\circ}\text{C}$.

In this regard, compared to silicon and other similar materials, silicon carbide (SiC), gallium nitride (GaN), and other wide band gap (E_g) materials seem to be the most promising options for usage in hostile environments. Thus, wideband semiconductor devices are necessary to fulfil the operational parameters. Importance of silicon carbide is basically because of advancements in the crystal quality and ease of access. SiC has a wide band gap, a large thermal coefficient, a low concentration of intrinsic carrier, a great breakdown electric field, and a high chemical inactivity, making SiC technology the best, and used in the processing of materials and production of electronic devices. Thus, researches are basically focused on improving the performance of SiC-based devices [1, 3, 5, 8, 10, 13, 14, 20]. Currently, Schottky diodes are discovered to be well suited for usage in radio frequency applications because of their fast-switching rates, high-frequency capabilities, power density, and lower system costs and also one of the promising devices utilised for applications needing high voltage and high temperature is silicon carbide (SiC)-based devices [2, 4, 7, 9, 11, 16, 19]. Some literature works reported that Schottky barrier diode temperature sensors based on SiC are good alternatives for temperature monitoring [2, 9, 18]. Due to its high thermal conductivity (3–5 W/cm $^{\circ}\text{C}$) and high critical electric field for breakdown ($E_c = 2\text{--}5\text{ MV/cm}$), SiC ($E_g = 3.2\text{ eV}$) has drawn a lot of interest in recent years as a suitable material for high-power applications. Therefore, in this work, simulation of the SiC-based Schottky diode temperature sensors is done within the temperature range 200–600 K for observing its thermal sensing characteristics, current–voltage characteristics and physical behavior.

2 Device Design

By providing engineers and researchers with established design IP (intellectual property), economical and competitive TCAD (technology computer-aided design) and EDA (electrical design automation) tools, Silvaco has overcome problems in semiconductor designing. Temperature sensitivity, electrical characteristics, physical behavior, etc., like useful details are obtained by the simulation of electronic devices. A wide range of physical device properties may be modeled using Silvaco

Fig. 1 Schematic diagram of the manufactured device which is to be simulated



International’s ATLAS device simulator. This software contains a large number of equations which are used to simulate the semiconductor device. Compared to practical experimentation, these simulations are significantly faster and less expensive to do. Exactness and correctness of the findings depend on the parameters such as bandgap of SiC, mobility of electrons and holes, permittivity, work function of Schottky metal, doping of the substrate, doping of epitaxial layer, device dimensions, diffusion lengths, etc. Figure 1 shows the schematic diagram of the fabricated device. The structure has a substrate, which is $n + \text{SiC}$, with a height of $30 \mu\text{m}$ and impurity concentration of $2 \times 10^{18} \text{ cm}^{-3}$. The Schottky metal used in this work has a work function 6.3 eV . Epitaxial layer or drift layer with a width of $10 \mu\text{m}$ having an impurity $= 5 \times 10^{16} \text{ cm}^{-3}$. Permittivity and thickness are the principal dielectric properties because they affect reverse breakdown voltage of the device. The backside contact is ohmic contact with metal Cr/Au. For SiC, the following parameters have been used; band gap $= 3.2 \text{ eV}$, electron affinity $= 4.12 \text{ eV}$, Schottky metal work function $= 6.3 \text{ eV}$, permittivity $= 9.6$, density of states in conduction band $= 1 \times 10^{19} \text{ cm}^{-3}$, density of states in valence band $= 1.2 \times 10^{19} \text{ cm}^{-3}$, and temperature $T = 300 \text{ K}$.

3 Result and Discussion

Figure 2 represents the characteristics of forward bias of the manufactured device. This figure shows that current increases exponentially with applied voltage and when temperature increases, the forward voltage drop in the device decreases.

Figure 3 shows semi-logarithmic forward bias characteristics corresponding to similar temperature range for the constructed sensor. As the curve is linear at the low bias regions suggests that thermionic emission current flow mechanism dominates over other current conduction mechanisms and series resistance effect seems as the biasing is increased and the curve starts bending.

As temperature increases, it is shown in Fig. 3 that current transportation starts at a lower bias range. This type of current transfer that depends on the temperature

Fig. 2 Current–voltage characteristics of the manufactured device within temperature range from 200 to 600 K

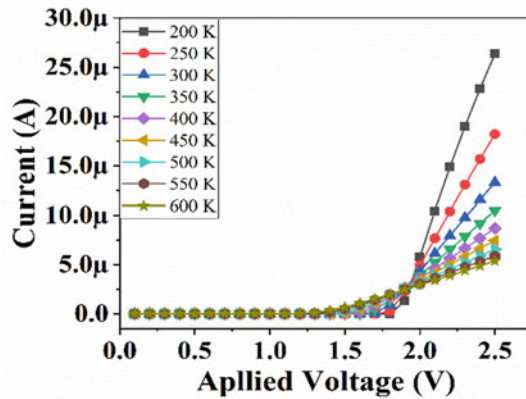
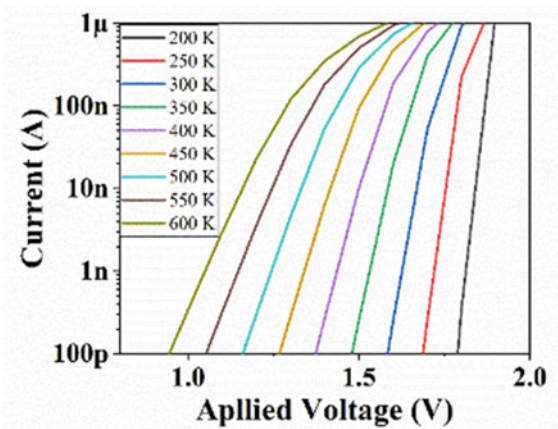


Fig. 3 Semi-logarithmic current–voltage plot corresponds to the same temperature range for the manufactured device



addressed in terms of thermionic emission as [15, 17]:

$$I_f = I_s \exp\left(\frac{q(V_f - I_f R_s)}{\eta k T}\right) \tag{1}$$

where

$$I_s = AA^* T^2 \exp\left(\frac{q\Phi_b}{kT}\right) \tag{2}$$

is the saturation current in the device.

Equation (1) can be rewritten to obtain the Schottky barrier as

$$\ln \frac{I_F}{T^2} = \ln(A_n A_J) - \frac{\Phi_{Bn} - \frac{V_E}{n}}{\frac{k}{q}} \frac{1}{T} \tag{3}$$

In Eqs. (1), (2), and (3), A_J is the area of the diode and A_n is Richardson’s constant, Φ_{Bn} is the Schottky barrier, R_s is the series resistance of the device, K is the Boltzmann constant (1.38×10^{-23} J/K), T is the temperature, q is the electronic charge, A is the Schottky contact area, and A^* is the effective Richardson constant ($146 \text{ A/cm}^{-2} \text{ K}^{-2}$). Furthermore, η and Φ_b are the ideality factor and the barrier height of the device, respectively. Merits and steadiness of barrier height and ideality factor are related to the technological process. At each temperature value, the slope and intercept of the linear \ln function may be found. Rearranging of Eq. (1) gives

$$V_f = \eta\Phi_b + I_f R_s + \frac{\eta k T}{q} \ln\left(\frac{I_f}{AA^*T^2}\right) \tag{4}$$

Current forward voltage is inversely dependent on the temperature as shown in Eq. (4). Figure 3 illustrates or follows the same pattern for constructed devices operating at elevated temperatures.

If two diodes are used in the device and biased via two known currents I_{D1} and I_{D2} , then the difference between the two diode voltages V_{D1} and V_{D2} is related to temperature T as

$$V_{D2} - V_{D1} = R_s(I_{D2} - I_{D1}) + \frac{kT\eta}{q} \ln\left(\frac{I_{D2}}{I_{D1}}\right) \tag{5}$$

where the symbols have their usual meaning.

In Fig. 4, the variation in forward voltage with temperature is plotted with temperature on the x -axis and voltage drop on the y -axis using Fig. 3, at specified current levels (i.e., 0.5–50 nA).

Forward voltage varies linearly with temperature at each specific current level that is displayed in Fig. 4. It shows that forward voltage decreases with increase in temperature for a selected current level. The manufactured sensor’s thermal sensitivity has its absolute value which can be determined by the equation [9]

Fig. 4 Variation in the forward voltage (V_f) with temperature ranging from 200 to 600 K at specified current levels of the fabricated device

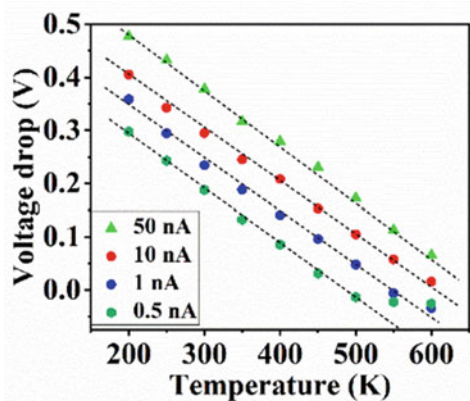
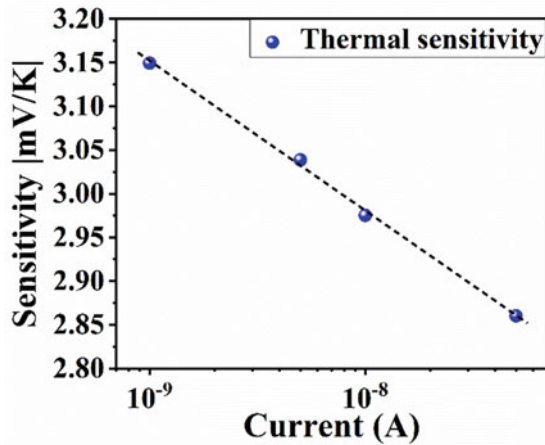


Fig. 5 Absolute values of thermal sensitivity of the sensor at selected current levels



$$|S| = \left| \frac{dV_f}{dT} \right| = \left| \frac{\eta K}{q} \left[\ln \left(\frac{I_f}{AA^* T^2} \right) - 2 \right] \right| \quad (6)$$

Figure 5 represents that slope of forward voltage drop versus temperature is used to determine the thermal sensitivity of the manufactured device.

The thermal sensitivity increases with decrease in the current level as shown in Fig. 5, which is similar to Eq. 6 corresponding to the specified current levels. The maximum value of sensitivity is calculated as 3.15 mV/K at 1 nA. These findings indicate that silicon carbide-based Schottky diode thermal sensors are suitable while working at low temperature. At some specific current levels, as shown in Fig. 4, thermal sensitivity is not ideally linear and it can be described on the basis of barrier height inhomogeneities present [15, 17] at the interface of fabricated Pt/4H-*n*SiC SBD temperature sensor. The nanometer-sized patches at the interface prevent charge carriers from flowing at low current levels, which prevents forward voltage from acting as it should. That's why researchers in this field, working on the possibilities that are concentrated on developing the methods which improve the interface of SiC-based Schottky devices [6, 10, 12]. On the other hand, the presence of more charge carriers in higher energy states will make it easier for the forward voltage drop to vary with temperature at high current and temperature levels.

4 Conclusions

In conclusion, SiC Schottky diode thermal sensor has been fabricated using the atlas module of Silvaco TCAD. This paper examines the thermal characteristics of silicon carbide Schottky diode. Its thermal sensitivity was determined using current measurements between 1 and 50 nA. The maximum value of thermal sensitivity is observed at 1 nA which is 3.15 mV/K. With lowering measurement current levels in

the devices, it is discovered that the absolute values of sensitivity of the manufactured device are rising. Moreover, current forward voltage is inversely dependent on the temperature. There is exponentially increase in current with applied voltage within a specified temperature range i.e., 200–600 K. Therefore, it is possible to create Schottky barrier diodes because broad bandgap Silicon Carbide (SiC) material has excellent electrothermal characteristics.

References

1. Baliga BJ (2006) Silicon carbide power devices. World Scientific. <https://doi.org/10.1142/5986>
2. Draghici F, et al (2019) 400 °C sensor based on Ni/4H-SiC Schottky diode for reliable temperature monitoring in industrial environments. *Sensors (Basel)* 19(10). <https://doi.org/10.3390/S19102384>.
3. Kranzer D, et al (2018) Applications of SiC devices. *Wide Bandgap Semicond. Power Devices Mater Phys Des Appl*, 345–371. <https://doi.org/10.1016/B978-0-08-102306-8.00010-1>
4. Kumar V et al (2014) Barrier height inhomogeneities induced anomaly in thermal sensitivity of Ni/4H-SiC Schottky diode temperature sensor. *J Vac Sci Technol B Nanotechnol Microelectron Mater Process Meas Phenom* 32(4):041203. <https://doi.org/10.1116/1.4884756>.
5. Kumar V et al (2016) Capacitance roll-off and frequency-dispersion capacitance-conductance phenomena in field plate and guard ring edge-terminated Ni/SiO₂/4H-nSiC Schottky barrier diodes. *Phys status solidi* 213(1):193–202. <https://doi.org/10.1002/pssa.201532454>
6. Kumar V et al (2022) Defect levels in high energy heavy ion implanted 4H-SiC. *Mater Lett* 308:131150. <https://doi.org/10.1016/j.matlet.2021.131150>
7. Kumar V, et al (2015) Diameter dependent thermal sensitivity variation trend in Ni/4H-SiC Schottky diode temperature sensors. *J Vac Sci Technol B Nanotechnol Microelectron Mater Process Meas Phenom* 33(5):052207. <https://doi.org/10.1116/1.4929890>
8. Kumar V, et al (2020) Electronic transport in epitaxial 4H-SiC based Schottky diodes modified selectively by swift heavy ions. *Mater Sci Semicond Process* 115. <https://doi.org/10.1016/J.MSSP.2020.105108>
9. Kumar V, et al (2020) Epitaxial 4H-SiC based Schottky diode temperature sensors in ultra-low current range. *Vacuum* 182. <https://doi.org/10.1016/J.VACUUM.2020.109590>
10. Kumar V et al (2020) Interface improvement of epitaxial 4H-SiC based Schottky diodes by selective heavy ion irradiation. *Appl Nanosci*. <https://doi.org/10.1007/s13204-020-01608-3>
11. Kumar V et al (2021) Interfacial and structural analysis of MeV heavy ion irradiated SiC. *Appl Nanosci*. <https://doi.org/10.1007/S13204-021-01921-5>
12. Kumar V, et al (2012) Simulation based analysis of temperature effect on breakdown voltage of ion implanted Co/n-Si Schottky diode. 4, 4pp, 4009. <https://essuir.sumdu.edu.ua/handle/123456789/30266>
13. Kumar V et al (2018) Tailoring surface and electrical properties of Ni/4H-nSiC Schottky barrier diodes via selective swift heavy ion irradiation. *Phys Status Solidi Appl Mater Sci* 215:5. <https://doi.org/10.1002/PSSA.201700555>
14. Kumar V, Maan AS, Improvement in reverse bias leakage current of Ni/4H-nSiC Schottky barrier diodes via MeV selective ion irradiation. <https://doi.org/10.1088/1757-899X/331/1/012016>.
15. Rhoderick EH (1982) Metal-semiconductor contacts. *IEE Proc I Solid State Electron Devices*. <https://doi.org/10.1049/ip-i-1.1982.0001>
16. Senesky DG (2013) Wide bandgap semiconductors for sensing within extreme harsh environments. *ECS Trans* 50(6):233–238. <https://doi.org/10.1149/05006.0233ecst>
17. Tyagi MS (1984) Physics of Schottky barrier junctions. In: *Metal-semiconductor Schottky barrier junctions and their applications*. https://doi.org/10.1007/978-1-4684-4655-5_1

18. Verma J et al (2022) Trench termination in Ga₂O₃-based power device: a simulation-based study. Appl Nanosci. <https://doi.org/10.1007/s13204-021-02219-2>
19. Zhang N et al (2014) Temperature sensor based on 4H-silicon carbide pn diode operational from 20 °C to 600 °C. Appl Phys Lett 104:7. <https://doi.org/10.1063/1.4865372>
20. Kumar V, et al (2013) Selective SHI irradiation for mesa type edge termination in semiconductor planar junction. J Phys Conf Ser 423(1):012057. <https://doi.org/10.1088/1742-6596/423/1/012057>

Design and Performance of a Circularly Polarized Planar Microstrip Antenna with Improved Gain



Shipra Tiwari, Pramod Sharma, and Shoyab Ali

Abstract This paper presents a simulated circularly polarized microstrip patch antenna resonating at a frequency of 2.4 GHz for wireless applications. We insert a reflecting surface over the antenna to improve its gain. The frequency bandwidth is 70.5 MHz and its return loss is -30.7676 dB at a frequency of 2.4 GHz. The axial ratio is less than 3 dB, which is 1.3202 dB, which shows a circular radiation pattern. The maximum gain of the antenna is 5.6083 dB without a reflector at the proposed frequency. We have used HFSS software for the simulation of the proposed antenna.

Keywords Circular polarization · Gain · Axial ratio · Frequency selective surface · Split ring resonator

1 Introduction

Many wireless devices use microstrip patch antennas owing to their compact size, conformal designs, and cost-effectiveness [1]. In the last few years, there is an increase in the demand for antenna with high gain, the lesser area covered, and avoids multipath fading, and mismatching of polarization effects. The preference for circularly polarized (CP) antennas more than other antennas because of low polarization loss and its easy installation process [2–4]. Various methods and ways have been proposed and suggested to design a single-feed circularly polarized (CP) microstrip patch antenna [5–7].

A square patch antenna with a single feed and two L-shaped slots was added at two opposite corners to get circularly polarized radiation for satellite application [8]. The circularly polarized antennas are preferred over linear polarized (LP) antennas because waves arriving at the receiving end of the antenna cannot maintain the same polarization as provided in a transmitted antenna, especially in handheld devices. This happens due to ongoing deforestation and urbanization [9].

S. Tiwari (✉) · P. Sharma · S. Ali
Regional College for Education Research and Technology, Jaipur, India
e-mail: shipra10.tiwari@gmail.com

The modern-day communication protocol requires circularly polarized (CP) wide bandwidth with high gain simultaneously.

The circular patch antenna was used to design a micro-strip patch antenna for circular polarization with a cross slot with different lengths [10]. RHCP radiation pattern over the band is shown in a well-defined way by the proposed antenna with L-shaped slits and truncated corners; this makes the design more appropriate for wireless communication [11].

The efficacy of the used antenna has been analyzed in terms of return loss, gain, axial ratio current distribution, etc. The electromagnetic tool HFSS has been used in it. The presented CP circularly polarized antenna is lightweight and compact in size but is characterized by high gain.

2 Geometry and Structure of Proposed Antenna

Figure 1 shows a schematic diagram of the antenna. The antenna is placed on the substrate and a reflecting surface of RT-Duroid material is placed 1 cm above the antenna. The reflecting surface consists of the matrices of split rings.

A simple circular patch antenna is designed on RT/duroid 5880 substrate having dimension $L_1 \times W_1$ and thickness T_1 mm and permittivity $\epsilon_r = 2.2$ with a loss tangent $\tan \delta = 0.004$ having ground on the lower side with same dimension $L_1 \times W_1$ and thickness T_2 mm and on the other side circular patch is designed with radius “ a ”. The values of these parameters are given below in Table 1. For circular polarization, the two opposite side of the circle is etched as shown in Fig. 2. Microstrip feed is given to the patch antenna. HFSS software is used to simulate and optimize the proposed antenna structure.

Where L_1 = Length of ground and substrate, W_1 = Width of ground and substrate, T_1 = Thickness of substrate, T_2 = Thickness of ground, a = Radius of the circular patch, and g = Air gap.

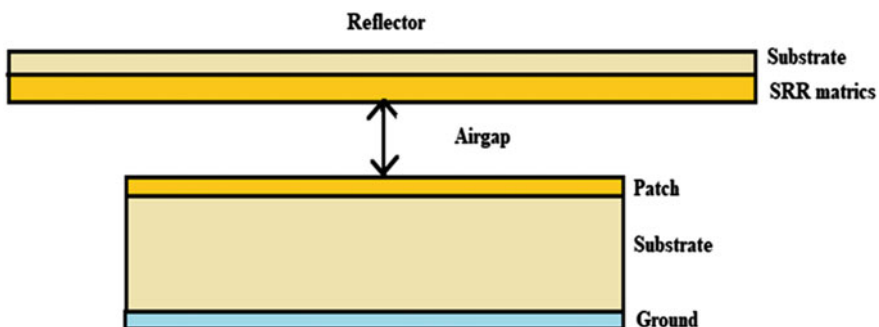


Fig. 1 Patch antenna

Table 1 Dimension of the proposed antenna

Parameters	L_1	W_1	T_1	T_2	a	g
Value (mm)	94.92	59.21	1.57	0.035	23.96	10

Table 2 Dimension of reflector

Parameters	L_2	W_2	T_3	S_0	S_1	G
Value (mm)	130	90	1.57	8	5	0.5

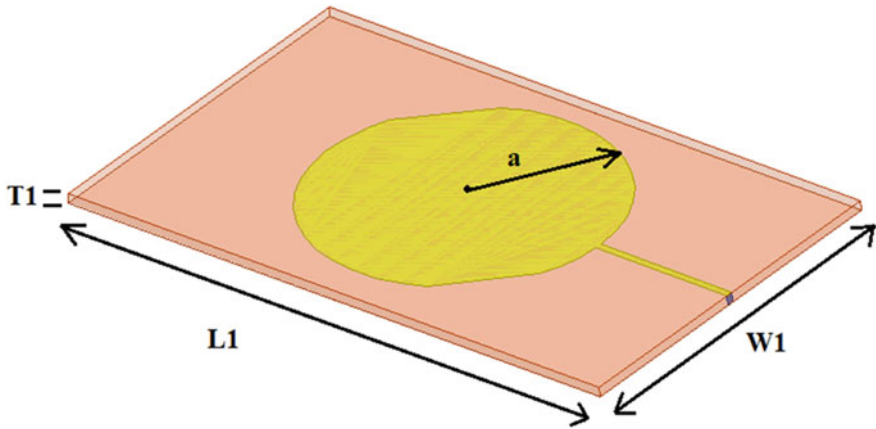


Fig. 2 Circular patch antenna

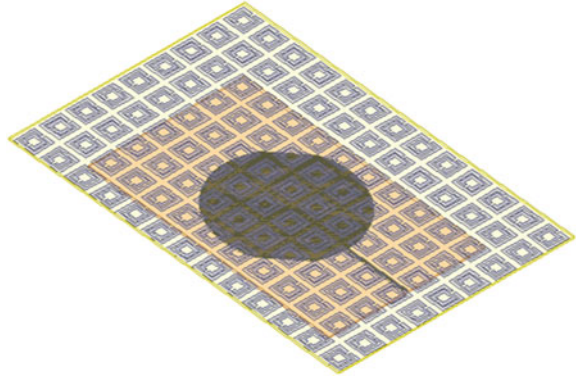
A reflector/Duroid that consists of a matrix of split rings is placed in front of the circular microstrip patch antenna. This reflector has dimensions $L_2 \times W_2$ and thickness T_3 .

Where L_2 = length of reflector, W_2 = width of reflector, T_3 = Thickness of reflector S_0 = length of outer split ring, S_1 = length of inner split ring, and G = gap. All the dimensions are in mm.

Reflector is made up of RT/Duroid material and the dimension is 130×90 mm. Bottom surface of the reflector has a matrix of split rings which create a frequency selective surface (FSS). There are 13×9 unit cells in the FSS. All these cells are 0.5 mm apart from each other. All the gaps are 1.5 mm. Dielectric substrate is RT/Duroid with a dielectric constant of 2.2 and a thickness of 1.57 mm.

These unit cells disturb the electric field and magnetic field comes from the circular patch antenna and modulate the antenna parameters. There are several applications of FSS like gain enhancement, filtering, wide banding, multibanding, etc. Figure 3 is showing the complete arrangement of the patch antenna along with the reflector. There is a 1 mm air gap between the reflector and patch antenna. The outer dimension of the frequency selective surface unit cell is 8 by 8 mm and the inner unit cell dimension is 5 by 5 mm. All the gaps are 5 mm. The split rings are made up of

Fig. 3 Matrix of metamaterial unit cell



conductors. These split rings generate the inductive behavior and the gap between the rings generates the capacity behavior. The frequency and electromagnetic behavior of the design fluctuate due to the venation of inductor and capacitor.

3 Result and Discussion

For the dimension and simulation of the proposed circularly polarized antenna, HFSS software is used which is based on the finite element method. For circularly polarized radiation, the circular patch is etched on both sides. The circularly patch is designed in such a way to resonate at 2.4 GHz as shown in Fig. 4. The maximum return loss is -42.30 dB at a frequency of 2.4 GHz. The axial ratio is plotted against the frequency having a minimum value of 2.44 dB at a proposed frequency as shown in Fig. 5. Since the axial ratio is less than 3 dB at a frequency of 2.4 GHz, the proposed antenna shows a circular radiation pattern. The left-hand circular polarised gain and the right-hand circular polarized gain in the XY and YZ planes are also shown in Fig. 7. They are also evidence that antenna behavior is circularly polarized.

The maximum gain of 5.6082 dB of the proposed antenna is obtained at a frequency of 2.4 GHz shown in Fig. 6. When we use the reflector over the antenna the results are as follows:

Resonant frequency = 2.4 GHz.

Return loss = -15 dB.

Bandwidth = 74 MHz.

Gain = 7.4 GHz.

S11 parameters and bandwidth are the same as the circular patch antenna without a reflector but there is a significant change in the gain. We found a gain of 7.4 dB. The radiation pattern is shown in Fig. 8.

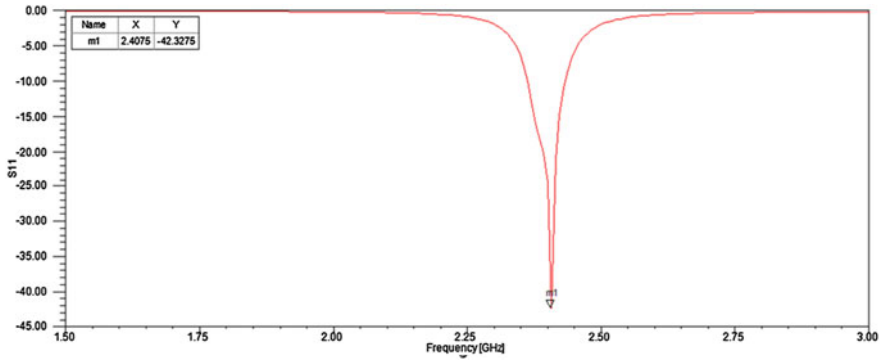


Fig. 4 Simulated return loss versus frequency 2.4 GHz

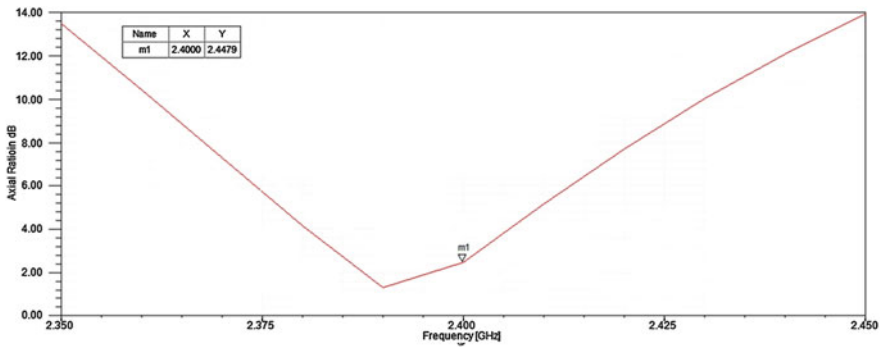
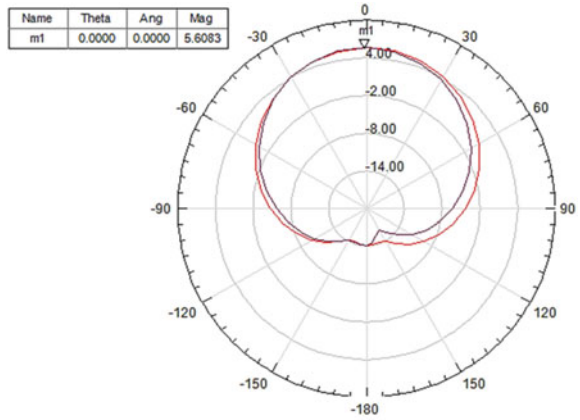


Fig. 5 Axial ratio versus frequency curve

Fig. 6 Gain in XY plane



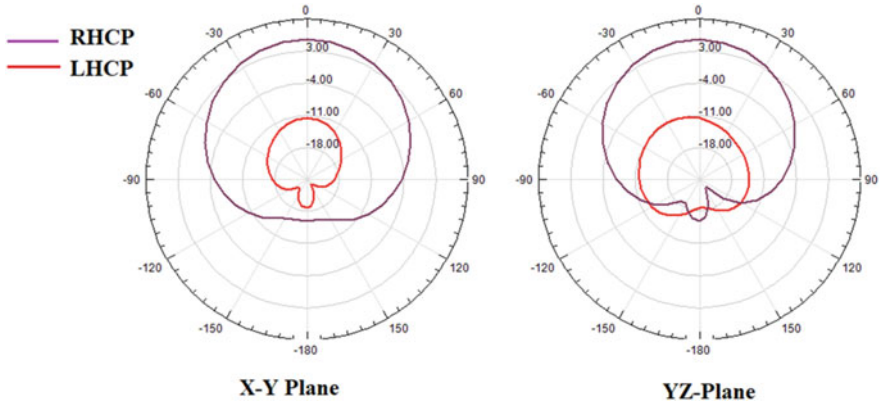
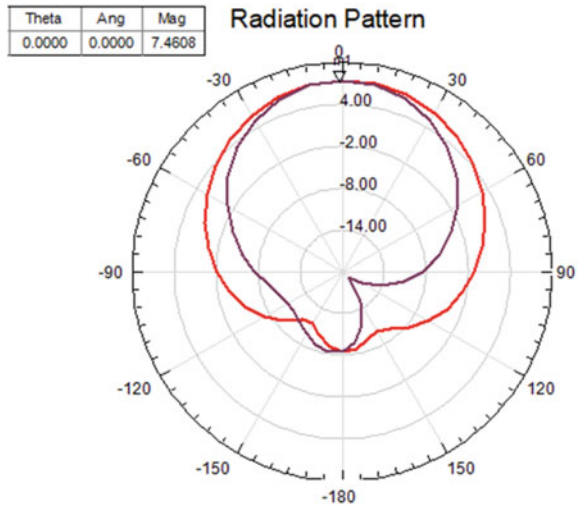


Fig. 7 RHCP and LHCP gain in XY and YZ planes

Fig. 8 Gain in XY plane



4 Comparison with Flexible Antenna

To fabricate a flexible antenna, there are various types of materials like conductive polymers, metal nanoparticles, graphene-based materials, liquid metals, etc. In conductive polymers, the conductor materials are polyaniline, polypyrrole, and polyacetylene, having a conductivity of between 52 and 1000 S/m, and in metal nanoparticles, the conductive materials are silver, copper, and gold. Graphene-based materials are paper, mesh fabric, and liquid metal, eutectic gain. Similarly, various substrates with thicknesses ranging from 0.8 to 3 mm are used in flexible antennas, such as wash cotton, kapton polyimide, fr4, jeans, and PDMS. Various fabrication

Table 3 Comparison between proposed antenna and flexible antenna

Ref	Antenna type	Dimension (mm ²)	Substrate	Resonant frequency (GHz)	Gain (dB)
[12]	Dipole	46 × 45	Kapton, polyimide, graphene flakes	2	2.38
[13]	MPA	40 × 35	Photo paper, Cu strips	2.43	2
	Proposed antenna	94.92 × 59.21	RT duroid	2.4	5.6

methods are screen printing, inkjet printing, and swing and embossing. Table 3 is showing the comparison between the proposed antenna and the flexible antenna.

From Table 3, we can conclude that the dimension of the proposed antenna is just double by the reference antenna but at the same time, approximately more than double also increase the gain. So flexible antenna can be used on those applications where less amount of gain is required.

5 Conclusion

In this paper, a circularly polarized patch antenna is designed and simulated for wireless application resonant at 2.4 GHz frequency. The maximum return loss is –30.7676 dB at the resonant frequency of 2.41 GHz obtained. Circularly polarized radiation is obtained by etched opposite sides of a circular patch antenna. The axial ratio is 1.3202 dB at 2.41 GHz. The maximum gain of the proposed antenna is 5.6083 dB at the resonance frequency.

When we add an FSS reflector in front of the antenna, we found a gain enhancement of approx. 2 dB. So we can say the FSS reflector can be used for gain enhancement. We can infer from Table 3 that the suggested antenna's size is just slightly larger than that of the reference antenna while simultaneously increasing gain by roughly a factor of two. Therefore, flexible antennas can be employed in applications where less gain is needed.

References

1. Collin R (1991) Field theory of guided waves, 2nd edn. IEEE Press, New York
2. Garg BR, Bahl PI, Ittipiboon A (2001) Microstrip antenna design handbook. norwood, M.A: Artech House
3. Lam KY, Luk KM, Lee KF, Wong H, KB, N.G.:Small circularly polarized U-slot wideband patch antenna. IEEE Antennas and Wireless Propagation Letters, Vol. 10, p. 87–90
4. Nasimuddin, Chen ZN, Qing X (2010) Asymmetric-circular shaped slotted microstrip antennas for circular polarization and RFID applications. IEEE Trans Antennas Propag 58:3821–3828

5. Iwasaki H (1996) A circularly polarized small-size microstrip antenna with a cross slot. *IEEE Trans Antennas Propag* 44(10):1399–1401
6. Yang YH, Sun BH, Guo JL (2019) A low-cost, single-layer, dual circularly polarized antenna for millimeter-wave applications. *IEEE Antennas Wirel Propag Lett* 18(4):651–655. <https://doi.org/10.1109/LAWP.2019.2900301>
7. Hao XU, Chen Z, Liu H, Chang L, Huang T, Ye S, Zhang L, Du C (2022) Single-fed dual-circularly polarized stacked dielectric resonator antenna for K/Ka-band UAV satellite communications. *IEEE Trans Veh Technol* 71(4):4449–4453
8. Hassan EL, Abo, M., Hussein, A., Fawzy, K., Kamal, A.H.: Microstrip antenna with LShaped slots for circularly polarized satellite applications. *The Institute of Engineering and technology*, vol. 2019, issue no. 12, pp 8428–8431.(2019).
9. Guthy S, NVSN S, Vakula D (2019) Gain and bandwidth improvement of the circularly polarised pentagonal patch antenna. 19(12):274–277
10. Akshay K, Ekanshi T, Anjali S, Ankit S, Gupta MRA (2014) circularly polarized smallsize microstrip antenna using a cross slot with enhanced bandwidth & gain. *IEE IOSR J Electron Commun Eng* 9:128–132. <https://doi.org/10.9790/2834-0925128132>
11. Mohammad I, Norbahiah M, Mohammed S, Zamri MNA (2010) Circularly polarized microstrip patch antenna. *Inf Technol J* 2(2):174–178. <https://doi.org/10.3923/itj.2010.363.366>
12. Scidà A, Haque S, Treossi E, Robinson A, Smerzi S, Ravesi S, Borini S, Palermo V (2018) Application of graphene-based flexible antennas in consumer electronic devices. *Mater Today* 21:223–230
13. Ullah M, Islam M, Alam T, Ashraf F (2018) Paper-based flexible antenna for wearable telemedicine applications at 2.4 GHz ISM Band. *Sensors* 18:4214

Cost–Benefit Analysis on Electrical Vehicle Charging Station Using the Vehicle-To-Grid Technology from Python Language



Naresh Kumar Golla , Suresh Kumar Sudabattula ,
Sai Nithika Yakkali , and Yerolla Harshith 

Abstract In the present scenario, most of the vehicles use an integrated combustion engine which consumes fossil fuels and pollutes the atmosphere. As fossil fuels are going to be depleted in the future, Vehicle electrification will have a positive impact on the system as electric vehicles have a low emission rate which in turn reduces global warming. Therefore, the usage of electric vehicles increases in the future. The huge penetration of electric vehicles is going to bring an additional load on the existing grid. Hence, there is a need to control and manage electric power wisely. To overcome this demand on the grid at peak times and to conserve energy, the vehicle-to-grid concept is introduced. Electric vehicle users can supply back the available power in their vehicle to the grid at peak times. This minimizes the load on the grid at peak times and users can be benefitted as they get paid by supplying power back to the grid. Hence, the vehicle-to-grid technology benefits both the user and the grid. To implement this vehicle-to-grid concept there is a need for an interface that connects both the user and the grid. This can be done by using an electric vehicle aggregator. In the proposed approach, an IEEE 33 bus system integrated with four electric vehicle charging stations (10, 14, 17 and 30) was considered to analyse the performance of the system for a 24-h horizon. Here, the Python coding is carried out for cost–benefit analysis based on the load demand and SoC constraints during off and peak load times for 24 h of the day.

Keywords Electrification · Vehicle to grid · Vehicle aggregator · Cost–benefit analysis · Electric vehicle charging station · Python

N. K. Golla (✉) · S. N. Yakkali · Y. Harshith
B. V Raju Institute of Technology, Narsapur, Medak 502313, Telangana, India
e-mail: nareshkumar.golla@gmail.com

S. N. Yakkali
e-mail: 18211a0296@bvrit.ac.in

Y. Harshith
e-mail: 18211a02c0@bvrit.ac.in

N. K. Golla · S. K. Sudabattula
Lovely Professional University, Phagwara 144411, Punjab, India

1 Introduction

In recent years, electric vehicles (EVs) have gained a lot of interest due to the diminishing of fossil fuels and the evolution of climate change. EVs are powered by batteries and can get a charge from the grid at respective charging stations. Through the usage of these electric cars, we have the potential to reduce our reliance on fossil fuels and cut down on emissions of greenhouse gases. On the other hand, increasing the number of EVs puts additional operating strain on the grid that is already in effect. Charging electric vehicles in a disorderly and unplanned manner may lead to an increase in load. This can be managed by co-ordinating the charging/discharging concerning demand and State of Charge (SoC) of EV. With this, the consumer can get economically benefitted and efficient operation is done to balance the demand on the grid.

There are two ways to use EVs as energy resources. One is the Vehicle to Grid (V2G) technology, in which the energy in the battery is discharged during the peak load times by co-ordinating charging/discharging to reduce the peak load and to benefit customers by minimizing charging costs. Another is the injection of Reactive Power Dispatch (RPD) from EVs for reducing losses, deviations in voltage and running expenses [13]. To assess the potential advantages of V2G provisions accessible from EVs while considering the implementation costs, the Cost–Benefit Analysis (CBA) is used in this context. Electric vehicles run on electricity only. They contain one or more electric motors powered by rechargeable batteries. Electric vehicles have a low running cost compared to normal vehicles as they have fewer moving parts because they use little or no fossil fuels. EVs convert 77% of electrical energy from the grid to power at wheels but conventional gas vehicles converts only 12–30% of gasoline to power. EVs provide a smoother experience of driving, improved acceleration and need less maintenance than internal combustion engine (ICE) vehicles.

There are different levels available for caring the EVs in the charging stations. Level-1, 120-V (V) AC is available only in domestic houses. Level-2, 240 V AC is mostly used by the end-user available both in houses and public stations. Level-3, 480 V DC fast charging is available only at public charging stations.

2 Literature Review

A lot of research is going on in the field of electric vehicles and many authors from around the globe provided a wide range of solutions on technical and economic approaches to decrease the losses on the grid and reduce the charging cost for the consumer.

Kamal Chellappan et al. propose an IEEE-33 bus system demand and SoC values of an EV in real time for 24 h in the day to determine the mode of operation of the electric vehicle [1]. The mode of operation is determined in such a way that

the user and the grid can be benefitted mutually with the maximum value. Along with the mode of operation generated power is calculated to formulate the battery of operation.

Seung Tae Cha et al. propose that, to calculate the SoC level of the electric vehicle, one must analyse the driving data and the driving patterns for different times of the day [2]. Distance and SoC values are analysed for 24 h of the day and are formulated. Driving data is obtained from Danish National Transport Survey (TU data). This obtained data is used for optimal electric vehicle charging to maximize the benefits for the customer and the grid.

Dai Wang et al. estimate the demand for the electric vehicle charging station and analyse the charging behaviour of the vehicle based on charging load profiles and the number of electric vehicles available. And this is done by using the trip chain model which has the information on the trips travelled by the electrical vehicle which can further be used to determine the travel pattern of that vehicle [3]. The simulation results obtained are used to calculate how demand and charging facilities can be met.

M. Bagheri Tookanlou et al. illustrate the need for electric vehicle scheduling, which mainly focuses on benefitting every individual participating in the V2G and G2V operation [4]. In this method, an electrical vehicle charging station finds the right time to buy from an electric supplier to get maximum benefits and similarly, electric vehicles find the shortest driving routes to accommodate cost–benefits for the users. For simulation, nine electrical vehicle charging stations and three electrical suppliers are used to visualize the cost–benefit for the given electric vehicle.

Mohammad Hossein Sarparandeh et al. propose that electric vehicles can work both as batteries and supply back power to the grid. In this way, there is a balance between the supply and demand of electricity. Hence, by using the V2G technology, both the customer and the electricity grid can be benefitted [5]. But it's unclear how the benefits are divided thus using Nash Bargaining Theory determines how to divide these benefits between the electric vehicle charging station and the customer.

Xinzhou Lia et al. illustrate that, for electric vehicle users and power grid operators, a sensitivity analysis was carried out to find critical factors that had an impact on costs and benefits. If the price of power being put into the grid is more than three times higher than the average price, V2G peak shaving services are profitable for electric car users. Users of electric vehicles that purchase batteries at a reduced cost will make more money [6]. Except for electric vehicles, there are no other participants whose advantages outweigh the power plants.

In Mahmoud Ghofrani et al., utilizing the vehicle-to-grid capabilities of electric cars, this study puts out a stochastic framework to reduce the negative impacts of uncertainty and improve the predictability of wind generation. To get optimal results while charging and discharging electric vehicles, a genetic algorithm is used in conjunction with a Monte Carlo simulation [7]. A cost–benefit analysis is used to determine whether it is economically feasible to integrate V2G services with wind power.

In Yosef Shirazi et al., there has been a global shift towards the use of alternative fuels for bus fleets in recent years. This shift has been prompted by concerns about the environment, public health and the economy. Compressed natural gas and electric

automobiles are two viable options that are becoming more popular. The marginal and fleet-wide situations are being investigated in this study. According to the findings, the marginal addition of either a small CNG bus or a small V2G-enabled electric bus is not cost-feasible at present given the existing costs. This study is the first to measure and incorporate the economic effects of extreme cold temperature on electric car battery operations, as well as the decreased V2G revenues [8].

In Zhuowei Luo et al., the development and management of a power infrastructure that accommodates electric vehicles (PEVs) present various obstacles. PEV charging loads may be calculated with the use of a modified Latin hypercube sampling approach for dealing with PEVs' stochastic nature. For this reason, we come up with a novel two-stage optimization approach for determining the best times of day to charge PEVs [9]. As a result of using this approach, it is possible to reduce peak load using PEV charging in the first stage while also reducing fluctuation in the second stage.

In Lance Noel et al., electric cars are becoming more popular as a solution to a variety of issues, including rising fuel prices, the negative health effects of diesel emissions and the effects of climate change. Vehicle-to-grid initiatives give additional economic incentives [10]. Several aspects, such as the expense of fuel, the cost of power and batteries, the health hazards and the market price for frequency control, were taken into consideration and analysed. There would be a substantial increase in the amount of money saved in the net present if all the school district's fleet were converted to electric buses capable of V2G operation. A sensitivity analysis was carried out so that we could assess the extent to which the variables affected the expenses and the benefits.

Nico Brinkel et al. illustrate that shared Evs reduce the grid congestion only at relatively low shared EV adoption and also charging cost proposed in this system is negligible [11]. B.K. Chaturvedi et al. propose that transition from EVs will impact the stakeholders, [12] but it's going to open new investment in this sector.

3 Problem Formulation

The main objective of this proposed work is to reduce the charging cost for an end-user and provide incentives, i.e. how the consumer can be benefitted by using EV as a DG from V2G technology based on the smart charging technique.

The power equation for the distribution system is given as

In Grid-to-Vehicle mode,

$$P_G = P_D + \sum_{i=1}^{24} P_{EV} + P_L \quad (1)$$

In Vehicle-to-Grid mode,

$$P_G + \sum_{i=1}^{24} P_{EV DG} = P_D + P_L \tag{2}$$

where P_G is the real power supply from grid, P_{EV} is the EV acting as a load (G2V), P_{DG} is the distributed generator, P_D is the existing base load, $P_{EV DG}$ is the EV acting as a source (V2G) and P_L is the real power loss.

EVs power charging–discharging limits

$$P_{ch,n,\Delta t} \leq P_{max_{ch,n}} \tag{3}$$

$$P_{disch,n,\Delta t} \leq P_{max_{disch,n}} \tag{4}$$

SoC limits of an EV

$$SoC_{min} \leq SoC_n \leq SoC_{max} \tag{5}$$

And, the value of SoC varies from 0.2 to 0.9. Hence, the efficiencies are taken as 90%.

$$SoC(t) = SoC(t - 1) + P_{batt}(t) * \Delta t * \eta_c \text{ charging mode} \tag{6}$$

$$SoC(t) = SoC(t - 1) + P_{batt}(t) * \Delta t * \eta_d \text{ discharging mode} \tag{7}$$

$$P_{batt}(t) = SoC(t) * E \tag{8}$$

$$\text{Initial Power} = \text{Generation Load} \tag{9}$$

Here, $SoC(t)$ is the State of Charge in the present hour.

$SoC(t - 1)$ is the State of Charge in the previous hour.

η_c, η_d are the efficiencies under charging and discharging modes.

E is the energy of the battery in kWh.

Δt is the respective time interval.

Based on the demand and SoC values, we can determine the mode of operation of the electric vehicle. When the demand is more and SoC value is high, the customer can discharge the power from the electric vehicle to the grid. When the demand is less and SoC value is low, the customer can charge the power from the electric vehicle to the grid. In all the other cases, electric vehicle remains neutral. This can be calculated by comparing P_D and P_G values along with SoC values with the range of SoC_{min} and SoC_{max} values.

4 Methodology

In the proposed approach an IEEE 33 bus system integrated with four electric vehicle charging stations (10, 14, 17 and 30) [14] was considered to analyse the performance of the system for a 24-h horizon.

The following fig shows the block diagram for the V2G operation. A utility grid supplies power to various loads like residential loads, commercial loads and electric vehicle charging stations. An AC–DC bidirectional converter is used to convert AC power from the grid to the DC bus. And to this, DC bus electric vehicle charging stations are connected to which electric vehicles are connected and charged. We know that electric vehicles can supply back power to the grid by using the vehicle to grid technology. Thus, the power is bidirectional from electrical charging stations to the grid (see Fig. 1).

To implement this vehicle-to-grid technology we need to first analyse the demand and the SoC values through which the mode of operation can be determined.

4.1 Mode of Operation

The mode of operation of the electric vehicle can be determined based on the demand and SOC values. When demand is higher and the customer has a high SoC value, the electric car can be used to discharge power to the grid. Customers can charge the power from the electric vehicle to the grid when demand is low, and the SoC value is low. In all other instances, an electric vehicle is considered neutral.

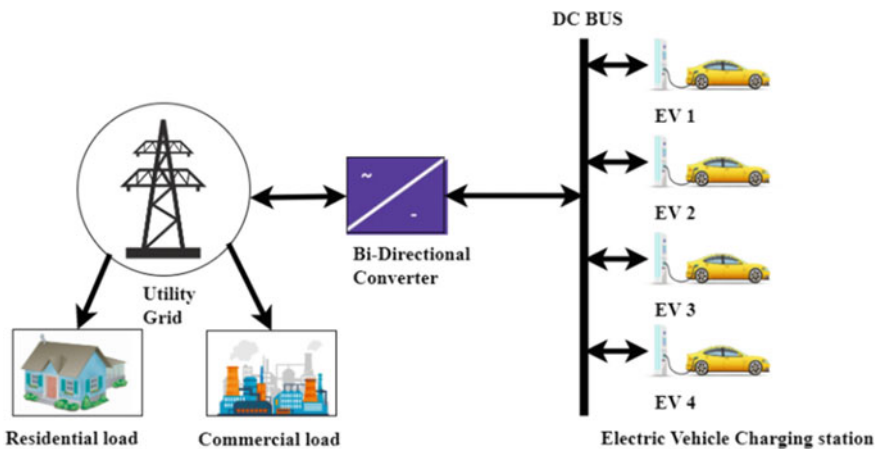


Fig. 1 Block diagram for the proposed model

4.2 Cost–Benefit Analysis

After analysing the demand and SoC, we determine the mode of operation. Based on this mode of operation, we can further analyse based on the cost. First, we need to analyse the cost variation in real time for 24 h of the day and cost varies with respect to the time. After obtaining the cost curve, we need to calculate the mean electricity price for 24 h. After obtaining the mean value, we must calculate the benefit factor with which we can obtain the net profit obtained for both vehicle-to-grid and grid-to-vehicle technology.

4.3 Python

Python is a programming language that is used to build various software and automated tasks. It is a high-level programming language and is a general-purpose language which can be used to perform various programs. In this project, we are using Python libraries like NumPy, pandas and matplotlib. NumPy, stands for numerical Python, is a Python library which is used for manipulating arrays and objects. Pandas is also a Python library which is used to analyse the data. Matplotlib is a plotting library and used to plot graphs and for visualization of the given data. We used Python to plot the graphs for cost–benefit analysis.

5 Results and Discussion

The optimal hourly electricity price supplied by the Energy Supplier (ES) to the EVCS for a 24-h horizon is given in the following Fig. 2.

Firstly, the SoC and demand are obtained through Python for a 24-h horizon, based on the SoC and demand constraints over a period of time the smart charging method is implemented. The following Fig. 3 shows its variations for 24 h of the day for the EVCS at the 10th bus.

At initial hours demand is high and SoC, value is more than the minimum value, thus the electric vehicle user discharges the power to the grid. After reaching the minimum SoC value which is 0.2, the user is in neutral condition. This is because the demand is high, and thus, the cost is higher to charge the vehicle. After the neutral operation when the demand decreases, the user can charge his vehicle at a cheaper price. After the user charges his vehicle and the SoC value reaches the maximum value which is 0.9, the user must again remain in the neutral state as the demand is low. And later when the demand increases, the user can discharge the power to get maximum profits. This cycle is repeated for different values of demand and SoC. Here, three modes of operation, charging, discharging and neutral, are considered based on the demand and SoC constraints for a 24-h period. When demand is high

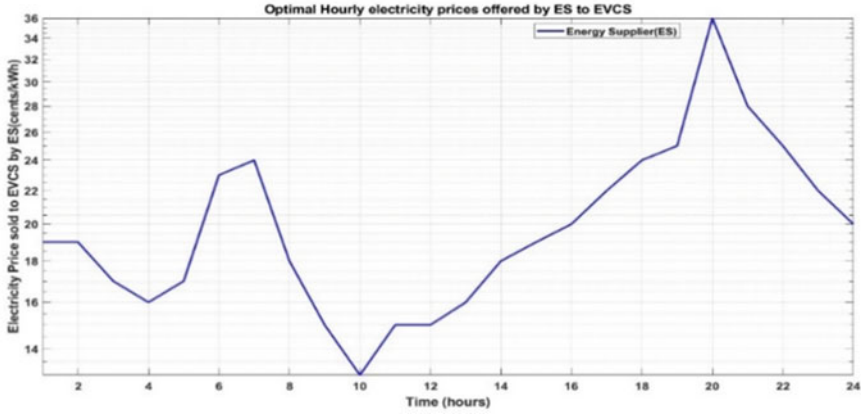
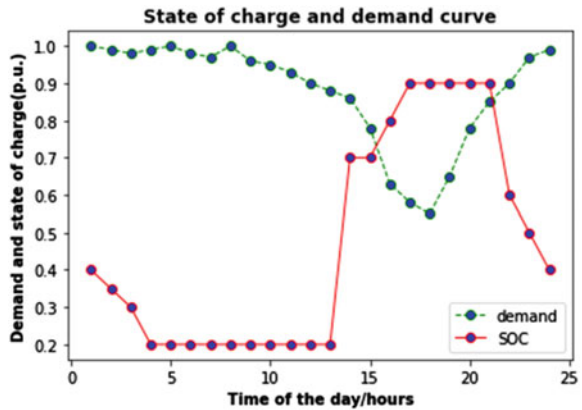


Fig. 2 Electricity Price supplied to EVCS by ES on 24-h horizon

Fig. 3 Demand, SoC curve of EVCS at bus 10



with the SoC is more than the minimum value and available power is low, then V2G mode is preferred (represented as 2), and when demand is low and SoC is less than the minimum value, then G2V mode is preferred (represented as 3). When demand is high with SoC low and when demand is low with SoC high with its available power, it operates the neutral mode (represented as 1) (see Table 1).

In a similar way, the following graphs are determined based on demand and SoC constraints for the EVCS at 14, 17 and 30th buses, respectively (see Figs. 4, 5 and 6).

Table 1 Demand, SoC and Power Constraints for EVCS 10

Time in hrs	Demand in PU	SOC in PU	Mode of operation	Power in PU
1	1	0.4	3	0.432
2	0.99	0.35	3	0.432
3	0.98	0.3	3	0.432
4	0.99	0.2	3	0.432
5	1	0.2	3	0.432
6	0.98	0.2	1	0.432
7	0.97	0.2	1	0.432
8	1	0.2	1	0.432
9	0.96	0.2	1	0.432
10	0.95	0.2	1	0.432
11	0.93	0.2	1	0.432
12	0.9	0.2	1	0.432
13	0.88	0.2	1	0.432
14	0.86	0.7	2	0.432
15	0.78	0.7	2	0.432
16	0.63	0.8	2	0.48
17	0.58	0.9	1	0.528
18	0.55	0.9	1	0.528
19	0.65	0.9	1	0.528
20	0.78	0.9	1	0.528
21	0.85	0.9	1	0.528
22	0.9	0.6	3	0.528
23	0.97	0.5	3	0.48
24	0.99	0.4	3	0.432

Fig. 4 Demand, SoC curve of EVCS at bus 14

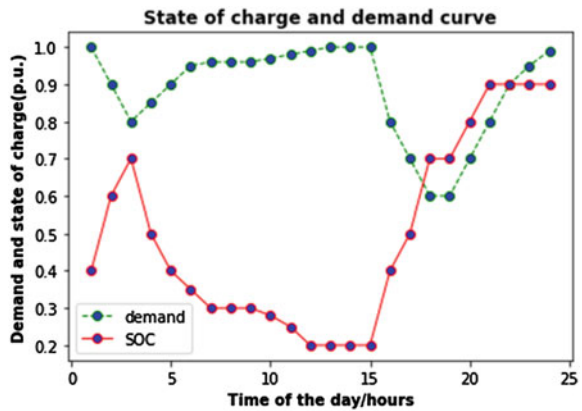


Fig. 5 Demand, SoC curve of EVCS at bus 17

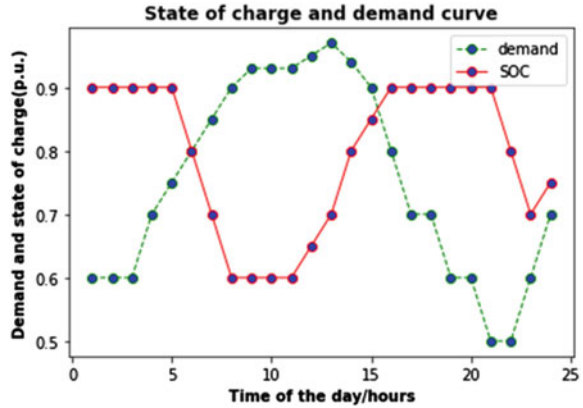
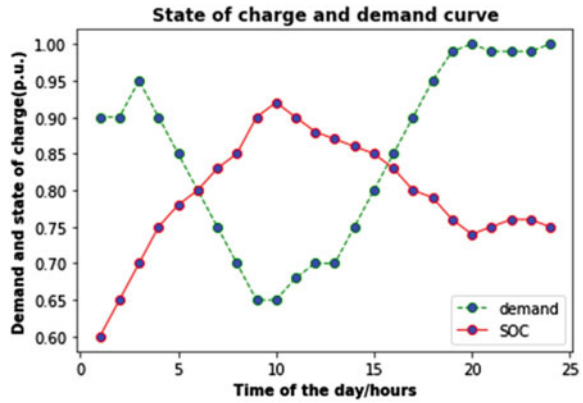


Fig. 6 Demand and SoC curve of EVCS at bus 30



5.1 Cost–Benefit Analysis

Based on the mode of operation and estimating the cost at different times of the day, the cost analysis can be carried out. To analyse the benefits of the end user, we need to first calculate the mean electricity value which is the average of the electricity price provided by the energy supplier to the EVCS for each time of the day. After obtaining the mean value, we need to calculate the benefit factor which is given by

$$\text{benefit factor} = (\text{power}/\text{SoC}) * \text{Demand}. \tag{10}$$

With benefit factor, the total electricity price can be estimated

$$\text{Total price} = (\text{mean price}) + \text{benefit factor} * \text{mean price}. \tag{11}$$

And net profit is obtained by subtracting the total price by mean price.

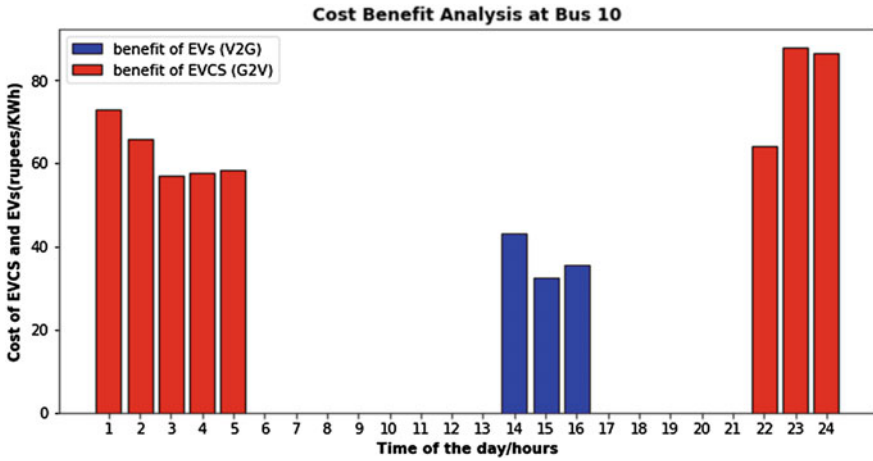
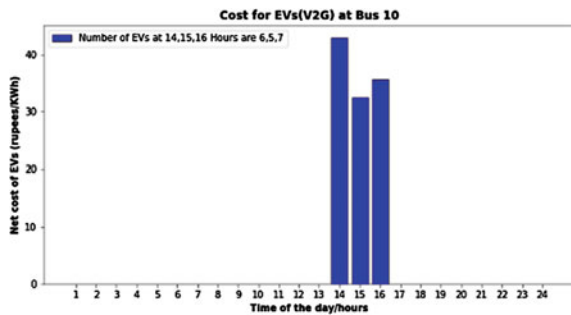


Fig. 7 Cost–benefit curve at bus 10

Fig. 8 Cost curve at bus 10



The following Fig. 7 shows the net profit earned by the G2V and V2G modes by the EVCS at the 10th bus and the end user based on the smart charging technique by considering the off and peak load times for a 24-h horizon with load demand and SoC constraints.

The following Figs. 8, 9, 10 and 11 show the cost–benefit analysis for V2G mode with respect to the EVs connected to the respective charging station.

Fig. 9 Cost curve at bus 14

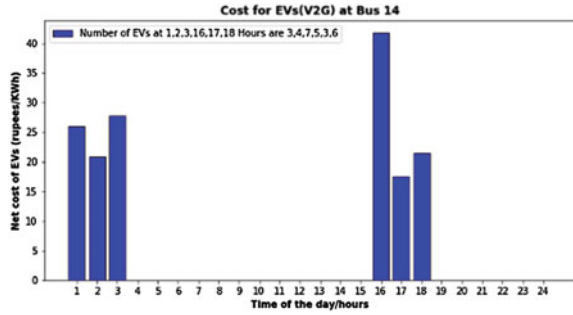


Fig. 10 Cost curve at bus 17

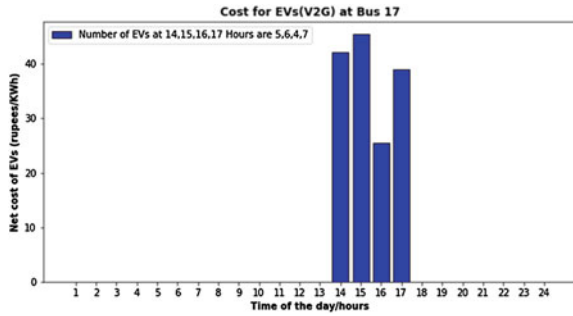
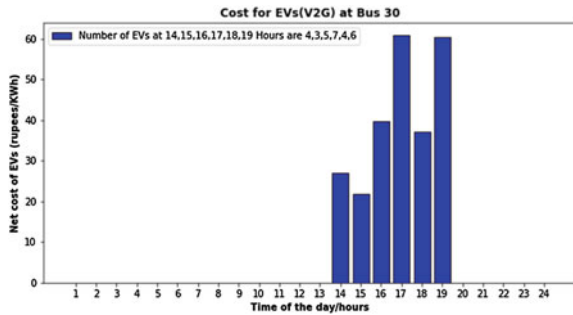


Fig. 11 Cost curve at bus 30



6 Conclusion

With the massive penetration of EVs, there is a huge impact on distribution system, so there is a need for DGs integrated into the system to minimize its effect. The stochastic nature of the DGs with renewable sources and its high capital cost, where the EV is chosen as a load, i.e. G2V and source, i.e. V2G operating in bi-directional mode with a smart charging technique based on the off and peak demand for a 24-h horizon. The mutual benefits of the electric vehicle charging station and EV end users are analysed through cost–benefit analysis. In addition, from the V2G technology

Smart charging technique is used during the charging/discharging mode based on the demand and SoC constraints. The cost analysis is carried out for four EVCS integrated with the IEEE 33 bus system and analysed the benefits obtained to the end user and EVCS from distribution system. Therefore, EV acting as DG is one of the promising opportunities to support the distribution system in the technical and economic benefits. For the extension of the research, the battery degradation is considered for the V2G operation in both the technical and economic aspects.

References

1. Chellappan K, Murty VSSCS, Krishnan N, Sharma G, Senjyu T (2021) Real power loss minimization considering multiple DGs and battery in distribution system. *Electr Power Compon Syst* 49(6–7):563–572. <https://doi.org/10.1080/15325008.2021.2011488>
2. Wu Q et al (2010) Driving pattern analysis for electric vehicle (EV) grid integration study. In: 2010 IEEE PES innovative smart grid technologies conference Europe (ISGT Europe), pp 1–6. <https://doi.org/10.1109/ISGTEUROPE.2010.5751581>
3. Wang D, Gao J, Li P, Wang B, Zhang C, Saxena S (2017) Modeling of plug-in electric vehicle travel patterns and charging load based on trip chain generation. *J Power Sources* 359:468–479. ISSN 0378-7753. <https://doi.org/10.1016/j.jpowsour.2017.05.036>
4. Bagheri Tookanlou M, Marzband M, Al Sumaiti A, Mazza A (2020) Cost-benefit analysis for multiple agents considering an electric vehicle charging/discharging strategy and grid integration. In: 2020 IEEE 20th mediterranean electrotechnical conference (MELECON), pp 19–24. <https://doi.org/10.1109/MELECON48756.2020.9140637>
5. Sarparandeh MH, Ehsan M (2017) Pricing of vehicle-to-grid services in a microgrid by nash bargaining theory. *Math Probl Eng* 2017: 11. Article ID 1840140. <https://doi.org/10.1155/2017/1840140>
6. Li X, Tan Y, Liu X, Liao Q, Sun B, Cao G, Li C, Yang X, Wang Z (2020) A cost-benefit analysis of V2G electric vehicles supporting peak shaving in Shanghai. *Electr Power Syst Res* 179:106058. ISSN 0378-7796. <https://doi.org/10.1016/j.epsr.2019.106058>
7. Ghofrani M, Arabali A, Etezadi-Amoli M, Fadali MS (2014) Smart scheduling and cost-benefit analysis of grid-enabled electric vehicles for wind power integration. *IEEE Trans Smart Grid* 5(5):2306–2313. <https://doi.org/10.1109/TSG.2014.2328976>
8. Shirazi Y, Carr E, Knapp L (2015) A cost-benefit analysis of alternatively fueled buses with special considerations for V2G technology. *Energy Policy* 87:591–603. ISSN 0301-4215. <https://doi.org/10.1016/j.enpol.2015.09.038>
9. Luo Z, Hu Z, Song Y, Xu Z, Lu H (2013) Optimal coordination of plug-in electric vehicles in power grids with cost-benefit analysis—Part I: enabling techniques. *IEEE Trans Power Syst* 28(4):3546–3555. <https://doi.org/10.1109/TPWRS.2013.2262318>
10. Noel L, McCormack R (2014) A cost benefit analysis of a V2G-capable electric school bus compared to a traditional diesel school bus. *Appl Energy* 126:246–255. ISSN 0306-2619. <https://doi.org/10.1016/j.apenergy.2014.04.009>
11. Brinkel N, Alskafif T, van Sark W (2022) Grid congestion mitigation in the era of shared electric vehicles. *J Energy Storage* 48:103806. <https://doi.org/10.1016/j.est.2021.103806>

12. Chaturvedi BK, Nautiyal A, Kandpal TC, Yaqoot M (2022) Projected transition to electric vehicles in India and its impact on stakeholders. *Energy Sustain Dev* 66:189–200. ISSN 0973-0826. <https://doi.org/10.1016/j.esd.2021.12.006>
13. Majhi R (2020) A systematic review of charging infrastructure location problem for electric vehicles. *Transp Rev*, 41. <https://doi.org/10.1080/01441647.2020.1854365>
14. Golla NK, Sudabattula SK, Suresh V (2022) Optimal placement of electric vehicle charging station in distribution system using meta-heuristic techniques. *Math Model Eng Probl* 9(1):60–66. <https://doi.org/10.18280/mmep.090108>

Performance Analysis of a 3.2-kW Solar PV Electric Vehicle Charging Station Under Variable Climatic Conditions



Bhuwan Pratap Singh, Sunil Kumar Goyal, and Shahbaz Ahmed Siddiqui

Abstract Due to an alarming situation of global warming across the world in the past few years, eco-friendly transportation system based on green (non-conventional) energy has been increasingly adopted across the world. However, the challenge in the adoption of this new emerging technology is its sustainable deployment on a large scale. In the past couple of years, Electric Vehicles (EVs) are commercialized on a large scale and are available in the market for consumers. The emission of greenhouse gases has been reduced nowadays with the replacement of internal combustion (IC) engines by the emission-free EVs. Therefore, charging of these EVs with solar photovoltaic systems (SPVS), i.e., PV-EV charging is an interesting option and attracting the attention of researchers throughout the world. In view of this, a PV-based charging methodology for EVs is proposed in this paper with SPVS, i.e., (PV-EV Charging). In this methodology, the power generation requirements through SPVS for charging EVs have been estimated based on the technical and performance specifications of different EVs (Cars) available in the Indian market. To charge the EVs effectively, an MPPT charge controller is implemented based on Perturb & Observe (P&O) technique along with the DC/DC boost converter to maximize the PV generation through SPVS. The simulation model is developed in MATLAB/Simulink environment. The performance analysis of SPVS with the P&O MPPT technique to charge EVs is studied under different operating conditions including actual (practical) climatic conditions.

Keywords PV-EV charging · Solar photovoltaic system (SPVS) · MPPT techniques · Perturb & Observe (P&O) · Variable climatic conditions

B. P. Singh · S. K. Goyal (✉) · S. A. Siddiqui
Manipal University Jaipur, Jaipur, Rajasthan, India
e-mail: sunilkumar.goyal@jaipur.manipal.edu

© The Author(s), under exclusive license to Springer Nature Singapore Pte Ltd. 2024
S. K. Goyal et al. (eds.), *Flexible Electronics for Electric Vehicles*, Lecture Notes
in Electrical Engineering 1065, https://doi.org/10.1007/978-981-99-4795-9_21

219

1 Introduction

The utilization of renewable energy sources (RES) is precipitously increasing worldwide at present to overcome the hazardous effects of conventional energy sources (CES) from environmental and economic perspectives. Mostly, the RES either comes directly or indirectly from the sun or wind. Among all RES, solar energy (energy directly received from the Sun) is one of the plentiful sources of renewable energy [1]. It has numerous applications, viz. heating, lightening homes, cooking, power generation, irrigation systems, street lights operation, electric vehicle charging, and a variety of industrial and commercial applications [2]. Solar photovoltaic (PV) systems are expected to deliver 5% of global energy demand by 2030 and rise up to 11% by 2050 [3].

Since the worldwide acceptance of electric vehicles (EVs) is nowadays increasing rapidly and attained a 2.6% market share in 2019 [4]. The expanding consumer base of EVs along with the attainment of market share presents a trend toward the electrification of transportation system [5]. As per the climatic conditions of different geographic locations like Europe, the electrification of transportation is also desirable due to the low carbon intensity in the electricity mix. Increasing adoption of EVs requires an increased demand for EV charging stations and electrical energy. For EVs acceptance and their worldwide adoption, it is essential to provide highly efficient charging infrastructure for EVs [6]. However, considerably a high capital investment is required to provide large scale highly efficient clusters of charging stations for EVs [7].

This paper analyses the performance of a stand-alone, off-grid solar PV system for EV charging under actual climatic conditions. The benefits of the proposed system are as follows:

1. The capital investment required for the installation of large-scale highly efficient charging stations for EVs would be reduced to a significant level by the elimination of grid power utilization.
2. The cost of local energy generation through grid would also be reduced with the reduced cost of electricity generation through solar PV systems for charging of EVs.
3. The charging of EVs would also be possible at locations with highly constrained grid infrastructure.

In this article, the power generation capacity of SPVS to charge the EVs effectively has been estimated based on the performance and technical specifications of the various EVs (Cars) available in the Indian market. Firstly, daily average running distance of the EV has been assumed and hence the requirement(s) of electricity is calculated for the charging of vehicles. To meet the power requirement(s), a stand-alone SPVS is developed in MATLAB/Simulink along with an MPPT charge controller to enhance the power generation through SPVS. Perturb & Observe (P&O) MPPT technique is selected for this purpose as it is user-friendly, most robust, easy to implement, and industrialized technique. The implementation of the MPPT technique

along with a DC/DC boost converter results in maximum utilization of available PV energy for electricity generation [8].

The SPVS is tested and its performance is analyzed under actual weather conditions. The actual solar irradiance and temperature data from 06:00 AM to 06:30 PM has been taken for a clear shiny day with gradual changes and for a rainy day with abrupt changes. The weather data is taken from National Solar Radiation Database (NSRDB) collaborated with The National Renewable Energy Laboratory (NREL) [9]. The location of Manipal University Jaipur, India, with longitude 75.565234 and latitude 26.843855 is selected for the live data. The foremost requirement of an EV charger circuit is to maintain a low ripple current and high power factor at the receiving end and the sending end, respectively. To perform this function and ensure effective operation, a DC/DC boost converter is implemented in the charger circuit cascaded with a PWM boost rectifier. The paper is followed by the system modeling, simulation results and discussion, conclusion, and future perspectives of the proposed work.

2 Charging of EVs

2.1 Charging Approaches for EVs

The availability of public charging infrastructure is not sufficient to meet the demand as the demand for EVs nowadays increasing rapidly day by day. Two types of charging facilities are available, one is personal chargers which are usually installed at the home location of the user and the other is public charging stations. It is expected that there will be 13 million public charging stations and 130 million personal charging points by the year 2030 [10]. Hence, this would include a great investment from global infrastructure point of view. Apparently, there are three types of charging methods for almost all EVs, viz. [11]:

Method I: For household purpose, a set of cords to be operated on single-phase AC supply is provided to the consumers which can charge EV in 7–30 h based on the sizing of battery.

Method II: Second is to charge the medium-sized EVs through AC supply, it took around 4–8 h to charge the EVs from 0 to 80%. But, this requires three-phase AC supply which is usually available at public places.

Method III: Third is most effective which is DC supply-based fast charger. It can provide up to 120 kW and can charge the EVs (with Li-ion battery) from 0 to 80% in just 30–50 min.

A stand-alone SPVS-based fast-charging (DC) station to charge EVs is designed in this paper, and its performance under actual weather conditions is investigated. Moreover, to ensure fast charging, an MPPT technique is also implemented for the extraction of maximum available instantaneous PV power.

2.2 Technical Estimations

A wide range of EVs is available in the Indian automobile market these days and many more manufacturers are under planning of launching various new and fully electrically operated EVs very soon in the Indian market. Since the operating and technical specifications of EVs are unlike IC engine-based vehicles, viz. fuel tank capacity, cubic capacity, engine displacement, etc. Hence, an overview is presented here about the operating and technical specifications of EVs available in the Indian automobile market. Table 1 shows the technical and operating specifications, viz. max. range in kms, motor capacity, battery capacity, type of charging, and charging time [12]. Based on the features available in the interior of the car, its max. driving range and the segment of car, the battery capacity varies from manufacturer to manufacturer.

The power generation requirements for SPVS to charge the EVs have been estimated based on the operating and technical specifications of various EVs given in Table 1. Based on the specifications of the Tata Nexon EV Car which is the most popular and highest-selling EV these days, the power generation requirements for SPVS have been calculated as follows:

$$\text{Energy consumption (kWH) for Tata Nexon EV is } \frac{312}{30.2} = 10.33 \text{ kms/kWH}$$

Daily average utilization of vehicle is assumed as 250 kms

$$\text{Consumption of energy per day: } \frac{250}{10.33} = 24.20 \text{ kWH}$$

Average time of solar insolation in a day: 8 hours

$$\text{SPVS capacity required for generating required kWH: } \frac{24.20}{8} = 3.025 \text{ kW}$$

Therefore, the capacity of SPVS required for generating the required kWH is 3.025 kw. To ensure the required PV power generation through installed SPVS, a 3.2 kW stand-alone SPVS has been developed in the proposed work.

3 System Modeling

A stand-alone SPVS of 3.2 kW capacity is developed in MATLAB/Simulink to generate the required electrical power based on the above calculation to charge the EVs effectively. A PV module of “Waaree Energies WS-270” is considered which is available in Simulink to develop the desired SPVS. The technical specifications and parameters of the selected PV module are presented in Table 2. Two strings of six

Table 1 Operating and Technical Specifications of Cars (EVs) [12]

S. No	Car model (EVs)	Manufacturer	Maximum driving range (kms)	Battery capacity (kWH)	Full charge time (fast charge with DC supply)	Maximum power (bhp)	Maximum speed (kmph)
1	Tigor EV	Tata Motors	213	21.5	65 min (0–80%)	40.23	80
2	Nexon EV	Tata Motors	312	30.2	60 min (0–80%)	127.0	120
3	Nexon EV Max	Tata Motors	437	40.5	56 min (0–80%)	141.04	140
4	Kona Electric	Hyundai Motor Company	452	39.2	60 min (0–80%)	134.1	167
5	MG ZS EV	MG Morris Garages	340	44.5	40 min (0–80%)	140.8	140
6	E Verito	Mahindra and Mahindra	110	21.2	90 min (0–80%)	41.57	86
7	EQC	Mercedes-Benz	455–471	80.0	90 min (10–90%)	402.3	180
8	Audi RS e-tron GT	Audi	401–481	93.4	22.5 min (5–80%)	636.98	266
9	Audi e-tron GT	Audi	388–500	93.4	22.5 min (5–80%)	522.99	245
10	Kia EV6	Kia Motors	500	77.4	18 min (10–80%)	225.86	192
11	BMW i4	BMW	493–590	83.9	31 min (0–80%)	335.25	225
12	Porsche Taycan	Porsche	354.431	93.4	22.5 min (5–80%)	321.84	260
13	Mini Cooper SE	Mini Cooper	270	32.6	35 min (0–80%)	181.03	150
14	Jaguar I-Pace	Jaguar	470	90	45 min (0–80%)	394.26	200
15	BMW iX	BMW	372–425	71	31 min (0–80%)	321.84	200

such modules in each string have been used to design the desired PV array; hence, 12 PV modules of “Waaree Energies WS-270” are used in the proposed system. The aforesaid designed PV array with 12 PV modules is capable to generate 3238.20 W (3.2 kW) electrical power which is slightly greater than the calculated power required to charge the EVs effectively and is sufficient to charge an EV overnight.

To step-up the voltage level of PV voltage, a DC/DC boost converter is implemented along with the SPVS [13]. It also ensures the maximum power extraction

Table 2 Technical specifications of PV module “Waaree Energies WS-270”

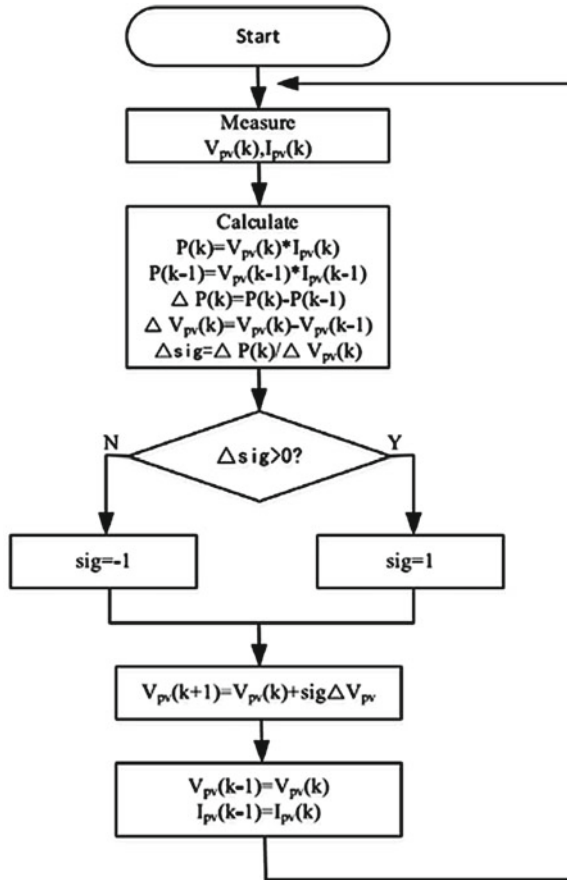
Parameters	Value
P_{mpp} (W)	269.85
I_{mpp} (A)	07.71
V_{mpp} (V)	35.00
I_{sc} (A)	08.37
V_{ocv} (V)	43.00
R_s (ohms)	0.34857
R_p (ohms)	111.839
N_s	72
kV _{OC} (%/°C)	- 0.359
kI _{SC} (%/°C)	0.062999
Number of strings	2
Number of PV modules in one string	6

from the SPVS along with the boost up in the voltage level [14]. An MPPT charge controller is also implemented in the DC/DC boost converter to generate desired duty cycle and trigger the converter. Perturb & Observe (P&O) MPPT technique is selected for this purpose as it is user-friendly, most robust, easy to implement, and industrialized technique. With the variation in climatic conditions, viz. irradiance and temperature, $I-V$ and $P-V$ curves of PV cells vary non-linearly, and hence, it is quite difficult to track the maximum power point (MPP) on the $P-V$ curve [15]. The main objective of MPPT techniques is to continuously track the MPP on the $P-V$ curve and with reference to the voltage at actual MPP, it generates the reference voltage for the DC/DC boost converter.

The reference voltage is calculated based on the error in the measured and calculated power in each iteration, and hence, it keeps on tracking the new MPP with the variation in climatic conditions at every instance. Figure 1 shows the flow chart of the P&O MPPT technique [16]. Figure 2 shows the complete SPVS developed in MATLAB/Simulink R2020a.

The SPVS is designed with a PV array of 3.2 kW, DC/DC boost converter, MPPT charge controller, and the load as shown in Fig. 2 [17]. The load in this system is assumed as an EV of desired capacity which can be charged overnight. The power generated by the SPVS during the day must be stored in an energy storage unit (ESU) for overnight charging or it can also be used directly to charge the vehicle if no vehicle is to be charged in the night.

Fig. 1 Traditional P&O MPPT technique: flow chart [16]



4 Simulation: Results and Discussion

The testing and analysis of the developed SPVS have been carried out under actual climatic conditions for two different weathers to test the ability of maximum power extraction from the PV array. To estimate the efficiency of the MPPT technique and the SPVS, the difference between generated and the delivered power and voltage are calculated and studied.

Case 1: The actual temperature and solar irradiance data in case-1 has been taken for a clear shiny day, i.e. 11 June 2022 from National Solar Radiation Database (NSRDB) collaborated with The National Renewable Energy Laboratory (NREL).

The location of Manipal University Jaipur, India, with longitude 75.565234 and latitude 26.843855 is selected for the live data. The irradiance and temperature both change (increase and decrease) gradually throughout the day from 06:00 AM to 06:00 PM. Figure 3 and Fig. 4 show the pattern of variable irradiance and temperature for case-1, respectively.

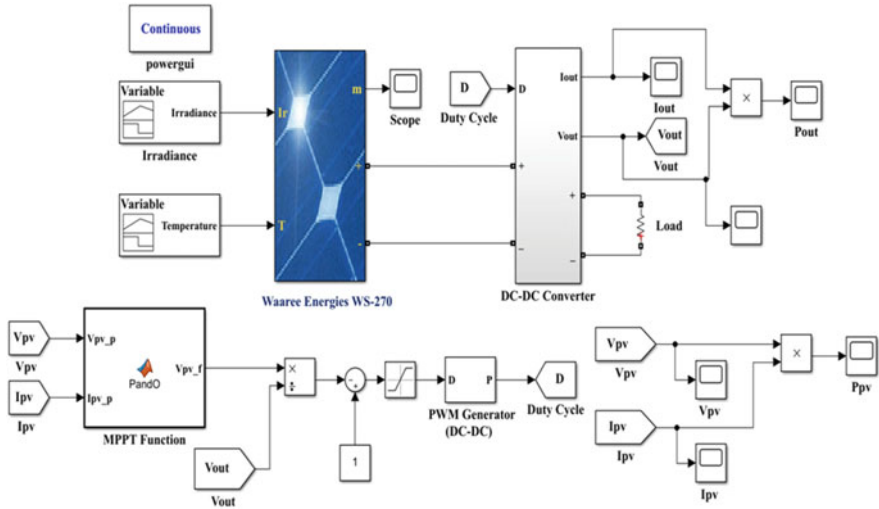


Fig. 2 Stand-alone SPVS of 3.2 kW capacity for EV charging

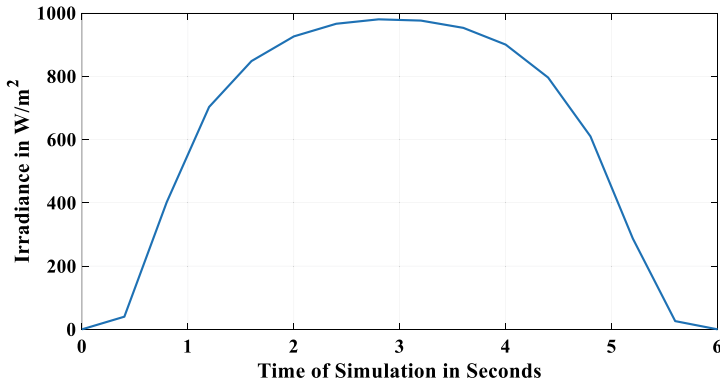


Fig. 3 Variation of solar irradiance for Case-1

Figures 5 and 6 show the variation in output power on the load side, i.e. P_{out} , and the variation in the generated voltage on the PV array side, respectively.

It is clear from Fig. 5 that, after convergence of MPPT at MPP, the maximum power received at the load is 2928.50 W and the expected maximum power at MPP is 3238.20 W. Hence, the tracking efficiency of the P&O MPPT technique is found as 90.44% in this case excluding the loss of power in transmission and converter.

The variation in the PV array voltage is shown in Fig. 6. It is seen from the figure that the maximum voltage extracted from PV array after the convergence of MPPT technique at MPP is 201.68 V, i.e., 96.03% of the actual expected maximum voltage, i.e., $35 \times 6 = 210$ V at MPP. Therefore, it is clearly observed in this case that

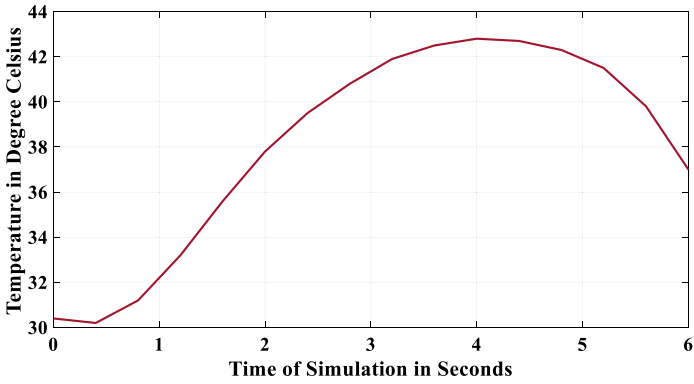


Fig. 4 Variation of temperature for Case-1

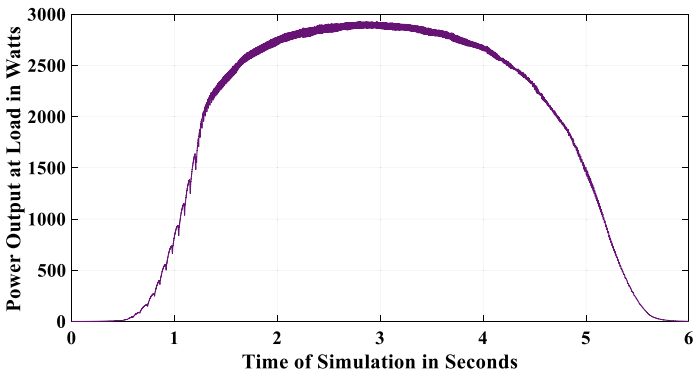


Fig. 5 Variation of output power (P_{out}) for Case-1

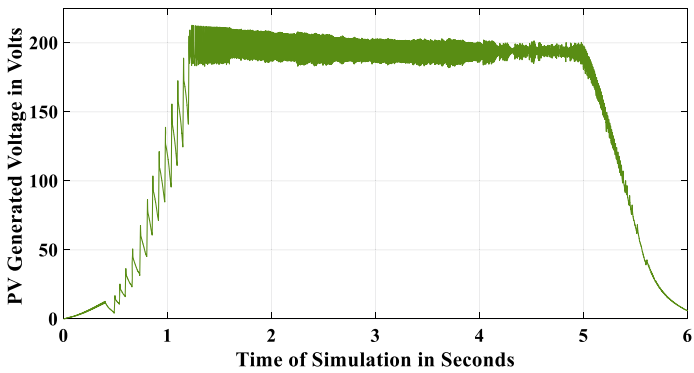


Fig. 6 Variation of generated PV voltage (V_{pv}) for Case-1

the tracking efficiency of P&O reduces with variations in climatic conditions. As under these conditions, the maximum available solar irradiance (G) is 980 W/m^2 at temperature (T) $40.8 \text{ }^\circ\text{C}$. However, the efficiency of the same algorithm is reported as 99.75% under STC conditions, i.e., at $G = 1000 \text{ W/m}^2$ and $T = 25 \text{ }^\circ\text{C}$.

Case 2: The actual temperature and solar irradiance data in case-2 has been for a rainy day, i.e., 15 June at Manipal University Jaipur, India, location with longitude 75.565234 and latitude 26.843855 . The irradiance and temperature both change (increase and decrease) gradually as well as rapidly when the clouds suddenly appeared with/without rain. Figures 7 and 8 show the pattern of variable irradiance and temperature from 06:00 AM to 06:00 PM for case-2, respectively.

The inputs to the SPVS have been provided as per the variations in irradiance and temperature as shown in Figs. 7 and 8, respectively, and the performance of the system has been studied. Figures 9 and 10 show the output power received on the load side, i.e., P_{out} and the voltage generated on the PV array side, i.e., V_{pv} , respectively.

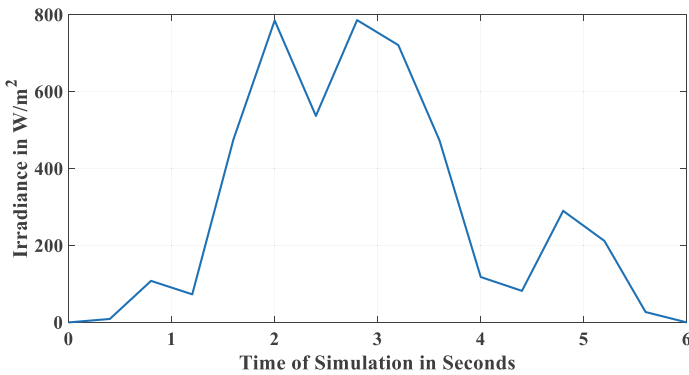


Fig. 7 Variation of solar irradiance for Case-2

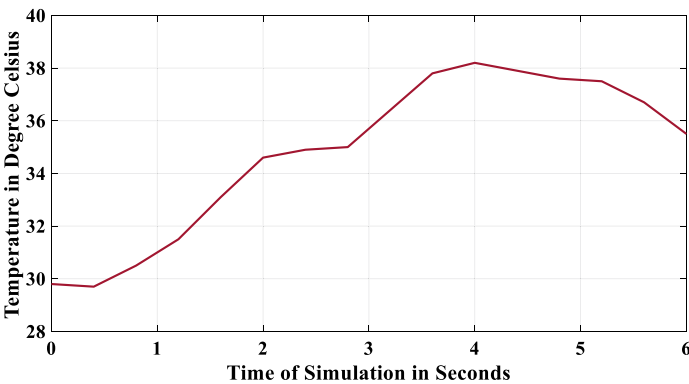


Fig. 8 Variation of temperature for Case-2

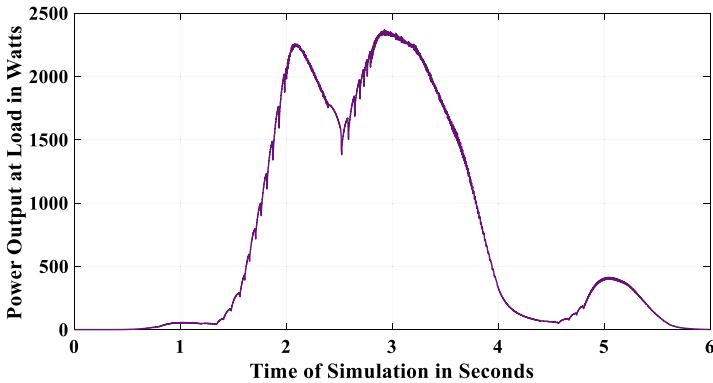


Fig. 9 Variation of output power (P_{out}) for Case-2

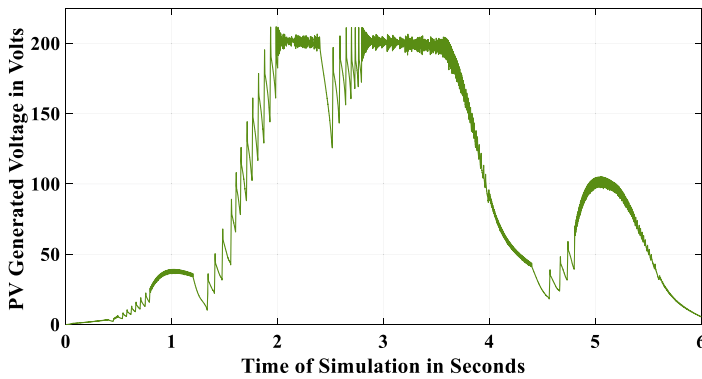


Fig. 10 Variation of generated PV voltage (V_{pv}) for Case-2

P&O is one of the most robust and conventional MPPT techniques which was developed a few decades back in the earlier days of challenging situation for MPP tracking. In the past few decades, numerous modifications and developments in its approach to track newer MPP have also been proposed by various researchers. It is seen under the variations in output power and generated PV voltage curves in Figs. 9 and 10 that the conventional P&O MPPT technique produces oscillations in the tracking of actual MPP before it settles down at new MPP with the abrupt variation in the irradiance and temperature. In Fig. 9 of output power variations, the maximum power received on the load side at 2.8 s is 2366.20 W, when the level of irradiance is maximum, i.e., 786 W/m² and the temperature is 35 °C which is only 73.07% of the actual expected power at MPP. The reason for this low extraction percentage is that the level of instantaneous temperature and irradiance are quite different from the desired values at STC. Also, the temperature and irradiance both are varying abruptly due to the sudden appearance of clouds with/without rain. Therefore, the

prediction of the desired reference voltage for newer MPP is quite a challenging task for an MPPT technique because the new MPP shifts to a newer position very quickly under abrupt changes in the input parameters.

Moreover, if the voltage generation at the PV array side is observed in Fig. 10, the oscillations in tracking the maximum voltage are present at the generation side also. The maximum voltage generated on the PV array side is 203.5 V at 2.8 s which is only 96.90% of the expected maximum voltage at MPP. Amplitudes of oscillations near MPP are not desirable though the efficiency to extract maximum voltage on the generation side under the abrupt changes in the level of irradiance and temperature is satisfactory. The drop in the efficiency on the generation side at 2.8 s is due to the low level of irradiance and a quite high temperature. Due to this reason, the researchers are still interested and are continuously working toward the performance enhancement of the well-known conventional MPPT technique, i.e., P&O, and also working toward the development of such new techniques. So that the new developments could handle these types of abrupt variations in the atmospheric conditions and extract maximum power from the SPVS. This will also result in the enhanced overall performance of the SPVS which will not be affected by abruptly varying climatic conditions.

5 Conclusion

EVs can easily be charged or refueled by the power generated through SPVS or other RES which results in reduced load on the utility grid. A stand-alone SPVS is thus developed in the proposed work for the electrical power generation required to charge the EVs. An MPPT charge controller along with a DC/DC boost converter is also implemented to ensure the maximum power generation by SPVS. To track MPP on the $P-V$ curve of SPVS, P&O MPPT technique is selected in this work. The SPVS developed in MATLAB/Simulink environment and its performance has been analyzed for the actual (practical) weather conditions. The weather data is taken from the National Solar Radiation Database (NSRDB) collaborated with The National Renewable Energy Laboratory (NREL) at Manipal University Jaipur, India, location for two different weathers. Under normal shiny days in case-1, the performance of SPVS with a tracking efficiency of 90.44% is satisfactory to track MPP. The lower efficiency results due to the continuous variation (gradual rise and fall) in the level of irradiance as well as the lesser maximum available irradiance, i.e., 980 W/m^2 at higher temperature, i.e., $40.8 \text{ }^\circ\text{C}$.

However, under abruptly changing climatic conditions, i.e., abrupt variations in the temperature and irradiance on a rainy day, the tracking efficiency of SPVS falls down to 73.07% in case-2. Moreover, the amplitude and frequency of oscillations have also been increased with reduced tracking efficiency as compared to the previous case. It can be concluded here that, under abruptly varying atmospheric conditions, the selected MPPT technique, i.e., P&O is inefficient. Therefore, further modifications and improvements in tracking algorithm are necessary to enhance its efficacy of

tracking actual MPP under actual (practical) atmospheric conditions. This would result in increased efficiency of tracking and would ensure maximum utilization of the available sunlight by extracting maximum power through PV array and as a result effective charging of EVs could be achieved.

References

1. Osório GJ, Gough M, Lotfi M, Santos SF, Espassandim HM, Shafie-khah M, Catalão JP (2021) Rooftop photovoltaic parking lots to support electric vehicles charging: a comprehensive survey. *Int J Electr Power Energy Syst* 133:107274
2. Singh BP, Goyal SK, Siddiqui SA (2019) Grid connected-photovoltaic system (GC-PVS): Issues and challenges. In: IOP conference series: materials science and engineering, vol 594, no 1. IOP Publishing, p 012032
3. Frankl P, Nowak S, Gutschner M, Gnos S, Rinke T (2010) International energy agency technology roadmap: solar photovoltaic energy
4. Abergel T, et al (2020) Global EV outlook 2020. International Energy Agency (IEA), Paris, France, p 276
5. Ghotge R, van Wijk A, Lukszo Z (2021) Off-grid solar charging of electric vehicles at long-term parking locations. *Energy* 227:120356
6. Hall D, Lutsey N (2017) Emerging best practices for electric vehicle charging infrastructure. The International Council on Clean Transportation (ICCT): Washington, DC, USA, 54.
7. Nicholas M (2019) Estimating electric vehicle charging infrastructure costs across major U.S. metropolitan areas. International Council on Clean Transportation, Washington DC, USA, p 11
8. Singh BP, Goyal SK, Siddiqui SA (2020) Analysis and classification of maximum power point tracking (MPPT) techniques: a review. *Intelligent computing techniques for smart energy systems*. pp 999–1008
9. <https://nsrdb.nrel.gov/data-sets/international-data>
10. Karthikeyan S, Bragruthshibu H, Logesh R, Srinivasan K, Tarjanbabu S (2021, March) Solar based fast tag charger for electrical vehicle. In: 2021 7th international conference on advanced computing and communication systems (ICACCS), vol 1. IEEE, pp 776–779
11. Shatnawi M, Ari KB, Alshamsi K, Alhammadi M, Alamoodi O (2021, February) Solar EV charging. In: 2021 6th international conference on renewable energy: generation and applications (ICREGA). IEEE, pp 178–183
12. <https://www.cardekho.com/compare/mg-zs-ev-and-tata-nexon-ev-and-hyundai-kona-and-tata-tigor-ev.html>
13. Singh BP, Goyal SK, Siddiqui SA, Kumar P (2020) A study and comprehensive overview of inverter topologies for grid-connected photovoltaic systems (PVS). *Intell Comput Tech Smart Energy Syst*, 1009–1017
14. Kumar P, Kour M, Goyal SK, Singh BP (2020) Multilevel inverter topologies in renewable energy applications. In: *Intelligent computing techniques for smart energy systems*. Springer, Singapore, pp 891–902
15. Goyal SK, Sungh BP, Kumar A, Kumar P, Saraswat A (2020) Modelling and simulation of a solar PV system: a comprehensive study. In: 2020 international conference on computation, automation and knowledge management (ICCAKM). IEEE, pp 367–372
16. Peng L, Zheng S, Chai X, Li L (2018) A novel tangent error maximum power point tracking algorithm for photovoltaic system under fast multi-changing solar irradiances. *Appl Energy* 210:303–316
17. Singh BP, Goyal SK, Siddiqui SA, Saraswat A, Ucheniya R (2022) Intersection point determination method: a novel MPPT approach for sudden and fast changing environmental conditions. *Renewable Energy* 200:614–632

Application of SEPIC Converter to Developed Electric Vehicle Charging Station Based on PV Source



Ram Niwash Mahia and Rajat Kumar

Abstract The ever-increasing concern about climate change as a result of emitting greenhouse gases has led to a greater emphasis on discovering and developing clean energy alternatives. It has played a significant part in the development of electrification in the transportation industry and has contributed to the rise in the popularity of electric cars. Therefore, a major benefit and degree of control for charging electric vehicles is afforded by a charging station that makes use of renewable energy sources. The purpose of this study was to demonstrate a solar energy power conversion system (SEPIC) based on a maximum power point tracking (MPPT) controller and a power and energy optimization (P&O) algorithm. The job was done for the sake of display. Photovoltaic (PV) systems require a constant voltage in order to regulate their output voltage and output power in response to varying levels of irradiance and temperatures. The operational voltage of a PV system is the consistent electric current it provides. This research makes use of data collected on solar irradiation at Ashok Leyland Bhandara, Maharashtra. Using a SEPIC converter allows for a high-voltage transformation ratio above the input voltage while minimizing loss across the switch. Improved energy conversion and increased convenience are the outcomes of combining solar cells with MPPT controllers, modernized P&O algorithms, and SEPIC converters. The PI paper controller is used with the SEPIC converter to maintain the duty cycle to be more efficient. In the proposed system, the MPPT P&O algorithm is written in a MATLAB functional block diagram and implemented in the simulation.

Keywords Perturb and observation algorithm · Maximum power point tracking · PI controller · SEPIC converter

R. N. Mahia (✉) · R. Kumar

Department of Electrical Engineering, NIT Hamirpur, Hamirpur, Himanchal Pradesh, India
e-mail: ram@nith.ac.in

R. Kumar

e-mail: er.rajatkumar08@gmail.com

1 Introduction

Global warming caused by carbon dioxide emissions necessitates the discovery of polluting alternative energy sources. And, due to the increases in demand for energy, use of solar power also increases. Solar panel receives sun rays and converts solar energy but the output power of solar panel depends on irradiance and temperature. Irradiance and temperature depends on climate conditions at this standard conditions Temperature (T) = 250 C and irradiance (Ir) = 1000 w/m² it provide rated output voltage. When weather is bad, it receives less irradiance, and due to which, its output power decreases. To overcome this problem, maximum power tracking point (MPPT) controllers are made [1, 2]. The MPPT charge controllers allow PV module to operate at maximum power point. To track this maximum power point, several algorithms are used like incremental conductance, perturb and observation, and fuzzy logic. In this paper, perturb and observation algorithms are used. The MPPT-based P&O method is widely used because of running time is less effective, and also the overall cost is less [3–5]. In this paper, PV panel is directly fed to dc-dc sepic converter and the advantage of using sepic converter its input and output voltage are same so there no need conversation of voltage and SEPIC converters results has been improved energy conversion and facilitates [6, 7]. SEPIC converter is more efficient than other converters. PI controllers are used in maintaining the duty cycle [8–11], and also designing multiple ports for EV charging stations for different voltage levels.

P&O method is to modify the operating voltage and current of PV panel until we achieve the maximum power from it. By using a modified P&O algorithm, the overall proposed system cost is less and efficiency is also improved [12, 13].

Purpose of this system designing is that the overall cost is less as compared to other systems [14, 15]. In Sect. 2, the block diagram representation of the proposed system and the basic circuit of PV energy conversion system are also discussed. Increase energy conversion from PV panel and their performance has been discussed in Sect. 2 and also discussed P&O and modified SEPIC converter topology are discussed in Sect. 2. The power electronics dc-dc converter and its performance discussed in sect. 2. After implementation of proposed system results and conclusion are discussed in Sect. 3.

2 Proposed System

Figure 1 shows PV panel input straight to SEPIC converter. Photovoltaic production depends on climatic conditions like temperature and sun irradiation. SEPIC converter acts as both buck and boost. The SEPIC converter acts as a boost converter when PV panel output voltage is low and a buck converter when PV panel voltage is high to maintain constant voltage and safeguard the system. Algorithms optimize PV unit power in various environmental situations using maximum power point tracking controllers. This proposed work presents an EV charging station energy management

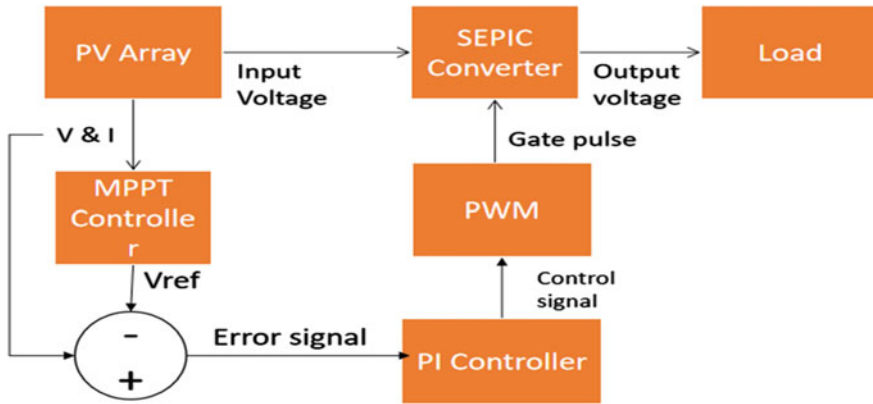


Fig. 1 Block diagram representation of the proposed system

system, a photovoltaic device production forecast, a usage prediction, and a peak demand reduction function to help create a charging station that can handle different voltage levels. Charging stations, a forecast for the generation of solar devices, a prediction of how electric vehicle charging stations will be utilized, and a function to decrease peak demand. By using solar energy and an maximum power transfer algorithm and also DC-DC converter to development of a charging station that can accommodate better efficiency. In PV energy conversion in the system, there are three main components: solar panel, MPPT controller, and DC-DC converter. The solar module basically consists of solar cells [1, 2]. The next section consists of designing PV cell for calculating series and parallel arrays [3, 4].

2.1 Designing of PV Cell

The analogous circuit of the PV module is displayed in Fig. 2, which exhibits the diagram. The value of the series resistance, denoted by R_s , is extremely low, while the value of the shunt resistance, denoted by R_{sh} , is extremely high. The photon current, denoted by I_{ph} , is denoted by I_d , and the diode current, denoted by R_s and R_{sh} , respectively. The photovoltaic module is made up of a certain number of cells connected in series and parallel [5].

The equations of diodes can be described as

$$I_d = I_o \left(\frac{qVd}{e^{akT}} - 1 \right) \tag{1}$$

where

T Temperature (k)

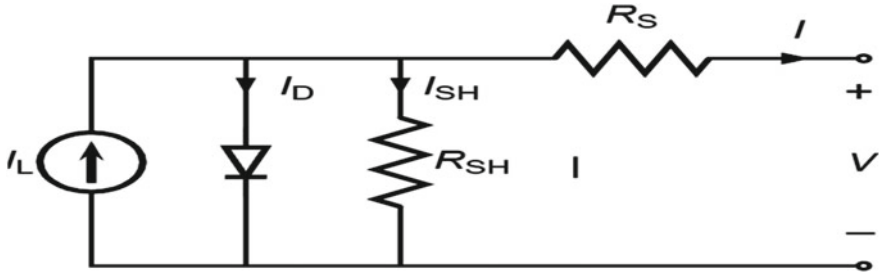


Fig. 2 Equivalent circuit configuration of PV cell

- q Charge of electron in columns (1.6×10^{-19})
- k Boltzmann constant (1.38×10^{-23} J/K)
- I_o Reverse saturation current of diode at T
- a Diode ideality factor.

The optimal PV cell can be defined from Eq. (1) as

$$I = I_{ph} - I_o \left(\frac{qVd}{e^{akT}} - 1 \right) \tag{2}$$

where

- I_{ph} Photon current at a certain irradiation and temperature (T) and
- V Voltage across the diode.

The entire PV model can be described as

$$I = I_{ph} - I_d - I_{Rsh} \tag{3}$$

We get the real current by putting in the value of I_d from Eq. (1).

$$I = I_{ph} - I_o \left(e^{\frac{q(V+R_s I)}{akT}} \right) - 1 \left(\frac{V + I R_s}{R_{sh}} \right) \tag{4}$$

2.2 Modified Perturb and Observe (P&O) Algorithm

Figure 3 shows the modified P&O method with certain modifications. The output of the PV array is entirely dependent on the temperature and irradiation level of each PV cell [6, 7]. If there was a change in the conditions of the atmosphere, then the temperature and irradiation levels would likewise change, as would the output of the PV array also changes. The P&O technique is the one that assesses maximum power

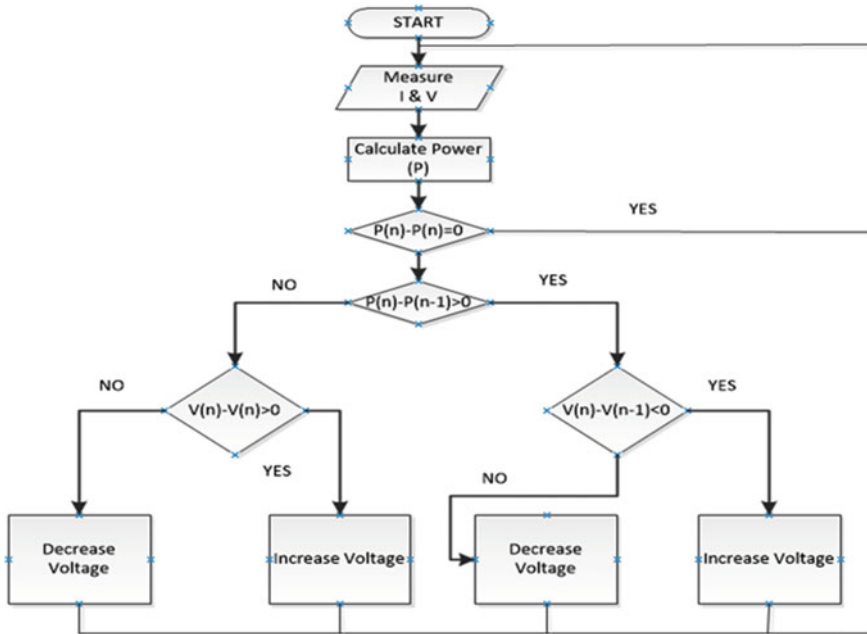


Fig. 3 Flowchart of perturb and observe algorithm

at a variety of points. Let’s look at three different scenarios to get better results when calculating maximum power.

For achieving maximum power,

$$\frac{\Delta P_{PV}}{\Delta V_{PV}} = 0 \tag{5}$$

$$\frac{\Delta P}{\Delta V} < 0 \text{ For } V < V_{pp} \tag{6}$$

$$\frac{\Delta P}{\Delta V} > 0 \text{ For } V > V_{pp} \tag{7}$$

In this paper, the purpose of using P&O method in this method is easy to implement and this complexity is less and low cost and also increases efficiency. The next section uses DC–DC SEPIC converters to regulate input voltage with constant voltage [8, 9].

2.3 DC–DC Single-Ended Primary Inductor Converter (SEPIC)

Operation of SEPIC converter is same as buck–boost converter. The polarities of input voltage and output voltage of SEPIC converter are similar which makes it much more effective. The SEPIC converter could be stepped up and stepped down input voltages [10, 11].

2.4 Modeling of Modified SEPIC Converter

Figure 4 shows that the modified SEPIC converter is a boost converter accompanied by a buck–boost converter. This type of converter is comparable to a standard buck–boost converter, but it has the additional advantage of offering non-inverted output performance. As a result, it is an excellent choice for applications that make use of renewable energy sources and have high static gain requirements. Figure 4 shows the modified SEPIC converter's functional block diagram.

Figure 4 shows that the PWM switching signal that will allow the switch to activate is being generated by the PI controller [12, 13]. The switching signal that is produced by the controller has an amplitude of less than 5 V. In the majority of situations, a switching signal with a minimum voltage of 20 V is necessary to activate a switch. Therefore, a PWM signal must be provided from the controller in order for switch to be switched on so that the switch can be turned on. The purpose of satisfying the criteria is required by the voltage on the load side. Parameters of PV module and SEPIC converter are shown in Table 1.

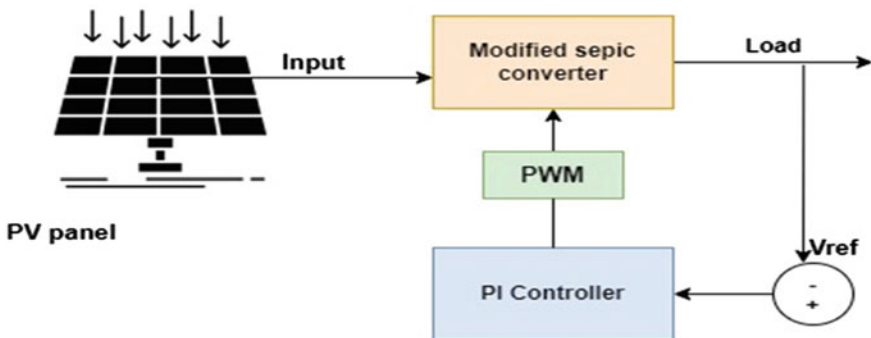


Fig. 4 Block diagram of modified SEPIC converter

Table 1 Parameter of PV module and SEPIC converter

PV module parameter		SEPIC parameters	
Parameters	Value	Parameters	Value
Maximum power (Watt)	250.2	Inductor L1 (H)	0.120
Series connected module per strings	4	Inductor L2 (H)	0.120
Parallel connected strings	5	Capacitor C1 (F)	4.28
Short circuit current Isc (A)	8.66	Capacitor C2 (F)	4.28
Shunt resistance Rsh (ohms)	224.18	Resistance (Ω)	6.4
Series resistance Rs (ohms)	0.237	Output voltage (V)	230.2
Open circuit voltage Voc (V)	37.3		

2.5 Designing of Multiple Ports

The purpose of this work is to design a charging station for EVs that can accommodate many voltage levels, including the more common voltage levels 1 (110–120 V) and 2 (200–220 V) [14].

Figure 5 shows that the power for the MPPT controller comes straight from the PV array. In addition, the PI controller receives input from the voltage and current sensors through a signal sent via the SEPIC converter. The duty cycle of the SEPIC converter is kept constant by a signal sent via the PI controller. By changing the duty cycle, it may function as a buck converter or a boost converter. The converter operates as a boost converter for duty cycles less than 0.5 and as a buck converter for duty cycles greater than 0.5. The SEPIC is wired directly to many different ports, and those ports all display voltage levels of 1 and 2.

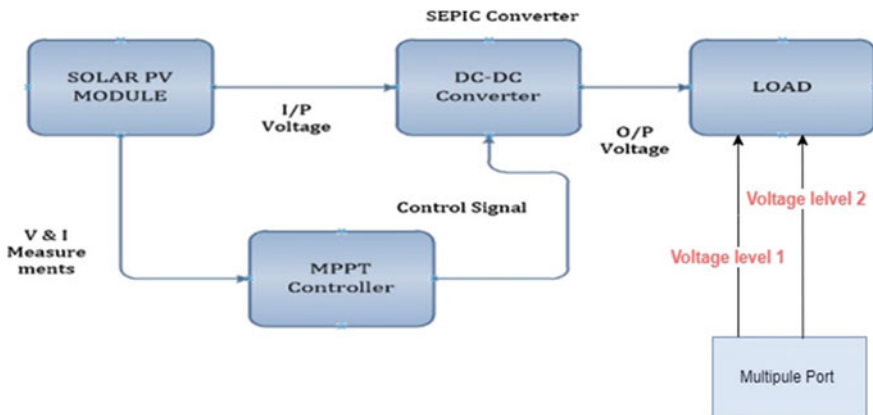


Fig. 5 Block diagram of multiple ports for electric vehicle charging station

2.6 Lithium-Ion Battery

In the proposed system, Li-ion battery is used for battery storage system. The Li-ion battery is directly fed through SEPIC converter for charging purpose. Design a multiple port for different - different voltage level like (110–120 V) (200–220 V) and also assessment of state of charge of lithium ion battery after maximizing power from PV under ambient circumstances [15].

2.7 Mathematical Modeling of Li-Ion Battery

The first stage in the estimate process is to make an educated guess as to the voltage and current of a Li-ion battery. Time required for charging at voltage level 1 (110–120 V) is given by

$$\text{Charging time of battery (T)} = \frac{Ah}{A}$$

where

Ah Battery Capacity

A Current in amperes.

For ideal case, losses = 10% Charging current for 200 Ah battery = $200 \times (10/100) = 20$ A.

For charging purpose, take 21 A current.

Charging time for 200 Ah battery = $200/21 = 9.52$ h.

For practical case, 40% of losses occur in the case of battery charging

$$200 \times 40/100 = 80$$

$$200 + 80 = 280(200 \text{ Ah} + \text{losses})$$

Charging time for battery = $Ah/A = 280/22 = 12$ h.

Similarly, for calculating for voltage level 2 for (200–220 V), the charging time of EVs is 15 h. Table 2 shows the battery parameters for voltage levels (110–120 V, 200–220 V).

Table 2 Modelling of li-ion battery

S. no	Battery parameter	Voltage level 1 (110–120 V)	Voltage level 2 (200–220 V)
1	Nominal voltage (V)	110	110
2	Rated capacity (Ah)	200	200
3	Initial SOC (%)	20	50
4	Voltage level (V)	110–120	200–220
5	Power level (Watt)	2.9	6.5
6	Charging capacity for (100%)	12 h	15 h

3 Simulation and Results

3.1 Maximum Power Tracking with the P&O Method Using the SEPIC Converter

The amount of input needed to maximize the output from a photovoltaic source is totally dependent on the weather, particularly temperature fluctuations and the amount of solar irradiation. Photovoltaic output is inherently unsteady as a result of this. Ashok Leyland Bhandara, in Maharashtra, India, provides data on sun irradiation relevant to this investigation. Figure 6 shows an example of active power production in relation to data on solar irradiation, and this is meant to serve as an illustration. Ashok Leyland’s records in Bhandara, Maharashtra, line up with this information. Solar panels with a combined peak output of 2 MW have been installed on this location’s four workshop roofs. Figure 6 shows the solar irradiance data collected over the course of 5 months at the location shown in Fig. 6. A Shop 2 detail is also displayed for the sake of completeness.

For designing an EV charging station with more than one port for 110–110 V. In the proposed system, two SEPIC converters are used. The first one is directly

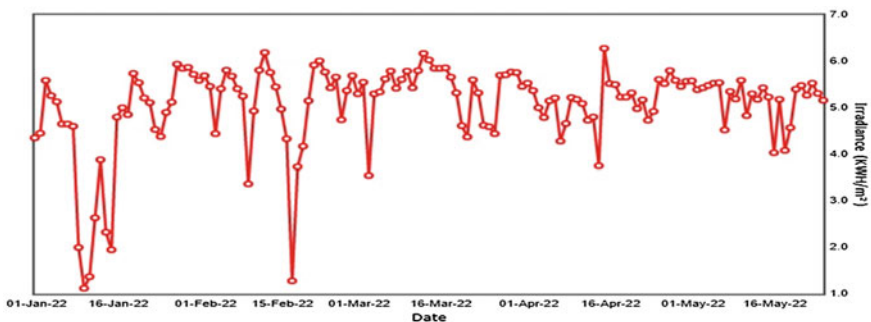


Fig. 6 Solar irradiance of ALB over a duration of 5 months

fed by the PV source, and the second one is connected to the drain source of the first one through the switch of the first one. This is done to get a higher voltage from the second converter. The output of the converter is connected to battery for charging of station battery. Different irradiances and constant temperatures have an effect on output power. At time = 0.5 s, the irradiance is 1000 W/m² with MPPT controllers controlling 900, 800, and 600 at t = 5. In Fig. 7, the power and output voltage waveforms for voltage levels 110–120 V are shown, and output current and irradiance are also shown in Fig. 8, that is to be controlled following the 50 V reference and congested to changes in ambient circumstances.

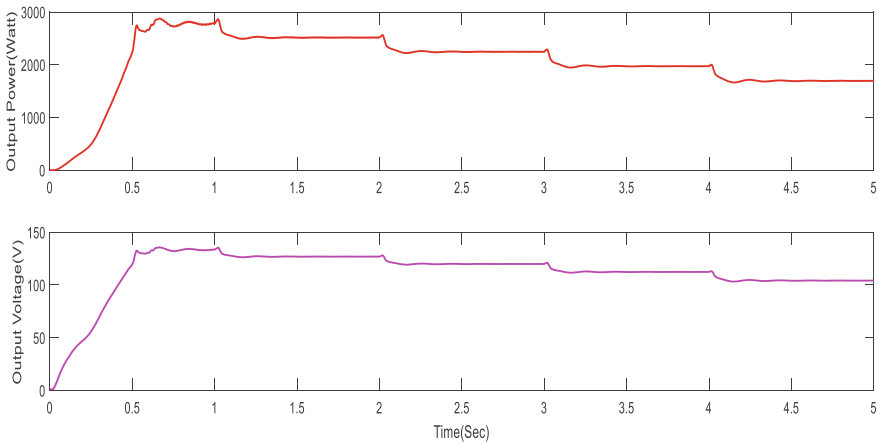


Fig. 7 Output waveforms of output power and output voltage for voltage level 1 (110–120 V)

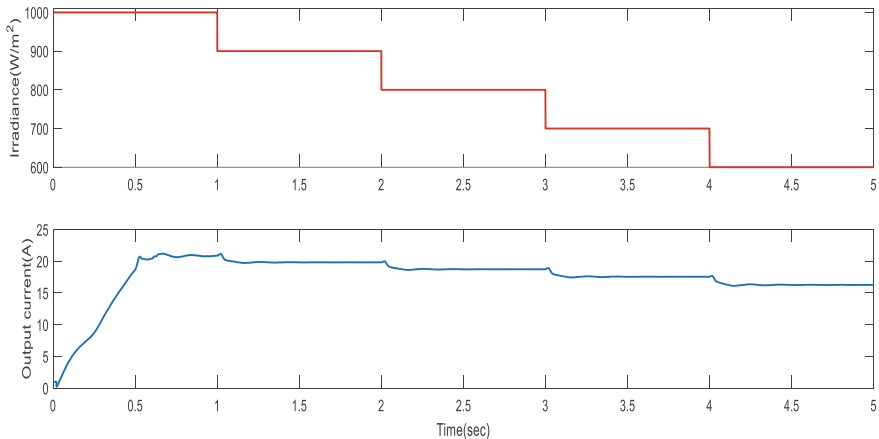


Fig. 8 Waveforms of output current and irradiance for voltage level 1 (110-120V)

The output power and voltage performance for voltage level 1 (110–120 V) and voltage level 2 (200–220 V) at various irradiances and constant temperatures are shown in Tables 3 and 4. The power and output voltage waveforms for voltage level 2 (200–220 V) are shown in Fig. 9, and output current and irradiance are also shown in Fig. 10. In regulated tracking, the given 50 V reference and congestive to change of atmospheric conditions are seen.

Table 3 Performance of output power, output voltage, and output current at different irradiance for voltage level 1 (110–120 V)

Parameters	Irradiance (w/m ²)	Output power (Watt)	Output voltage (V)	Output current (A)
1	1000	2889	127.9	21.68
2	900	2784	127.3	20.56
3	800	2587	125.4	19.45
4	700	2459	121.3	18.78
5	600	2321	119.2	17.01

Table 4 Performance of output power, output voltage, and output current at different irradiance for voltage level 2 (200–220 V)

Parameters	Irradiance (w/m ²)	Output power (Watt)	Output voltage (V)	Output current (A)
1	1000	5854	228.3	36.68
2	900	5689	201.5	31.55
3	800	4973	186.3	29.37
4	700	4765	171.3	26.58
5	600	4213	158.5	25.45

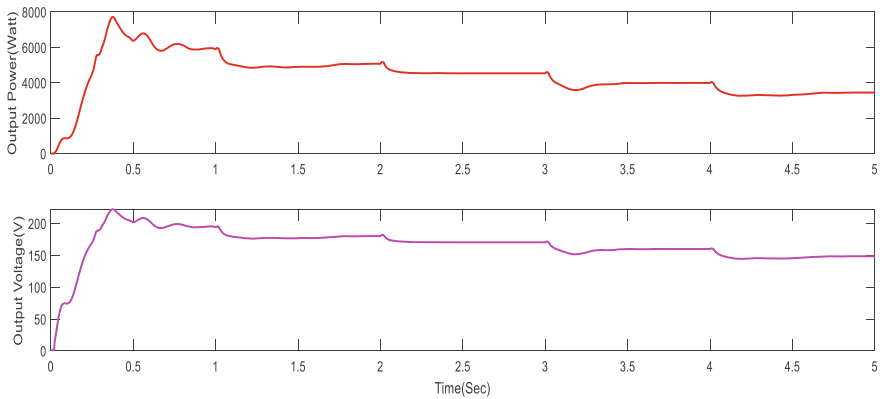


Fig. 9 Output waveforms of output power and output voltage level 2 (200–220 V)

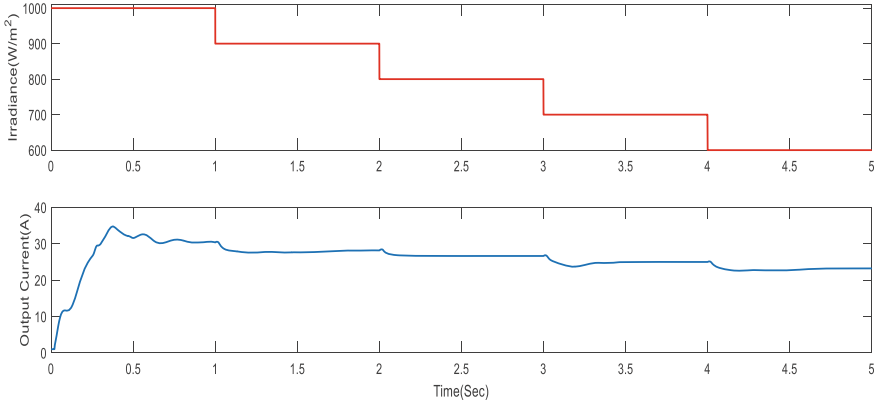


Fig. 10 Waveforms of output current and irradiance for voltage level (200–220V)

3.2 Estimation of (SOC) Li-Ion Battery

The states of coherence are given as a percentage, with 0% meaning a state that is empty and 100% meaning a state that is full. The percentage for empty states is 0, and the percentage for full states is 100. In this proposed system, two LI-ion batteries with a rated capacity of 200 Ah are used to measure the SOC, with initial losses of 10% being taken into account. At first, the charging current for a 200 Ah battery is 20 A, but it takes 21 A to charge it. At this current, the battery takes 9.2 h to charge. For a practical case, losses happen when the battery is under load, so assume that 40% of the battery is lost at the point where it is being charged. Figures 11 and 12 show the waveforms of SOC at 20% for voltage level 1 and SOC at 50% for voltage level 2.

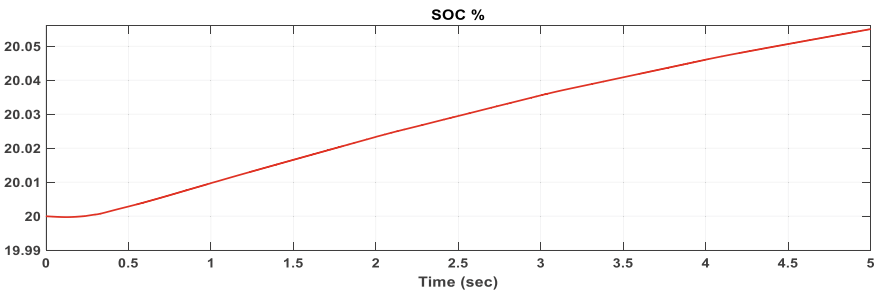


Fig. 11 Waveform of SOC at 20%

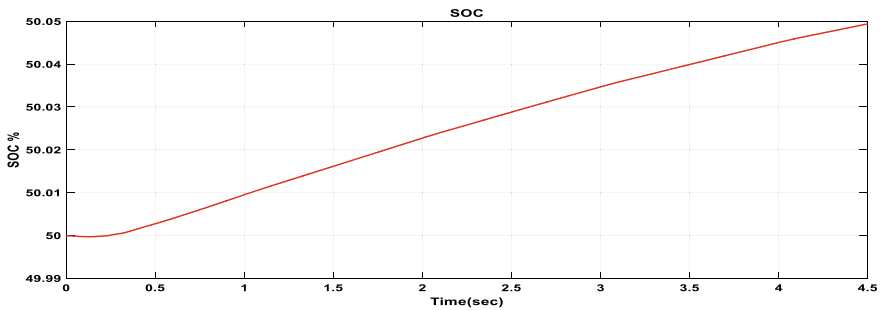


Fig. 12 Waveform of SOC at 50%

4 Conclusion

Currently, EVs are expanded quickly as needed zero emission from the world. In particular, the release of CO₂ into the atmosphere is a big concern in a large city; thus, in order to overcome this problem and maximize the advantages to owners of electric vehicles, a charging station for electric vehicles to be designed. For the purpose of this investigation, we will make use of the data on the solar irradiance that is collected from Ashok Leyland Bhandara in the Indian state of Maharashtra. The purpose of this work is to present an MPPT controller and P&O algorithm-based SEPIC converter that was developed with the goal of extracting the maximum amount of electricity possible from solar panels. When utilizing a SEPIC converter, the objective is to deliver a huge voltage transformation ratio that is higher than the input voltage while simultaneously lowering loss across the switch. This is accomplished by using a SEPIC converter. This specific combination of solar cells, MPPT controllers, updated P&O algorithms, and SEPIC converters has produced enhanced energy conversion. The energy management system for charging stations for electric vehicles has been proposed for multiple voltage levels, such as (110–120 V) and (200–220 V), for reducing the demand during peak hours. The suggested system maintains 97.3% efficiency no matter what the load is, even while it is operating during the peak off time.

References

1. Al-Rubaye MJM, Gino Morais Araujo V, Kadhim Abed J, Van den Bossche A (2018) Review different types of MPPT techniques for photovoltaic systems
2. Pakkiraiah B, Sukumar GD (2016) Research survey on various MPPT performance issues to improve the solar PV system efficiency. *J Sol Energy* 2016
3. Geethalakshmi B, Sreeram P (2014) Modeling and analysis of an integrated PV array and SEPIC converter
4. Mishra S, Ziar H, Isabella O, Zeman M (2019) Selection map for PV module installation based on shading tolerability and temperature coefficient. *IEEE J Photovolt* 9(3):872–880

5. Kineavy F, Duffy M (2016) Smart EV charging system for maximising power delivery from renewable sources
6. Singh HK, Kumar N (2020) Solar PV array powered ON board electric vehicle charging with charging current protection scheme
7. Shariff SM, Alam MS, Ahmad F, Rafat Y, Asghar MSJ, Khan S (2020) System design and realization of a solar-powered electric vehicle charging station. *IEEE Syst J* 14(2):2748–2758
8. Lakshmi Praba B, Seyezhai R (2021) Simulation and hardware implementation of interleaved SEPIC converter with valley-fill circuit for HBLED system. In: *Lecture notes in mechanical engineering*. Springer, Singapore, pp 335–353
9. Duranay ZB (2021) Output voltage regulated sepic converter for photovoltaic systems
10. Rashmi MJ, Rajesh KS (2016) A comparative study and performance analysis of synchronous SEPIC converter and synchronous Zeta converter by using PV system with MPPT technique
11. Perianayagi M, Prabha NR, Gnanavadeivel J (2019) Design and analysis of single switch dual output DC-DC SEPIC converter for PV applications
12. Wu T-F, Kuo C-L, Sun K-H, Hsieh H-C (2014) Combined unipolar and bipolar PWM for current distortion improvement during power compensation. *IEEE Trans Power Electron* 29(4):1702–1709. <https://doi.org/10.1109/tpel.2013.2265399>
13. Zhang Y, He J, Ionel DM (2019) Modeling and control of a multiport converter based EV charging station with PV and battery
14. Danko M, Adamec J, Taraba M, Drgona P (2019) Overview of batteries state of charge estimation methods. *Transp Res Procedia* 40:186–192. <https://doi.org/10.1016/j.trpro.2019.07.029>
15. Such MC, Hill C (2012) Battery energy storage and wind energy integrated into the smart grid

Regenerative Braking Integrated with Anti-lock Braking Mechanism in Electric Vehicle



Gagneet Kour and Surbhi Gupta

Abstract Commercialization in a profitable way with rapid adoption toward the electrified vehicles has made the reduced consumption of petroleum. In order to secure energy, the advancement in transportation systems has been made which makes the best use of electricity for running the vehicles which in turn minimizes the environmental impacts and limits the non-renewable resource usage. It is difficult to shift away from petroleum in the intensive transport energy sector as high energy and density in power make petroleum an ideal running fuel. However, the recent frontier of research in electric vehicles is the implementation of regenerative braking system. The integration of regeneration braking alongside anti-lock braking system which is studied upon safety heading will increase the battery life and add mileage to the vehicle. Both these concepts work hand in hand to enhance the energy which is required while driving operation. The idea of using regenerative braking technique tends to recover the amount of energy which gets wasted while braking, and on the other hand, anti-lock braking employed in vehicles improves safety by minimizing the longitudinal distance of breaking. These two methods make the vehicle efficient and safer to use.

Keywords Anti-lock braking · Electric vehicle · Efficiency · Kinetic energy · Pulse width modulation · Regeneration · Torque

1 Introduction

The clear alternative for the internal combustion engine (ICE) is an electric vehicle which does not use fossil fuels like petrol and diesel. With the rapid dwindling of non-renewable resource of energy, there occurs a need to search for alternative

G. Kour (✉)

M.E Department, Chandigarh University, Mohali, Punjab, India
e-mail: kourneet123@gmail.com

S. Gupta

Chandigarh University, Mohali, Punjab, India
e-mail: surbhi.e9023@cumail.in

energy sources which can lessen the consumption of fossil fuels as demand and usage is increasing day by day due to population explosion and vehicle production. The conventional form of braking leads to the wastage of energy which can be used again if recovered successfully and reusing the same energy to increase the mileage of the vehicle [1]. The benefits of electric vehicles and their eco-friendly nature make them worthy to use, and also the use of regenerative braking system allows storage of energy as well. The use of regenerative braking technique and anti-locking braking system makes vehicles more efficient and safer to use while increasing the mileage of the vehicle. The kinetic energy or energy in motion of the wheels is usually lost during the braking in heat form because of the friction in between brake pads. Therefore, this lost energy can be recovered and regenerated by using regenerative braking system. This method of braking uses capacitor banks for temporarily storing energy and supplies back to the battery in case of need and emergency. This system of braking increases battery life via recharging battery with stored energy. Hence, a vehicle can travel more distance on single charge of battery [2]. Various accidents occur when brakes are applied in hard mode, this leads to the locking up of the wheels. At this time, driver loses control over steering and hence the direction of the car remains same. In anti-locking braking system, a phenomenon of pulse width modulation uses a non-continuous braking system where brakes are applied in interval which prevents the wheels from getting locked up [3]. Because of such type of braking systems, wheels of vehicles can grip better the surface of roads and stopping distances can also be decreased on a significant note.

2 Overview of Regenerative Braking

The word regeneration symbolizes restoration or renewal of some material from its parent part with the help of an external agent or any equipment. The use of regenerative braking system is a great initiative for reducing the dependency on oil and petroleum as non-renewable sources are on the verge of extinction within a few more years. Therefore, it has become a necessity for both public and private sectors to move away from petroleum fuel so as for energy security. The phenomenon of regenerative braking is based on the regeneration of energy which gets lost while braking operation in vehicles [4]. Energy is neither created nor destroyed, it can simply transform from one state to another. During braking, there is a considerable amount of kinetic energy is wasted in heat form because of the friction between disc pads. The wasted energy could be recovered with the use of regenerative braking technique. This kind of braking system allows recollection of kinetic energy and then conversion of this energy into electrical form which is stored for future use. Moreover, efficiency of the vehicle is also increased by the use of regenerative brakes. During driving operation, an automobile involves so many events in which brakes are applied [5]. With the implantation of regenerative brake, the energy can be recovered while slowing the motion with the conversion of the kinetic energy to some other form of energy that can be put into use immediately or at the time of emergency. The

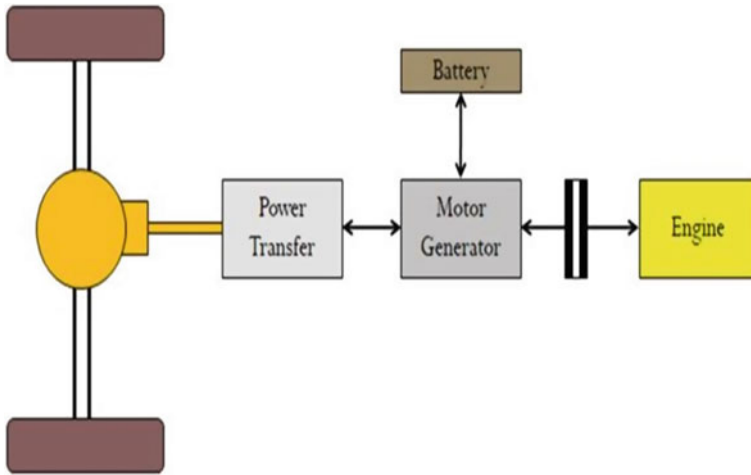


Fig. 1 Regenerative braking technique

energy which is normally dissipated into brakes of vehicle is directed via a system of power transmission toward auxiliary battery while the process of deceleration taking into action. This energy which is stored could be changed again into motion energy and is put into use when the need of accelerating vehicle occurs. At lower speeds, the regenerative brakes are less effective as compared to higher vehicular speeds. As a result, friction brakes are required in order to stop the car fully during failure in the event of regenerative braking (Fig. 1).

3 Overview of Anti-lock Braking System

Anti-locking braking system which is also known as Pulse Width Modulation (PWM) braking is employed in vehicles for safety allowing the vehicles to keep an attractive touch with surface of roads while brake operation, avoiding the wheels to get locked and thus preventing an uncontrolled form of skidding. The process takes much less time while the driver can control the steering [6, 7]. It significantly increases the control over vehicle by decreasing the distance of stopping on dry or any wet surface. The recent development has evolved the use of ABS in many ways which not only controls locking of wheel but also controls the front–rear brake bias electronically. The concept of anti-lock braking system is generally simple which helps in providing grip to the wheel while slipping. The contact between car and road is due to the contract patch. While the skidding takes place, vehicles tend to move out of control and do not stop. At this moment, ABS comes into action and gives the control of the vehicle back to driver (Fig. 2).

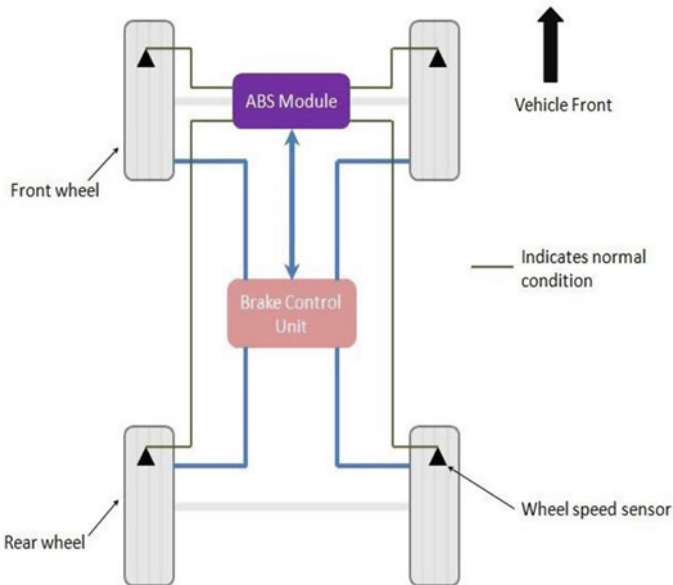


Fig. 2 Anti-lock brake system

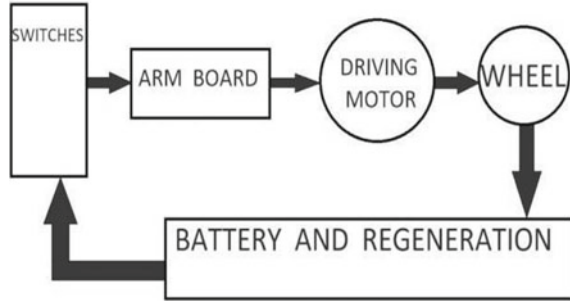
Furthermore, the ABS circuit consists of four main parts i.e. sensors for speed, pump, valve, and controller. The information regarding any skid is provided to the system via sensors which are employed for speed detection on each wheel or at differential positions. The regular monitoring is done with the help of controller that can be a computer or any electronic device with screen for controlling valves. At the time of instance braking, there is a sudden type of deceleration is observed by controller and the controller leads to a decrease in the pressure on that particular brake unless it sees any acceleration [8]. This continues till controller observes any acceleration again. The whole action takes place before it comes to any notice. In 1 s, approximately 15–20 times brake is applied and this entirely feels like a pulsation in the pedal of brake as the valve opens and closes quickly while releasing the pressure at the same time.

4 Working Methodology

This section describes the block diagram with components used and the working of prototype which has been designed with regenerative braking system along with anti-lock braking system (Fig. 3).

The functioning of the prototype has been divided into five components which are described as given below:

Fig. 3 Block diagram for the system



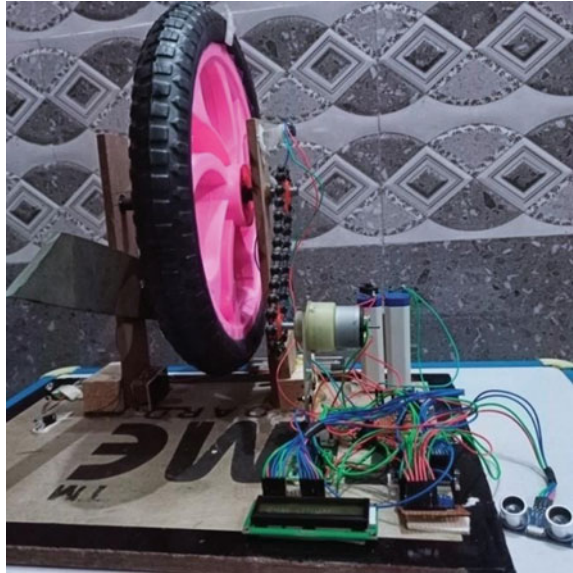
- i. Switches
 - ii. ARM board
 - iii. Battery and Regeneration block
 - iv. Driving motor
 - v. Wheel.
- A. Switches: For turning ON/OFF the prototype, switches are being placed.
 - B. ARM board: This block has two functions to perform:
 - Anti-lock braking works by managing the speed of a DC motor
 - To continuously sensing an impending obstruction and responding swiftly to control the motor's speed, either slowing the wheel down or totally stopping it [9]. These choices are contingent on a set of predetermined criteria.
 - C. Battery and Regeneration block: When the brakes are engaged, this block is activated. The DC motor in this block acts as a generator (changing the K.E. of the wheel to electrical energy) and stores the charge in are chargeable battery, allowing the circuitry to run longer.
 - D. Driving motor: This motor is used to modify the wheel's speed (through PWM input) and stop it, as well as to operate the anti-lock braking system.
 - E. Wheel: A flywheel is attached to wheel, that stores translational energy as rotational energy. Thus, flywheel sends rotational kinetic energy to the motor, which initiates the regenerative motion [10].

4.1 Working of Prototype

The implementation of Regenerative Braking System (RBS) and Anti-lock Braking System (ABS) together in an EV system with ultrasonic sensors in order to detect any obstacle can be termed as a system of smart-braking (Fig. 4).

The brakes of this prototype are applied either conventionally; by applying brakes manually or automatically; when the sensor senses any obstacle. The distance from an obstacle in front gets sensed with the help of ultrasonic sensor installed in the system. Depending upon the output from sensor which is given to microcontroller, the

Fig. 4 Prototype of the system



calculation of the distance is done and then it is compared with the standard distance value taken as reference. However, if the distance value comes under defined critical limits, activation of brake control mechanism comes into action by the command of microcontroller, and vehicle gets slowed down or brought to a halt. The track of obstacle accounted by the sensors fitted at the front is given as an input to the microcontroller. Based on the value of distances, different duty cycle pulses are provided to the vehicle. The distance is measured again when the value of velocity comes out to be zero. Thus, pulses are applied at intervals until the change in the distance ceases. This system is termed ABS braking system. Additionally, during the braking operation (manual only), the translational energy is stored in the flywheel as rotational energy. This rotational K.E. is further transferred to motor to work as generator. The generated electricity recharges the batteries.

Therefore, we are able to gather the K.E. by combining regenerative braking with ABS. The findings of this research contribute to the technical advancement and improvement of hybrid vehicle braking quality. The ability to combine ABS and regenerative braking to achieve high performance has been demonstrated. We have created a capacitor bank that can store enough energy to power modest loads or charge small batteries. This research also explains how to improve a hybrid vehicle's efficiency and reduce its fuel consumption. And it will assist our future generations in reducing the impact of fuel scarcity. The trade-off between performance and cost must therefore be justified based on the indicated environment and internal considerations.

Table 1 Readings from the model

RPM before brake pedal pressed	RPM after brake pedal pressed	Voltage output
100	20	9
200	160	9.5
300	260	9.8
400	330	10
500	420	10.2
600	530	10.4
700	620	11

5 Results from the Hardware Model

The following table represents the readings from the working of the model and the graphical representation has also shown (Table 1).

With the motor specifications of 12 V, 800 RPM, 2 kg cm, 400 ma current, the testing of prototype was done. RPM before brake pedal pressed was noted and then RPM after applying brake was noted at intervals. The output voltage in correspondence to the RPM applied was recorded and it shows the increase in the voltage at the end of the testing through a digital voltmeter.

The readings from the experimental apparatus and its implementation demonstrated the collection of the KE using the regeneration braking scheme alongside ABS. The results which are displayed and presented from the hardware of the project lead to technical enhancement and its extension for improving the quality of electric vehicles. The techniques of RBS and ABS with ultrasonic detection are feasible in utilizing this technology in order to get higher performance of EVs. The desired outputs were gathered from the system (Fig. 5).

6 Advantages and Disadvantages of Regenerative Braking System and Anti-lock Braking System

6.1 *Advantages and Disadvantages of Regenerative Braking System*

6.1.1 Advantages of RBS

1. It enhances the vehicle's fuel economy.
2. Traditional friction-based brakes are possible—To ensure that a vehicle can stop in time, a friction-based braking system is combined with the regeneration system [11, 12].

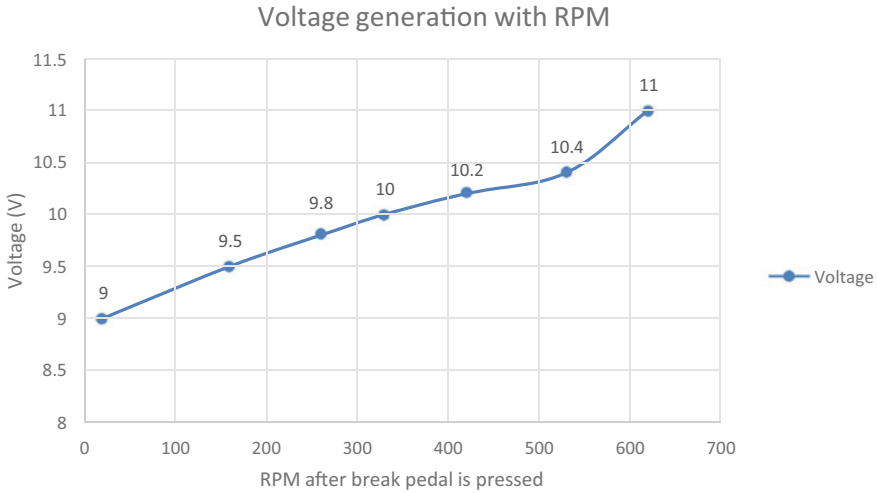


Fig. 5 Graphical representation of readings from model

3. It extends the battery charge—Once energy gets caught by regenerative brake, it is used for recharging vehicle’s battery. However, this energy would otherwise be lost during braking, every car can have a longer charge than before while traveling.
4. It decreases braking system wear and tear—Because this system includes an electric drive train; the increased braking effectiveness allows the vehicle’s brakes to last longer. There is no way to get this benefit with conventional friction brakes.

6.1.2 Disadvantages of RBS

1. It provides a sliding scale of benefits- Regenerative braking effect decreases as vehicle’s speed increases. To bring most cars to a complete stop at low speeds, friction brakes are required. This indicates that energy is still being wasted.
2. It provides a unique driving experience—Regenerative braking systems provide a unique driving experience for drivers who are used to traditional braking systems [13, 14]. Many drivers characterize the vehicle’s brake pedal as “mushy”. Some people may have doubts about their brakes’ abilities until they get adjusted to the new technology.
3. It has a high maintenance cost—Because additional equipment is necessary for regeneration control and equipment and machine protection, both the initial and ongoing costs are higher.
4. It drives up the equipment’s overall cost—Because the DC machines necessary for regenerative braking are larger and more expensive than those commonly used, the locomotive’s weight, as well as the mechanical strength and cost, rise [15].

The pros and cons of a regenerative braking system provide new benefits and cost-saving options to drivers. The demand for friction-based brakes in low-speed circumstances is one of its key limitations.

6.2 *Advantages and Disadvantages of ABS*

6.2.1 Advantages of ABS

1. Shortened stopping distances—If we need to stop quickly to avoid an accident, ABS can assist you to reduce the time and distance it takes to come to a halt. On slick road surfaces, this is especially advantageous.
2. Enhanced control—When driving on wet or slippery roads, you run the risk of skidding or losing control of your vehicle. ABS gives you more vehicle control and improves traction between tires and road [16].
3. Fewer accidents—Both of the aforementioned benefits reduce the odds of being involved in a traffic accident, making the road a safer place for everyone.
4. Lower premiums: In addition to the safety benefits, ABS can help in saving money on insurance premiums. Because having ABS installed reduces the chances of being involved in an accident, most insurance companies provide cheaper premiums as a result of it [17].

6.2.2 Disadvantages of ABS

Anti-lock brakes have been demonstrated to be the safest feature and they provide lower risk of hazardous situations in a vehicle; however, not all drivers are sold on this very option [18]. Here are a few drawbacks that drivers encounter while using this type of braking technology.

1. Unpredictable stop timings: These brakes are designed for braking safely in slick instances. But some of the drivers claim that ABS increases the stopping distance during normal conditions because of the fault in system circuitry or clunking/ noise of ABS plays its role while the driver cannot apply brake at same rate.
2. Expenditure: Maintenance of an ABS can be expensive. The sensors on each tyre tend to lose their accuracy because of repeated usage and are required to be recalibrated and also develop issues due to environmental factors and cost huge amount of money for repair. Therefore, it becomes uncertain to add ABS system in some vehicles [19, 20].
3. Advanced systems: Through tampering with brakes, it becomes an easy task to produce an issue in ABS system. Disorientation of an ABS occurs if compensating brake sensor causes car to tremor while making high-tone noises, or overall brake worse, can be one of the issues [21].

7 Recent Developments in Regenerative Braking System

The regenerative braking system has been able to regenerate the energy from capturing it before it could leave the vehicle and hence mileage of the vehicle increases. The energy generated from this system is stored in energy storage systems which are pre-installed in the vehicle so that, in single charge of battery, more distance can be traveled [22]. Recent developments in RBS technique are discussed below.

The system of RBS has also been used in conjunction with fuel cell vehicles for solving the problems of the energy requirement and reduction in air pollution [23]. The simulation model for this fuel-based electric vehicle has been testified and results from this system show that it is capable of increasing the efficiency of the vehicle.

RBS has been employed in the electric bike which tends to broaden an area of implementation and its study. As RBS is being installed and used in several cars and trucks but the installation of RBS in scooters and bikes (particularly in two-wheelers) is pending, the proposed methodology gives skilled knowledge regarding RBS installation in E-bike for improving the economy of the nation as most of the market filled with two-wheelers is presented.

Some studies show that RBS has been used in an automobile engine. During the braking operation, an alternator gets activated via magnetic clutch and the utilization of lost energy is made to generate electric power [24]. An experimental setup has been made and represented so as to make use of wasted energy. Results from the experiment show that 2.9KW energy can be recovered and transmitted back to battery as chemical energy.

A strategy for increasing the efficiency of the vehicle through fuzzy logic with a series of regenerative braking has also been proposed. The theory of vehicle stability of brakes analyzes the mechanical as well as electrical system of braking [25]. The research is conducted through MATLAB/SIMULINK and results are verified for safety purpose of intelligent vehicles. The strategy proposed in this paper has helped vehicle to distribute the forces, i.e., braking and mechanical force of front as well as rear axles for obtaining better recovery of braking energy.

Advanced control fuzzy algorithms helped in saving the energy demand with the need of boosting voltage to give reverse current to the battery when back emf drops during lower speeds [26].

8 Conclusion

The twenty-first century can be termed as the final era where ICE (internal combustion engines) is being used frequently in vehicles. However, with the beginning of electric vehicles, alternative energy carriers for generating energy are being found out and will be commonly used in the vehicles in the coming years. Carriers like electric battery, hydrogen fuel and compressed air have marked great success in producing energy and also they have shown their ability for storing the energy when combined with

certain equipments. The kind of brakes being discussed and presented in this project allows the use of batteries for a prolonged time without even plugging them into an external charger. The method of regenerative braking leads to the capturing of energy which can be stored and used in time of emergency or requirement along with ABS and ultrasonic sensor that is placed in front of the system detects the object and passes signal for avoiding any collision which therefore prevents accidents and unwanted situations thereby prolonging the life of drivers. In fact, cars like Tesla Roadster run entirely on battery power which uses regenerative form of braking system. The description of increasing the efficiency of the vehicle thereby reducing the use of fuel has been discussed for mitigating the shortage of fuel for future generations. With the advancement and more familiarization with the regenerative braking system, designers and engineers will make the best use of utilizing regeneration technology for recapturing energy.

References

1. Chen J (2008) Panasonic makes electric bike with regenerative braking. Gizmodo
2. Gitlin JM (2008) McLaren and free scale partner up for regenerative braking. ArsTechnica
3. John S, Pedro JO (2013) A comparative study of two control schemes for anti-lock braking systems. In: Proceedings of the 9th IEEE Asian control conference
4. HybridCars.com (2006) Hydraulic Hybrids
5. Celentano G, Iervolino R, Porreca S, Fontana V (2003) Car brake system modeling for longitudinal control design. IEEE
6. Pacejka HB, Bakker E (1991) The magic formulae tire model. In: Proceedings 1st International colloquium on tire models for vehicle dynamics analysis, Delft (WE)
7. Chanthanumataporn S, Lerspalungsanti S, Pimsarn M (2011) Design of regenerative braking system for an electric vehicle modified from used car. In: Second TS ME international conference on mechanical engineering
8. Husain I (2010) Electric and hybrid vehicles: design fundamentals. CRC press, Taylor and Francis Group, USA
9. Gao Y, Chen L, Ehsani M (1999) Investigation of the effectiveness of regenerative braking for EV and HEV. SAE Paper 1999-01-2910
10. Kumar S, Saxena (2009) Automobile engineering. Laxmi publications Pvt Ltd., India
11. Miller JM (2004) Propulsion systems for hybrid vehicles. Institute of Electrical Engineers, UK.
- Chen J-X, Jiang J-Z, Wang X-J (2003) Research of energy regeneration technology in electric vehicle, vol. 7, no 2. Shanghai University Press
12. Regenerative braking boosts green credentials. Railway Gazette International. 2 July 2007. Accessed 11 Mar 2014
13. Hui L, Channxue Song (2011) Design of a fuzzy logic controller for abs of electric vehicle based on amesim and simulink. In: Proceedings of the IEEE international conference on transportation, mechanical and electrical engineering
14. Iqbal IM, Rosli MH, Abu MA, Kornain Z (2012) Automated car braking system using neural network system via lab view environment. In: Proceedings of the IEEE international conference on open systems
15. Zhou K, Wang X, Zhang C, Liu J (2010) Data acquisition system based on lab view for abs dynamic simulation test stand. In: Proceedings of the IEEE international conference on information and automation
16. Torrens R (2008) Regenerative braking. 4QD

17. Gover J A tutorial on hybrid electric vehicles: EV, HEV, PHEV and FCEV. IEEE, Fellow Professor of Electrical Engineering Kettering University
18. Robert Bosch GmbH (2011) Chassis systems control, reduce consumption, protect the environment, regenerative braking systems, Gerlingen, Germany
19. Cody J, Göl Ö, Nedic Z, Nafalski A, Mohtar A (2009) Regenerative braking in an electric vehicle. University of South Australia.
20. Cikanek SR, Bailey KE (2002) Regenerative braking system for a hybrid electric vehicle. In: Proceedings of the American control conference, Anchorage
21. Jo C, Lee S, Song H, Cho Y, Kim I, Hyun D, Kim H (2010) Design and control of an upper-wedge-type electronic brake. *J Automob Eng* 224(11): 1393–1405
22. Baslamisli SC, Köse IE, Anlas G (2007) Robust control of anti-lock brake system. *Veh Syst Dyn* 45(3):217–232.
23. Chaturvedi L, Yadav DK, Pancholi G (2017) Regenerative braking energy storing phenomena in fuel cell based electric vehicle. Rajasthan Technical University, Kota
24. Suyambazhahan S (2016) Experimental study of regenerative brakes used in an automobile engine. ABET Accredited University
25. Zhe L, Ling Z, Yue R, Wei Y, Yinong L, Fengl G, Yusheng L, Zhoubin X (2016) A control strategy of regenerative braking system for intelligent vehicle. State Key Laboratory of Mechanical Transmission, College of Automotive Engineering, Chongqing University, Chongqing 400044 2 Changan Automotive Engineering Institute, Chongqing 401120
26. Bhurse SS, Bhole AA (2018) A review of regenerative braking in electric vehicles. ICCPEIC

Investigating Opto-Electronic Performance of RbSiBr₃ Multi-junction Solar PV Material: A Path Toward Sustainable Development



Hansraj Karwasara, Karina Khan, Mamta Soni, Amit Soni,
and Jagrati Sahariya

Abstract The cubic inorganic metal halide perovskite compound RbSiBr₃ is thermodynamically and mechanically stable because of its good absorption of photons. The present work is oriented on finding optoelectronic properties of the RbSiBr₃ compound by simulation tool: DFT (density functional theory) which is compiled in Wien2k code. All simulation works of finding the optoelectronic properties are carried out by TB-mBJ (Tran-Blaha-modified Becke Johnson) exchange–correlation potential. The electronic computations announced the 0.84 eV band gap of this compound that shows its handiness in the lower layer of multi-junction solar cells. The analysis of optical properties gives lower reflection and high absorption coefficient that proves its adaptation in optoelectronic applications.

Keywords Multi-junction solar cell · Optical properties · Electronic properties · DFT

H. Karwasara · K. Khan
Department of Physics, Manipal University Jaipur-303007, Jaipur, India

M. Soni
Faculty of Management and Commerce, Manipal University Jaipur, Jaipur-303007, Rajasthan, India

A. Soni (✉)
Department of Electrical Engineering, Manipal University Jaipur-303007, Jaipur, India
e-mail: amitsoni_17@yahoo.co.in

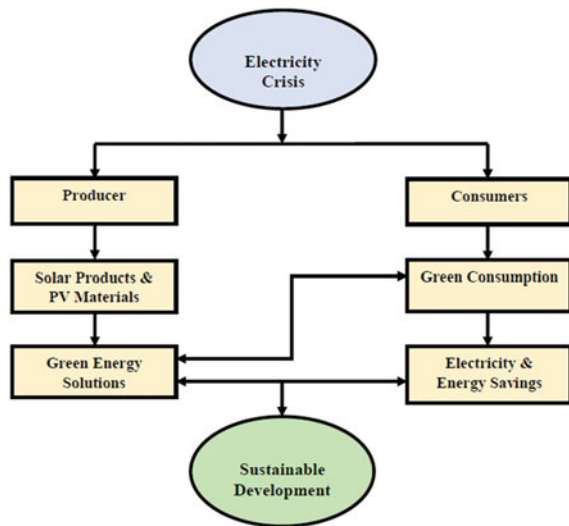
J. Sahariya (✉)
Department of Physics, NIT Uttarakhand-246174, Srinagar, Uttarakhand, India
e-mail: jagrati.sahariya@gmail.com

1 Introduction

As we have been stepping towards the ladder of developments and advancements, we are unknowingly and knowingly creating critical paths of global warming, water crisis, ecological imbalance, pollution of all kinds, and many more such global threatening issues for future generations. Because of global warming and overpopulation, the usage of electricity has been increased leaving us with the problem of electricity crisis [1–4]. This problem of electricity is not nation-specific, rather it is a global issue now, for which solutions have been pursued with the adaptation of renewable energy sources. But to seek solutions with the support of producers’ level is not enough [3, 4]. To overcome the crisis of electricity, it is required to look for solutions on both the fronts, i.e., producer as well as consumer. Figure 1 depicts the solutions on both sides that will lead us toward sustainable development. The energy framework is significantly relies upon non-renewable energy sources in the extant world, and their available accessibility on earth is adequate yet it won’t dependable as these non-renewable energy sources require almost a long period of production. Alongside the fossil fuels’ exhaustible nature and non-eco-accommodating nature additionally gravely issues globally [5–7].

Therefore, it is smarter to turn on environmentally friendly power sources to oppose the non-renewable ones [8, 9]. Researchers focusing around to reap the sustainable source into helpful structure in a legitimate manner and its gathering takes minimal expense and is positive for the climate [9]. Solution from the producer side will encourage manufacturing of solar products, execution of solar plants, research on PV materials improving solar cells efficiency, etc. All these producer-oriented steps will give green energy solutions in the form of green energy production practices and green energy products at the consumers’ front, ultimately guiding consumers

Fig. 1 Flowchart representing the process of achieving sustainable development



towards green energy consumption. Green consumption practices will forward to the path of electricity savings for present and future needs. Green energy solutions from producers and green energy consumption practices by consumers together will lead to sustainable development. To talk about producers' front, it has been researched that they found green production practices to be a costlier affair at the initial stage of product life cycle (PLC) as there exists less demand at this stage of PLC and hence non-profitable also. However, with consumers' support system, economies of scale can lead producers toward large-scale production and help them to overcome the non-profitable state as economies of scale reduce per unit cost [10, 11].

For this, solar cell modules are utilized to convert the solar energy into its electrical structure. Alongside the transformation of energy, solar cells utilized should be highly efficient, non-harmful, and having optimum band gap material. The multi-junction solar cells are used in order to obtain the high efficiency of solar cells, and in this, the stacking of solar cell materials with various bandgaps has been performed to retain the visible spectrum of sunlight [12–14]. To meet this enormous number of necessity of present, lower layer multi-junction solar cells are made of inorganic halide perovskite with general formula ABX₃ and are colossally investigated because these compounds have high magnificence in the optoelectronic devices [15]. The electronic behavior of halide perovskite CsPb/Sn/Ge/SiX₃ (X = Br, Cl, I) has been studied to show their utility in optoelectronic instruments [16, 17]. Korbel et al. [18] researched all basic properties like magnetic, optical, and electronic approaches to acting of tin halide perovskite structure ASnX₃ by DFT. The VASP computational tool has been utilized to examine the fundamental properties like thermodynamic and electronic properties of Cs/RbSnI₃ compounds in their all possible structure [19]. In the same context, Mao et al. [20] computed the bandgap of several inorganic perovskite compounds through computational screening. Jiang et al. [21] performed the ionic exchange in CsSnX₃ by Rb to determine their outcomes by DFT for showing photovoltaic utilization. Radha and Lambrecht [22] registered the energy gap of CsSiCl₃ which is optimum for semiconductor photovoltaic material. Jain et al. [23] played the computational screening method to compute the bulk of perovskite samples to analyze their structural and electronic properties. Yunsheng et al. [24] assessed the optoelectronic characteristic of RbSnCl₃ by the GGA-HSE approach. The Wien2k code has been utilized to process perovskites like CsGeBr₃ and CsSnBr₃ [25]. The cubic and orthorhombic phases of RbSnBr₃ have been explored for comparing their stability and properties [26]. Yi et al. [27] revealed in their paper that K/RbSnBr₃ has the reasonable band gap for solar cell devices. Further, the phonon computation has been performed on several perovskites belonging to the ABX₃ inorganic group [28]. Khan et al. [29] handled the optoelectronic behavior of K/RbSnCl/Br₃ by using PBE-GGA and TB-mBJ approach under DFT.

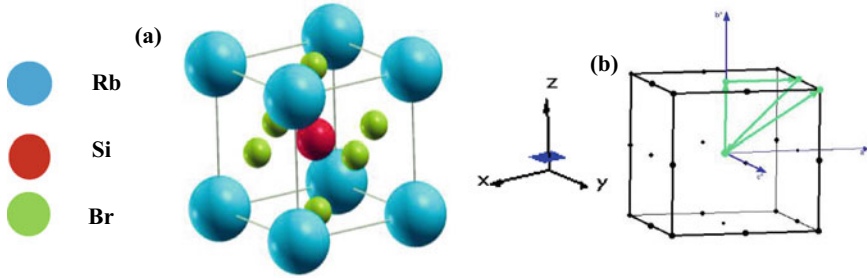


Fig. 2 a Crystal structure b Brillouin zone of cubic RbSiBr₃

2 Computational Details

This research work depends on the calculations of optoelectronic properties of ternary inorganic halide perovskite RbSiBr₃ using Wien2k code that is established on DFT and taking on FP-LAPW (full potential linearized augmented plane wave) method that is developed to solve the basis set [30, 31]. To attain the accuracy in the results, we have used the most promising TB-mBJ exchange–correlation functional for solving exchange–correlation term of Kohn–Sham equation [32]. This work has involved the lattice of 1000 k points to accomplish precision in the outcomes. The values of other inputs like l_{\max} , G_{\max} , $R_{\text{MT}} \times K_{\max}$, and energy cutoff are taken as 10, 12, 7, and -6Ry, respectively. Initially, we have taken the lattice constant of cubic RbSiBr₃ with space group 221 (Pm3m) from recently published work [29] and then compute out the volume optimization which yields $a = b = c = 5.82 \text{ \AA}$ with atomic positions Rb (0,0,0); Si (1/2,1/2,1/2); and Br (1/2,1/2, 0). The crystal structure and Brillouin zone are shown in Fig. 2a and b.

3 Results and Discussion

3.1 Electronic Properties

The TB-mBJ potential is utilized to process the electronic characteristics of RbSiBr₃ by band structure, which is portrayed in Fig. 3a in which the fermi energy level is set to 0 eV and we gauge the 0.84 eV band gap that portrays its semiconductor nature. As the band gap of this compound is lower than 1.5 eV, this compound is utilized as multi-junction solar cells. Through this structure, we come to realize that this compound has a direct band gap too as the top of the valence energy band (below fermi energy level) and the least point of conduction band (above fermi energy level) emerge at a common k point, i.e., at R. All the different color bands in Fig. 3a show the inhabitation of the electrons in different energy levels in which the electrons get transfer after absorbing energy. To elaborate this explanation of the

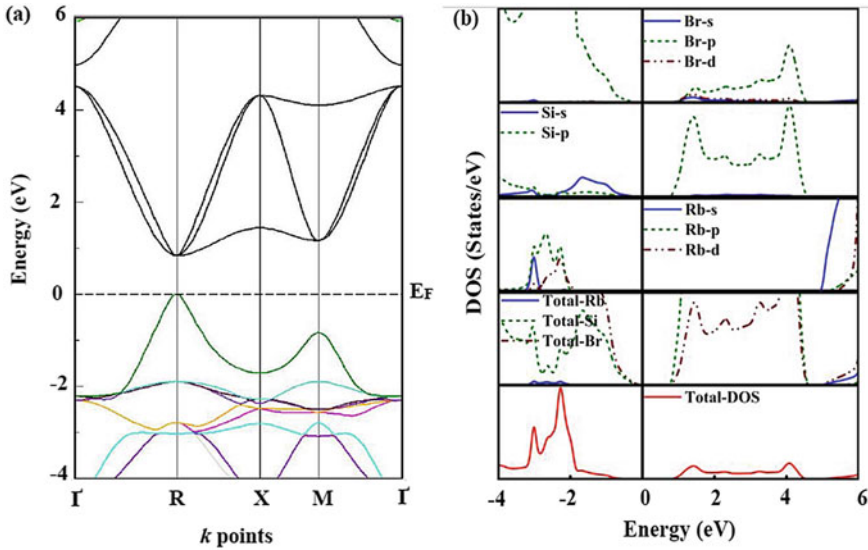


Fig. 3 a Band structure b DOS of cubic RbSiBr₃

electronic properties, the DOS (density of state) spectra, depicted in Fig. 3b, have been studied which are computed by TB-mBJ exchange–correlation potential. The band gap obtained by band structure is affirmed through DOS spectra. Through the DOS, it is clearly visible that valence energy band is situated beneath the fermi level (0 eV).

This can be seen in the DOS spectra in Fig. 3b that the band gap formation is majorly due to the Si and Br atoms. In the valence band region, the main contribution comes from the mixing of the “s” state of Si and “p” state of Br, while, in the conduction energy band region, it comes from the mixing of “s” state of Br and Rb with “p” state of Si. The partial covalent bonding can be observed in Si and Br as these are overlapped with each other at some energy ranges.

3.2 Optical Properties

The optical properties are essential for proving the utility of the compound in the optoelectronic device because optical factors arise due to the mobility and recombination of electrons after the incident of photons on the material. All the optical spectra are depicted in Fig. 4a-e up to the energy range of 10 eV, which are computed

through TB-mBJ exchange–correlation potential. The real and imaginary dielectric tensor spectra presented in Fig. 4a and b are the function of the wave vector. The real dielectric tensor spectra through which we get its static value $\epsilon_1(0) = 5.38$ is helpful for getting energy stockpiling and polarization. The imaginary dielectric tensor spectra presented in Fig. 4b depict the transition of electrons from one energy state to another which peaks at 2.4, 2.9, 3.9, and 9.0 eV arise due to the electron transitions. Figure 4c addresses the absorption graph of RbSiCl_3 , this optical parameter is utilized to enlighten us on the quantity of absorbed photons. In addition, through the absorption spectra, we viewed that a large portion of photon intensity lies in the 3–5 eV range of visible electromagnetic waves. The calculated value of the IAC (integrated absorption coefficient) is $126.47 (\times 10^4 \text{ eV/cm})$ that indicates the better absorption of photons on the material. The absorption of the material additionally relies on the surface of interface and this is analyzed by reflectivity spectra shown in Fig. 4d which yield the 15–23% low reflectance in the energy range–to 10 eV. The refractivity spectra given in Fig. 4e used to tell about the morphology of the material, i.e., its transparency and smoothness and the static value of refraction is 2.23. The compound exhibits a cubic structure and the physical properties of the compound is same in all directions, which indicated its isotropic nature. All optical properties affirm the utilization of the compound in multi-junction solar cell and optoelectronic device.

4 Conclusion

We arrive at the conclusion that, after examining the optoelectronic behavior of ternary inorganic perovskite RbSiBr_3 utilizing DFT typified in Wien2k code in the FP-LAPW method, RbSiBr_3 could be used as a lower layer in multi-junction solar cell as its band gap is lower than the optimum band gap for the solar cells. It is analyzed through the energy band structure and DOS that RbSiBr_3 perovskite has a semiconductor and direct band gap nature. In addition, its optical properties affirm that RbSiBr_3 has a prominent intensity in the visible range of electromagnetic spectra with high absorption and low reflectance. All optical properties also prove the isotropic nature of the compound. Based on electronic and optical properties, this compound can be used for optoelectronic applications.

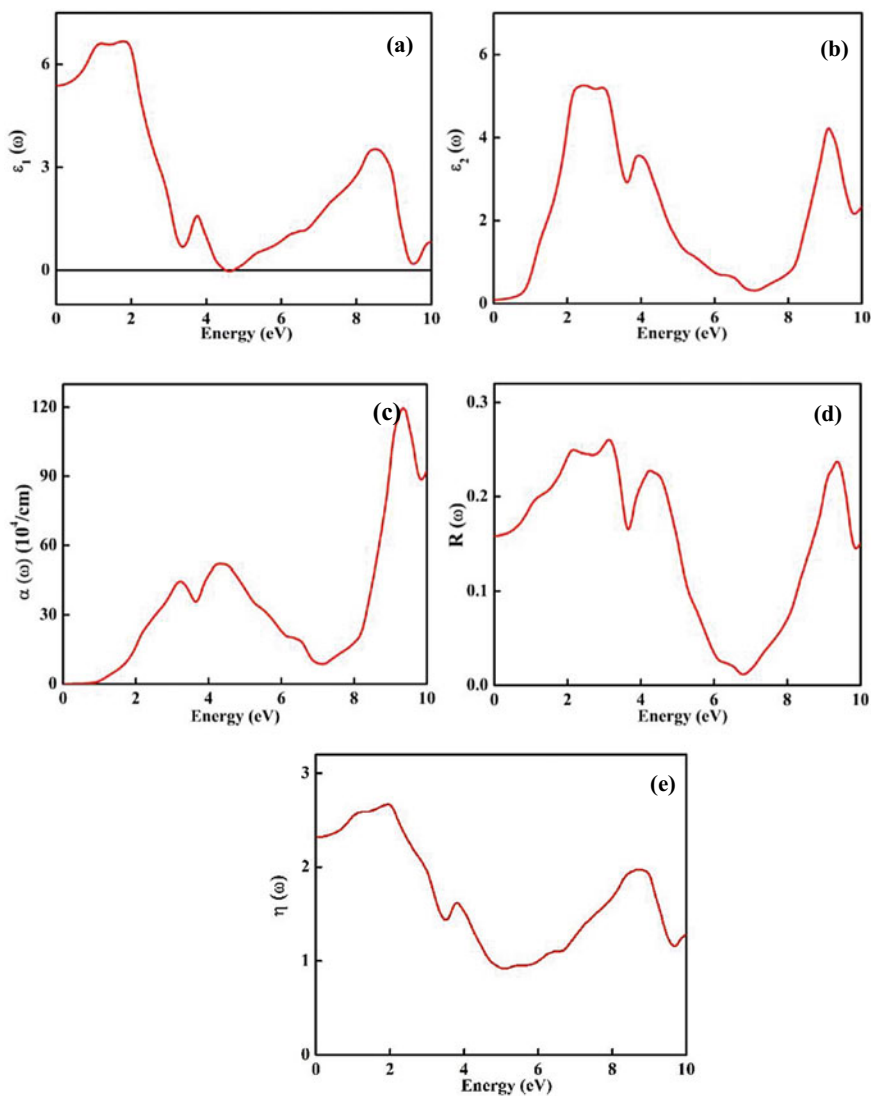


Fig. 4 a Real dielectric tensor b Imaginary dielectric tensor c Absorption d Reflectivity e Refractivity spectra of cubic RbSiBr₃

Acknowledgements We acknowledge Prof. Peter Blaha for giving the Wien2k code for examining the material. We are beholden to Manipal University Jaipur for giving all necessary adds. Monetary help provider is DST-SERB, New Delhi (India), vide grant number EMR/2017/005534.

References

1. Bhattacharya PC (2002) Urbanisation in developing countries. *Econ Polit Wkly* 4219–4228
2. McGee T (1994) The future of urbanisation in developing countries. The case of Indonesia. *Third World Plan Rev* 16: iii
3. Bocquier P (2008) Urbanisation in developing countries: is the ‘cities without slums’ target attainable. *Int Dev Plan Rev* 30:i–vii
4. Harris N (1990) Urbanisation, economic development and policy in developing countries. *Habitat Int* 14:3–42
5. Kurbatova T, Khlyap H (2015) State and economic prospects of developing potential of non-renewable and renewable energy resources in Ukraine. *Renew Sustain Energy Rev* 52:217–226
6. Nyambuu U, Semmler W (2014) Trends in the extraction of non-renewable resources: The case of fossil energy. *Econ Model* 37:271–279
7. Heiberg S, Wellmer F-W (2012) Stretching the availability of non-renewable resources. In: *Non-renewable resource issues*. Springer, pp 183–194
8. Güney T (2019) Renewable energy, non-renewable energy and sustainable development. *Int J Sust Dev World* 26:389–397
9. Shahzad U (2012) The need for renewable energy sources. *Energy* 2:16–18.
10. Kabir E, Kumar P, Kumar S, Adelodun AA, Kim K-H (2018) Solar energy: potential and future prospects. *Renew Sustain Energy Rev* 82:894–900
11. Lewis NS (2007) Toward cost-effective solar energy use. *Science* 315:798–801
12. Lee TD, Ebong AU (2017) A review of thin film solar cell technologies and challenges. *Renew Sustain Energy Rev* 70:1286–1297
13. Yamaguchi M (2002) Multi-junction solar cells and novel structures for solar cell applications. *Physica E* 14:84–90
14. Lim EL, Yap CC, Jumali MHH, Teridi MAM, Teh CH (2018) A mini review: can graphene be a novel material for perovskite solar cell applications? *Nano-Micro Lett* 10:1–12
15. Luxová J, Šulcová P, Trojan M (2008) Study of perovskite compounds. *J Therm Anal Calorim* 93:823–827
16. Huang L, Lambrecht WRL (2016) Electronic band structure trends of perovskite halides: beyond Pb and Sn to Ge and Si. *Phys Rev B* 93:195211
17. Gou G, Young J, Liu X, Rondinelli JM (2017) Interplay of cation ordering and ferroelectricity in perovskite tin Iodides: designing a polar halide perovskite for photovoltaic applications. *Inorg Chem* 56:26–32
18. Körbel S, Marques MAL, Botti S (2016) Stability and electronic properties of new inorganic perovskites from high-throughput ab initio calculations. *J Mater Chem C* 4:3157–3167
19. Jung Y-K, Lee J-H, Walsh A, Soon A (2017) Influence of Rb/Cs cation-exchange on inorganic Sn halide perovskites: from chemical structure to physical properties. *Chem Mater* 29:3181–3188
20. Mao X, Sun L, Wu T, Chu T, Deng W, Han K (2018) First-principles screening of all-inorganic lead-free ABX₃ perovskites. *J Phys Chem C* 122:7670–7675
21. Jiang J, Onwudinanti CK, Hatton RA, Bobbert PA, Tao S (2018) Stabilizing lead-free all-inorganic tin halide perovskites by Ion exchange. *J Phys Chem C* 122:17660–17667
22. Radha SK, Lambrecht WRL (2019) Band gaps and stability of CsSiX₃ halides. *Phys Status Solidi A* 216:1800962
23. Jain D, Chaube S, Khullar P, Goverapet Srinivasan S, Rai B (2019) Bulk and surface DFT investigations of inorganic halide perovskites screened using machine learning and materials property databases. *Phys Chem Chem Phys* 21:19423–19436
24. Li Y, Gong X, Zhang P, Shao X (2019) Structural, electronic and optical properties of RbSnCl₃: a first-principles calculation. *Chem Phys Lett* 716:76–82
25. Mahmood Q, Yaseen M, Hassan M, Rashid MS, Tili I, Laref A (2019) The first-principle study of mechanical, optoelectronic and thermoelectric properties of CsGeBr₃ and CsSnB₃ perovskites. *Mater Res Express* 6:045901

26. Benyahia K (2019) First principle calculations of phases stability and electronic structure of the trihalide perovskite RbSnBr₃. PSBJ 3
27. Yi Z, Ladi NH, Shai X, Li H, Shen Y, Wang M (2019) Will organic–inorganic hybrid halide lead perovskites be eliminated from optoelectronic applications? *Nanoscale Adv* 1:1276–1289
28. Yang RX, Skelton JM, da Silva EL, Frost JM, Walsh A (2020) Assessment of dynamic structural instabilities across 24 cubic inorganic halide perovskites. *J Chem Phys* 152:024703
29. Khan K, Sahariya J, Soni A (2021) Structural, electronic and optical modeling of perovskite solar materials ASnX₃ (A = Rb, K; X = Cl, Br): first principle investigations. *Mater Chem Phys* 262:124284
30. Blaha P, Schwarz K, Tran F, Laskowski R, Madsen GKH, Marks LD (2020) WIEN2k: an APW+lo program for calculating the properties of solids. *J Chem Phys* 152:074101
31. Blaha P, Schwarz K, Sorantin P, Trickey SB (1990) Full-potential, linearized augmented plane wave programs for crystalline systems. *Comput Phys Commun* 59:399–415
32. Tran F, Blaha P (2009) Accurate band gaps of semiconductors and insulators with a semilocal exchange–correlation potential. *Phys Rev Lett* 102:226401

An Overview of Distributed Generation Integration Techniques, Present Trends and Future Scope



Deepak Porwal , Manoj Fozdar (SMIEEE), and Rajive Tiwari

Abstract Distributed generation integration is a new booming and fast-adopting technology. The small rating components, compactness, local power demand fulfilment and renewable-based input energy sources are the attractive features of distributed energy resources. They offer a reliable and secure supply at distribution level. The system as a whole is relieved from heavy power congestion with the presence of these local energy sources. However, DERs suffer from low inertia issues, power quality problems and changing input energy and load patterns. This paper reviews the DG technologies in service, their contribution in total energy demands and need for active distribution networks and future challenges.

Keywords Distributed energy resources · Active distribution networks · Radial distribution system · Optimal Volt-VAr Control

1 Introduction

With the development of increasing electricity-driven devices, the world relies more on uninterruptible supply. In the past few decades, a number of blackouts have been reported throughout the world [1, 2]. This further strengthens the urge for a reliable and secure power. Rapid industrialization, fuel-based transportation, use of bio-harmful materials and lack of pollution awareness have all together affected the local environment seriously. It has increased the carbon emissions into the surrounding atmosphere and thus raised the global warming to an alarming stage. Worldwide, Countries are taking global warming and energy crisis as a major challenge. Several nations are allocating a large sum of budget to curb the emission only. Power utilities are also focused on decarbonizing the power system, framing new grid reinforcement techniques to withstand new climate patterns and cyber-physical attacks. Secondly, it

D. Porwal (✉) · M. Fozdar (SMIEEE) · R. Tiwari
Department of Electrical Engineering, Malaviya National Institute of Technology, Jaipur,
Rajasthan 302017, India
e-mail: deepakporwal1512@gmail.com

facilitates customers with clean energy choices and network operators with improved service performance.

Sustainable and clean energy sources are being seen as long-term solutions for an eco-friendly power system. Renewable-based energy plants are attracting both utilities and customers due to their green-clean feature, advancing research, sophisticated compact design, increasing market competition and promotions, various government schemes and subsidies. The distributed generation (DG) units are small in size, flexible in control and low inertia systems. They depend on locally available input energy sources like solar, wind, hydro, etc. Their capacity is governed by local topographical conditions, type of user and usage duration. The DGs contribute to improving system security, reliability, efficiency and power quality; all these make them more suitable for low- and medium-power applications [3].

Power electronics and advanced control-based systems are enormously supporting in DG operations and integrating them into the main system. Conventional power system is already ageing with old infrastructure and components, traditional mechanism of unidirectional power transfer and prevailing distribution level voltage fluctuations. Secondly, there is a requirement of restructuring and modernizing the grid with recent technologies like distributed energy resources (DERs) to better integrate and utilize them optimally. All these has led to shifting on the new generation small rating power plants.

Based on the fuel input, Distributed Generators (DGs) can be categorized into dispatchable and non-dispatchable systems [4]. These DGs are able to supply stand-alone systems and feed the inaccessible areas and remote villages efficiently. The DG power in these areas can be utilized for illumination purposes, heating applications, running small-scale industrial units and communications. In terms of performance, DG integration positively contributes to distribution system. This is because of lower network losses, enhanced voltage security margin, improved system reliability and indirect contribution to reduction in polluting emissions [5]. However, DG connection causes to raise the short-circuit fault levels. In order to mitigate such problems, fault current limiter is installed [6]. With the increasing share of DGs, long-term voltage stability is gaining interest and relatively improved functioning and good controllability methods are being explored. Power system planners and network operators are continuously working on automated distribution technologies. The automated distribution systems (ADS) provide a reliable and efficient control to strategize optimal operation by controlling line switches and enabling controllable devices. It includes active participation of DERs with changing load profiles. It manages and upgrades the system and increases power-sharing capacity of DERs [7–9].

The introduction of DG-based system forms a new revenue-generating entity and new jobs are also generated. This results in improved efficiency, better knowledge sharing, higher energy usage and enhanced interaction between organizations and people. DG output varies largely based on energy volume, form and type of DG applications. It may take long time for small and simple load supply, while short time with peak loads. The efficiency of DG mainly depends on the form of DC or AC it generates, the converters used and other controlling equipments. Due to the

increasing penetration of distributed generation-based plants, both transmission and distribution systems are responsible for voltage security problems. Now, DG units are actively participating in power generation and system security [10].

2 Distributed Generation

The energy generated from small-scale power units and distributed to nearby load centres is called distributed generation. These power units extract energy mainly from wind, photovoltaic (PV) cells, micro- and small hydro storage, geothermal energy banks and microturbine mechanism. The power generation at the local end level eliminates the heavy costs of power transmission and distribution over long distance. These DGs can produce power from 1 to 100 MW comprising many small units. These units can be easily mounted on low- or medium-voltage networks. Such systems improve the stability of the system by releasing the transmission capacities and supplies as spinning reserves during peak load conditions.

Based on power levels, distributed generation can be the following types:

1. **Small local type:** This is specified as per site and used to generate electricity using a cluster of small generators producing power enough to serve limited customers. It can be in grid-connected mode or totally isolated.
2. **Microlocal type:** This is a much smaller level and is generally installed by individual energy consumer. Such a system is termed as micro-level distributed generation. These systems can be grid-connected, where they can feed excess power generated to the grid. Thus, works as prosumers of energy, i.e. a power producer and consumer.

DG-embedded systems can meet the power demand exactly as they are well-sized, well-coordinated and can be installed in small discrete units. DG systems supply power to the grid, reduces the demand and the energy price by lowering the burden on main grid [11–13]. The concept of DG-based system increases the service life of the equipments used and decreases the cost associated with fuel. It also removes the requirement of specific fuel for power generation. The DG installation removes the need of new power plant construction and enables healthy market competitiveness for growing load demands. DGs are diversified systems and hence find wide acceptance where local resources are available and cost of long transmission is high.

Small-sized distributed generators offer several benefits compared to the conventional centralized power system:

- Reduction in overall transmission and distribution network losses.
- Reduction in peak load generation shortage conditions.
- Connecting inaccessible areas and remote rural villages.
- Quick response to daily fluctuating power demands.
- Better power management with enhanced security and improved supply reliability.
- Easy correction in power, voltage and frequency at regular intervals.

Table 1 Different types of DG Technologies

S. no	Technology	Output type	Features
1	Photovoltaics (PV)	DC	No emissions, reliable, no minimal maintenance cost
2	Wind turbines	AC	Best suited for remote applications like hill areas
3	Small hydro	AC	Provides good inertia, pollution-free
4	Fuel cells	DC	Good for small power applications, stationary
5	Micro-turbines	AC	Best suited for high-speed, low inertia applications
6	Reciprocating engines	AC	Continuous power supply or backup emergency power
7	Combustion gas turbines	AC	Low cost of installation, lower amount of emissions, require lesser maintenance

- Better congestion management with the integration of several other devices like energy storage devices.

The distributed generation techniques, their topology and benefits are given in Table 1.

PV arrays, wind plants and hydro-generating plants generally provide active power and require a reactive power source within the system. Wind energy is available in plenty at hilly areas and water bodies. It is uniformly distributed at site-specific locations and can be harnessed throughout the year. The wind-based power generation can be performed the whole day [14]. Hydroelectric plants are further categorized as per their capacity into micro plants (less than 100 kW), mini plants (100–1 MW) and macro plants (1–25 MW). It is free of any type of fuel input and serves multiple purposes such as controlling soil erosion, canal formation, water supply for irrigation, reserving water for scarcity situations, etc. They have the longest life and higher capacity compared to other renewable-based sources. Fuel cell uses hydrogen and oxygen for electricity generation. Fuel cell work without any interruption if reactants and flow of oxidant is controlled properly. There is no rotating part in fuel cell, and this results in lower vibrations and highly silent operation.

3 Role of Distributed Generation

Distributed generations constitute today's modern grid. Local-level generation helps to meet peak load requirements, thus better management of system is achieved. DGs can feed their surplus power back to the utilities, and this makes it a revenue generation mechanism. The need of new transmission lines is avoided and economic saving is achieved with local renewable-based power generation. The wind, solar and

other such distributed generation systems can be conveniently utilized, with reduced line losses.

DG-enabled systems can be isolated from the main grid without disrupting the loads. So, the grid remains intact even during disconnection of DGs. Once, the normal operating condition is attained again, the local DG grid can resynchronize with the main grid. The growth of such systems depends on all the participants of power delivery process like utilities, transmission channels, distribution system operators, market managers and service providers. The old DG integration philosophy of 'Fit and Forget' may not suit the present situations [15–18].

4 Active Distribution Networks (ADNs)

The increasing penetration of DGs has led to the evolution of active distribution networks (ADNs). Coordinated control of all the power generators, tap-changing transformers and voltage regulators is termed active distribution network management [19]. With large DG integration, the voltage rise problem has become common in distribution networks [16]. At the interconnection point, DG units shall not actively participate in voltage regulation [20]. Secondly, rising complexity of operation and control of these networks is also a challenge [19]. In view of this, ADNs must properly coordinate with the transmission grid to eliminate the over-voltage problem. Nowadays, DG technologies like synchronous machines, doubly fed induction generators (DFIGs) are able to provide dynamic reactive power response. This can be used to enhance overall system stability and security. Active distribution network automation also helps to improve the distribution system performance.

Distribution system automation controls the automatic switches as well as the dispatchable devices [21]. Dispatchable Distributed Generators (DDGs), even SVCs are controlled by distribution system operator (DSO) via communication systems. Automatic switches via secure communication protocols are used for automation purpose [22]. Distribution management system (DMS) can well coordinate Renewable Energy Sources (RESs), dynamic loads and Energy Storage Systems (ESS) with the help of advanced communication techniques. Data transfer technologies along with electrical grid are used to build an effective automated active distribution system. Distribution systems are tested for network losses, voltage stability margin and emission index. Due to high network losses, utility companies incur huge financial losses [23]. The system planners and network operators are aiming for improved technical and economic performance. With different DG technologies integrated into the system, power quality problem is becoming a major challenge. Several fixed and variable switched topologies of capacitor banks along with DGs are being experimented for satisfactory operation. Smart DG integration techniques are required to guarantee overall secure and reliable operation [24–47].

5 Future Challenges of Renewable Energy Sources-Based Generation

1. Promote the use of distributed generation technologies, particularly in remote and inaccessible locations.
2. Provide local, feasible and decentralized DG facilities with flexible and smooth control.
3. Encourage utilities to derive new tariff schemes and demand-side management programmes for further boosting distributed generation at consumer level.
4. Devise smart real-time monitoring and control system by using intelligent electronic devices (IEDs) for network operators to collect and analyse the information.
5. Identify the most suitable DG size and locations at the distribution level.
6. Enable DGs to withstand contingency conditions by proper system planning and design.

References

1. Mousavi OA, Bozorg M, Cherkaoui R (2013) Preventive reactive power management for improving voltage stability margin. *Electr Power Syst Res* 96:36–46
2. Eremia M, Shahidehpour M (2013) *Handbook of electrical power system dynamics: modeling, stability, and control*. Wiley
3. EU Commission Task Force for Smart Grids (2010) Functionalities of smart grids and smart meters. [Online]. <http://ec.europa.eu/>
4. Tolba MA, Rezk H, Al-Dhaifallah M, Eisa AA (2020) Heuristic optimization techniques for connecting renewable distributed generators on distribution grids. *Neural Comput Appl* 32(17): 14195–14225. <https://doi.org/10.1007/s00521-020-04812-y>
5. Essallah S, Khedher A, Bouallegue A (2019) Integration of distributed generation in electrical grid: optimal placement and sizing under different load conditions. *Comput Electr Eng* 79. Art. no. 106461. <https://doi.org/10.1016/j.compeleceng.2019.106461>
6. El-Ela AAA, El-Sehiemy RA, Shaheen AM, Ellien AR (2021) Optimal allocation of distributed generation units correlated with fault current limiter sites in distribution systems. *IEEE Syst J* 15(2): 214–2155. <https://doi.org/10.1109/jsyst.2020.3009028>
7. Yinger R, Robert S (2017) Modernizing the California grid: preparing for a future with high penetrations of distributed energy resources. *IEEE Power Energy Mag* 15(2): 20–28
8. Southern California Edison (2018) Southern California edison company's (U-338-E) annual report on the status of the electric program investment charge program
9. Yinger R (2018) Integrated grid project (IGP). In: EPIC winter symposium
10. Ettahadi M, Ghasemi H, Vaez-Zadeh S (2012) Voltage stability based DG placement in distribution networks. *IEEE Trans Power Delivery* 28. <https://doi.org/10.1109/TPWRD.2012.2214241>
11. PecasLopes JA, Hatziaargyriou N, Mutale J, Djapic P, Jenkins N (2007) Integrating distributed generation into electric power systems: a review of drivers, challenges and opportunities. *Int J Elect Power Syst Res* 77:1189–1203
12. Cuffe P, Smith P, Keane A (2014) Capability chart for distributed reactive power resources. *IEEE Trans Power Syst* 29(1):15–22

13. \bibitem{b13} (2008) IEEE application guide for IEEE Std 1547. In: IEEE standard for interconnecting distributed resources with electric power systems
14. Shaheen AM, Elsayed AM, El-Sehiemy RA, Abdelaziz AY (2021) Equilibrium optimization algorithm for network reconfiguration and distributed generation allocation in power systems. *Appl Soft Comput* 98, Art. no. 106867. <https://doi.org/10.1016/j.asoc.2020.106867>
15. Hooshmand E, Rabiee A (2019) Energy management in distribution systems, considering the impact of reconfiguration, RESs, ESSs and DR: a trade-off between cost and reliability. *Renew Energy* 139:346–358. <https://doi.org/10.1016/j.renene.2019.02.101>
16. Tonkoski R, Turcotte D, El-Fouly THM (2012) Impact of high PV penetration on voltage profiles in residential neighborhoods. *IEEE Trans Sustain Energy* 3(3):518–527
17. Milanovic JV, Mat Zali S (2013) Validation of equivalent dynamic model of active distribution network cell. *IEEE Trans Power Syst* 28(3):2101–2110.
18. Yuquan L, Meng Y, Ke W, Ming G (2014) Research on transmission and distribution network reactive power/voltage coordinated control technology of large receiving-end urban power grid. In: 2014 IEEE international conference on mechatronics and automation. pp 1990–1994
19. Ghazavi Dozein M, Ansari J, Shahbazi HR, Kalantar M (2013) Optimal distribution voltage control through a sub-framework in the reactive power management on the smart grid. In: 2013 smart grid conference (SGC). pp 153–159
20. Siirto OK, Safdarian A, Lehtonen M, Fotuhi-Firuzabad M (2015) Optimal distribution network automation considering earth fault events. *IEEE Trans Smart Grid* 6(2):1010–1018. <https://doi.org/10.1109/TSG.2014.2387471>
21. Fetouh T, Elsayed AM (2020) Optimal control and operation of fully automated distribution networks using improved tunicate swarm intelligent algorithm. *IEEE Access* 8:129689–129708. <https://doi.org/10.1109/ACCESS.2020.3009113>
22. McGranaghan M, Goodman F (2005) Technical and system requirements for advanced distribution automation. In: Proceedings of 18th international conference and exhibition on electricity distribution (CIRED). pp v5–93. <https://doi.org/10.1049/cp:20051374>
23. Ranamuka D, Agalgaonkar AP, Muttaqi KM (2019) Innovative Volt/VAR control philosophy for future distribution systems embedded with voltage-regulating devices and distributed renewable energy resources. *IEEE Syst J* 13(3):3153–3164
24. Teshome D, Xu W, Bagheri P, Nassif A, Zhou Y (2019) A reactive power control scheme for DER-caused voltage rise mitigation in secondary systems. In: 2019 IEEE power & energy society general meeting (PESGM). Atlanta, GA, USA, p 1
25. Hu S, Xiang Y, Zhang X, Liu J, Wang R, Hong B (2019) Reactive power operability of distributed energy resources for voltage stability of distribution networks. *J Mod Power Syst Clean Energy* 7(4):851–861. <https://doi.org/10.1007/s40565-018-0484-3>
26. Modarresi J, Gholipour E, Khodabakhshian A (2016) A comprehensive review of the voltage stability indices. *Renew Sust Energy Rev* 63:1–12
27. Meena NK, Swarnkar A, Gupta N et al (2017) Multi-objective Taguchi approach for optimal DG integration in distribution systems. *IET Gener Transm Distrib* 11(9):2418–2428
28. Yuvaraj T, Devabalaji KR, Ravi K (2015) Optimal placement and sizing of DSTATCOM using harmony search algorithm. *Energy Procedia* 79:759–765
29. Maksić M, Matvoz D (2014) A practical case of determining the maximum allowed PV plant connection power using different reactive power control concepts. In: 2014 IEEE power engineering society general meeting
30. Weckx S, Driesen J (2016) Optimal local reactive power control by pv inverters. *IEEE Trans Sustain Energy* 7(4):1624–1633
31. Yang G, Marra F, Juamperez M et al (2015) Voltage rise mitigation for solar PV integration at LV grids. *J Mod Power Syst Clean Energy* 3:411–421
32. Lee TL, HuYu SH, Chan H (2013) D-STATCOM with positive-sequence admittance and negative-sequence conductance to mitigate voltage fluctuations in high-level penetration of distributed-generation systems. *IEEE Trans Ind Electron* 60: 1417–1428
33. Zhang Z, Ochoa LF, Valverde G (2018) A novel voltage sensitivity approach for the decentralized control of dg plants. *IEEE Trans Power Syst* 33(2):1566–1576

34. Ali ES, Abd Elazim SM, Abdelaziz AY (2016) Ant lion optimization algorithm for renewable distributed generations. *Energy* 116, Part 1: 445–458
35. Sannigrahi S, Ghatak S, Acharjee P (2019) Strategically incorporation of RES and DSTATCOM for techno-economic-environmental benefits using search space reduction based improved CSA. *IET Gener Transm Distrib* 13. <https://doi.org/10.1049/iet-gtd.2018.5220>
36. Poornazaryan B, Karimyan P, Gharehpetian GB et al (2016) Optimal allocation and sizing of DG units considering voltage stability, losses and load variations. *Int J Electr Power* 79:42–52
37. Murty VVSN, Kumar A (2015) Optimal placement of DG in radial distribution systems based on new voltage stability index under load growth. *Int J Electr Power* 69:246–256
38. Arcidiacono V, Chiandone M, Sulligoi G (2011) Voltage control in distribution networks using smart control devices of the distributed generators. In: 2011 international conference on clean electrical power (ICCEP). pp 738–743
39. Rocha L, Castro R, Jesus JMF (2016) An improved particle swarm optimization algorithm for optimal placement and sizing of STATCOM. *Int Trans Electr Energy* 26(4):825–840
40. Hedayati H, Nabaviniaki SA, Akbarimajd A (2008) A method for placement of DG units in distribution networks. *IEEE Trans Power Del* 23(3):1620–1628
41. Etehadhi M, Ghasemi H, Vaez-Zadeh S (2013) Voltage stability based DG placement in distribution networks. *IEEE Trans Power Del* 28(1):171–178
42. Masters CL (2002) Voltage rise: the big issue when connecting embedded generation to long 11kV overhead lines. *Power Eng J* 16(1):5–12. <https://doi.org/10.1049/pe:20020101>
43. Esmailian HR, Fadaeinedjad R (2015) Energy loss minimization in distribution systems utilizing an enhanced reconfiguration method integrating distributed generation. *IEEE Syst J* 9(4):1430–1439
44. Liu Y, Li J, Wu L (2018) Coordinated optimal network reconfiguration and voltage regulator/DER control for unbalanced distribution systems. *IEEE Trans Smart Grid*. <https://doi.org/10.1109/TSG.2018.2815010>.
45. Pe´rez-London˜o S, Rodrı´guez LF, Olivar G (2014) A simplified voltage stability index (SVSI). *Int J Electr Power* 63:806–813
46. Balamourougan V, Sidhu TS, Sachdev MS (2004) Technique for online prediction of voltage collapse. *IEE Proc Gener, Transm Distrib* 151(4):453–460
47. Dođanşahin K, Kekezođlu B, Yumurtacı R, Erdinç O, Catal˜ao J (2018) Maximum permissible integration capacity of renewable DG units based on system loads. *Energies* 11:255. <https://doi.org/10.3390/en1101025>

Design and Control of Battery Management System for Electric Vehicle



Bharat Singh, Deepanshu Rawat, Pulkesh Parwani, Rhytham Gupta, and Tisha Kapoor

Abstract The battery management system (BMS) serves the purpose of controlling the functional limits of the battery packs, thermally and electrically, and is critical for accident protection. The BMS also helps in optimal operation of the battery pack, which helps to prolong the battery life, benefitting the lifecycle and the cost. This paper addresses the future challenges in BMS and focuses on the possible solutions. This paper encompasses cell balancing automation, which equalizes the voltage and SoC among the cells when the cells are at distinct SoC thereby improving the battery life, and SoC estimation, which estimates the approximate driving range of the electric vehicle. This paper focuses on the control of cell balancing function of battery management system, MATLAB model is designed performing the cell balancing of six cells for different states of charge values. A comprehensive technical review of the BMS is done and an evaluation of components and architecture of BMS is also presented along with the major simulations.

Keywords Electric vehicles · Battery management system · State of charge · Cell balancing

1 Introduction

As the electric vehicle industry is picking up the pace, there is an increased push by the government in the form of production-linked incentive (PLI) schemes which in turn encourages people to switch to electric vehicles. The Indian electric vehicle market was valued at USD 1,434 billion in 2021, and it is expected to reach USD 15,397 billion by 2027, registering a CAGR of 47.09% during the forecast period (2022–2027). There have been many research and development in the sector but

B. Singh · D. Rawat (✉) · P. Parwani · R. Gupta · T. Kapoor
Bharati Vidyapeeth's College of Engineering, New Delhi, India
e-mail: deepanshurawat2k@gmail.com; deepanshurawat.eee1@bvp.edu.in

P. Parwani
e-mail: parwanipulkesh@gmail.com; pulkeshparwani.eee1@bvp.edu.in

many more are yet to be done for the sales of electric vehicle (EV) to surpass the IC engine vehicles and become mainstream. The primary reason masses are hesitant to switch to EVs is the driving range uncertainty. The battery pack, which is responsible to power the drivetrain, also determines the driving range of the vehicle. Being one of the major cost contributors to EVs, battery pack requires a Battery Management System (BMS) which helps prolong the battery pack life, control the functional limits of the pack, optimize the use of battery, and in turn, maximize the range.

A basic requirement of a BMS is that it should provide an accurate estimation of the state of charge (SoC), configure cells according to real-time operation conditions, handle cell–cell unbalance conditions, maximize energy efficiency, and ensure safety of the battery pack.

2 Battery Management System

The electric mobility industry is at a crucial stage given how the electric vehicle (EV) ecosystem is rapidly developing in India and abroad. The Li-ion battery packs are one of the most important components of an EV and constitute a major chunk of the cost of the vehicle; hence, the protection of the battery pack by a well-designed battery management system (BMS) is imperative.

2.1 Battery Pack Layout

A battery pack can be defined as the set of several identical batteries or individual battery cells. They can be connected in a series, parallel, or a combination of two (preferably nPmS module) to deliver the desired voltage, current, or power. The battery pack consists of various cell modules, battery management system, insulation monitoring device, pre-charge circuit, balancing circuits, current sensors, and service disconnect/fuses [1].

2.2 Importance of Battery Management System

Apart from controlling the functional limits of the battery pack both electrically and thermally, BMS is also crucial to accident prevention. BMS helps in optimal operation of battery pack which helps to prolong life of the battery pack, benefiting in lifecycle & cost. BMS predicts the SoC to provide driver with distance to zero km which aids in timely charging. BMS generates reports regarding pack abuse and warranty period status.

2.3 Function of a BMS

Battery Management System has a vital role in cell monitoring and measurement of parameters such as voltages, current, temperatures (Cell and Ambient) as well as pressure (Cell and Ambient). In an event of detection of some abnormal/abuse condition, it disconnects the battery from the load. Acting as a safety tool it tends to provide protection against over charge, over discharge, short circuit, temperature, and polarity. It logs and communicates over charge as it dispatches status to other components via CAN [2] and SPI. It also consists of state estimation algorithms like State of Health (SOH) and State of Charge (SOC) [3].

2.4 Thermal Management

It is one of the most crucial elements for any battery to operate properly, the temperature of the battery must be maintained to a certain temperature. If the battery temperature exceeds that certain temperature, then the cooling system needs to be activated [4]. The cooling system can be managed by the BMS model. At every different temperature, performance and behavior of the battery may also differ.

2.5 BMS Architecture

The architecture of BMS can be broadly categorized into two configurations, namely, packs with single BMS and packs with slave–master BMS configuration. For the packs with single BMS, at the lowest level of hierarchy, we have the cell monitoring unit (CMU) which monitors the cell and communicates the cell parameters with the module management unit (MMU) which, in turn, transfers the data to the pack management unit (PMU), which finally sends the data to the controller which takes the controlling action [5]. For the packs with slave–master BMS configuration, the CMU can work independently and can take several minor decisions just like BMS (Fig. 1).

3 Simulations/Automations

3.1 Cell Balancing Automation

Six batteries each of 3.6 V and 4A rating were taken from the library browser. State of charge (SoC) of the first battery was kept at 75%, the second at 65%, the third at 55%, the fourth at 45%, the fifth at 35%, and the last one at 25%. The SoC of

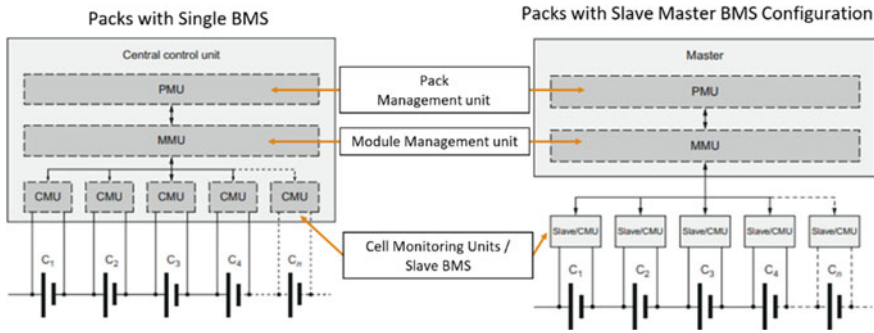


Fig. 1 Figure demonstrating the architecture of the battery management system

all the batteries was kept at different levels to model the cell balancing [6]. Six bus selectors were taken for measuring the battery parameter and were connected to each bus selector with each of the batteries. Six scopes were taken and each of them was connected with the bus selector for each battery. To measure the SoC of every block, six Goto blocks (labeled as SoC-1, SoC-2, SoC-3, SoC-4, SoC-5, and SoC-6, respectively) were taken and connected to the respective initial SoC of the batteries. The batteries were in discharge mode; hence, six resistive loads were connected with 4 V nominal voltage and 0.1 Hz frequency. Each battery is connected to the load. In order to control the switching operation of the loads, six ideal switches were taken, and each switch was connected between the battery and the load. Further, a control signal was generated to achieve the proper discharge mode. For this purpose, six switches (S1, S2, S3, S4, S5, and S6) connecting each switch with ideal switch were taken. To add logic to the circuits, a MATLAB function was constructed which used the six SoCs (SoC-1, SoC-2, SoC-3, SoC-4, SoC-5, and SoC-6) as the input and generated corresponding control signals as per the code which were further fed as the gate pulse to the six switches (S1, S2, S3, S4, S5, and S6) [7]. The code for the MATLAB function is shown in the pages before. A scope, a display, and a mux block were taken to view all the six SoCs. The SoCs were connected with the input of the scope and mux, respectively, and the output of the mux was connected to the display on which the result was displayed. The SoC for each battery came out to be 63.5 which means that all the six batteries got discharged and achieved the same level of SoC (Cell Balancing) [8, 9]. This vividly indicates that the simulation is operating in accordance with the theoretical interpretation and hence ideal for industrial applications (Figs. 2 and 3).

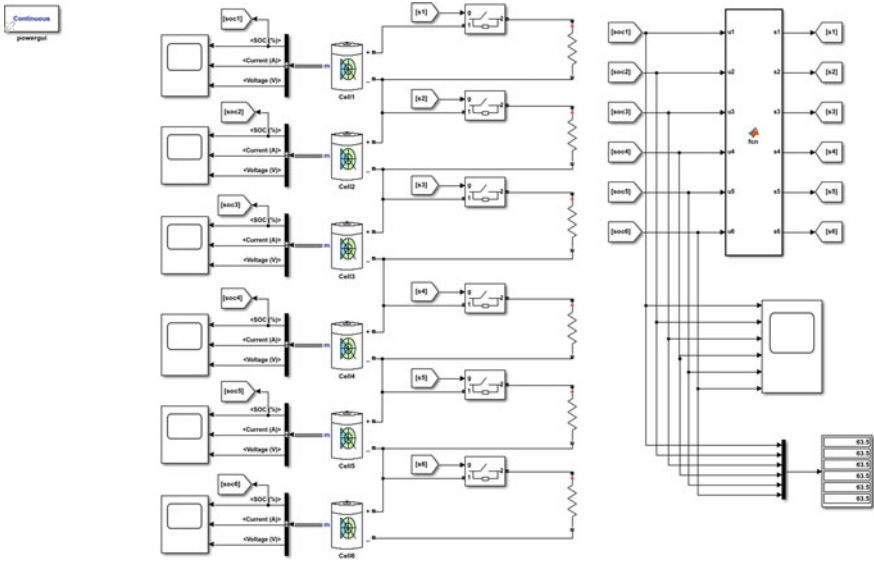


Fig. 2 MATLAB/Simulink figure to demonstrate cell balancing using six cells at different SoCs

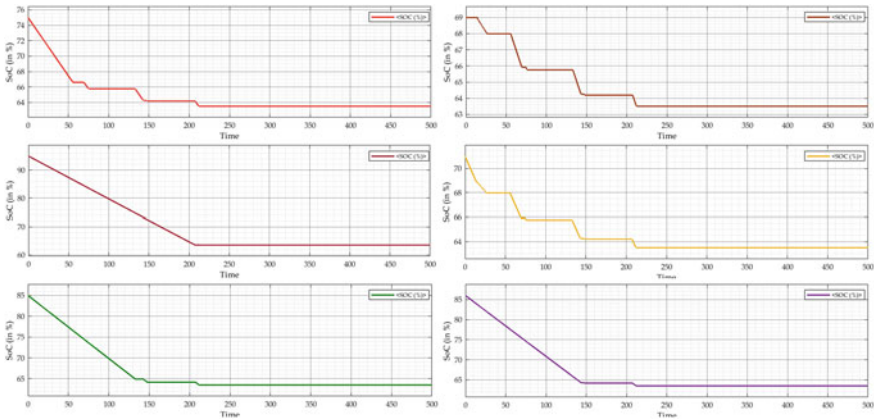


Fig. 3 MATLAB/Simulink scope output for Fig. 2

3.2 SoC Estimation Automation Using Coulomb’s Law

3.2.1 SoC Estimation Automation with Load Drawing Constant Current

A battery model was taken which can feed the battery capacity as per the data sheets with 100 V nominal voltage and 50Ah rating. A current sensor (by measuring it we

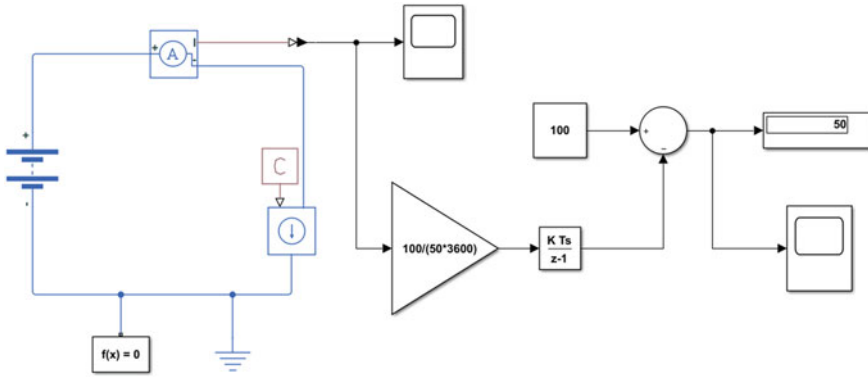


Fig. 4 MATLAB/Simulink figure to demonstrate the computation of SoC using Coulomb’s law (assuming that load is drawing constant current from the battery)

can get the output) and a current-controlled source (to withdraw a controlled current of 25 A from the battery) were taken. The current sensor with the positive terminal of the battery and current-controlled source with the negative terminal was taken.

A PS Constant was taken and connected to the current controlled source to withdraw a constant current (25 amperes). Solver configuration block was taken along with an electrical reference. PS-simulink converter, a scope, and a gain block (with a value of $100/(50*3600)$) were taken as a coulomb function. The converter along with current sensor and scope and gain block with the converter was connected as shown in the Simulation. A discrete-time integrator (with sample time = 0.1) was taken and connected with the gain block [10].

The integrator portion was modeled and the initial state of charge (in this example, it is 100%) was added. For this purpose, a constant block (with value = 100) was taken. A sum block was taken and connected with constant block and discrete time integrator. Finally, a scope and a display block were taken to understand the SoC of the battery and were connected with the sum block. The graph came out to be a straight line starting from 100 to 50 which means that initially state of charge (SoC) of the battery is 100% and after 1 h, state of charge (SoC) of the battery comes to 50%. This can theoretically be computed using the formula, $SoC(t) = SoC(t - 1) + 1/C \int_0^t I(t)dt$ (Eq. 1). Substituting the values in Eq. 1, the SoC after 1 h can be computed to be 50% [11] (Fig. 4).

3.2.2 SoC Estimation Automation with Constant Load

A battery model was taken which can feed the battery capacity as per the data sheets with 12 V nominal voltage and 100Ah rating. A current sensor (by measuring it, we can get the output) and a resistive load of 1.2 ohms (to withdraw a continuous current from the battery) were taken. The current sensor with the positive terminal of the battery and resistor with the negative terminal was taken.

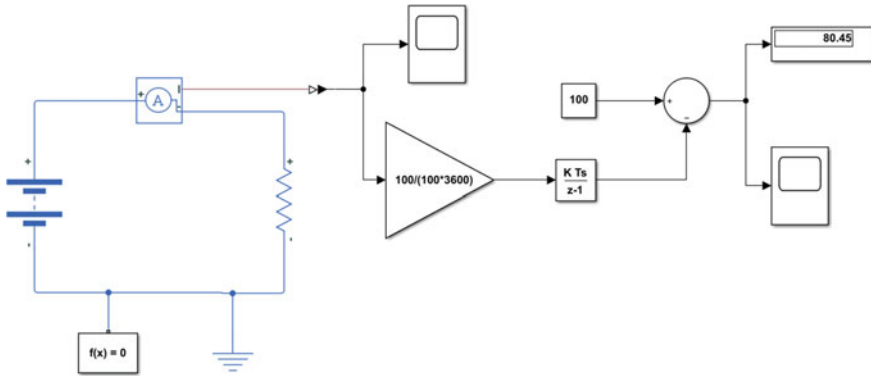


Fig. 5 MATLAB/Simulink figure to demonstrate the computation of SoC using Coulomb’s law (assuming a constant load condition)

Solver configuration block was taken along with an electrical reference. PS-simulink converter, a scope, and a gain block (with a value of $100/(100*3600)$) were taken as a coulomb function. The converter along with current sensor and scope and gain block with the converter was connected as shown in the Simulation. A discrete-time integrator (with sample time = 0.1) was taken and connected with the gain block.

The integrator portion was modeled and the initial state of charge (in this example, it is 100%) was added. For this purpose, a constant block (with value = 100) was taken. A sum block was taken and connected with constant block and discrete-time integrator. Finally, a scope and a display block were taken to understand the SoC of the battery and were connected with the sum block. The graph came out to be a straight line starting from 100 to 80 which means that, initially, state of charge (SoC) of the battery was 100%, and after 2 h, state of charge (SoC) of the battery comes to 80.45%. This result can be theoretically computed using Coulomb’s formula, (Refer to Eq. 1). Substituting the values in Eq. 1, the SoC after 2 h can be theoretically computed to be 80% which matches the value in the display of simulation in Fig. 5. This clearly implies that the simulation is operating according to the theoretical interpretation and hence ideal for industrial applications.

4 Conclusion

In this paper, a comprehensive study was done on different aspects of Battery Management System using MATLAB/Simulink. This paper encompassed cell balancing automation, which equalizes the voltage and SoC among the cells when the cells are at distinct SoC and keeps the SoC within a specific range and helps enhance the battery life, and SoC estimation, which help us to figure out the approximate range of the EV.

This estimation provides an aid in keeping some parts of the battery reserved for auxiliary systems like geofencing, central locking, etc. In addition, we investigated the design with the help of MATLAB simulations and outputs to simplify the existing design. Based on the previous work, particular challenges faced by BMS, and their feasible solutions were presented as a concrete foundation for upcoming research. Due to changing situations in real-world applications, an ideal solution was not required. Based on the particular situation, different strategies must be implicated to enhance and optimize the performance of BMS in future EVs.

References

1. Emanet B, Kiyak İ (2021) Performance effective battery management system(BMS) design of mini electric vehicles. In: 2021 5th international symposium on multidisciplinary studies and innovative technologies (ISMSIT). pp 744–749. <https://doi.org/10.1109/ISMSIT52890.2021.9604678>
2. Gabbar HA, Othman AM, Abdussami MR (2021) Review of battery management systems (BMS) development and industrial standards. *Technologies* 9:28. <https://doi.org/10.3390/technologies9020028>
3. Ci S, Lin N, Wu D (2016) Reconfigurable battery techniques and systems: a survey. *IEEE Access* 4:1175–1189. <https://doi.org/10.1109/ACCESS.2016.2545338>
4. Xing Y, Ma EWM, Tsui KL, Pecht M (2011) Battery management systems in electric and hybrid vehicles. *Energies* 4:1840–1857
5. Aiello O, Crovetto P, Fiori F (2015) Susceptibility to EMI of a battery management system IC for electric vehicles. <https://doi.org/10.1109/ISEMC.2015.7256257>
6. Xu D, Wang L, Yang J (2010) Research on Li-ion battery management system. *Int Conf Elect Control Eng* 2010:4106–4109. <https://doi.org/10.1109/iCECE.2010.998>
7. Sugumar HS (2021) Overview of cell balancing methods for Li-ion battery technology energy storage. 3 <https://doi.org/10.1002/est2.203>
8. Duraisamy T, Kaliyaperumal D (2020) Active cell balancing for electric vehicle battery management system. *Int J Power Electron Drive Syst (IJPEDS)* 11:571 <https://doi.org/10.11591/ijpeds.v11.i2.pp571-579>
9. Daowd M et al (2011) Passive and active battery balancing comparison based on MATLAB simulation. In: *IEEE vehicle power and propulsion conference (VPPC)*. Chicago USA, pp 6–9
10. Gao Z, Chin CS, Toh W, Chiew J, Jia J (2017) State-of-charge estimation and active cell pack balancing design of lithium battery power system for smart electric vehicle. *J Adv Transp* 2017:1–14. <https://doi.org/10.1155/2017/6510747>
11. Zhou W, Pan ZY, Lu Q (2021) Review on the battery model and SOC estimation method. *Processes* 9:1685. <https://doi.org/10.3390/pr9091685>

Current Conduction in Nichrome/p-Si Schottky Diode



Ekta Sharma, Ankit Panchal, Reena Rathi, Vamshi Krishna Dasarraju, and Suman

Abstract Schottky diodes are widely explored in the last few years due to their high sensitivity, low operating temperature, high selectivity and low working cost. High efficiency, low forward voltage drop and low capacitance make Schottky diodes suitable for using in voltage clamping devices, solar panels, power rectifiers, radio frequency mixtures, detector diode and switched-mode power supplies. Much work has been done on metals and their silicides as Schottky diodes; however, as far as we can tell, there is a lack of insight using alloys as Schottky diodes. In the present work, the development and characterization of a silicon-based Schottky diode based on a nichrome alloy are discussed. Electron beam deposition technique was used to fabricate a wire-shaped nichrome alloy with composition Ni-80 wt%: Cr-20wt%. Capacitance–voltage and current–voltage measurements at room temperature were used to examine the electrical properties of nichrome/p-Si Schottky connections, confirming that the alloy is compatible with conventional silicon fabrication techniques. Calculations of crucial device parameters, including ideality factor, trap centres' energy level and density and barrier height, were made in an effort to understand the observed current conduction mechanism in diode that had been manufactured.

Keywords MS interface · Ideality factor · Barrier height and current conduction mechanism

E. Sharma · A. Panchal (✉) · R. Rathi
Chaudhary Ranbir Singh University, Jind 126102, India
e-mail: ap21284@gmail.com

V. K. Dasarraju
Northern Illinois University, Dekalb, IL 60115, USA

Suman
Department of Physics, Government College for Women, Rohtak 124001, India

1 Introduction

A growing number of possible technological applications have made metal–semiconductor (MS) interfaces of interest. The characteristics of the barrier created at the contact interface heavily influence the Schottky diode's performance. The ideality factor and Schottky barrier height are used to assess the diode's quality. The ideal Schottky diode should have the same barrier height throughout the temperature range, and the ideality factor should be practically constant. Numerous hypotheses, such as the theory of thermionic emission and the theory of the Gaussian distribution of the barrier height inhomogeneities present at the metal–semiconductor contact, may only partially explain the experimental data [5, 25]. New trials are therefore required in order to gain additional knowledge about the mechanisms governing barrier height. To describe the charge transport mechanism in different materials, there are numerous models available, including Schottky, Poole–Frenkel and space charge-limited conduction mechanisms [28]. The existence of carrier trapping centres in forbidden band gaps has a significant impact on the electrical characteristics of semiconductor materials [4, 8, 10, 20, 26].

Researchers explore issues involving frequently used elemental metals, such as Schottky contact on silicon. Problem of ageing effect and oxidation of Al at low temperature, and the poor adhesion of gold and silicon due to diffusion of Si into gold, limit the use of Al and Au as Schottky diodes [7, 11, 13]. Metals such as Ti and Cu were used as barriers to diffusion, but the desired efficiency of the device was not achieved [2, 6, 16]. Platinum is anti-resist and highly efficient; however, it is cost and not suitable for CMOS processing. Along with metals, in order to create abrupt contacts, numerous metal silicides were also used; however, these materials also had some drawbacks [17]. The problem of interface roughness in cobalt silicide causes junction leakage. Additionally, the CoSi_2 phase needs a high temperature to develop, which has an impact on how activated implanted impurities are distributed throughout the material [9, 12, 15]. Furthermore, it was observed that Pd metal is highly reactive and may combine with silicon to create amorphous silicide even at ambient temperature. Rarely does a silicon–silicide interface have crystal alignments that are identical to the stress-free silicon crystal structure [21]. The layer may crack due to stress. Some alloys like PtSi, PdSi, GdPt, NiPt, GdV, PbEr, TiW, etc., have been described in order to investigate the metal–silicon system more closely, for example, to control the barrier heights, make shallow connections and study the chemical properties of the interaction of binary alloy systems with silicon [1, 3, 18, 19, 23, 24].

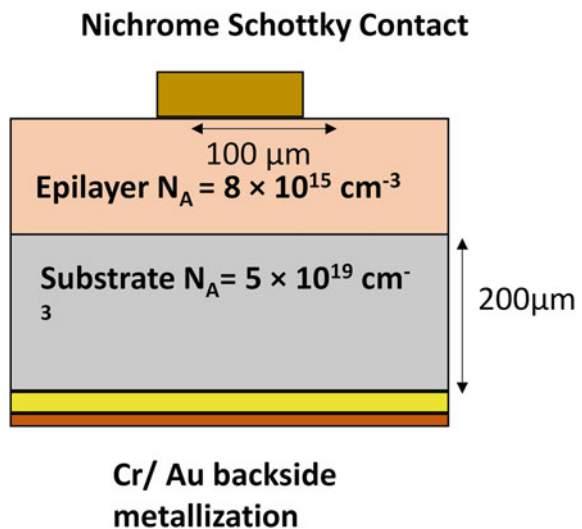
As far as we are aware, there has not been much research on nichrome alloy as a Schottky contact metal. The characteristic qualities of nichrome alloy are anti-oxidant, anti-resist, high thermal stability, affordability and device compatibility. Future electronic devices employed in severe environments, such as gas sensors, particle detectors and temperature sensors, may benefit greatly from these features [14, 22, 27]. In this study, an E-beam deposition procedure was used to create a Schottky diode on p-type silicon wafers that was based on a nichrome alloy. The

space charge limiting current, Poole–Frenkel and Ohmic conduction mechanisms were used to investigate the electrical properties of manufactured diode.

2 Experimental

The Schottky diode was fabricated using p/p⁺ Si < 100 > epitaxial wafers having resistivity $2 \pm 0.2 \Omega\text{-cm}$. Warm TCE, acetone and methanol were used to thoroughly wash wafers prior to metal deposition. Wafers were also cleaned using the conventional RCA cleaning procedure, which removes organic and inorganic impurities using solutions of NH₄OH: H₂O₂: H₂O (1:1:5 volume at 600 °C) and HCl: H₂O₂: H₂O (1:1:6 volume at 850 °C), respectively. After that, silicon wafers were dipped in a solution of 5% HF to eliminate native oxide. Ni-80 wt%: Cr-20 wt% nichrome wire was utilized as a source to create Schottky contacts. A crucible inside the e-beam chamber was filled with nichrome wire that had been bent into a circle. Ion pumps were used to maintain a vacuum on the order of 2×10^{-7} Torr, after which nichrome was evaporated using an e-beam. A diode of 1.0 mm was fabricated with the help of a metal mask. Tally Step was used to measure the nichrome film thickness, which yielded a result of about 2 μm. A composite Cr/Au layer was formed on the silicon wafers’ reverse side in order to create Ohmic contact (Fig. 1). Using a Keithley 236 I–V analyzer at room temperature, the diode’s current–voltage (I–V) properties were determined (Fig. 2).

Fig. 1 Schematic diagram of fabricated Nichrome/p-Silicon schottky diode



3 Results and Discussion

Figure 2 shows the forward bias electrical properties of nichrome/p-Si Schottky diodes that were obtained at room temperature. The I–V characteristics were obtained by varying the DC bias voltage in steps of 1 mV, from 0 to 0.6V. Both Schottky diodes exhibit rectifying behaviour, as seen in Fig. 2. Current conduction in Schottky diodes, for example, will adhere to the thermionic emission theory. This hypothesis suggests that the current in a diode will be mostly derived from charge carriers occupying energy levels higher than the potential barrier.

$$J = J_0 \left[\exp\left(\frac{qV}{\eta kT}\right) \right] \text{ if } V \gg \frac{3kT}{q} \quad (1)$$

where

$$J_0 = A^{**} T^2 \exp\left(\frac{-q\Phi_{b0}}{kT}\right) \quad (2)$$

is known as the saturation current density, A^{**} is known as the effective Richardson constant, Φ_{b0} is known as the barrier height and η is the ideality factor of the diode.

Barrier height and ideality factor can be calculated using the relation:

$$\Phi_{b0} = \frac{kT}{q} \ln\left(\frac{A^{**} T^2}{J_0}\right) \quad (3)$$

and

$$\eta = \frac{q}{kT} \left(\frac{dV}{d(\ln J_0)} \right) \quad (4)$$

Fig. 2 Forward bias characteristics of the fabricated diode

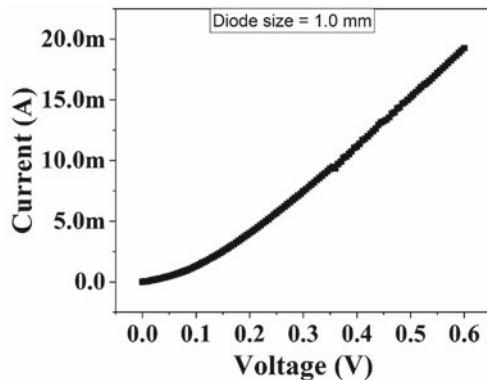
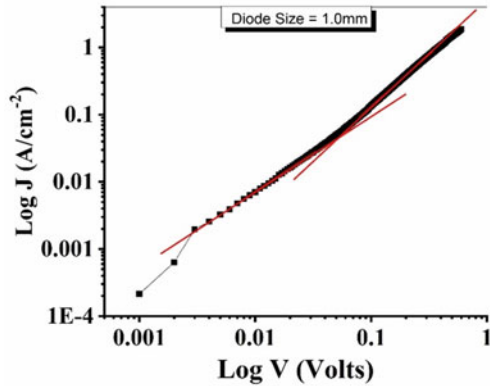


Fig. 3 LogJ-LogV graph for Nichrome/p-Silicon Schottky diode of diameter 1.0 mm



Saturation current and ideality factor values are given, respectively, by the semi-logarithmic J–V graph’s intercept and slope. Devices were found to have ideality factors that were more than one ($\eta > 1$), indicating the existence of conduction mechanisms other than thermionic emission. The value of barrier height is obtained as 0.56 eV and the value of 1.31 was obtained for the ideality factor. Numerous researchers have noted that non-ideality is the root cause of phenomena like Schottky emission, the Poole–Frenkel mechanism, the space charge limiting current, etc. A logarithmic scale was used to represent the forward characteristics of the diode. With the help of power-law type relationship $I \propto V^m$, the consistencies of curves were investigated. The value of power (m) of the logJ–logV graph in Fig. 3 was used to interpret the relative dominance of the aforementioned mechanisms.

Ohmic conduction will be predominant when $m = 1$, whereas $m > 2$ suggests space charge restricting current conduction. Additionally, the fact that m is between 1 and 2 suggests that either the Schottky or Poole–Frenkel conduction mechanism is responsible for the conduction [30].

3.1 Conduction Mechanism in Fabricated Diode

In p-type manufactured diodes, we have investigated the dominance of the above-mentioned conduction pathways. In Fig. 3, logJ–logV curve for 1.0 mm Nichrome/p-Si Schottky diodes, two linear regions can be seen. Both of these locations were categorized as having a smaller electric field region with a power of $1 < m < 2$, and a higher electric field region with a power of $m \geq 2$. The fact that the value of m falls between 1 and 2 in the lower electric field area suggests that either Schottky emission or the Poole–Frenkel effect may be the mechanism for current conduction [29]. For the Schottky effect and the PF effect, the theoretical computed value of β was 1.1×10^{-5} and 2.19×10^{-5} , respectively. Lower electric field region of the fabricated diode with a diameter of 1.0 mm exhibits the Ohmic conduction mechanism, but higher

electric field region exhibits dominance of Poole–Frenkel conduction mechanism. The experimentally computed value of β comes out to be greater than the Schottky and Poole–Frenkel effect having a value of 1.39×10^{-5} .

4 Conclusion

Ni-80 wt%: Cr-20 wt% alloy-based Schottky on p-type silicon diode was successfully fabricated and characterized. It is anti-oxidant, anti-corrosive and inexpensive. It is revealed to be compatible with common silicon fabrication methods and does not require an additional sticky layer. The e-beam evaporation metallization technique was used to deposit nichrome film. The calculated value of barrier height and ideality factor are 0.56 eV and 1.31, respectively. The initial section of the LogJ–LogV graph's slope indicates that current will flow owing to ohmic conduction. This is because there are sufficient numbers of charge carriers in thermal equilibrium to support current flow. Under stronger electric fields, Poole–Frenkel conduction was seen to predominate in the fabricated diode.

References

1. Aboelfotoh MO (1987) Schottky-barrier behavior of a Ti-W alloy on Si(100). *J Appl Phys* 61(7):2558–2565. <https://doi.org/10.1063/1.337933>
2. Card HC (1976) Aluminum—Silicon Schottky barriers and ohmic contacts in integrated circuits. *IEEE Trans Electron Devices* 23(6):538–544. <https://doi.org/10.1109/T-ED.1976.18449>
3. Eizenberg M et al (1981) Formation of shallow Schottky contacts to Si using Pt-Si and Pd-Si alloy films. *J Appl Phys* 52(2):861–868. <https://doi.org/10.1063/1.328850>
4. Hiraki A (1983) Low temperature reactions at Si/metal interfaces; what is going on at the interfaces? *Surf Sci Rep* 3(7):357–412. [https://doi.org/10.1016/0167-5729\(84\)90003-7](https://doi.org/10.1016/0167-5729(84)90003-7)
5. Kumar V et al (2014) Barrier height inhomogeneities induced anomaly in thermal sensitivity of Ni/4H-SiC Schottky diode temperature sensor. *J Vac Sci Technol B, Nanotechnol Microelectron. Mater, Process, Meas, Phenom* 32(4):041203. <https://doi.org/10.1116/1.4884756>
6. Kumar V et al (2016) Capacitance roll-off and frequency-dispersion capacitance-conductance phenomena in field plate and guard ring edge-terminated Ni/SiO₂/4H-nSiC Schottky barrier diodes. *Phys status solidi* 213(1):193–202. <https://doi.org/10.1002/pssa.201532454>
7. Kumar V et al (2022) Defect levels in high energy heavy ion implanted 4H-SiC. *Mater Lett* 308:131150. <https://doi.org/10.1016/j.matlet.2021.131150>
8. Kumar V et al (2015) Diameter dependent thermal sensitivity variation trend in Ni/4H-SiC Schottky diode temperature sensors. *J Vac Sci Technol B, Nanotechnol Microelectron. Mater Process Meas Phenom* 33(5):052207. <https://doi.org/10.1116/1.4929890>
9. Kumar V et al (2020) Electronic transport in epitaxial 4H–SiC based Schottky diodes modified selectively by swift heavy ions. *Mater Sci Semicond Process* 115:105108. <https://doi.org/10.1016/j.mssp.2020.105108>
10. Kumar V et al (2020) Epitaxial 4H–SiC based Schottky diode temperature sensors in ultra-low current range. *Vacuum* 182:109590. <https://doi.org/10.1016/j.vacuum.2020.109590>

11. Kumar V et al (2020) Interface improvement of epitaxial 4H-SiC based Schottky diodes by selective heavy ion irradiation. *Appl Nanosci*. <https://doi.org/10.1007/s13204-020-01608-3>
12. Kumar V et al (2021) Interfacial and structural analysis of MeV heavy ion irradiated SiC. *Appl Nanosci*. <https://doi.org/10.1007/s13204-021-01921-5>
13. Kumar V et al (2013) Selective SHI irradiation for mesa type edge termination in semiconductor planar junction. *J Phys Conf Ser* 423:012057. <https://doi.org/10.1088/1742-6596/423/1/012057>
14. Kumar V et al (2012) Simulation based analysis of temperature effect on breakdown voltage of ion implanted Co/n-Si Schottky Diode. *J Nano-Electron Phys* 4(4):04009. <http://essuir.sumdu.edu.ua/handle/123456789/30266>
15. Kumar V et al (2018) Tailoring surface and electrical properties of Ni/4H-nSiC Schottky barrier diodes via selective swift heavy ion irradiation. *Phys status solidi* 215(5):1700555. <https://doi.org/10.1002/pssa.201700555>
16. Kumar V, Maan AS (2018) Improvement in reverse bias leakage current of Ni/4H-nSiC Schottky barrier diodes via MeV selective ion irradiation. *IOP Conf. Ser. Mater. Sci. Eng.* 331:012016. <https://doi.org/10.1088/1757-899X/331/1/012016>
17. Li SS Metal–semiconductor contacts. In: *Semiconductor physical electronics*. Springer New York, New York, NY, pp. 284–333. https://doi.org/10.1007/0-387-37766-2_10
18. Nava F et al (1982) The interaction of Ni-Pt alloy with silicon. *Thin Solid Films* 89(4):381–386. [https://doi.org/10.1016/0040-6090\(82\)90315-7](https://doi.org/10.1016/0040-6090(82)90315-7)
19. Ottaviani G et al (1983) Interaction of Pd–Er alloys with silicon. *J Appl Phys* 54(8):4614–4622. <https://doi.org/10.1063/1.332617>
20. Petersson S et al (1977) Evaluating PtSi front contact to surface barrier detectors. *Nucl Instruments Methods*. 143(3):525–535. [https://doi.org/10.1016/0029-554X\(77\)90242-7](https://doi.org/10.1016/0029-554X(77)90242-7)
21. Petrovic S et al (2006) Structure and surface composition of NiCr sputtered thin films. *Sci Sinter* 38(2):155–160. <https://doi.org/10.2298/SOS0602155P>
22. Rölke J (1981) Nichrome thin film technology and its application. *Electrocompon Sci Technol* 9(1):51–57. <https://doi.org/10.1155/APEC.9.51>
23. Thomas S, Terry LE (1976) Composition profiles and Schottky barrier heights of silicides formed in NiPt alloy films. *J Appl Phys* 47(1):301–307. <https://doi.org/10.1063/1.322316>
24. Thompson R et al (1981) Schottky contacts of Gd-Pt and Gd-V alloys on n -Si and p -Si. *J Appl Phys* 52(11):6763–6768. <https://doi.org/10.1063/1.328629>
25. Tyagi MS (1984) Physics of Schottky barrier junctions. *Met Schottky Barrier Junctions Their Appl* 1–60. https://doi.org/10.1007/978-1-4684-4655-5_1
26. Verma J et al (2022) Trench termination in Ga₂O₃-based power device: a simulation-based study. *Appl Nanosci* 2021:1–7. <https://doi.org/10.1007/S13204-021-02219-2>
27. Weiser K (1970) *Semiconductor technique: current injection in solids*. Murray A. Lampert and Peter Mark. Academic Press, New York, 1970. xiv, 354 pp., illus. \$18. *Electrical Science series*. *Science* (80-) 170(3961):966–967. <https://doi.org/10.1126/science.170.3961.966.b>
28. Yakuphanoglu F et al (2007) Space charge-limited conduction in Ag/p-Si Schottky diode. *Phys B Condens Matter* 392(1–2):188–191. <https://doi.org/10.1016/j.physb.2006.11.018>
29. Yoon Y et al (2012) Deep level transient spectroscopy and minority carrier lifetime study on Ga-doped continuous Czochralski silicon. *Appl Phys Lett* 101(22): 222107. <https://doi.org/10.1063/1.4766337>
30. Yüksel ÖF et al (2011) A detailed analysis of current-voltage characteristics of Au/perylene-monoimide/n-Si Schottky barrier diodes over a wide temperature range. *J Appl Phys* 110(2):024507. <https://doi.org/10.1063/1.3610394>

III & V Group Elements and Heterostructures for Optoelectronics: A Survey



Jayesh Jain, Amit Rathi , and Priya Chaudhary

Abstract III–V semiconductors have a lot of promise for new optoelectronic applications. A survey of different research led us to that heterostructure devices are framed by the thin film deposition of III and V semiconductors. A heterojunction is an interface formed by two different semiconductor layers or areas. A heterostructure is the arrangement of numerous heterojunctions in a device. Heterojunction devices in view of III–V expected possibility for the manufacture of effective solar cells. Semiconductor diode lasers are used in the manufacture of many applications like DVD and CD players, as well as fiber optic handsets. In the synthesis of lasing heterostructures, rotating layers of different III–V compound semiconductors are utilized. This paper presents types of various heterojunctions with a collection of optical and electronic properties of various III & V compound semiconductors.

Keywords III–V semiconductors · Heterojunction · Heterostructure · Optical and electronic properties

1 Introduction

Semiconductors are substances with properties somewhere between conductor and insulator. ‘Its leading properties may be changed in important ways by introducing pollutants (“doping”) into the crystal structure’[1]. Right when two contrastingly doped regions exist in a comparative crystal, a semiconductor intersection is made. The approach to acting of charge carriers, which integrate electrons, particles, and electron openings (holes), at these intersections is the reason for diodes, semiconductors, and latest devices.’ A few instances of semiconductors are silicon, germanium, gallium arsenide, etc. Gallium arsenide is the second most popular semiconductor after silicon and is utilized in microwave-repeat consolidated circuits, solar-based cells, laser diodes, and other applications. Silicon is an important component in

J. Jain · A. Rathi (✉) · P. Chaudhary
Department of Electronics and Communication, Manipal University Jaipur, Jaipur, Rajasthan,
India
e-mail: amitrathi1978@gmail.com

Table 1 III–V compound semiconductor

Group III	Group V
B	N
Ga	Sb
Al	As
In	P

the manufacture of most electronic circuits but it is an indirect bandgap semiconductor. For the emission of light direct bandgap semiconductor is required direct bandgap semiconductor having the same alignment of a maximum energy level of valance band with the minimum energy level of the conduction band with respect to the momentum, for example, gallium arsenide (GaAs), indium gallium arsenide (InGaAs), gallium nitride (GaN), gallium phosphide (GaP), aluminum arsenide (AlAs), gallium arsenide phosphide (GaAsP), etc. Aside from doping, changing the temperature and pressure of a semiconductor can control its optical and electrical properties.

A heterojunction is generated by connecting two separate semiconductors with varying lattice constants as well as bandgap. At the point of interaction, a heterojunction shapes a 2D channel transporter. Heterojunctions' exceptional transport feature has been commonly used to manufacture high-performance field-effect semiconductors. In optical devices such as semiconductor lasers, heterojunction devices are used.

A semiconductor heterojunction is shaped by synthetic holding at the point of interaction. Heterojunction is generally shaped by the technique for epitaxy and there shapes a nonconformist between the two semiconductors [2]”.

We will majorly focus on the III and V group semiconductors which are shown in Table 1.

III–V compound semiconductors play a basic impact on the improvement of optoelectronic contraptions for a broad degree of purposes. Basic reasons for GaAs or InP-based III–V compound SC are contraptions for optical fiber correspondences, infrared and evident LEDs/LDs, and high-capability solar energy cells. For short recurrence light emitters used, areas of strength in lighting structures GaN-based compounds are fundamental for short recurrence light emitters.

Optoelectronic devices consolidate the relationship between photons and electrons. Direct bandgap semiconductors that show solid ingestion/spread attributes are awesome for such applications.’The bandgap of the compound semiconductors can be arranged by alloying them. Bandgap arranging draws in the progress of heterojunctions that is basic for a plan of prevalent execution optoelectronic devices like lasers and LED [3]. The interest in III–V compound semiconductor identifiers advanced at first due to the scope of frequencies that could be distinguished because of, the various energy gaps available with different semiconductor materials. Presently, we going to talk about the most recent band boundaries for all of the III–V gathering semiconductors ~InAs, GaAs, AlAs, GaP, GaAsP, etc.

2 Survey of III–V Compounds

The most significant and commonly used compound semiconductor material is gallium arsenide (GaAs). Many more band structure boundaries are precisely understood in GaAs than in any other compound semiconductor [4, 5]. The negative sign in deformity potential refers to how the band hole widens when the crystal is compacted. Wei and Zunger's first-standards calculations reveal that the energy of the valence band's most extreme increases as the unit cell volume decreases for various III–V semiconductors including GaP, GaAs, InP, GaSb, InSb, and InAs though it has the contrary sign in different materials. It is used with other semiconductors including InGaAs, AlGaAs, and others as a substrate for epitaxial growth whatever the bearing of the valence band is greatest, it is for the most part concurred that the conduction band moves a lot quicker with pressure. It has higher electron mobility, and higher saturated electron velocity which allows its transistor to work in excess of 250 GHz frequency' [6, 7].

Aluminium arsenide (AlAs) is one of the most critical optoelectronic and electronic materials due to its subsequent fusion into GaAs-based heterostructures. AlAs, like GaAs, is a winding opening semiconductor with X-L- Γ mentioning the minima of conduction valley. It has a larger band gap than GaAs and very little induced strain, allowing it to grow arbitrarily thick for other quantum well devices while still maintaining great performance and electron mobility. Majorly used to manufacture LEDs' [7, 8].

Gallium Phosphide (GaP) it's another III–V compound semiconductor with a lattice constant of 5.4500 Å and an indirect bandgap is 2.260 eV through Si has a lattice constant of 5.431 Å, and this outcome in lattice mismatch of 0.35%, which is significantly low when compared with GaAs and Si. This is done by optical and morphology studies on GaP/Si heterojunctions using hydride vapor phase epitaxy (HVPE) in two-step method, initially low-temperature GaP buffer layer growth on Si and then over-layer GaP growth at high temperature. Its refractive index varies from 3.2 to 5.0 which is higher than almost other semiconductors. It is used to design orange, green, and low-cost red LEDs, pure form of GaP emits green light of 555 nm wavelength [7].

Gallium arsenide phosphide, GaAs_{1-x}P_x, is a ternary compound semiconductor. The properties such as bandgap and lattice constants can be tuned by varying the composition(x), due to the property of changing composition this especially works for tandem solar cell applications. The GaP buffer layer was first produced at low temperatures, and then the GaAs_{0.75}P_{0.25} layer was grown on top of it at high temperatures [7, 9].

Indium arsenide (InAs) is a semiconductor with such a small band gap with a melting point of 942 °C, it is a direct band gap material of 0.35 eV bandgap. It is used to manufacture infrared detectors within the 1–3.8 μm wavelength range and is also used in designing laser diodes, majorly known for narrow energy bandgap and high electron mobility.

Table 2 Structure information: zincblende vital statistics [14]

Formula	ZnS
Cell parameters	Lattice constant (a) = 5.41 Å, Z = 4
Crystal system	Cubic
Lattice type	Face-centered
Atomic position	S:0,0,0 Zn:0.25,0.25,0.25
Melting point and density	1020 degrees C and 4.102

Indium phosphide (InP) has a zincblende structure which is obtained by reacting indium iodide and white phosphorous at 400°C and also by thermal decomposition of phosphine and trialkyl indium compound. Because of its high electron velocity with respect to other semiconductors, it is used in high-frequency and power electronics and its direct band gap make it useful for optical devices like laser. InP-based optical devices like lasers and LEDs can emit light at a high wavelength range of 1200 nm–12 μm which is used for datacom applications and telecom in the digital world and many more applications like optical sensing, high-speed electronics, photovoltaic applications, etc.

A III-nitride compound semiconductor is created by mixing a gathering III element, such as indium, gallium, aluminum, or boron with a gathering Vth group element, nitrogen. Their band hole energies range from 0.70 eV for indium nitride (InN) to 6.20 eV for aluminum nitride (AlN) and 3.40 eV for gallium nitride (GaN). “Because of their very attractive intrinsic characteristics, III-nitride semiconductors have made significant progress. The extraordinary accomplishments being developed of LDs, blue/bright (UV) LEDs, high-recurrence semiconductors working at high temperatures and powers” [10–12]. III-nitride-based electronic devices are likewise more harmless to the ecosystem they don’t contain poisonous components, for example, arsenic that is used to manufacture other compound semiconductors like gallium arsenide. The wide band hole energy spectrum further makes these materials a strong option for protection layers in solar cells. The optical properties of the III-nitride put-together devices depend with respect to a few significant factors, for example, refractive file and dielectric steady of the materials [13] (Tables 2 and 3).

Table 3 Zinc blend nitride binaries [15–17]

Parameters	AlN	InN	GaN
Energy gap e_g (eV)	4.9	1.94	3.299
Effective mass m_0	0.25	0.12	0.15
Electron spin resonance e_p (eV)	27.1	25.0	25.0
Deformation potential a (eV)	−9.4	−3.35	−7.4
Wavelength (nm)	253	639	376
Frequency (tera hz, 10^{12} Hz)	1186	469	798

A survey of optical and electrical properties of these semiconductor compounds and some of the ternary alloys of antimonides, arsenide antimonide, arsenide phosphide, and so on has been shown at the last of this survey in Tables 5, 6, 7, 8 and 9. Next part of this survey is related to the study of the main structure compound (III–V) semiconductor, after a basic literature survey of some important compound semiconductors (Figs. 1 and 2).

The wurtzite crystal structure is a crystalline arrangement for several matching compounds, named just after the mineral wurtzite. It is a delineation of a hexagonal crystal system.” It is gotten from a hexagonal closely packed (hcp) exhibit of anions and has two unbalanced units in its unit cell as we can see in Fig. 3. “Wurtzite

Fig. 1 a $3 \times 3 \times 3$ Lattice of zinc blende b A single-unit cell of zincblende

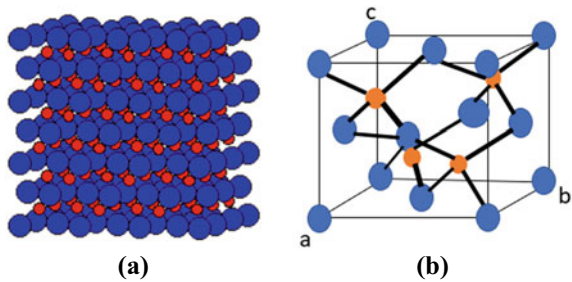


Fig. 2 a The (110) plane of zincblende (ZnS). b The (111) plane of zincblende (ZnS)

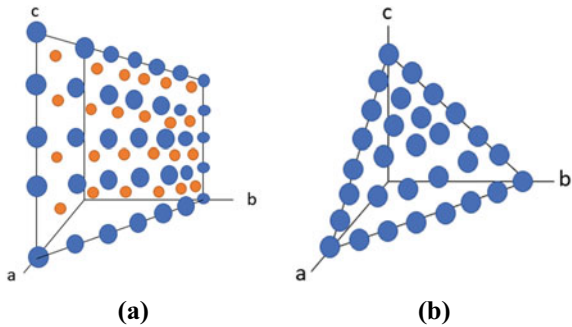


Fig. 3 Unit cell construction of a wurtzite cross section. Sulfur particles are displayed in red (enormous), Zinc atoms are displayed in green (little) and the unit cell is represented by the dashed lines

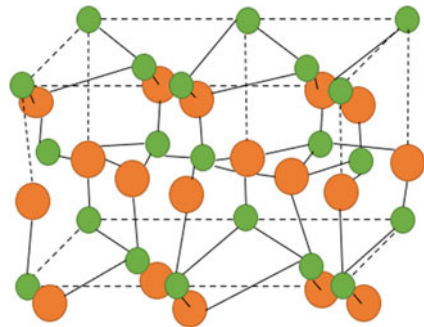


Table 4 Wurtzite nitride binaries [23, 24]

Parameters	GaN	AlN	InN
Energy gap e_g (eV)	3.507	6.23	1.994
Effective mass m_e (m_0)	0.20	0.28	0.12
Electron spin resonance e_p (eV)	14.0	14.5	14.6
Deformation potential a (eV)	-18.3	-18.0	-7.0
Wavelength (nm)	354	199	628
Frequency (tera hz, 10^{12} Hz)	847	1507	478

itself is one of the combinations that can take on the wurtzite structure (ZnS with up to 8.0% iron rather than zinc)” CdS, AgI, α -SiC, ZnO, GaN, CdSe, AlN, InN, and other semiconductors [18–22]. Some of the optical and electrical parameters of these compounds are shown in Table 4 [14].

Table 5 Properties of binary compound semiconductor [7, 30]

Parameters	AlAs	GaP	InP	GaSb	AlSb	InSb	GaAs	InAs	AlP
Energy gap e_g (eV)	3.099	2.886	1.4236	0.812	2.386	0.235	1.591	0.417	3.63
Effective mass m_e (m_0)	0.15	0.13	0.0795	0.039	0.14	0.0135	0.067	0.026	0.22
Electron spin resonance e_p (eV)	21.1	31.4	20.7	27.0	18.7	23.3	28.8	21.5	17.7
Deformation potential a (eV)	-8.11	-9.9	-6.6	-8.3	-5.9	-7.3	-8.33	-6.08	-8.7
Wavelength (nm)	400	430	871	1527	520	5277	779	2974	342
Frequency (tera hz, 10^{12} Hz)	750	698	344	196	577	57	385	101	877

Table 6 Antimonides compound semiconductor

Parameters	GaInSb	AlInSb	AlGaSb
Energy gap e_g (eV)	0.415	0.43	-0.044 + 1.22x
Wavelength (nm)	2989	2883	1054
Frequency (tera hz, 10^{12} Hz)	100	104	285

Table 7 Arsenides antimonides compound semiconductor

Parameters	GaAsSb	InAsSb	AlAsSb
Energy gap e_g (eV)	1.43	0.67	0.8
Effective mass m_e (m_0)	0.0447	0.035	0.021
Wavelength (nm)	867	1850	1550
Frequency (tera hz, 10^{12} Hz)	346	162	194

Table 8 Phosphides antimonides compound semiconductor

Parameters	GaPSb	AlPSb	InPSb
Energy gap e_g (eV)	2.7	2.7	1.9
Wavelength (nm)	459	459	653
Frequency (tera hz, 10^{12} Hz)	654	654	459

Table 9 Ternary alloys Arsenide compound semiconductor

Parameters	AlGaAs	GaInAs	AlInAs
Energy gap e_g (eV)	0.14–0.66	0.477	0.7
Effective mass m_0	0.063	0.041	0.049
Electron spin resonance e_p (eV)	–	–1.480	–4.810
Deformation potential a (eV)	–	2.61	–1.4
Wavelength (nm)	1879	2600	1771
Frequency (tera hz, 10^{12} Hz)	160	115	169

There are two types of zinc sulfide, zinc blende and wurtzite. The vital distinction between zinc blende and wurtzite is that zinc mix is cubic, though wurtzite has a hexagonal design.

3 Types of Heterojunctions

Various strategies have been utilized to manufacture heterojunction devices by utilizing thin films of semiconductors over silicon like vacuum thermal evaporation technique. Salwan et al. [25], spray pyrolysis [26], chemical bath deposition (CBD) [27], alloying technique epitaxial growth from vapor phase, microreactor-assisted solution deposition (MASDP) [28], and Sintering [29].

There are basically two types of heterojunctions. An anisotype heterojunction is formed by two semiconductors with different conductivities. The P-type semiconductor used has a small energy bandgap compared to the N-type material, which has a large bandgap. A basic frame structure is shown in Fig. 4.

An isotype heterojunction is generated when two semiconductors with the same conductivity but differing lattice constants and bandgaps are connected. A basic frame structure of isotype heterojunction is shown in Fig. 5.

The way of behaving of a semiconductor intersection significantly relies upon the arrangement of the energy groups at the point of interaction. “There are three types of heterostructure according to their band alignments: straddling gap (type I), staggered gap (type II), and broken gap (type III) as shown in Fig. 6.”

- Type I structures have band offsets of opposite sign in the case of GaAs/AlGaAs, GaSb/AlSb, and GaAs/GaP.

Fig. 4 The band outline of the singular semiconductors, before they are combined to form heterojunction, is displayed” [2]

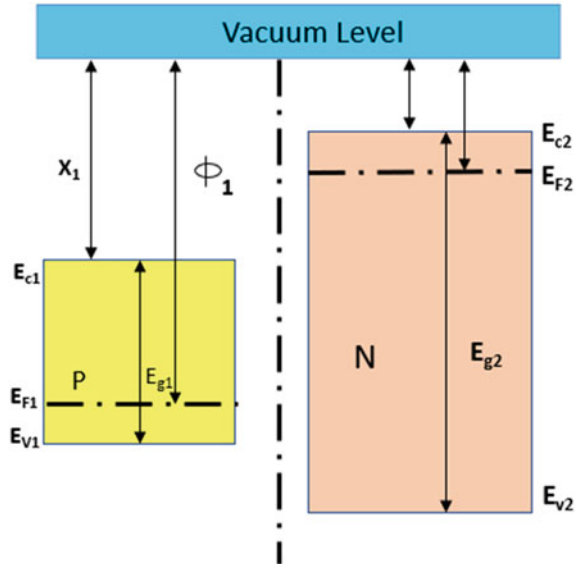
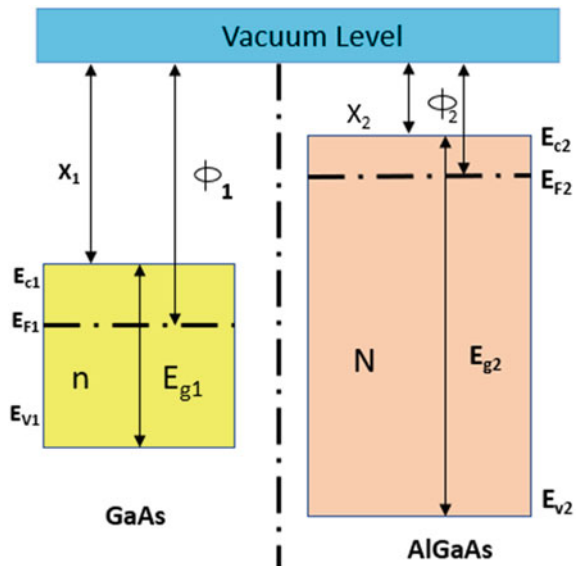


Fig. 5 An isotype heterojunction with two n-type semiconductors having bandgaps E_{g1} and E_{g2} has been displayed” [2]



- Type II The band offsets have the same sign and the examples are $In_xGa_{1-x}As/Ga_xSb_{1-x}As$ and $Al_xIn_{1-x}As/InP$ systems.
- Type III also has the band offsets of the same sign, but the offsets are so large that the gaps in the two materials do not overlap and the example is $InAs/GaSb$ [6].

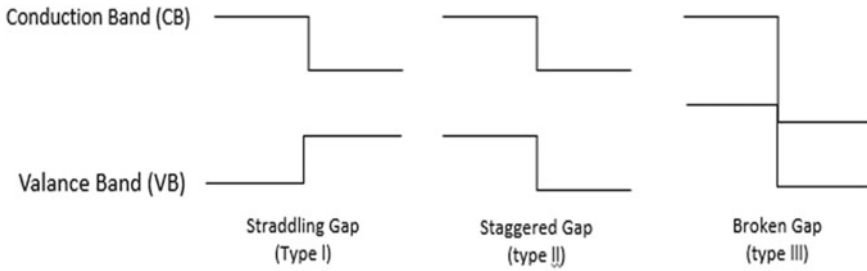


Fig. 6 Three types of heterojunctions are organized by band alignment

A metal–semiconductor connection is the most frequent type of heterojunction. Metal contacts are often put on the top of semiconductor surfaces to allow semiconductors to interact with the outside environment. Today, it is very common that semiconductor devices are given both Ohmic and non-Ohmic contacts an example is field effect transistors. This is one of the biggest benefits of heterojunctions. The main disadvantage with heterojunctions is the lattice mismatch-induced defects that generally degrade the performance of the device. It is sensible to expect that the connection point is highly stressed. Relies upon the size of the pressure and the thickness of the layers, the point of interaction can be loose by shaping imperfections like dislocations and other undesirable deformities if any. Such deformities overall corrupt the exhibition of the device fabricated [8].

4 Survey of Different Semiconductor Properties

We have concentrated on the accessible data about band structure boundaries for significant III–V semiconductors and their ternary alloys. Similarly, we studied how the proposed boundaries fit into the band structure calculations. And to calculate the wavelength of materials, we have used $E_g = hc/\lambda$.

5 Conclusion

As we examined above, ongoing exploration show that utilization of heterostructure ideas and development strategy for advancement for cross section consistent and quantum very much in light of III–V components are capable to a great extent for the outcome of examination, heterostructure addresses a procedure for the amalgamation of new kind of material called heterosemiconductor.

Considered figures of legitimacy are frequencies, transconductance, commotion at high and low frequencies, and quantum efficiencies. It is directed at how to upgrade those by material and plan. Extrapolations to the future capability of heterodevices

are made, simply by thinking about the guaranteed scaling of horizontal aspects. Field of utilizations is introduced, where heterodevices offer selective characteristics, for example, high recurrence transmission and sensors, and new blended frameworks. On account of rationale, the pattern goes to nanoscale devices and ICs focusing on nanoelectronics past conventional hardware. Heterostructure layers permit a vertical nanoscaling and, in this way, give an extra level of opportunity for planning and optimization. We conclude that semiconductor devices are more compact and lighter than other devices, these devices have much longer life as compared to the life of others but are very sensitive to changes in temperature and not able to handle much power.

References

1. <https://www.hitachihightech.com/global/products/device/semiconductor/about.html>
2. Tanmoy Biswas Department of Computer Science, Syamaprasad College, 92, S P Mukherjee Road, Kolkata - 700026 tanmoybiswas.ece@gmail.Com
3. Mokkalapati S, Jagadish C (2009) III-V compound SC for optoelectronic devices. *Mater Today* 12(4):22–32
4. Adachi S (1994) GaAs and related materials: bulk semiconducting and superlattice properties. World Scientific, Singapore
5. Blakemore JS (1982) Semiconducting and other major properties of gallium arsenide. *J Appl Phys* 53(10):R123–R181
6. Wei S-H, Zunger A (1999) Predicted band-gap pressure coefficients of all diamond and zinc-blende semiconductors: chemical trends. *Phys Rev B* 60(8):5404
7. Vurgaftman I, Ćr Meyer J, Ćr Ram-Mohan L (2001) Band parameters for III–V compound semiconductors and their alloys. *J Appl Phys* 89(11):5815–5875
8. Adachi S (ed) (1993) Properties of aluminium gallium arsenide, vol 58. INSPEC, London
9. Hayashi K, Soga T, Nishikawa H, Jimbo T, Umeno M (1994) MOCVD growth of GaAsP on Si for tandem solar cell application. In: Proceedings of 1994 IEEE 1st world conference on photovoltaic energy conversion-WCPEC (a joint conference of PVSC, PVSEC and PSEC), vol 2, pp 1890–1893. IEEE
10. Acharya AR (2014) Group III–nitride semiconductors: preeminent materials for modern electronic and optoelectronic applications. *Himal Phys* 5:22–26
11. Strite AS, Morkoç H (1992) GaN, AlN, and InN: a review. *J Vac Sci & Technol B: Microelectron Nano Meter Struct Process, Meas, Phenom* 10(4):1237–1266
12. Mohammad SN, Morkoç H (1996) Progress and prospects of group-III nitride semiconductors. *Prog Quantum Electron* 20(5–6):361–525
13. Gil B (ed) (1998) Group III nitride semiconductor compounds: physics and applications. Clarendon Press
14. Togo A, Chaput L, Tanaka I (2015) Distributions of phonon lifetimes in Brillouin zones. *Phys Rev B* 91(9):094306
15. Powell RC, Lee N-E, Kim Y-W, Greene JE (1993) Heteroepitaxial wurtzite and zinc-blende structure GaN grown by reactive-ion molecular-beam epitaxy: growth kinetics, microstructure, and properties. *J Appl Phys* 73(1): 189–204
16. Vidal MA, Ramírez-Flores G, Navarro-Contreras H, Lastras-Martínez A, Powell RC, Greene JE (1996) Refractive indices of zincblende structure β -GaN (001) in the subband-gap region (0.7–3.3 eV). *Appl Phys Lett* 68(4):441–443
17. Petalas J, Logothetidis S, Boultaidakis S, Alouani M, Wills JM (1995) Optical and electronic-structure study of cubic and hexagonal GaN thin films. *Phys Rev B* 52(11):8082

18. Riyaj M, Quraishi AM, Hasan PMZ, Darwesh R, Kattayat S, Josey S, Kumar S, Ezzeldien M, Rathi A, Alvi PA (2022) Tuning the responsible parameters for gain characteristics of the novel type-II D-QW (InGaAs) heterostructure. *Mater Sci Semicond Process* 140:106377
19. Vijay J, Singh AK, Rathi A (2021) Near-infrared range tuneability in GaAs-based type-II nanoscale heterostructure emitter. *J Nanophotonics* 15(4):046009
20. Singh AK, Singh R, Singh K, Rathi A (2021) Optical gain enhancement and wavefunction confinement tuning in AlSb/InGaAsP/GaAsSb heterostructures. *Eur Phys J B* 94(6):1–5
21. Vijay J, Singh AK, Jain PK, Alvi PA, Singh K, Rathi A (2021) Optical gain characteristics of GaAs based type-II AlAsSb/InGaAs/GaAsSb nanoscale heterostructure for near infrared applications. *Optoelectron Adv Mater-Rapid Commun* 15:114–119
22. Riyaj M, Vijay JP, Khan AM, Kattayat S, Kaya S, Ahmad MA, Kumar S, Alvi PA, Rathi A (2020) Band dispersion and optical gain calculations of staggered type GaAs_{0.4}Sb_{0.6}/In_{0.7}Ga_{0.3}As/GaAs_{0.4}Sb_{0.6} nano-heterostructure under electric field and [100] strain. *Superlattices Microstruct*:106694
23. Vurgaftman I, Meyer JR (2003) Band parameters for nitrogen-containing semiconductors. *J Appl Phys* 94(6): 3675–3696
24. Vurgaftman I, Meyer JR (2007) Electron band structure parameters. *Nitride Semicond Devices: Princ Simul*: 13–48
25. Al-Ani SKJ, Ismail RA, Al-Ta'ay HFA (2006) Optoelectronic properties n: CdS: In/p-Si heterojunction photodetector. Springer
26. Godbole B, Badera N, Shrivastav SB, Ganesan V (2009) A simple chemical spray pyrolysis apparatus for thin film preparation. *J Instrum Soc India* 39–1
27. Khudruj SMA (2011) CdS thin film photoelectrochemical electrodes: combined electrochemical and chemical bath depositions. An-Najah National University, Faculty of Graduate studies
28. Ramprasad S, Su YW, Chang C, Paul BK, Palo DR (2012) Cadmium sulphide thin film deposition: a parametric study using microreactor assisted chemical solution deposition. *Sol Energy Mater & Sol Cells* 96:77–85. Elsevier
29. Kumar I V, Sharma DK, Bansal MK, Dwivedi DK, Sharma TP (2011) Synthesis and characterization of screen-printed CdS films. *Sci Sinter* 43:335–341
30. Hazama H, Sugimasa T, Imachi T, Hamaguchi C (1986) Temperature dependence of the effective masses in III–V semiconductors. *J Phys Soc Jpn* 55(4):1282–1293

Load Shedding Technique for Maintaining Voltage Stability



Prashant Kumar Sharma, Akash Sharma, and Rajive Tiwari

Abstract Recently, energy and power industries have under-went considerable changes, because of intervention of DG's in the existing conventional system, the operational, management, and control of the power system is becoming ever so more complicated and tedious along with several challenges. The earlier distribution structure has under-went huge modification in the past few years as power systems are no more regulated by a single hand. The involvement of variable large and small private players has complicated the situation further. The system operator is facing more challenges as now the flow of power in both the directions, i.e., from generator end to consumer end and vice versa. The spatially Distributed Generation (DG) has provisioned facility of clean energy and reduction of emissions safe guarding environment and has considerably improved the efficiency and performance of power system. However, inclusion and integration of DGs in the conventional power system have side effects towards reliability of the system. The introduction of DGs gives rise to poor power quality, faulty operation of protection systems or devices, and may even lead to voltage sag or swell, all of which are undesirable effects of penetration of DGs.

Keywords PSO · DG · UFLS · RES · p-best · G-best GA

1 Introduction

The distribution system has a major problem of power losses and low voltage profile which is needed to be resolved by using several optimization technologies. Integration of Distributed Generators (DGs) in the main Grid is one such solution. The optimal DG location and size which could be used immensely improve the profile of voltage and result in reduction in losses. Extensive research work has been done and still going on, in the past few years to establish the various related aspects/ attributes of the power system structure like reliable supply, stability, and protection system employed

P. K. Sharma (✉) · A. Sharma · R. Tiwari
Malviya National Institute of Technology, Jaipur, Rajasthan, India
e-mail: 2020pes5656@mnit.ac.in

© The Author(s), under exclusive license to Springer Nature Singapore Pte Ltd. 2024
S. K. Goyal et al. (eds.), *Flexible Electronics for Electric Vehicles*, Lecture Notes
in Electrical Engineering 1065, https://doi.org/10.1007/978-981-99-4795-9_29

305

to integrate distributed generation with our conventional system has many problems like stability, reliability, low-voltage profile, and losses [1]. So, in this research, more focus is on the improvement of the profile of voltage and loss reduction by employing load shedding and distributed generation penetration [2, 3].

2 Literature Review

Frequency resilience and voltage stability of low inertia power system are considerably improved with penetration of high wind power RES-based load shedding mechanism [4]. “Under Frequency Load Shedding techniques” may not function satisfactorily when there is an extensive network owing to considerable time delay and short of extensive employment of phase measurement units in the real-time power system networks [4]. Pascal’s triangle rule is used to formulate the general expression of load shedding quantity, on the basis of margin of reactive power and increased % of load shedding when applied on the weaker buses [5, 6]. Laghari has described under frequency load shedding technique based on different modules center of inertia frequency calculator module and load shed amount calculator modules [7]. In 2012, Rugthaicharoencheep discussed a feeder reconfiguration technique for loss reduction in distribution system [8]. Changgang Li briefly explained about a new continuous UFLS scheme is proposed to shed loads proportional frequency deviation [9].

3 Methodology

3.1 Particle Swarm Optimization

The “Particle Swarm Optimization technique” for improvement in the convergence characteristics and reduction in the computation time in comparison to Genetical Algorithm (GA) technique [1, 10]. The validation of the effectiveness of problem-solving using particle swarm optimization is carried out on “IEEE 33-bus system,” The objective function is the reduction of power loss using Eq. (1) having below-mentioned definite constraints in Table 1.

$$P_{DG,M} = P_{\text{loss}} + \sum P_{D,M} \quad (1)$$

With every upcoming iteration in the algorithm, the position and velocity of individual particles are updated to their new value using below-mentioned Eqs. (2) and (3) till the desired criterion is achieved [1, 8, 10–12].

$$v_{id}^{k+1} = w * v_{id}^k + c_1 * rand(\cdot) * (pbest_{id} - x_{id}^k) + c_2 * rand(\cdot) * (gbest_d - x_{id}^k) \quad (2)$$

Table 1 Objective function and equality constraint

Objective function	Equality constraint on bus real & reactive power
Minf = min (Tloss)	$P_{DG,M} = P_{loss} + \sum P_{D,M}$
	<i>Inequality constraint on bus real & reactive power</i>
	$2 \leq DGPosition \leq nbuses$
	$V_M^{min} \leq V_M \leq V_M^{max}$
	$0 \leq P_{DG,M} \leq 0.3 \sum_{i=1}^n P_{load}$

$$x_{id}^{k+1} = x_{id}^k + v_{id}^{k+1}$$

where

i = 1,2,.....n,

d = 1,2.....m

n: No. of particle

m: No. of members in the particle

d: Dimensional space

rand(): Random values (range of 0–1)

v_{id}^k, x_{id}^k : “velocity and position” of particle I during the kth iteration.

K: iteration no.

M: “inertia weight factor”

c_1 and c_2 : Acceleration constants.

In accordance with the equation, the inertia weight “w” is typically set.

$$w(k + 1) = w_{max} - \frac{w_{max} - w_{min}}{K_{max}} * k \tag{3}$$

K_{max} : Maximum permissible iterations.

K: Current iteration.

w_{max} and w_{min} : Max. & Min. of inertia weights (Fig. 1).

3.2 Objective Function and Equality Constraint

where,

$P_{DG,M}$ & $Q_{DG,M}$: Injection of Real & Reactive powers at bus M (by DG).

$\sum P_{D,M}$ & $\sum Q_{D,M}$: Value of total Real power & Reactive Power at the M_{th} bus.

$\sum_{i=1}^n P_{load}$: Value of total real power demanded by the network.

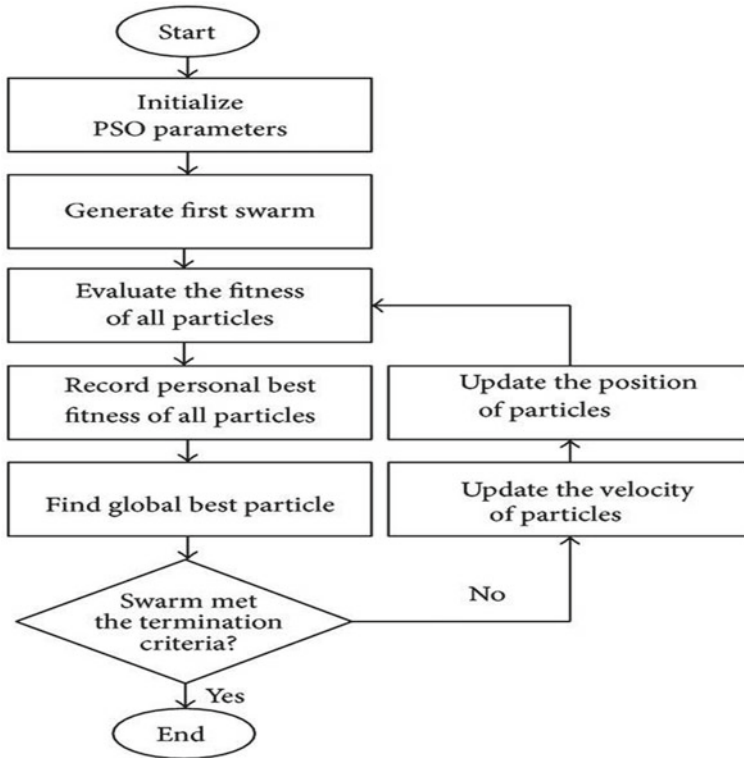


Fig. 1 Flowchart of particle swarm optimization (PSO)

3.3 Load Shedding Technique

The objective of this research work is the development of methodology, i.e., load shedding for improvisation of the voltage profile especially when we have grids with less inertia by the attainment of adequately reasonable profile of voltage stability. However, the traditional “Under-Frequency Load Shedding (UFLS) strategy,” results in increased deflection in frequency [4]. Other than the traditional “UFLS technique”, a high quantity of load shedding is employed on buses which are weak in terms of voltage stability for the recommended procedure. A generalized expression for quantifying load shedding is derived, on the basis of margin in reactive power, which is categorized to index the stability in voltage [10]. It is also ensured that the proposed strategy has adaptability towards various load levels [13].

A. Margin of Reactive Power

The margin of reactive power indicates what further increment in the loading of a specific bus could be achieved before exhausting its loading limit and collapse of voltage [14].

$$I = E / (Z_{line} + Z_{load})$$

$$Q_r = V I \sin\theta = \frac{z_{load}}{A} (E / z_{line})^2 \cos\theta \tag{4}$$

where

E= Generator voltage in a two-bus system

V= Load voltage in a two-bus system

Z_{line}= Line impedance.

The relationship between the load voltage V and the reactive power Q_R could be determined using Eq. 1.

3.4 Proposed Load Shedding Scheme

Let the “number of load-buses be N” and “the inverse of reactive power margins of load bus-1 to load bus-N, respectively, be “Q_{m1}, Q_{m2}, . . . , Q_{mN}” [15].

Thus, the calculation of the margin factor of Q of the i-th load bus (r_i) could be calculated with the help of Eq. 2.

$$r_i = \frac{Q_{mi}}{Q_{m1} + Q_{m2} + Q_{m3} \dots \dots \dots Q_{mn}} \frac{Q_{mi}}{\sum_{j=1}^N Q_{mi}} \tag{5}$$

$$LS_{i,1} = r_i L_i \tag{6}$$

where

The total load at i – thbusbe L_i

in the n-th stage, the load shedding amount, imposed on the i-th load bus can be expressed using Eq. 3 [16]:

$$LS_{i,n} = (1 - r_i)^{(n - 1)} * r_i * L_i \tag{7}$$

A. Steps for Implementation

Step-1: Calculate the reactive power for all the load bus.

Step-2: For all load buses, calculation of the inverse values of reactive power is made.

Table 2 Load shedding at the optimized location of DGs

Bus	Load shed without DG (pu)	Load shed with DG (pu)
4	0.23516	0.11239
7	0.35220	0.26078
25	0.568492	0.24768
30	0.214412	0.17473

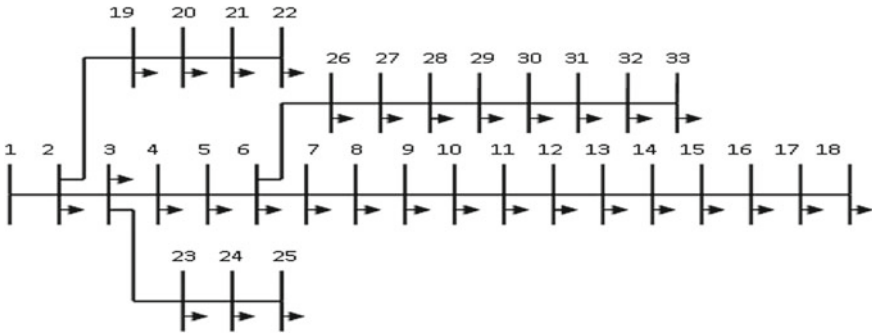


Fig. 2 IEEE 33 bus system

Step-3: Calculation of the reactive margin factors of load buses with the help of Eq. 2, to achieve normalization of the above values.

Step-4: Calculate load shedding factors for load buses using Eq. 3.

Step-5: Shed $LS_{i,1}$ amount of load at i th bus by Eq. 3 from the i -th load bus.

The proposed methodology is validated on the test system “without DG” and “with DG,” By using L-Index, the buses arrived for the best-optimized location of DGs are 4, 7, 25, and 30 (Table 2).

4 Result and Discussion

4.1 Case1 IEEE 33 Bus System

B. Voltage profile improvement analysis on IEEE 33 Bus system.

DG Specification

Base case “Real power & Reactive Power” demand = 3715KW & 2300KVAR.

Penetration = $30/100 = 0.3$;

Power Factor = 0.85 (Figs. 2, 3 and 4) (Tables 3, 4, 5 and 6);

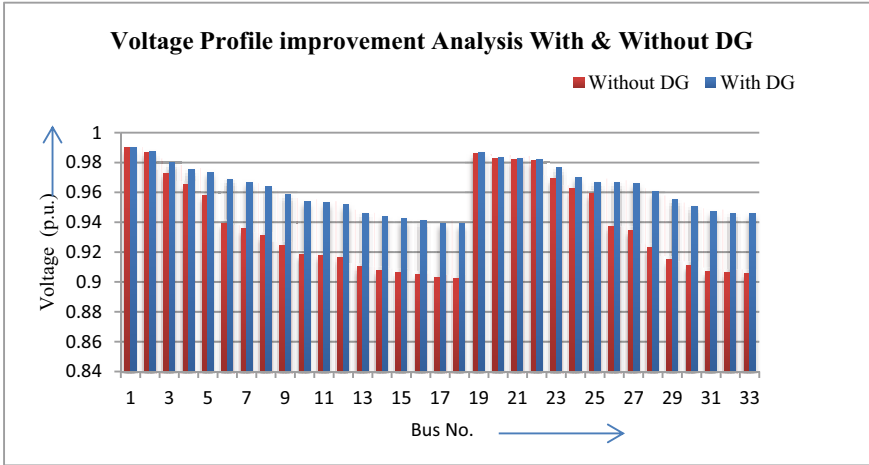


Fig. 3 Voltage profile improvement analysis on IEEE 33 bus system

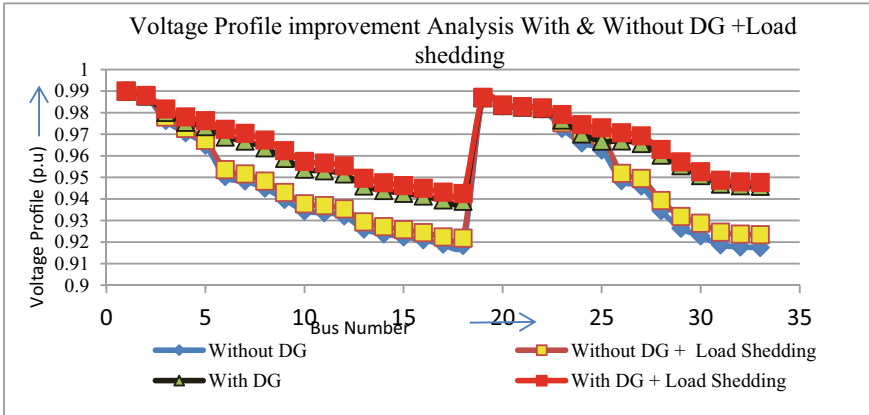


Fig. 4 Voltage profile improvement analysis with & without DG + Load shedding

Table 3 Final result with and without DG + Load shedding

Base case real power loss (KW):	206 KW
Base case reactive power loss (KVAR):	137.90 KVAR
Base case real power loss with load shedding:	181.15KW,
Base case reactive power loss with load shedding	79.65KVAR
Optimal real power loss with DG + PSO (KW):	75.7777 KW
Optimal reactive power loss with DG + PSO (KW):	49.76 KVAR
Real power loss with DG + Load shedding:	61.383 KW
Reactive power loss with DG + Load shedding:	41.288 KVAR
Percent reduction:	70.20

Table 4 Load flow results of IEEE 33 bus system with DG + PSO

S.No	P_{Loss} (KW)	Q_{Loss} (KVAR)	Voltage
1	7.241494526	3.691434303	0.99
2	15.05333988	7.667127066	0.987721177
3	7.550774529	3.845531072	0.980135656
4	1.536490357	0.782557802	0.975530233
5	2.716145757	2.344707021	0.973539803
6	0.565357467	1.868820517	0.968739777
7	1.99376553	0.658889902	0.966790026
8	2.547233775	1.83005145	0.963694694
9	2.58185637	1.83005145	0.958784322
10	0.476743949	0.157621346	0.953825223
11	0.757208106	0.250380244	0.953027016
12	2.285133213	1.797907944	0.951636496
13	0.624050061	0.821427785	0.945980927
14	0.304743674	0.271227026	0.94388747
15	0.239920313	0.175206446	0.942584713
16	0.214168514	0.285945705	0.941323161
17	0.045200685	0.035444253	0.939457841
18	0.260830181	0.253420233	0.938898542
19	0.835953321	0.753258298	0.986863539
20	0.101145795	0.118163976	0.983279709
21	0.04377427	0.057877871	0.982574454
22	3.065903554	2.094898195	0.981936711
23	4.94829729	3.907391546	0.976616319
24	1.234319146	0.96582718	0.97007506
25	2.260076893	1.151191876	0.966820639
26	0.945906011	0.481606614	0.966946245
27	4.134852053	3.645619794	0.965654292
28	4.210651301	3.668219723	0.960341734
29	5.440576743	2.771210026	0.955405681
30	1.367754236	1.351752185	0.950762324
31	0.18283761	0.213104448	0.946914901
32	0.011288076	0.017551137	0.946069238
33	75.77779319	49.76542444	0.945807332

Table 5 Improvisation of voltage after DG connection + Load shedding

Base case	Improvisation after DG connection	Improvisation after DG connection load Shedding
Minimum voltage at bus @ 18 = 0.902353 pu	Minimum voltage at bus @18 = 0.93889 pu	Minimum voltage at bus @18 = 0.9425 pu
Maximum voltage at bus @ 1 = 1 pu	Maximum voltage at bus @1 = 1 pu	Maximum voltage at bus @1 = 1 pu

Table 6 Tail end voltage improvement scenario

Tail end nodes	Base case voltage (pu)	Voltage with DG (pu)	Voltage with DG + Load shedding	% Voltage profile improvement
18	0.9023	0.9389	0.9425	4.05
22	0.9811	0.9819	0.9822	0.08
25	0.9590	0.9668	0.9730	0.813
33	0.9058	0.9458	0.9476	4.41

5 Conclusion

In the base case, real and reactive power losses (without load shedding) are 206 KW, 137.90 KVAR, respectively, and in the base case, real and reactive power losses (with load shedding) are 181.15KW and 79.65 KVAR, real and reactive powers losses with DG are 75.7777 KW and 49.76 KVAR, and real and reactive power losses with DG (load shedding) are 61.383 KW and 41.288 KVAR. We have found optimal location and size of DG using PSO are Bus No. 29 and 1310.805 KVA, respectively.



References

1. El-Zonkoly M (2011) Optimal placement of multi-distributed generation units including different load models using particle swarm optimization. *IET Gener Transm Distrib* 5(7):760–771
2. Shekari T, Aminifar F, Sanaye-Pasand M (2016) An analytical adaptive load shedding scheme against severe combinational disturbances. *IEEE Trans Power Syst* 31(5):4135–4143
3. Ching-Tzong S, Lee C (2003) Network reconfiguration of distribution systems using improved mixed-integer hybrid differential evolution. *IEEE Trans Power Del* 18(3):1022–1027
4. Masood N, Shazon MH, Deeba SR (2021) A frequency and voltage stability based load shedding technique for low inertia power system. *IEEE J* 9(3):78947–78961
5. Mahdad B, Srairi K (2019) Adaptive differential search algorithm for optimal location of distributed generation in the presence of SVC for power loss reduction in distribution system. *Eng Sci Technol, Int J* 19(3):1266–1282
6. Manson S, Zweigle G, Yedidi V (2014) An adaptive under- frequency load-shedding system. *IEEE Trans Ind Appl* 50(3):1659–1667
7. Laghari JA, Mokhlis H, Karimi M, Abu Bakar AH, Mohamad H (2015) A new under-frequency load shedding technique based on combination of fixed and random priority of loads for smart grid applications. *IEEE Trans Power Syst* 30(5):2507–2515

8. Rugthai Charoencheep N, Sirisumrannukul S (2009) Feeder reconfiguration for loss reduction in distribution system with distributed generators by tabu search. *GMSARN Int J* 3(2):47–54
9. Li C, Wu Y, Sun Y, Zhang H, Liu Y, Liu Y, Terzija V (2020) Continuous under-frequency load shedding scheme for power system adaptive frequency control. *IEEE Trans Power Sys* 35(2):950–961
10. Moradi MH, Abedini M (2012) A combination of genetic algorithm and particle swarm optimization for optimal DG location and sizing in distribution systems. *Int J Electr Power Energy Syst* 34(1):66–74
11. Yuan-Kang WU, Lee C-Y, Liu L-C, Tsai S-H (2010) Study of reconfiguration for the distribution system with distributed generator. *IEEE Trans Power Delivery* 25(3):110–112
12. Lalitha MP, Reddy VCV, Usha V, Reddy NS (2010) Optimal DG placement for minimum real power loss in radial distribution system using PSO. *ARNP J Eng Appl Sci* 5(4):30–37.
13. Manson S, Zweigle G, Yedidi V (2014) Case study: an adaptive under-frequency load-shedding system. *IEEE Trans Ind Appl* 50(3):1659–1667
14. Tang J, Liu J, Ponci F, Monti A (2013) Adaptive load shedding based on combined frequency and voltage stability assessment using synchrophasor measurements. *IEEE Trans Power Syst* 28(2):2035–2047
15. Mortaji H, Ow SH, Moghavvemi M, Almurib HAF (2017) Load shedding and smart-direct load control using internet of things in smart grid demand response management. *IEEE Trans Ind Appl* 53(6):5155–5163
16. Wiszniewski A (2007) New criteria of voltage stability margin for the purpose of load shedding. *IEEE Trans Power Del* 22(3):1367–1371

Implementation of Renewable Sources for Designing EV Charging Station with Hybrid Storage Device as Reserve Source



K. N. D. V. Sai Eswar  and M. Arun Noyal Doss 

Abstract A worldwide temperature alteration has prompted the immense reception of Electric Vehicles (EVs) seem to be the best substitution for ICE motors. Charging the vehicles with petroleum/fuel-based grid isn't conservative and productive. Due to the increased number of EVs in transportation sector, implementation of electric vehicle charging stations (EVCS) is fundamental to empower huge reception as it will lessen "range anxiety" concerns about the distance. Then, at that point, EV could travel before battery runs out. Subsequently, a renewable power-based charging station views as massive potential and control for electric vehicle charging. An effective plan of charging station (CS) with the utilization of solar power of 25KW, wind power of 20KW, and storage devices (battery and super-capacitor) is developed. MPPT control procedure, DC appropriate converters, and current control methodologies used for the optimal power management for the designed sources. Super-capacitors, batteries, and grid stays the optional energy storage devices/delivering devices for the EVs in the charging station. By coordinating these renewable sources, it produces electric energy to charging vehicles as well as huge decrement in the dependence on the over-burdened grid. Simulation results are realized with the help of MATLAB/Simulink for the designed system.

Keywords Renewable energy source plants · Electric vehicles · Charging stations · MPPT · DC–DC converters

1 Introduction

Electric vehicles are intense options in contrast to ordinary vehicles with zero fossil fuel by-products during operation, EVs can decrease complete environmental impact, and contamination discharges completely. As fossil fuels are creeping out to a greater degree, the requirement for biofuels would be equally reduced. The quantity of EVs

K. N. D. V. S. Eswar · M. A. N. Doss (✉)
SRM Institute of Science and Technology, Kattankulathur, India
e-mail: arunoyal@gmail.com

out and about in 2010 was a couple hundred this number rose to roughly 3,000,000 in the year 2017 and around 6,000,000 in mid-2019 [1]. Although electric vehicles have a high price tag, they have low maintenance costs and utilize significantly less energy than ordinary vehicles. Regardless the effectiveness of an electric motor lessens the maintenance cost and CO₂ outflows contrasted with the ICE. It would likewise address a maintainable progression towards a clean climate. Electric motors have an efficiency of 80–95% settling on them is a more engaging decision than Combustion Vehicles (CVs), which have an efficiency of under 20% [2]. By contrast, assuming the EVs are charged through current fossil fuel generating stations, they will adversely influence the distributed networks. EV owners re-energize the batteries from residential connection prompts to power quality issues like harmonics in the line currents, phase imbalance, voltage deviations, DC offset, phantom loading, stray flux, and line losses when it was associated with the utility grid [3]. In numerous countries of the world, electric vehicles are turning out to be dynamically more famous. In any case, the shortfall of charging stations restricts the broad acceptance of EVs by consumers around the world.

1.1 Related Works

As per the Ministry of New and Renewable Energy, in India, environmentally friendly power generation represents around 20% of the total power generation. An overview directed in [4] shows that assuming renewable power was presented in EVCS, there will be a 433% expansion in the utilization of these stations by EV drivers. Environmentally friendly power sources like wind and solar are probably the best answers to bridge this shortage faced by local electricity networks, possibly supporting the EV charging infrastructure [5]. High effectiveness, low network cost, simple arrangement, and less power conversion levels are the benefits when it is well chosen for one-time establishment [6].

Solar and wind energies are unreservedly open and are more profitable than different sources for power generation [7]. A large portion of the literature showed that the establishment of PV solar and wind energy conversion systems with the power grid has progressed and is feasible [8], the energy storage system's usage is to balance out the power grid [9]. It is challenging that the developing number of EVs implies enormous charging demand and burdens the grid load in the peak hour [10]. The fast or quick charging stations are the people who execute controlled rectification and have sufficient ability to charge electric vehicles within less time [11]. In [12], to meet acceleration and regenerative braking using HESS, energy management mechanism is used to split the demand. Relative factors [13] like cost, size, weight, reduced ripple current, and efficiency parameters are derived with frequency doubling property in [14]. Magnitude fluctuations and current peak factors of the battery and SC are solved using GA and factor was decreased by 3–9% in [15, 16]. For managing the energy for HESS developed two H_∞ controllers are designed

in [17]. Combination of battery and SC results in the increase in battery life by decreasing the load on battery alone results in improved battery life by 3.91% [18].

Problem statement. Main attributes like low contamination and emissions, EVs have immense possibilities for improvement. Designing a charging station with zero emissions is the crucial factor. CS is designed in such a way that it should benefit the consumers with less cost per unit, reliable, loss-free, large parking area, and should have less time to charge the EVs. Grid burden to be lessened which further not to disturb the distributed loads. For simple design factors like less maintenance and robust installation, CS should be built. Only renewable energy sources along with HESS can be an effective solution to make this charging station operates at a reasonable cost for the consumers.

2 Employment of Energy Sources for EVCS

The main motto of this work is to plan an EVCS that guarantees to provide the load while limiting the expenses and the system outflows. Sources utilized to design a charging station are (a) Photovoltaic system, (b) Wind energy system, and (c) Hybrid storage systems used as a backup source in crisis cases, yet for restricted charging time because of its lesser storage limit. Each source is associated with a Common DC-Link. From that point, this power is transmitted to the EVCS through DC converters and bi-directional converters which not only boost the supply but also change the nature of the supply. The utility grid is taken as an optional source at required times. Inventory from the RECS doesn't meet the expected load. It is planned that a cost-effective and reliable system can be designed by the appropriate administration of sustainable power generation and load demands (Fig. 1).

2.1 Photovoltaic System

A photovoltaic system can create power by harnessing sun energy and converting into electric energy. Just a limited quantity of solar radiation falling on the Solar Photovoltaic (SPV) boards is changed into power, and the rest is switched completely to heat [19].

$$I_{pv} = I_{ph} - I_0 \left\{ e^{\frac{q(V_{pv} + R_s I_{pv})}{AKT}} - 1 \right\} - \frac{V_{pv} + R_s I_{pv}}{R_{sh}} \quad (1)$$

Accordingly, the impact of solar radiation alongside temperature on output power is thought of. For the most part, the photovoltaic system works in the maximum power point tracking (MPPT) mode to understand the exceptionally proficient use of the renewables. Because of the presence of the photovoltaic system, the charging station can freely deliver surplus energy which can be moved to the utility grid.

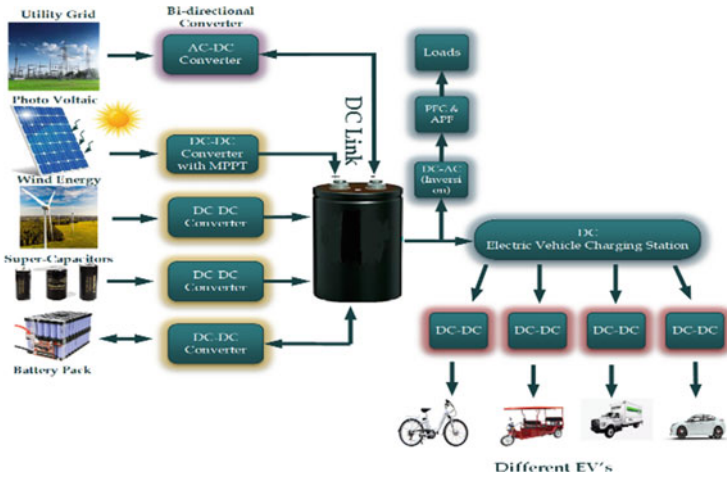


Fig. 1 Overview of charging station with RECS as the main source

This diminishes the stress on the main grid power system. Nonetheless, the power generation of the photovoltaic system is connected straight with the ongoing solar irradiance.

$$P_{pv}(k) = A \times \frac{G(k)}{1000} [1 + \gamma_{pv} \times (T_{amb} - 25)] \times \eta_{DA} \tag{2}$$

where I_{ph} is the photocurrent developed by irradiation from solar, I_0 is the saturation current of diode when operated in reverse mode, d is the forward diode current, I_{sh} is the shunt current flowing through branch resistor, R_{sh} and R_{se} are the shunt and series resistance, respectively, I_{pv} is the developed net current by solar PV system, V_{pv} is the output voltage of the PV cell, q is the electron charge, A and K are the fitting factor and Boltzmann constant (1.38×10^{-23} J/K) parameters, respectively.

2.2 Wind Energy Conversion System

Wind energy is a natural resource having many benefits like it uses long-permanent magnets in generators. In basic, kinetic energy is taken as input for the turbine and later it changes to electric power with the help of a generator. Variable speed is preferred to reduce the fluctuations in the output as well as to improve the reactive power. Finally, which is fed to a permanent magnet synchronous generator (PMSG) and double fed induction generator (DFIG) [20].

The produced kinetic energy and torque for the wind turbine is

$$P_w = \frac{1}{2} A C_P(\lambda, \beta) \times (V_\omega)^3 \quad (3)$$

$$T_m = \frac{P_m}{\omega_m} = \frac{\frac{1}{2} \cdot C_P \cdot \rho \cdot A \cdot V_\omega^3}{\omega_m} \quad (4)$$

where P_w is the kinetic energy generated (Watts), A is the blade swept area (m^2), C_P is the rotor power co-efficient (no dimensions), λ is the tip-speed ratio, β is the turbines blade pitch angle, V_ω is the velocity of the wind speed (m/s), P_m is the mechanical power (Watts), T_m is the mechanical torque (N-m), ρ is the air density (kg/m^3), and ω_m is the mechanical angular speed (rad/s).

The tip-speed ratio of the wind turbine relies upon the rotor angular velocity (ω), rotor range (R) and speed of the wind (V_ω) as addressed in (2).

$$\lambda = \frac{\omega_\omega R}{V_\omega} \quad (5)$$

By considering the torques of the electrical and mechanical along with the masses present in the generator and turbines, angular speed is given by

$$J \frac{d\omega_m}{dt} = T_e - T_m \cdot B \cdot \omega_m \quad (6)$$

T_e is the electromagnetic torque, T_m is the mechanical torque, J is the combined inertia, and B is the rotor friction.

2.3 Hybrid Energy Storage Systems (HESS)

Due to irregularity of the photovoltaic and wind power generation, storage systems are required. Batteries and supercapacitors (SC) are considered here for storing the energy when surplus power is generated from the hybrid sources. During an emergency case, these will be acting as an additional source to the primary source.

Battery. Batteries have high energy density and low power density. By considering all the requirements and satisfying the energy load demand Li-ion battery is chosen with an energy density value of 80–170 h/kg value and a power density of 0.8–12 kW/kg. The charge and discharge cycles are nearly 1200. Interestingly, the State of Charge (SOC) is used to demonstrate the current energy present in the battery. Thus, the deterministic discrete-time SOC model of the battery can be given by [4].

$$SOC(k) = SOC(k-1) - \frac{\eta I_{bat}(k) \Delta t}{Q} \quad (7)$$

Super-Capacitor. Due to inherent characteristics like high charge storage capacity and low equivalent series resistance, electric double-layer capacitor is used. In general, SC has a high power density, and the value is selected between 4 and 10(kW/kg) and a low energy density of 20–30(wh/kg). The delivery power from the Supercapacitor is too low, but the charge/discharge cycles are more than one million, which is more when compared to the batteries.

The current equation for the SC is given by

$$L \frac{d_{isc}}{dt} = V_{sc} - \alpha V_{Bus} \quad (8)$$

where L is the inductor value of the filter and α represents the duty cycle of controller.

2.4 DC Link and Utility Grid

It is assessed that the DC bus design decreases the overall conversion losses from around 32% to under 10% when contrasted with the AC bus structure. The stability of the DC bus up-front relies upon the size of DC capacitance which needs to support the DC ripples must be low or requires a large value of capacitance. Here, a 650 V DC link is interlinked between the sources and the charging station. Whenever EV power demand decrements and renewable power generation doesn't satisfy the need, then EV takes power from the utility grid called grid to vehicle (G2V).

3 Operation and Control of Charging Station in Different Cases

The charging station includes a dual converter, charging slots, and EVs. A microgrid controller is needed to control the power flow in the charging station at a particular time. EVs can be charged by their state of charge (SOC), characterized as the proportion of the available capacity to its maximum limit when a battery is charged [21]. If PV production exceeds the consumption and battery storage capacity, the PV will stop working. Every moment of generated power is tracked from the solar,

wind, and batteries. Power received from the grid or sent to the grid is also monitored from time to time. The total power delivered to the EV station and the power utilized by all the components in the charging station is also calculated and should be equated clearly. Proper energy management can be done by considering all the above-mentioned factors.

3.1 Operating Modes at Different Cases

Case 1. Solar Photovoltaic system alone acting as a source

In this scenario, the system generates power through irradiance and temperature from the sun. It is alone sufficient to supply the EVs connected to the charging point, then the surplus energy from the solar is used to charge the storage devices. Even if it is excess to batteries, it will be connected to dummy loads to balance the system.

$$\text{Solar}_{power}(t) = \text{EV}_{load}(t)$$

$$\text{Solar}_{surpluspower}(t) > \text{BESS}_{charges}(t) + \text{OtherEmergencyloads}$$

Case 2. Wind Energy Conversion System alone acting as a source

In this case, the wind energy conversion system alone acts as a source, and if it meets the load requirements no excess energy can be utilized from other sources. Even if generated power is surplus from batteries, it transfers to dummy loads to maintain stability.

$$\text{Wind}_{power}(t) = \text{EV}_{load}(t)$$

$$\text{Wind}_{surpluspower}(t) > \text{BESS}_{charges}(t) + \text{OtherEmergencyloads}$$

Case 3. Solar as a primary source and WECS as a secondary source

If the system meets the required load, Case 1 satisfies the relation. Due to any climatic change, if the solar PV system is not able to generate the required amount of power to meet the load, then it will add the WECS along with the solar where

load demand gets satisfied. Surplus power is fed to the storage devices to perform charging action and these are ready to act as an additional source to the primary source when needed.

$$\text{Solar}_{\text{primarypower}}(t) + \text{Wind}_{\text{Secondarypower}}(t) = \text{EV}_{\text{load}}(t)$$

$$\begin{aligned} \{\text{Solar}_{\text{primarypower}} + \text{Wind}_{\text{Secondarypower}}\}_{\text{Surplus}}(t) &> \text{EV}_{\text{load}}(t) \\ &> \text{BESS}_{\text{charges}}(t) + \text{Other Emergency loads} \end{aligned}$$

Case 4. Deficit of power from hybrid sources, Usage of storage devices and grid supply as a main source

Day-time solar can generate energy by taking the sun as the main source. In the same way, if the wind flow is more, the power generated from the wind is also more. Due to any light failure or no wind flow, hybrid source becomes zero. Then hybrid storage devices already charged during Case 1 and Case 2 now get discharged by supplying to loads. But the power from the batteries doesn't deliver much longer time remaining power is borrowed from the grid.

$$\text{Solar}_{\text{primarypower}}(t) + \text{Wind}_{\text{Secondarypower}}(t) < \text{EV}_{\text{load}}(t)$$

$$\text{Solar}_{\text{primarypower}}(t) + \text{Wind}_{\text{Secondarypower}}(t) + \text{BESS}_{\text{charges}}(t) < \text{EV}_{\text{load}}(t)$$

$$\text{Solar}_{\text{primarypower}}(t) + \text{Wind}_{\text{Secondarypower}}(t) + \text{BESS}_{\text{discharges}}(t) + \text{Grid}_{\text{borrowedpower}}(t) < \text{EV}_{\text{load}}(t)$$

3.2 MPPT Control Technique

Perturb and Observe (P&O) calculation-based DC converter is used for solar photovoltaic and wind energy systems to tracking the most extreme power fluctuations. Necessary steps and methods are taken to acquire the objective of this system. Various sorts of calculations are used in the MPPT strategy which mainly objected from PV modules and wind Systems. The duty cycle of the operated hybrid system is acquired, with the assistance of the MPPT, and necessary signals are sent to the PID regulator. This, further makes the proper action and summarizes the actual value, and keeps up with the consistent voltage at the DC bus. Similarly, energy management between the battery and super-capacitor is made with the assistance of the central controller where the generated power is adjusted at the DC-link. The boost converter is employed to charge and discharge modes of the energy devices. These are charged when it arrives

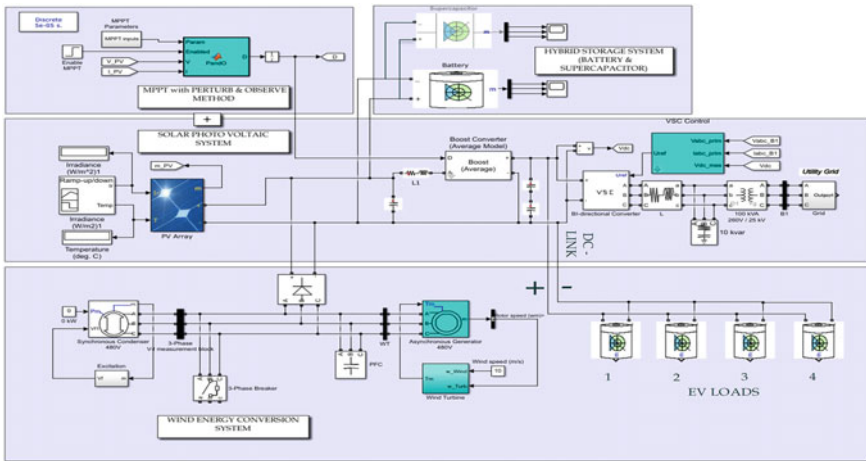


Fig. 2 Simulation overview of charging station

at their lower current limit and charges until their set value is reached to maximum, treated as boost operation. A control strategy is utilized to monitor the situation with the condition of charge (SoC), voltage, and current limits. A controlled way is planned where the expected power command is taken from the EVCS and it will divide the voltage flowing in it and the actual current is estimated. The actual current is compared with the reference current if error permits it is sent to the PID controller. Finally, signals and switching operations are controlled by the PWM generator thus, charge/discharge happens. Here mainly, the SC can act as a low pass filter which diminishes the extra additional filtering equipment to the system.

4 Simulation Results and Discussions

The developed system includes the renewable sources and energy storage systems which are modelled under MATLAB Simulink which is shown in Fig. 2.

For developing the simulation, concerned parameters and data are given in Table 1 (Figs. 3, 4, 5 and 6).

Table 1 Simulation parameters

Hybrid Source, Storage and Converter specifications					
Solar PV panel	Maximum power in watts(W)	25,000	Battery	Ampere hour (Ah)	240
	Maximum voltage in volts(V)	54.7		Voltage in volts(V)	48
	Maximum current in amperes(A)	5.58		Energy capacity in(KWh)	11.52
	Open circuit voltage in volts(V)	64.2		Type and variant of battery	Li.ion
	Short circuit current in amperes(A)	5.96	Dc-Link	DC bus voltage in Volts (V)	650
	Number of panels connected in series and parallel	12*7	Converters	Power in watts(W)	37,200
Wind turbine	Rated power in watts(W)	20,000		Voltage(Vin)min in volts(v)	50
	Cut-in speed in(m/s)	12		Output voltage (Vo) in volts(v)	400
	Beta	0		Switching frequency(fs)	20,000
	Power coefficient Cp	0.4		Duty cycle(D)	0.88
	Blade length in(m)	52		Ripple voltage(DV)	2
	Air density in(kg/m ³)	1.23		Ripple current(DI)	50
Super-capacitor	Capacitor in farads(F)	75	Inductor in henries(H)	2.734*10 ⁻⁵	
	Voltage in(V)	60	Capacitor in farads(F)	1.1*10 ⁻³	
	Current in amperes(A)	300	Efficiency of converters	90%	

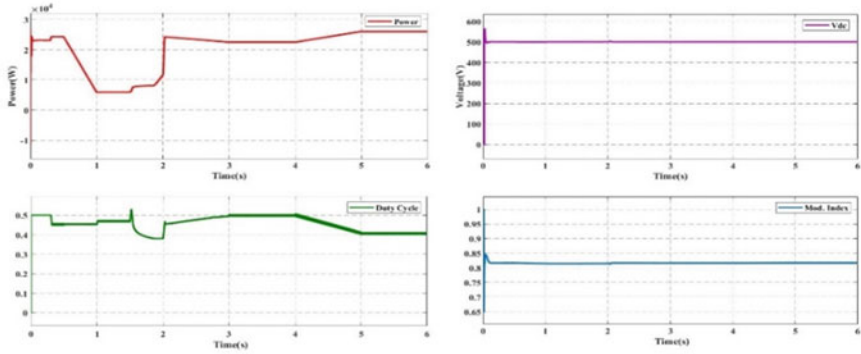


Fig. 3 Performance behavior of the solar PV system shows the total power generated, DC link voltage, duty cycle, and modulation index of the converter

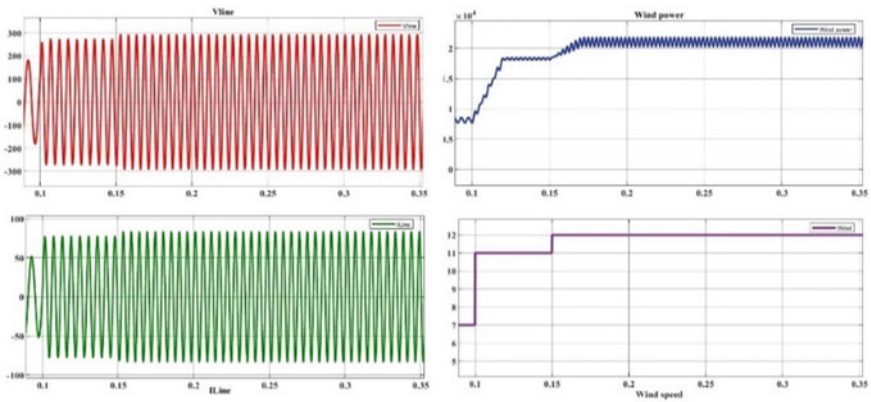


Fig. 4 Performance behavior of the wind energy conversion system shows the generated grid voltages and currents, generated power and its wind speed

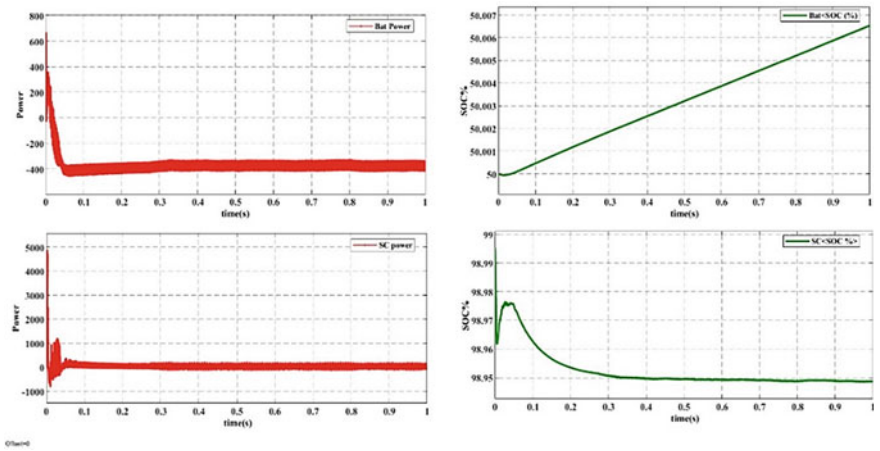


Fig. 5 Performance behavior of the hybrid energy storage systems shows the amount of energy generated from battery and its state of charge, as well as for the super-capacitor and its state of charge

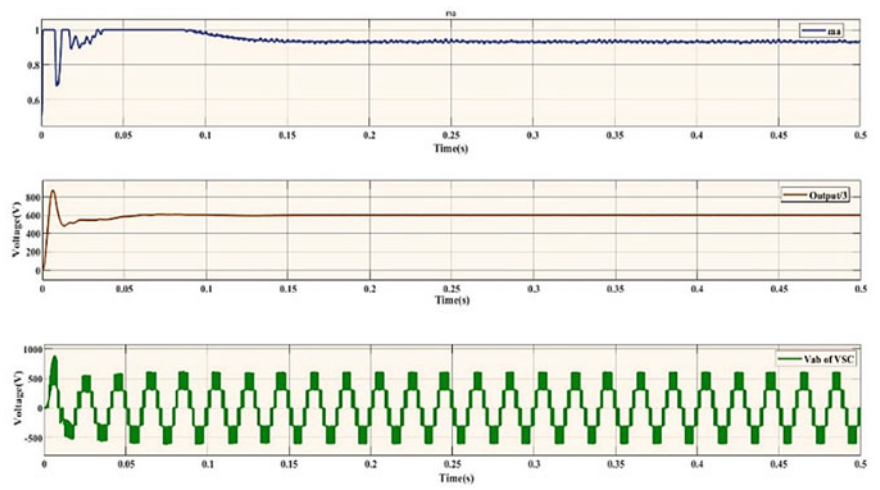


Fig. 6 Performance behavior of the converter shows its modulation index value, Vdc voltage maintaining constant at DC link along with voltage produced at VSC

5 Conclusion

Due to the increased number of EVs in the transportation sector, the effective way to develop the electric vehicle charging station is built by considering renewable sources like solar and wind. Hybrid energy storage systems play a vital role with an optional parameter like a grid system. So, it will be a robust solution for charging EVs and

maintains stable condition during peak loads, which also lessen the burden and cost on the grid network. MPPT integrated with PID Current controller is employed to perform the operational converter by maintaining the constant voltage at DC link. A single bi-directional converter is used for the energy management of hybrid storage systems which makes the circuit effective. The design part of the charging station is analyzed with the help of the simulation, results are validated using MATLAB. This design structure will be a productive solution for commercial outlets and parking lots.

References

1. Biradar SK, Patil RA, Ullegaddi M (eds) (1998) Energy storage system in electric vehicle. Power Qual 98
2. Falvo MC, Sbordone D, Bayram IS, Devetsikiotis M (2014) EV charging stations and modes: international standards. In: 2014 international symposium on power electronics, electrical drives, automation and motion
3. Khan W, Ahmad F, Alam MS (2019) Fast EV charging station integration with grid ensuring optimal and quality power exchange. EngSci Technol, Int J 22(1):143–152
4. Zhang J et al (2018) A non-cooperative game based charging power dispatch in electric vehicle charging station and charging effect analysis. In: 2018 2nd IEEE conference on energy internet and energy system integration (EI2)
5. Ben Salah I, Bayoudhi B, Diallo D (2014) EV energy management strategy based on a single converter fed by a hybrid battery/supercapacitor power source. In: 2014 first international conference on green energy ICGE 2014
6. Biya TS, Sindhu MR (2019) Design and power management of solar powered electric vehicle charging station with energy storage system. In: 2019 3rd international conference on electronics, communication and aerospace technology (ICECA)
7. Alkaws G, Baashar Y, Abbas UD, Alkahtani AA, Tiong SK (2021) Review of renewable energy-based charging infrastructure for electric vehicles. Appl. Sci 11(9):3847
8. Singh S, Chauhan P, Singh NJ (2021) Feasibility of grid-connected solar-wind hybrid system with electric vehicle charging station. J Mod Power Syst Clean Energy 9(2):295–306
9. Venkatachalam K, Saravanan V (2020) Performance evaluation and load demand management of grid connected hybrid wind-solar-battery system. Int J Appl Power Eng (IJAPE) 9:223
10. Ostadi A, Kazerani M, Chen S (2013) Hybrid energy storage system (HESS) in vehicular applications: a review on interfacing battery and ultra-capacitor units. In: 2013 IEEE transportation electrification conference and expo (ITEC). pp 1–7
11. Zhuge K, Kazerani M (2014) Development of a hybrid energy storage system (HESS) for electric and hybrid electric vehicles. In: 2014 IEEE transportation electrification conference and expo (ITEC). pp 1–5
12. Zhang H, Ye K, Li P, Li H (2020) Optimization of hybrid energy storage system control strategy for pure electric vehicle based on typical driving cycle. Math Probl Eng 1024–123X. Hindawi
13. Bai Z, Yan Z, Wu X et al (2019) H_{∞} control for battery/supercapacitor hybrid energy storage system used in electric vehicles. Int J Automot Technol 20:1287–1296
14. Waseem M, Sherwani AF, Suhaib M (2019) Integration of solar energy in electrical, hybrid, autonomous vehicles: a technological review. SN Appl Sci 1:1459
15. Xavier LS, Amorim WCS, Cupertino AF et al (2019) Power converters for battery energy storage systems connected to medium voltage systems: a comprehensive review. BMC Energy 1:7
16. Conte F (2006) Battery and battery management for hybrid electric vehicles: a review. Elektrotech Inftech 123:424–431

17. Masih-Tehrani M, Yazdi MRH, Esfahanian V et al (2019) Wavelet-based power management for hybrid energy storage system. *J Mod Power Syst Clean Energy* 7: 779–790
18. Liang J, Zhang J, Zhang X et al (2013) Energy management strategy for a parallel hybrid electric vehicle equipped with a battery/ultra-capacitor hybrid energy storage system. *J Zhejiang Univ Sci A* 14:535–553
19. Domínguez-Navarro JA, Dufo-López R, Yusta-Loyo JM, Artal-Sevil JS, Bernal-Agustín JL (2019) Design of an electric vehicle fast-charging station with integration of renewable energy and storage systems. *Int J Electr Power Energy Syst* 105(2):46–58
20. Morris B, Federica F, Carola L, Michela L (2020) Electric vehicles charging technology review and optimal size estimation. *J Electr Eng & Technol* 15(6):2539–2552
21. Aldhanhani T, Al-Durra A, El-Saadany EF (2017) Optimal design of electric vehicle charging stations integrated with renewable DG. In: 2017 IEEE innovative smart grid technologies-Asia (ISGT-Asia). pp 1–6

A Cost-Efficient Energy Management of EV Integrated Community Microgrid



Divya Mathur, Neeraj Kanwar, and Sunil Kumar Goyal

Abstract The use of energy management in community microgrid is essential for load fulfillment and to cope up with the varying power output of renewable energy sources. Nowadays, electric vehicle is a good opportunity as it can act as both energy source and load according to optimum cost and available energy. If the systems have extra renewable energy, they can be utilized for EV charging. Scheduling of EV charging with respect to excess generated power and varying electricity prices is considered in this paper. The proposed system helps in energy management of community microgrid integrated with the residential EV charging points. The cost is optimized using biogeography-based optimization method with a given load profile, generated renewable energy, and real-time price of electricity. The limits of EV owner priority are also kept considered. The results show that with the higher electricity cost, EV is either kept idle or being charged with minimum charging rates, while for lower electricity cost, EV is charged with higher rates.

Keywords Community microgrid · Cost optimization · Vehicle to Grid (V2G) method · Electric vehicle charging schedule

1 Introduction

In recent years, uses of grid-connected energy storage are emerging as an important step towards demand fulfillment with economic aspects. Also, it helps in peak shaving, quality improvement, self-dependent, demand-side flexibility, etc. [1]. A community microgrid consists of various distributed energy sources, like solar, wind,

D. Mathur · N. Kanwar (✉) · S. K. Goyal
Department of Electrical Engineering, Manipal University Jaipur, Jaipur, Rajasthan, India
e-mail: nk12.mnit@gmail.com

D. Mathur
e-mail: divya.199209604@mun.manipal.edu

S. K. Goyal
e-mail: sunilkumar.goyal@jaipur.manipal.edu

along with battery storage devices and variable loads. They improve grid stability if connected by acting as a sustainable and quality electric power supplier. Because of the variable output power from renewable energy sources due to weather conditions and time of day, the continuity of power generation is not guaranteed. The unpredictable electricity demand adds complexity to the control of power system [2]. Also with increasing electricity demand, different strategies of energy generation are being developed.

In a similar way, growing oil price and increasing CO₂ emission lead to the growth of more development in electric vehicles. The charging of these vehicles also increases the load on power system [3]. The irregular and unknown charging of electric vehicles will lead to unexpected overload on power system. Thus, it is required to have a coordinated vehicle charging system. The electric vehicle spends a high duration in parking where they are being charged for getting ready for the next ride [4]. Like in India, most vehicles are on road only during office timing of 8–10 h. For rest of the duration, the vehicle is parked in the residential parking. This gives a great opportunity to EVs to serve as energy storage or add to the load. Therefore, a proper charging and discharging of EVs can not only smooth the load profile but also helps in reduction electricity cost. This intelligent and coordinated connection between grid and vehicle is called Vehicle to Grid (V2G) connection [5]. This article focuses on fulfilling the load demand with the obtained energy from renewable energy sources but if RESs are not able to fulfill it, the electric vehicle will act as an alternate source. This will lead to continuous charging and discharging of battery and thus will harm the battery lifespan. The expert energy management system will help in reducing abrupt charging and discharging of battery and also supplying load demand with optimum cost requirements [6]. On the basis of the frequently changing load demand of system, and generating renewable energy, the different charging rates decisions are made to make the system cost-effective [7]. The EVs can be charged both from the electric utility and renewable energy sources (RESs) and should be charged in such a way that the least operational cost occurs.

In this paper, variable load demand and renewable energy generated are considered in a community microgrid which is connected to the electric vehicle for charging/discharging purposes. The priority of CMG is to fulfill load demand, so charging rates can be reduced or increased in accordance with the availability of renewable energy or reduced electricity price. The EVs are first charged through extra renewable energy sources and after that charging rates are optimized according to retail electricity price.

2 Mathematical Modeling

2.1 A Model of Community Microgrid

In this paper, a community microgrid is modeled with renewable energy sources of solar and wind farm for optimum charging strategy with respect to varying electricity retail price. A residential load of 20 houses with maximum demand of 1.8 kWh connected with ten solar and five wind farms with total installed capacity of 65 kW. The community microgrid is capable of working in both grid-connected and isolated forms [8]. An aggregator with DSO controlling unit integrated with community microgrid, to control the flow of energy from utility, solar and wind farm, and battery energy storage, as shown in Fig. 1.

The aggregator takes input of energy generated through solar and wind farms, instantaneous electricity price, and load profile to control the flow of energy and generates the optimum charging/discharging rates of EVs. The so-decided charging/discharging rates are then sending to respective electric vehicle if connected to the system. The EVs rate of charge/discharge is maintained only in the limits of desired SOC and the requirement of EV owner. When the renewable energy is in excess, the vehicle is charged through it, but during low generation, the decision depends on the rate of electricity. During low price, batteries of EVs can be charged with higher rates, while, during higher rates, these can be charged with slower charging rates or even can be kept idle [9]. There is also a limitation from EV owners to reach to required SOC so as to be ready for the next ride. This process of continuous charging and discharging of battery will affect the life of the battery [10]. So, the batteries are continuing to charge till their maximum limit, i.e., 90% SOC or the required SOC

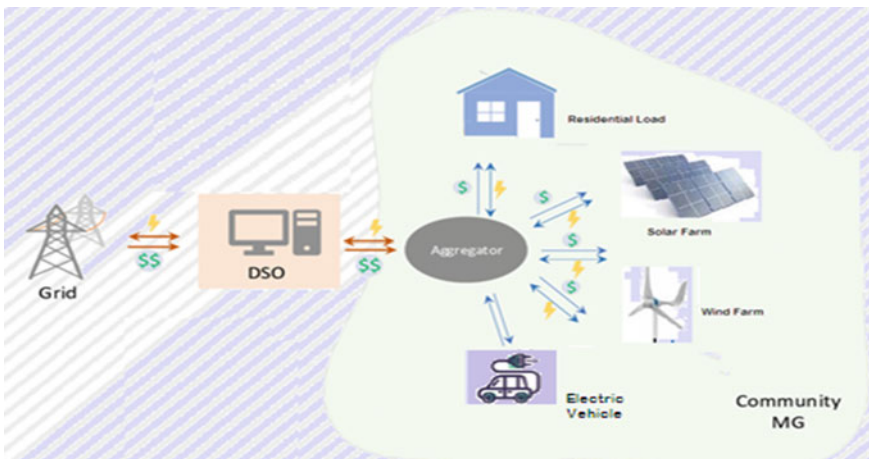


Fig. 1 Model of community microgrid

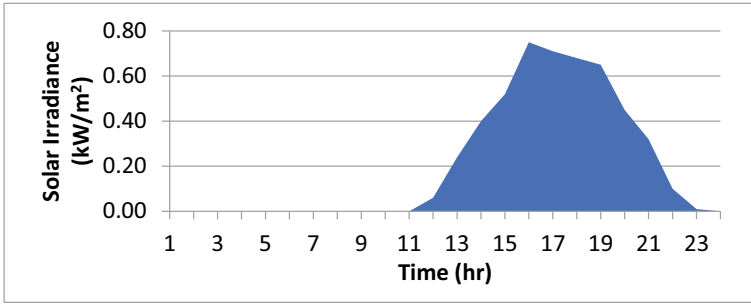


Fig. 2 Variation of solar irradiance in a day

prescribed by EV owner and continue to discharge till the minimum limit, i.e., 20% SOC.

2.2 Modeling of Solar PV Farm

A solar generator is a portable power station with solar panels and an inverter with controller to supply maximum ac output power. The area of cross section of solar generator is taken here as 20 m² to generate maximum solar power of 4 kW with conversion energy 18%. The output power of solar generator is a function of PV size and instantaneous irradiation (*I*) [11]. The PV output can be calculated as

$$P_{sT} = \eta_{conv} * Area * I(1 - 5 \times 10^{-3}(t - 27)) \tag{1}$$

where η_{conv} = % conversion efficiency

Area = solar panel area in m²,

and *t* shows the surrounding temperature (30 °C).

The power output of 24 h of solar array is shown in Fig. 2 [7].

2.3 Wind Power Modeling

The power output from wind generator is a function of the surrounding wind speed and the power rated. It also depends upon the velocity of wind, *v* (m/s), according to the following relation [12]:

$$P_{wT} = \eta_{conv} * \begin{cases} 0 & \text{for velocity lesser than cut - in and greater than cut - off velocity} \\ P_{rated} \times \frac{v^2 - (cut-in velocity)^2}{rated\ velocity^2 - (cut-in velocity)^2} & \text{from cutin to rated velocity} \\ P_{rated} & \text{from rated to cutout velocity} \end{cases} \tag{2}$$

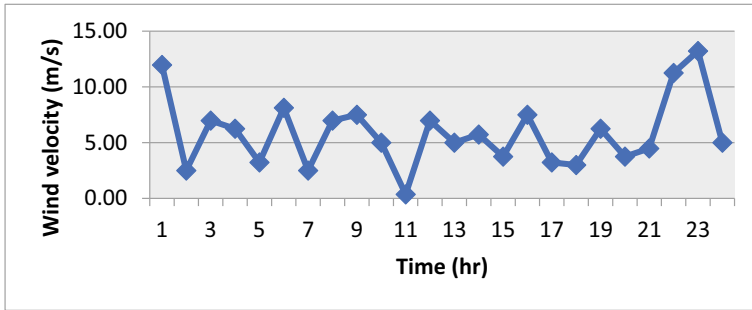


Fig. 3 Wind velocity in a day [7]

where P_{rated} is the rated power of wind generator assumed to be 25 kW,
 cut-in velocity is assumed as 3 m/s,
 rated velocity is assumed as 10 m/s,
 cut-off velocity is assumed 25 m/s,
 and η_{conv} is the efficiency of conversion of wind generator = 95%.
 The wind velocity variation over 24 h is shown in Fig. 3.

2.4 Electric Vehicle

Mostly, lead-acid or lithium-ion batteries are used in electric vehicles for better life span, performance, and costing. Due to repeated charging/discharging, the battery life of EV reducing, so, if required, the battery can be discharged to limited SOC [13]. In this paper, two EVs with the following (Table 1) battery specification is used.

Only 90% of battery capacity can be considered for optimization of battery life, i.e., 36 kWh and 40.5 kWh, respectively. Also, up to the minimum of only 20% of the capacity of battery can be discharged. So, the minimum available battery capacity will be 8 kWh and 9 kWh, respectively. The aggregator manages the charging/discharging rates of EVs in consideration of optimization of the electricity price and the priority of EV owner. If the departure time of EV is near, then it is charged to the prescribed limit on priority irrespective of electricity price, thus EV will act as an important load for the system. It also lowers the effect of varying behavior of RESs. It decides charging/

Table 1 Specification of EVs connected

	Arrival time	Departure time	Battery capacity (kWh)	Battery capacity at the time of arrival (kWh)	Battery capacity required at the time of departure (kWh)
EV1	6:00 AM	10:00 PM	40	18	23
EV2	10:00 PM	11:00 AM	45	16	30

discharging rates for optimal operation of CMG, depending on the instantaneous price of electricity, RESs power generation, and varying load requirements. The battery of EVs will be charged either from RES if it is higher than load or from utility when the price of electricity is lower. In case of urgency, if battery is required to charge from utility during peak rates of electricity, then the charging rates will be lower; otherwise, battery will be discharged at this time. The imposed limits on the charging/discharging rates for optimum battery lifetime are

$$\min SOC < SOC_{inst} < \max SOC \quad (3)$$

where $\min SOC$ and $\max SOC$ are taken as 0.2 and 0.9 times of full battery capacity, respectively.

SOC_{inst} is the instantaneous SOC of EV battery.

Instantaneous the battery energy levels BL can be represented as [1]

$$BL(t + 1) = BL(t) \pm \Delta t * ch(t) * \eta_c \text{for charging} \quad (4)$$

$$BL(t + 1) = BL(t) \pm \Delta t * dch(t) * \eta_d$$

for discharging.

where Δt is the time taken for charge/discharge (1 h in this case).

η_c, η_d are the charging and discharging efficiencies, respectively (assumed 100% in this case).

The charging and discharging rates are assumed to be varied between + 6 and – 6 kWh.

2.5 Loads Profile

As the household appliances are not flexible with time usage, thus load profile is not changed and is kept on priority. For the available set of residential load connected with the community microgrid, the hourly variations of load [13] are shown in Fig. 4.

2.6 Utility Pricing

As per the generated energy from RESs, the electricity can be bought or sold every hour. In general, buying electricity from utility at higher price is restricted. The rate of electricity consumption and distribution is taken same. It is shown in Table 2.

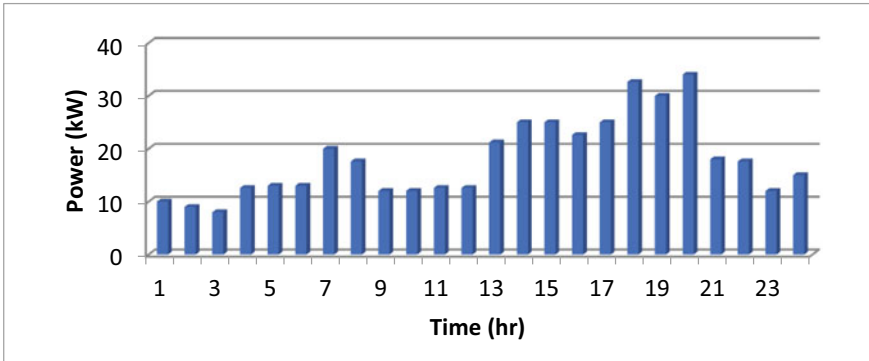


Fig. 4 Hourly load profile [7]

Table 2 Variable electricity price on hourly basis [7]

Time	Hourly electricity price (cents/kWh)	Time	Hourly electricity price (cents/kWh)
1	17.50	13	32.50
2	12.50	14	27.50
3	14.00	15	29.00
4	17.50	16	30.00
5	22.50	17	35.00
6	30.00	18	36.00
7	30.00	19	37.50
8	36.25	20	38.00
9	31.25	21	25.00
10	30.00	22	22.50
11	30.00	23	17.50
12	33.75	24	12.50

3 Objective Function Formulation

The main aim of this paper is to minimize the cost of electricity. The total cost of electricity can be obtained as

$$Total_Cost = RTP(t) * \{Load(t) - (P_{sT}(t) + P_{wT}(t) - ch(t))\} \tag{5}$$

subjected to

$$chmax > ch(t) > 0$$

$$dchmax < dch(t) < 0$$

where ch_{max} is the maximum charging rate, i.e., 6kWh.

and dch_{max} is the maximum discharging rate, i.e., -6 kWh (negative symbol for discharge).

also

$$BL_{min} < BL + ch(t) < BL_{max}$$

$$BL_{min} < BL - dch(t) < BL_{max}$$

and energy balance

$$P_{exch}(t) + P_{sT}(t) + P_{wT}(t) = Load(t) + ch(t)/dch(t) \quad (6)$$

where $P_{exch}(t)$ is the power exchange with grid,

$P_{sT}(t)$ is solar output from Eq. 1,

$P_{wT}(t)$ is wind output from Eq. 2,

$Load(t)$ & $ch(t)/dch(t)$ are instantaneous load and charging/discharging rates,

$RTP(t)$ is the instantaneous real-time pricing of electricity.

4 Results

The CMG modeled here is accessed for cost minimization and for fulfilling the load with the scheduling of EVs. The renewable power so generated is optimally used for this purpose. When the generated power is higher than the load demand, the EV is charged by renewable energy at the time of lower electricity rates. But if the electricity price is higher, then it is beneficiary to sell the stored energy to the utility if available in EVs. The power generated from the given renewable energy sources, i.e. solar and wind generators are shown in Fig. 5.

The control of charging/discharging rates of EVs with respect to the variable electricity price is the main aim in this paper. The initial battery level at the time of starting is assumed to be 18kWh and 16 kWh, respectively. The limits of battery energy and SOC are taken care while optimizing the cost of electricity. The departure SOC of EV battery is maintained according to the owner's priority. If the generated power is greater than the load demand, then the EVs are charged with maximum rates. But, if the power so generated is lesser than load demand, then EVs will be discharged if it has sufficient energy to do so; otherwise, it is charged with a slower rate on peak pricing if priority of owner occurred. The varying battery level of EVs in accordance with load, price, and generated power is given in Fig. 6.

It is observed that the generated power left after the fulfillment of load demand is distributed to battery taken consideration of maximum charging/discharging rates to be 4kWh. The optimum cost obtained after optimization is \$ 26.4743. Also, it is being observed that during lower price of electricity the battery is charged with

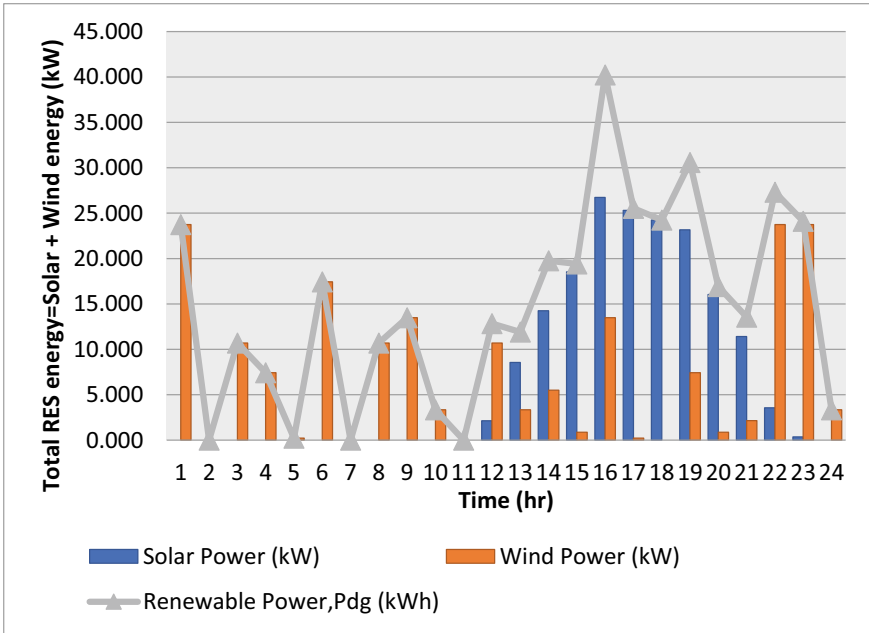


Fig. 5 Renewable power generated

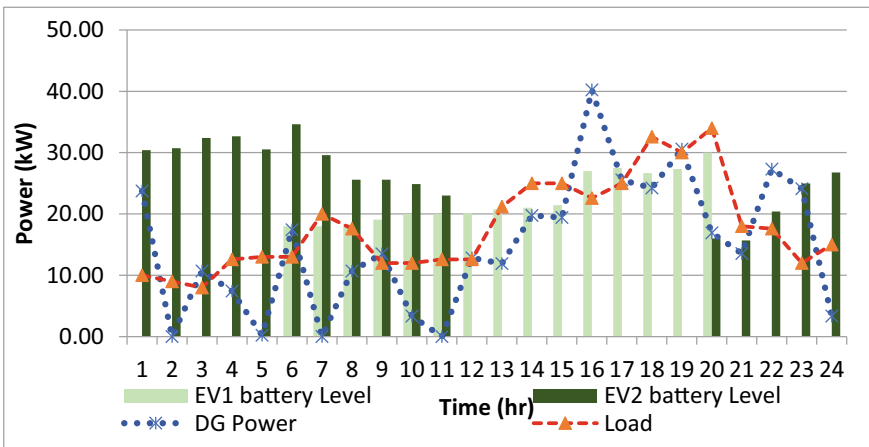


Fig. 6 Battery level of two EVs

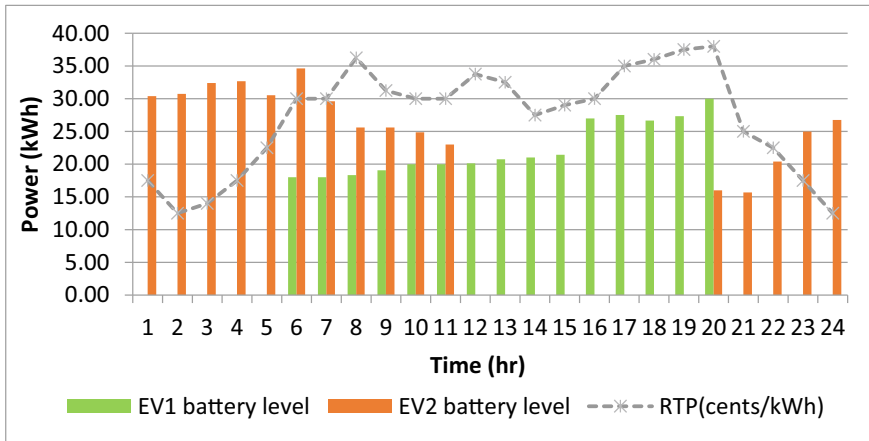


Fig. 7 Variation of EVs battery level with electricity price

higher rates as compared to that of higher price intervals. While for higher electricity price, it is kept idle or used as an alternate source for load fulfillment. For the time of departure, the battery level of EV is kept at the owner's priority. This can also be observed in Fig. 7. This is to be noted here that price of selling and buying of electricity is assumed to be same in this calculation.

5 Conclusions

This paper represents the energy management of a community microgrid in which cost of electricity is optimized and load demand is fulfilled. The community microgrid so proposed is integrated with electric vehicle charging stations at residential load. In the proposed system, the cost of CMG is optimized by reducing unprofitable charging/discharging rates and optimally scheduling the electric vehicles. The coordination of community microgrid with its load demand and variable renewable energy generated is to maintain here with the fulfillment of EV demand. Also, the dynamic nature of EVs is also considered here. The cost-effective charging/discharging rates are obtained for that. The results show that during higher generated power the EV is charged faster, while, during lower generated power, it is done in accordance with the price of electricity of utility.

References

1. Jasim M, Al Essa M (2018) Management of charging cycles for grid-connected energy storage batteries. *J Energy Storage* 18: 380–388

2. Mathur D, Kanwar N, Goyal SK a. pp 1–8
3. Mousavi-agah M, Abbasi A (2012) The impact of charging plug-in hybrid electric vehicles on residential the impact of charging plug-in hybrid electric vehicles on residential distribution transformers
4. Nguyen HK, Bin Song J (2012) Optimal charging and discharging for multiple PHEVs with demand side management in vehicle-to-building. September 2016
5. Singh M, Member S, Kumar P, Kar I (2013) A multi charging station for electric vehicles and its utilization for load management and the grid support.
6. Venayagamoorthy GK et al (2016) for a smart microgrid. *IEEE Trans Neural Networks Learn Syst* 27(8):1643–1656
7. Hossain A, Roy H, Squartini S, Zaman F, Muttaqi KM (2018) Energy management of community microgrids considering degradation cost of battery. *J Energy Storage* 22:257–269
8. Khooban M, Niknam T, Shasadeghi M (2017) Load frequency control in microgrids based on a stochastic non-integer controller 3029(c):1–9
9. Ahmad F, Member S, Alam MS, Member S, Shariff SM (2019) A cost-efficient approach to EV charging station integrated community microgrid. *IEEE Trans Transp Electrif PP(c):1*
10. Vetter J, Nov P, Wagner MR, Veit C (2005) Ageing mechanisms in lithium-ion batteries 147:269–281
11. Rafique S, Member S (2021) Energy management systems for residential buildings with electric vehicles and distributed energy resources. 9
12. Wang W, Liu L, Liu J, Chen Z, Soc EV (2021) Energy management and optimization of vehicle-to-grid systems for wind power integration 7(1):172–180
13. Wang X, Member S, Liang Q, Member S (2015) Energy management strategy for plug-in hybrid electric vehicles via bidirectional vehicle-to-grid. 1–10

Automatic Target Recognition from ISAR Images: A Review



Hari Kishan Kondaveeti, Rakesh Kancharla, K. Raja Sravan Kumar, and Valli Kumari Vatsavayi

Abstract Inverse Synthetic Aperture Radar (ISAR) is one of the promising imaging radar technology used in military applications mostly. ISAR picture productions are extremely good at predicting common radar targets such as aircraft, missiles, military vehicles, battleships, and space objects. Even though extensive research work is going on the classification/recognition of targets from ISAR imagery, no study has been performed to compile and compare those works. This paper presents a review of research works done on Automatic Target Recognition/Classification (ATR/ATC) from ISAR imagery. This work will be helpful for the researchers to have a comprehensive overview of the research progress.

1 Introduction

Automatic Target Recognition (ATR) systems that depend on ISAR technology take up images of targets moving in a non-cooperative way as input [40] and classify same based on features calculated from the image [3]. ATR systems are crucial in military surveillance in making tactic decisions accurately in real time. However, the difficulties faced by ATR systems are challenging the researchers to develop accurate mechanisms.

A two-dimensional ISAR representation is generated from the distribution of electromagnetic energy scattered from a target of interest. The pictures generated by the ISAR are processed by operators trained with knowledge in processing. The identification procedures require that a long amount of time be invested before a diagnosis

H. K. Kondaveeti (✉) · K. R. S. Kumar
School of Computer Science and Engineering, VIT-AP University, Vijayawada, Andhra Pradesh, India
e-mail: kishan.kondaveeti@vitap.ac.in

R. Kancharla
Sasi Institute of Technology and Engineering, Tadepalligudem, Andhra Pradesh, India

V. K. Vatsavayi
Department of CS & SE, AUCE (A), Andhra University, Visakhapatnam, Andhra Pradesh, India

is made by the operator. Besides the difficulty associated with ISAR processing, it is also rigorous and time-consuming.

1.1 Typical Target Recognition Procedure

Figure 1 depicts the typical target recognition procedure. It involves data acquisition and image generation, image preprocessing, feature extraction, classification, and final decision-making.

ISAR images when generated include deformations brought about by lots of noise and clutter. Noise and clutter must be eliminated prior to the extraction of important features to guarantee the validity of classification processes. Preprocessing methods entail noise reduction and alignment of orientation.

Noise reduction and Target Extraction

The noise that could be observed in ISAR images can be divided generally into two, the speckle and granular. The noise associated with ISAR images has a self-multiplying capacity. Threshold-based techniques [14] are simple and straightforward techniques used to deal with speckle noise when the SNR and SCR are high. Mean intensity of all the image pixels is considered as threshold. However, universal applicability of this threshold selection method is questionable. A slightly improvised threshold selection method [30] is employed in [40] for better noise suppression. They used area selection operation for removing the outliers, for target extraction. In [17], a combination of homomorphic and wavelet filtering techniques is used for target extraction. Other target extraction methods include watershed segmentation [39], Gradient Vector Flow (GVF) [36], combination of Smallest Univalve Segment Assimilating Nucleus (SUSAN), and Variation Level Sets (VLS) [37].

Feature Extraction

After preprocessing, features are extracted from the images for classification of targets. Figure 2 depicts the features used in target recognition from ISAR images.

Classification

Classification methods follow through processes made possible by the building of a training database and testing database. The information set comprising an example of a target's ISAR images would be broken into the training and test images. The

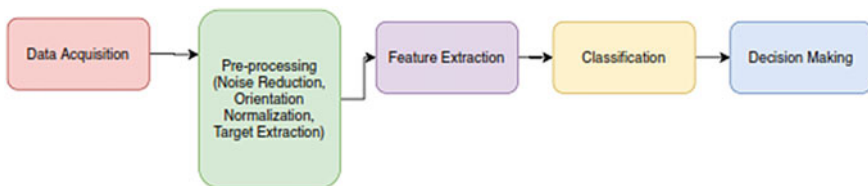


Fig. 1 Typical target recognition procedure

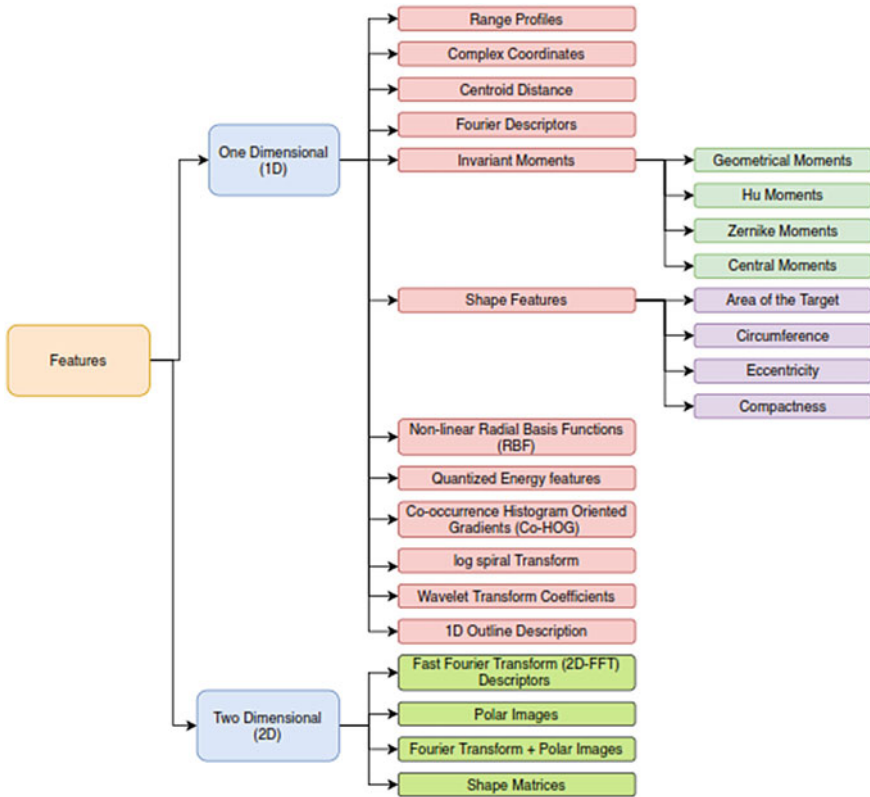


Fig. 2 Typical features used for target recognition from ISAR imagery

images are processed where the features are extracted and stored in the database using a label attached to them. When the testing phase has been carried out, images subjected to rotation and scaling functions are given as inputs. The features of the test images are also obtained. The distance/similarity between test image features is calculated.

with trained image features stored in the database. Test image is recognized as a target whose training images are nearer to it or with which the degree of similarity is more.

Even though extensive research work is being carried out on target recognition/ classification using ISAR imagery, very few researchers attempted to summarize the findings. Kurowska [21] reviewed the ship target classification mechanisms. This work compiled all the classification methods that focus on single-ship target images. He emphasized on the methods that depend on shape and length estimation of the ship targets. However, this paper summarized the works related to the classification of ship targets alone.

Park et al. [32] presented a comparative study on the capabilities of various ISAR imaging algorithms in classifying the targets efficiently. This study focused on a few high-resolution spectral estimation techniques and was not comprehensive.

This study focused on compiling the research works related to all kinds of targets such as aircraft, ships, military vehicles, and space objects. We reviewed the literature extensively from the beginning and tried to present them in a clear and precise manner. This study will be helpful for the researchers working on target recognition applications.

2 Target Recognition/Classification

Most of the researchers depend on the 2D/3D pattern-matching mechanism to classify the targets. After extracting the feature vectors from the images, they used similarity measures [17], template matching [38], correlation mechanisms [10, 14, 33, 41, 42], and nearest neighbor classifiers [3, 4, 8].

Manikandan et al. [26] evaluated the efficiency of edge detection methods such as Prewitt, Canny, and Log in automatic target recognition systems that work on data acquired from various sensors such as infrared sensors and radars.

2.1 Object Recognition

Maskall [27] used nonlinear radial basis functions and nearest neighbor classifiers for classifying armored vehicles. Kawakami et al. [12] used support vector machines to classify the cone and cylinder objects. In recent works, Yang et al. [49] and Zhou et al. [51] used deep neural networks for the classification of space objects. Xue et al. proposed new methods [43, 44] based on the deep relation graph learning to classify the real-world objects. Table 1 presents a summary of features, classifiers, and types of targets used in the literature.

To facilitate a quick recognition of space targets in ISAR images Yang et al. [49] built a system that depends on low dimensional structural features.

2.2 Ship Target Recognition

Yang et al. [47] proposed an analytical model to estimate the length of ship targets in ISAR images. They used the position of mainmast and center line's differential Doppler to estimate the length accurately. In general, least squares method, Hough, and radon transform are the dominant methods for center line. Du et al. [7] proposed a new method to extract the center line of a ship. To accurately identify the center line, the authors added a width character.

Table 1 Summary table of various target recognition mechanisms using ISAR images

Work	Features	Classifier	Targets
Li et al. [18]	Chirplet-based adaptive signal representation	Autocorrelation analysis	Aircraft, walking person data
Maskall [21]	Nonlinear radial basis functions	Nearest neighbour classifier	Armored vehicles
Kawakami et al. [10]	2D ISAR images	Support vector machines	Cone, cylinder
Xue et al. [36]	2D ISAR images	Deep relation graph learning	Real-world objects
Xue et al. [35]		Advanced region proposal networks (ARPNs)	Real-world objects
Yang et al. [40]	2D ISAR images	Deep Convolution neural networks (P-DCNN)	Space objects
Zhou et al. [42]	Deformation-robust features	Inverse compositional spatial transformer networks (IC-TANs)	Space objects

Table 2 Summary table of ship target recognition mechanisms

Author	Features	Classifier
Xie et al. [34]	Length, projected image features	Correlation coefficient
Yamamoto et al. [38]	Geometric characteristics	Pattern matching
Musman et al. [22]	Geometric characteristics	Constrained mutual subspace method
Cooke et al. [4]	3D scatterer model	Radon transform, bidirectional code
Kawahara et al. [11]	CoHOG	Random ensemble metric (REMetric)

The methods described in [1, 2, 6, 23–25, 28, 34, 35, 42, 46] focus on ship target classification. They cannot be applied directly to missiles and aerospace objects as they rely on 3D wire-frame models and geometrical characteristics of the ships such as ship length height, position of the mainmast, etc.

Bachmann et al. [2] investigated the ability of backward propagation and lateral inhibition neural networks in distinguishing the commercial/auxiliary ships and combat ships in the simulated ISAR image Database. The authors used local range-bin moments as input to the network. Rice et al. [35] proposed a classification method depending on the comparison of range-Doppler images to 3D ship reference models. Kawahara et al. [13] used CoHOG features and random ensemble classifier for ship classification. Table 2 summarizes the works done on ship target classification using ISAR images.

In [23], a multi-frame algorithm was found to efficiently take images of moving ships despite their instability due to motion, and constrained mutual subspace method (CMSM) was found to successfully identify a ship from the image taken, while the image was in motion and possibly swaying from side to side. The study is built around ISAR successfully reconstructing the image despite the incompleteness of information reflected in the image.

Musman et al. [28] introduced a system that can automatically detect ships using ISAR technology's capability to detect images. It describes how images are extracted, segmented, and classified by ISAR's multi-frame algorithm. Similar systems if fully developed can be used to automatically identify both cruise ships and military boats.

Zhao et al. [50] proposed a deep learning approach using transfer learning which is capable of handling the small data problem. An unknown class issue was addressed with the help of an output layer known as OpenMax.

2.3 Aircraft Target Recognition

Template matching is the simplest technique for target classification [11]. Template matching is a digital image processing technique that tries to compare if a small part of an image will match a template image, that is, it determines the matching between range or Doppler profiles.

In [9], the authors used Two-dimensional Fast Fourier Transform (2D-FFT) descriptors to feed backward propagation neural networks to classify the aircraft targets from ISAR images. In [10], authors applied two different correlation filters on one-dimensional short wavelength radar range profiles used for aircraft target identification. Both et al. [3] reported the performance of recognition system using geometrical and Hu moments, shape features, and quantized energy strips. They compared the accuracy of the recognition system on nearest neighbor classifier and neural network and concluded that neural network classifier performed better in their experimental analysis.

Zhang et al. [38] followed a learning-from-examples approach to construct recognition models. They used four features global orientation, vectors of persistent scatterers, Euclidean distance of vector of persistent scatterers, and local orientation vector of persistent scatterers to construct structural models of the objects for target recognition.

Li et al. [22] applied chirplet-based adaptive signal representation for the joint time–frequency localization of the signals for the target classification. Table 3 summarizes the works done in aircraft target recognition from ISAR imagery.

The authors of [16, 18, 19] developed enhanced versions of shape matrices for a more accurate two-dimensional representation of the targets.

In recent works [45, 48, 52], the researchers tried to apply Convolution Neural Networks (CNN) to deal with automatic classification problems. Other recent works can be seen in [5, 31, 50]

Table 3 Summary table of aircraft target recognition mechanisms

Author	Features	Classifier
Hudson et al. [8]	1D Short wavelength radar range profiles	Correlation mechanism
Gao et al. [7]	Two dimensional fast fourier transform (2D-FFT)	Backpropagation neural networks
Botha et al. [2]	Geometrical moments, Hu moments, shape features, quantized energy strips	Neural networks, Nearest neighbor classifier
Botha et al. [3]	1D down range profiles 2D ISAR images	Nearest neighbor classifier
Ning et al. [23]	Log-spiral transform	Multi-layer feedforward neural network classifier
Fulin et al. [6]	Fourier and wavelet transform coefficients	Nearest neighbor classifier
Kumar et al. [16]	Fourier and wavelet transform coefficients	Neural network classifier
Kondaveeti et al. [14]	SIFT features	LIBLINEAR
Kishan et al. [13]	Shape matrices	Nearest neighbour classifier
Kondaveeti et al. [15]	Shape matrices	Nearest neighbour classifier
Vatsavayi et al. [33]	Shape matrices	Nearest neighbour classifier
Kim et al. [12]	2D polar images	Nearest neighbour classifier
Park et al. [27]	2D fourier transformed polar images	Nearest neighbour Cclassifier

3 Conclusion

These related works dealing mostly with Inverse Synthetic Aperture Radar (ISAR) image classification have been reviewed because of the relevance of their importance to the topic of ISAR image classification. The considered literature and the theories in them could be used to understand the capabilities and limitations of the existing algorithms and to develop new algorithms to suit image classification systems that could be used to classify and recognize images of ships, aircraft, and space objects.

References

1. Maki A, Fukui K, Kawawada Y, Kiyu M (2002) Automatic ship identification in ISAR imagery: an on-line system using CMSM. In: Proceedings of the 2002 IEEE radar conference. pp 206–211. IEEE.
2. Bachmann C, Musman S, Schultz A (1992) Lateral inhibition neural networks for classification of simulated radar imagery. In: IEEE international joint conference on neural networks (6th IJCNN'92), vol 2, pp 115–120

3. Botha E (1994) Classification of aerospace targets using super-resolution ISAR images. In: Proceedings: South African Symposium on communications and signal processing. pp 138–145
4. Botha EC, Barnard E, Barnard CJ (1996) Feature-based classification of aerospace radar targets using neural networks. *Neural Netw* 9(1):129–142
5. Cao TT, Rosenberg L (2022) An improved clean algorithm for isar. In: 2022 IEEE radar conference (RadarConf22). IEEE, pp 1–6
6. Cooke T, Martorella M, Haywood B, Gibbins D (2006) Use of 3D ship scatterer models from ISAR image sequences for target recognition. *Digit Signal Process: Rev J* 16(5):523–532
7. Lin-lin D, Yu-lin X, Zeng-ping C (2010) A new algorithm for ship centerline extraction in isar image. In: 2010 2nd international conference on advanced computer control, vol 2. pp 213–216
8. Fulin S, Li D, Ni L, Huadong S (2004) Feature extraction and selection based on ATR of ISAR image. In: Proceedings 7th international conference on signal processing, 2004. Proceedings. ICSP '04. 2004
9. Gao X, Liu Y (1993) BP nets applied to ISAR object recognition. In: Proceedings of TENCON'93. IEEE region 10 international conference on computers, communications and automation. vol 45. IEEE, Beijing, China, pp S–102
10. Hudson S, Demetri P (1993) Correlation filters for aircraft identification from Radar range profiles. *IEEE Trans Aerosp Electron Syst* 29(3):741–748
11. Jain A, Duin R, Mao J (2000) Statistical pattern recognition: A review. *IEEE Trans Pattern Anal Mach Intell* 22(1):4–37
12. Kawakami K, Hidetoshi Tanaka KY (2004) 3D object recognition using ISAR image. In: SICE annual conference. pp 673–677
13. Kawahara T, Toda S, Mikami A, Tanabe M (2012) Automatic ship recognition robust against aspect angle changes and occlusions. In: 2012 IEEE Radar conference. pp 0864–0869
14. Kim K, Seo D, Kim H (2005) Efficient classification of ISAR images. *IEEE Trans Antennas Propagat* 53(5):1611–1621
15. Kondaveeti HK, Vatsavayi VK (2016) Robust isar image classification using abridged shape matrices. In: 2016 international conference on emerging trends in engineering, technology and science (ICETETS). pp 1–6
16. Kondaveeti HK, Vatsavayi VK (2017) Abridged shape matrix representation for the recognition of aircraft targets from 2d ISAR imagery. *Adv Comput Sci Technol* 10(5):1103. <https://doi.org/10.37622/acst/10.5.2017.1103-1122>
17. Kondaveeti HK, Vatsavayi VK (2018) Automatic target recognition from inverse synthetic aperture radar images. In: Computer vision. IGI Global, pp 2307–2332. <https://doi.org/10.4018/978-1-5225-5204-8.ch101>
18. Kondaveeti HK, Vatsavayi VK (2021) Ameliorated shape matrix representation for efficient classification of targets in isar imagery. In: Bhattacharyya S, Nayak J, Prakash KB, Naik B, Abraham A (eds) International conference on intelligent and smart computing in data analytics. Springer Singapore, Singapore, pp 183–188
19. Kondaveeti HK, Vatsavayi VK et al (2021) Automatic classification of isar images. *Des Eng* 298–314
20. Kumar BK, Prabhakar B, Suryanarayana K, Thilagavathi V, Rajagopal R (2006) Target identification using harmonic wavelet based ISAR imaging. *Eurasip J Appl Signal Process* 2006:1–13
21. Kurowska A (2016) The preliminary survey of ship recognition algorithms using ISAR images. In: Proceedings International Radar Symposium 2016-June (2016)
22. Li J, Ling H (2002) ISAR feature extraction from targets with non-rigid body motion using adaptive chirplet representation. In: IEEE Antennas and Propagation Society, AP-S International Symposium (Digest) 4:294–297
23. Maki A, Fukui K, Onoguchi K, Maeda K (2001) Isar image analysis by subspace method: automatic extraction and identification of ship profile. In: 11th international conference on image analysis and processing. pp 523–528
24. Maki A, Fukui K (2004) Ship identification in sequential ISAR imagery. *Mach Vis Appl* 15(3):149–155

25. Maki A, Fukui K, Onoguchi K, Maeda KI (2001) ISAR image analysis by subspace method: automatic extraction and identification of ship profile. In: Proceedings-11th international conference on image analysis and processing, ICIAP 2001. pp 523–528
26. Manikandan J, Venkataramani B, Jayachandran M (2007) Evaluation of edge detection techniques towards implementation of automatic target recognition. In: International conference on computational intelligence and multimedia applications (ICCIMA 2007), vol 2. pp 441–445
27. Maskall G (2002) An application of nonlinear feature extraction to the classification of isar images. In: IET conference proceedings. pp 405–408(3). <https://digital-library.theiet.org/content/conferences/10.1049/cp20020317>
28. Musman S, Kerr D, Bachmann C (1996) Automatic recognition of ISAR ship images. *IEEE Trans Aerosp Electron Syst* 32(4):1392–1404
29. Ning W, Chen W, Zhang X (2003) Automatic target recognition of ISAR object images based on neural network. In: International conference on neural networks and signal processing, 2003. Proceedings of the 2003. IEEE, Nanjing, pp 3–6
30. Otsu N (1979) A threshold selection method from gray level histograms. *IEEE Trans Syst, Man Cybern* 9:62–66
31. Pandey N, Ram SS (2022) Classification of automotive targets using inverse synthetic aperture radar images. *IEEE Trans Intell Veh*
32. Park JI, Kim KT (2010) A comparative study on ISAR imaging algorithms for radar target identification. *Prog Electromagn Res* 108:155–175. <https://doi.org/10.2528/pier10071901>
33. Park S, Jung J, Kim S, Kim K (2015) Efficient classification of ISAR images using 2d fourier transform and polar mapping. *IEEE Trans Aerosp Electron Syst* 51(3):1726–1736
34. Pastina D, Spina C (2009) Multi-feature based automatic recognition of ship targets in ISAR. *IET Radar Sonar Navig* 3(4):406–423
35. Rice F, Cooke T, Gibbins D (2006) Model based ISAR ship classification. *Digit Signal Process* 16(5):628–637. <https://doi.org/10.1016/j.dsp.2006.01.007>
36. Saidi MN, Daoudi K, Khenchaf A, Hoeltzener B, Aboutajdine D (2009) Automatic target recognition of aircraft models based on ISAR images. *Int Geosci Remote Sens Symp (IGARSS)* 4:685–688
37. Saidi MN, Toumi A, Hoeltzener B, Khenchaf A, Aboutajdine D (2009) Aircraft target recognition: a novel approach for features extraction from ISAR images. In: 2009 international radar conference “Surveillance for a safer world”, RADAR 2009
38. Zhang S, Bhanu B (1996) Automatic model construction for object recognition using isar images. In: Proceedings of 13th international conference on pattern recognition, vol 4. pp 169–173
39. Toumi A, Hoeltzener B, Khenchaf A (2007) Using watersheds segmentation on ISAR image for automatic target recognition. In: 2007 2nd Int Conf Digit Inf Manag, ICDIM 1:285–290
40. Vatsavayi VK, Kondaveeti HK (2018) Efficient isar image classification using mecm representation. *J King Saud Univ-Comput Inf Sci* 30(3):356–372. <http://www.sciencedirect.com/science/article/pii/S1319157816300490>
41. Wu H, Li G, Zhou J (2019) High-resolution range profiles recognition based on SAR/ISAR images. In: Proceedings of 2019 IEEE 3rd advanced information management, communicates, electronic and automation control conference, IMCEC 2019. pp 1514–1518
42. Xie SD, Pan M, Li D (2019) Robust method for ship recognition based on ISAR imaging using 3D model. *J Eng* 2019(20):6777–6780
43. Xue B, Tong N (2019) DIOD: fast and efficient weakly semi-supervised deep complex ISAR object detection. *IEEE Trans Cybern* 49(11):3991–4003
44. Xue B, Tong N (2019) Real-world ISAR object recognition and relation discovery using deep relation graph learning. *IEEE Access* 7:43906–43914
45. Xue R, Bai X, Cao X, Zhou F (2022) Sequential isar target classification based on hybrid trans-former. *IEEE Trans Geosci Remote Sens* 60:1–11
46. Yamamoto K, Iwamoto M, Kirimoto T (2001) A new algorithm to calculate the reference image of ship targets for ATR using ISAR. *Ocean Conf Rec (IEEE)* 4:2601–2607

47. Yang H, Su F, Gao J (2014) The length estimation of ship targets in isar images. In: 2014 12th international conference on signal processing (ICSP). pp 1910–1913
48. Yang H, Zhang Y, Yin C, Ding W (2022) Ultra-lightweight cnn design based on neural architecture search and knowledge distillation: a novel method to build the automatic recognition model of space target isar images. *Def Technol* 18(6):1073–1095
49. Yang H, Zhang Y, Ding W (2020) Multiple heterogeneous P-DCNNs ensemble with stacking algorithm: a novel recognition method of space target ISAR images under the condition of small sample set. *IEEE Access* 8: 75543–75570
50. Zhao W, Heng A, Rosenberg L, Nguyen ST, Hamey L, Orgun M (2022) Isar ship classification using transfer learning. In: 2022 IEEE radar conference (RadarConf22). IEEE, pp 1–6
51. Zhou X, Bai X (2019) Robust ISAR target recognition based on IC-STNs. In: 2019 6th Asia-Pacific conference on synthetic aperture radar, APSAR 2019. pp 1–5
52. Zhou X, Bai X, Wang L, Zhou F (2022) Robust isar target recognition based on adrisarnet. *IEEE Trans Aerosp Electron Syst*

A Survey Study and Comparison of Drones Communication Systems



Charalampos Koulouris, Piromalis Dimitrios, Izzat Al-Darraj, Georgios Tsaramirsis, Alaa Omar Khadidos, Adil Omar Khadidos, and Panagiotis Papageorgas

Abstract Drones have become more popular in recent years and this technology has dramatically advanced. Drones are starting to become essential tools in many operations such as surveillance, delivery, and more. A communication system is an essential challenge in drones that determines the drone's capabilities of guiding, positioning, controlling, and transmission of information remotely. This paper introduces the current drone Radio Frequency (RF) communication technologies by specifying and explaining their features. These technologies represent IoT devices, Satellites, Global System for Mobile (GSM), Automatic Dependent Surveillance-Broadcast (ADS-B), Remote control, Bluetooth, WiFi, and Global Navigation Satellite System (GNSS). Furthermore, a comparison of ability in working in various environments is provided between the RF communication systems such as urban areas, remote areas, sea, and high altitude. It is found that each RF communication system is useful for a different scenario. Thus, a drone has to use a combination of RF communication systems in order to be remotely effectively communicated and guided.

C. Koulouris · P. Dimitrios

Industrial Design and Production Engineering Department, University of West Attica, 12244 Egaleo, Greece

I. Al-Darraj (✉)

Automated Manufacturing Department, Al-khwarizmi College of Engineering, University of Baghdad, Baghdad, Iraq

e-mail: izzat.a@kecbu.uobaghdad.edu.iq

G. Tsaramirsis

Abu Dhabi Womens's College, Higher Colleges of Technology, Abu Dhabi, UAE

A. O. Khadidos

Department of Information Systems, Faculty of Computing and IT, King Abulaziz University, Jeddah, Saudi Arabia

A. O. Khadidos

Department of Information Technology, Faculty of Computing and IT, King Abulaziz University, Jeddah, Saudi Arabia

P. Papageorgas

Department of Electrical and Electronics Engineering, University of West Attica, 12244 Egaleo, Greece

Keywords Drones · RF communications · IoT devices · Global system for mobile · Automatic dependent surveillance-broadcast · Remote control

1 Introduction

Drones are considered as an essential aerial, land, water, and underwater equipment that has been utilized widely in our daily purposes ranging from entertainment to industry. Unmanned Aerial Vehicles (UAVs), are the most popular type of “Everyday” drones, and are used for taking photos, carrying medical equipment in emergency health situations, monitoring for security purposes, and so on. Drones are becoming, day after day, more important for our life and are applied as necessary tools for people, companies, and governments. Drones were used a few decades ago by militaries to spy on enemies and later to carry small rockets to hit targets [1]. These military drones had and still have first-person view capabilities such that militaries remotely can pilot them from a thousand miles away. This first-person view capability was achieved mostly with satellite connections. Militaries are able to use satellite constellations using big satellite modems inside drones to offer high bandwidth connectivity on every point of the earth and at high altitudes. In the last decade, a new type of drone are used by civilians to take photos and pilot them for fun [1]. These later types of civilian drones can be of various types based on their physical properties such as shape, number of engines, frame, and other characteristics [2, 3]. Some of these are bi-copters, tri-copters, quad-copters, hex-copters, quad-copters, and so on, depending on the number of engines [2]. Figure 1 shows the design of a quadcopter. An aeroplane-looking-type drone is shown in Fig. 2.

Quadcopters and hex-copters are common among civilians because they are more stable to guide, hover over a specific area very well, can make a vertical takeoff and landing, can be used inside urban areas to carry things and make deliveries, take photos and videos, and many other applications [4]. Civilian drones can even be manufactured by the process of 3D printing in maker spaces [5]. Quadcopters and hex-copters have only one drawback, they consume a lot of energy because they have many copter motors and don’t have much air drag since their body is not an aerodynamic drag design. Also, drones were limited by battery performance [6]. Advancements in battery technology have enhanced its lifetime [7]. Hence, drones now can fly twice the time with new battery technology and smart energy-consuming software. Aeroplane-shaped drones are able to fly for many hours and in large distances, they can carry a camera, Internet of Things (IoT) devices, Communications systems, and many other devices [8, 9]. Drone Radio Frequency (RF) communication systems are as important as the control system of the drone itself. Without an appropriate RF communications system, the drone is not able to be guided or position itself in the sky through. There are a variety of RF communications systems, traditional remote control with or without first-person view, Global System for Mobile (GSM) communications with 4G/5G, satellite communications, Automatic Dependent Surveillance-Broadcast (ADS-B), and IoT devices. In the next sections, we will examine all of

Fig. 1 Quadcopter civilian drone

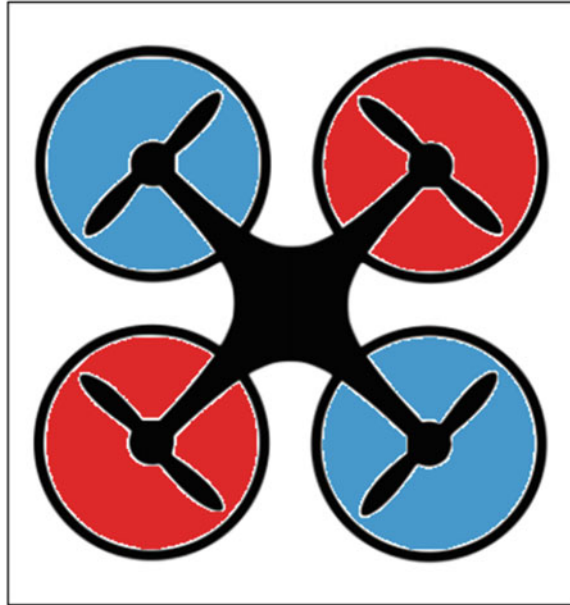


Fig. 2 Aeroplane shape drone



them one by one. It is essential to establish a legal and technical framework which guarantees the flight of drones safely by the interested users. Consequently, it is important to find a solution that enables the use of drones effectively. One of the solutions to this issue is to use a combination of RF communication systems. In this paper, we examine the different RF communications systems available that can be used to communicate with the drone, in order to get information about its drone and guide it in a perfect way without problems.

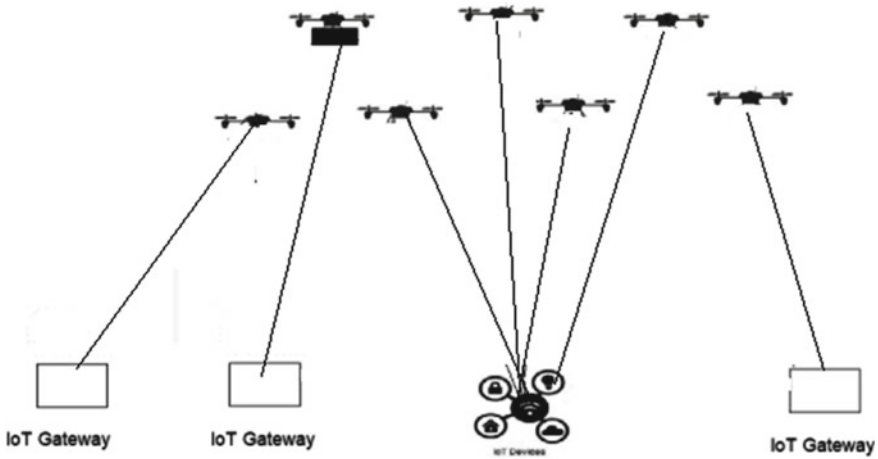


Fig. 3 An IoT drone connectivity model

2 Drone RF Communication Systems

2.1 IoT Devices

IoT devices are becoming more and more useful that can be used with a drone. In spite of the fact that IoT devices shown in Fig. 3 can transmit little information; They are a very good option in remote areas especially when the drone wants to save battery energy.

Long-range IoT devices, like LoRa [10], can transfer information with very little energy up to 10 km and more. IoT devices in drones can be used to both send and receive information. They are applied to send information about the drone's location, name, and unique electronics ID. On the other hand, information can be received through IoT devices in order to collect IoT data from devices on earth or other drones. There is also a possibility to use IoT devices through satellites. This technology of integrating IoT devices with satellites is quite new which can produce a commercial modem of the same size of a laptop. Thus, currently, it is not possible to use this new technology, due to size issue, for a commercial drone. But, this issue may be soon solved by using the swarm IoT M138 modem which has the ability to be connected with a Swarm of satellites in network approach [11].

2.2 Satellites

Satellite connections for drones are widely used to control them. Military drones are using big satellite modems to connect to satellite constellations, as shown in

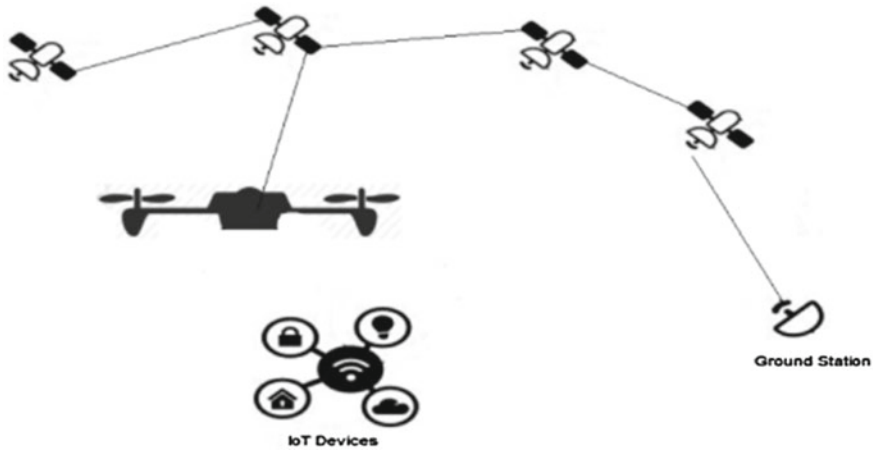


Fig. 4 A drone communication with satellites and possible communication with IoT devices on earth and other RF systems

Fig. 4. This configuration offers a very high bandwidth with very good first-person view capabilities to users. A small factor satellite modem which can be used in small drones is the Iridium 9603 [12, 13]. Iridium 9603 is a machine-to-machine communication satellite modem that provides a small amount of data transmitted. Nevertheless, it is still enough to give basic guiding commands to a drone and transmit its electronic ID.

2.3 GSM

GSM RF communications are the most advanced telecommunications systems currently available in the market. They offer high bandwidth internet connection and many other capabilities. The GSM, shown in Fig. 5, is the 4G/5G version of RF communications that can be used in almost all earth locations with human activity.

Drones equipped with a 4G GSM modem can be guided and offer an almost first-person view capability. The 5G GSM modem has very high bandwidth communication, but it is limited in range (1–2 km). It can be used for very high bandwidth internet connection even for laptops in houses. 5G GSM modem also can offer a possible IoT device integration. The next generation of GSM modem, the 6G, will possibly offer more IoT and drone IoT capabilities. It is estimated that the drones can participate in the 6G network and act as ad hoc IoT hubs [14]. 5G services recently deployed in all central cities are working in a spectrum called the C-band [15], causing problems to the aviation industry because of interference with the radio aircraft altimeters. As a result, the airlines warned authorities to stop the deployment of 5G close to the

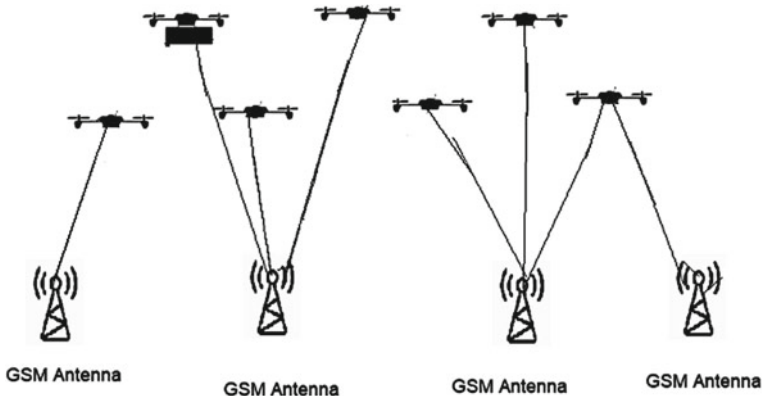


Fig. 5 A GSM connectivity model for drones

airports until the Federal Aviation Administration (FAA) determines which radio altimeters can be used in a 5G-covered area [15].

2.4 ADS-B

ADS-B uses a GPS receiver to get the position of the aircraft and then broadcast its position. Air Traffic Control (ATC) uses ADS-B to receive information about an aircraft's identity and its position. So, they can guide the aircraft, especially inside populated aircraft areas and airports. Aircraft on the other hand can receive information about surrounding aircraft and weather information. There are two types of ADS-B, ADS-B IN which an aircraft receives information, and ADS-B OUT which an aircraft transmits information. ADS-B is operating at 1090 MHz frequency [16]. Some drone manufacturers have included ADS-B in their drones, especially for drones over 250 g, though they use only ADS-B IN to receive information about nearby aircraft and not ADS-B OUT to transmit information. It is not yet mandatory to include an ADS-B IN in a drone and it is prohibited to include an ADS-B OUT in a drone in the USA.

2.5 Remote Control

Remote control is the most common form of RF communication with a drone. Users holding a joystick equipped with an antenna can control their drone up to 50 km with most commercial remote controllers like DJI drones [17] providing up to 4 km range and operating in 2.4–5.85 GHz. With remote controls, drone pilots can give guiding commands and get a First-Person View (FPV) video from the camera of their

drone, while the remote controllers are usually connected to a smartphone. Therefore, remote control is very useful for the average drone user, but, is not a solution for professional drones, since it is limited by range, and it can be used only by the drone operator and not by any other third party.

2.6 *Bluetooth and WiFi*

Drones equipped with a small computer like Raspberry Pi [18] can carry wifi network cards and Bluetooth modem cards [19]. So, they can be connected to a mobile or a computer in the network through wifi to update their software through the internet. FAA in April 2021 requested all drones above 0.55 pounds to transmit their remote ID via radio frequency, like Bluetooth or wifi [20]. Before remote ID drones had the requirement to carry license plates, but drone ID license plate stickers are not able to read in distance, while the drone is flying [14]. Bluetooth has also been used for communication between drones, a system called BloothAir [21]. Its Bluetooth cannot be received in distance, since it is limited in the range of 10 m [22].

A possible scenario of drone connectivity, shown in Fig. 6, can be applied to receive signals from satellites, GSM networks, GPS, and IoT gateways and to collect IoT signals acting as ad hoc devices in the 6G network. The drone ID can be transmitted through all these networks in combination.

2.7 *GNSS*

GPS, Glonass, and Galileo are a special type of RF system and are widely used by drones. In fact, they are an essential component for knowing their position and navigation in a terrain. Satellite position systems are so important, that drones almost cannot fly without them in a non-line-of-sight situation. Especially for many applications for geo-referencing [23], autonomous navigation and first-person view navigation, it is impossible to do them without GNSS. Geo-referencing is done with GPS/Glnass and is used by commercial drones to determine if they are able to fly in a restricted area [23]. Commercial drones are restricted to fly close to airports and users are not able to use them in all restricted areas [1]. Controlling a drone with Proportional Differential Derivative (PID) controllers and stabilizing is also done with the help of GPS/Glonass [24, 25]. One special function of the GNSS is to synchronize the clocks of the drones, and this is very crucial for computer systems, because they synchronize the exchange of messages and information.

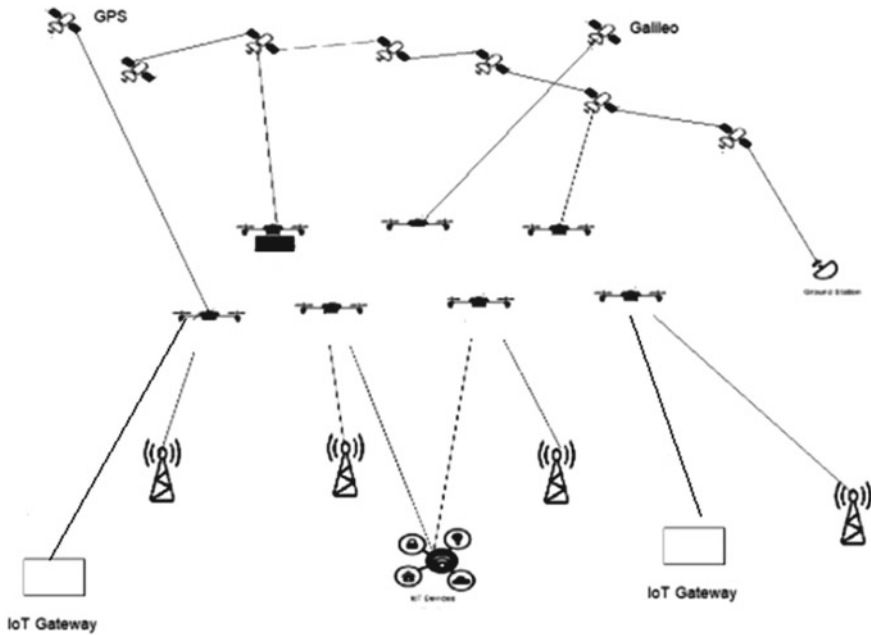


Fig. 6 Utilizing drones in parallel, IoT devices, satellites, and LTE

3 Discussion

Due to the limitations of all the RF systems; a single current RF system is not possible to provide full RF drone coverage and provide a Drone ID solution. Satellite communications are relatively expensive and most of them have big modems that cannot be used in all drones. Militaries use satellite first-person view communications but for big drones and with very high budgets. Iridium 9603 is the best current satellite solution, but it is also expensive for the average user. In addition, it cannot provide high bandwidth.

IoT devices, especially LoRa, are the best solution for long-range IoT communications. The main drawback of IoT devices is the very low bandwidth as in Iridium 9603 [12, 13]. In addition, IoT devices offer very little data. Hence, IoT devices and Iridium 9603 cannot be used to continuously guide a drone. They only can be applied to give a command if the IoT device has a duplex asynchronous communication. The most promising IoT device currently offering suitable satellite communication for a drone is the swarm M138 modem [11]. Practically, it is a very new device, the swarm M138 modem is not yet tested in a drone up to now. GSM has a long range and internet data which can be used outside cities too. Thus, it is the best solution in urban areas, especially the ones that use 4G. GSM is applied widely by operators of small and large drones to give commands and for guiding with first-person view drone capabilities. ADS-B IN/OUT is a very good solution for aircraft and it will

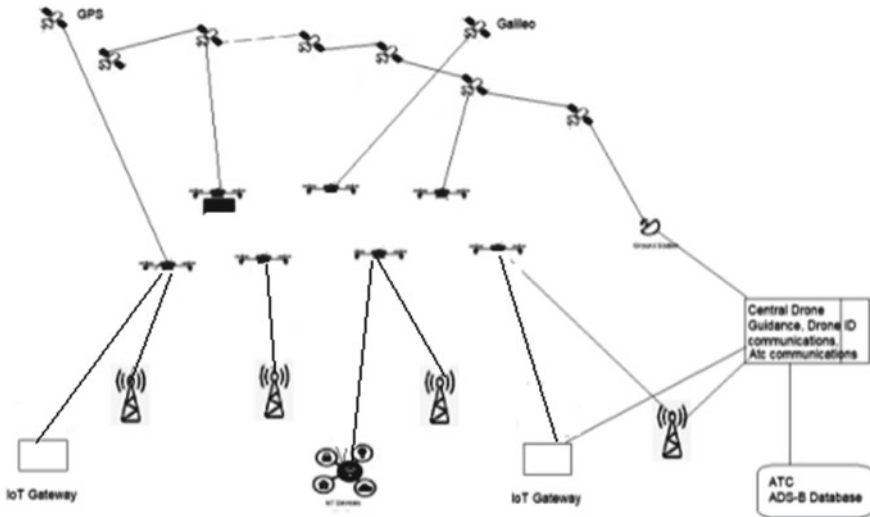


Fig. 7 A complete RF communications scenario

be included in the NEXTGEN project by federal aviation authorities [15]. ADS-B offers very good information about aircraft position and identity. Moreover, ADS-B can guide the aircraft by aircraft traffic control. Though ADS-B is not yet used in drones, only one manufacturer (DJI) includes “ADS-B IN” in their drones [17]. Hence, drones receive information about big aircraft traffic. ADS-B is not capable to guide remotely an aircraft since it is not designed to be a first-person view technology and is also limited by range. Finally, traditional remote control is a very good option for first-person view drone guidance, especially for amateur drone operators. However, traditional remote control is limited by the range. The reason for range limitation is due to either RF systems transfer signals up to 50 km, or RF signals cannot be propagated further enough because of earth curvature and natural obstacles. A complete scenario for a drone RF Communications system that offers IoT connectivity, satellite connectivity, GSM, GPS, and ADS-B is presented in Fig. 7.

Figure 7 shows a possible solution to communicate with drones and guide them in all scenarios and terrains. It includes Satellite communications, LTE for 4G/5G in urban areas, IoT devices in urban areas for both transmitting and receiving messages and commands, remote control, drone electronic ID, and ATC.

4 Conclusion

This paper covered a number of RF drone systems. Based on this study, we can conclude that due to the limitations of all the RF systems; a single current RF system is not possible to provide full RF drone coverage. Hence, different systems are

recommended based on the specific drone properties and operational environment. In general, satellite communication can be expensive and require big modems. Iridium 9603 is the best current satellite solution, but it is also expensive for the average user. In addition, it cannot provide high bandwidth. GSM can be used inside Urban areas where 4G/5G is reachable. IoT devices can be applied to transmit commands through earth-based IoT devices and IoT satellite modems (LoRa) when the drone needs to save power. ADS-B IN and/or ADS-B OUT is used to communicate with larger aircraft to exchange information with aircraft and to avoid collision with them. Satellite communications, such as iridium 9603 or other bigger satellite modems, can be used in high altitudes and oceans where the other RF systems are not useful or reachable. The main limitation of this work is that the electronic identification of drones was not covered in length as this focused more on communications. As future work, we will focus on various technologies for electronic identification of drones.

References

1. Mohammed F, Idries A, Mohamed N, Al-Jaroodi J, Jawhar I (2014) UAVs for smart cities: opportunities and challenges. In: 2014 international conference on unmanned aircraft systems (ICUAS), Orlando, FL, USA, May 27–30, 2014
2. Van der Geer J, Hanraads JAJ, Lupton RA (2000) The art of writing a scientific article. *J Sci Commun* 163:51–59
3. Kardasz P, Doskocz J, Hejduk M, Wiejkut PÅ, Zarzycki H (2016) Drones and possibilities of their using. *J Civil Environ Eng* 6:1–7
4. Elmeseiry N, Alshaer N, Ismail T (2021) A detailed survey and future directions of unmanned aerial vehicles (UAVs) with potential applications. *Aerospace* 8:363. <https://doi.org/10.3390/aerospace8120363>
5. Al-Darraj I, Derbali M, Tsaramirsis G (2021) Tilting-rotors quadcopters: a new dynamics modelling and simulation based on the Newton-Euler method with lead compensator control. In: 2021 8th international conference on computing for sustainable global development (INDIACom), 2021, pp 363–369. <https://doi.org/10.1109/INDIACom51348.2021.00063>
6. Kantaros A, Diegel O, Piromalis D, Tsaramirsis G, Khadidos AO, Khadidos AO, Khan FQ, Jan S (2022) 3D printing: making an innovative technology widely accessible through makerspaces and outsourced services. *Mater Today Proc* 49(Part 7):2712–2723. ISSN 2214-7853. <https://doi.org/10.1016/j.matpr.2021.09.074>
7. Banerjee A, Roychoudhury A (2017) Future of mobile software for smartphones and drones: energy and performance. In: IEEE/ACM 4th international conference on mobile software engineering and systems
8. Rimpas D, Kaminaris SD, Aldarraj I, Piromalis D, Vokas G, Papageorgas PG, Tsaramirsis G (2021) Energy management and storage systems on electric vehicles: a comprehensive review. *Mater Today Proc*
9. Al-Darraj I, Derbali M, Jerbi H, Khan FQ, Jan S et al (2021) A technical framework for selection of autonomous uav navigation technologies and sensors. *Comput Mater Contin* 68(2):2771–2790
10. Al-Darraj I, Piromalis D, Kakei AA, Khan FQ, Stojmenovic M, Tsaramirsis G, Papageorgas PG (2021) Adaptive robust controller design-based RBF neural network for aerial robot arm model. *Electronics* 10(7):831. <https://doi.org/10.3390/electronics10070831>. Accessed 16 January 2022
11. <https://www.bis.doc.gov/index.php/documents/>. Accessed 16 January 2022

12. Sarker VK, Pena Queralt J, Gia TN, Tenhunen H, Westerlund T (2019) A survey on LoRa for IoT: integrating edge computing. In: Fourth international conference on fog and mobile edge computing (FMEC). Published in IEEE
13. <https://www.iridium.com/products/iridium-9603/>. Accessed 16 January 2022
14. Ehresmann M, Baumann J-P, Behnke A, Franz J, Friedrich L, Gaessler B, Galla D, Grabi F, Hiessl R, Koller M, Kumpf P, Mueller M, Papanikolaou A, Rieser J, Schäfer F, Schoeneich V, Seiler H, Siedorf M, Starlinger V, Laufer R (2016) Micro return Capsule 2- REXUS experiment results
15. <https://swarm.space/swarm-m138-modem/>. Accessed 16 January 2022
16. <https://www.faa.gov/5g>. Accessed 21 January 2022
17. Mozaffari M, Lin X, Hayes S (2021) Towards 6G with connected sky: UAVs and beyond
18. <https://www.dji.com/>. Accessed 16 January 2022
19. <https://www.raspberrypi.org/>. Accessed 16 January 2022
20. Gharibi M, Boutaba R, Waslander SL (2016) Internet of drones. IEEE
21. Swinney CJ, Woods (2021) RF detection and classification of unmanned aerial vehicles in environments with wireless interference. In: International conference on unmanned aircraft systems (ICUAS)
22. https://www.faa.gov/uas/getting_started/remote_id/. Accessed 16 January 2022
23. Li K, Lu N, Zheng J, Zhang P, Ni W, Tovar E (2021) BloothAir: a secure aerial relay system using bluetooth
24. Tsira V, Nandi G (2014) Bluetooth technology: security issues and its prevention. *Int J Comput Technol Appl* 5(5):1833–1837; Jacobs IS, Bean CP (1963) Fine particles, thin films and exchange anisotropy. In: Rado GT, Suhl H (eds) *Magnetism*, vol III. Academic, New York, pp 271–350
25. Aziz D, Algburi S, Alani S, Mahmood S (2020) Design and implementation of GPS based quadcopter control system, IMDC-SDSP, EAI. <https://doi.org/10.4108/eai.28-6-2020.2297931>

Studying the Optoelectronic Properties of NaSnCl₃ Solar PV Material: A Step Towards Sustainable Development



Shikha Sharma, Hansraj Karwasara, Karina Khan, Mamta Soni, Amit Soni, and Jagrati Sahariya

Abstract The halide perovskites appear as new-generation semiconductors in the last few years. The goal of the current work is to govern the optoelectronic characteristics of NaSnCl₃ by using DFT which is incorporated in Wien2k code. The Tran-Blaha modified Becke Johnson exchange–correlation potential (TB-mBJ) is used for all simulation work in order to determine the optoelectronic properties. The compound band gap value of 0.91 eV demonstrates its usefulness in the field of multi-junction solar cells. Low reflection and high absorption coefficients revealed by an investigation of optical properties demonstrate, this material’s suitability for optoelectronic applications.

Keywords Metal Halide Perovskites · Optoelectronic properties · Density functional theory

1 Introduction

One of the key scientific developments in the realm of photovoltaic technology is the study of solar cells using organo-metal perovskite as a light absorber. Researcher’s interest in metal halide perovskite materials has grown significantly in the last few years due to their remarkable optoelectronic properties, which include a wide spectrum of absorption, improved optical absorption, an adaptive band gap, enlarge charge diffusion, and good charge carrier mobility [1, 2]. Furthermore, metal halide

S. Sharma · H. Karwasara · K. Khan
Department of Physics, Manipal University, Jaipur 303007, Rajasthan, India

M. Soni
Faculty of Management & Commerce, Manipal University, Jaipur 303007, Rajasthan, India

A. Soni (✉)
Department of Electrical Engineering, Manipal University, Jaipur 303007, Rajasthan, India
e-mail: amitsoni_17@yahoo.co.in

J. Sahariya
Department of Physics, NIT, Srinagar 246174, Uttarakhand, India

perovskites are inexpensive and widely accessible on the planet. Clean and sustainable energy sources have gained a lot of attention because of environmental pollution and the global energy problem. In recent years, ternary halide perovskites, also known as ABX_3 perovskites, have emerged as new-generation semiconductors [3–6]. These are well known for having high power conversion efficiencies, making them suitable for a number of optoelectronic applications, such as solar cells, photodetectors, LED, lasers sensors, and PV detectors [8–11] due to their superior structural, electronic, photovoltaic, and charge transport capabilities. The PV cells also have exceptional optoelectronic characteristics, including an adjustable band gap, strong optical absorption, a broad absorption spectrum, low carrier effective masses, a controlling point defect, and long charge diffusion lengths [1, 12]. Idrissi et al. [13] used the Quantum Espresso software to study the structural and electrical characteristics of the solar perovskites photovoltaic material $CsPbCl_3$, $CsSnCl_3$, and $CsGeCl_3$. For $ASnX_3$ where A represents Rb and K, while X represents Cl and Br, Khan et al. [14] investigated its properties through TB-mBJ. Krishnamoorthy et al. [15] performed DFT calculations for lead-free halide perovskite compounds to show their potential candidacy for photovoltaic applications. Young and Rondinelli [16] studied the bromide- and iodide-based perovskite compounds to determine superior arrangements and preferred rotation patterns. In order to investigate the potential of inorganic and hybrid perovskite compounds as prospective solar cell absorbers, Travis et al. [17] evaluated stability factors for these compounds. The investigation of the photovoltaic, piezoelectric, and magnetic behavior of solar perovskite compounds by Korbel et al. [18] demonstrates the exceptional competency of these compounds. Gou et al. [19] to explore the optical characteristics of perovskite compound $CsSnI_3$ by first principle theory have used first principle theory. In order to achieve the high efficient solar cell applications, Jung et al. [20] investigated the optoelectronic characteristics of Pb-free perovskite (Rb, Cs) SnI_3 . First principle studies for (K, Rb) $SnCl_3$ inorganic Pb-free metal halide perovskite compounds have been carried out by Mao et al. [21]. By the DFT-based CASTEP software, Islam et al. [22] investigated the optoelectronic, elastic, and electrical characteristics of $CsSnCl_3$ under hydrostatic pressure. The non-toxic $CsSnCl_3$ perovskite has ductility, according to the mechanical characteristics investigation by Roknuzzaman et al. [23]. Huang et al. [24] determined the band structure and binding energies of $CsSnY_3$, (Y=I, Cl, and Br) perovskites.

2 Computational Details

This study utilized the developed FP-LAPW method to solve the basis set system and DFT based on the Wien2k code for the ternary inorganic halide perovskite $NaSnCl_3$. This depends on the calculation of photoelectron properties [25, 26]. To obtain the accuracy of the results we solved the exchange–correlation term of the Kohn–Sham equation using the TB-mBJ exchange–correlation function [27]. This work includes a grid of 1000 k points to get the accuracy of the results. Other input values such as $R_{MT} \times K_{max} = 7$ were chosen as the energy cutoff, where K_{max} is the maximum

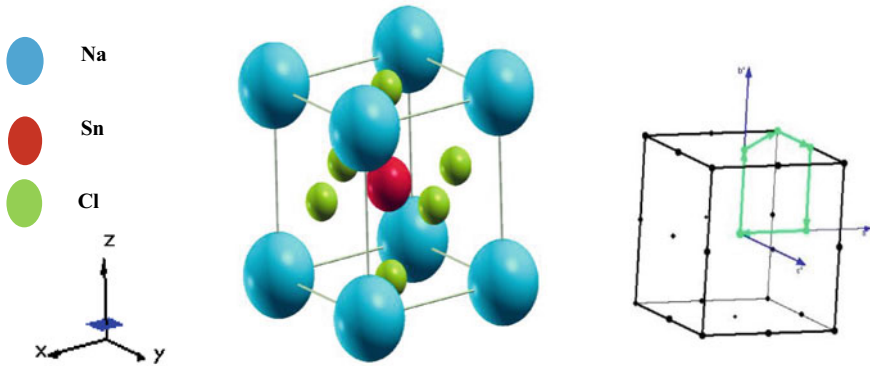


Fig. 1 Crystal structure and Brillouin zone of NaSnCl₃

value of the reciprocal lattice vectors employed in the plane wave expansion. The l_{\max} and G_{\max} will take 10 and 12, respectively. We consider the energy value for the separation of core and valence states is -6Ry. The size of the basis sets used in the calculations is controlled by these parameters. The lattice constant of NaSnCl₃ having space group (Pm3m) and no. 221 taken as $a = b = c = 5.82 \text{ \AA}$ with Wyckoff positions Na (0, 0, 0); Sn (1/2, 1/2, 1/2); Cl (1/2, 1/2, 0) which is shown in Fig. 1.

3 Results and Discussion

The basic properties of any material basically depend on its electron structure. The TB-mBJ potential was used to manipulate the NaSnCl₃ electronics properties. The compound structure and its Brillouin zone are shown in Fig. 1. We computed a band gap of NaSnCl₃ 0.91 eV, which represents its semiconductor nature. The band gap value is observed from the NaSnCl₃ band structure. But to elaborate its detailed interpretation, we examined the DOS spectra from the TB-mBJ potential shown in Fig. 2. DOS clearly represents that the valence band lies below the Fermi level (0 eV). From Fig. 2, we found that, from the energy value -4 to 6 electron volts, three bands are formed. The first band is core band is lies from -4 to 2.7 eV, the second band is valance band from -2.7 to 0 eV, and the third band is conduction band from 0.94 to 6 eV. The main contribution in the band gap region comes from the emerging from the mixing of “p” state of Cl-atom and Na-atom, while, in the conduction region, the mixture is with the “s” state of Na-atoms and “p” state of Sn-atom. The band gap of various metal halide perovskite compounds is compared in Table 1.

Optical properties are one of the crucial properties to demonstrate the effectiveness of compounds in optoelectronic devices as optical variables result from the movement and recombination of electrons after photons enter the material. Figure 3a-e shows a curve that was plotted for the dielectric tensor, absorption, reflection, and refraction.

Fig. 2 Density of state (DOS) of NaSnCl₃

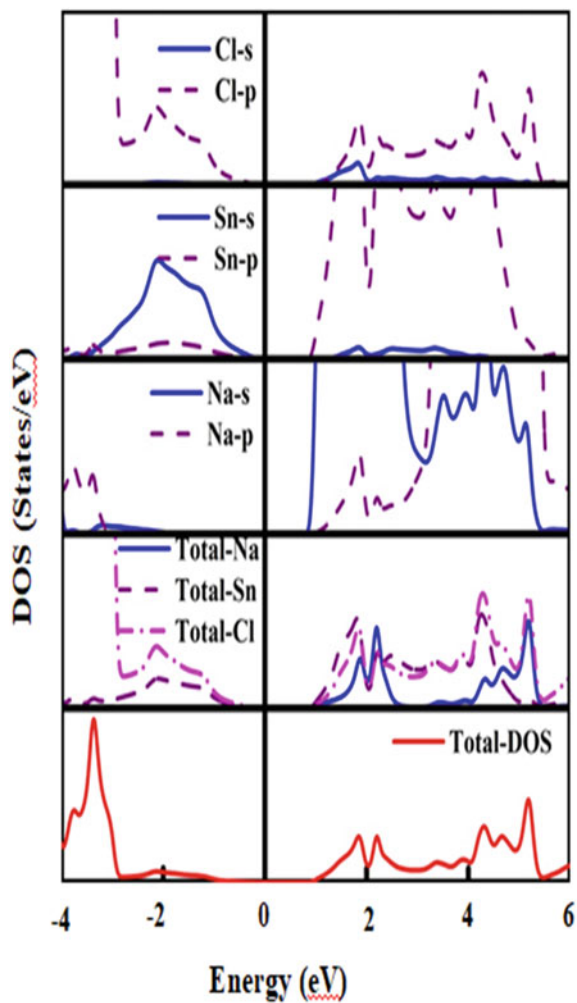


Table 1 The band gap for various metal halide perovskite compounds

Compound	Band gap (eV)
CsSnCl ₃	1.9 ¹⁴
CsPbCl ₃	2.6 ¹⁴
CsGeCl ₃	1.95 ¹⁴
CsSnBr ₃	1.6 ²⁵
CsSnI ₃	1.35 ²⁵
NaSnCl ₃	0.91 (our work)

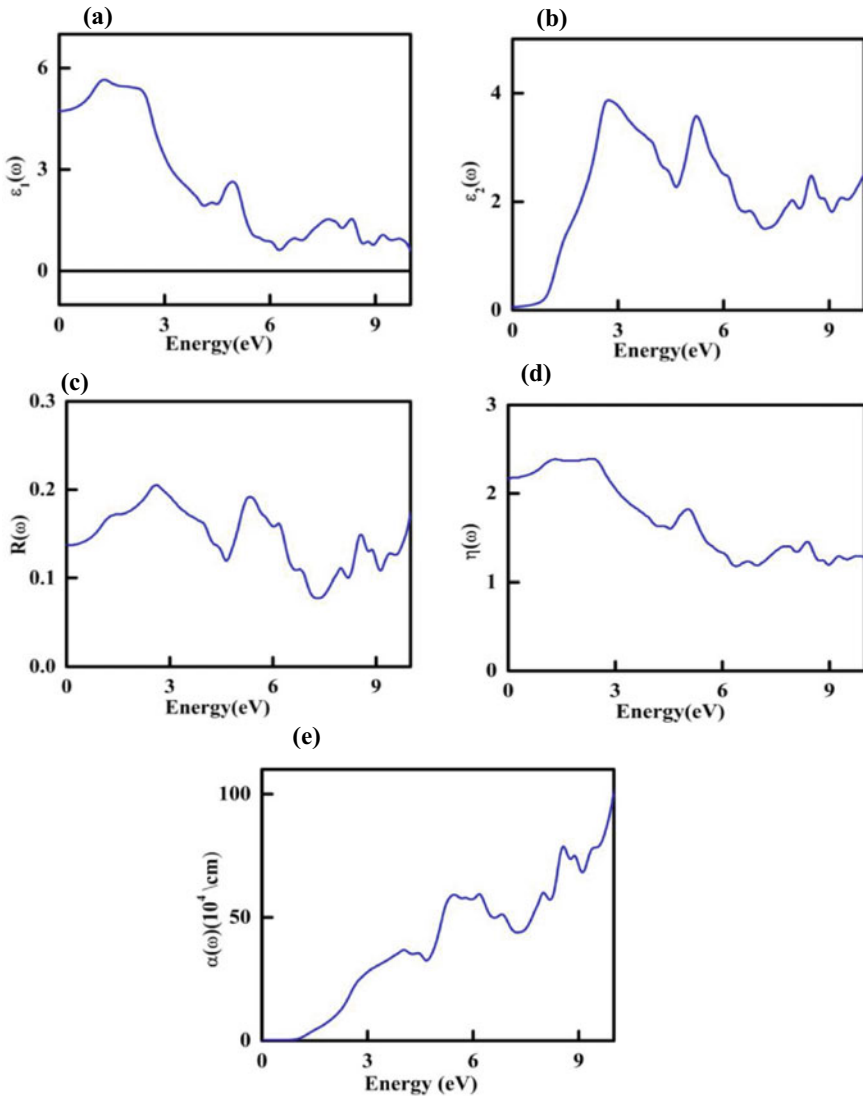


Fig. 3 a Real dielectric tensor, b imaginary dielectric tensor, c reflectivity, d refractivity, e absorption spectra of NaSnCl₃

The TB-mBJ exchange potentials up to 10.0 eV were captured in Fig. 3a–e. The complex dielectric function $\epsilon(\omega)$ must be studied in great detail in order to calculate compounds’ optical characteristics. Figure 3a–b shows real and imaginary components of the dielectric tensor spectra which is a function of the wave vector.

Since TB-mBJ computations are the most exact so, we choose them to evaluate the optical properties of the NaSnCl₃. Real dielectric tensor spectra at 0 eV have an

absolute value of 4.78. The imaginary portion of the dielectric function is indicated in Fig. 3b. The imaginary component of the dielectric function $\epsilon_2(\omega)$ is shown in Fig. 3b. It helps to study the changes that take place between the occupied and unoccupied states. The $\epsilon_2(\omega)$ spectra depict the motion of free electrons from valence to the conduction band and emerged peaks are (3.85, 3.55, and 2.47 eV). The reflectance and refractivity spectra of the compound NaSnCl_3 are shown in Fig. 3c–d and at 0 eV, obtained values are 0.138 and 2.17, respectively. The integrated absorption coefficient, which is determined to be $92.85 (\times 10^4 \text{ eV/cm})$ is shown in Fig. 3e as a spectrum to illustrate the level of material absorption for the incident photon. Therefore, we came to the conclusion that the metal halide perovskite NaSnCl_3 is suitable for optoelectronic applications based on the computed values.

4 Conclusion

After analyzing the optoelectronic behavior of NaSnCl_3 ternary inorganic perovskites through the Wien2k code by the FP-LAPW method, we conclude that NaSnCl_3 can be used for multi-junction solar cells. The observed band gap value of 0.91 eV shows their semiconductor nature and which is analyzed by DOS spectra. Furthermore, the optical properties show that NaSnCl_3 has a significant intensity which lies in the visible electromagnetic spectrum and it has a high absorption value of $92.85 (\times 10^4 \text{ eV/cm})$. Therefore, based on the electronic and optical properties, the compound can be used for optoelectronic applications.

Acknowledgements We thank Prof. Peter Blaha for providing the Wien2k code to check the material. We believe that Manipal University Jaipur will provide all the extra services we need. Financial Assistance Provider DST-SERB New Delhi (India) Application Number EMR/2017/005534.

References

1. Yin WJ, Shi T, Yan Y (2014) Unique properties of halide perovskites as possible origins of the superior solar cell performance. *Adv Mater* 26:4653–4658
2. Akkerman QA, Gandini M, Stasio FD, Rastogi P, Palazon F, Bertoni G, Ball JM, Prato M, Petrozza A, Manna L (2016) Strongly emissive perovskite nanocrystal inks for high-voltage solar cells. *Nat Energy* 2:1–8
3. Liang J, Wang C, Wang Y, Xu Z, Lu Z, Ma Y, Zhu H, Hu Y, Xiao C, Yi X, Zhu G, Lv H, Ma L, Chen T, Tie Z, Jin Z, Liu J (2016) All-inorganic perovskite solar cells. *J Am Chem Soc* 138:1–6
4. Chen Q, Wu J, Ou X, Huang B, Almutlaq J, Zhumekenov AA, Guan X, Han S, Liang L, Yi Z, Li J, Xie X, Wang Y, Li Y, Fan D, Teh DBL, All AH, Mohammed OF, Bakr OM, Wu T, Bettinelli M, Yang H, Huang W, Liu X (2018) All-inorganic perovskite nanocrystal scintillators. *Nature* 561:88–93

5. Yu H, Tian G, Xu W, Wang S, Zhang H, Niu J, Chen X (2018) Green light-emitting devices based on perovskite CsPbBr₃ quantum dots. *Front Chem* 6:1–6
6. Wang Y, Li X, Song J, Xiao L, Zeng H, Sun H (2015) Quantum dot light-emitting diodes based on inorganic perovskite cesium lead halides (CsPbX₃). *Adv Mater* 27
7. Abrusci SD, Stranks P, Docampo HL, Yip AKY, Jen HJ (2013) High-performance perovskite-polymer hybrid solar cells via electronic coupling with fullerene monolayers. *Nano Lett* 13
8. Ramasamy P, Lim DH, Kim B, Lee SH, Lee MS, Lee JS (2016) All-inorganic cesium lead halide perovskite nanocrystals for photodetector applications. *Chem Commun* 52
9. Zhang X, Xu B, Zhang J, Gao Y, Zheng Y, Wang K, Sun XW (2016) All-inorganic perovskite nanocrystals for high-efficiency light emitting diodes: dual-phase CsPbBr₃-CsPb₂Br₅ composites. *Adv Funct Mater* 26:4595
10. He X, Liu P, Zhang H, Liao Q, Yao J, Fu H (2017) Patterning multicolored microdisk laser arrays of cesium lead halide perovskite. *Adv Mater* 29:1604510
11. Guney T (2019) Renewable energy, non-renewable energy and sustainable development. *Int J Sust Dev World* 26:389–397
12. Zhang W, Eperon GE, Snaith HJ (2016) Metal halide perovskites for energy applications. *Nat Energy* 1:16048
13. Idrissi S, Ziti S, Labrim H, Bahmad L (2021) Band gaps of the solar perovskites photovoltaic CsXCl₃ (X = Sn, Pb or Ge). *Mater Sci Semicond Process* 122:1–8
14. Khan K, Sahariya J, Soni A (2021) Structural, electronic and optical modeling of perovskite solar materials ASnX₃ (A = Rb, K; X = Cl, Br): first principle investigations. *Mater Chem Phys* 262(124284):1–9
15. Krishnamoorthy T, Ding H, Yan C, Leong WL, Baikie T, Zhang Z, Sherburne M, Li S, Asta M, Mathews N, Mhaisalkar SG (2015) Lead-free germanium iodide perovskite materials for photovoltaic applications. *J Mater Chem* 3:23829–23832
16. Young J, Rondinelli JM (2016) Octahedral rotation preferences in perovskite iodides and bromides. *J Phys Chem Lett* 5:918–922
17. Travis W, Glover ENK, Bronstein H, Scanlon DO, Palgrave RG (2016) On the application of the tolerance factor to inorganic and hybrid halide perovskites: a revised system. *Chem Sci* 7:4548–4556
18. Korbel S, Marques MAL, Botti S (2016) Stability and electronic properties of new inorganic perovskites from high-throughput ab initio calculations. *J Mater Chem C* 4:3157–3167
19. Gou G, Young J, Liu X, Rondinelli JM (2017) Interplay of cation ordering and ferroelectricity in perovskite tin iodides: designing a polar halide perovskite for photovoltaic applications. *Inorg Chem* 56:26–32
20. Jung YK, Lee JH, Walsh A, Soon A (2017) Influence of Rb/Cs cation-exchange on inorganic Sn halide perovskites: from chemical structure to physical properties. *Chem Mater* 29:3181–3188
21. Mao X, Sun L, Wu T, Chu T, Deng W, Han K (2018) First-principles screening of all-inorganic lead-free ABX₃ perovskites. *J Phys Chem C* 122:7670–7675
22. Islam J, Akther Hossain AKM (2020) Semiconducting to metallic transition with outstanding optoelectronic properties of CsSnCl₃ perovskite under pressure. *Sci Rep* 10:1–11
23. Roknuzzaman M, Ostrikov K, Wang H, Du A, Tesfamichael T (2017) Towards lead-free perovskite photovoltaics and optoelectronics by ab-initio simulations. *Sci Rep* 7:1–8
24. Huang L, Lambrecht WRL (2013) Electronic band structure, phonons, and exciton binding energies of halide perovskites CsSnCl₃, CsSnBr₃, and CsSnI₃. *Phys Rev B* 88:1–12
25. Blaha P, Schwarz K, Tran F, Laskowski R, Madsen GKH, Marks LD (2020) WIEN2k: an APW+lo program for calculating the properties of solids. *J Chem Phys* 152:074101
26. Blaha P, Schwarz K, Sorantin P, Trickey SB (1990) Full-potential, linearized augmented plane wave programs for crystalline systems. *Comput Phys Commun* 59:399–415
27. Tran F, Blaha P (2009) Accurate band gaps of semiconductors and insulators with a semilocal exchange-correlation potential. *Phys Rev Lett* 102:226401

Overview of India's Battery-Swapping and Charging Infrastructure for Electric Vehicles



Devjani Bhattacharya  and Kumud Kumar Sharma

Abstract In this study, an overview of the current state of electric vehicle (EV) technology in India is provided. This paper introduces the beginning of electric vehicles which are shifting from traditional engine vehicles. EVs have a number of advantages, including increasing the use of clean energy by using less oil and fossil fuels, helping to meet climate change commitments by reducing harmful emissions, reducing pollution lower public risks, and the introduction of new technologies leads to infrastructure and economic growth. Comparisons are made between different types of battery systems. This highlights major government initiatives and standards for the battery charging infrastructure in India. The paper also covers ease of doing business, i.e., Battery Swapping System (BSS) which is convenient and less time-consuming.

Keywords Electric vehicle · Traction batteries · The battery swapping system · EV charging infrastructure

1 Introduction

1.1 Overview of Electric Vehicle

Electric vehicles are rapidly gaining traction as the only practical option for lowering pollution and conserving non-renewable resources. Fossil fuel stocks are dwindling quickly, as we are all aware. We must therefore explore electric vehicles. Research and development into batteries for electric and hybrid vehicles is becoming increasingly popular because of the rise in the demand for fossil fuels on the global market and the expansion of internal combustion engine vehicles is causing environmental issues to get worse. Given the need to reduce air and noise pollution as well as

D. Bhattacharya (✉) · K. K. Sharma
DPG Institute of Technology and Management, Gurugram, Haryana, India
e-mail: devjani.bhattacharyabanerjee@gmail.com

Table 1 Characteristics that set apart the various electric vehicle technologies in the market

Vehicle type	Electric vehicle	Gasoline-powered (internal combustion)	Plug-in hybrid (PHEV)	Hybrid (HV)
Energy source	Electric only	Gasoline only	Main: electric	Main: gasoline
			Main: gasoline	Sub: electric
Propulsion mechanism	Motors	Engine		Combination of motor + engine
CO ₂ emissions	None	Yes	Yes	Yes
Fuel facility locations	Charging stations	Gas stations	Gas stations, chargers	Gas stations
Tax liability	Low	High	Low	Low
Cruising distance	Short	Long	Long	Long

greenhouse gas emissions, these vehicles may be a future development in the field of road transportation [1, 2] (Table 1).

1.2 Types of Batteries Used in Electric Vehicles

We now have access to a range of electric vehicle batteries. There are six main battery types to take into account in electric vehicles.

1.2.1 Lithium-Ion (Li-On)

Regarding electric vehicles, the most popular battery type is a lithium-ion battery since it provides advantages like:

High energy efficiency.

Even in extreme temperatures, the battery performs well.

Excellent ratio of weight to power even in its diminutive size, it has a large capacity for holding charges. Low self-discharge level; excellent charge retention even when inactive for extended periods of time.

Li-Ion batteries' disadvantage is that they operate at high temperatures, which could reduce their lifespan and operational safety [3].

1.2.2 Nickel–Metal Hybrid (NiMH)

Nickel–metal due to its advantages over conventional batteries, hybrid batteries are a better choice for hybrid electric vehicles (HEVs).

Offer higher tolerance to harsh conditions and are a safer alternative to lead-acid batteries. There are some difficulties on the other side:

High self-discharge rates, heat production at high temperatures, and higher manufacturing costs.

These difficulties make scaling up to full-fledged EVs using NiMH batteries far less feasible and therefore only possible for hybrid vehicles.

1.2.3 Solid-State Batteries (SSB)

With the exception of using solid electrolytes rather than liquid electrolyte solutions, SSBs are predominantly li-ion batteries. SSBs have a lower risk of catching fire when heated and even more energy density and longevity than Li-ion batteries.

This technology is still under experimental stages which pulls it back when it comes to applicability.

1.2.4 Lead–Acid Batteries

Prior to the discovery of Li-ion batteries, lead–acid batteries were the most practical option. These are known as the oldest rechargeable battery technology. Despite the low cost of production for these batteries, they drain quickly due to their hefty weight.

1.2.5 Aluminum-Ion (AI-Ion)

India is one of the countries which has bauxite (aluminum ore) in large quantities. In the long run, this may benefit the country as the need of AI-Ion for batteries will rise with the increased EV production.

AI-Ion batteries have future use as it is a worthy replacement for Li-ion because of their various pros—a large capacity, quick charging, and safer handling; improved energy density. Its adoption may face challenges because of its high manufacturing.

1.2.6 Ultracapacitors

Between the electrode and the electrolyte, ultracapacitors (supercapacitors) store polarized liquid. Due to the exceptionally high-power supply of super-capacitors, which increases during regenerative braking, and start–stop acceleration moments, it can be employed as a secondary storage device in EVs, possibly as a NiMH battery replacement (Table 2).

Table 2 Comparison of different battery types

Categories	Li-ion	NiMH	SSB	Lead-acid	Al-ion	Super-capacitors
Reliability	High	Very high	High	Decent	Very high	High
Capacity	High	Decent	High	Decent	Very high	High
Life cycle	High	Very high	High	Decent	Decent	High
Performance	High	Low	High	Decent	Very high	Very high
Efficiency	High	Low	High	Decent	Very high	Decent
Cost	Low	High	Very high	Low	Very high	Very high

1.3 Rechargeable Batteries

A rechargeable battery known as an electric vehicle battery (EVB, often referred to as a traction battery) powers the electric motors in a battery electric vehicle (BEV) or hybrid electric vehicle (HEV). High electric charge (or energy) capacity is often taken into consideration while manufacturing lithium-ion batteries.

Electric car batteries use deep-cycle batteries, which are designed to provide power for a long time as opposed to Starting, Lighting, and Ignition (SLI) batteries. Because they reduce vehicle weight and hence improve performance, smaller, lighter batteries are desirable. Electric car batteries stand out due to their high specific energy and energy density. The maximum all-electric range of the cars is frequently impacted by the fact that the majority of modern battery technologies have significantly lower specific energies than liquid fuels [3].

1.3.1 Battery Swapping System

The Battery Swapping System's Composition

The usage of a battery changeover truck illustrates a significant difference in how EV batteries are turned over. As a result, the specific duties and roles that each person performs will change. To lessen the effects of these changes and offer a reliable and effective EV battery-changing service, each participant's function and role, as well as any modifications they have undergone, are identified. The processes of battery manufacturing, charging, transportation, storage, and replacement, as well as communication, are all explained. Following that, as shown in Fig. 1, each member's relationship is described [4]

1.3.2 Battery Swapping Station (BSS)

An EV is typically the primary everyday form of transportation for commuters. With infrequent stops to the grocery store and other places during the day, an EV is utilized

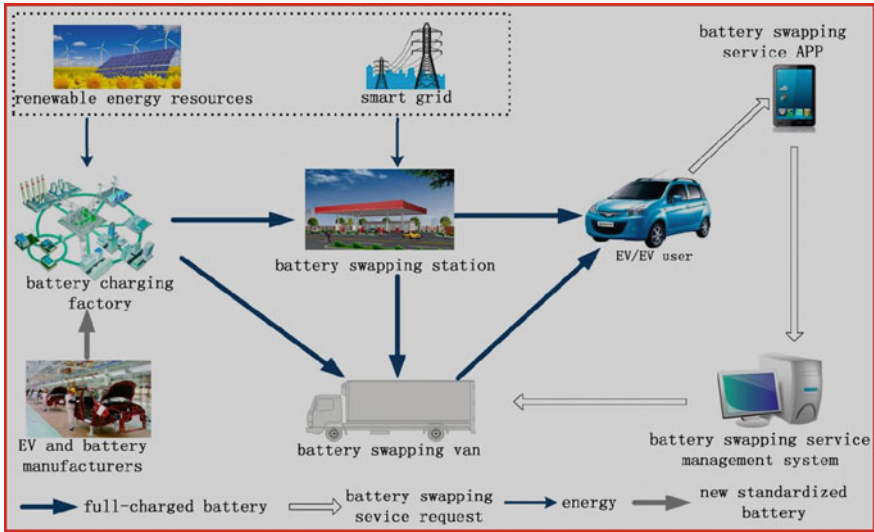


Fig. 1 Member relationship description

for both the morning journey to work and the evening commute home. Because energy consumption is quite high during peak travel periods, there is a substantial demand for battery swapping. Due to the restricted capacity of the fully charged battery store in the battery swapping station, it might not be sufficient to simply replenish the totally charged battery storage using the battery logistics system. EV customers cannot utilize this battery charging method because it is only available for batteries that have been changed [4].

1.3.3 Major challenges of BSS

Let's talk about changing the batteries; this device's main benefit is speed. The entire procedure could be completed in less than five minutes, which is about how long it currently takes many people to fill up their cars at gas stations. Another benefit is that users don't need to deal with potentially messy or tangled connections or get out of their cars [5].

1.4 Interchangeability

Brand interoperability and cross-platform capabilities guarantee the technology's appeal and standing as a dominant market trend. A battery-changing system won't be widely used until identical interchangeable battery packs are produced by multiple

different manufacturers. The manufacturer's consent is required for this simple modification. This could, however, limit inventiveness, individuality, and adaptability of products created by a single manufacturer. The primary cell producers will be compelled to develop standardized cells in order to supply comparable cells to the following manufacturing unit, which will be the only means of further standardizing production and limiting the creation of new goods [6].




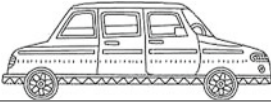
1.4.1 Electric Vehicle Charging Infrastructure (EVCI)

To enable quicker uptake, EVCI should be deployed a little before EVs. Due to low public awareness in India, EVCI installations are essential if EV adoption is to be accelerated. The installation of EVCI, whose power input will be connected to the utility grid, will take place across a substantial area of the nation. This has an impact on a variety of elements, including grid handling capacity, distribution system upgrades, transformer loads, component deterioration, installation location, load consumption pattern, time of use, and others. Prior to their creation and installation, the EVCI must be tested and evaluated for quality by comparing them to national and international standards that are outlined [7].

2 Highlights of Indian Standards for Charging Infrastructure

The nation is building EV charging infrastructure in addition to EV acceptance and innovation. Public sector businesses like NTPC, EESL, BHEL, and others have set up electric vehicle charging stations all around India. Electric vehicle owners can plug in and recharge their batteries at these locations. The Bureau of Indian Standards (BIS), which formed the Committee of Electro Technical Division (ETD) 51, is primarily the responsibility of creating Indian Standards (IS) for EV charging stations. The earliest IEC and ISO standards for EV charging stations were developed by IEC and ISO groups, which are known as the ISO 15118 series of standards and IEC 61851 series of standards respectively. The IEC 61851 series of standards served as the foundation for the IS 17017 family of standards, which also assisted in their development (not all are similar). For India's needs, standards in the IS/ISO 15118 series have been directly adapted. The Department of Heavy Industries (DHI) develops and publishes significant standards for EV and EVCS, BIS, and Automotive Industry Standards (AIS). The DH unveiled the Bharat Chargers AC-001 (AC Charging System) and DC-001 (DC Charging System) in 2017. They are based on GB/T (Chinese) standards but have had the ambient temperature adjusted to cater for climatic conditions in India. The replacement ambient temperature is between 0 and 55 degrees Celsius. The AIS 138-1, 138-2, and additional EVCS testing standards are added to the IEC 61851 series and made available by AIS [8–15].

Table 3 Electric vehicles capacity and battery voltage range [16]

Vehicle segment	Battery capacity	Battery voltage
E-2W 	1.2–3.3 kWh	48–72 V
E-3W (passenger/goods) 	3.6–8 kWh	48–60 V
E-cars (1st generation) 	21 kWh	72 V
E-cars (2nd generation) 	30–80 kWh	350–500 V

2.1 Battery Details for Various EV Sector Models

Since the battery receives power at the appropriate voltage and current levels to enable charging, electric vehicle charging requirements are to be determined by the specifications of electric car batteries. According to Table 3, the typical EV battery voltage and capacity varies depending on the EV segment [16]

2.2 Charging Techniques

Conductive charging comes in two flavors: AC and DC. Should an AC EV charging infrastructure exist, the onboard charger of the EV receives the AC power and converts it to DC. By converting power from the outside and transferring DC power directly to the battery, DC EV charging infrastructure eliminates the onboard charger. AC and DC both include three separate AC charging options and one DC charging mode.

In Modes 1 and 2, a cable and plug can be used to connect an EV to a standard socket outlet as depicted in Fig. 2.

Mode 1, also referred to as dumb charging, should not be used because it obstructs the EV’s and EVSE’s ability to communicate. The portable cable used in Mode 2 is typically used for in-home charging and features built-in protection and control. In Modes 3 and 4, which are used in commercial or public charging situations, better control systems are available, but they are more expensive, require a separate charger, and give EV electricity [16].

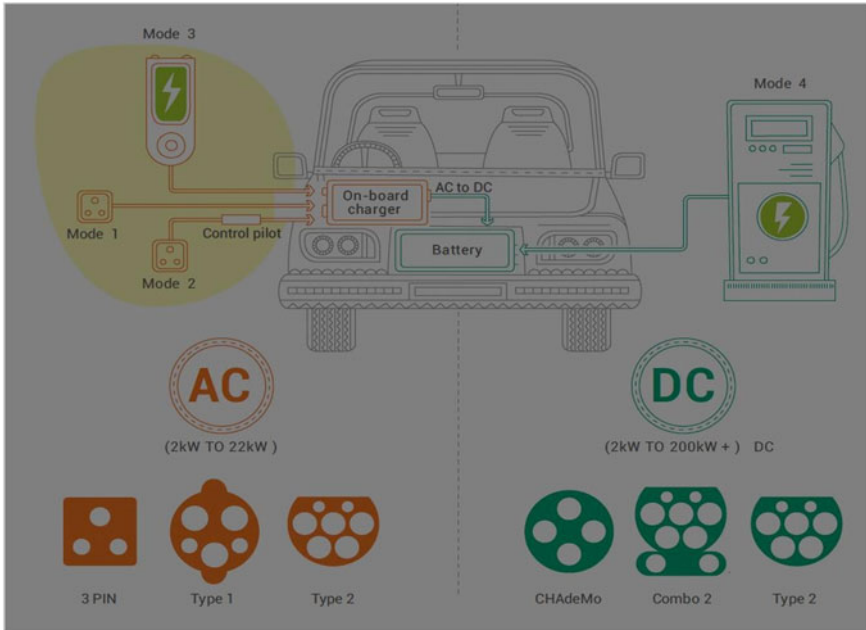


Fig. 2 Connection of EV in modes 1 and 2

2.3 Major Challenge of EV Charging Infrastructure

An electric car battery may often be fully charged in up to 8 h. The necessity of having enough charging ports to fulfill demand is a source of concern. Many organizations all throughout the world use different EVCS test standards. With a clear goal in mind, overcoming technical and cultural gaps can let EVs charge safely wherever. The solution is to create a global testing and certification standard that is all-inclusive [18]. A list of installed electric vehicle charging stations is provided as of June 2020 [17].

3 Conclusion

Electric vehicles are the future of the globe for transportation. Given that EVs have many advantages, one of which is increasing the usage of clean energy by consuming less oil and fossil fuels, helping fulfill climate commitments by reducing harmful emissions, reduction in pollution serves public risks and this advent of new technologies results in economic growth and infrastructure. However, there are some technical and procedural challenges to overcome before the acceptance of EVs. The

deployment of EV will be useful and is in line with many climate actions. Therefore, the use of renewable energy (RE) in the transportation industry is urgently needed. Many countries have increased funding and established the infrastructure for developing RE in order to enhance their share in the sector.

Battery swapping system is a new technology that will be used to upgrade the battery system for EVs. This cutting-edge modular low-voltage system will make sure that the EVs have access to the necessary electricity. Empty batteries can be exchanged for charged ones at battery replacement locations. At last, countries need to constantly work on the enhancement of smart grid from which energy flows to charging stations. As, during the peak hours of power demand rise, we need to distribute the energy to the storage system with balance.

References

1. Brady J, O'Mahony M (2011) Travel to work in Dublin. The potential impacts of electric vehicles. *Transp Res Part D: Transp Environ* 16(2):188
2. Hawkins TR, Singh B (2012) Comparative environmental life cycle assessment of conventional and electric vehicles. *J Ind Ecol* 17(1):53
3. Doughty D, Roth EP (2012) A general discussion of li ion battery safety. *Electrochem Soc Interface* 21(2):37
4. <https://www.mdpi.com/1996-1073/10/10/1667/htm>, p 3
5. 'Challenges for battery swapping station (2017). <https://getsetojo.com/blogs/blog/challenges-for-battery-swapping-over-charging-stations-for-evs-in-india>. Accessed 10 January 2019
6. Mahoor M, Hosseini ZS, Khodaei A (2017) Electric vehicle battery swapping station. In: CIGRE grid of the future symposium, Paris, France, pp 1–5
7. <https://doi.org/10.1049/iet-stg.2019.0059>, p 3
8. Central Electricity Authority (Technical Standards for Connectivity to the Grid) (Amendment) Regulations (2019) Ministry of power, notification (New Delhi, dated 6th February 2019) Part-III Section 4
9. Central Electricity Authority (Measures relating to Safety and Electric Supply) (Amendment) Regulations (2019) Ministry of power, notification (New Delhi, dated 28th June 2019) Part-III Section 4
10. IS 17017: Part 1: 2018, Electric vehicle conductive charging system Part 1 general requirements. Bureau of Indian Standards
11. IS 17017: Part 2: Sec 2: 2020, Electric vehicle conductive charging system Part 2 plugs, socket outlets, vehicle connectors, and vehicle inlets Section 2: dimensional compatibility and interchange ability requirements for A.C. Pin and contact-tube accessories, Bureau of Indian Standards
12. IS 17017: Part 21: Sec 1: 2019/IEC 61851-21-1: 2017, Electric vehicle conductive charging system Part 21 electromagnetic compatibility (EMC) requirements section 1 on-board chargers, Bureau of Indian Standards
13. IS 17017: Part 21: Sec 2: 2019/IEC 61851-21-2: 2018, Electric vehicle conductive charging system Part 21 electromagnetic compatibility (EMC) requirements Section 2 off-board chargers, Bureau of Indian Standards
14. Letter No. August 23, 2018-R&R dated April 13, 2018 issued by the ministry of power.
15. Clause 2.2 of the charging infrastructure for electric vehicles (EV)–revised guidelines and standards, 2019
16. NITIAAYOG, Handbook of electric vehicle charging infrastructure implementation, Version–1

17. Ministry of Power, Central Electricity Authority, R&D division, electric vehicle charging reports, June 2020
18. Jeykishan Kumar K, Kumar SR. <https://doi.org/10.1002/est2.261>

Real-Time Network Traffic Analysis for Threat Detection



Yogesh Gupta, Amit Saraswat, and Sunil Kumar Goyal

Abstract Wi-Fi is now ubiquitous in most populated areas, and the way the devices communicate leaves a lot of “digital exhaust”. Usually, a computer will have a Wi-Fi device that’s configured to connect to a given network, but often these devices can be configured instead to pick up the background Wi-Fi chatter of surrounding devices. There can always be good reasons as well as bad ones for the same, but the matter is all about the intentions. So, now imagine how many packets are flowing in a network and how harmful or useful they can be. Keeping the bad part aside, this can be used for ethical purpose as done in this work. This work follows certain steps to detect, analyze and then finally visualize the pattern of the network protocols or the data packets flowing. It also revolves around the analysis and hence, can be detected on a real-time basis.

Keywords Wireshark CLI (tshark) · Zookeeper · Kafka · Logstash · Elasticsearch · Kibana

1 Introduction

The messages sent or received in any network generally flow at a rate of 100 k per hour (approximately 30 per second). Somewhat that can’t be considered as “Big Data”, but it isn’t insignificant either. Likewise, it becomes important to monitor computer networks of majorly every network operator. The captured valuable information about utilization and status of a network infrastructure can go into wrong hands during the monitoring stage. But keeping network security in mind, safety of users and their respective data is the key to a safe and ethical environment. In the literature,

Y. Gupta

School of Engineering and Technology, BML Munjal University, Gurugram, India

A. Saraswat (✉) · S. K. Goyal

Department of Electrical Engineering, Manipal University, Jaipur, Rajasthan, India

e-mail: amit.saraswat@jaipur.manipal.edu

few researchers put their efforts for network traffic monitoring and threat detection [1–5]. Also, few efforts have been made on streaming data in literature [6–10].

Due to the sheer volume of data that is transferred through modern network infrastructures, monitoring systems mainly collect traffic information in smaller flow logs. These traditionally consist of network addresses, ports, timestamps, channels, radio signals, and volume information. This data can be used in accounting or in statistical analysis to improve any situational awareness or to detect anomalies. Every such data packet, which contains such information can be extremely harmful (if gone in black hands). So, it becomes crucial to analyze such packets on a regular basis to trace out the real black hat. With rising threats, cybersecurity becomes very important in today's era. But when we talk about the amount of data that we get, it is also important to take the term "Big Data" into consideration. Moreover, streaming it in near-real time becomes the tip of the iceberg. Cybersecurity itself has no meaning if not done in real time. But for this research, let's keep "Cybersecurity" as the tip of the iceberg and emphasize more towards streaming real-time data and further analyze/visualize streamed (captured) data packets using the "Big Data Technologies".

This work follows certain steps to detect, analyze, and then finally visualize the pattern of the network protocols or the data packets flowing. To get a clear view of the steps, this research will take you through the methodology, where all the terminologies and their respective usage will become clear with appropriate examples, pertaining to step-by-step demonstration (using appropriate figures/tables). Process flow diagram with appropriate notations (tools) are also used to make the process more clear and easily understandable.

The remainder of the paper is structured as follows: Sect. 2 states the problems that motivate and require a solution provided in this research work. Section 3 describes the related work which helps to gain a deeper understanding of the problem. The methodology of this work is elaborated in Sect. 4, which provides an analysis on the various aspects of the problem and its solution. Section 5 discusses the derived results in detail. At the end, conclusion and future work is drawn in Sect. 6, that will go into perfecting as well as updating the system with constant feedback checking.

2 Problem Statement

In this section, the problem is defined in detail including motivations as follows.

2.1 Motivation and Respective Solution

Due to the colossally increasing flow of data packets [11], it has become extremely important to dissect and examine a certain protocol inside the network traffic captured. So, the major reasons for analyzing the network traffic in real time are:

- By collecting this type of traffic, it can be possible to track and analyzes behavior in ways that we may or may not feel comfortable with.
- Improving public transport as Transport for London (TFL) [12] is already done by collecting Wi-Fi connection data to get a far better understanding of how customers move through stations. Moreover, the traffic captured is not used to identify any specific individuals or monitor anyone's personal browsing history. Everything done is just for analyses purpose and obviously a good cause.
- Not likely but tracking customers in-store [13] could be used to provide the customers with the best offers and hence, analysis is to be done in real time, which we normally consider near-real time.

Another reason is the rising number of cyber threats and cybercrimes, it has become crucial to get an eye on its numbers. Many other reasons may involve the analysis done with streams of Wi-Fi packet capture (pcap) data. As already mentioned earlier, these packets carry very critical information of the host. Such information can become vulnerable and can be captured to analyze the user behavior and predict the hacker (passive or active) in some or the other way. This research basically analyzes the user behavior and detects the black guy, who is trying to trace, harm, or deny the victim from using the services. This denial of service is also referred to as DoS (Denial-of-Service) or DDoS (Distributed Denial-of-Service) attack. Further, many types of man-in-the-middle (MITM) attacks can be predicted with such an enhanced solution as provided in this report.

2.2 Solving Specific Problem

Solving a specific problem can never be the right way for problem solvers. Rather, making the solution that can be widely used must be the right approach. Keeping that thought, this research provides a vast knowledge base to the analysts for performing different types of analyses over the captured dataset and then finally predicting [14] the untrustworthy users as per their convenience and analytical skills in real time (precisely near-real time).

2.3 Detailed Explanation

The main problem begins when the black hats try to hook or trace out a victim. Keeping the cybersecurity and all the protocols in mind, this research helps all types of analysts to gather vast information accurately belonging to those black guys. This is easily done with the help of event streaming and further using the right pipelining framework to analyze and predict different cyber-attacks, black hats, and middleware (man-in-the-middle attackers). Also, Fig. 1, as given in Sect. 4, describes the whole scenario from capturing the flowing data packets (in any network within range) to

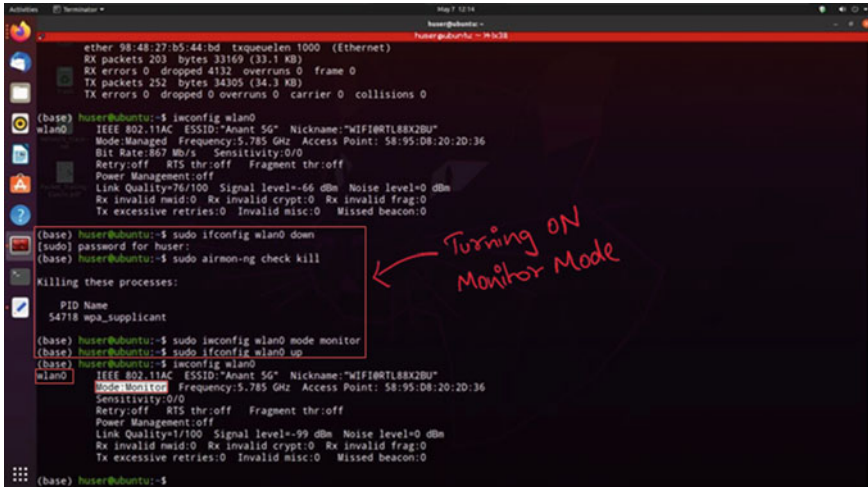


Fig. 1 wlan0 in monotor mode

finally giving it a shot for perfect visualizations and future predictions. Performing such steps can have a good as well as a bad intention. Keeping all the evils aside, this research tends to take it in a direction where every single analysis is done to gain information only for a constructive resolution, that too only for educational and research purposes [15].

3 Related Work

Various methods for the detection of black hats are present like “Wireshark API.” But taking it a step forward towards analyzation and visualization makes it much more powerful and easily noticeable for analysts to perform different predictions and hence, trace out the black guy in real time. The authors presented a similar approach which considered a hybrid scenario for emulating networks on one or more PCs with the CORE demonstrations keeping the wired as well as wireless settings [16]. Their system yielded good results but, at the same time, the process became very technical and required more of network-based knowledge, whereas it should be simple and should be available and understandable by the data scientists as well to apply their knowledgebase and make it more powerful than ever. In [17], the author states an innovative approach for real-time network traffic classification. The developed model adopts a new approach for the relaxation of the hypothesis of independence between the attributes of the Naive Bayes algorithm. As a result, the proposed system becomes a promising alternative to be applied in real-time scenarios. Similarly, the authors listed down the real-time diagnoses of network anomaly based on statistical traffic analysis by experimentally showing the developed mechanism to

alert the DDoS attack schemes within a short response time [18]. Another framework as anticipated by authors in references [19, 20] for network traffic analysis focused on handling high-speed network traffic with links working at 100 GB/s. The author proposed a flow-based modular Network Measurements Analysis (NEMEA) system to overcome the situation. Their system also yielded good results but, at the same time, there are some drawbacks related to the server's resources.

4 Methodology

This section provides an explanation of how this work solves the above-discussed problem. The process is started with capturing the live data packets to finally analyzing it in various forms for future predictions (at real time). The data is being immensely generated at every single moment and that too at a reckless pace, it becomes very important to collect that data. But the main procedure starts when the data cleaning takes place. It is the most critical step for every analyst as it is very important to filter out the needful data and trash the rest. After perfectly collecting and cleaning the recorded or live-streamed data, it turns out to be the right time for entering the analyzation phase.

4.1 *Technical Specifications*

As the process starts with capturing or tracing out the live data packets with “Tshark” (Wireshark CLI), a widely used network protocol analyzer. It acts as a producer for “Kafka.” Kafka is very powerful for event streaming and maintaining logs. To view the live packets being streamed in Kafka, Kafka-consumer provides a very efficient CLI as well as API. Now, the packets as consumed in Kafka are sent to “Elasticsearch” where the JSON formatted data is indexed and stored in a very easy and reliable format for performing different analyzations in “Kibana” via “Logstash”, which is yet another free and open source server-side data processing pipeline that ingests data from a multitude of sources (Kafka in our case), transforms it, and then sends it to your favorite “stash” (Elasticsearch in our case). Finally, exploring and analyzing the data with stunning visualizations in Kibana makes the process complete and starts the job for the analysts.

4.2 *Hardware and Software Components*

Aiming for generating, collecting, processing, cleaning, visualizing/analyzing, and then finally concluding with the utmost accurate predictions at real-time, becomes very important to have the perfect hardware as well as the software components. In

this work, hardware comprises of 4 CPU cores and 8 GB of memory on a single server (Linux) is used to perform all the experiments. Network packet capturing (pcap) comes under the umbrella of cyber security, hence, making it a collaborative work for the “Ethical hackers” and “Data Scientists”. In view of the software requirements, the combination of open-source CLIs like Tshark, Kafka, and APIs like the ELK stack (Elasticsearch, Logstash, and Kibana) are used in this research.

Believing over the new technology has always been treated as an effective solution. But the trust develops once the innovation is implemented and gives the most successful results. Analyzations and predictions made over such effectual results make the technology utmost effective. Comparing the power of Tshark, Kafka streams, and ELK stack with the closest technology, it is necessary to include the hardware requirements as well as their respective efficiencies to create a great difference. Keeping this concern in mind, the accuracy of Tshark packet capturing (pcap), the fleetness of Kafka streams (streaming different topics at the same time and inviting all sorts of developers with its wide acceptance), and with the precision of the ELK stack (the perfect pipelining, indexing, and visualizing/analyzing framework), it becomes very difficult to compare it with other open-source tools or applications (either CLIs or APIs).

5 Result and Discussion

In this paper, the analysis is done using different graphs such as vertical as well as horizontal bar or line graphs, pie charts, tree maps, and various other helpful visualizations. Following steps are designed for real-time network traffic analysis for threat detection.

5.1 *Starting and Examining ELK Stack Daemons (Running)*

Checking the state of ELK stack by the following commands.

- `sudo systemctl status logstash.services`
- `sudo systemctl status elasticsearch.services`
- `sudo systemctl status kibana.services`.

5.2 *Starting and Examining Kafka Daemons (Running)*

Checking the kafka daemons by “jps” command and ensuring that the state of zookeeper and kafka (3 brokers) is up with their respective “ProcessIDs” and “Port numbers”.

- “kafka-topics.sh--list--zookeeper localhost:2181” for listing all the available kafka topics with presence of zookeeper on localhost port number 2181.
- “kafka-topics.sh--describe--zookeeper localhost:2181”—topic test_pcap for describing the “test_pcap” kafka topic with presence of zookeeper on localhost port number 2181, a replication factor of 3 and partitions count 3.

5.3 Retrieving Server Ports with “netstat”

Getting the details of the server port numbers for Kafka brokers (9092, 9093, and 9094), Zookeeper (2181), and the ELK Stack (9600 for Logstash, 9200 for Elasticsearch, and 5601 for Kibana) running on localhost using the command “netstat -plntu”.

5.4 Configuring Logstash Pipeline

Keeping the input as “kafka” and output as “elasticsearch” for the logstash (pipeline) configuration file. In addition to that, setting the bootstrap servers (localhost:9092, localhost:9093, and localhost:9093), the topic name (test_pcap), and the encoding of the captured data (JSON) for kafka. Similarly, for elastic search, keeping its respective host (localhost:9200) and the encoding of the data (JSON) to be indexed at “pcap” for further analyzations to be done in the Kibana application.

5.5 “ifconfig” Before External W-Fi Adaptor

Using “ifconfig” for getting the interface configurations (broker0, docker0, eth0, lo) without the external Wi-Fi adaptor.

5.6 “ifconfig” After External W-Fi Adaptor

Using “ifconfig” for getting the interface configurations (broker0, docker0, eth0, lo) after inserting the external Wi-Fi adaptor (known as wlan0).

5.7 External W-Fi Adaptor in Managed Mode

Default state (Managed) of the external W-Fi adaptor (wlan0) using “iwconfig wlan0” command.

5.8 Configuring “wlan0” in Monitor Mode

Enabling monitor mode on wlan0 with the following set of commands (in sequence) as shown in Fig. 1.

- “sudo ifconfig wlan0 down” for making the wlan0 down.
- “sudo airmon-ng check kill” for killing unnecessary services that may harm the monitoring interface.
- “sudo iwconfig wlan0 mode monitor” for setting the mode for wlan0 as monitor.
- “sudo ifconfig wlan0 up” for finally making the wlan0 in upstate with enabled monitor mode.

Hence, performing “iwconfig wlan0” to check whether the set of commands executed successfully or not.

5.9 Configuring “wlan0” in Monitor Mode

Using the following set of commands (Fig. 2) for capturing (with tshark) and streaming (using “kafkacat”) the data packets (in any network within range) in kafka.

The resolved distribution of MAC addresses of senders is referred to as “sa” and that of receivers are “ra” or “da” (enhanced results with resolved names). The most common filter traffic (wlan.fc.type and wlan.fc.type_subtype) can be referred to the Wireshark Display Filters. Similarly, for the other commands, tshark man-pages and kafkacat man-pages would be really helpful as in [21].

Finally, using “kafka-console-consumer.sh--bootstrap-server localhost:9092--topic test_pcap” for consuming and streaming the captured packets in Kafka consumer console. An example of a packet consumed (in real time) is highlighted in Fig. 2.

5.9.1 Discovering Live Data Using Kibana (With Examples)

As a result, getting the consumed data packets are indexed in elastic search and hence, inspecting it in real-time using the Kibana application (on localhost:5601). Figures 3, 4, 5 and 6 show some of the examples of live streaming of data as indexed

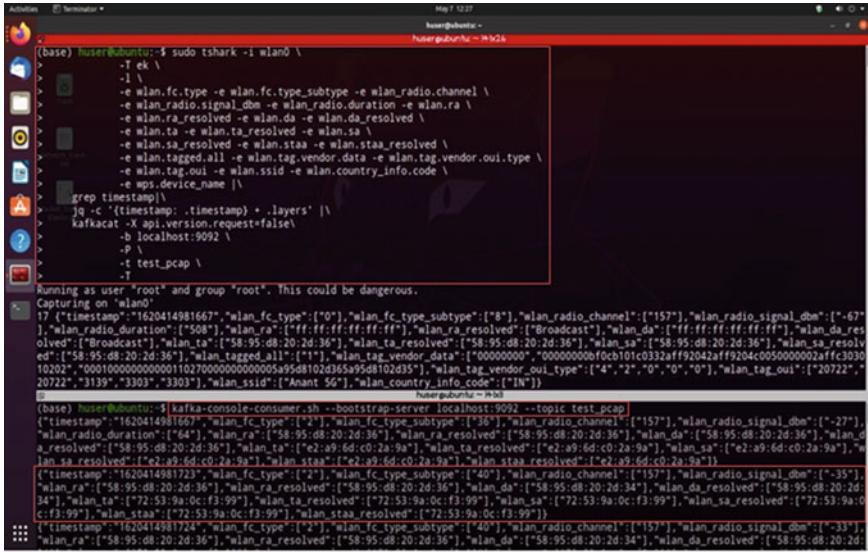


Fig. 2 tshark and kafka-consumer

(in raw format as well as in filtered-out tabulated format) in elastic search (on the kibana's discover console). Using filters is clearly mentioned in Fig. 2.

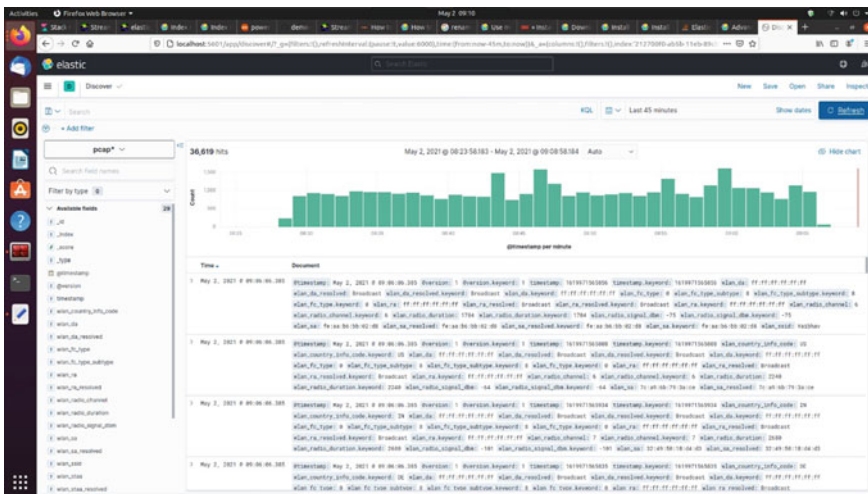


Fig. 3 Streaming raw data in Kibana

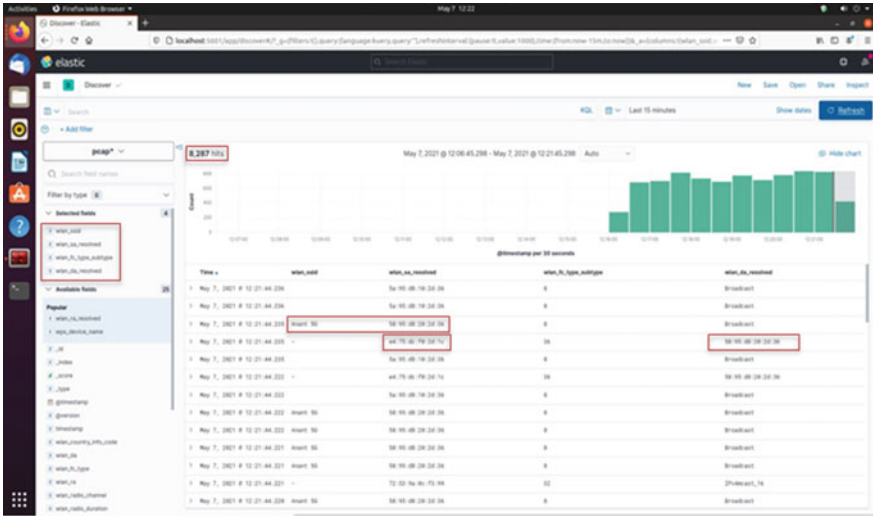


Fig. 4 Filtering out useful data in tabulated form

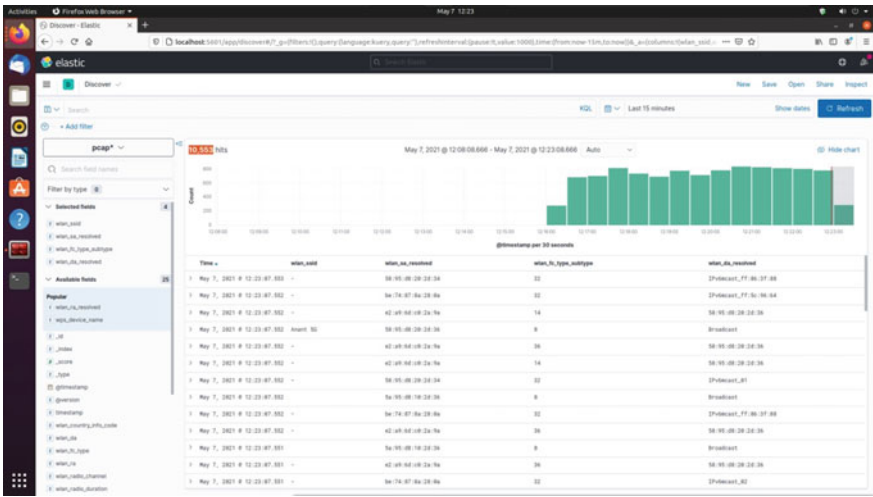


Fig. 5 Some interesting “da” receivers with resolved names

5.9.2 Visualizing Data Using Kibana in Different Time Frames

Figures 7 and 8 present the heat map visualization, generated in different time frames in Kibana by specifying the metrics, terms, and many more useful fields.

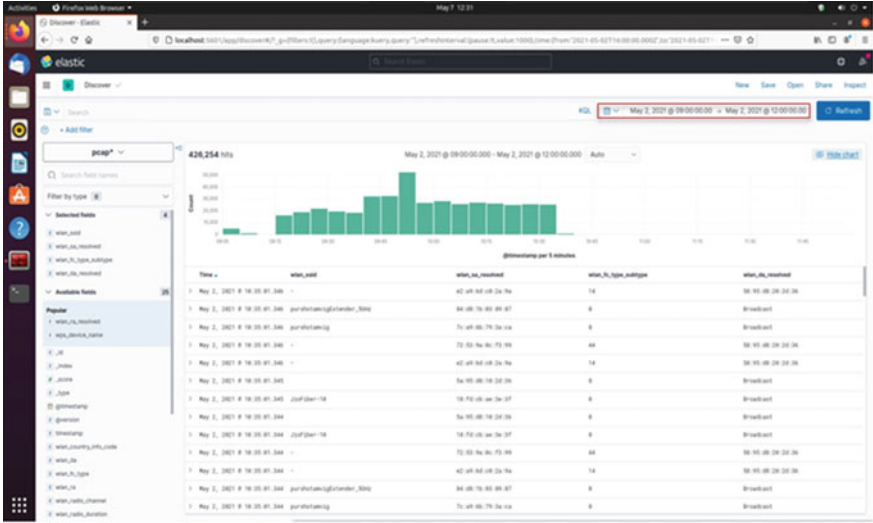


Fig. 6 Filtering captured data for certain time frame

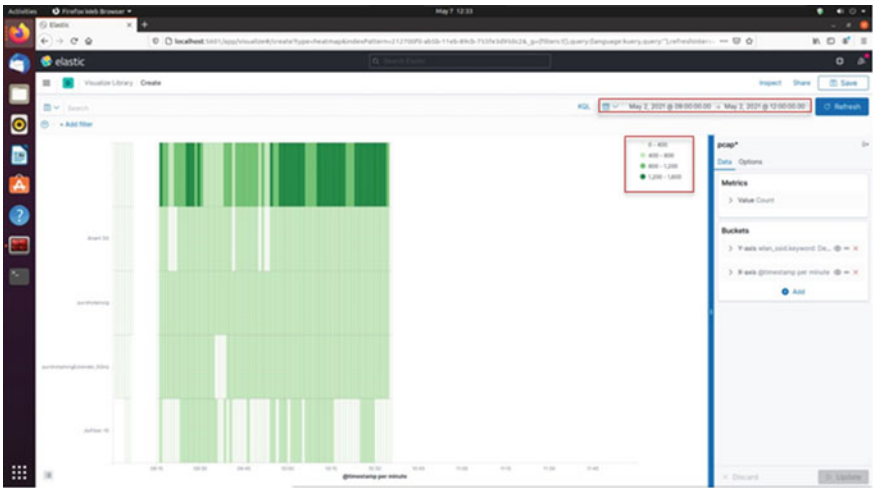


Fig. 7 Heat map of data usage for up to 5 available Wi-Fi devices

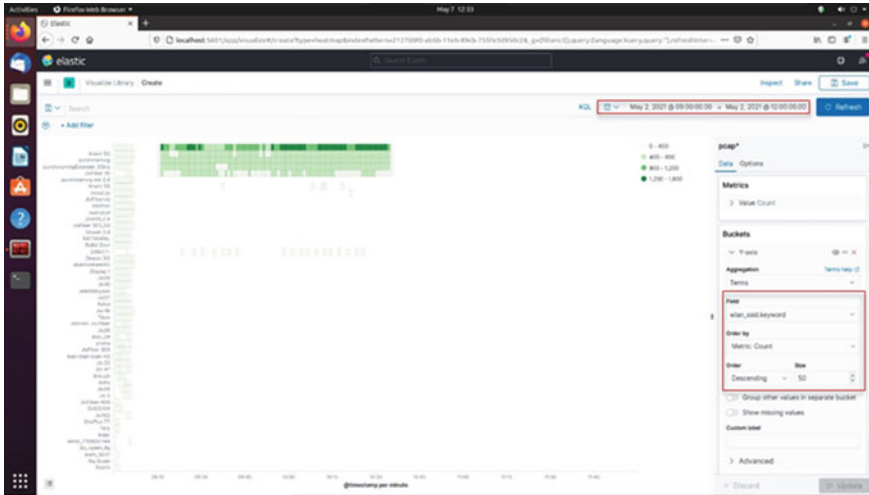


Fig. 8 Heat map for up to 50 available Wi-Fi devices

5.9.3 Analyzing and Making Predictions Using Custom Kibana Dashboards

Finally, analyzing the dataset and making precise predictions with the help of various visualizations as offered by Kibana. Figure 9 shows an example of a custom dashboard built to analyze the data in a rich format and predict the attacker with accurate predictions and secure the environment by constantly examining the case.

6 Conclusion and Future Work

In this paper, an analysis is made on real-time network traffic data for threat detection. With the power of Tshark, the flowing data packets in the range of the external Wi-Fi adaptor (wlan0) are captured. Whereas streaming and indexing the data (JSON formatted) resulted out to be trouble-free with the immensity of kafkacat (Kafka CLI) and the ELK stack respectively. Kibana framework is used in this paper for visualization. Using the latest and strongest chipset of the adaptor is also used to increase the bounds of the packet capture (pcap).

Predicting and catching out the cybercriminals in any network turns out to be the focus of research. Always performing such activities for ethical reasons becomes the most important takeout. So, the cybercrime is at stake, and efficient analysts are in demand. At last, it can be concluded that “Cybersecurity” can be the tip of the iceberg in the world of “Big Data.”

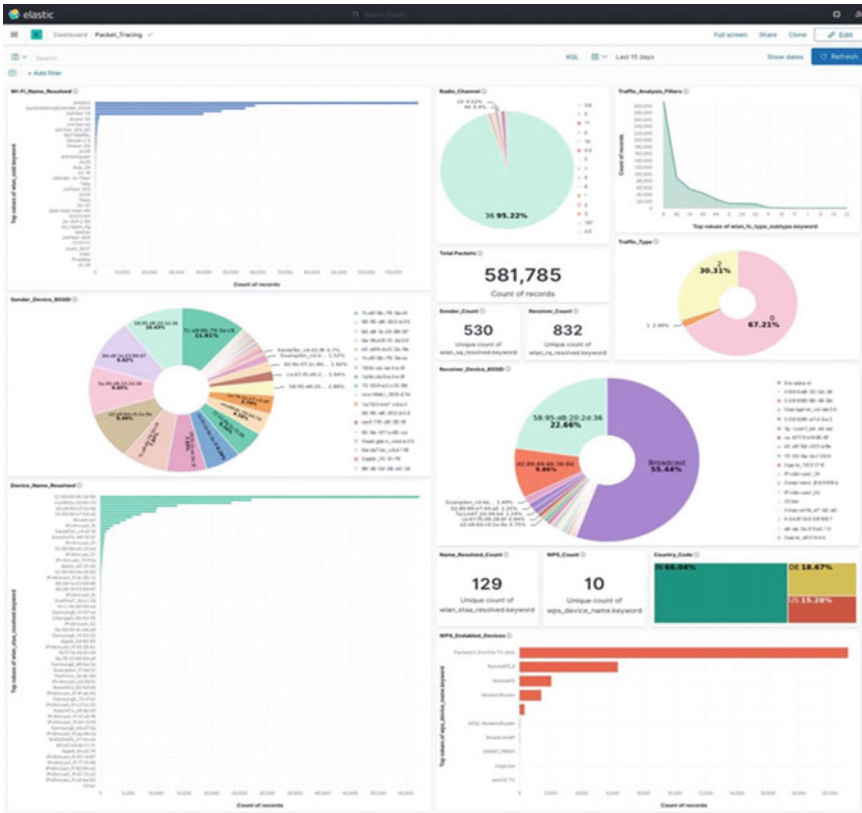


Fig. 9 Custum dashboard

References

1. Bailey M, Cooke E, Jahanian F, Nazario J, Watson D (2005) The internet motion sensor: a distributed blackhole monitoring system. In: Proceedings of network and distributed system security symposium (NDSS)
2. Xu G, Yu W, Chen Z, Zhang H, Moulema P, Fu X, Lu C (2015) A cloud computing-based system for cyber security management. *Int J Parallel Emergent Distrib Syst* 30(1):29–45
3. Yegneswaran V, Barford P, Jha S (2004) Global intrusion detection in the domino overlay system. In: Proceedings of the 11th IEEE network and distributed system security symposium (NDSS)
4. Yu W, Xu G, Chen Z, Moulema P (2013) A cloud computing-based architecture for cyber security situation awareness. In: Proceedings of 4th international workshop on security and privacy in cloud computing (SPCC)
5. Yu W, Zhang N, Fu X, Bettati R, Zhao W (2010) Location leakage of internet threat monitors: modeling and defense. *IEEE Trans Comput (TC)* 59(12):1655–1668
6. Guo H, Li Y, Jajodi S (2007) Chaining watermarks for detecting malicious modifications to streaming data. *Inf Sci* 177(1):281–298
7. Li X, Agrawal G (2005) Efficient evaluation of xquery over streaming data. In: Proceedings of the 31st international conference on very large data bases (VLDB)

8. Nehme RV, Rundensteiner EA, Bertino E (2008) A security punctuation framework for enforcing access control on streaming data. In: Proceedings of 24th international conference on data engineering (ICDE)
9. Zikopoulos P, Eaton C (2011) Understanding big data: analytics for enterprise class hadoop and streaming data
10. Guan Y, Fu X, Xuan D, Shenoy PU, Bettati R, Zhao W (2001) NetCamo: camouflaging network traffic for QoS-guaranteed mission critical applications. *IEEE Trans Syst Man Cybern Part A: Syst Humans* 31(4)
11. Eisenman SM, Fei X, Zhou X, Mahmassani HS (1964) Number and location of sensors for real-time network traffic estimation and prediction. *Transp Res Rec J Transp Res Board* 1:2006
12. Kim S, Reddy A (2005) A study of analyzing network traffic as images in real-time
13. Joshi MR, Hadi TH (2005) A review of network traffic analysis and prediction techniques. *Computer Science*
14. Khater N, Overill RE (2016) Network traffic classification techniques and challenges. In: Proceedings of 10th international conference on digital information management, pp 43–48
15. Ahrenholz J, Danilov C, Henderson T, Kim J (2008) CORE: a real-time network emulator
16. Dias K, Pongelupe M, Caminhas W, Errico L (2019) An innovative approach for real-time network traffic classification. *Comput Netw* 158:143–157
17. Liu L, Jin X, Min G, Xu L (2012) Real-time diagnosis of network anomaly based on statistical traffic analysis
18. Cejka T, Bartos V, Svepes M, Rosa Z, Kubatova H (2016) NEMEA: a framework for network traffic analysis
19. Goodall JR, Lutters WG, Rheingans P, Komlodi A (2006) Focusing on context in network traffic analysis. *IEEE Comput Graphics Appl* 26(2):72–80
20. Karimi A, Niyaz Q, Sun W, Javaid A, Devabhaktuni V (2016) Distributed network traffic feature extraction for a real-time IDS. In: Proceedings of international conference on electro information technology, pp 522–526
21. Sullivan M, Heybey A (2021) Tribeca: a system for managing large databases of network Traac

Machine Learning-Based DC Microgrid Control for Electric Vehicle Charging Stations



Anirudh Pratap, D. K. Palwalia, Mohit Tepan, Nikhil Jain, Anjali Kumari, and Anil Mina

Abstract The use of Renewable energy sources to construct modern-day DC microgrids which have various implementations, one such implementation is an Electric vehicle charging station. The demand for EV is increasing throughout the world and the seamless transition of this kind in the automobile industry requires the construction of EV charging stations, maybe more in numbers than the conventional fuel stations. Therefore, a wide network of EV charging points needs to be created even in remote locations, the use of DC microgrids with grid integration seems to be a proper solution for this problem. This paper presents a machine learning-based energy distribution system for the DC microgrid to be implemented for EV charging station. The designed system is tested in MATLAB/Simulink environment and is compared with conventional control systems.

Keywords EV charging station · DC microgrid · ML-based control

1 Introduction

The increasing adoption of electric vehicle in the automobile industry, demands a better network of EV charging stations throughout the country. In India, there will be 80% electric two- and three-wheelers, 40% electric buses, and 30–70% electric automobiles by 2030. Electric transportation is receiving funding and attention as the country works toward its “Zero-emission” 2070 goal. By 2027, the Indian electric vehicle industry is anticipated to reach USD 15,000 billion [1].

It is impossible to provide generate a market for electric vehicles in countries such as India without an EV charging station network, which can be constructed by either integrating the already existing fuel stations with EV charging points and slowly

A. Pratap (✉) · D. K. Palwalia · M. Tepan · N. Jain · A. Kumari · A. Mina
Rajasthan Technical University, Kota, India
e-mail: anirudhppurohit@gmail.com

D. K. Palwalia
e-mail: dkpalwalia@rtu.ac.in

converting them into complete EV charging station or to create new EV charging stations all together. Although the first option of integrating the fuel stations with EV charging stations sounds more economical and suitable option there in one problem, the high amount of electricity generated and used by EV charging point creates a lot of problems if kept close to fuel discharge units as the static charge generated or plugging and unplugging can create sparks which can lead to fatal accidents in the filling stations [2].

Then the only suitable solution is to construct new EV charging stations [3] which is not very is to do, especially at distant highways and rural areas, even in cities the grid integration of charging stations is quite challenging if multiple sources are used to power the station. In this situation, a DC microgrid comes out as a viable solution for powering the EV charging station. A DC microgrid with multiple sources such as solar photovoltaic (PV), energy storage system (ESS), and wind power is used to generate power and function at remote locations both in stand-alone and grid-connected mode. DC microgrids are more resilient than present AC infrastructure, in addition to their capacity to island, that is why they are idle for powering an EV charging station.

The adaptation of DC microgrid to power the remote and urban EV charging stations has various advantages such as:

- Utilization of green energy at remote locations as it uses renewable energy sources making them environmentally friendly and can be made more resistant to hard weather due to its smaller construction.
- As the load is close to the generation, therefore, there are very low transmission losses which makes the system low loss system.
- The converter system is less expensive which provides additional cost efficiency.
- The power output is high and there is no reactive current in the DC microgrid.
- Controlling a DC microgrid is very easy compared to the AC grid which has complexity like synchronizing, frequency control, harmonics, etc.

State-of-the-art EV charging station has come up with various viable solutions for problems such as grid integration, stable standalone operation of the MG, and various infrastructural solutions [4, 5]. Considering the unique characteristics of a DC-based design, it can be deduced from the literature study that the elements of optimum size and operation, EV-oriented reliability evaluation, and ESS dimensioning have seldom been examined in an organic manner for microgrids using EVs.

In this paper, we present a DC microgrid for EV charging station which uses machine learning algorithm-based controller for optimal energy distribution and stand-alone/islanded operation of the DC microgrid for EV charging station. The grid integration of solar PV, wind turbine, and ESS system is used to power two separate EV charging station which initially runs in grid-connected mode and then is islanded to run as the only source to serve the load. For this purpose, various EV charging station technologies are reviewed beforehand for a better understanding of the problems. In order to take into consideration the techno-economic specifics of various DC microgrid structures, the process for DC microgrid optimum planning, including sizing and operation, is enhanced.

The paper is organized as follows: Sect. 2 addresses the microgrid control and stability problems along with state-of-the-art solutions. Machine learning algorithm-based controller designing is discussed and elaborated in Sect. 3. In Sect. 4, results for the test case scenario are illustrated and discussed. The paper is concluded in Sect. 5.

2 Microgrid Control and Stability

The transient stability of an electrical system is defined as its ability to regain its original state of equilibrium after being subjected to an abrupt disturbance [6, 7]. Tests of transient stability within power system are conducted for a minimum period of time equal to the time necessary for one swing, which is roughly 1 s or less. If the system is stable during the initial swing, it is assumed that the disturbances will decrease in succeeding swing, and the systems will be stable thereafter. The microgrid consists of various sources such as solar PV, ESS, and wind turbine which provide the load power, the optimal energy distribution of these sources is important and is achieved via various state-of-art topologies which are discussed here.

The system parameters are stated in Table 1.

2.1 PV Control

The areas of research for solar PV power generation have been (a) efficiency improvement [8], (b) cell characteristics modeling, (c) grid integration [9], and most importantly, (d) maximum power point tracking techniques [10, 15]. Over the last decade, many contributions to research have been seen in the field of MPPT algorithm [15] these techniques can be broadly divided into two categories: (i) conventional and (ii) modern soft computing algorithm techniques.

The most popular conventional technique is the P&O algorithm which is very capable of tracking maximum power only under uniform irradiation but fails when the partial shading of the PV module occurs, i.e., panels receive unequal irradiation [11]. The importance of the MPPT algorithm is that it can track the maximum power output

Table 1 System parameters

Parameters	Variables
Change in power generation	ΔP_m
Change in wind power generation	ΔP_W
Wind turbine time constant	T_{WT}
Change in solar power generation	ΔP_{PV}
Solar time constant	T_{PV}

Table 2 PV parameters

Designation	Specification
Max. power	249 W
Open circuit voltage (V_{oc})	38.5 V
Short circuit current (I_{sc})	8.85 A
Current at max. power	8.11 A
Voltage at max. power	30.7 V

that can be derived from a solar PV array at certain given irradiation and temperature. The more recent control algorithm is based on the soft computing techniques such as fuzzy logic, swarm optimization, generic algorithm controller, etc., which are the prime choice for nonlinear optimization such as the MPPT. The significant downside of the fuzzy logic technique is that once the rules are created, they cannot be modified [12]. Additionally, these algorithms struggle mightily to obtain the global maximum under partly shadowed situations. The PV data is presented in Table 2.

2.2 ESS Control

Energy Storage Systems (ESS) Fig. 1 is another main component of the DC microgrid and has its implementations for ESS charging stations for various purposes. The ongoing ESS technologies make use of ultracapacitors, flywheel, and most commonly batteries to store power and provide energy during transients. The battery is critical in ensuring that the load receives uninterrupted power. The battery control system’s goal is to control the battery current so that the required power can be obtained. The model also includes charging/discharging current limits, as well as maximum SOC limits.

The controlling of the battery is done by a bidirectional buck–boost DC–DC converter which connects it to the grid. The amount of charge cycles a battery may go through at a given depth of drain before failing to achieve the capacity or efficiency performance criteria. A battery rack is a supporting framework for a set of batteries

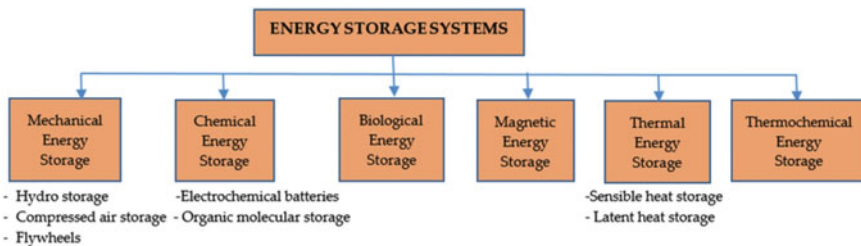


Fig. 1 Energy storage systems

as well as battery cells. In the field of photovoltaics, a captive electrolyte battery is a battery with an immobilized electrolyte. A backup power system is a backup device that can provide enough power to operate crucial technology until grid power comes back to a home, business, or industry (See EPS (Emergency Power System); UPS (Uninterruptible Power Supply); ESS for further information) (Energy Storage System).

2.3 Wind Energy Control

The technical method for converting wind energy into electrical energy is referred to as wind energy converters. The combined electrical and mechanical elements, which have been balanced together within control circuits, must be described in order to convert wind energy into useful electrical energy.

The extensive data analysis of wind energy generation is calculated and provides the predictions for the use of wind power for the use of EV charging station with enabled fast charging [13]. The grid integration of wind power with the other DC sources is also to be carried out. Wind energy grid integration is essentially the sum of all efforts connected to linking WPPs to a grid. Based on when the activity takes place, they are divided into three categories. The first phase, planning, entails activities that take place prior to the integration of a WPP.

Wind turbine used in the model is connected through auto main failure switch; this AMF panel turns on the wind turbine supply when it detects that the microgrid is disconnected from the utility grid. This connects the wind turbine directly to the load, which is an optimal operation for the wind turbine to avoid the generator harmonics to disrupt the flow in the utility grid. The automatic switching of the wind turbine provides the extra power required for the smooth operation of the EV charging station even during the night time.

The actions that take place during in the actual connection of a wind turbine to the grid are referred to as physical connection. System operations are the actions that take place after the WPP has been linked to the grid.

3 ML-Based Control

The anticipation of future responses of the dependent variables using a set of methods known as machine learning (ML), which learns from the training dataset. The relationships between covariates and response variables in the training dataset are modeled by a specific ML technique. Multiple sample points make up the training dataset [14].

ML can be used to develop a dynamic model without solving the equation, it can also be used to train a dynamic model on same form. All parameters, with the

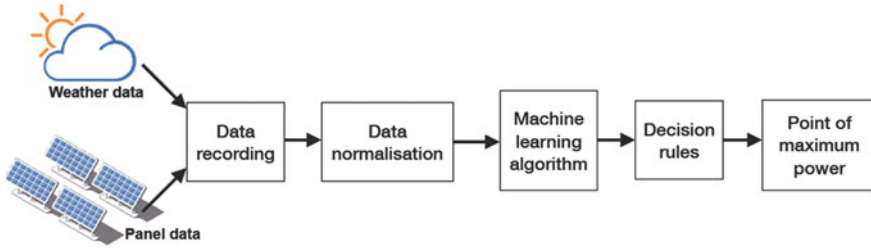


Fig. 2 Implemented flowchart

exception of the hydrodynamic damping parameters, can be estimated with sufficient accuracy using standard methods in most circumstances Fig. 2.

The ML algorithm used for the tracking of the maximum power point of operation of the solar PV array is the Bayesian regularization function Fig. 3, with the objective function of tracking the point of maximum power output $P_d(t)$. The inputs are varying values of irradiance from 1 to 1000 ($Rad_d(t)$) and temperature ranging from 15 to 35 degree Celsius ($T_d(t)$), which forms the weather information vector $W_d(t)$, each input sample of the training dataset consists of

$$T_d(t), W_{d-1}(t), W_{d-2}(t), W_{d-3}(t), W_{d-4}(t), W_{d-5}(t) W_{d-i}(t) = \{Rad_{d-i}(t), Temp_{d-i}(t)\},$$

$$i = 1, 2, \dots$$

We can regulate the variance of the network and prevent overfitting [11]. The ML-based MPPT of the PV array is effective in all types of irradiation conditions, and provides accurate solutions, without consuming much computational power. Next, we see the battery control using the similar ML algorithm which takes the grid-generated voltage V_{dc} and reference value of battery current $I_{battery_{ref}}$ which directs the flow of current through the bidirectional DC-DC converter. This energy storage system provides the excess energy required during high load requirements and stores power during low load requirements.

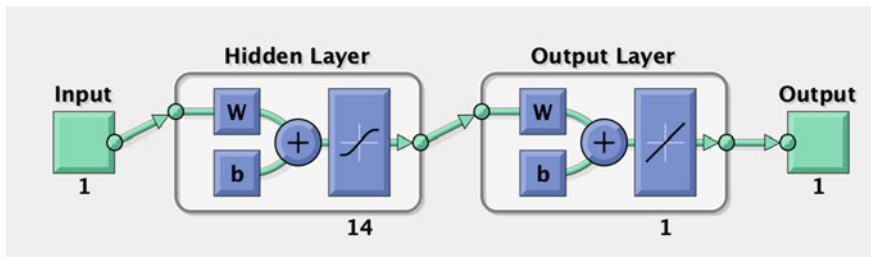


Fig. 3 Neural network model

4 Results and Discussion

The DC microgrid data is validated in the MATLAB/Simulink environment for the proper testing and execution in real-world scenarios. Isolated DC microgrids must be able to supply a continuous, stable power source in comparison to grid-connected microgrids. This research offers a DC microgrid for EV charging station that maximizes storage capacity while being incredibly sensitive to changing irradiances. The microgrid's charging and discharging processes are also enhanced by the deployment of an energy management control system (EMCS).

The following results Figs. 4, 5 and 6 show that the grid can provide power to the load even in islanded conditions where the power is provided only by the DC microgrid sources, i.e., the solar PV, battery ESS, and the wind turbine. After the microgrid being disconnected from the main utility grid at $T = 0.5$ the wind turbine is connected with the use of AMF (Auto Mains Failure) panel. When the utility grid is disconnected due to any reason the AMF panel switches the load from the grid to the secondary generating unit which in the undertaken case is the wind turbine.

The solar PV power is controlled by the ML-based control for maximum power output at a given temperature and irradiance the basic plot of PV power shows the power generated within the DC microgrid before and after the islanding.

The designed microgrid can run on standalone mode which is very important for the EV charging station constructed at remote locations. Energy storage system battery control is also executed by using the ML algorithm for better accuracy and robust operation of the microgrid. The grid power can be seen to regain the original power level within a very short range of time (milliseconds) which shows the robust nature of the system. Microgrid's generated DC voltage gets optimally equal to the load required voltage with the DC load sharing or drooping technique [14].

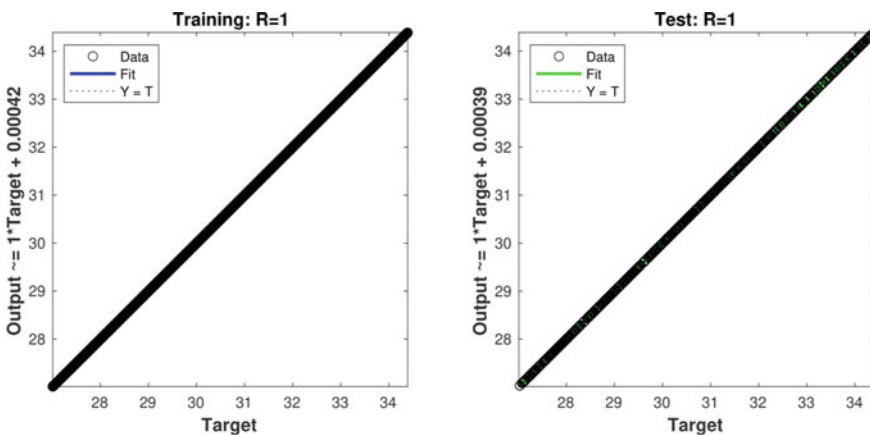


Fig. 4 Training and testing

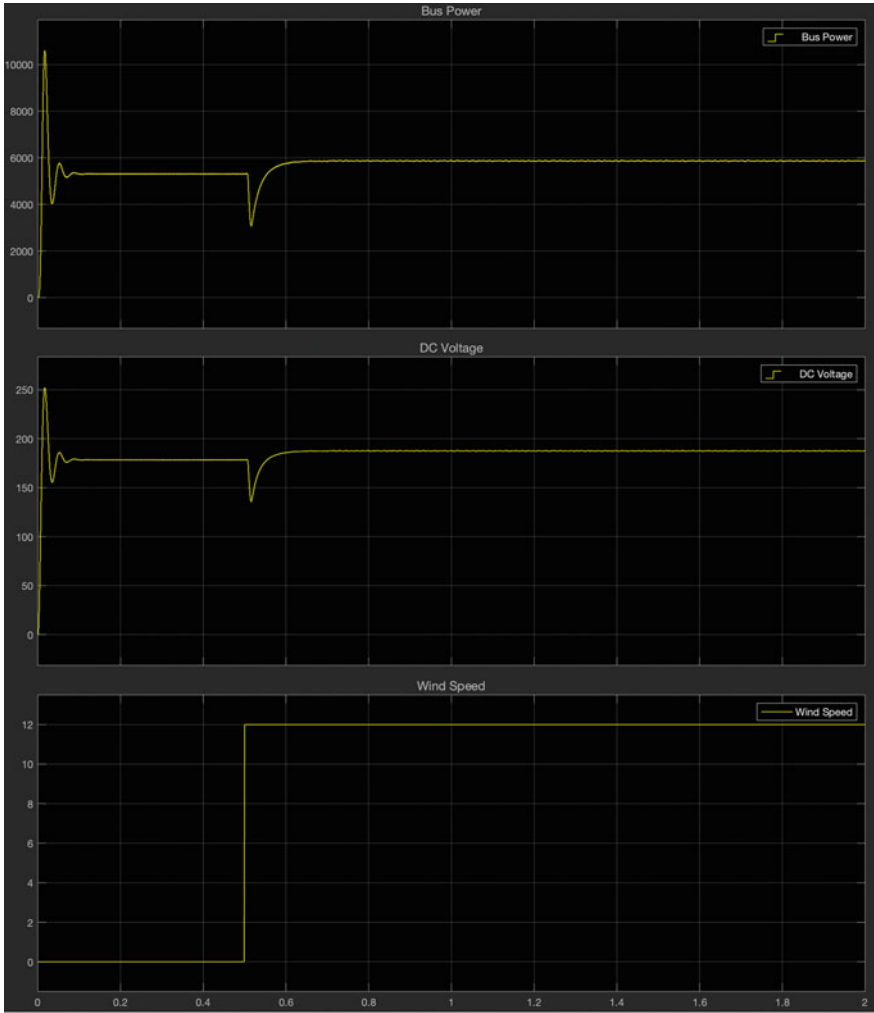


Fig. 5 Results

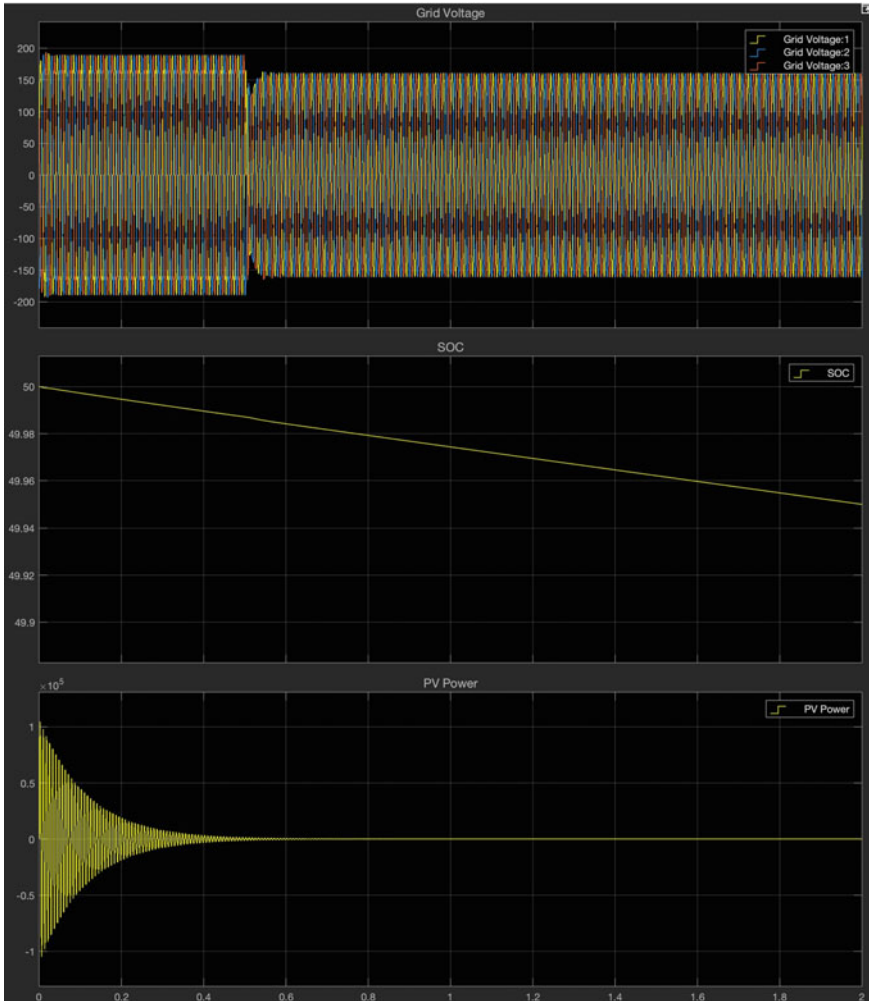


Fig. 6 Results

5 Conclusion

The proposed system of DC microgrid for EV charging station is a proper implementation of state-of-art technologies including machine learning algorithm-based controlling and DC load sharing for the microgrid operation.

The implementation of high-end machine learning technologies such as reinforcement learning approach and adaptive neural network controlling can prove to be an overkill which requires high computational complexity for an average-sized dataset for battery control and maximum power point tracking for a PV array. This experimental setup proves to be a viable solution for the implementation of DC

microgrid in EV charging stations which can be implemented in countries like India with low complexity. Although further research is promoted to design more efficient and less power-consuming artificial neural network controller designing using analog integration for a wide range of implementation for EV charging stations.

References

1. Cosentino V, Favuzza S, Graditi G, Ippolito MG, Massaro F, Riva Sanseverino E, Zizzo G (2012) Smart renewable generation for an islanded system. Technical and economic issues of future scenarios. *Energy* 39(1):196–204
2. Ahmed W et al (2020) Machine learning based energy management model for smart grid and renewable energy districts. *IEEE Access* 8:185059–185078. <https://doi.org/10.1109/ACCESS.2020.3029943>
3. Al-Ali AR, El-Hag A, Bahadiri M, Harbaji M, Ali El Haj Y (2012) Smart home renewable energy management system. *Energy Procedia* 12:120–126
4. Khan A, Memon S, Sattar TP (2018) Analyzing integrated renewable energy and smart-grid systems to improve voltage quality and harmonic distortion losses at electric-vehicle charging stations. *IEEE Access* 6:26404–26415. <https://doi.org/10.1109/ACCESS.2018.2830187>
5. Kabalci E, Kabalci Y (2019) Smart grids and their communication systems. Springer, Singapore
6. Locment F, Sechilariu M (2015) Modeling and simulation of DC microgrids for electric vehicle charging stations. *Energies* 8:4335–4356. <https://doi.org/10.3390/en8054335>
7. Alagoz BB, Kaygusuz A, Karabiber A (2012) A user-mode distributed energy management architecture for smart grid applications. *Energy* 44(1):167–177
8. Wang D, Locment F, Sechilariu M (2020) Modelling, simulation, and management strategy of an electric vehicle charging station based on a DC microgrid. *Appl Sci* 10:2053. <https://doi.org/10.3390/app10062053>
9. Sechilariu M, Wang B, Locment F (2013) Building integrated photovoltaic system with energy storage and smart grid communication. *IEEE Trans Ind Electron* 60:1607–1618
10. Kumar Panwar L, Srikanth Reddy K, Kumar R, Panigrahi BK, Vyas S (2015) Strategic energy management (SEM) in a micro grid with modern grid interactive electric vehicle. *Energy Convers Manag* Dec 106:41–52
11. Aluisio B, Conserva A, Dicorato M, Forte G, Trovato M (2017) Optimal operation planning of V2G-equipped microgrid in the presence of EV aggregator. *Electr Power Syst Res* 152:295–305
12. Shekari T, Golshavannaz S, Aminifar F (2017) Techno-economic collaboration of PEV fleets in energy management of microgrids. *IEEE Trans Power Syst* 32:3841
13. Chandra Mouli GR, Bauer P, Zeman M (2016) System design for a solar powered electric vehicle charging station for workplaces. *Appl Energy* 168:434–443
14. Jain A, Jain S, Palwalia DK (2016) Stability enhancement of DC-DC converters using robust droop control scheme and circulating current elimination in DC micro-grid. In: 2016 IEEE 7th power India international conference (PIICON), pp 1–6. <https://doi.org/10.1109/POWERI.2016.8077192>
15. Prasanth Ram J, Sudhakar Babu T, Rajasekar N (2017) A comprehensive review on solar PV maximum power point tracking techniques. *Renew Sustain Energy Rev* 67:826–847. ISSN 1364-0321. <https://doi.org/10.1016/j.rser.2016.09.076>
16. Kundar P et al (2004) Definition and classification of power system stability. *IEEE Trans Power Syst* 19(4):2124

Tree Shaped Nature-Inspired Ultra-Wideband Antenna for Wireless Body Area Networks Applications



Laxmi Narayan Balai

Abstract This paper describes a nature-inspired tree-shaped antenna with a defective ground structure for high-speed wireless communication at frequencies spanning from 1.79 to 4.16 GHz. The suggested antenna has a gain of 4.6 dB and an efficiency of more than 90%, making it suitable for wireless body area network applications, which are presently a prominent topic among researchers because of the COVID 19 therapy. Since the suggested antenna is simple, low profile, and planar, it is appropriate for industrial applications.

Keywords Nature-inspired antenna · Ultra-wideband antenna · Wireless personal area networks

1 Introduction

Wireless body area networks (WBANs) have a wide range of applications, including medical, personal entertainment, athletics, military, and intelligent systems. Ultra-wideband (UWB) is seen as a viable candidate in this sector [1–3]. WBAN systems are popular due to their low signal strength and low cost. UWB considers the majority of obstacles, which frequently reflect waves with limited bandwidth and a bigger mapping [4, 5]. Its transmission frequencies extend from 3.1 to 10.6 GHz and have a higher degree of attenuation. The gain of an antenna is dramatically affected when its bandwidth is increased. It is incredibly challenging for researchers to obtain a broad bandwidth, high gain, low profile, and planar structure all at the same time [1, 6–8]. Several research articles have been studied in an attempt to fill the afore-said research gap. The research [9, 10] examines several bandwidth improvement approaches with steady gain. Antennas inspired by natural architecture give good efficiency in their constructions [11–15]. The article [16] discusses several efficiency increase approaches for microwave antennas. This study makes use of a large slot in the ground with a parasitic element that provides ultra-wideband characteristics.

L. N. Balai (✉)
Yagyavalkya Institute of Technology, Jaipur, India
e-mail: lnbalai@yahoo.com

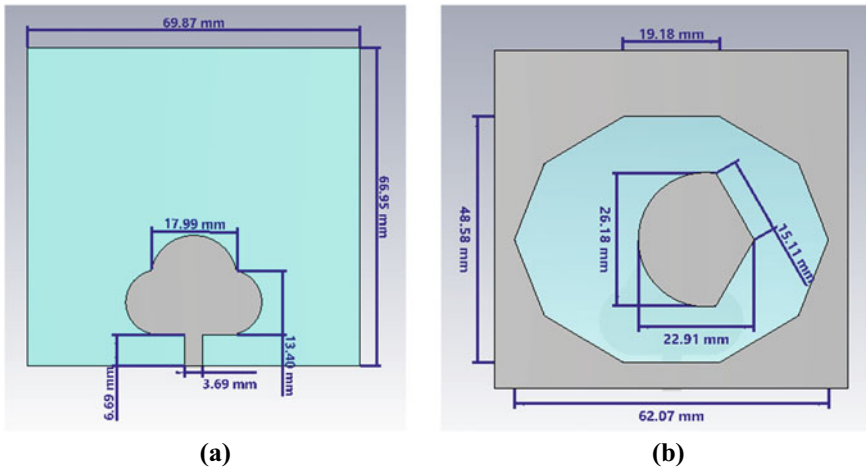


Fig. 1 Geometry of tree shaped antenna **a** top view, **b** back view

This research presents a nature-inspired tree-shaped antenna with outstanding efficiency. This study presents a pentagon-shaped slot with a sectored ground to attain ultra-wideband characteristics.

2 Antenna Design

Figure 1 depicts the proposed antenna's geometry. The 50Ω microstrip line powers the tree-shaped patch. FR4 Substrate with a dielectric constant of 4.3 and height of 1.6 mm is employed. The thickness of the conductive layer is 0.035 mm. Figure 1a depicts all of the front layer design parameters. Figure 1b depicts the backside ground plane. To obtain ultra-wideband properties and consistent gain, a pentagon-shaped slot is carved from the ground and a parasitic element is placed in the middle of the ground slot. Because the patch is tree-shaped and inspired by natural formations, it has efficient radiation characteristics.

3 Results and Discussions

Computer Simulation Technology Software [17] is used to simulate the proposed antenna. Figure 2 depicts the planned antenna's electric field distribution. It should be noticed that the electric field is strongest near the patch's boundaries. The maximum electric field density is 82.78 dB (V/m), indicating that the antenna is radiating efficiently.

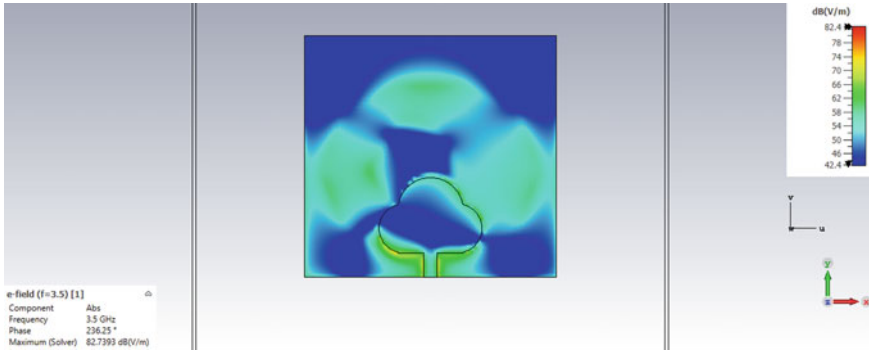


Fig. 2 Electric field distribution of tree shaped antenna

Figure 3 depicts the surface current distribution of the proposed antenna. It should be noted that the largest surface current is spread at the boundaries of the ground slot, the parasitic element in the ground, and the edges of the tree-shaped patch. At 3.5 GHz, the maximum surface current density is 32.6 dB (A/m).

Figure 4 presents the proposed antenna’s reflection coefficient (S11) versus frequency plot. It should be mentioned that the suggested antenna has a frequency range of 1.79–4.16 GHz and has a 69.09% impedance bandwidth at 3.43 GHz. S11 at the resonant frequency is -31.16 dB, indicating low return loss and good impedance matching.

The suggested antenna’s Smith chart is presented in Fig. 5, and it shows that the impedance at the resonant frequency is 52.16Ω , which is extremely near to 50Ω , indicating effective impedance matching.

Figure 6 shows an efficiency versus frequency plot. It implies that the radiation efficiency is extremely near to one and the overall efficiency is about 0.9, indicating that the antenna construction has minimal losses.

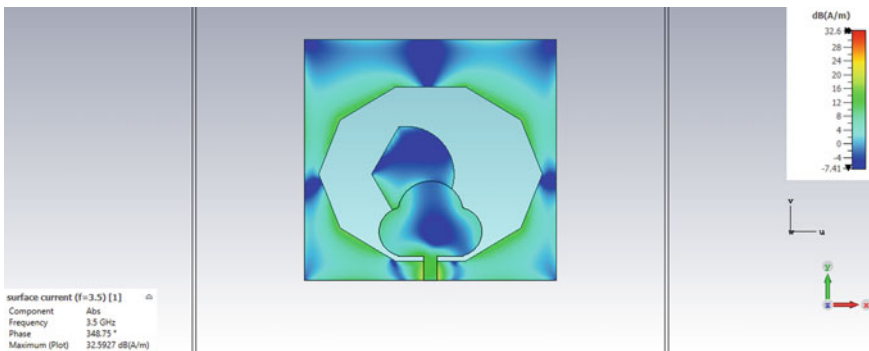


Fig. 3 Surface current distribution of tree shaped antenna

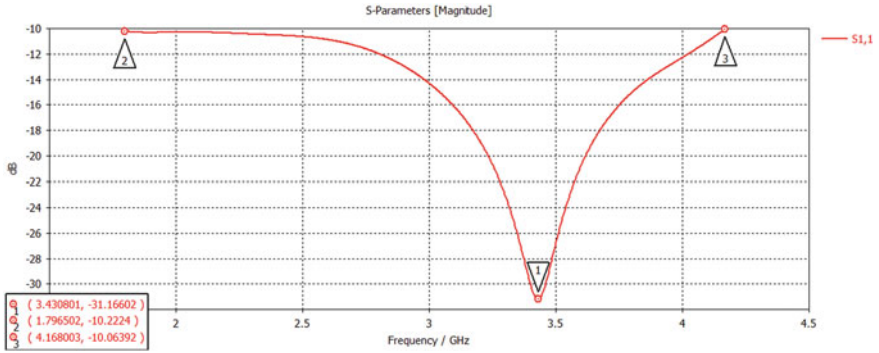


Fig. 4 Reflection coefficient versus frequency plot of tree shaped antenna

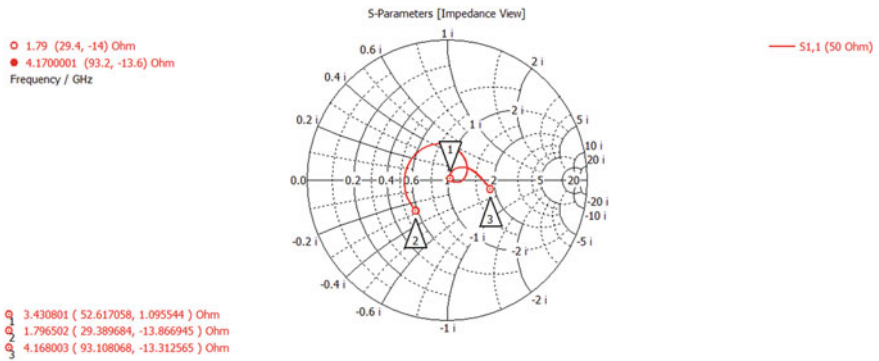


Fig. 5 Smith chart plot of tree shaped antenna

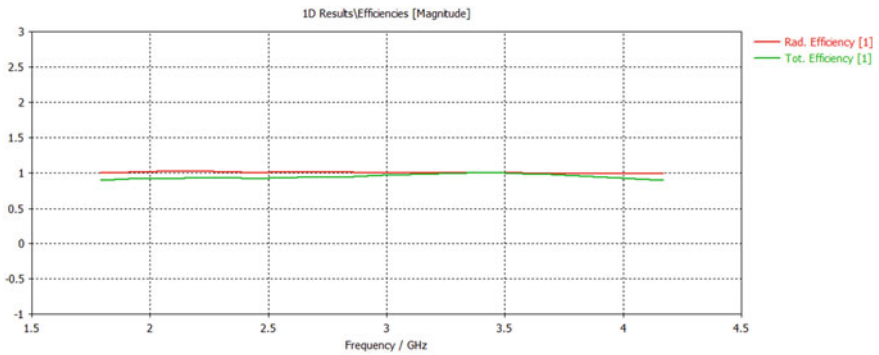
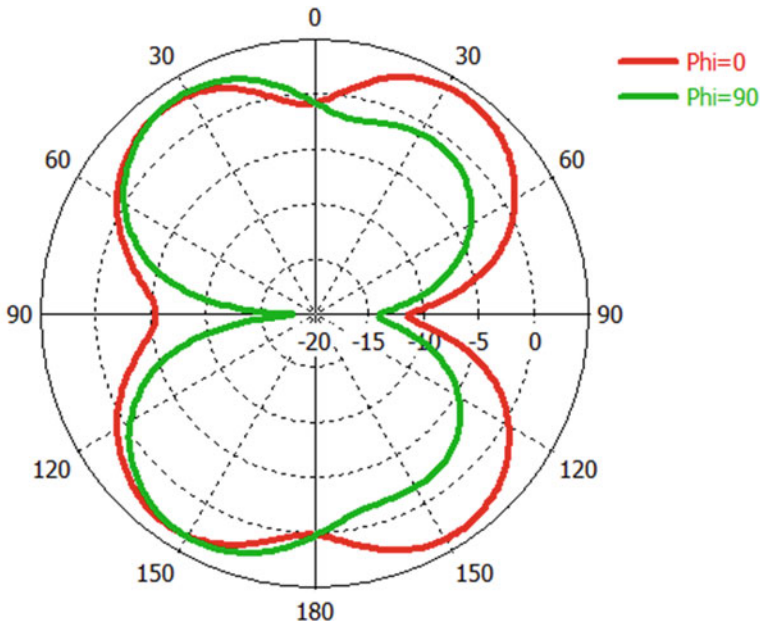
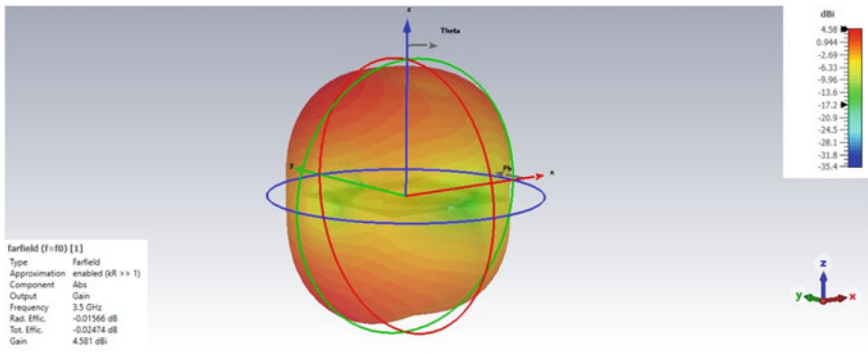


Fig. 6 Efficiency versus frequency plot of tree shaped antenna

Figure 7 represents the proposed antenna's radiation pattern. Figure 7a depicts the radiation pattern at $\Phi = 0$ and $\Phi = 90$, indicating that it is quasi-bidirectional and radiates at the broadside of the antenna shape and the antenna has a decent coverage range. Figure 7b depicts a three-dimensional radiation pattern, indicating a clear understanding of the antenna's radiation process. At the resonance frequency, the maximum gain is 4.58 dB.



Theta / Degree vs. dBi
(a)



(b)

Fig. 7 Radiation pattern of tree shaped antenna at 3.43 GHz **a** one-dimensional radiation pattern at $\Phi = 0$ and $\Phi = 90$, **b** three-dimensional radiation pattern

Table 1 Performance comparison with reported antennas

Works	Bandwidth (%)	Resonant frequency (GHz)	Minimum S11 (dB)	Maximum gain (dB)
Proposed	69	3.43	-31.16	4.58
[2]	16.25	2.44	-18	1.42
[18]	4.5, 3.8	2.4, 5.8	-12.5	1.1
[19]	33, 19.8	3.5, 5.5	-30 to -35	2.5, 2.6

4 Performance Comparison with Reported Antennas

The performance of the proposed antenna is compared with the reported antenna in Table 1. It may be observed that the proposed antenna provides better bandwidth, good impedance matching, and maximum gain in comparison to reported antennas.

5 Conclusion

This research proposes a nature-inspired tree-shaped antenna with super wideband characteristics and 69% bandwidth at 3.5 GHz with a gain of 4.581 dB. The proposed antenna has an efficiency of more than 90% thanks to a construction inspired by natural plants that receive efficient solar radiation. Because of its high gain and ultra-wideband properties, it is well suited for high-speed, low-latency communication applications. The proposed antenna has applications in wireless personal area networks, military, defense, biological monitoring, and a variety of other fields. The antenna construction is simple, planar, low profile, and low cost, allowing for affordable large-scale fabrication.

References

1. Afruz U, Kabir MA (2021) Design of wearable microstrip patch antenna for wireless body area network. In: 2021 24th international conference on computer and information technology (ICCIT), pp 1-5. <https://doi.org/10.1109/ICCIT54785.2021.9689901>
2. Liu P, Meng Z, Wang L, Zhang Y, Li Y (2020) Omnidirectional dual-polarized saber antenna with low wind drag. *IEEE Trans Antennas Propag* 68(1):558-563. <https://doi.org/10.1109/TAP.2019.2934566>
3. Savci H, Sajjad H, Khan S, Kaburcuk F (2021) A compact multi-band antenna on textile for wearable body area network devices. *Balk J Electr Comput Eng* 9(3):255-260. <https://doi.org/10.17694/bajece.849699>
4. Ali WAE, Ibrahim AA (2017) A compact double-sided MIMO antenna with an improved isolation for UWB applications. *AEU - Int J Electron Commun* 82:7-13. <https://doi.org/10.1016/j.aeue.2017.07.031>

5. Ahad A, Tahir M, Sheikh MA, Ahmed KI, Mughees A, Numani A (2020) Technologies trend towards 5G network for smart health-care using IoT: a review. *Sensors (Switzerland)* 20(14):1–22. <https://doi.org/10.3390/s20144047>
6. Jhang W-C, Sun J-S (2021) Small antenna design of triple band for WIFI 6E and WLAN applications in the narrow border laptop computer. *Int J Antennas Propag* 2021:7334206. <https://doi.org/10.1155/2021/7334206>
7. Zhang S, Ying Z, Xiong J, He S (2009) Ultrawideband MIMO/diversity antennas with a tree-like structure to enhance wideband isolation. *IEEE Antennas Wirel Propag Lett* 8:1279–1282. <https://doi.org/10.1109/LAWP.2009.2037027>
8. Tapan Nahar SR (2021) Cost efficient low profile MIMO antenna for 5G communicationse. In: *Intelligent computing techniques for smart energy systems: proceedings of ICTSES 2021. Lecture notes in electrical engineering*, vol 862, p 726
9. Nahar T, Rawat S (2021) Survey of various bandwidth enhancement techniques used for 5G antennas. *Int J Microw Wirel Technol* 1–21. <https://doi.org/10.1017/S1759078720001804>
10. Masoodi IS, Ishteyaq I, Muzaffar K (2022) Extra compact two element sub 6 GHz MIMO antenna for future 5G wireless applications. *Prog Electromagn Res Lett* 102:37–45. <https://doi.org/10.2528/PIERL21100303>
11. Keshwala U, Rawat S, Ray K (2020) Nature inspired 21 branches sneezewort/Achillea ptarmica plant growth pattern–shaped antenna for Ku-band applications. *Int J RF Microw Comput Eng* 30(8):e22240. <https://doi.org/10.1002/mmce.22240>
12. Naga Jyothi Sree G, Nelaturi S (2021) Design and experimental verification of fractal based MIMO antenna for lower sub 6-GHz 5G applications. *AEU - Int J Electron Commun* 137:153797. <https://doi.org/10.1016/j.aeue.2021.153797>
13. Babu K, Das S, Varshney G, Naga Jyothi Sree G, Madhav B (2021) A micro-scaled graphene based tree-shaped wideband printed MIMO antenna for terahertz applications
14. Patel A et al (2022) Inverted-L shaped wideband MIMO antenna for millimeter-wave 5G applications. *Electron* 11(9):1–16. <https://doi.org/10.3390/electronics11091387>
15. Olawoye TO, Kumar P (2022) A high gain antenna with DGS for sub-6 GHz 5G communications. *Adv Electromagn* 11(1):41–50. *SE-Research Articles*. <https://doi.org/10.7716/aem.v11i1.1670>
16. Nahar T, Rawat S (2022) Efficiency enhancement techniques of microwave and millimeter-wave antennas for 5G communication: a survey. *Trans Emerg Telecommun Technol* e4530. <https://doi.org/10.1002/ett.4530>
17. CST Microwave Studio. <http://www.cst.com/products/cstmws>
18. Hsieh CY, Wu CH, Ma TG (2015) A compact dual-band filtering patch antenna using step impedance resonators. *IEEE Antennas Wirel Propag Lett* 14:1056–1059. <https://doi.org/10.1109/LAWP.2015.2390033>
19. Jin G, Deng C, Yang J, Xu Y, Liao S (2019) A new differentially-fed frequency reconfigurable antenna for WLAN and sub-6 GHz 5G applications. *IEEE Access* 7:56539–56546. <https://doi.org/10.1109/ACCESS.2019.2901760>

Machine Learning-Based Model for Predicting Failure of Physical Machines in Cloud Computing



Priti Kumari , Vandana Dubey , Meenal Jain , and G. R. Mishra 

Abstract Cloud computing is a form of computing that makes use of the internet to provide a wide range of services and scalable computing resources. It is a commonly used technique because it enables the integration of software and hardware resources. However, when compared to traditional computer systems, the possibilities of letdown in a cloud-based system upsurge. One of the most important parts for achieving high dependability and accessibility for the cloud computing architecture is fault tolerance (FT). To achieve cloud computing reliability, failures must be investigated and rectified immediately. As a result, in this research, we investigated machine learning's predictive capabilities by employing a variety of methods to improve the accuracy of failure prediction. We used machine learning (ML) and constructed a failure prediction model for forecasting physical machine (PM) failure in the cloud data center, as well as comparison-based testing on prediction accuracy. The procedures we considered are Support Vector Machine (SVM), K Nearest Neighbor (KNN), Gaussian Naive Bayes (GNB), and Random Forest. Precision, recall, F1-measure, and accuracy were used to measure the effectiveness of machine learning approaches. According to the simulation, KNN, SVM, and Random Forest performed well on the datasets.

Keywords Cloud computing · Physical machine · SVM · KNN · Gaussian Naïve Bayes · Random forest · K-mean

P. Kumari
Ashoka Institute of Technology and Management, Varanasi, U.P., India

M. Jain
Bennett University, Greater Noida, U.P., India

G. R. Mishra
Dr. Rammanohar, Lohia Avadh University, Faizabad, U.P., India

V. Dubey (✉)
C. Byregowda Institute of Technology, Kolar, Karnataka, India
e-mail: vandanashuklaec05@gmail.com

1 Introduction

The term Cloud computing makes use of the internet to provide a wide range of services and scalable computing resources. Due to the features that permit distribution and multiplexing system resources across several tenants, cloud reliability has expanded a widespread foothold in recent epochs. However, the widespread adoption of cloud services is due to the ability to deliver resources flexibly and elastically based on user needs on a pay-per-use basis. It is no longer necessary for users to purchase, manage, or update their computer resources [1]. Instead, they may access a variety of information technology capabilities as services, such as computation, storage, memory, networks, software, and so on, at reasonable costs and without the difficulties of owning or managing the resources. On the other side, cloud service providers benefit from the scalability of their services and the concept of multi-tenancy. A multitenant architecture enables a cloud provider to share resources among numerous consumers, lowering costs. A user can also request specialized resources, although they will be more expensive [2].

Even though cloud services are utilized for a wide range of applications, there are uncertainties about breakdowns and performance deterioration in the cloud. Many businesses are adopting the cloud computing paradigm because of its benefits such as high scalability, on-demand services, and low-cost maintenance [1]. The cloud computing-based infrastructure as a service (IaaS) concept virtualizes PMs into virtual machines to execute various sorts of tasks given by customers [2, 3]. However, due to hardware or software failures, PMs in cloud environments where VMs are run might frequently stop operating or fail when completing user requests. According to the presented model, PM failures have a massive influence on performance, scalability, revenue, and user confidence. To handle the failure of PM, FT procedures are used to enable the cloud system to work uninterruptedly in the existence of a fault [2–4]. The causes of failure are depicted in Fig. 1.

This paper presents a proactive FT strategy to predict failure in advance. Our suggested work's significant contribution is as follows:

- Proposes a model for predicting physical machine failures in cloud data centers.
- In the projected model, we have applied ML procedures like SVM, KNN, GNB, and Random-forest to detect PM failures.
- We have performed simulation and compared the result of each ML technique in terms of precision, recall, F1-measure, and accurateness.

The remaining part of the transcript is systematized as follows: The Related Work on FT and ML techniques is discussed in Sect. 2. The projected method is defined in



Fig. 1 Causes of failure

Sect. 3. The machine learning training model is described in Sect. 4. The simulation consequences are deliberated in Sect. 5. This paper is concise in Segment 6.

2 Related Work

Fault tolerance (FT) is required for the cloud system to provide required services even if one or more components fail. According to the literature, there are two sorts of FT methods: reactive and proactive. Reactive FT is a technique for reducing the impact of failures that have already happened. The proactive FT refers to the process of anticipating a defect and replacing the questionable component with a functional component [2, 4].

In cloud computing, many strategies have been implemented to deal with failure reactively. Machine Learning methods, on the other hand, are better at predicting cloud computing failure. Islam et al. [5] used machine learning approaches to forecast application failure in cloud computing. The authors have proposed a forecast strategy constructed on a special kind of Recurrent Neural Network entitled the LSTM to recognize application breakdowns in the cloud (LSTM). It gathers resource utilization statistics or presentation data for individual job or task in order to forecast whether they will be terminated. Li et al. [6] suggested a machine learning-based methodology for forecasting node failure. Liu et al. [7] conducted a statistical study of workload at the node, job, or task levels in terms of resource consumption. The LLFT system introduced by Zhao et al. [8] is a reactive middleware for enduring letdowns in distributed systems.

Li et al. [9] have tried to minimize the functioning costs of external and internal letdowns and for that they have proposed an approach named as FTS. Azaiez et al. [10] proposed a hybrid FT technique that incorporates the benefits of replication. In Attallah et al. [11], major goal of the suggested model is to keep track of variations in CPU consumption and make a conclusion once a high charge of CPU consumption is found. Ragmani et al. [12] invented a methodology to deal with disc failure, and they used artificial neural networks to forecast failure in advance. The existing FT models are deliberated in Table 1.

Moreover, the existing models have focused on the reactive and some of the work considered proactive fault tolerance methods. Many of the existing proactive models aim to predict the failure of applications, disk, CPU utilization, etc. However, there is no significant work is done to predict the failure of physical machines in the cloud data center. In this work, we have proposed a model to predict the failure of PM in the cloud data center to improve the reliability of the cloud systems.

Table 1 Preceding FT models comparison

Existing fault tolerance models	FT methods	Description
LLFT [8]	Reactive	The suggested strategy focuses on replicating applications that are operating on the cloud
FTS [9]	Reactive	The proposed approach focuses to minimize the cost
Hybrid FT [10]	Reactive	The proposed scheme is based on a checkpoint and replication technique that focuses on VM failure
PLBFT [11]	Proactive	The proposed method aims to focus on CPU utilization or balancing the load of virtual machines
Adaptive fault tolerance model for improving cloud computing performance using ANN [12]	Proactive	The proposed model used the ANN algorithm to predict the disk failure
LSTM [5]	Proactive	The proposed approach has used the RNN algorithm to predict application failure in the cloud environment
AIOps [6]	Proactive	The authors have suggested a machine learning-based methodology for forecasting node failure. The aim is to reduce the cost

3 Proposed Model

In the cloud environment, several virtual machines or tasks are executed on the PMs to serve the client's requests. The paper proposes a failure prediction model to forecast the failure of PMs in the cloud environment. The proposed prediction model is demonstrated in Fig. 2. The proposed model consists of six stages such as (1) uploading the failure dataset, which is unlabeled, (2) extracting some useful feature from the dataset for predicting failure, and (3) once feature extraction is done then performing data cleaning. (4) Applying the K-Means clustering technique to deal with the unlabeled dataset. (5) Foreseeing the failure using the machine learning model. (6) Once the failure is predicted then it will be managed by the cloud service providers.

- **Uploading Dataset:** For predicting the failure, the dataset we have used here is the NERSC [18]. This dataset consists of data related to the past occurrences of PM failures and disk failures in the PM respectively.
- **Feature Extracting:** From that data set we have extracted some features such as the cause of failure, the downtime throughout a failure, and PM's category and its purpose. The cause of fault indicates whether a fault is likely to recur or not.
- **Cleaning Dataset:** It is the procedure of making raw data for analysis by eliminating corrupt data, unifying the raw data, and filling the null values. The focus of this research is to deal with missing values in certain rows and columns.

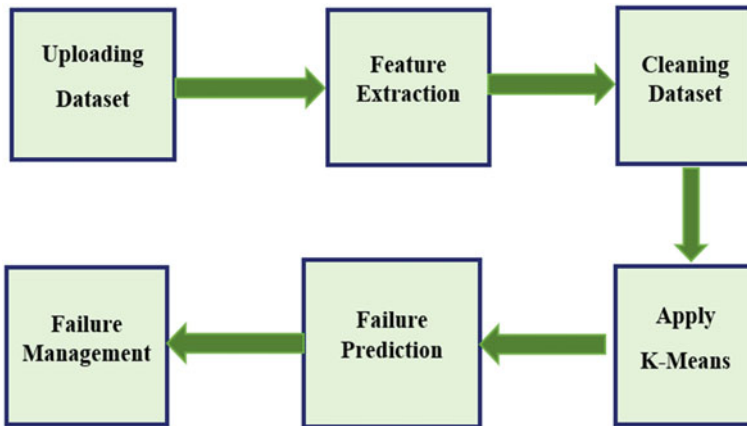


Fig. 2 Proposed failure prediction model

- **K-Means procedure:** This technique is used to cluster failure data in an unsupervised fashion. It's a non-parametric algorithm that doesn't presuppose any kind of definite data distribution, therefore it's good for real-world failure data. The data is also unlabelled; thus K-Means is utilized to divide the data into three groups based on feature similarity [13].
- **Failure Prediction:** We applied a variety of machine learning models to anticipate PM failure in a cloud data center, including SVM, KNN, GNB, and Random Forest.
- **Failure Management:** Once a failure has been successfully anticipated, cloud service providers will manage it by replacing the suspected component with a working component, hence increasing the reliability of cloud-based services.

4 Machine Learning (ML) Model Training

Today, machine learning is in use. The term machine learning (ML) refers to the ability of computers to learn without being explicitly programmed. It is, without a doubt, one of the most captivating technologies ever devised. As the name implies, it gives the computer characteristics that make it more human-like: The capacity for learning.

This section defines the several modeling decisions during the model training phase. We investigated four ML procedures in our projected solution: SVM [14], KNN [15], GNB, and random forest [5]. To perform an impartial comparison, we have executed all four ML procedures.

- **SVM (Support Vector Machine):** It is a type of supervised ML procedure, i.e., used for both classification as well as regression. The motive of the SVM procedure

is to search for a hyperplane in an N-dimensional interplanetary that categorizes the data points [14].

- **KNN (K Nearest Neighbor):** This algorithm adopts the resemblance among the new arrived data and existing data and places the novel data into class, i.e., utmost comparable to the existing classes. This procedure keeps all the existing data and labels a novel data point based on the resemblance, which means whenever a new case appears then it will be simply categorized into a good suite group [15].
- **GNB (Gaussian Naïve Bayes):** This is a basic but effective probabilistic classification-based model in ML that draws impact from Bayes Theorem [16].

$$\text{Probability } (X|Y) = \frac{\text{Probability } (Y|X) \cdot \text{Probability } (X)}{\text{Probability } (Y)} \quad (1)$$

where X and Y are two events, Probability ($X|Y$) is the possibility of event X provided event Y has previously occurred, Probability ($Y|X$) is the likelihood of event Y provided event X has previously occurred, Probability (X) is the independent likelihood of X , and Probability (Y) is the independent likelihood of Y .

- **Random Forest:** On any given dataset, this classifier comprises many decision trees on numerous subcategories and receipts the average to advance the prognostic correctness of that dataset. It is a supervised ML algorithm, i.e., used extensively in both classification and regression. It makes decision trees on diverse trials or samples and receipts their common vote and average for classification and regression, respectively [17].

5 Performance Evaluation

We have executed a proof-of-perception model of our forecast system and estimated its performance with the NERSC datasets [18]. The NERSC dataset contains data related to the past occurrences of PM failures. The work has used the following attributes of the dataset: the cause of failure, the downtime during a failure, and the physical machine's type and its purpose.

In this segment, we have presented our experimental outcomes. The simulation experiments are accomplished on a system having an Intel® Core (TM) CPU i5-7200 computer with a CPU speed of 2.7 GHz and storage of 8 GB.

5.1 Results

To examine the excellence of a proposed forecast system, firstly, need to stipulate the assessment parameters. The objective of this study is to project an effectual predictor to foresee failure appropriately and shelter as many failure actions as possible while

producing very insufficient false positives. In this work, we have used the subsequent list of parameters to assess the performance of projected model: Precision, Recall, Accuracy, and F1 Score. We perform an evaluation using different sizes of training data and test data. For Assessment 1, we have considered 80% and 20% data for training and testing respectively (see Table 2). For Assessment 2, we have used 75% of data for training and 25% for testing (see Table 3). For assessment 3, we have considered 70% of data for training and 30% for testing (see Table 4). The predicted value for Assessment 1, Assessment 2, and Assessment 3 is shown in Figs. 2, 3, and 4, respectively.

The KNN, SVM, and Random Forest algorithms all provide comparable accuracy for the given data set, based on the results. However, the Random Forest machine learning model is best suitable for predicting the failure in cloud computing (Fig. 5).

Table 2 Training data is 80% and testing data is 20%

Assessment 1				
Parameter	KNN (%)	SVM (%)	GNB (%)	Random forest (%)
Precision	100	100	98	100
Recall	100	100	96	100
F1-score	100	100	97	100
Accuracy	100	100	97	100

Table 3 Training data is 75% and testing data is 25%

Assessment 2				
Parameter	KNN (%)	SVM (%)	GNB (%)	Random forest (%)
Precision	100	100	98	100
Recall	100	100	96	100
F1-score	100	100	97	100
Accuracy	99	99	96	100

Table 4 Training data is 70% and testing data is 30%

Assessment 3				
Parameter	KNN (%)	SVM (%)	GNB (%)	Random forest (%)
Precision	100	100	98	100
Recall	100	100	96	100
F1-score	100	100	97	100
Accuracy	100	99	97	100

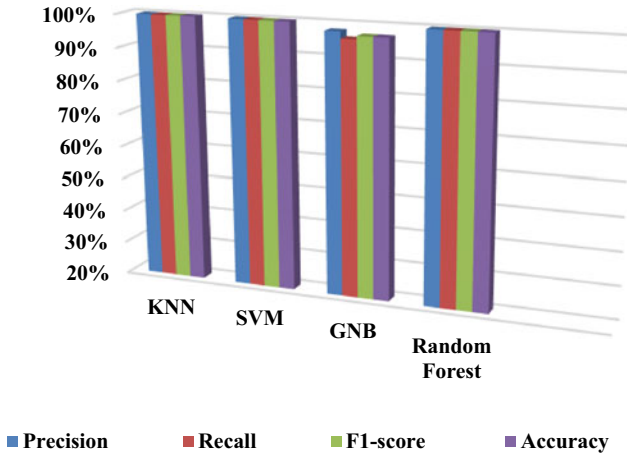


Fig. 3 Predicted value for Assessment 1

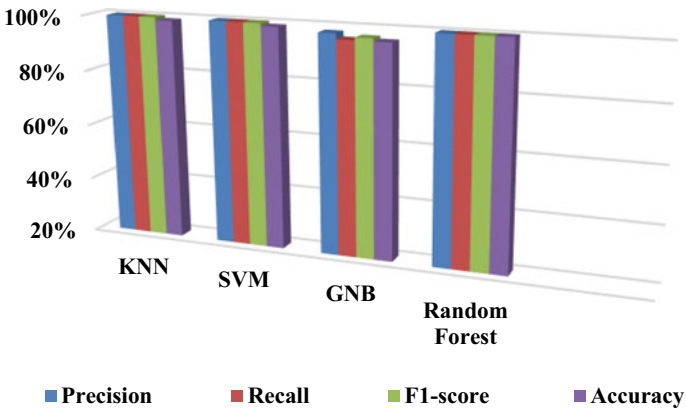


Fig. 4 Predicted value for Assessment 2

6 Conclusion and Future Scope

This research provides a failure prediction model for cloud data center physical machine (PM) failure. SVM, KNN, GNB, and Random Forest were the approaches we explored. The performance of machine learning approaches was evaluated using precision, recall, F1-measure, and accuracy. KNN, SVM, and Random Forest all performed well on the presented dataset, according to the simulation. We plan to use deep learning techniques on this and other datasets in the future to anticipate the breakdown of physical devices in cloud computing.

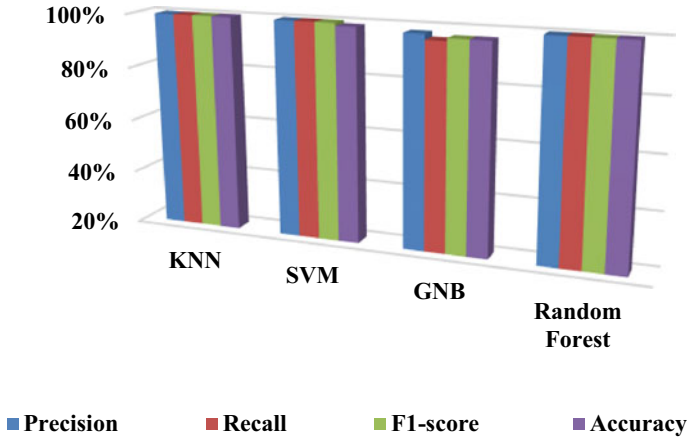


Fig. 5 Predicted value for Assessment 3

References

1. Kumari P, Kaur P (2020) Topology-aware virtual machine replication for fault tolerance in cloud computing systems. *Multiagent Grid Syst* 16(2):193–206
2. Kumari P, Kaur P (2021) A survey of fault tolerance in cloud computing. *J King Saud Univ Comput Inf Sci* 33(10):1159–1176
3. Liu J, Wang S, Zhou A, Kumar SA, Yang F, Buyya R (2016) Using proactive fault-tolerance approach to enhance cloud service reliability. *IEEE Trans Cloud Comput* 6(4):1191–1202
4. Buyya R, Yeo CS, Venugopal S, Broberg J, Brandic I (2009) Cloud computing and emerging IT platforms: vision, hype, and reality for delivering computing as the 5th utility. *Futur Gener Comput Syst* 25(6):599–616
5. Islam T, Manivannan D (2017) Predicting application failure in cloud: a machine learning approach. In: 2017 IEEE international conference on cognitive computing (ICCC). IEEE, pp 24–31
6. Li Y, Jiang ZM, Li H, Hassan AE, He C, Huang R, Zeng Z, Wang M, Chen P (2020) Predicting node failures in an ultra-large-scale cloud computing platform: an aiops solution. *ACM Trans Softw Eng Methodol (TOSEM)* 29(2):1–24
7. Liu Z, Cho S (2012) Characterizing machines and workloads on a Google cluster. In: Proceedings of the 41st international conference on parallel processing workshops, pp 397–403
8. Cheraghlou MN, Khadem-Zadeh A, Haghparast M (2016) A survey of fault tolerance architecture in cloud computing. *J Netw Comput Appl* 61:81–92
9. Li Z, Yu J, Hu H, Chen J, Hu H, Ge J, Chang V (2018) Fault-tolerant scheduling for scientific workflow with task replication method in cloud. In: Paper presented at: international conference on internet of things, big data and security, pp 95–104
10. Azaiez M, Chainbi W, Ghedira K (2019) Hybrid fault tolerance model for cloud dependability. In: Paper presented at: international conference on high performance computing and communications, pp 2436–2444
11. Attallah SM, Fayek MB, Nassar SM, Hemayed EE (2021) Proactive load balancing fault tolerance algorithm in cloud computing. *Concurr Comput Pract Exp* 33(10):e6172
12. Ragmani A, Elomri A, Abghour N, Moussaid K, Rida M, Badidi E (2020) Adaptive fault-tolerant model for improving cloud computing performance using artificial neural network. *Procedia Comput Sci* 170:929–934

13. Mahendiran A, Saravanan N, Subramanian NV, Sairam N (2012) Implementation of K-means clustering in cloud computing environment. *Res J Appl Sci Eng Technol* 4(10):1391–1394
14. Catak FO, Balaban ME (2012) CloudSVM: training an SVM classifier in cloud computing systems. In: Joint international conference on pervasive computing and the networked world. Springer, Berlin, Heidelberg, pp 57–68
15. Ghosh P, Shakti S, Phadikar S (2016) A cloud intrusion detection system using novel PRFCM clustering and KNN based Dempster-Shafer rule. *Int J Cloud Appl Comput (IJCAC)* 6(4):18–35
16. Fekade B, Maksymyuk T, Jo M (2016) Clustering hypervisors to minimize failures in mobile cloud computing. *Wirel Commun Mob Comput* 16(18):3455–3465
17. Hur JH, Ihm SY, Park YH (2017) A variable impacts measurement in random forest for mobile cloud computing. *Wirel Commun Mobile Comput* 2017
18. <https://www.nersc.gov/research-and-development/data-analytics>

Solar Inverter Equipped with a Battery Management System



Babu Naik Gugulothu , Moinuddin Pasha, P. Deepa, K. Y. Kusuma, and Ponnam Naga Roopa

Abstract This paper examines the development of solar power inverters and focuses on the integration of packaging and functionality in solar inverter technology. Efficiency and losses, as well as the mean time between failures and inverter prices, are the three most crucial metrics for assessing inverter technological advancements. High dependability, a long life, and lower costs are all correlated with high integration levels. The study discusses the current status of inverter design and trends toward higher functional and packaging integration. Regarding integration level, which will be defined by several metrics, many generations of medium power inverters are compared. The battery management system, a crucial component, is required for both hybrid and electric vehicles. The BMS completes the required tasks by integrating more than two processes, such as choosing the temperatures and voltages of the battery cells in a battery module as well as gathering the voltage and current of the battery, balancing the voltages of the cell, and figuring out the state of charge. This article will include the investigation on battery temperature, battery voltage, battery current, and cell voltage sampling. using a sensor to measure battery temperature, cell voltage, and cell balance. We'll talk about specialized integrated circuits. The difficulties with sampling the voltage across the many hundreds of cells in a Li-ion battery are solved by this technique. Based on the experimental data, we compare two methods for calculating the battery current integral findings and decide which is optimal.

Keywords Solar panel · BMS · Protection system

B. N. Gugulothu (✉) · M. Pasha · P. Deepa · K. Y. Kusuma · P. N. Roopa
Department of Electrical and Electronics Engineering, BMS Institute of Technology & Management, Bengaluru, Karnataka, India
e-mail: babunaikg@bmsit.in

1 Introduction

Over the past 10 years, the solar business has seen tremendous growth, and it is anticipated that this pattern will hold going forward. By the end of 2008, the cumulative total capacity was approaching very near to 15 GW. Europe is currently in the lead with more than 9 GW, or more than 65% of the total installed PV capacity worldwide. Japan (2, 1 GW) and the US are not far behind, making up 15% and 8% of the world's total installed PV power, respectively (1, 2 GW). SMA Solar Technology AG is the active market leader for solar inverters and has shown its innovations for more than 25 years. Over 4 GW of solar energy has been installed globally by SMA Solar Technology AG. Due to the rising popularity of electric and hybrid vehicles, SMA creates and manufactures the BMS, which is today one of the most important parts of a car. Due to the benefits of its power density and high energy, lack of memory effect, reduced self-discharge, and long cycle life, lithium-ion batteries are rising in popularity. This paper presents the results of recent research on the dynamic Li-ion battery management system [1]. The management system for Li-ion batteries is under a lot of strain due to the highly sophisticated way they are used in hybrid electric vehicles [2]. Since there are many cells—often up to 100 cells—in a dynamic Li-ion battery, calculating the voltage of the cells might be challenging. Estimates of the state of charge have historically been used extensively in battery management research [3–5]. Accurate battery current integration calculations are necessary for performing an accurate SOC assessment [6, 7]. This essay explores the following key themes: If system administration costs are kept to a minimum, BMS can acquire battery signal characteristics in challenging situations that satisfy systematic accuracy criteria [8]. Some of these indications are battery temperature, voltage and current integration, and cell voltage and current integration. Would, through detailed experiment data, produce a result that was more precise and accurate [9, 10]. When Solar Systems Connected to the Grid: The main function of a solar inverter is to convert the DC output voltage of a solar generator into an AC output voltage that is compatible with the grid. The majority of solar inverters on the market right now are grid linked, or configured to feed AC power to the grid. Solar inverters are substantially less necessary for installations on islands. Efficiency has become the most important aspect to take into account when contrasting solar inverters over time. Today's solar inverter specs are becoming increasingly complex.

2 Solar Inverter

2.1 Condition for Solar Inverter

Modern inverters may do more than just convert DC to AC power; they can also, among other things, assess DC or AC properties, keep an eye on and protect the entire solar system, interact with users or the grid, and run solar generators. In summary,

a solar inverter is a “high-tech” gadget in every sense today. For instance, the entire internal microprocessor is equivalent to the power of a modern laptop.

2.2 Fundamental of Solar Inverters

A block diagram showing the operation of a solar inverter. Power semiconductors arranged in the best feasible architecture serve as an inverter’s brains. There are means for DC protection and switches, as well as an EMI and DC filter, between the solar generator and the power semiconductor configuration. On the AC side, EMI and Sinus filters, AC Protection, and switches to the grid are installed. Equipment for monitoring electrical parameters on the DC and AC sides interacts with hardware components and controller units. A control device, the controller Device for interfacing, monitoring, control, and generation of pulse patterns. Thermal connections are made between dissipating components like semiconductors and magnetics and a cooling system that is either attached to or integrated into the housing [11].

2.3 Increased Output Power Inverters

The need for higher output power from solar inverters has necessitated further developments of the idea of second-generation inverters. One is an even better thermal management system. A front compartment house and a vented rear compartment are shown in the design of this better cooling concept based on the Opto-couple concept in Fig. 1. More components that are appropriately situated are in the back compartment.

3 Battery Management System (BMS)

Depending on the application, BMS has many definitions. BMS, generally speaking, is a management strategy that keeps an eye on, regulates, and improves a person’s performance or the performance of a number of battery modules in an energy storage system. In the event of abnormal circumstances, the BMS has the ability to control the detachment of the module(s) from the system. When the appropriate safety precautions are performed inside a system, it is used to enhance battery performance. BMS is employed in a power system application to track, manage, and supply the battery’s power at its most effective level. BMS is used in automotive applications to regulate energy at various system interfaces and to protect the system from dangers. BMS is made up of many functional structural elements. All of the other parts of the organized system, including the controllers, a grid, and other dispersed resources, are connected to the batteries through the functional blocks of the BMS.

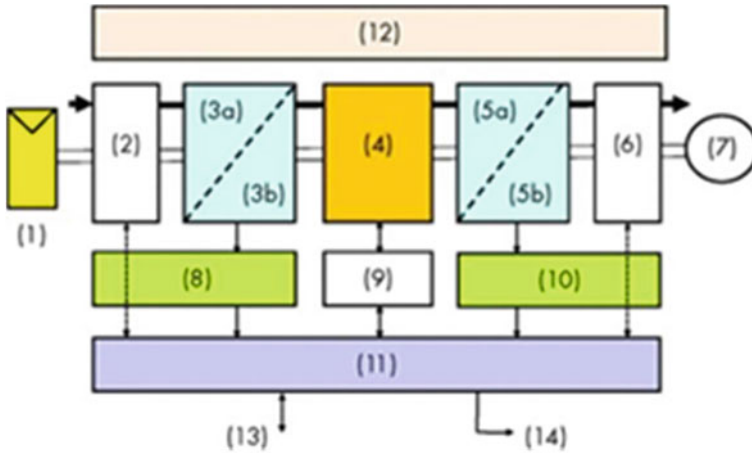


Fig. 1 Solar inverter diagram

With the correct architecture, practical building blocks, and cutting-edge electronics, the system battery life may be extended. There are numerous commercial BMSs available. For instance, NUVATION Energy offers a modular-based, versatile, and reliable BMS for stationary and mobile energy storage applications (Fig. 2).

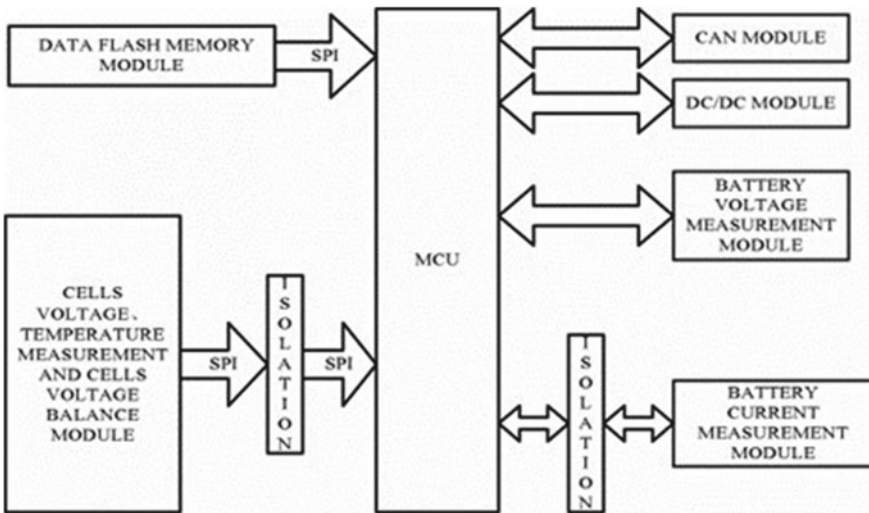


Fig. 2 Solar inverter diagram

3.1 Structure of BMS

The bulk of BMS components is classified as the following: main controller module, data FLASH memory module, battery voltage measurement module, cell voltage measurement module, and another CAN-bus module [12, 13]. To connect to other controllers and communicate with them, a CAN-bus module is utilized. The 12 V power supply is converted into a 5 V power source using a DC/DC module. An isolated power supply that enhances disturbance rejection is the DC/DC module. The charge and discharge current of batteries is measured using a battery. Module for measuring current. A battery voltage measuring module is used to gauge the voltages of each series-connected cell. The surface of each cell is examined by a temperature measurement module. Data FLASH memory modules are used to store measurement data. The measurement data may be retained for a maximum of 30 days. The main controller must communicate with all of the aforementioned modules in order to oversee the appropriate operation of all components.

3.2 Development of Software Structure

Multiple tasks are supported by the BMS software architecture [8]. In the past, it was not practical to complete two tasks at once; one work had to be placed on hold in order to complete the other. The new BMS software design now allows for the uninterrupted completion of multiple tasks in parallel. The early responsibilities of a software architect for a BMS use to measure voltage/current, over current/voltage protection, and monitor temperature and protective relay actuation must be finished as soon as is practically possible in order to ensure the safety of the BMS. To carry out real-time operations, the real-time operating system (RTOS) is integrated into the BMS software architecture. The architecture of the BMS software is shown in Fig. 3.

3.3 Functions of BMS

See Fig. 4.

4 Monitoring BMS

The voltage/current, temperature, cell voltage, isolation, and interlocks of the battery pack are the main targets of the BMS. A broken voltage regulator or battery charging mechanism might cause overvoltage in the battery system. While an overcharge

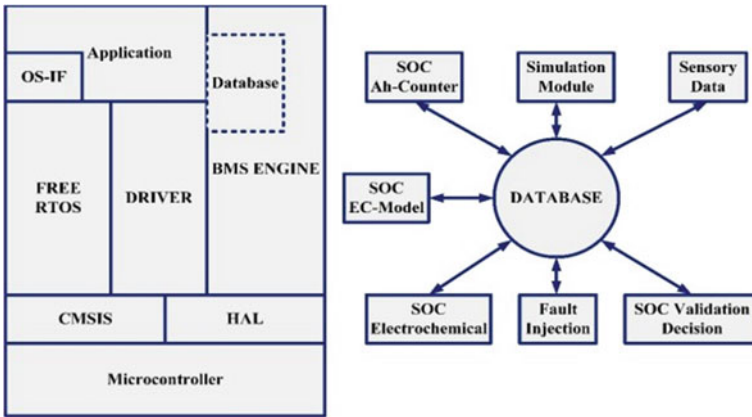


Fig. 3 Software structure



Fig. 4 Function BMS

causes the cell to vent, an excessive voltage or current might permanently harm the battery system [14]. Combustible gases that are evacuated pose a serious threat to public safety. Low voltage or current can also have a big effect on how well a battery works. The BMS has a crucial role in isolating the main battery system, especially in high-voltage systems. The current from a malfunctioning high-voltage battery will pass through a human body and result in death if it comes into contact with it. To shield the battery system from dangers, a BMS is necessary to safeguard includes, among other things, figuring out the system’s working state, establishing fault criteria, authenticating and identifying the device, anticipating pack/cell overvoltage and overcurrent, foreseeing the isolation fault, and detecting high/low temperatures. Because changes in the cell/pack parameter are brought on by the external environment of the battery pack, a BMS is required to safeguard the battery system against external occurrences.

4.1 Management of Charging and Discharging

Each battery can only be charged and discharged a certain number of times; as the number of cycles rises, the battery life decreases. The charge level has a significant impact on battery life. It is necessary to confirm the most efficient procedure for charging and discharging activities. Ensure management in this area by running the pre-charge process, limiting dynamic power, conducting active and passive balancing, and controlling the charger current [15].

4.2 Diagnosis

Depth of discharge (DOD), state of charge (SOC), battery capacity, regular monitoring of cell temperature, state of fitness (SOF), available energy, charging time, remaining runtime, remaining useful life (RUL), inner cell impedance, and current capability are all parameters that are measured by BMS [16]. BMS is in charge of monitoring as well. Examples of faults include limiting the consequences of fault effects, thermal runaways, fires, and explosions. Defect diagnosis is therefore an essential BMS feature. Calculating the depth of discharge is necessary to establish the optimal battery cycle and may shorten battery life. The longevity of lead-acid batteries is shortened if the depth of discharge exceeds 50%, for this reason. In order to avoid, the DOD of the BMS should be kept current.

5 Results and Discussion

To maximize the energy of solar radiation we must use MPPT (Maximum Power Point Tracking) to maximize the solar radiation accessible in order to harvest the most energy possible from it (Figs. 5, 6 and 7).

5.1 A DC-AC Inverter

Utilizing an inverter and a transformer, 12 V from a battery are converted to 230 V (Figs. 8 and 9).

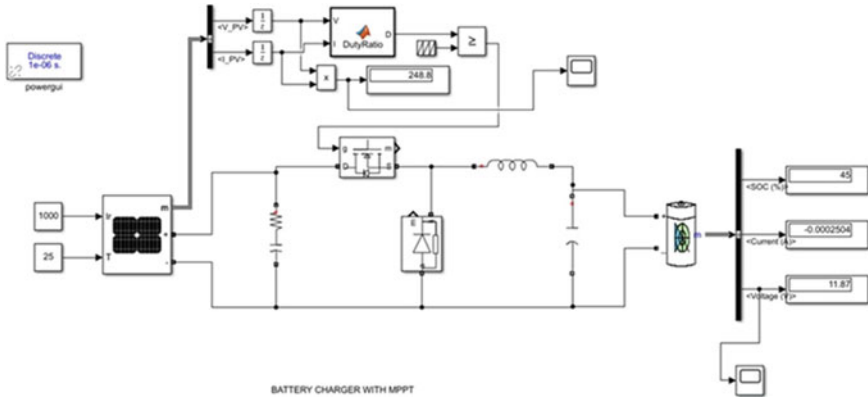


Fig. 5 Circuit for MPPT

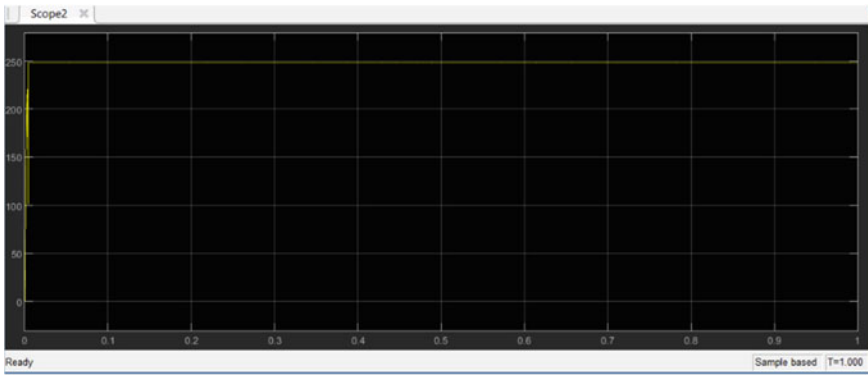
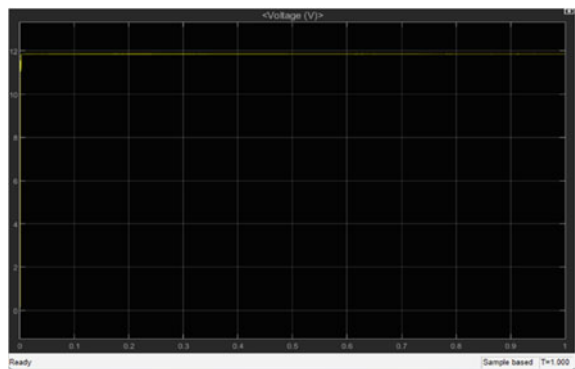


Fig. 6 Maximum power obtained using MPPT

Fig. 7 DC output obtained in solar panel



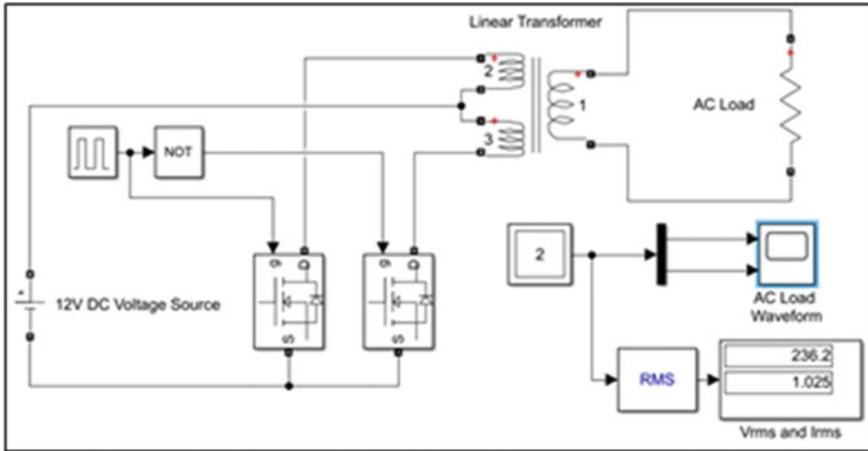


Fig. 8 Circuit of 12–230 V inverter

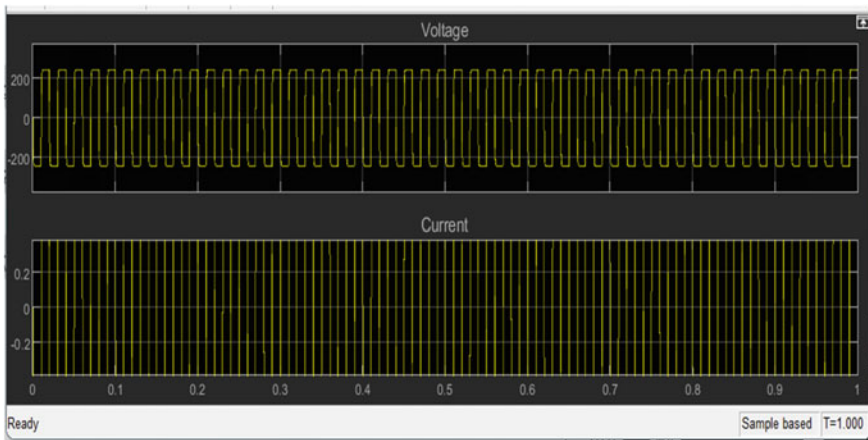


Fig. 9 Output waveforms of inverter

5.2 Approaches of BMS Evaluation

Techniques for evaluating BMS include CC-metric. The accuracy of a BFG’s SOC estimates is assessed using the CC-metric. It is well known that Coulomb counts’ use of the SOC calculation approach leads to incorrect results. However, if the battery capacity and initial SOC are known, the Coulomb counting method will provide a very accurate estimate of SOC. The CC-metric advises using unique BFG validation load patterns that enable precise assessment of the battery’s starting state of charge and capacity in order to assess the BFG process. It must be emphasized once more that the TTV measure simultaneously quantifies the accuracy of the subsequent BFG

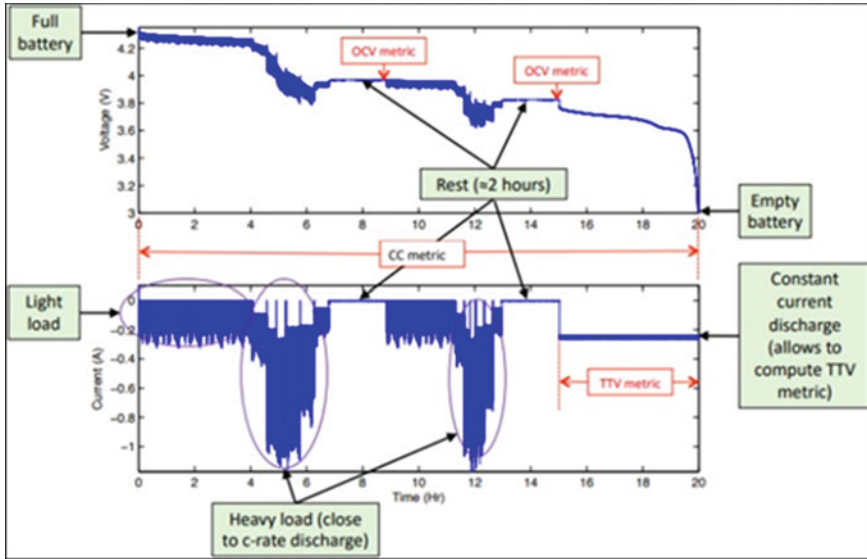


Fig. 10 BMS evaluation

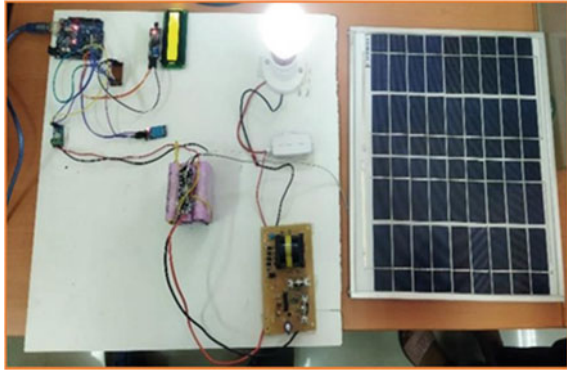
estimations, such as those of SOC, battery capacity, and ECM parameter. A particular load profile known as the BFG evaluation profile must be applied to the battery in order to calculate the BFG evaluation metrics. Demonstrates a BFG assessment profile created to calculate the three parameters mentioned above for a battery with a 1.5 Ah of nominal capacity [17] (Fig. 10).

BFG estimate from SOC. It is important to recognize that the CC-metric is a laboratory-based measurement and cannot be used in real time while the battery is being used by the end user. The idea behind OCV-metric is that the genuine SOC may be ascertained by using the OCV curve, which can then be used to confirm the SOC estimate produced by a BFG. The battery must be rested before the OCV can be measured directly, hence the OCV-SOC metric is also a lab-based metric like the CC-metric. The most exact method for assessing the precision of a BFG algorithm is the TTV (Time to Voltage) Metric. This statistic assesses a BFG’s various qualities simultaneously.

5.3 Prototype Solar Inverter with BMS

See Fig. 11.

Fig. 11 Prototype of solar inverter with BMS



6 Conclusion

This article focused on the functional and packaging integration for solar inverters as it relates to power electronic packaging. The primary driver of cost and reliability improvements in solar inverters is power electronic packaging. Over the course of the upcoming inverter generation, functional and packaging integration will play a bigger role. However, the complexity and power of solar inverters are continually rising, posing a challenge for power electronic packaging. The article provides an overview of the current standards landscape, evaluates it, and, when necessary, makes technical and safety recommendations for the new BMS standard. The BMS is one of the core elements of electrical energy storage systems. A safe BMS on both fronts is necessary for the correct operation of an electrical system since BMS reacts to both internal and external events. This study focuses on the specifics of BMS for stationary (large-scale) energy storage applications and electrical transportation. Numerous BMS for energy storage system elements, such as testing, components, functionality, topology, operation, architecture, and safety considerations, are included in the analysis.

References

1. Jiang J, Zhang C (2015) Fundamentals and applications of lithium-ion batteries in electric drive vehicles. Wiley, HobokenNJ, USA
2. Sung W, Shin CB (2015) Electrochemical model of a lithium-ion battery implemented into an automotive battery management system. *Comput Chem Eng* 76:87–97
3. Ahmadi L, Fowler M, Young SB, Fraser RA, Gaffney B, Walker SB (2014) Energy efficiency of Li-ion battery packs re-used in stationary power applications. *Sustain Energy Technol Assess* 8:9–17
4. Ahmadi L, Yip A, Fowler M, Young SB, Fraser RA (2014) Environmental feasibility of re-use of electric vehicle batteries. *Sustain Energy Technol Assess* 6:64–74
5. EV Sales Forecasts. <https://evadoption.com/ev-sales/ev-sales-forecasts/>. Accessed on 10 February 2019

6. Pop V (ed) (2008) Battery management systems: accurate state-of-charge indication for battery powered applications. Springer, Dordrecht, The Netherlands
7. Cheng KWE, Divakar BP, Wu H, Ding K, Ho HF (2011) Battery-management system (BMS) and SOC development for electrical vehicles. *IEEE Trans Veh Technol* 60(1):76–88. <https://doi.org/10.1109/TVT.2010.2089647>
8. Balasingam B, Avvari G, Pattipati B, Pattipati K, Bar-Shalom Y (2014) A robust approach to battery fuel gauging, part II: Real time capacity estimation. *J Power Sources* 269:949–961
9. Dey S, Mohon S, Pisu P, Ayalew B (2016) Sensor fault detection, isolation, and estimation in lithium-ion batteries. *IEEE Trans Control Syst Technol* 24:2141–2149
10. Kang Y, Duan B, Zhou Z, Shang Y, Zhang C (2020) Online multi-fault detection and diagnosis for battery packs in electric vehicles. *Appl Energy* 259:114170
11. U.S. Department of Energy (2014) Energy storage safety strategic plan—December 2014. Energy.gov. <https://www.energy.gov/oe/downloads/energy-storage-safety-strategic-plan-december-2014>. Accessed on 18 November 2020
12. Balasingam B, Avvari G, Pattipati K, Bar-Shalom Y (2015) Performance analysis results of a battery fuel gauge algorithm at multiple temperatures. *J Power Sources* 273:742–753
13. Avvari G, Pattipati B, Balasingam B, Pattipati K, Bar-Shalom Y (2015) Experimental set-up and procedures to test and validate battery fuel gauge algorithms. *Appl Energy* 160:404–418
14. Pattipati B, Balasingam B, Avvari G, Pattipati K, Bar-Shalom Y (2014) Open circuit voltage characterization of lithium-ion batteries. *J Power Sources* 269:317–333
15. Hussein HH, Batarseh I (2011) A review of charging algorithms for nickel and lithium battery chargers. *IEEE Trans Veh Technol* 60:830–838
16. Wang Z, Hong J, Liu P, Zhang L (2017) Voltage fault diagnosis and prognosis of battery systems based on entropy and Z-score for electric vehicles. *Appl Energy* 196:289–302
17. Eddahech A, Briat O, Bertrand N, Delétage JY, Vinassa JM (2012) Behavior and state-of-health monitoring of Li-ion batteries using impedance spectroscopy and recurrent neural networks. *Int J Electr Power Energy Syst* 42:487–494

Optimal Power Sharing in a Meshed MTDC Grid Through Robust Current Flow Controllers



Lokesh Garg and Sheetla Prasad

Abstract The two main challenges in meshed MTDC grids are protection from dc faults and managing the line power flows. In order to control the line power flow and the protection against dc faults DC current flow controllers can be used. The function of current flow controller is to control/balance the branch currents between the transmission lines in meshed multi-terminal HVDC grid system by increasing or decreasing the magnitude of the current as well as it is also possible to reverse the direction of current. However, the stability of the system may affect by the introduction of a DC current flow controller also increases the system size, overall cost, and complexity of the system. In this paper, the dynamic characteristics of the system with the introduction of a current flow controller on a four-terminal HVDC system have been discussed. The proposed scheme is simple and easily implemented and also it is very effective as it maintains the reliability security and stability of the system, whenever there is a change in load or if there is any fault in any line. To ensure proper power sharing and maintain the stability of the system time domain simulation is done on four terminals meshed MTDC grid in the presence of CFC by using MATLAB. The simulation result shows that the proposed system can effectively work by the introduction of a proposed optimal controller and application of current flow controllers which provide a solution to power flow issues in meshed MTDC grids.

Keywords Multi-terminal direct current (MTDC) · High-voltage direct current (HVDC) · Voltage source converter (VSC) · HVDC · Current flow controller · Droop control (CFC) · Modular multilevel converter (MMC)

L. Garg · S. Prasad (✉)
DEECE, Galgotias University, Greater Noida, India
e-mail: sheetla.prasad@galgotiasuniversity.edu.in

1 Introduction

Due to continuous increment in power demand and limited natural resources, the conventional power stations cannot be minimized the power mismatch between generation and demand. However, the generation and transmission line efficiencies can be increased by controlling the power within the system [1]. The need for high voltage DC (HVDC) transmission increasing day by day due to its many advantages over HVAC transmission. The main advantages of HVDC transmission lines are listed such as asynchronous grid interconnection, power exchange capability, low cost for long distance, easily underground transmission, and also the integration of scattered power plants like offshore renewable energy sources such as wind farms. Mesh grid has the limitation that the branch currents are not fully controlled through a converter station in the case of mesh grid [2]. Due to the advancement in power electronics application, HVDC uses alternating current which is converted into direct current, and bulk of DC power is used to transfer economically via long overhead transmission lines. Power flow in DC grid as well as in AC grids depends on the grid cable resistances. For reliable and safe operation, in the presence of any sudden load change, then, the cables must have carried extra current under their thermal limits otherwise for a long duration with overload capacity the cable may damage. Therefore, in order to limit current below the thermal limits of the cables current flow controllers are used in DC grids.

First time VSC-MTDC technology was introduced in Japan in 1999 which consist of three VSC terminals having back-to-back connections that were used for power exchange [3]. The main features of an MTDC system are used to regulate voltage, power, and current using several DC-to-DC converters economically [4]. In MTDC grid converter stations are usually used to operate in DC voltage control mode and power control mode. MTDC system improves system reliability, improves system flexibility, and easily integrates different types of renewable energy. On the basis of topology, MTDC systems are mainly connected in three modes, namely, radial MTDC system, ring or meshed MTDC system, and series connected MTDC system. In case of disturbance in meshed DC grid, e.g., short circuit, sudden loss of a DC terminal then other lines becomes overloaded and the overall system may lead to collapse. To control the voltage in the MTDC system, several methods were developed such as active load sharing, i.e., master–slave method, passive load sharing, i.e., voltage droop method, voltage margin methods, etc. The basic advantage of the droop control method is that it has the capability of independent load sharing with improvement in terms of reliability [5]. If there is a large disturbance then the output power with fixed droop control of the VSC station hit its boundary limits which results in the reduction of the DC voltage control ability of the entire MTDC system. Traditionally the use of MTDC technology was used only for radial system, but nowadays with the applications of power electronics devices, it is used for meshed or ring main system as results reliability of the system is more in ring main system as compared to radial system.

In MTDC grids, it is essential to maintain DC line currents within thermal limits and electric stress. If there is a continuous operation of overloaded lines, then there may be a chance that the cable may damage as well as it may lead to permanent failure of the cable. In order to avoid transmission breakdown with improvement in reliability and efficiency of the DC grid, the transmission line must have a good current distribution which can be done by using a current flow controller (CFCs). In CFC, a small DC voltage is injected in series with the DC line. The value of this injected voltage is normally 1–2% of the rated system voltage which changes the current flow as the impedance is modified [6]. If the number of converter terminals and DC lines increases then it will reduce the effectiveness of the system. The main functions of current flow controllers are the effective power flow regulation and balance cable current flow, which results in the protection of cables from overload. [7]-[8]. Current flow controllers can be operated in Buck mode or Boost mode [9]. In the HVDC transmission grid for meshed or ring main system, there are two main drawbacks namely protection against DC faults and line power flow. In order to minimize these drawbacks in meshed or ring main system, current flow controllers are used to balance cable currents and also used to restricting over all power flow in the grid by preventing individual line capacity limit. For the protection of HVDC grids from DC faults, direct current circuit breakers are also required. For MTDC grid system stability, security, and the reliability must be required which can be achieved by the droop control method in case of any disturbances in the grid system. The main advantage of the droop control method over master–slave control method is that it has shared active power as well as DC voltage according to capability [10].

The main obstacle in meshed MTDC grid is that due to the resistance of the transmission lines effective regulation of power or current flow in the DC system cannot be achieved. In order to overcome the resistance of the transmission lines CFCs are used in meshed MTDC grid for the effective power flow regulation [11]. VSC-MTDC system and modular multi-level converter system can be interconnected between offshore and onshore power sources. The main advantage of interconnection is that it improves the flexibility of the AC and DC system for processing high power level and there is no need for filter link on AC side and also improves the overall reliability of the system [12].

The rest of the paper is as follows. Section 2 describes four terminals meshed MTDC system and the need of CFC system. Section 3 shows a mathematical representation of meshed four-terminal HVDC system with current flow controllers. In Sect. 4 system analysis with proposed controller system design is given. In Sect. 5 simulation results and discussions are given followed by conclusion in Sect. 6. System control strategies and related parameters are given in the appendix.

2 System Description

The single-line diagram of a meshed four-terminal modular multi-level converter-based multi-terminal high voltage direct current (MMC-MTDC) system is shown in Fig. 1 and the associated data is given in Appendix. There are four terminals T_1 , T_2 , T_3 , and T_4 . IGBT switches with capacitors, freewheeling diodes are used for the current flow controller (CFC). In each cable four IGBT are inserted in series. A capacitor is connected across both cables. The main purpose of the capacitor is to charge or discharge the cable. The capacitor will charge by the cable, which carry higher current and discharge by the other cable which carry the lesser current [4], respectively. It is not possible to regulate the DC current of every branch in MMC when they are connected in parallel. However, they can regulate the power at the converter terminal [2]. During the unbalanced conditions in parallel transmission lines each line carries the different currents, in some cases one or more lines may carry the current beyond their maximum current limits, i.e., overloaded. Three types of current flow controller are used in the MTDC system to achieve current flow regulation. The first method is to use insert variable resistance in the DC transmission line, the branch current can be varied by on/off the variable resistance. This system has the limitations that there is power loss in the resistor and some cooling devices are required to dissipate the heat. Second method to control the current is to insert active DC power sources into the transmission line in order to get the active power absorbed or generated [2, 9]. However, the limitation of this method is that isolation transformers are required which increases the overall capital cost and running cost of the system and also more space required to accommodate the additional equipment [9, 10, 19]. In the third method, an equivalent voltage source is inserted in the DC line which is used to control the current/power flow. The dual H-bridge CFC used for current flow regulation has advantages over the above two methods as it not required any isolation transformer and there is no power loss [2, 10, 11]. There are two methods used to prevent the transmission lines from overloading, either to increase the delivering capacity for the transmission lines or to reduce the transmission level for the whole system. However, the limitations of these two methods are an increase in cost as well as a decrease in the efficiency of the HVDC system. In order to overcome these limitations additional devices like CFC are used to regulate the branch current.

The generalized meshed MTDC grid system is represented in Fig. 1a and the detailed network connections are also given in Fig. 1b for a terminal T_i . The mathematical equation dynamics can be derived for the terminal T_i as given as

$$L_{in} \frac{di_{in}}{dt} = v_i - v_n - R_{in} i_{in} \quad (1)$$

$$C_i \frac{dv_i}{dt} = i_i - \sum_{n=1}^4 i_{in} \quad (2)$$

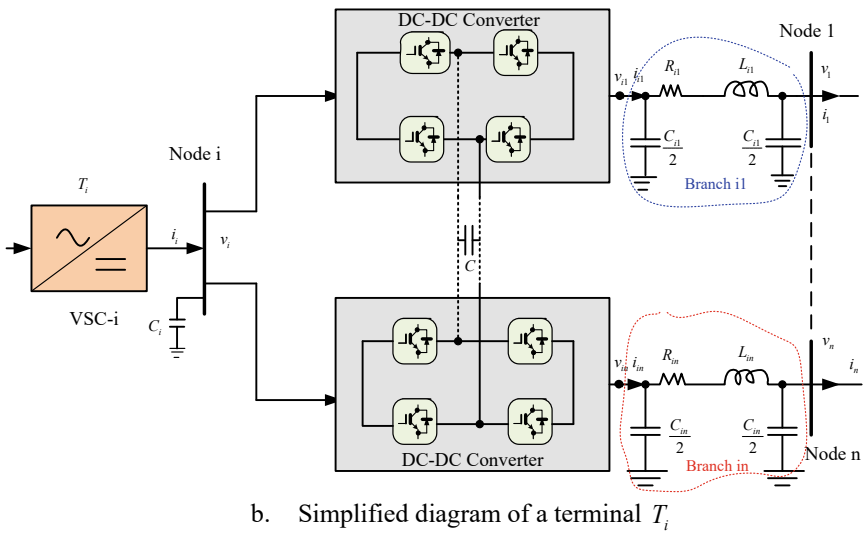
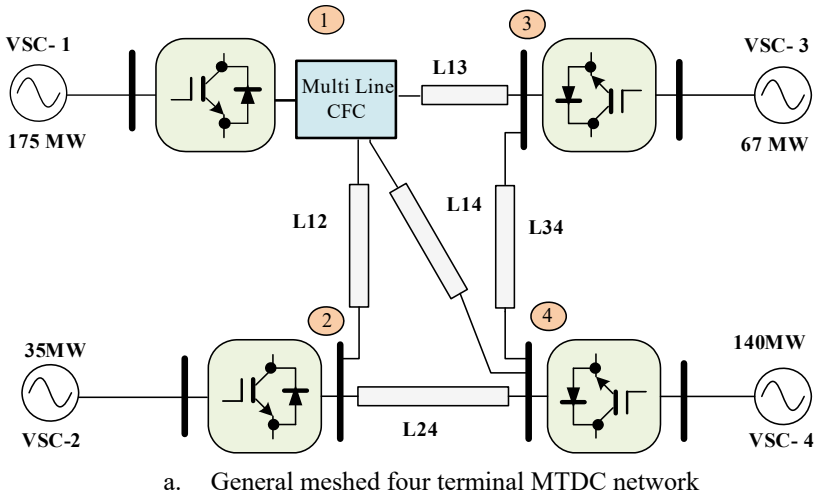


Fig. 1 Meshed four-terminal HVDC system under test

where $n = 1, 2, 3, 4$. All variables of the pi-transmission line network are given in Fig. 1b.

Using Eqs. (1) and (2), the mathematical equation with fixed droop constant-based meshed four-terminal MTDC can be written as

$$\frac{dv_1}{dt} = \frac{1}{C_1} [i_1 - i_{12} - i_{13} - i_{14}] \tag{3}$$

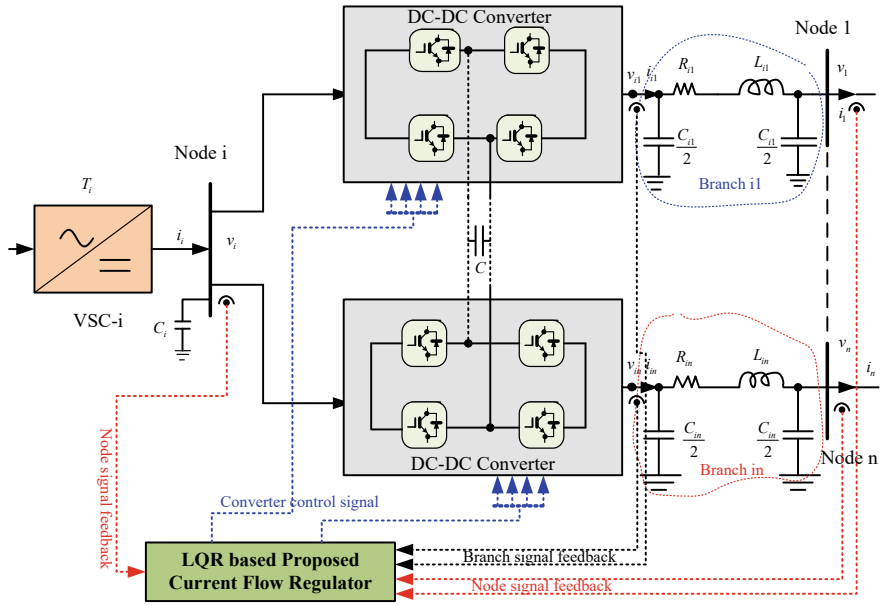


Fig. 2 Proposed control scheme for terminal T_i

$$\frac{dv_2}{dt} = \frac{1}{C_2} [i_2 + i_{12} - i_{24}] \tag{4}$$

$$\frac{dv_4}{dt} = \frac{1}{C_4} [i_{14} - i_{24} - i_{34} - i_4] \tag{5}$$

$$\frac{di_{12}}{dt} = \frac{1}{L_{12}} [v_1 - v_2 - R_{12}i_{12} - u_{c1}d_{a1}] \tag{6}$$

$$\frac{di_{13}}{dt} = \frac{1}{L_{13}} [v_1 - v_3 - R_{13}i_{13} - u_{c1}d_{a1}] \tag{7}$$

$$\frac{di_{14}}{dt} = \frac{1}{L_{14}} [v_1 - v_4 - R_{14}i_{14} - u_{c1}d_{a1}] \tag{8}$$

$$\frac{di_{24}}{dt} = \frac{1}{L_{24}} [v_2 - v_4 - R_{24}i_{24}] \tag{9}$$

$$\frac{di_{34}}{dt} = \frac{1}{L_{34}} [v_3 - v_4 - R_{34}i_{34}] \tag{10}$$

$$\frac{du_{c1}}{dt} = \frac{1}{C_{cfc}} [i_{12}d_{a1} + i_{13}d_{a1} + i_{34}d_{a1}] \tag{11}$$

The state-space equations for fixed droop constant-based meshed four-terminal MTDC are given as

$$\dot{x}(t) = Ax(t) + Bu(t) + F \Delta P_d(t) \quad (12)$$

Here state-space parameters $x(t)$, $u(t)$ and $\Delta P_d(t)$ are considered as system states variable, input variable, and reference variable, respectively. The matrices of system parameters are given as $A \in \mathfrak{R}^{n \times n}$, $B \in \mathfrak{R}^{n \times k}$, $F \in \mathfrak{R}^{n \times q}$.

$$A = \begin{bmatrix} 0 & 0 & 0 & -\frac{1}{C_1} & -\frac{1}{C_1} & -\frac{1}{C_1} & 0 & 0 & 0 \\ 0 & 0 & 0 & \frac{1}{C_2} & 0 & 0 & -\frac{1}{C_2} & 0 & 0 \\ 0 & 0 & 0 & 0 & 0 & \frac{1}{C_4} & \frac{1}{C_4} & \frac{1}{C_4} & 0 \\ \frac{1}{L_{12}} & -\frac{1}{L_{12}} & 0 & -\frac{R_{12}}{L_{12}} & 0 & 0 & 0 & 0 & -\frac{d_{a1}}{L_{12}} \\ \frac{1}{L_{23}} & 0 & 0 & 0 & -\frac{R_{13}}{L_{23}} & 0 & 0 & 0 & -\frac{d_{a1}}{L_{13}} \\ \frac{1}{L_{14}} & 0 & -\frac{1}{L_{14}} & 0 & 0 & -\frac{R_{14}}{L_{14}} & 0 & 0 & -\frac{d_{a1}}{L_{14}} \\ 0 & \frac{1}{L_{24}} & \frac{1}{L_{24}} & 0 & 0 & 0 & -\frac{R_{24}}{L_{24}} & 0 & 0 \\ 0 & 0 & -\frac{1}{L_{34}} & 0 & 0 & 0 & 0 & -\frac{R_{34}}{L_{34}} & 0 \\ 0 & 0 & 0 & -\frac{d_{a1}}{C_{cfc}} & -\frac{d_{a1}}{C_{cfc}} & -\frac{d_{a1}}{C_{cfc}} & 0 & 0 & 0 \end{bmatrix},$$

$$B = \begin{bmatrix} \frac{1}{C_1} & 0 & 0 & 0 \\ 0 & \frac{1}{C_1} & 0 & 0 \\ 0 & 0 & 0 & -\frac{1}{C_1} \\ 0 & 0 & 0 & 0 \\ 0 & 0 & -\frac{1}{L_{13}} & 0 \\ 0 & 0 & 0 & 0 \\ 0 & 0 & 0 & 0 \\ 0 & 0 & \frac{1}{L_{34}} & 0 \\ 0 & 0 & 0 & 0 \end{bmatrix}$$

$$x(t) = [v_1 \ v_2 \ v_4 \ i_{12} \ i_{13} \ i_{14} \ i_{24} \ i_{34} \ u_{c1}]^T, u = [i_1 \ i_2 \ v_3 \ i_4]^T$$

3 Linear Quadratic Regulator (LQR)

Optimal control is used to find the minimum cost. When the dynamics of the system are represented by a set of linear differential equations and the cost is described by a quadratic function then it is called a linear quadratic problem. LQR is a type of optimal control that is based on state-space representation. The advantage of the LQR method is that it reduces the work done by the control system engineer who wants to optimize the controller. It is used for the complex system in which differential equations are linearized into the linear system. LQR is an approximate

state feedback controller, i.e., there is not a clear relationship between the controller parameter and control behavior. The main challenges regarding LQR are to find the right weighted factors and in order to get the desired result we need to modify the performance index of the weighted matrix.

In the controller design and performance domain, the linear quadratic regulator (LQR) based controller is a well-known control strategy that changes the trajectories of a nonlinear or linear network by use of a regular control signal. The state-input control law is not a persistent continuous function of time. All things being said, it can change starting with one continuous system and then going to the next dependent on the current situation in the state-space. Subsequently, it can be optimized easily through linear matrix inequalities (LMIs) optimization platform [20]. The weights of LQR control approach are optimized linearly via a derived quadratic criterion function with states dynamic and control efforts. To achieve both fast state trajectory speed and effective control signal simultaneously, the quadratic function criteria are selected as

$$\Upsilon_{\min} = \int_0^{\infty} (x^T Q x + u^T R u) dt \tag{13}$$

where positive definite matrices are defined as $Q = Q^T > 0, R = R^T > 0$, and obtained using proper optimization. The weights matrices Q and R are optimized to improve fast responses and reduce penalty factor in control efforts. In most of the research work in the literature, weight matrices Q and R are considered as unity value to give a moderate response and equal penalty on each control efforts, respectively. In this study, the control law is designed and selected as

$$u(t) = -K x(t) \tag{14}$$

The state feedback gain K is optimized using LMI optimization.

Proof: Let the LQR objective Lyapunov function is considered as

$$\kappa = x^T(t) P x(t) \tag{15}$$

After time derivative with respect time of Eqs. (13) and (15), the optimal solution can be written below using Eq. (14).

$$x^T(t) \{ Q + K^T R K \} x(t) = - \frac{d}{dt} (x^T(t) P x(t)) \tag{16}$$

From microgrid state-space Eq. (12) substitution in the above equation, it is written as

$$x^T(t) \{ Q + K^T R K \} x(t) = -x^T(t) \{ (A - BK)^T P + P(A - BK) \} x(t) - x^T(t) 2PF \Delta P_d(t) \tag{17}$$

$$x^T(t)\{A^T P + PA + Q - K^T RK - K^T B^T P - PBK\}x(t) - x^T(t)2PF \Delta P_d < 0 \quad (18)$$

Using lemma given in [20], term $\{-K^T RK + K^T B^T P + PBK\} \cong -B^T PR^{-1}PB$ and substitute in the above equation.

$$x^T(t)\{A^T P + PA + Q - B^T R^{-1}PB\}x(t) - x^T(t)2PF \Delta P_d(t) < 0 \quad (19)$$

To achieve accurate convergence $\dot{\kappa} < 0$, the above equation may be converted in LMI using a lemma in [20].

$$\{A^T P + PA + Q - B^T R^{-1}PB\} < 0 \quad (20)$$

Thus, closed-loop system state trajectories converge asymptotically.

The Eq. (15) is transferred into LMI using Schur complements [20] to obtain the optimized value as

Select positive definite matrix P and R so that following LMIs holds simultaneously with a minimum of γ_{\min}

$$P > 0$$

$$Q > 0$$

$$R > 0$$

$$A^T P + PA + Q - B^T R^{-1}PB < 0 \quad (21)$$

After the calculation of optimized parameters, the effective control law is obtained.

$$u = [i_1 \ i_2 \ v_3 \ i_4]^T = -R^{-1}PBx(t) \quad (22)$$

Thus, this completes proof and optimization.

4 Results and Discussions

The simulation is done on four-terminal meshed MTDC grid by using MATLAB/SIMULINK. A CFC is introduced in the system. Results shown in Figs. 3, 4 and 5 give the system performance after the disturbance. Figure 3 shows the voltage deviation at grid terminal 1, grid terminal 2, grid terminal 3, and the current flow deviation between branches 1 and 2. The results show that the voltage at respective

grid terminals is constant after the disturbance, which can be achieved by Current Flow Controllers Fig. 4 shows the current deviation between the lines 1 and 3, between the lines 1 and 4, between the lines 2 and 4, and between the lines 3 and 4. The results show that the current between the respective branches is constant after the disturbance, which can be achieved by Current Flow Controllers. Figure 5 shows deviations in capacitor voltage at terminal 1 and control efforts responses. From the result, it shows that the capacitor voltage at terminal 1 is constant after the disturbance. Results show that CFC is effectively works after the disturbance as it maintains constant current at various branches and constant grid voltage at various terminals.

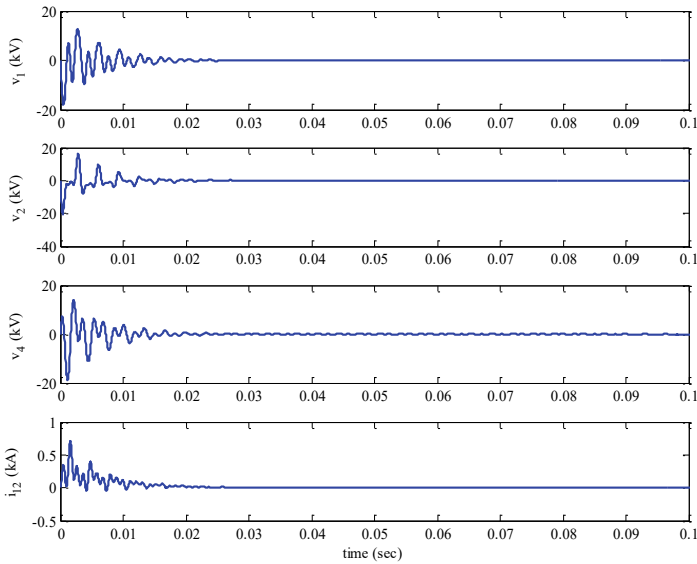


Fig. 3 Terminals 1, 2, 3 voltage deviations and line 1 to 2 current flow deviation responses

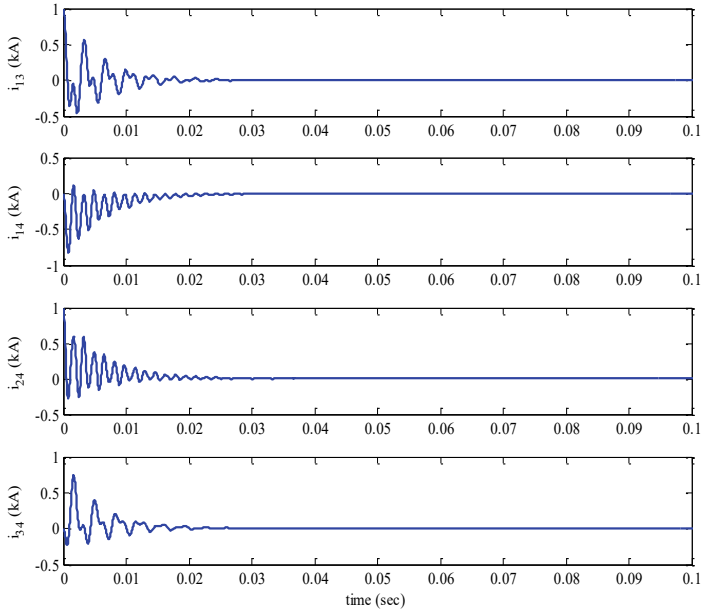


Fig. 4 Current deviations in lines 1 to 3, 1 to 4, 2 to 4, and 3 to 4 responses, respectively

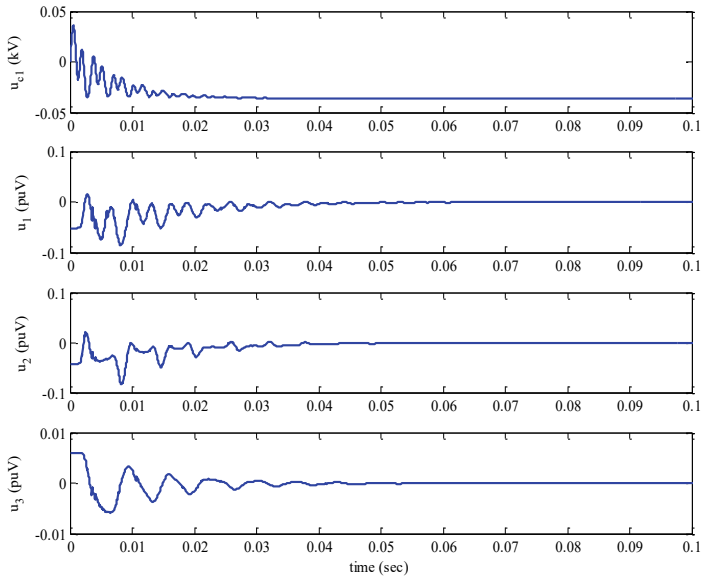


Fig. 5 Deviations in capacitor voltage at terminal 1 and control efforts responses

5 Conclusion

In this paper operation, control and simulation results are given here on four-terminal meshed MTDC grids with the introduction of CFC in the system. In a meshed MTDC grid current flow controller CFC is used which is capable to do effective power flow regulation/current regulation by inserting a variable dc voltage source connected in series with the dc line. The simulations are done on four-terminal meshed VSC-MTDC systems with the proposed controller. The proposed controller can work effectively for the optimal power sharing whenever there is any disturbance in the system and it also enhances the stability, security, and reliability of the DC grid. The performance of the proposed strategy enhances in terms of time response characteristics and its applicability. CFC improves the dc grid reliability by limiting the line currents below their thermal ratings. The proposed control scheme has been verified via time domain simulation in MATLAB. From the results, it has been concluded that by the use of current flow controller in a meshed MTDC grid the optimal power sharing can be achieved.

Appendix

T1: Control Strategies and Ratings of AC/DC Terminals

Terminals	1	2	3	4
VSC control strategy	P, Q	P, Q	V_{dc} , Q	P, Q
Rated power/voltage [MW/MVAR/KV]	175	35	100	140

T2: Parameters of the DC Branches/Lines

Branches	L_{12}	L_{13}	L_{14}	L_{24}	L_{34}
Distance in KM	75	125	200	150	175
Resistance in Ω	0.75	1.25	2.00	1.50	1.75
Inductance in mH	5.25	8.75	14	10.5	12.25
Capacitance in μF	3.75	6.75	10	7.5	8.75
Current limits in KA	1.20	1.20	1.20	1.00	0.60

References

1. Mohammed Mabrook Alharbi (2016) Modelling of multi-terminal VSC-based HVDC systems. MTech Thesis, Missouri University of Science and Technology, 2014; Deng N, Wang P

- (2016) Small signal stability analysis and control system design of a meshed multi-terminal high-voltage direct current grid with a current flow controller. *Electric Power Compon Syst* 44(10):1126–2113
2. Mulugeta T (2012) Control, dynamics and operation of multi terminal VSC-HVDC transmission system. PhD thesis Norwegian University of Science and Technology
 3. Diab HY, Marei MI (2016) Reduced switch count topology of current flow control apparatus for MTDC grids. *J Power Electron* 16(5):1743–1751
 4. Zhang B, Gao (2022) An AC/DC-coupled droop control strategy for VSC-based DC microgrids. *IEEE Trans Power Electron*
 5. Balasubramaniam S, Ugalde-Loo CE (2019) Power flow management in MTDC grids using series current flow controllers. *IEEE Trans Ind Electron* 66(11):8485–8497
 6. Liu W, Li C, Ugalde-Loo CE, Wang S, Li G, Liang J (2020) Operation and control of HVDC circuit breaker with current flow control capability. *IEEE J Emerg Select Top Power Electron*
 7. Cwikowski O, Sau-Bassols J (2015) Integrated HVDC circuit breakers with current flow control capability. *CSEE J Power Energy Syst* 1(1)
 8. Liu W, Ugalde-Loo C, Liang J, Li C, Frederic (2019) Modelling and frequency analysis of a dual H-bridge current flow controller in meshed HVDC systems. In: *EPE*
 9. Wang P, Deng N (2018) Droop control for a multi-line current flow controller in meshed multi-terminal HVDC grid under large DC disturbances. *IEEE Power Energy Technol Syst J* 5(2)
 10. Liu W, Ugalde-Loo CE, Li C, Li G, Yang P (2019) Level-shift modulation and control of a dual H-bridge current flow controller in meshed HVDC systems. *IEEE Energy Convers Congr Expos*
 11. Ahmad J, Liu C (2020) MMC based MTDC grids: a detailed review on issues and challenges for operation, control and protection schemes. *IEEE Access* 8:168154–168165
 12. Balasubramaniam S, Liang J (2019) Series current flow controllers for DC grids. *IEEE Access* 7:14779–14790
 13. Deng N, Wang P (2015) A DC current flow controller for meshed modular multilevel converter multiterminal HVDC grids. *CSEE J Power Energy Syst* 1(1)
 14. Khudair M, Ravi Kumar C (2017) A novel technique of power flow controller by using a DC current flow controller for meshed modular multi-level converter three-terminal HVDC grid. *Int J Res Innovat* 670–679
 15. Wu W, Wu X, Zhao Y (2020) An improved multiport DC power flow controller for VSC-MTDC grids. *IEEE Access* 8:7573–7586
 16. Balasubramaniam S, Ugalde-Loo CE (2017) Experimental validation of dual H-bridge current flow controllers for meshed HVDC grids. *IEEE Trans Power Deliv.* <https://doi.org/10.1109/TPWRD.2017.2752301>
 17. Khaledian A, Aliakbar Golkar M (2017) Original analysis of droop control method in an autonomous micro grid. *J Appl Res Technol* 7
 18. Veilleux E, Ooi BT (2012) Multi-terminal HVDC with thyristor power flow controller. *IEEE Trans Power Deliv* 27(3):1205–1212
 19. Kumars Rouzbehi and Seyed Saeid Heidary Yazdi (2018) Power flow control in multi-terminal HVDC grids using a serial-parallel DC power flow controller. *IEEE Access* 6:56934–56944
 20. Boyd S, Ghaoui EL, Feron E, Balakrishnan E (1994) Linear matrix inequalities in system and control theory. Society for industrial and applied mathematics. Philadelphia, version 5.2. <https://web.stanford.edu/~boyd/lmibook/lmibook.pdf>

Design of EV Charging Station with Integrated Renewable Energy Sources



Devarakonda Ashwin Kumar  and Natarajan Karupiah 

Abstract The increase of electric vehicles (EVs) is leading to an increase in electric vehicle charging stations, due to this spread the load on the existing power system is being increased and power quality disturbances are increasing. Using renewable energy is the best possibility to reduce stress and increase eco-friendliness. With the increasing electric mobility V2G/G2V is growing rapidly, V2G system helps in load leveling, voltage regulation, and improvement of grid stability. This paper introduces the detailed modeling of a multiport converter for EV charging by integrating renewable sources, to handle the sudden load disturbances the converter also incorporates a supercapacitor, which helps in overcoming frequency fluctuations, this helps in increasing battery life and reducing the energy storage system size. The detailed control system with all sources for improving stabilization such as power balancing, and voltage profile. The key aspects of the converter are less number of switches, a simple control structure, and balancing power between sources. Using renewable sources reduces the load on the power grid and the charging demands of EVs are fulfilled. To improve the efficiency of the converter, SiC devices are used, and the efficiency and power loss are compared by the simulation to the conventional Si devices. For different modes of operations, the simulation results are presented.

Keywords Multiport converter · EV charging · Renewable energy

1 Introduction

As many countries have kept a target of reducing carbon emissions in the future, the best alternatives are renewable energy sources, due to this demand electric vehicles are the best alternative to conventional automobiles [1]. The EV charging stations

D. A. Kumar (✉) · N. Karupiah
Vardhaman College of Engineering, Hyderabad, Telangana, India
e-mail: devarakondaashwinkumar21ped@vardhaman.org

N. Karupiah
e-mail: natarajankarupiah@vardhaman.org

consume a lot of power during the fast and super-fast charging process, creating stress on the grid, the power quality disturbances like voltage sag, stability issues, etc. are occurring in the power grid [2]. So there is a need to develop a good charging infrastructure such that the power quality issues are decreased and reliability is increased [3], so that consumers do not face issues while charging vehicles. So, manufacturers and EV charging providers are mainly focused on converters with a compact size, which is modular and has less electromagnetic interference [4]. Solar and wind are abundant in nature, so the combination can solve long-term problems, but as they are not constant, a battery is needed for reliability, but the power fluctuations may cause stress on the battery, in some cases battery sizing gets increased for this cause [5]. This may affect the battery life. So, to compensate for these, a supercapacitor in addition to these sources can help in reducing the size of the battery, handling fluctuations, and improving battery life [6]. The configuration as in Fig. 1 suffers from poor transient sharing of power, more ripples, more cost, and a complex control structure. As shown in Fig. 2, this configuration has good system performance, and power-sharing, with high utilization of supercapacitor, but with individual converters cost, control complexity increases.

Multiport converters have high-power density and high-efficiency advantages. Generally, there are (1) AC-bus and (2) DC-bus topologies of charging architectures. As most of the elements are DC, a DC-bus station is preferred, which also minimizes the losses, reduces cost, and improves efficiency [7]. In addition to the multiport converter, an additional grid connection port has been provided in the architecture, in case of the absence of renewable energy sources, for enabling V2G and G2V

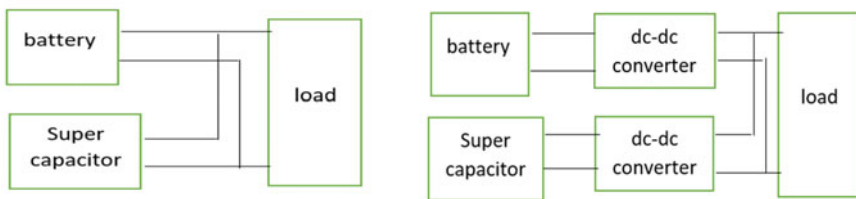
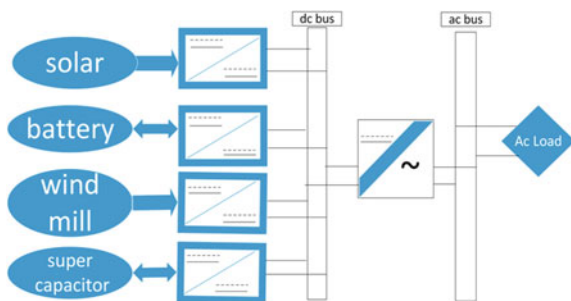


Fig. 1 Different energy converter configurations

Fig. 2 Individual converter configuration



operations. Generally, integration is done in isolated, non-isolated modes in isolated modes, a converter operation with transformer action is the basic principle, in non-isolated modes the converter operates by using buck, and boost mode operations offer a high-power density, high efficiency, compact, and modular design [8]. In this paper, the proposed converter has addressed the above issues with individual converters and complex control. The highlights of the proposed converter are (1) integrating sources with the low number of switches, (2) good voltage regulation, and (3) inherent power-sharing of battery and supercapacitor [9]. In addition to this work, the converter is also leveraged with silicon carbide switches to improve the efficiency and reduce power losses of the converter in place of normal switches; silicon carbide switches are used [10].

2 Proposed Multiport Converter Configuration

In the proposed converter configuration Fig. 3 2 uni-directional sources, 2 bi-directional sources, load with a grid interfacing port are present. [grid-port (later discussed).] As in the proposed configuration, more than one bi-directional sources are present, they help maintain DC-link voltage, and power balance is maintained, in the proposed configuration the sources-solar PV, battery and supercapacitor (combines energy source-CES) are connected by using DC-DC buck-boost converter configurations.

Wind power is connected by using a boost converter. In this converter L_s , L_w , L_{bat} are inductances of PV array port, wind-port, and CES-port. V_{pv} , V_{bat} , V_{scp} , V_{ces} , V_w , and V_{load} are the PV voltage, battery voltage, supercapacitor voltage, CES voltage, wind voltage, and load voltage. i_{pv} , i_s , i_b , i_{scp} , i_w , and i_{load} are PV, L_s , battery, supercapacitor, wind and load current. R_{load} , r_{bat} , and r_{scp} are load resistance, battery

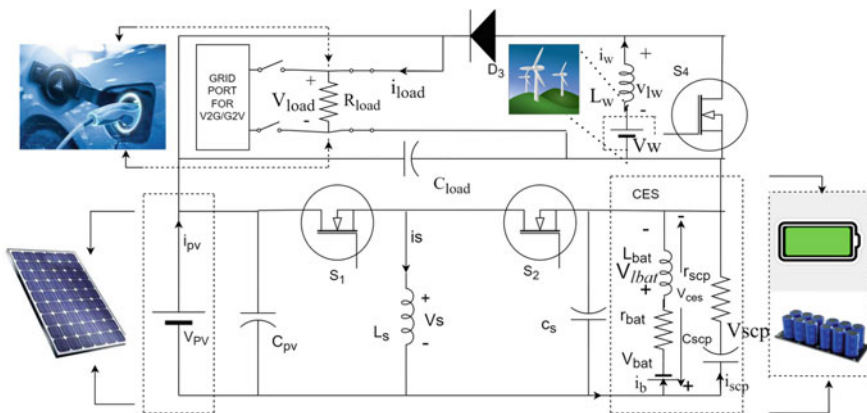


Fig. 3 Proposed multiport converter with integrated renewable energy sources and grid interfacing

internal resistance, and supercapacitance-resistance. S_1, S_2 are the PV array, CES side converter switches, D_3, S_4 are the wind side converter switches, and D_s, D_w are duty ratios of PV, CES, and wind converter.

2.1 Working of Converter

In this converter when solar energy is available PV operation and battery charging/discharging are done by operating S_1, S_2 switches. If PV is not available the voltage of C_{pv} is kept constant by CES so that load voltage is regulated by the (reference voltage) V_{loadr} this is done by controlling S_1, S_2 . Similarly, the wind is operated at MPP (maximum power point) by using D_3 and S_4 switches. Power sharing is done with respect to DC-link voltage in case of deficient/excess power average power is taken by the battery and oscillatory power is taken by the supercapacitor. The sharing depends on the $L_{bat}, C_{scp}, r_{scp}, r_{bat}$. If S_1 is ON the circuit equivalent is as Fig. 4a, under this mode.

$$V_{pv} = V_s; \quad V_{load} = V_{pv} + V_{ces} \tag{1}$$

If S_2 is ON the circuit equivalent is as Fig. 4b, under this mode

$$V_{ces} = V_s; \quad V_{load} = V_{pv} + V_{ces} \tag{2}$$

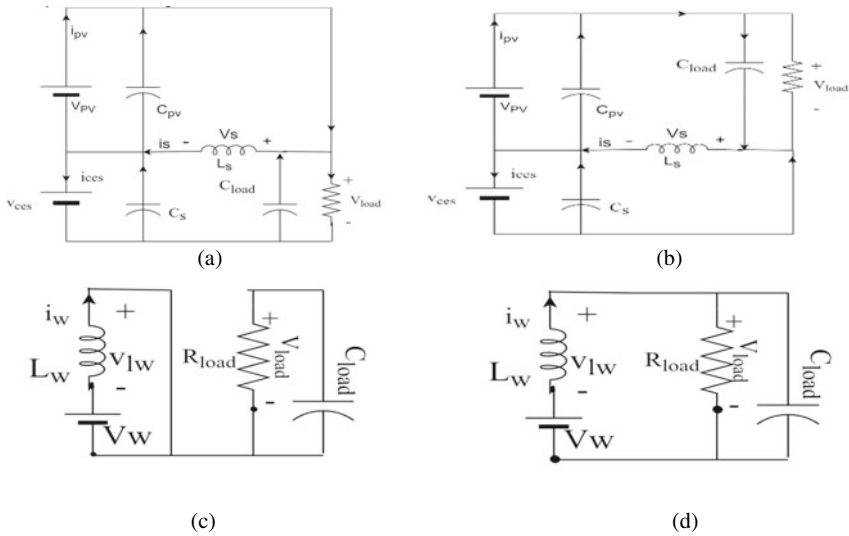


Fig. 4 a Equivalent circuit on S_1 ON, b equivalent circuit on S_2 ON, c equivalent circuit of S_4 in ON, d equivalent circuit of D_3 in ON

In these 2 modes, the load voltage is the sum of CES & PV voltages. By this we observe the inherent boosting of the converter. For a time period of T_s , the CES voltage is given as

$$V_{ces} = \frac{D_S}{1 - D_S} V_{pv} \tag{3}$$

when S_4, D_3 are ON the circuit equivalent is as Fig. 4c, d, g. So, the load voltage is given as

$$V_{load} = \frac{V_w}{1 - V_w}. \tag{4}$$

At steady state

$$I_s = I_{ces} + I_{pv} \tag{5}$$

so, by controlling inductor current (i_s) i_{pv} and i_{ces} are controlled.

In the circuit while S_1 and S_4 are ON S_2 is OFF, inductor L_S charges to current slope V_S/L_S , L_W charges to current slope V_w/L_W . During this period load is supplied by C_{load} , as C_S discharges through CES. When S_2 is ON and S_1, S_4 are OFF the inductors L_W, L_S discharge through CES and load, during this period load, DC-link is supplied power by PV through L_S . It can be seen under steady state that supercapacitor and battery voltages are equal, so for a good voltage regulation supercapacitor with high voltage rating than the battery is chosen, in the converter, DCM (discontinuous conduction mode) is avoided by allowing negative current through the inductor so that circuit operates in CCM (continuous conduction mode). By selecting a rated value of inductor DCM is avoided, the load voltage is properly maintained at a value by PV and CES (Figs. 5 and 6).

Fig. 5 Waveforms for control of switches

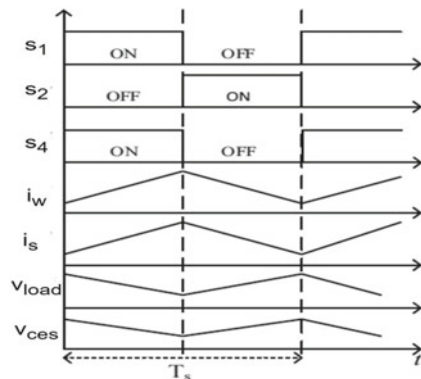
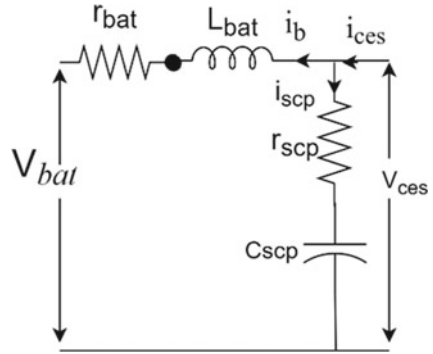


Fig. 6 Equivalent circuit of ces



3 Grid Interfacing and Circuit Description

When all the renewable sources are not able to supply load, or for V2G operation, a bi-directional buck-boost converter for V2G, G2V operation is realized [6, 9] (Fig. 7).

In this circuit, the switches S_1 , S_2 , S_3 , and S_4 are used for rectification operation during the G2V mode, as inverter operation during V2G mode. The LCL filter is used to remove harmonic content from the circuit. This filter reduces the electromagnetic interference with the grid, the DC-DC converter is a full bridge (zvs) circuit with a phase shifting control. The voltage ripples in the circuit are reduced by increasing the capacity of the voltage link (V_{DC} -bus). The circuit operates at a unity power factor, and the conversion efficiency is also good, ranging from medium to high power.

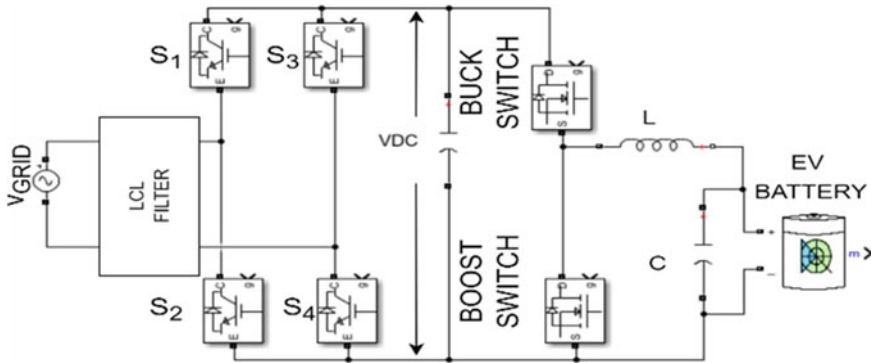


Fig. 7 Circuit diagram of grid port

4 Control System

4.1 For Multiport Converter

In designing the control system, a proportional-Integral(pi) controller is adopted to the control system for the operation of PV, and CES is given in Fig. 8a, the dual loop control structure is used for this, for wind a single loop control is adopted, it is the controller given in Fig. 8b. In this control system to get maximum power out of PV, wind maximum power point techniques are used, the MPP algorithm-perturb and observe (P&O) algorithm is used in this control due to its low cost and ease of implementation.

In wind control, the voltage (V_w), and currents (i_w) are given to the mppt algorithm, by this, a current signal is generated which is given as reference (i_{WR}) to the next summing point. Current (i_w) and the generated reference (i_{WR}) are compared, then the error signal is supplied to the PI controller. It produces a duty ratio such that error is minimized, then to produce switching pulses the signal (d_w) is compared to a high-frequency carrier signal, whose result is switching pulses (S_4). In PV and CES controller, if PV is available, by using PV voltage (v_{PV}), current (i_{PV}), a voltage reference (v_{pvr}) is generated by using the mppt algorithm, this reference is given to the voltage controller which adjusts the voltage reference, and the reference voltage and actual voltage (V_{PV}) of PV are compared to get error signal, it is given to pi block, this generates the current reference (i_{sr}) so that voltage is maintained at MPP. Next, the generated current reference and actual current (i_s) are compared to get an error signal and this error pulse is fed to the pi block to get (d_s), which is followed by a PWM generator, the PWM generator compares the (d_s) with a high-frequency ramp signal to generate (S_1), for a gate signal of CES switch S_1 signal is negated (Fig. 9).

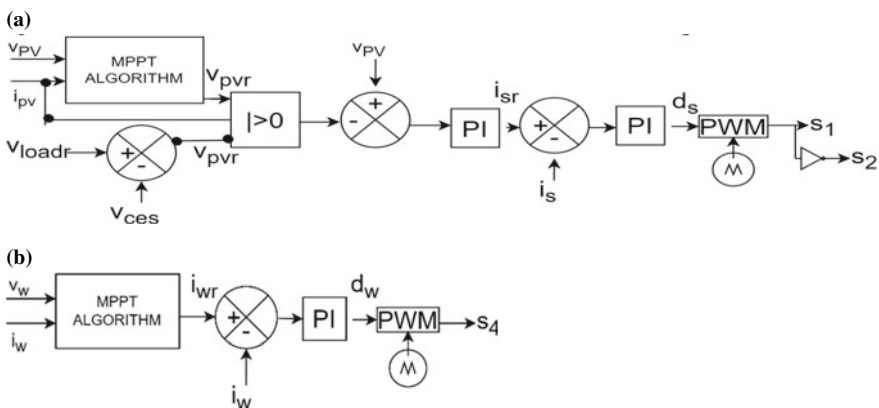


Fig. 8 a Proposed control for PV&CES. b Proposed control for wind

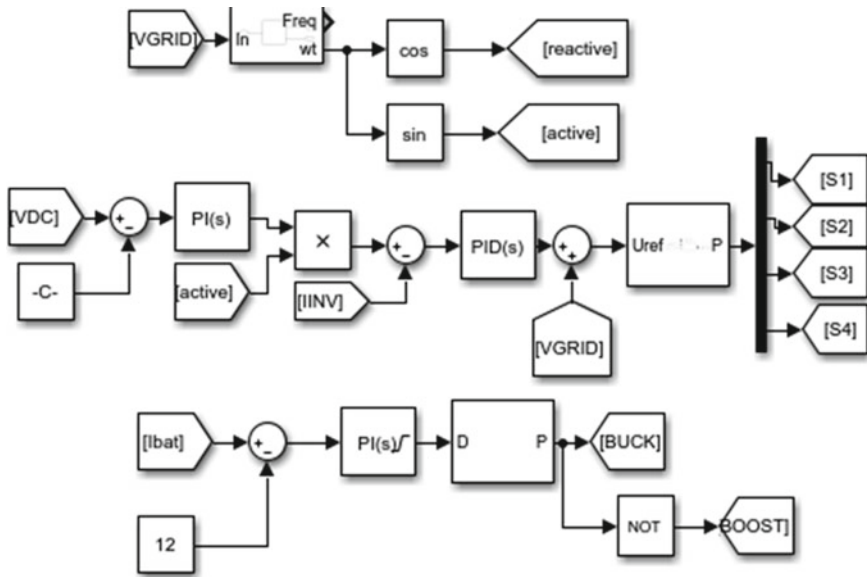


Fig. 9 Controller for V2G/G2V operation

4.2 Grid Interfacing Operation Controller

For injecting power into the grid, the main criteria are having the same level of voltage and frequency. so the circuit should operate at unity power factor, so power factor correction should be done in the circuit, mainly the operation of V2G/G2V is based on the sign of current reference given to the battery current controller, initially, the active component of voltage is extracted from the grid voltage (V_{grid}) by using a phase locked loop, because charging/discharging depends on the phase shift angle. In the next step, based on DC-link voltage a reference is generated which is passed from a PI controller, to this signal multiplying the active voltage component a current reference is generated, then by reducing errors, followed by a PWM generator S_1, S_2, S_3, S_4 pulses are generated (Table 1).

Table 1 Circuit parameters

Component	Value	Component	Value
PV source: MPP: voltage, current	16.8 V, 2.5 A	L_{BAT}, L_S, L_W	2, 5, 2 mH
Supercapacitor: terminal voltage, capacitance	40 V, 9 F	C_{PV}, C_S, C_W	2000, 2000, 1000 μ F
Battery: terminal voltage, capacity	36 V, 32 Ah	Load: R_{load}	(10–100) Ω
Wind source: MPP: voltage, current	30 V, 3 A		

5 Simulation Procedure and Results

5.1 Multiport Converter Simulation

As various sources are present, many cases are possible and each case has been realized in simulation. The inputs to the solar, wind, and resistive load are varied at particular intervals, the inputs and load are varied to check if the system is able to supply load under different operating conditions. PV, wind sources can be connected/disconnected but the battery, and supercapacitor are present in the circuit. The various operating modes are

Inputs parameters for source: PV array-irradiation, inputs 1000, 800, 600, 400 W/m², Time in 0, 2, 4, 6 s, Wind -current reference 1, 2, 3, 4 A, Time in 0, 3, 5, 9 s.

The load is also changing in order of $50 \pm 10 \Omega$ at time: 0, 2, 4, 6 s.

Case 1: PV and wind unavailable: Fig. 10. As both sources are absent the load has to be supplied from the storage unit only, we can observe that as the load changes with respect to time, the transient power is given by the supercapacitor and stable power is given by the battery, and load voltage is maintained almost constant. Case 2: PV source present, wind absent: Fig. 11. In this load gets power from PV, battery, and supercapacitor, the input is varied at an even number of seconds during the simulation time and the load disturbances are also created, the current of PV at few points $t = 2$ s changes, irradiance is also dropping at 200 w/m², due to changes in the load and PV power the load voltage also changes but we can observe that there is only a slight variation, a good amount of voltage regulation is observed. Case 3: wind source present, PV absent: Fig. 12, the load is supplied from wind, CES wind disturbances are created at an odd number of seconds in simulation, the load disturbances are created at regular intervals, and we can observe that only a few changes are present in load voltage, the supercapacitor, battery supplied transient and steady power during disturbances. Case 4: all sources are turned ON: Fig. 13: at regular intervals, PV, wind disturbances are created along with load changes, we can observe that load voltage is almost maintained constant we can clearly see that a good power balance is achieved between all the sources under all the disturbances. Power sharing between all the sources is also plotted in Fig. 16, we can observe that most of the load power is supplied from PV, and the rest of the power is shared between other sources.

6 Vehicle to Grid/Grid to Vehicle (V2G/G2V) Operation

The operation of V2G is shown in Fig. 14. As the current reference is positive, we can see that V2G operation occurs, and the grid voltage and current are out of phase showing the successful injection of power to the grid. The operation of G2V is shown in Fig. 15, as the current reference is negative, G2V operation occurs, and the grid

Fig. 10 PV and wind unavailable

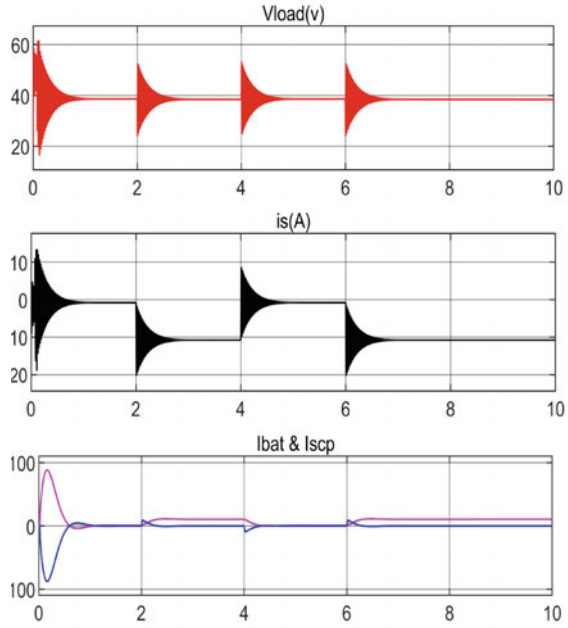


Fig. 11 PV source present, wind absent

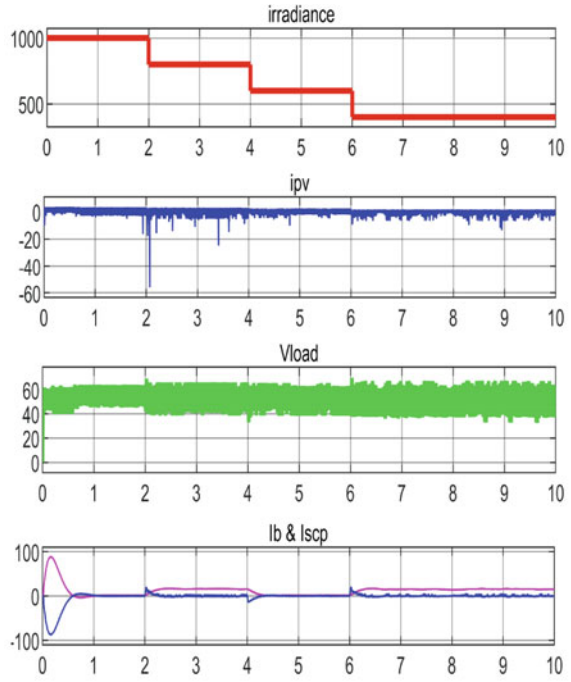


Fig. 12 Wind source present, PV absent

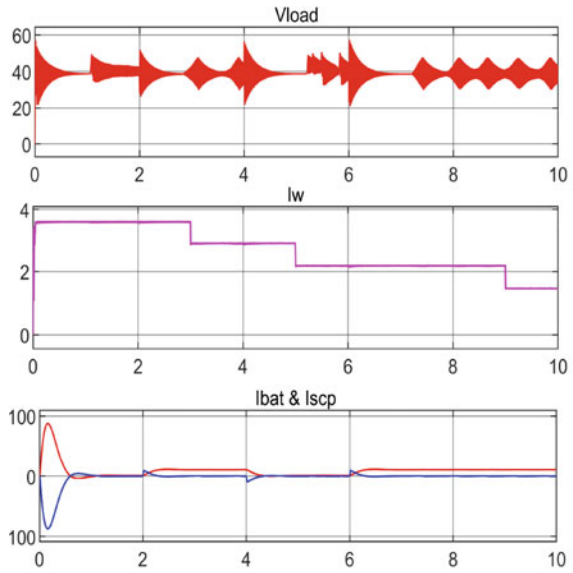


Fig. 13 All sources are turned ON

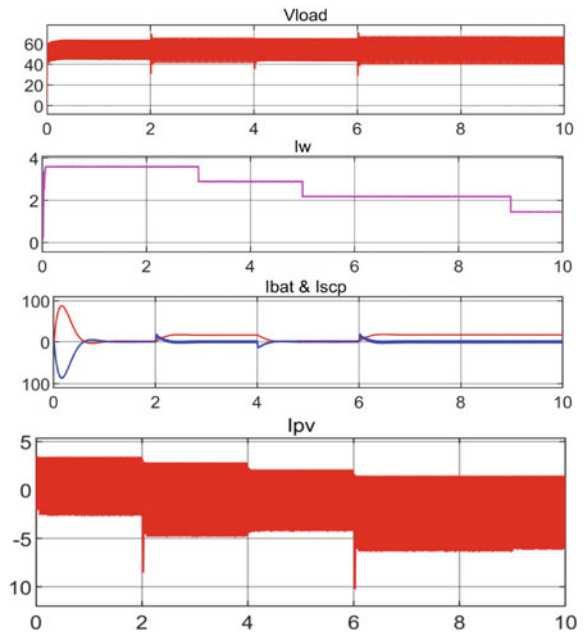


Fig. 14 V2G operation

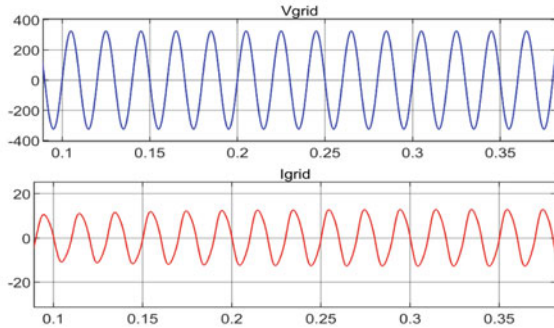
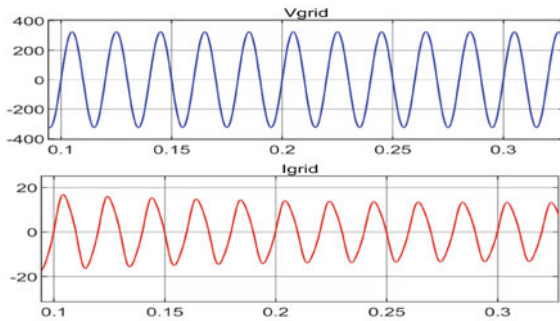


Fig. 15 G2V operation



voltage and current are in phase showing G2V operation, we can also observe that the battery current follows the reference value in both cases (Fig. 16).

7 Comparison and Improvement of Efficiency

The proposed work's load voltages have been compared with earlier works and the results are shown in Table 2 and Fig. 17. From the simulation results Fig. 17 we can see that the proposed converter has maintained a stable load voltage as compared to another one [5].

To improve the power density, efficiency of the proposed converter work has been done by incorporating SiC MOSFETs [10]. The losses such as conduction and switching losses for normal Si-MOSFET and SiC-MOSFET at various loads are calculated.

We can observe from Fig. 18 that losses of the designed converter are decreased, as a result, the efficiency of the charging station is increased. Efficiency plots are shown in Fig. 19 which clearly show an increase in efficiency. The losses and efficiency of the converter are calculated by using functions in MATLAB. From the results, it is

Fig. 16 Power sharing

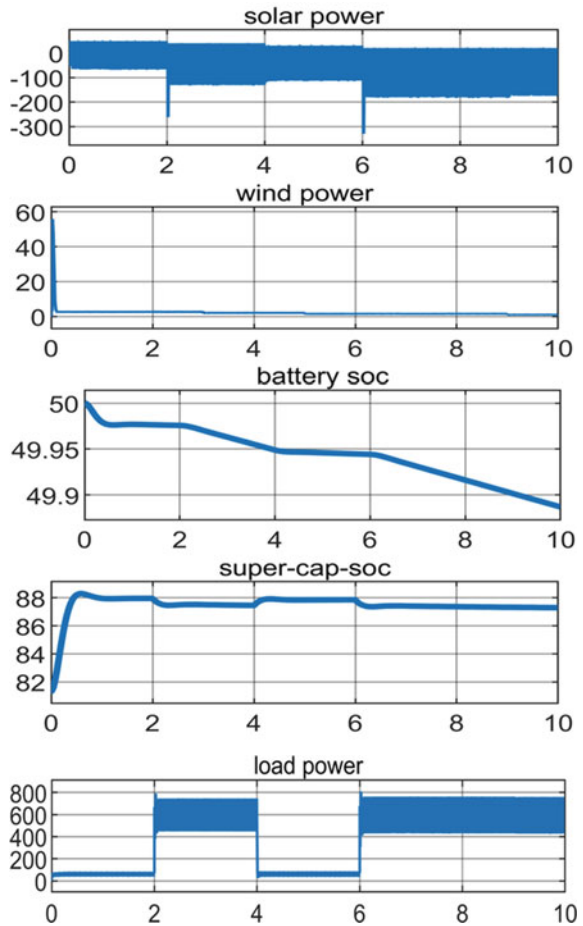
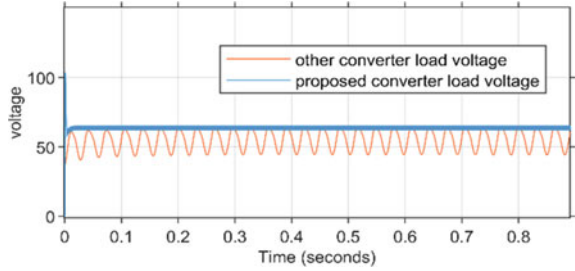


Table 2 Comparison of various parameters

Parameters	Reference [5]	Reference [4]	[Proposed]
PV supply	Present	Present	Present
Wind supply	Present	Absent	Present
Storage units	Present	Present	Present
Switch count	8	6	3
Inductors count	4	3	3
Sharing of Power	Combined	Combined	Inbuilt
Voltage regulation	Combined	Combined	Inbuilt

Fig. 17 Comparison of proposed converter load voltage with previous work



observed that for each mode of operation of the converter at various load values the efficiencies are increased, and the conduction and switching losses are reduced.

Fig. 18 Power losses under various modes, loads compared between Si and SiC switches

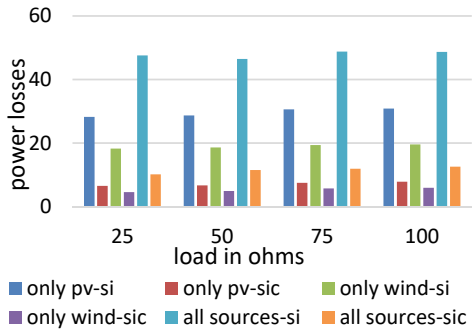
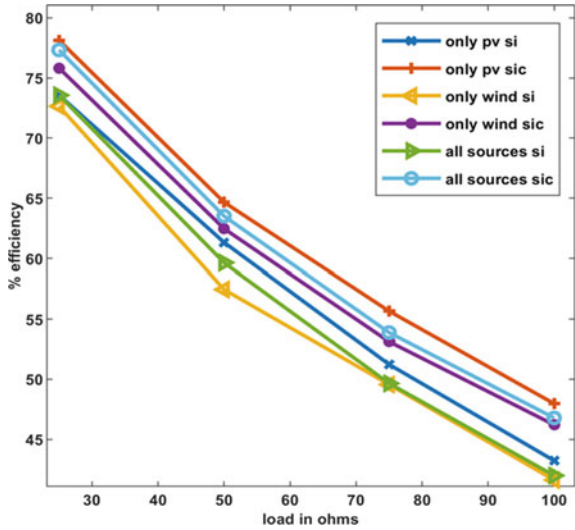


Fig. 19 Comparison of efficiencies of converter by both types of switches, at various load and operation modes



8 Conclusion

In this paper, a multiport converter for EV charging by integrating renewable energy sources is designed and the converter is tested under various conditions of load and source disturbances. It was able to supply constant power to load under various disturbances also, as a result of all sources integration the power-sharing between the sources was good. The proposed converter was easy to design with less number of elements, due to the low number of switches the losses were less and efficiency was good when compared with similar circuit topologies. To improve the performance of the circuit the sic mosfets were also incorporated by which circuit efficiency has been increased.

References

1. Song Y, Yang X, Lu Z (2010) Integration of plug-in hybrid and electric vehicles: experience from China. In: IEEE PES general meeting, 2010, pp 1–6. <https://doi.org/10.1109/PES.2010.5589926>
2. Tani A, Camara MB, Dakyo B (2015) Energy management in the decentralized generation systems based on renewable energy—ultracapacitors and battery to compensate the wind/load power fluctuations. *IEEE Trans Ind Appl* 51:1817–1827. <https://doi.org/10.1109/tia.2014.2354737>
3. Du Y, Zhou X, Bai S, Lukic S, Huang A (2010) Review of non-isolated bi-directional DC-DC converters for plug-in hybrid electric vehicle charge station application at municipal parking decks. Twenty-fifth annual IEEE applied power electronics conference and exposition (APEC) 2010:1145–1151. <https://doi.org/10.1109/APEC.2010.5433359>
4. Kollimalla SK, Mishra MK, Narasamma NL (2014) Design and analysis of novel control strategy for battery and supercapacitor storage system. *IEEE Trans Sustain Energy* 5(4):1137–1144. <https://doi.org/10.1109/TSTE.2014.2336896>
5. Zhang N, Sutanto D, Muttaqi KM (2015) A four-port DC-DC converter to integrate energy storage system and solar PV to supply the grid and local load demand. In: 2015 Australasian universities power engineering conference (AUPEC), pp1–6. <https://doi.org/10.1109/aupec.2015.7324811>
6. Zgheib R, Al-Haddad K, Kamwa I (2016) V2G, G2V and active filter operation of a bidirectional battery charger for electric vehicles. *IEEE international conference on industrial technology (ICIT) 2016*:1260–1265. <https://doi.org/10.1109/ICIT.2016.7474935>
7. Krishnamoorthy M, Raj P, Suresh S, Natarajan K (2019) Techno economic analysis of hybrid renewable electrification system in different climatic zones. *Lecture notes in electrical engineering*, pp 151–166. https://doi.org/10.1007/978-981-13-8942-9_14
8. Verma A, Singh B (2020) Multimode operation of solar PV array, grid, battery and diesel generator set based EV charging station. *IEEE Trans Ind Appl* 56(5):5330–5339. <https://doi.org/10.1109/TIA.2020.3001268>
9. Ravivarman S, Natarajan K, Raja Gopal RB (2019) Non-isolated modified quadratic boost converter with midpoint output for solar photovoltaic applications. In: *E3S web of conferences*, vol 87. EDP Sciences, p 01025. <https://doi.org/10.1051/e3sconf/20198701025>
10. CREE C3M0065090D: SiC-mosfet. <https://www.wolfspeed.com/c3m0065090d>

Impact on Solar Energy Generation with Dual-Axis Solar Tracking System Including Different Weather Conditions



Rajendra Singh and Neeraj Tiwari

Abstract The term solar energy refers to the radiation in light energy and the heat of the sun is received in high amounts. The solar energy that is received from the sun reaches the surface from the 6 surface or layers that travel from the sun to power the environment. Light from the sun travels 93 million miles per kilometer from the sun to the various atmospheric layers 51% of the solar energy is absorbed by the land and ocean and the remaining energy is transmitted from one form to another form that can be utilized in another form of the energy. The energy of the sun that is emitted in the daytime depends on the surface latitude angle which is a tilt on the surface. The solar energy of the sun is available in the form of radiation at different levels according to the time variation and location, earth's surface that changes according to time to time, day by day, and year by year. This energy can be utilized by using semiconductor devices like PN junction semiconductor materials that are made of silicon, and germanium. Silicon semiconductor materials are utilized to fabricate the semiconductor chips and repair the computers and other electronic devices. Solar cells are made of semiconductor material for the production of energy this process at cell fabrication. A p–n junction semiconductor device made of silicone is generally used to fabricate semiconductor chips for computers and other electronic devices. When sunlight hits the cells, the solar cell generates direct current (DC) electric power. SPV module is a single mono-block unit having a fixed number of solar cell strings (36, 72, etc.), which is the fundamental building block of SPV systems. It consists of Solar cell strings sealed between the layers of Ethyl Vinyl Acetate (EVA). Solar energy generation can be increased by the tracking of the solar Self through the solar tracking power system in terms of the dual axis. 18% efficiency at the solar system can be increased through the tracking system. Solar energy can be used for the heating of water, heating of the building, drying agriculture and animal products, electric power generation through Solar radiation through the sun, thermal power production, solar pumping, and utilization of electric vehicles through solar energy.

R. Singh (✉) · N. Tiwari

Department of Electrical Engineering, School of Engineering and Technology, Poornima University, Jaipur 303905, India

e-mail: rajendra.singh@poornima.org

Keywords Solar panel · Radiation energy · SPV module · Ethyl vinyl acetate · E-vehicle in transport · Solar drying of agriculture · Solar pumping · Power production

1 Introduction

Solar energy generation by photovoltaic plants but also it is generated by semiconductor devices, these devices are called solar cells and a combination of the cells is called a solar array. According to the customer services and requirements capacity of the solar power generation can be changed (increase or decrease) at the particular desired level [1]. A number of different technologies have utilized the control and achieve the goal quality of the energy. Reduction of the faults and the loss of power energy an effective solution is achieved for quick correction [2]. A number of the electronics equipment and elements provide better results for controlling the cost, performance, output result, monitoring of the plant operation, easy for controlling and easy for installation and controlling. These alternative energies are required for better management and security for the remote control of the power system [3].

Photovoltaic systems can be Generated solar energy according to the intensity of the radiation, actual energy production is very lower as compared to the energy distributed by the sun on earth. Fundamental to keep the plant and monitor the generation of energy proves the system.

Some of the points are associated with the maximum generation of energy through solar.

1. Plants should be kept clean remove the dust particle from solar plates
2. It should be justifying the production of energy according to the requirement.
3. Data of the system can be accessed by anyone; it should be controllable under the plant data.

1.1 *Components of a Solar SPV System*

The output of the system change with the operation of the machine and the solar radiation, input of the supply, and variation of the frequency. The output value of the supply of the system depends on the different components like the number of cells in the PV array, the controlling system, and conditions. So some major components of the solar system can be described here the power system.

- (1) PV array of the solar system—it utilizes for converting solar energy into a direct supply of electricity.
- (2) Controlling units—this unit is utilized for the controlling the supply components like voltage, current, harmonics, and fluctuation of the supply.

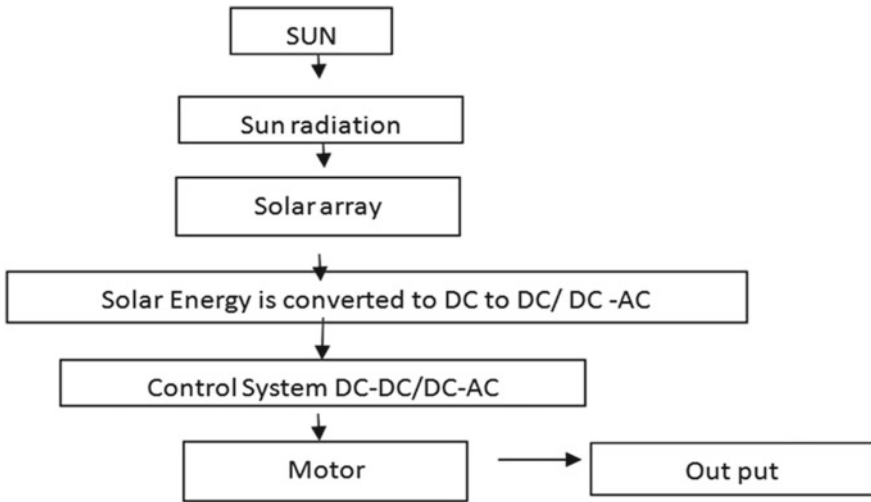


Fig. 1 Generation and utilization of solar energy block diagram [4, 5]

- (3) Convertor units—these units are used for converting the energy form from one form to another form of energy at the desired levels [4, 5].

Solar array systems have different types of components like a single phase of power supply that have 220 V to 440 V, 50 Hz grid connected. Conventional system operator on fixed 50 Hz power supply. This system has drawn a constant power supply from the grid. The power supply Flow from the grade to the load center in terms of the AC and DC supply. Electrical machines draw the power supply from the source as a constant value of the current and voltage (Fig. 1).

In the supply, the permanent magnet is controlled through a DC or AC motor that maybe PV modules are connected in the combination of the series and parallel strings... The solar system consists of a number of parallel and series combinations of photovoltaic cells that are called module [6] (Fig. 2).

Controller. A number of modules are connected in series for increasing voltage at a desired level and a number of sales are connected in parallel for increasing the rating of current for a solar cell. So the series and parallel combination are including generating a desired level of voltage and current for the respective drive and motor. The capacity of the solar cell in a given kVA. Every solar power plant has a controller for controlling the voltage and current and frequency of the applied system.

The controllers have maximum efficiency and add the tracking point which is the maximum PowerPoint tracker (MPPT) that provides the maximum output of the solar cell. On the other hand, the controller protects the unit from overvoltage and under current conditions. The size of the motor is depending on the load and the configuration of the input data. The controller system also consists of electronic units for the monitoring of the system and a remote system for operating performance. The



Fig. 2 Solar array

controlling system also includes the inverter units and synchronizes for the constant power supply at the inverter unit [7] (Fig. 3).

Locating and Mounting the Controller. Controller units are connected near the load center. It is recommended for the installing unit; the controller box and pipe of the solar array should be near each other and connected to the tightly controlled unit on the opposing side of the solar panel.

If the load center has some distance from the generating unit then it will be preferable so it should avoid the loss in the DC power supply [8] (Fig. 4).



Fig. 3 Controller panel



Fig. 4 Controller under solar panel

2 A Structure of the Solar Panel

A structure of the solar panel depends on the tracking system add adaptive intelligent solar trackers are utilized to generate the electricity in the electrical system and this electricity can be utilized for different purposes.

The solar panels have different parts like.

1. Solar panel
2. Controlling unit of the system which is utilized is number of the gears at the different sizes of the motors and ratings.
3. Solar trackers are utilized to track the direction of solar panels in the direction of the sun. Solar trackers r depend on the height, direction, Flow of air, intensity of the solar radiation, linear actuator, and unit of controlling, batteries (Fig. 5).
4. Biaxial solar tracker—This type of solar tracker is utilized to track the sun's direction in both directions horizontally and vertically, east to best [9].
5. Some of the batteries are installed in a small size horizontally; small batteries of the solar cell are utilized to monitor the current and voltage at a particular position with a precise orientation.

2.1 Algorithm for Solar Tracking System

A solar tracking system has an algorithm for the tracker biaxial solar tracking system. After initializing the controller TTL units or modules are utilized to track the system.

In the next step the real time for the request of the operation in the variables as well as the controller of the sunlight tracking systems at a particular time period is utilized then it is necessary to determine the sun rising time t_{SR} and the sunset time t_{SS} in the order of interval at a particular time. If the condition of the $t_{SR} > t_C > t_{SS}$ is a full film then the controller calculates the number of the art for the necessary

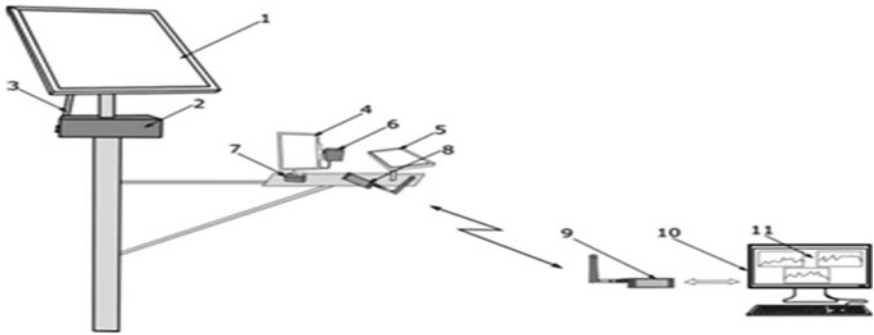


Fig. 5 An adaptive intelligent solar tracking system

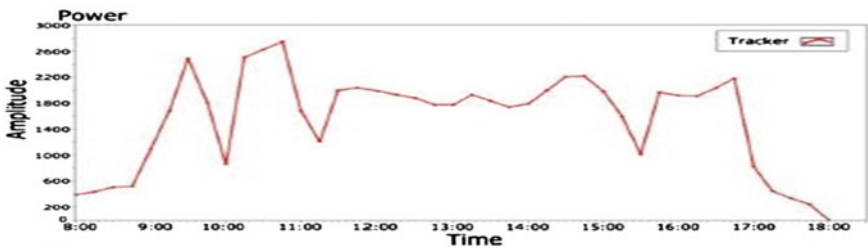


Fig. 6 Power achieving through solar tracker during a cloudy day

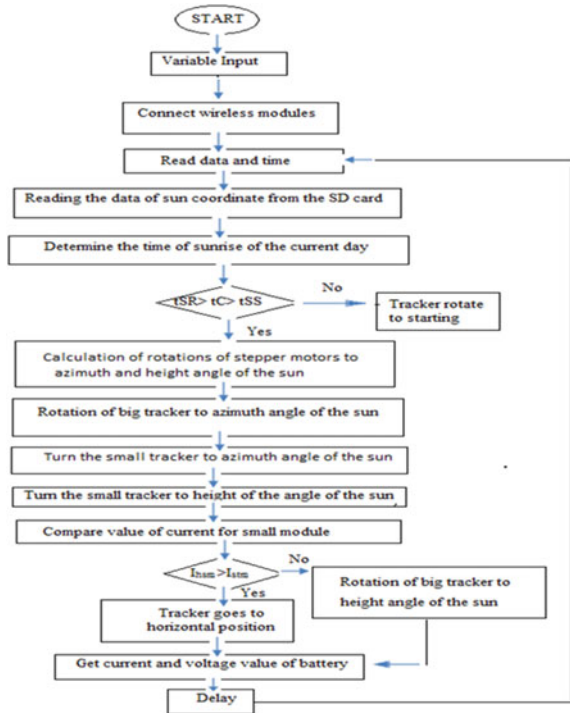
in-bring format tracker to the desired position. Then the stepper motor is utilized for tracking the sun which rotates in a particular direction it may be a horizontal plane (Figs. 6 and 7).

Now if the current is very small then the amplifier is utilized to generate the current and store it in the batteries. If the value of the current each higher at the desired level then it is utilized indirectly. And the current and voltage of the battery and the voltage at sent to the wireless channel to the dispatcher for the data processing and presentation of a convenient form. One of the short periods of time cycle is begun in a new way [10, 11].

3 Result and Conclusion

In this paper, we have discussed the solar power plant and solar energy generation through the dual-axis solar tracking system. Through the dual-axis solar tracker system the energy generation can be increased and the quality of the power also increases. Through the solar tracking system generation of voltage depends on the radiation of the solar, intensity, the direction of the sun, the timing of sunrise and sunset, and the position of the solar tracker horizontally and vertically, different other

Fig. 7 Adaptive intelligent solar tracking system's algorithm



components of the system also affect the generation of the power like solar cells, Photovoltaic array, azimuth angle, the horizontal and vertical direction of the solar face, rating of the PV array system. A flow chart of the system is defined at the starting point to the endpoint when the generation of the solar energy is achieved sun rising to sunset time. The generation of the solar system also depends on the condition of the weather, if the sun facing time period is high then the generation of the power is high and if the sun-facing time is less then the generation of the energy is very less.

References

1. Kuttybay N et al (2019) An automated intelligent solar tracking control system with adaptive algorithm for different weather conditions. In: International conference on automatic control and intelligent systems (I2CACIS 2019), pp 315–320
2. Mousazadeh et al (2009) A review of principle and sun-tracking methods for maximizing solar systems output. *Renew Sustain Energy Rev* 13(8):1800–1818
3. Nadia ALR et al (2018) Advances in solar photovoltaic tracking systems. A review. *Renew Sustain Energy Rev* 82:2548–2569

4. Saymbetov et al (2018) Intelligent energy efficient wireless communication system for street lighting. In: 2018 international conference on computing and network communications (CoCoNet). IEEE, pp 18–22
5. Alexandru et al (2010) Simulation of a dual-axis solar tracker for improving the performance of a photovoltaic panel. *Proc Inst Mech Eng (J Power Energy)* 224(6):797–811
6. Koussa et al (2011) Measured and modelled improvement in solar energy yield from flat plate photovoltaic systems utilizing different tracking systems and under a range of environmental conditions. *Appl Energy* 88(5):1756–1771
7. Kelly et al (2011) Increasing the solar photovoltaic energy capture on sunny and cloudy days. *Solar Energy* 85(1):111–125
8. El Kadmiri et al (2015) A novel solar tracker based on omnidirectional computer vision. *J Solar Energy* 1025–1030
9. Khan et al (2010) Design and construction of an automatic solar tracking system. In: International conference on electrical & computer engineering (ICECE 2010), pp 326–329
10. Ferdous et al (2014) Energy efficient hybrid dual axis solar tracking system. *J Renew Energy* 560–570
11. Yazidi et al (2006) Low cost two-axis solar tracker with high precision positioning. In: 2006 first international symposium on environment identities and Mediterranean area. IEEE, pp 211–216

Semantic Normal Form for Performance-Critical Databases



Adil Khadidos, Alaa Khadidos, Yasser Ades, and Mohammad Yamin

Abstract Semantic Normal Form (SNF) compliant software is software that is immune to malignant change. SNF software extends and adapts to business needs without recourse to database restructuring or the rewriting of associated software. This stability eliminates most software maintenance costs while also enabling Just-in-Time systems implementation. SNF software is achieved largely because it embodies an SNF compliant conceptual database schema. SNF compliant database schemas consist of tables with a simple uniform structure; however, SNF schemas tend to have many more tables than non-SNF compliant versions. This means that SNF compliant schemas necessitate the frequent use of multiple query joins in data manipulation. This raises the question about the technical feasibility of building high-performance database transactions for SNF compliant systems. In this paper, we measure the performance premium for SNF compliant software by comparing the performance of an SNF system with a non-SNF version. The SNF version was indeed a little slower but a deeper analysis of both the comparison results and our experience with industrial SNF systems suggests that not only is it possible to achieve high-performance SNF compliant systems, but that SNF compliance is particularly desirable for large complex performance critical databases.

Keywords Semantic Normal Form (SNF) · Third Normal Form · Conceptual schema stability · SQL queries · Database performance analysis

A. Khadidos (✉)

Department of Information Technology, Faculty of Computing and Information Technology, King Abdulaziz University, Jeddah, Saudi Arabia
e-mail: akhadidos@kau.edu.sa

A. Khadidos

Department of Information Systems, Faculty of Computing and Information Technology, King Abdulaziz University, Jeddah, Saudi Arabia

Y. Ades

Department of Business Administration, Faculty of Economics and Administration, King Abdulaziz University, Jeddah, Saudi Arabia

M. Yamin

Independent Management Consultant, Melbourne, Australia

1 Introduction

Databases are the heart of computer-based information systems, and their conceptual design is crucial to their functionality and adaptability to changing user requirements. William Kent correctly anticipated in his 1978 seminal work, 5 that getting the conceptual database schema right would emerge as the most critical and challenging task in the construction and maintenance of enterprise information systems [1]. Critical because the conceptual database schema 1 is like the structure of a building—quite expensive to × once the software is commissioned and challenging because getting it right early in the system life 10 cycle is difficult. When Hoberman was tasked to update Kents Data and Reality for republication in 2012 [2], he lamented in the preface that the book remains up-to-date some 34 years after its publication. This, sadly, reacts on the paucity of progress in systems analysis research. When practitioners talk about getting the conceptual database schema right, they mean getting it stable. 15 Stability 2 is a characteristic of conceptual schemas which allows the schema to grow and adapt with minimal impact on legacy software and minimal database restructuring. In industry, we use two informal approaches to achieving this quality pattern reuse and Stability Analysis. Stability Analysis involves the review by experienced analysts of the conceptual schema before it is used as 20 a foundation for physical database design and subsequent analysis and design activity. Pattern reuse brings to bear the experience of expert analysts at the start of the conceptual schema design process. Neither of these two approaches singularly or in combination have addressed the challenge identified by Kent. Empirical research conducted by Sjoberg [3, 4] suggested that the problem of 25 unstable conceptual schemas is now both endemic and chronic in large enterprises. We continue to suffer from high information system project failure rates, high maintenance costs, and software in exibility that we, in hindsight, attribute to the initial design of our conceptual schemas. At the core of this challenge is that we cannot measure stability except contingently—i.e., when it is too late 30 for a business. A few years after the publication of Kents Data and Reality Stamper postulated the existence of a semantic theory the Semantic Normal Form (SNF) that correlates with stability. He published his postulate in 1979 [5]. His research team, initially based at the London School of Economics UK, continued to 35 works on perfecting and testing the theory using Poppers most severe scientific method. The significance of the discovery of the SNF for enterprise software quality is that 1. we now know, empirically, that SNF compliance correlates with intrinsic database schema stability [6, 7], 40 2. we can objectively determine if a database conceptual schema is SNF compliant or not up front [7] in the same way that we can determine if a database schema is relational normalized [8, 8–13] or not. How does SNF compliance relate to relational normalization? SNF schemas are relationally speaking in 3rd normal form but not all relational 3rd normal 45 form schemas are SNF compliant. Moreover, all higher relational normal forms, including BCNF, are not SNF compliant as they usually increase instability, i.e., they increase the malignant assumptions in the conceptual schemas by embedding business rules in the data structure. It is noteworthy that practitioners rarely venture beyond the

relational 3rd normal form, 50. The strongest claim against SNF compliance, as a quality objective, is the conjecture that SNF may undermine transaction performance in the same way that a relationally 3rd normal form schema may sometimes undermine transaction performance. This analogy is reinforced by the orthodox claim that relational normalization itself correlates with stability. This correlation is unfounded as we know from experience [3, 4] and the analogy is unsound. Relational normalization is an internal software characteristic relating to certain contingent properties of data whereas semantic normalization is an external software characteristic. It means almost nothing to a business whether the database schema is relationally normalized or not. Relational normalization is a characteristic that deals with the anomalies of updating instances in the database. Semantic normalization is a characteristic that deals with the anomalies of updating the conceptual database schema. When trading relational normalization for performance we are trading an external software quality 3 that is tangible for the business 65 performance with an internal software quality relational normalization. Not surprisingly, we do sometimes relationally deformalize for the sake of performance. However, when comparing performance with Semantic normalization we are trading two external software quality goals stability vs performance. In section VI we articulate in progressively stronger arguments that SNF compliance 70 does not undermine performance and demonstrate that SNF and performance are not just reconcilable, but in the context of large organizational information systems SNF compliance is desirable for performance critical transactions.

Before articulating this position let us just assume that stability (immunity to malignant change) is not a significant quality objective and then ask 75 what the performance premium of SNF compliance is anyhow. We develop two working relational schemas one that is SNF compliant and another that has departed significantly from SNF but is nonetheless relationally 3rd normal form compliant. We then compare their performance. The case applications are for an online shop and their corresponding database 80 schemas are implemented in the MySQL database management system. The databases tables are populated with 350,000 records each and the response time is measured for a variety of typical transactions. In Sect. 2 we briefly describe relational normalization. In Sect. 3 we present the two database schemas. In Sect. 4 we present the empirical results 85 and in Sect. 5 we analyze these results. In Sect. 6 we analyze the underlying assumptions of our empirical work together with old experience with the performance of industrial SNF systems.

2 Normalization

Relational normalization is a well-known process of analyzing a given set of 90 data attributes according to their functional dependencies [13, 14]. A relational database schema organizes the attributes in tables (called relations in Relational theory) in such a way as to minimize data redundancy thereby reducing update anomalies. Intuitively, the simplest way to describe the objective of relational normalization is to organize

the data so that one fact is stored in only one 95 places. A schema is considered in 1st relational normal form (1NF) if the values of non-key attributes are uniquely identified by the primary key that is there are no multivalued attributes in 1NF compliant schema. Any relation which satisfies 1NF and has no partial dependencies is considered as second normal form (2NF). Any relation which satisfies 2NF and does not contain any transitive dependencies is considered as third normal form (3NF). Relational analysts are averse to using surrogate keys as primary keys. They call them artificial keys and prefer to use user defined “natural keys,” but relational theory cannot exclude them in principle. Relational theory recognizes a key as a primary key only if it is unique, singular, and non-null.

3 The Database Schemas

To measure the performance premium of SNF compliance, we developed a database to hold the sales of an e-commerce system. The system stored the items sold and to whom. The following shows the tables before normalization.

Initially, three tables as shown in Figs. 1 and 2 were extracted from this sales table, namely a table for items, a table for customers, and a table for the actual sales.

Item_id	Item_id	Item_name	Item_price	Qty_in_stock	Customer_id	Customer_name	Customer_contact	Customer_address	Qty_sold	Total_bill
---------	---------	-----------	------------	--------------	-------------	---------------	------------------	------------------	----------	------------

Fig. 1 Sales table before normalization

SHOP_ITEM

Item_id	Item_name	Item_price	Qty_in_stock
---------	-----------	------------	--------------

CUSTOMER

Customer_id	Customer_name	Customer_contact	Customer_address
-------------	---------------	------------------	------------------

SALES

Customer_id	Item_id	Qty_sold	Total_bill
-------------	---------	----------	------------

Fig. 2 The 3rd relational normal form schema but non-SNF

The diagram in Fig. 3 shows the non-SNF compliant relation database schema for the e-sales system in graphical form. The schema of Fig. 3 was 115 implemented in MySQL and each table was populated with auto-generated data. We now turn our attention to the SNF compliant version of this application. The conventional approach to generate SNF compliant schemas quickly and reliably is to use the semantic analysis method [7, 15] but there are alternative ways that allow conventional analysts to leverage their skills in stability analysis to approach SNF compliance. It is outside the scope of this short paper to explore the diverse ways to achieve SNF compliance, we are only concerned with measuring and evaluating the performance premium of SNF compliance. Figure 4 is the SNF compliant version of this application. This is the version that is intrinsically stable or immune to malignant change. For example, in 125 Fig. 3 the item table has name and price. In a SNF schema both the name and price are read and represented by a separate table, with start and finish time. This is because both the name and the price may change over time. Also, because the same item may have different prices in different currencies. Transforming the schema of Fig. 3 into SNF compliant schema will result in 130 the database schema of Fig. 4.

As can be seen from Fig. 4, the SNF compliant schema has significantly more tables. You will also notice that the SNF schema uses surrogate ids as the primary key for all tables. In practice, most database management systems can generate them automatically.

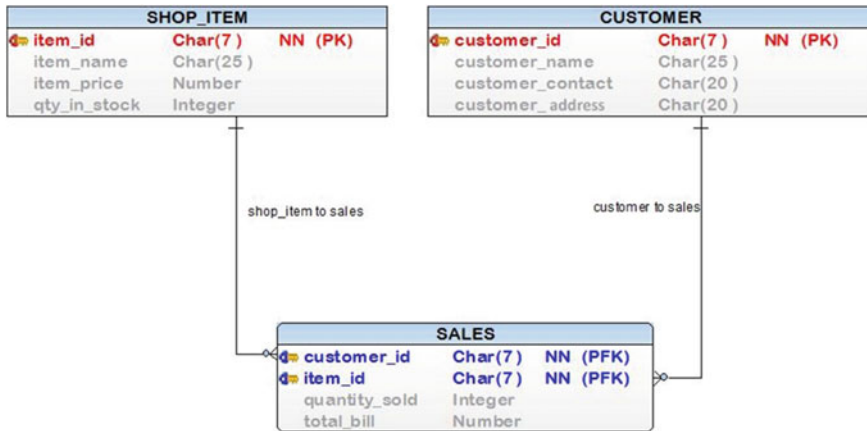


Fig. 3 The e-sales database schema

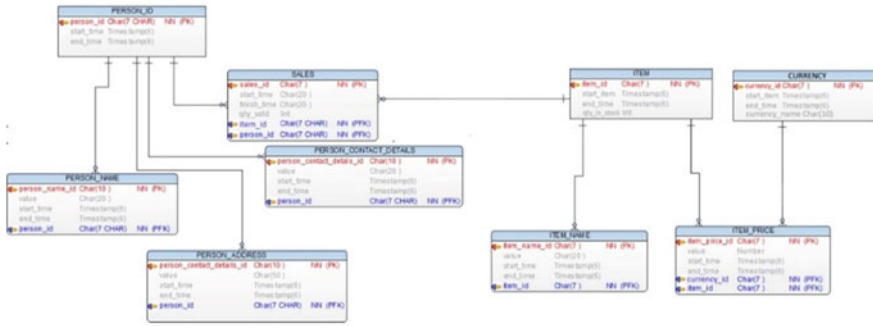


Fig. 4 The SNF-compliant e-sales system

4 Running the Performance Tests

Running the performance tests were executed, both systems were loaded with 350 thousand auto-generated records per table except for the tables of SNF that were extracted from attributes such as item name, price, and so on. Both databases were hosted locally in the memory drive of a desktop, with an Intel i7-140 6700 @ 4.00 GHz, 32 GB of DDR4 ram, and MSI gaming motherboard. MySQL was installed on a RAM drive of 8 GB to maximize response time. The non-SNF compliant system was populated with rest and then its data were converted to the SNF version. This meant that both systems had similar data. After both systems were populated, the following SQL queries were executed. 145 select an individual item by name. In both databases, the query was executed in 0.00 s. Select all active items in the SNF compliant version that corresponds to items with a finish time of null/present.

Here the execution of the query on the SNF database was slower, 0.04. 150 instead of 0.01 s. Update the price of all items that had price between 7 and 8. There were 2000 such items in the databases. Here the execution of the query in SNF was also slower, 0.07 instead of 0.03 s. 155 Increase the price of all items by 1. The execution of the query in SNF was also slower, 0.09 instead of 0.04 s. Delete items with price 7. The execution of the query in SNF was 0.03 the non-SNF database response 160 time was 0.02 s. For deleting individual records, the execution time was the same for both systems: 0.00 s. For inserting an added item the execution time was the same for 165 systems: 0.00 s.

5 Comparison

The diagram in Fig. 5 summarizes the performance differences between the two schemas. As can be seen, the non-SNF compliant system was faster due 170 to the reduced number of query joins but the SNF performance premium is not substantial. If performance optimization was applied to the SNF database, the difference will

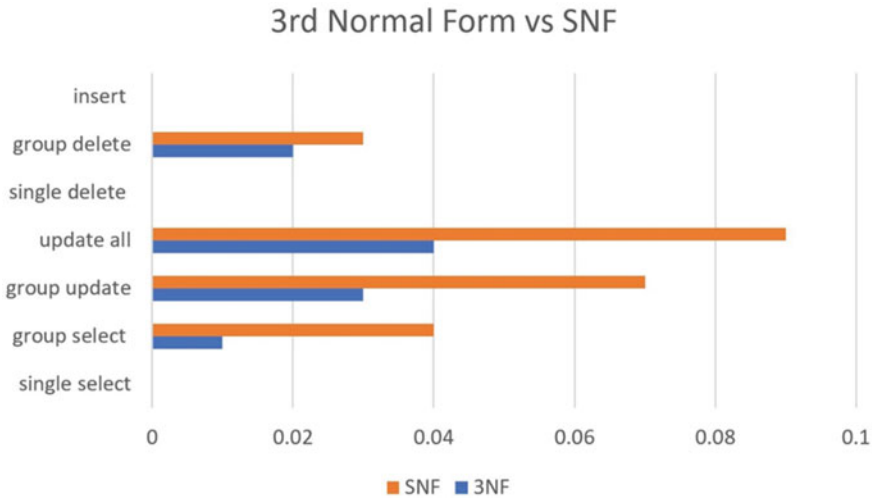


Fig. 5 Performance summary

be even smaller. But there is a deeper reason why even this small difference is inconsequential. We have compared the performance of two systems with different capabilities.

Two different requirement specifications one with an eye to providing hooks for system evolution and one that was oblivious to system evolution.

6 How is SNF Compliance Desirable for Performance Critical Applications?

In Sect. 4 we assumed that stability was not a quality criterion of any 180 significance. This is clearly an unrealistic assumption. In this section, we remove this assumption to reveal the importance of SNF compliance especially for performance critical applications.

6.1 Make the Trade Between Performance and Stability Consciously

Stability (or SNF compliance) is a substantive quality criterion for organizational information systems. We should not sacrifice it for performance lightly or unconsciously. To compromise stability for the sake of performance presupposes the existence of an SNF compliant schema on paper. For the sake of keeping this argument

simple, we will just assume in the first stage of the argument that SNF compliance and performance are irreconcilable qualities. 190 It is not unusual for the cost of implementing a requirement change that involves a malignant conceptual schema change, to be totally out of proportion with the size of the requirement change. It is these types of changes that 10 we should aim to minimize. Business managers rightfully expect us not to create impediments for their business ability to grow and adapt to the changing 195 environment. Whenever we depart from the ideal of SNF compliance in our implementation for the sake of performance we must justify that. To make the argument more concrete let us suppose that a systems analysis team specified a stable data model fragment for a share settlement system that can be easily extended to support settlement in multiple currencies. For them to 200 compromise the stability of their model by removing the capability to support multiple currencies it is reasonable that they must be convinced that: a change request to support multiple currencies is remote. a multicurrency capability will affect performance critical transactions. the performance benefits are worth the risk of instability. 205 Finally, the decision to sacrifice multiple currency support must be taken explicitly and in writing by an authority that can be made accountable, months or even years, after implementation. The attitude advocated above would lead us to a sound trade-o between SNF compliance and performance. Schema instability creates an impediment of 210 significant magnitude. These should be identified and traded-o against performance consciously by the analyst and decided explicitly by an authority that can be held accountable for its actions. To identify all the impediments created by departure from SNF require us to start with an SNF compliant model. The weakest argument in support of SNF as a quality goal is that we need it even 215 if we do not embody it in software simply so that we can identify malignant assumptions and assess departure.

6.2 SNF Releases Technical Sta to Work on Performance Tuning

The argument above is sufficient to keep stability as a goal for system analysis at least. It assumes that one may have to sacrifice SNF for the sake of 11 220 performance critical transactions. It assumed that these qualities are irreconcilable that is we cannot always have both SNF and high-performance transaction processing. We now remove this unjustifiable assumption. We argue that you should embody the SNF data model into the database conceptual schema. There are three key facts that we ignored in the argument above. 225 Firstly, one can make an SNF compliant system faster with the application of human resources. Secondly, a system based on a stable (i.e., SNF) schema releases maintenance stats that would otherwise be bogged down dealing with an endless stream of change requests. Thirdly, the dominant database management systems in the industry have succeeded in achieving physical data 230 independence [14]. This means that designers can always go back to tune

or redo the physical database design to improve performance without affecting their investment in application code. This combination of high stability and high performance was demonstrated in one of the first major industrial SNF system projects [6]. 235 The system was a university student information system called NAMAT [16]. NAMAT was based on a stable conceptual schema. After it was in production for about 6 months, the need for improving the performance of one transaction the course registration transaction was requested. A team was put to work on a database performance re-engineering project. The result was a 240 high-performance system with a stable (SNF) conceptual database schema. Postponing a major investment in database performance engineering is sometimes possible and in the above project desirable. Re-engineering the database physical design several months after delivery of the NAMAT 1 system allowed the team to measure performance factors precisely, identify bottlenecks accurately, focus on the performance engineering project, and avoid wasting resources over engineering the non-critical. SNF made human resources available for work on the performance critical parts. The additional human resources needed for building fast systems are made possible by SNF compliant software because they are an order of magnitude less expensive to maintain 12 250.

6.3 The Desirability of Stability for the Performance of Critical Transactions

At the start of this section, we assumed a concession that SNF may have to be sacrificed for the sake of performance on occasions. We then assumed that performance is a quality that can be bolted on after implementation. Now we argue that neither a trade-o for performance at the expense of SNF nor a shift 255 of performance engineering cost to post delivery is necessary. In the context of large-scale systems, SNF and high performance are not just reconcilable, but that SNF is desirable. Specifically, we argue that SNF is desirable for transactions that must achieve high degrees of performance on the day of delivery. This may seem strange but consider the following logic. 260 The fact that an unstable database schema fragment supports performance critical transactions does not mean that users will therefore refrain from generating requirement changes that affect that fragment. A performance critical part is not immune from requirement changes. The larger and more complex the project the greater is the probability that the malignant assumptions, inherent in schemas that depart from SNF, will surface even before delivery often referred to by project managers as requirement creep (or function creep or feature creep). Herein lays the desirability of SNF compliance to the performance critical transactions. Performance critical transactions on exceptionally large database systems require the 270 applications of considerable human resources for physical database design. A malignant alteration of the conceptual schema in a part that is performance critical not only affects the application programs but also the investment made in physical database design. For example, the consequences of the malignant change to the core of the

Australian Customs Data Model were aggravated by 275 the fact that it affected a performance critical part. The project resisted the alteration but the imperatives for change were overwhelming. This malignant change occurred during development and long before scheduled delivery; yet its consequences were severe. The larger the project the higher is the probability of a malignant change occurring prior to delivery [17]. 280 We have no evidence from practice that suggests that stability is consciously 13 compromised for the sake of reducing the cost of developing high-performance transactions in large database projects. Our experience suggests that the analysts, despite the Data Architects scrutiny, introduce instability unconsciously and it is not the physical database designers who introduce instability in the 285 conceptual schemata. The physical database designer's attention should and in practice is directed not at adding with the conceptual schema but embodying it faithfully in the physical schema. The physical designers' degrees of freedom are in the selection of access methods, distribution and replication strategies, storage media, encoding algorithms, hardware configuration, DBMSs, and communication channels. The problems of database base administration are complex enough that they do not need the headache caused by conceptual schema instability.

Acknowledgements This work would have not been possible without the initial work of the deceased Mohamed Assslam Madathilakath, who contributed to the empirical research reported in this paper.

References

1. Kent W (1978) Data, and reality: basic assumptions in data processing reconsidered. Amsterdam
2. Kent W (2012) Data and reality: a timeless perspective on perceiving and managing information. Technics publications
3. Sj_berg D (1993) Quantifying schema evolution. *Inform Softw Technol* 35(1):35–44
4. Marche S (1993) Measuring the stability of data models. *Eur J Inform Syst* 2(1):37–47
5. Stamper R (1979) Towards a semantic normal form. *Lond School Econ Polit Sci*
6. Stamper R, Ades Y (2004) Semantic normal form, and system quality. In: IEEE conference on requirements engineering
7. Stamper YA (1987) Semantic normal form, in: *Proceedings of Informatics conference. Meaning: the frontier of informatics*, Kings College, Cambridge: Aslib
8. Ho_er JA, Prescott MB, McFadden FX, Topi H (2009) *Modern database management*. Pearson, Boston
9. Elmasri R, Navathe S (2010) *Fundamentals of database systems*. Addison-Wesley Publishing Company
10. Price J (2013) *Oracle database 12c SQL*. McGraw-Hill Osborne Media
11. Ades Y, Sani NK, Nistazakis M, Poernomo I, Yamin M, Tsaramiris G (2009) Implementing SNF-compliant software: MDA and native technology. *Proceedings of ICISO2009, Beijing*
12. Poernomo I, Tsaramiris G, Zheng N (2009) Coarse-grain architectures from business requirements: an organisational semiotics approach. In: *ICISO2009*
13. Poernomo I, Tsaramiris G (2008) Prototype generation from ontology charts. In: *The fifth international conference on information technology: new generations*, vol. 17. Citeseer

14. Kent W (1983) A straightforward guide to 3rd normal forms in relational database theory. *Commun ACM* 26(2):120–125
15. Codd EF (1990) *The relational model for database management: version 2*. Addison Wesley
16. Ades Y, Umar FB, Poernomo I, Tsaramirsis G (2007) Mapping ontology charts to UML: a SNF preserving transformation. *ICOS2007*
17. Ades Y, Eid A et al (1989) *Namat user manual*. Doha, University of Qatar
18. Ades Y (1984) *Customs enterprise data model: Data retention policy*. In: Department of Industry Technology and Commerce, Canberra, Australia

Wireless Charging for Electric Vehicles: A Review



Tushar Mehndiratta and Rakesh Kumar

Abstract In terms of performance and range, electric vehicles (EVs) have lately improved. Several commercial models are now on the market, and the number of EVs on the road is constantly rising. Although the majority of electric vehicles are currently charged via electric cables, the companies like Tesla, BMW, and Mercedes Benz have started to design and manufacture electric vehicles that are charged wirelessly and that do not necessitate the use of inconvenient wires. Wireless charging further broadens the scope of dynamic charging, which includes charging when driving. When this is discovered, EVs' electric driving range will be unrestricted, and battery capability requirements will be drastically reduced. This has been emphasized and endorsed around the world, with the United Kingdom, Germany, and South Korea leading the way. This study provides a comprehensive analysis of the literature on electric vehicle wireless charging. Wireless charging's key technological components are summed up and equated, including compensation configurations, coil styling, and connectivity. To boost the charging power, a novel way to using superconductivity materials in coil designs is examined, as well as their possible effects on wireless charging. Besides that, the health and safety risks associated with wireless charging, and the rules that regulate them, are addressed. From an economic aspect, the costs of various wireless charging technologies have also been summed up and analyzed.

Keywords Wireless Charging · Electric Vehicle · Wireless Power Transfer · Coupled Magnetic Resonance · Infrastructure Allocation · Charging Station

1 Introduction

Transportation is a major cause of climate change and carbon dioxide emissions. In 2017, transportation accounted for about 60% of global oil usage, necessitating the development of a clean alternative. Electric vehicles (EVs) are a critical component

T. Mehndiratta · R. Kumar (✉)

Automobile Engineering Department, Manipal University Jaipur, Jaipur 303007, India
e-mail: rakesh.kumar@jaipur.manipal.edu

© The Author(s), under exclusive license to Springer Nature Singapore Pte Ltd. 2024
S. K. Goyal et al. (eds.), *Flexible Electronics for Electric Vehicles*, Lecture Notes
in Electrical Engineering 1065, https://doi.org/10.1007/978-981-99-4795-9_46

485

in the transformation to a green power society [1]. In terms of reliability and range, electric vehicles have come a long way recently. Several models are currently available for purchase on the car market. With the growing number of electric vehicles on the road, figuring out how to power them rapidly and easily remains a difficulty, putting a strain on electric networks. Electric cables are used to charge almost all current electric vehicles. For charging, whether at home or on the road, cables must be physically attached to the EVs [2–4].

The very first wireless device, a wireless lightning lamp, was invented by Nicola Tesla in the late 1800s. Tesla used alternating current (AC) potentials among two metal plates that were near but not touching to power the bulb. This innovation helped pave the way for new wireless charging options. Unresolved technological issues, such as low powered density and low transfer efficiency as distances rise, have hampered the development of this WPT technology [5].

Two advancements in Wireless power transfer technology have enabled wireless charging over ranges greater than 2 m using strongly linked coils after two decades. Inductive and capacitive power transfer are the two most common WPT technologies. Power can be transferred without the use of sturdy links using WPT, which consists of conductive power transfer and inductively power transfer [5, 6].

Several types of wireless charging systems for electric vehicles are static, semi-dynamic, and the dynamic systems of charging. Static charging technologies are equivalent to existing plug-in chargers, but they have several perks, such as the ability to “park and charge” [7]. The conductive charging method is replaced by an on-board acquiring device and a peripheral charging device in the asphalt. While vehicles are in motion, Dynamic WPT systems charge them. According to sources, the necessary capacity of the battery can be lowered by up to 25%, decreasing the upfront cost of a new electric vehicle. As a result, WPT appeals to EVs and has the potential to boost EV adoption [7–9].

Wireless charging system (WCS) can provide additional benefits in terms of simplicity, dependability, and accessibility when compared to plug-in charging solutions. Wireless charging systems have the drawback of being able to be used only when the automobile is stopped or in a static mode, for instance, in parking lots, car ports, or at red lights [10]. Furthermore, stationary Wireless charging system must contend with issues like electromagnetic compatibility (EMC), low power transfer, hefty constructions, shorter range, and higher efficiency. The WCS for EV’s interactive method of functioning has been investigated so as to boost the two aspects of range and battery storage capacity. This technology allows for the charging of battery memory modules when the vehicle is moving. The car has a larger range of transportation and requires less expensive battery storage volume [11, 12].

This study focuses on apparently-dynamic and dynamic wireless charging, as previously indicated. While there are a couple of effective electric vehicle systems with wireless charging in the market, like the “KAIST On-Line Electric Vehicle”, which are designed specifically for adaptable wireless charging, the bulk of apparent and dynamic Electric vehicle systems that are charged wirelessly have been converted from fixed wireless charging apparatus or are based on static advances. As a result, for some prototypes and simulation designs, distinguishing the type of wireless charging

is difficult. This section discusses some of the treatments that were created for static charging but are now frequently addressed in wireless charging research.

2 State of Art in Research

A variety of obstacles are preventing EV development and adoption. The battery is simultaneously the most vital and the most dangerous component of an electric car. Current electric vehicle batteries are expensive, have a short life duration, have a restricted driving range, and take a long time to charge as compared to ICEV batteries [13]. Additionally, batteries are still frequently large and underutilized, resulting in additional weight, volume, and inventory costs. Battery technology could help enhance battery longevity, power efficiency, and cost-effectiveness [5, 14].

The transfer of energy between an electrical outlet and an electric vehicle during wireless charging is accomplished using an electromagnetic field. There is no direct interaction between the electric vehicle and the source of power when using this charging methodology [15]. The leading disadvantage of this method is that it is less efficient than conductive charging and is more expensive. Wireless charging innovation, on the other hand, has been depicted to be approx. 85% efficient in charging points [15–18]. The main requirement for charging electric vehicles remains the distance it can transmit the charge. Inductive charging, Coupled Magnetic Resonance (CMR), laser, and radio wave are just a few of the charging innovations that have already been established for electric vehicle's batteries. [19].

To charge an electric vehicle wirelessly, the magnetic induction coupling employs the principle of electromagnetic induction. Its configuration consists of two coils. The acquiring coil sends a current to the transmitter coil, which stimulates a current in the transmitting coil, which can be used in charging of the electric vehicle. The transmitting and receiving coils must be close to one other and well linked to increase inductive coupling efficiency [20–22].

Environmental conditions have no effect on IPT systems, making them perfect in any situation and removing the need for maintenance. Due to core failures, the IPT requires ferrites for thermal assistance, requiring this to perform at lower frequency and resulting in a smaller size [23, 24]. Besides that, magnetic induction technology wirelessly transmits power from a stationary transmitter to a large number of relocating secondary receivers [25]. The magnetic coupling effect between the coils varies due to the huge air separation between the transmitter and reception coils. This leads to a loss in system stability due to the changing charging loops of the electrical characteristics. Because of the power requirements, it can hardly be a one-phase or three-phase supply. A wireless power transfer mechanism normally includes the following components: battery, transmitting coil, receiving coil, electrical grid, microcontrollers, sensors system, and related circuit. IPT modules are disseminated or endured based on the magnetic configuration of the coil [25, 26].

The current state of research is examined from a variety of angles:

- Infrastructure allocation for charging.
- Analytical and evaluation techniques for wireless charging technology for extending the driving range.
- A cost–benefit survey of wireless charging for electric vehicles versus alternative modes of transportation.

3 Charging Infrastructure Allocation

In traditional EV systems and operations research, the subject of charging infrastructure distribution or allocation is one of the most effectively addressed subjects. This also applies to electric vehicles that can be charged wirelessly [27]. The allocation problem poses a challenge in providing logistical perspectives to produce reports aimed at ideal charging framework distribution. The allocation issue is divided into two categories: microscopic allocation models and macroscopic allocation models, depending on the extent of the modeling. The microscopic allocation model, also known as micro-allocation, aims to locate the best charging infrastructure position on a vehicle's route or path. The design contemplates scenarios in which electric vehicles (EVs) with wireless charging only move along a defined route or path. The prototype is exemplified with a passenger bus (Fig. 1) [28]. More detailed modeling can be constructed on the basis of this micro-allocation. When determining critical areas for wireless charging routes or power outlets throughout the design stage of a wireless charging transport vehicle, micro-allocation techniques are very effective [29]. The model's goal is to provide a technical tool to help with mechanism findings for the wireless charging-based transport station. The macro-allocation version, often known as macro-allocation, looks at things at a higher level. The main objective of this form of modeling is to deliver scientific glimpse into the wireless charging electric vehicle as a whole, as well as to examine how the integration of EVs into larger transit networks impacts overall traffic behavior [30, 32]. Arithmetical optimization is frequently applied to solve allocation issues, whether they are macroscopic or microscopic. This methodology approach is used to either instantly find charging infrastructure sites or to provide alternative stages of the project of identifying the appropriate allotment. The use of an optimization technique to assess the user equilibrium assignment is an example of the latter circumstance [33, 34]. Despite the fact that Wireless Power Transfer has a variety of technical implementations, their conceptual setups are slightly different from the one shown in the figure, which can be used for both dynamic and quasi-dynamic wireless charging Electric vehicles. The following provides an explanation of the standard configuration's definitions and purposes:

Power Transmitting Unit The charging unit that transmits power to the vehicle via electromagnetic field or magnetic coupling from the grid is referred to as a power transmitting system. It is composed of a transmitting unit—the long track used to transmit power that is typically installed beneath the road—and a power supply unit that transfers grid power to the power track.

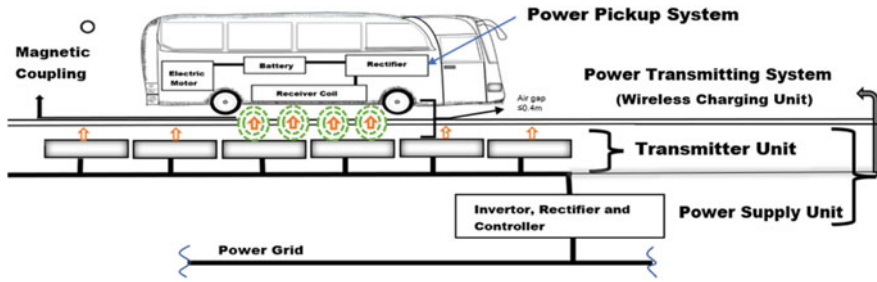


Fig. 1 Configuration of wireless power transfer in EV [20]

Table 1 The distance covered and time needed to fully charge the EV [31]

Scenario speed (km/h)	One coil receiver		Two coils receivers	
	Needed distance (km)	Needed time (h)	Needed distance (km)	Needed time (h)
10	166	40	833	20
100	400	83	2000	41

Power Pickup System The part that acquires power from the power transmitting unit is referred to as the power pickup system. It consists of a receiving coil or the pickup unit that is attached to the underside of the vehicle to obtain power and additional units like rectifiers and regulators that transfer power from the pickup to the traction motor and battery.

According to Table 1, if the lower speed is chosen and two receivers will be used, it will take 20 h to fully charge the vehicle. However, if only one receiver is used, 40 h would be required, assuming that the path is 1666 km long, has a WPT system, and that there is a 1.5 m space between each pair of transmitters. If two receivers are used, the vehicle can only be fully charged on a road that is 833 km long and has a WPT system with the same spacing between the transmitter coils that is 1.5 m. Based on these statistics, the suggested solution can assist in lowering the cost of Wireless power transfer pavement infrastructure and aid in proficiently charging the electric vehicles [31].

4 Driving Range Extension Analyses

This study makes use of a basic driving cycle, which is defined as an acceleration characteristics of a particular type of automobile offered by a government or organization that reflects driving styles. This article provides experiments in which the cost of charging infrastructure is calculated using a generalized driving cycle with the acceptance that the charging infrastructure is ideally assigned [35]. The goal of boosting is

to shorten the charging lane's overall length while increasing the life of battery. The model predicts that the amount of protection necessary for power tracks changes dramatically depending on the driving conditions of the vehicles. A car equipped with 8 KWH batter requires only 0.47% reporting under the typical driving cycle condition, however, a heavily loaded vehicle in a mountain terrain needs up to 64.5% of the coverage [35, 36]. Despite the fact that the research does not look at financial expenses, it does analyses the notion of the power track availability in aspects of the reportage of road to obtain a desired range of driving. A case study is conducted out to ascertain the preliminary expenditure of a running of wireless charging electric buses with a driving range of 400 km. The study proposes a sound cost model for investment projects. Simulations and regression are used to determine the expenditure of the power track. Standard driving cycles are first simulated with varied parameters. Regression analysis is then used to analyze the connection between the proportion of charging station coverage over the mandatory road and the status of the battery at the end of the ride using the simulated results. Several scenarios are assessed using various characteristics, including charging facility road coverage, battery capacity, halting periods, and charging power level a 500-kilowatt-hour battery is suggested in the analysis [37]. A dynamic Electric vehicle with wireless charging with a 24 kWh battery is put to the test on three different traffic road contexts, each with its own traffic flow that is intensity speed and length. According to the analysis, the energy delivered to the EV in the city is roughly 0.6 kWh/km on average, but 0.25 kWh/km on the highway [37, 38].

5 Evaluation of Battery Stand by Time

As smaller batteries can be used by the wireless charging electric vehicles, so their adoption may not guarantee the system's long-term economic efficiency [39]. According to studies, the batteries which are too tiny have an adverse impact on battery performance as a whole because they are more susceptible to more-discharging cycles, which accelerate the depletion of battery, and batteries that have short life will need to be replaced more frequently, resulting in higher overall battery costs. As a result, larger batteries could save money in the long term. This little example emphasizes how important it is to consider battery life while constructing wireless charging EV systems. The capacity of a battery diminishes dramatically with time, according to independent studies. As a result, unlike when modeling wireless charging devices in the past, studies no longer consider battery capability as a parameter. Battery capability, on the other hand, must be viewed as a dynamic metric that declines over time [39, 40].

The issue of battery drain was first investigated, but few follow-up studies have been published, owing to the fact that Incorporating battery life into the model results in a strong nonlinear property, rendering the review mathematically irreconcilable and making the development of standard costing and optimal allocation models particularly difficult. Incorporating battery life into the study also demands specialist

knowledge of different battery kinds and capabilities. This necessitates increased coordination between battery experts, activities, and systems investigators [41].

6 Conclusion

This report offers the first comprehensive overview of the current status in wireless charging EV operations and systems research. Investigations of present research efforts are crucial since technology and operations and systems-related research are still in their early stages. This surveying has a wide range of applications for researchers, industry, regulatory authorities, and policy experts. This section also goes over the notations, terms, and definitions used in the existing publications before delving deeper into the components of the wireless charging Electric vehicle. Because these ideas and classifications are not yet standardized, technology surveys at this level require precise design. It also demonstrates how variable terms and concepts are utilized in other polls.

The study's primary section reviewed existing journal articles from five distinct points of view: charging infrastructure appropriation, enhancement of the range of driving, evaluations of cost and benefits, existing parameters, and various view-points. A single article can be evaluated from multiple perspectives using the perspective-based review method. The most advanced research topic is charging allocation evaluations, which suggest methodologies for ideal charging infrastructure distribution.

Almost all of the journals studied saw dynamic wireless charging as a feasible choice for future electric vehicles. Rapid charging has the potential to reduce the cost of wireless charging infrastructure by simply increasing the charging amount per distance of wireless charging road, allowing as much power to be transmitted with a shorter recharging road. Another crucial topic is the impact of rapid charging on the economics of wireless charging electric vehicles. To summarize, wireless power transfer used to electric cars poses several risks and opportunities. Investigating these difficulties with analytical rigor will be a challenge for the future.


References

1. Global IE (2018) Energy & CO₂ status report
2. Outlook BE (2017) Country and regional insights-India. <http://www.bp.com>
3. Adnan N, Nordin SM, Rahman I, Vasant P, Noor MA (2018) An overview of electric vehicle technology: a vision towards sustainable transportation. *Intell Transp Planning: Breakthroughs Res Pract* 292–309
4. Sachan S (2018) Stochastic charging of electric vehicles in smart power distribution grids. *Sustain Cities Soc* 1(40):91–100
5. Tesla N (1914) Inventor. Apparatus for transmitting electrical energy. United States patent US 1,119,732. 1914 Dec 1
6. Kurs A, Karalis A, Moffatt R, Joannopoulos JD, Fisher P, Soljacic M (2007) Wireless power transfer via strongly coupled magnetic resonances. *Science* 317(5834):83–86
7. Chopra S, Bauer P (2011) Driving range extension of EV with on-road contactless power transfer—a case study. *IEEE Trans Industr Electron* 60(1):329–338
8. Fuller M (2016) Wireless charging in California: Range, recharge, and vehicle electrification. *Transp Res Part C: Emerg Technol* 1(67):343–356
9. Hu X, Jiang J, Cao D, Egardt B (2015) Battery health prognosis for electric vehicles using sample entropy and sparse Bayesian predictive modeling. *IEEE Trans Industr Electron* 63(4):2645–2656
10. Du J, Chen J, Song Z, Gao M, Ouyang M (2017) Design method of a power management strategy for variable battery capacities range-extended electric vehicles to improve energy efficiency and cost-effectiveness. *Energy* 15(121):32–42
11. Musavi F, Edington M, Eberle W (2012) Wireless power transfer: a survey of EV battery charging technologies. In: 2012 IEEE energy conversion congress and exposition (ECCE). IEEE, pp. 1804–1810
12. Cheon S, Kim YH, Kang SY, Lee ML, Lee JM, Zyung T (2010) Circuit-model-based analysis of a wireless energy-transfer system via coupled magnetic resonances. *IEEE Trans Industr Electron* 58(7):2906–2914
13. Liu X (2015) Qi standard wireless power transfer technology development toward spatial freedom. *IEEE Circ Syst Mag* 15(2):32–39
14. Vilathgamuwa DM, Sampath JP (2015) Wireless power transfer (WPT) for electric vehicles (EVs)—present and future trends. In: *Plug in electric vehicles in smart grids 2015*. Springer, Singapore, pp 33–60
15. Imura T, Hori Y (2011) Maximizing air gap and efficiency of magnetic resonant coupling for wireless power transfer using equivalent circuit and Neumann formula. *IEEE Trans Industr Electron* 58(10):4746–4752
16. Suh NP, Cho DH (eds) (2017) *The on-line electric vehicle: wireless electric ground transportation systems*. Springer
17. Suh NP, Cho DH (2017) Wireless power transfer for electric vehicles. In: *The on-line electric vehicle*. Springer, Cham, pp 17–34
18. Suh NP, Cho DH, Rim CT (2011) Design of on-line electric vehicle (OLEV). In: *Global product development*. Springer, Berlin, Heidelberg, pp 3–8
19. Tavakoli R, Jovicic A, Chandrappa N, Bohm R, Pantic Z (2016) Design of a dual-loop controller for in-motion wireless charging of an electric bus. In: 2016 IEEE energy conversion congress and exposition (ECCE). IEEE, pp 1–8
20. Jang YJ (2018) Survey of the operation and system study on wireless charging electric vehicle systems. *Transp Res Part C: Emerg Technol* 1(95):844–866
21. England H, Jones A (2015) Off road trials for ‘electric highways’ technology
22. Sarker MR, Pandžić H, Ortega-Vazquez MA (2014) Optimal operation and services scheduling for an electric vehicle battery swapping station. *IEEE Trans Power Syst* 30(2):901–910
23. Xiao C, Cao B, Liao C (2021) A fast construction method of resonance compensation network for electric vehicle wireless charging system. *IEEE Trans Instrum Meas* 1(70):1–9

24. Bayram IS, Ismail M (2019) A stochastic model for fast charging stations with energy storage systems. In: 2019 IEEE transportation electrification conference and expo (ITEC). IEEE, pp 1–5
25. Zhang Y, Yuan X, Duan L, Jiang L, Xu Y, Lan F, Lin Y (2021) Energy flow of a plug-in electric vehicle under the new European driving cycle. *J Energy Eng* 147(6):04021049
26. Hasan MK, Mahmud M, Habib AA, Motakabber SM, Islam S (2021) Review of electric vehicle energy storage and management system: standards, issues, and challenges. *J Energy Storage* 1(41):102940
27. Ahmad A, Alam MS, Chabaan R (2017) A comprehensive review of wireless charging technologies for electric vehicles. *IEEE Trans Transp Electrification* 4(1):38–63
28. Armghan H, Ahmad I, Ali N, Munir MF, Khan S, Armghan A (2018) Nonlinear controller analysis of fuel cell–battery–ultracapacitor-based hybrid energy storage systems in electric vehicles. *Arab J Sci Eng* 43(6):3123–3133
29. Yang B, Zhu T, Zhang X, Wang J, Shu H, Li S, He T, Yang L, Yu T (2020) Design and implementation of Battery/SMES hybrid energy storage systems used in electric vehicles: a nonlinear robust fractional-order control approach. *Energy* 15(191):116510
30. Napoli G, Polimeni A, Micari S, Andaloro L, Antonucci V (2020) Optimal allocation of electric vehicle charging stations in a highway network: part 1. Methodology and test application. *J Energy Storage* 27:101102
31. Mohamed N, Aymen F, Alqarni M, Turkey RA, Alamri B, Ali ZM, Aleem SH (2022) A new wireless charging system for electric vehicles using two receiver coils. *Ain Shams Eng J* 13(2):101569
32. Al-Obaidi A, Khani H, Farag HE, Mohamed M (2021) Bidirectional smart charging of electric vehicles considering user preferences, peer to peer energy trade, and provision of grid ancillary services. *Int J Electr Power Energy Syst* 1(124):106353
33. Grande LS, Yahyaoui I, Gómez SA (2018) Energetic, economic and environmental viability of off-grid PV-BESS for charging electric vehicles: case study of Spain. *Sustain Cities Soc* 1(37):519–529
34. Kouka K, Masmoudi A, Abdelkafi A, Krichen L (2020) Dynamic energy management of an electric vehicle charging station using photovoltaic power. *Sustain Energy, Grids Netw* 1(24):100402
35. Li Y, Han M, Yang Z, Li G (2021) Coordinating flexible demand response and renewable uncertainties for scheduling of community integrated energy systems with an electric vehicle charging station: a bi-level approach. *IEEE Trans Sustain Energy* 12(4):2321–2331
36. Jeung YC, Lee DC (2018) Voltage and current regulations of bidirectional isolated dual-active-bridge DC–DC converters based on a double-integral sliding mode control. *IEEE Trans Power Electron* 34(7):6937–6946
37. Tian MW, Talebizadehsardari P (2021) Energy cost and efficiency analysis of building resilience against power outage by shared parking station for electric vehicles and demand response program. *Energy* 15(215):119058
38. Schroeder A, Traber T (2012) The economics of fast charging infrastructure for electric vehicles. *Energy Policy* 1(43):136–144
39. Miller JM, Onar OC, Chinthavali M (2014) Primary-side power flow control of wireless power transfer for electric vehicle charging. *IEEE J Emerg Selected Topics Power Electron* 3(1):147–162
40. Zhao J, Cai T, Duan S, Feng H, Chen C, Zhang X (2016) A general design method of primary compensation network for dynamic WPT system maintaining stable transmission power. *IEEE Trans Power Electron* 31(12):8343–8358
41. Fujita T, Yasuda T, Akagi H (2017) A dynamic wireless power transfer system applicable to a stationary system. *IEEE Trans Ind Appl* 53(4):3748–3757

Optimal Reactive Power Dispatch Problem Using Novel Wild Horse-Based Optimizer



Gaurav Gangil , Sunil Kumar Goyal , Amit Saraswat ,
and Yeshpal Gupta

Abstract This study presents the new strategy for ORPD issues for modern power system problems. ORPD is most essential for maintaining a stable, secure, and economic management of electrical power system. This ORPD problem is a highly constrained, mixed integer non-linear (MINLP) problem. In order to satisfy the active and reactive power restrictions, the primary goal of the ORPD problem is to reduce active power losses in the system. Numerous optimization techniques have previously been used to address this type of problem. In this work, four optimization approaches are applied for reactive power dispatch problem for the considered system. The optimization approaches used for the ORPD problem are PSO, GA, MAPSO, and Novel algorithm named as Wild Horse Optimizer (WHO). These four algorithms are tested & evaluated for ORPD issues in IEEE-30 bus system. For load flow analysis MATPOWER software is used with MATLAB. Several comparisons have been made on account of computation time, Active and Reactive power savings, and performance comparison. The simulation results show that the proposed algorithm converges quicker than other techniques and illustrates superior performance in comparison with others and is well efficient for reactive power dispatch problems.

Keywords ORPD · Wild horse Optimizer · PSO · MAPSO · GA · MATPOWER

1 Introduction

In modern power system, active and reactive power dispatch optimization is essential for maintaining a secure, stable, and healthy operation in electrical power system [1, 2]. ORPD is also a part of OPF, which optimizes all controlled variables like Generator Voltages, Transformer Tap settings, and shunt compensators and manages a set of

G. Gangil · S. K. Goyal (✉) · A. Saraswat
Department of Electrical Engineering, Manipal University Jaipur, Rajasthan, India
e-mail: sunilkumar.goyal@jaipur.manipal.edu

Y. Gupta
Lincus Inc, Arizona, USA

operating constraints, in order to reduce transmission power losses [3]. The optimal reactive power dispatch problem is a non-linear type of problem. The transformer tap positions and shunt compensator are discrete values else are continuous values. So, the ORPD issues may be designed as a MINLP model with a collection of discrete and continuous variables [4–6].

Numerous optimization strategies have previously been used to address this type of issue. In [7, 8], author has used MAPSO (multi-agent PSO) technique for ORPD issues considering transmission power loss as the objective function. Additional comparison has been made with PSO and standard GA with the MAPSO approach. In [9], author has used two variants of GA, three variants of DE, and four variants of PSO algorithms that have been compared with the seeker optimization algorithm (SOA) and the test system considered are standard 57 bus and 118 bus systems. In [10], author has used a differential evolution algorithm for solving the constrained ORPD problem considering transmission power losses, voltage stability index, and voltage deviation as the objective for resolving the SO-Optimization of the ORPD problem. In [11, 12], author has used the harmony search algorithm & EMA for resolving the constrained ORPD problem considering power losses, and voltage deviation as the objective, for standard 30 and 57 bus as the system for resolving the optimization of the ORPD problem. In [13] author has used the PCA-RCGA algorithm for power loss minimization in ORPD problems considering other optimization approaches [14–18].

2 Problem Formulation

In (ORPD) Optimal Reactive power dispatch, the objective of the problem is to reduce the transmission power losses of the system. The mathematical formula for estimating active power losses is shown in Eq. 1.

$$P_{loss} = f(x_1, x_2) = \sum_{k \in N_E} g_k (V_i^2 + V_j^2 - 2V_i V_j \cos \theta_{ij}) \quad (1)$$

Here $\times 1$ represents the controlled variable vector $[V_G, T_K, Q_C]$ and $\times 2$ represents the dependent variable vector $[V_L, Q_G, F_L, P_R]$, V_G represents the generator voltage (continuous variable), T_K represents the Transformer tap position (Integer), Q_C represents the shunt compensator values (Integer), V_L is the load bus voltage, Q_G represents the reactive power outputs of the generators, F_L represents the flow limits of the transmission line, and P_{Rbus} represents the active power limits of the reference bus or slack bus.

$$P_{gi} - P_{di} = \sum_{j=1}^{N_b} V_i V_j (G_{ij} \cos \theta_{ij} + B_{ij} \sin \theta_{ij}) \quad (2)$$

$$Q_{gi} - Q_{di} = \sum_{j=1}^{N_b} V_i V_j (G_{ij} \sin \theta_{ij} - B_{ij} \cos \theta_{ij}) \quad (3)$$

Here power flow equations are considered as equality constraints as shown in (Eqs. 2–3) and other real and reactive power limits, transformer taps limits and bus voltage limits, flow limits of transmission line are considered as inequality constraints. So, the optimal reactive power dispatch optimization satisfies the equality and inequality constraints and offers optimum solutions. The inequality constraints are shown in (Eqs. 4–8). The voltage magnitude of each bus is

$$V_i^{\min} \leq V_i \leq V_i^{\max}, \quad i \in N_B \quad (4)$$

The Reactive power generation limit is

$$Q_{gi}^{\min} \leq Q_{gi} \leq Q_{gi}^{\max}, \quad i \in N_g \quad (5)$$

The Reactive power output of the compensator is

$$Q_{ci}^{\min} \leq Q_{ci} \leq Q_{ci}^{\max}, \quad i \in N_c \quad (6)$$

The Transformer tap-setting constraint is

$$T_k^{\min} \leq T_k \leq T_k^{\max}, \quad i \in N_T \quad (7)$$

The power flow limit of each transmission line

$$S_i \leq S_i^{\max} \quad (8)$$

where i is bus number & k is the branch number and N_B is the number of buses, and N_g is the number of generators, and N_c is the number of capacitors.

$$f = P_{loss} + \lambda_V \sum_{N_V^{\lim}} \Delta V_L^2 + \lambda_Q \sum_{N_Q^{\lim}} \Delta Q_G^2 \quad (9)$$

3 Wild Horse Optimizer

In the last decades, most of the optimization algorithms are based on bird, human, plant, and animal behavior. The wild horse optimizer algorithm was originally proposed by Naruei in the year 2021 [15]. In this article, a novel algorithm known as

Wild Horse Optimizer is based on the social behavior of horses. Wild horses generally live in the form of clusters which comprises stallion and many mares and foals. Horses possess several behaviors like grazing and mating. The main motivation of such an algorithm is the gracious behavior of the horses. Wild horses comprise stable family groups which possess a stallion having one or more mares and their children. In this study, this algorithm utilizes grouping behavior, graze, mate, dominate, and leader quality to improve this algorithm. This algorithm was evaluated on various test functions and compared with popular algorithms [15].

The first step of this algorithm is to initialize the pop and then split the population into several groups. Firstly, the population is divided into several groups. In this algorithm, stallion is the leader of all horses and is present in all groups. Initially, the leader is chosen at random, and finally at a later stage, it is evaluated based on the fitness function.

$$\vec{X}_{i,G}^j = 2Z \cos(2\pi RZ) \times (\text{Stallion}^j - X_{i,G}^j) + \text{Stallion}^j \tag{10}$$

Here, $\vec{X}_{i,G}^j$ represent the position of foal or mare, Stallion^j represents the position of leader. Z represent the coefficient evaluated by Eq. 10. And R used for random number lying between $[-2, 2]$, where P is an integer comprised of 0 and 1, R_1 , R_2 and R_3 are random integers that lie in the range of $[0,1]$. TDR begins with value 1 and scales back the algorithm’s execution. and at last, the value is 0.

$$TDR = 1 - \text{iter}x(1/\text{max iter}) \tag{11}$$

In this process, the mating concept is discussed which comprises separating the foal from groups and the mating process begins. Foals dispersed from the pack and joined another one. When the two foals of male and female and no familiar relation between them so they can mate. This loop is repeated for all groups. Figure 1 shows the mating behavior of foals and the reproduction of child.

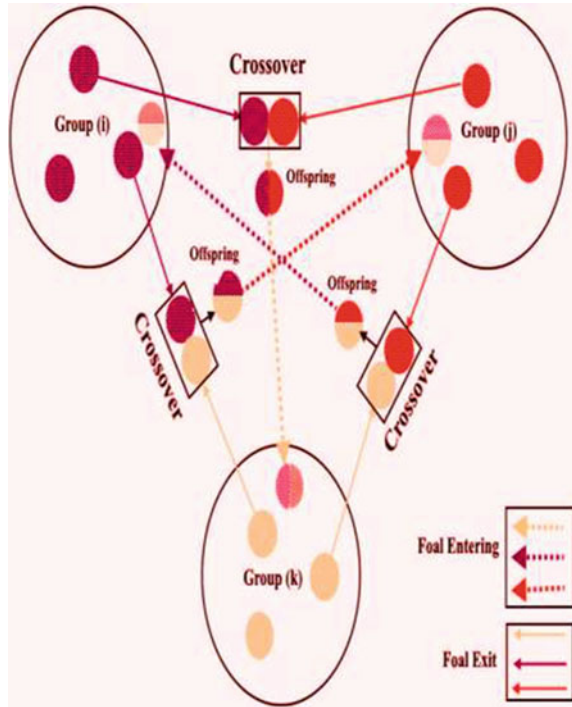
$$\text{Stal}_{Gi} = \left\{ \begin{array}{l} 2Z \cos(2\pi RZ)(WH - \text{Stal}_{Gi}) + WH \text{ if } R_3 > 0.5 \\ 2Z \cos(2\pi RZ)(WH - \text{Stal}_{Gi}) - WH \text{ if } R_3 < 0.5 \end{array} \right\} \tag{12}$$

$$\text{Stal}_{Gi} = \left\{ \begin{array}{l} X_{G,i} \text{ if } \cos t(X_{G,i}) < \cos t(\text{Stal}_{Gi}) \\ \text{Stal}_{Gi} \text{ if } \cos t(X_{G,i}) > \cos t(\text{Stal}_{Gi}) \end{array} \right\} \tag{13}$$

The next step will involve systems for choosing and exchanging leaders. Initially, leader is selected at random, and later on based on fitness function change the position of the leader so that an optimal solution is obtained. Figure 2 displays the proposed algorithm’s flowchart.

$$P = \vec{R}_1 < TDR; \text{IDX} = (P == 0); Z = R_2 o \text{IDX} + \vec{R}_3 o(\sim \text{IDX}), \tag{14}$$

Fig. 1 Working concept of wild horse optimizer [15]



4 Results and Discussion

To assess the viability of the suggested optimization strategy named wild horse optimizer (WHO), All optimization approaches are designed in MATLAB version 9.1, and for load flow analysis and MATPOWER version 7.1 are used. All numerical simulation is done on Windows 10, 4 GB ROM Laptop. Figure 3 displays the IEEE-30 bus system’s one line diagram. This system consists of 41 transmission lines, 6 PV Buses (PV buses including 01 slack bus), 30 Busbars, and 24 load buses (PQ buses). Four branches are linked with transformer tap positions and their position are (6–9), (6–10), (4–12), and (27–28). The reactive power installation is done at three bus positions 3, 10, and 24.

The generator bus position is 2, 5, 8, 11, and 13, and one slack bus is on Bus 01 position. The upper and lower voltage limits of the PV buses, Transformer settings, and Shunt compensator limits are shown [1]. The shunt compensator and transformer tap ratios are discrete variables. The power system data is shown [7]. The system active and reactive load demand at base case is 2.834 per unit and 1.262 per unit. The generator bus voltages and transformer tap at the base case are taken as 1.0. The total power generations which include real power generation are 2.893 per unit and reactive power generations are 0.980 per unit and power loss at base case is $P_{loss} =$

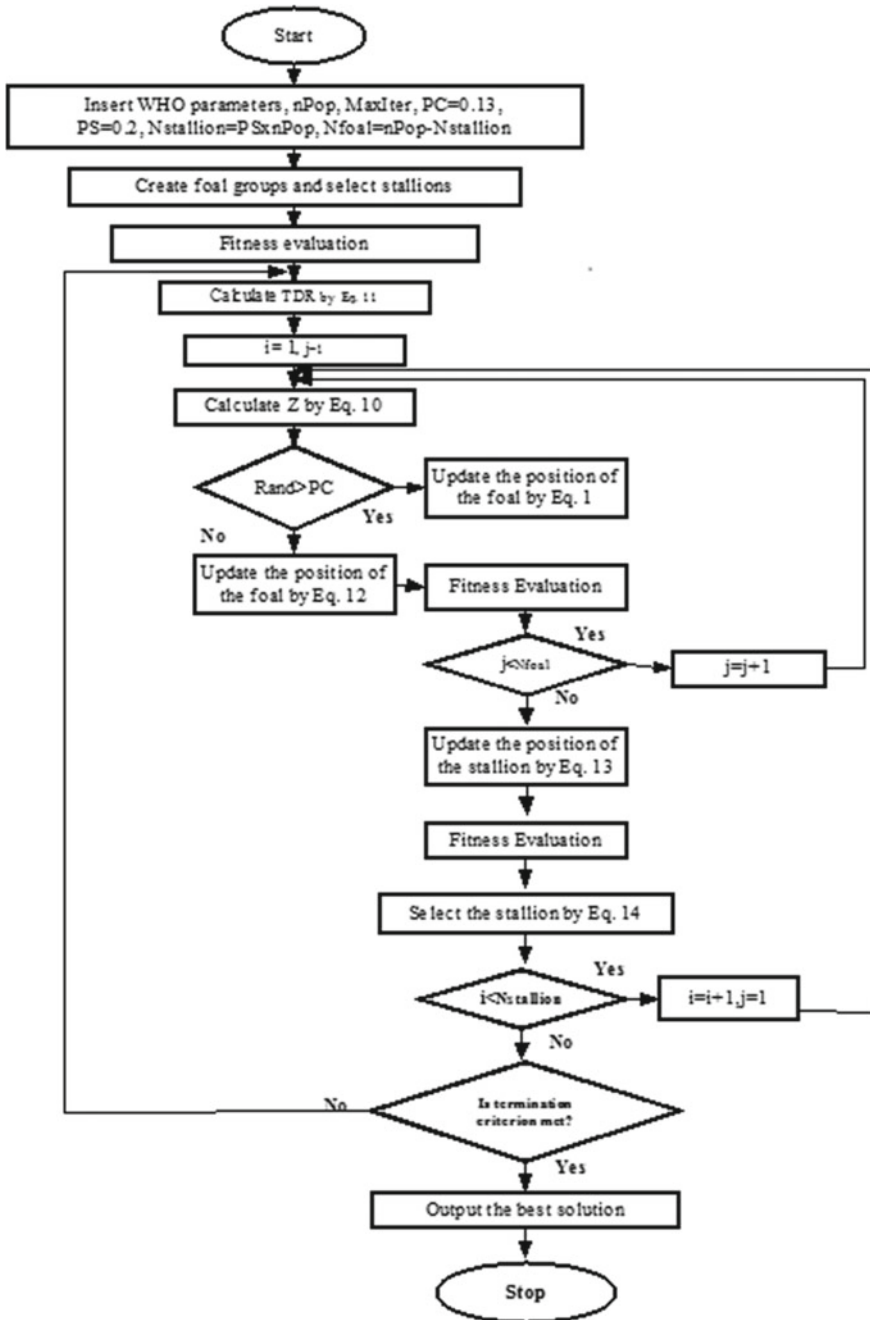


Fig. 2 Flowchart of novel wild horse optimizer for ORPD problem

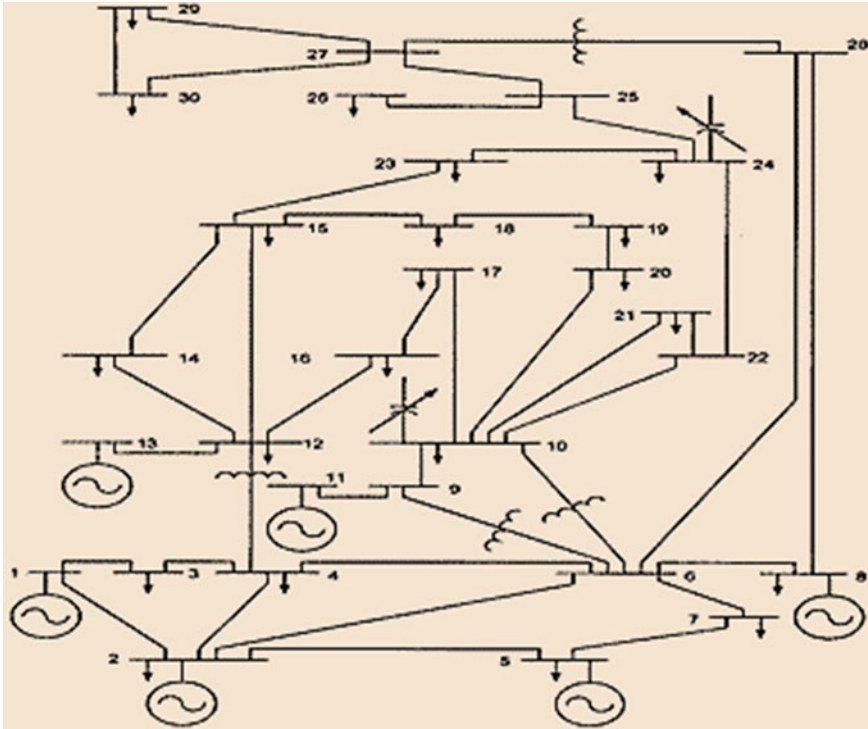


Fig. 3 one line diagram of IEEE-30 bus system

0.059 879 per unit, $Q_{loss} = -0.064 327$ per unit. Table 1 shows the parameters used for all optimization algorithms.

Table 3 shows the power generations and power losses by various optimization techniques. In this table, considering the active power generation by all optimization

Table 1 Optimization algorithm parameter comparison

S. no.	Algorithm	Parameter	Value
1	PSO	Inertial weight W Correlational Coefficient C_1, C_2	Linearly decrease from 0.9 to 0.4 $C_1=2.05, C_2=2.05$
2	GA	Selection Crossover Mutation	$P_c = 0.95$ $P_m = 0.05$
3	MAPSO	L_{size} Same as PSO	$L_{size} \times L_{size} = N_{pop}$
4	WHO	Crossover percent Stallion percent Crossover	$P_c = 0.13$ $P_s = 0.2$

Table 2 Optimized values of decision variables after Optimization by four Approaches

Decision variables	Basecase	SPSO	SGA	MAPSO	WHO
V1	1.06	1.0740	1.0679	1.0731	1.0737
V2	1.045	1.0648	1.0579	1.0640	1.0646
V5	1.01	1.0427	1.0355	1.0417	1.0424
V8	1.01	1.0429	1.0350	1.0422	1.0427
V11	1.082	1.0567	1.0748	1.0505	1.0541
V13	1.071	1.0682	1.0626	1.0675	1.0692
T 6–9	0.978	1.0142	1.0022	0.9979	0.9953
T 6–10	0.969	1.0050	0.9823	1.0322	1.0405
T 4–12	0.932	0.9961	0.9853	0.9950	0.9987
T 28–27	0.968	0.9703	0.9701	0.9675	0.9688
QC3	0	−8.0067	3.5434	−6.2043	−7.9587
QC10	0	25.3275	13.5405	28.6386	28.6144
QC24	0	10.7112	13.7303	10.6058	10.6172
Active power losses	5.4852	4.8985	4.9464	4.8997	4.8980

Table 3 Optimal transmission loss comparison by different approaches

Algorithms	Active power generation	Reactive power generation	Active power loss	Reactive power loss	Percentage power saving (%)
SPSO	288.2985	80.7447	4.8985	−45.4553	10.69605
SGA	288.3464	78.4664	4.9464	−47.7336	9.822795
MAPSO	288.2997	75.2981	4.8997	−50.9019	10.70332
WHO	288.2985	77.3495	4.8980	−48.8505	10.69545

approaches are nearly the same. But the reactive power generation slightly differ depending on optimization approaches. The percentage of power saving by all algorithms is shown in the last column of Table 3. The percentage of power saving varies by individual optimization approaches. Table 2 shows the control variables of all four optimization approaches including the proposed approach named as wild horse optimizer (WHO) in modified IEEE-30 bus system for reactive power issues while considering the equality and non-equality constraints.

A total of 30 simulation runs are used in this work, to compare the outcomes of all four algorithms. Table 4 shows the statistical comparative analysis of all four algorithms implemented in MATLAB. After learning from the findings that the WHO strategy outperforms all other optimization approaches. The Voltage profile by all four algorithms for all 30 buses is shown in Fig. 4.

Table 4 Comparing the outcomes of the 30 bus system simulations

Algorithms	Best	Worst	Average	Std. dev
SPSO	4.8985	4.9080	4.9012	0.00228
SGA	4.9464	5.3248	5.111	0.09784
MAPSO	4.8997	4.9074	4.9027	0.00239
WHO	4.8980	5.0137	4.9119	0.02509

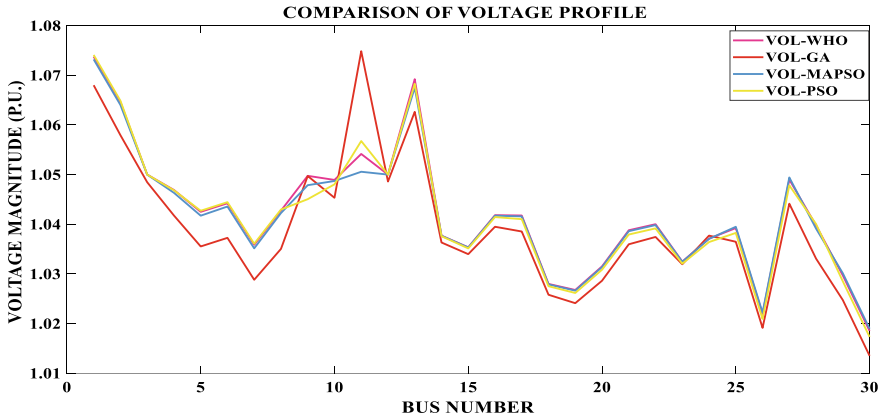


Fig. 4 Voltage Profile comparison of four approaches in IEEE-30 bus system

5 Conclusion

In this study, various optimization approaches are presented for resolving the ORPD problem. This study presents a wild horse optimizer technique used for solving the ORPD problem in 30 bus systems considering the total transmission loss as the objective. The proposed method benefits from the gracing and mating behavior of wild horses. This algorithm has an additional advantage that it is easy to understand and implement for various optimization problems. An additional optimization approaches used are PSO, GA, and multi-agent particle swarm optimization (MAPSO) is used for comparative analysis and proved that the proposed algorithm shows quicker and more effective results. The computation time of the proposed algorithm is lower than other optimization approaches to be used in the literature. The proposed algorithm has an effective and efficient algorithmic structure to get the best optimum results. On seeing the results of the test system, it indicates that the proposed algorithm is superior to other optimization approaches and can be applied to further engineering optimization issues.

References

1. Das T, Roy R, Mandal KK (2020) Optimal reactive power dispatch based on modified JAYA algorithm. In: 2020 international conference on computer, electrical & communication engineering (ICCECE), pp 1–7
2. Daqaq F, Ellaia R, Ouassaid M (2020) A constrained chaotic flower pollination algorithm for solving ORPD problem. In: 2020 international symposium on advanced electrical and communication technologies (ISAECT), pp 1–6
3. Gafar MG, El-Sehiemy RA, Hasanien HM (2019) A novel hybrid fuzzy-JAYA optimization algorithm for efficient ORPD solution. *IEEE Access* 7:182078–182088
4. Das T, Roy R (2018) Optimal reactive power dispatch using JAYA algorithm. *Emerg Trends Electron Dev Comput Tech (EDCT)* 2018:1–6
5. Jithendranath J, Babu BY (2014) Solving ORPD problem with modal analysis by differential evolution. In: 2014 IEEE 2nd international conference on electrical energy systems (ICEES), pp 51–55
6. Barakat AF, El-Sehiemy RA, Elsayd MI, Osman E (2019) An enhanced Jaya optimization algorithm (EJOA) for solving multi-objective ORPD problem. In: 2019 international conference on innovative trends in computer engineering (ITCE), pp 479–484
7. Dai C, Chen W, Zhu Y, Zhang X (2009) Reactive power dispatch considering voltage stability with seeker optimization algorithm. *Electr Power Syst Res* 79(10):1462–1471
8. Dai C, Chen W, Zhu Y, Zhang X (2009) Seeker optimization algorithm for optimal reactive power dispatch. *IEEE Trans Power Syst* 24(3):1218–1231
9. El Ela AAA, Abido MA, Spea SR (2011) Differential evolution algorithm for optimal reactive power dispatch. *Electr Power Syst Res* 81(2):458–464
10. Khazali AH, Kalantar M (2011) Optimal reactive power dispatch based on harmony search algorithm. *Int J Electr Power Energy Syst* 33(3):684–692
11. Saraswat A, Saini A (2014) Principal component analysis-based real coded genetic algorithm for optimal reactive power dispatch. *Int J Power Energy Convers* 5(2):135–154
12. Rajan A, Malakar T (2016) Exchange market algorithm based optimum reactive power dispatch. *Appl Soft Comput J* 43:320–336
13. Wei Y, Zhou Y, Luo Q, Deng W (2021) Optimal reactive power dispatch using an improved slime mould algorithm. *Energy Rep* 7:8742–8759
14. Shaheen MAM, Hasanien HM, Alkhuayli A (2021) A novel hybrid GWO-PSO optimization technique for optimal reactive power dispatch problem solution. *Ain Shams Eng J* 12(1):621–630
15. Naruei I, Kaynia F (2021) Wild horse optimizer: a new metaheuristic algorithm for solving engineering optimization problems. *Eng Comput* 1–32
16. Goyal SK, Gangil G, Saraswat A (2022) Simulation of solar-grid charging of electric vehicle using PI controller. In: 2022 2nd international conference on innovative practices in technology and management (ICIPTM), pp 247–252
17. Gangil G, Goyal SK, Srivastava M (2020) Optimal placement of DG for power losses minimization in radial distribution system using backward forward sweep algorithm. In: 2020 IEEE international conference on advances and developments in electrical and electronics engineering (ICADEE), pp 1–6
18. Gangil G, Goyal SK, Saraswat A, Soni A, Srivastava M (2021) Power quality improvement using DSTATCOM in distribution network. In: 2021 international conference on control, automation, power and signal processing (CAPS), pp 1–6

An Insight into Algorithms and Self Repair Mechanism for Embedded Memories Testing



Vinita Mathur , Aditya Kumar Pundir , Sudhanshu Singh, and Sanjay Kumar Singh 

Abstract This paper covers the critical review of algorithms related to Memory built-in self-test and repair based on key parameters including area overhead for spare register, memory row/column size, local bits, main memory sizes, testing time penalties, and repair rate. This paper reviews the concept of memories testing BIST and built-in self-memory repair BISR using different RA algorithms in brief. In MBIST March C, March C- and March LR are simulated for different Memory sizes. March LR shows better fault coverage and requires less testing time. For MBISR different repair redundancy algorithms are simulated for various cases of Spare row/column size. CRESTA shows the optimal repair rate as compared to other repair algorithms. In this paper, we have simulated the co-design of MBIST and MBISR March C, March C-, and March LR as base testing algorithms for MBIST and MBISR ESP with a spare row/column of one row and one column with a memory size of $6*6*1$. With this implementation, we found that March LR requires less testing time and co-designing of hardware reduces the hardware penalty.

Keywords Built-in self testing · Built-in self repair · Built-in redundancy analysis · March algorithms · MATLAB · Xilinx ISE 9.2i

1 Introduction

Memories are an integral part of IC technology as they are used to store data [1]. Embedded memories are the integrated on-chip memory that provides high performance, high speed with high bus width capacity. Embedded memories are the main part of the VLSI system with an add-on advantage it eliminates inter-chip communication [2]. There are two types of embedded memories SRAM and DRAM. Dynamic

V. Mathur (✉) · S. Singh · S. K. Singh
Amity University Rajasthan, Jaipur, India
e-mail: vinita.mathurdec@gmail.com

A. K. Pundir
Arya College of Engineering & IT, Jaipur, India

memories are low cost and highly suitable for high capacity memories requirement, but they are slower as compared to static memories. Static memories are faster in processing and require less power, but the complex structure of memory makes them highly expensive.

An advancement in integrated circuit designing led to increased memory capacity and memory density. Hence, memory density increases its fault occurrence possibility also increases [1–3]. These faults are classified into two parts: Static and dynamic faults [7–10, 13, 20].

For these faults diagnosis, memory testing is required. Memory testing is done through the classical method and March test method. Classical requires more test time whereas the March test algorithm is very convenient and efficient for diagnosing the memories, and it is typically used for less test time [1, 2]. March-based tests are MATS, MATS+, Marching 1/0, March C, March C-, March LR, March SS, March Y, March AB, March A, March B, and soon. These March tests are conducted with ATPG (Automatic test pattern generator), but this approach requires a long testing time and the cost of hardware is very high. Hence, inbuilt testing circuits are designed which contain the hardware and software modules. These modules are known as MBIST (Memory built-in self-test) and MBISR [12–20]. MBIST has only one limitation regarding area but it can be compromised in place of other benefits [4–6]. MBISR (Memory Build in self Repair) [10, 11] is the repair module that repairs faulty rows and columns. This module is designed in two-phase. In the first phase, fault diagnosis is done through MBIST [1, 11], Controller and in the second phase, repair signature is determined to repair the faults in memories. The specific method is there which are used in MBISR [4, 10, 12–20] with MBIST and MBIRA for memory repair and testing.

This paper is categorized into 8 sections as follows. Section 2 describes the types of memory faults Models that occur in memories. Section 3 describes how to diagnose the fault with different fault testing strategies. Section 4 describes the Conventional designing and testing of MBIST. Section 5 describes the Memory build-in self-repair algorithms. Section 6 describes the Conventional designing and testing of MBISR. Section 7 describes the proposed Co-Design of MBIST and MBISR. Finally, Sect. 8 concludes the paper with a result analysis.

2 Memory Fault Models

Memory fault models are classified as single cell faults and two-cell faults (coupling cell faults). To define these faults, faults primitives are used. For a single cell, the fault primitive symbol is <P/F/R> and for two cells, the fault primitive symbol is <PA;PB/F/R>. Here, P is the faulty cell, PA is the aggressor cell; PB is the victim cell [9, 16]. There are various types of memory faults which are described below

- **Stuck at Fault (SAF):** These faults arise when the memory cell is stuck at a value of 0 or 1 and never changes its value again is known as stuck at zero/stuck at one fault, i.e., <SA-0/SA-1> [1, 2].
- **Transition Fault (TF):** These faults occur when the memory cell is unable to transit its memory cell value from 0 to 1 or 1 to 0, i.e., <1/0> or <0/1> .
- **Coupling Fault (CF):** Transition in memory cell i cause an unwanted change in memory cell j, i.e., <1/0/1>

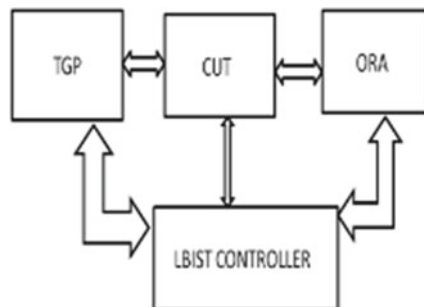
3 Fault Diagnosis Strategies

There are two methods used for fault diagnosis LBIST (Logical build self-test) and MBIST (Memory build-in self-test).

LBIST: Fig. 1 shows traditional LBIST using SOBIST (Structure offline BIST technique). Here, TGP produces a pattern for CUT, and this pattern is given to the output response analyzer (ORA) which compressed the pattern into the signature. LBIST controller provides the clock, timing, and scan signal for controlling the system [4, 6].

MBIST: It is the most effective method for memory testing. MBIST is widely used for fault diagnosis in memories. Figure 2 shows the MBIST structure for the Static RAM array which is the main memory on which testing is conducted. The address decoder unit selected the address through multiplex which is provided by the SRAM. The multiplexer is used to select data which is compared to SRAM and test pattern storage in MBIST mode. The Checker unit compares the data with the anticipated output and shows the result P/F (pass/fail) [5, 10, 20].

Fig. 1 LBSIT architecture



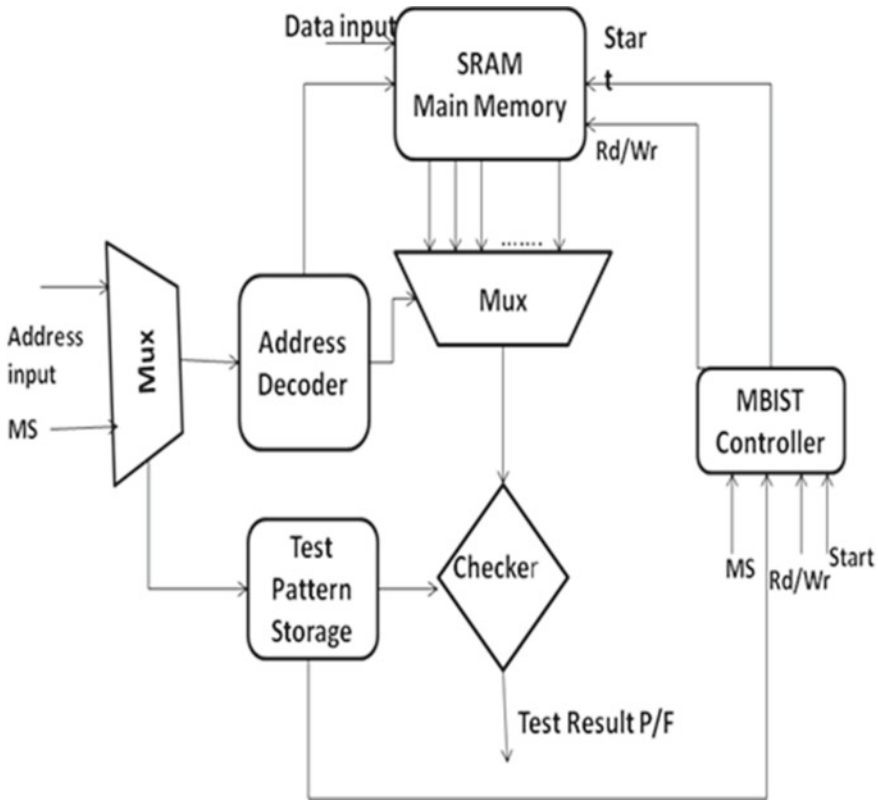


Fig. 2 MBIST architecture

4 Conventional Designing and Testing of MBIST

As shown in Fig. 3, we are having a Static RAM as MUT (Memory under Test) for testing different fault locations. This MUT contains SAF, SOF, AF, TF, and coupling fault at the edges. Table 1 shows the Trade-off performance of memories using different March test algorithms with fault coverage at different test lengths on MATLAB. Table 2 shows the trade-off performance of different Memories based on testing time with different march test algorithms on Xilinx.

After doing the critical review of [9, 13, 16, 20] cases, we have analyzed the trade-off performances based on the testing time of memory under test for fault detection with 6*6*1 memory Size as shown in Figs. 4 and 5.

These analyses are conducted on MATLAB and Xilinx ISE Suite Software. Here, N defines the address length.

A comparison chart between these March tests is shown in Figs. 4 and 5. March LR shows the optimized testing time and covers the wide number of faults as compared to March C and March C-.

Fig. 3 6*6*1 memory matrix

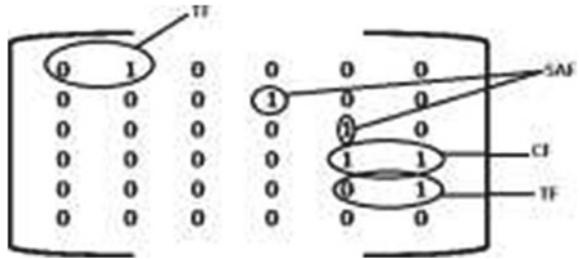


Table 1 Trade-off performances of memories based on testing time

S. no.	Algorithms	Memory size/address length	Tool used	Testing time	Fault detected
1	MARCH C	6*6*1(10N)	MATLAB	1.232s	SAF, SOF, AF, TF
2	MARCH C-	6*6*1(10N)	MATLAB	0.058s	SAF, SOF, AF, TF, and CF
3	MARCH LR	6*6*1(14N)	MATLAB	0.053s	SAF, SOF, AF, TF, CFid, CFin

Table 2 Trade-off Performances of Memories based on testing time

S. no.	Algorithms	Memory size	Language/tools/ device used	Testing time in Xilinx(ns)	Fault detected
1	MARCH C	128*8*1	VHDL/Xilinx/ Virtex 5	2.386	SAF, SOF, AF, TF
		256*8*1		3.928	
		1024*8*1		5.932	
2	MARCH C-	128*8*1		2.823	SAF, SOF, AF, TF, and CF
		256*8*1		4.225	
		1024*8*1		5.974	
3	MARCH LR	128*8*1	3.122	SAF, SOF, AF, TF, CFid, CFin	
		256*8*1	4.672		
		1024*8*1	6.027		

Fig. 4 Comparison using MATLAB

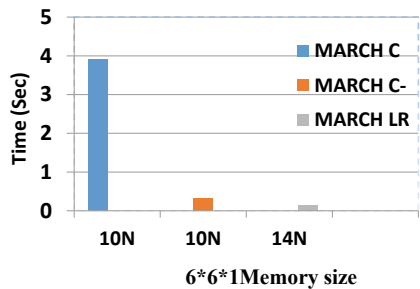
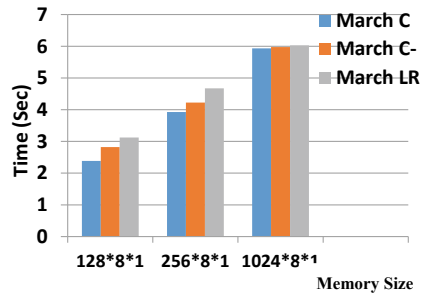


Fig. 5 Comparison using XILINX



5 Memory Build in Self Repair

Figure 6 shows the structure of MBISR in which the MBIST controller detects the faults in the main memory during a read operation. The multiplexer is used for data out which will provide only the correct data that it receives from the spare memory location. MBISR works on RA (Redundancy Algorithms) which are LRM, ESP, and CRESTA.

LRM: This algorithm uses a local bit map. It allocates the redundancy in parallel with MBIST controller operation with the help of a local bit map. Selecting the faulty column/row consumes more time because it takes more than one line for repair. Repair rate is also limited by the bitmap size [14, 18–20].

ESP: It is improved and simple to implement the algorithm, as the fault collection starts with marking of row/column pivot. When the row/column pivot is marked repair solution is provided. It consumes less area and tracing of row/column both are conducted. But for large fault analysis, requires more time. It also not works for predefined fault dictionaries [10, 18–20].

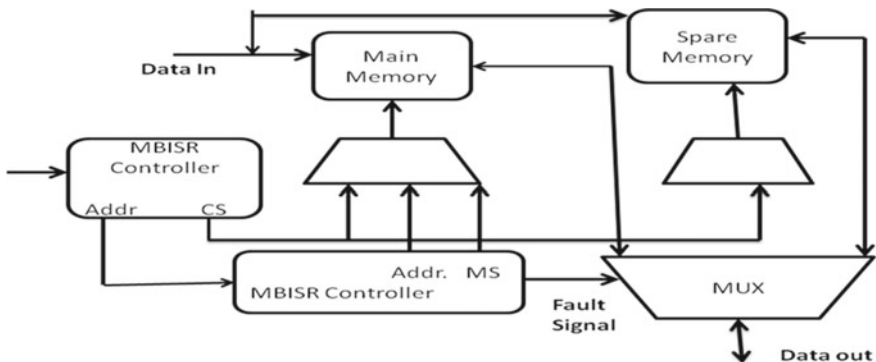


Fig. 6 Block diagram of memory build in self repair

CRESTA: It is a Comprehensive real-time exhaustive search test and analysis with optimal repair rate. It provides a guaranteed repair solution for the repair memory [13, 15].

6 Conventional Designing and Testing MBISR

A comparative study of selected papers is reviewed in this section based on methodology, implementation, and gaps described in Table 3. Table 4 describes the testing time required by the BIST to test the memory with its Repair rate, Area overhead that how much area is occupied by the BISR and BIST modules. It shows that the [13] acquire Zero penalty delay compared to others, and [14] have testing time 1.3 faster. The repair rate of [18] and [13] is higher than others.

After doing the critical review of [13] and [16] cases, we have analyzed the performance criteria of MBIRA based on area overhead, spare rows/columns, and repair rate with the various number of faults. Comparing these parameters, we have taken these equations (1)–(9) [13]. It shows that CRESTA provides better fault coverage and area requirement than the other algorithms. Table 5 shows the case for the spare rows/columns.

Table 3 Methodology and implementation of BIST and BIRA

Author’s name	Methodology	Implementation	GAP
Wooheon Kang et al. [13]	(CRESTA) Exhaustive search using RA for BIRA And MARCH C-Algorithm for BIST	RTL Verilog HDL and synthesis it on gate level by Synopsys design vision with 90 nm library	They have not explored 3D spare architecture
Wooheon Kang et al. [16]	(a) BIST and wrapper Module for multiple memories. MARCH C BIRA using RA algorithm with	RTL Verilog HDL and synthesis it on gate level by Synopsys design vision with 90 nm library	They serially repair the memory, which slows down the repair time
Chih-Sheng and Hou et al. [14]	RCB (row/column/bit) with Local repair most (LRM) RA analysis	90 nm standard cell library	This process Algorithm is time-consuming

Table 4 Testing time, repair rate, and area overhead

Author’s name	Testing time	Repair rate	Area overhead
Wooheon Kang et al. [13]	Delay:2.5 ns	Guarantees an optimal repair	Reduce up to 33.9%
Wooheon Kang et al. [16]	1.3 times faster	Optimal	Reduce up to 49.6%
Chih-Sheng Hou et al. [14]	Delay:0.08 ns	0.48% to 11.95%	0.44%

Table 5 Cases for Spare Rows/Columns

Cases	Memory size	Software used	Spare rows (SR)	Spare columns (Sc)
Case I	6 × 6x1	MATLAB	4	4
Case II	6 × 6x1	MATLAB	5	5
Case III	6 × 6x1	MATLAB	6	6

The equations taken for analysis are as follows (1)–(9) [13]

$$\mathbf{ASR} = [(\log_2 MM + 1) \times SR + (\log_2 MN + 1) \times Sc] \quad (1)$$

$$\begin{aligned} \mathbf{ALRM} = Mm \times Mn + [(\log_2 MM + 1) + (\log_2(Mn + 1))] \\ \times Mm + [(\log_2(MN + 1) \\ + (\log_2(Mm + 1)))] \times Mn + \mathbf{ASR} \end{aligned} \quad (2)$$

$$\mathbf{AESP} = (SR + Sc) \times (\log_2 MM + 1 + \log_2 MN + 1) + \mathbf{ASR} \quad (3)$$

$$\mathbf{ACRESTA} = \mathbf{ASR} \times (SR + Sc)! / (SR! \times Sc!) \quad (4)$$

$$\begin{aligned} \mathbf{AISF} = 2 SR Sc \times (\log_2 MM + \log_2 MN + 1) \\ + 2 SR Sc \times (\log_2 SR + \log_2 Sc) + \mathbf{ASR} \end{aligned} \quad (5)$$

$$\begin{aligned} \mathbf{ASFCC} = (SR + Sc) \times (\log_2 MM + \log_2 MN + 1) \\ + (SR + Sc) \times (\log_2 SR + \log_2 Sc) \\ + (SR \times (Sc - 1) + Sc \times (SR - 1)) \\ \times (\log_2(\max(MM, MN)) + \log_2(SR + Sc) + 2) + \mathbf{ASR} \end{aligned} \quad (6)$$

$$\begin{aligned} \mathbf{ABRANCH} = (SR + Sc) \times (\log_2 MM + \log_2 MN + 3) \\ + (SR + Sc) \times (\log_2 SR + \log_2 Sc) \\ + (SR \times (Sc - 1) + Sc \times (SR - 1)) \\ \times (\log_2(\max(MM, MN)) + \log_2(SR + Sc) + 2) \end{aligned} \quad (7)$$

$$\mathbf{AWhooneon} = 2SRSc \times (\log_2 SR(Sc + 1) + \log_2 Sc(SR + 1)) + \mathbf{ASSR} \quad (8)$$

where,

$$\mathbf{ASSR} = SR \times \log_2 SR(Sc + 1) + Sc \times \log_2 Sc(SR + 1) \quad (9)$$

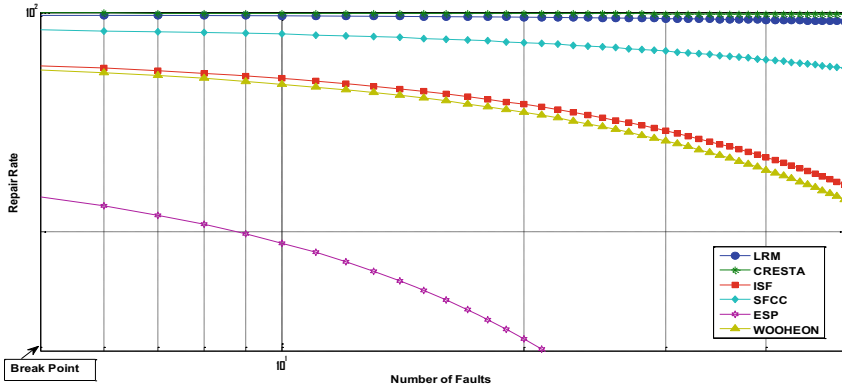


Fig. 7 Case I repair rate and numbers of fault

$$Mm = (SR \times (Sc + 1) + SR)Mn = (Sc \times (SR + 1) + Sc) \tag{10}$$

Here, ASR = Area overhead for spare register, MM = Memory row size, MN= Memory column size, Mm = Memory of row local bit, Mn = Memory of column local bit, SR = Spare row, Sc = Spare column, ALRM = Area of Local Repair Most, AESP = Area of Essential Spare Pivoting, ACRESTA = Area of CRESTA, AISF = Area of ISF, ASFCC = Area of SFCC, ABRANCH= Area of Branch, AWhooneon = Area of Wooheon, ASSR= Area of small_spare_register.

Case I: $S_R = 04$ and $S_c = 04$, Fig. 7 showcase 1 here we have used four spare columns, and the results show the better repair rate Range of repair rate is 10^3 .

Case II: $S_R = 05$ and $S_c = 05$, Fig. 8 shows case II here we have used five spare columns, and the results show a better repair rate than the four spare rows. The range of repair rates is 10^3 .

Case III: $S_R = 06$ and $S_c = 06$, Fig. 9 shows case III here we have used six spare columns and the results show a better repair rate than the four/five spare rows. The range of repair rates is 10^3 .

7 Proposed Co-design of MBIST and MBISR

Co-design of memory testing and repair is shown in Fig. 10. Here, the main memory (SRAM) is tested using the MBIST controller and if any fault arises then the faulty row/column address is sent to the MBISR controller. This controller repairs the faulty row/column and provides fault-free memory. But if the fault is not repairable then it sends to unreparable memory.

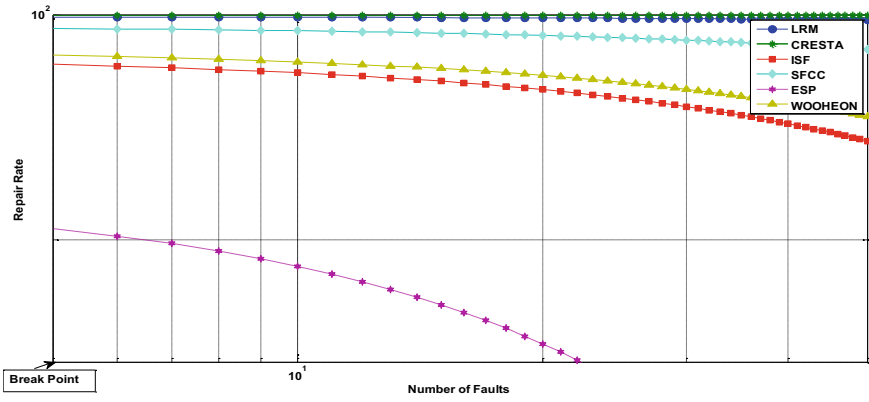


Fig. 8 Case II repair rate and numbers of faults

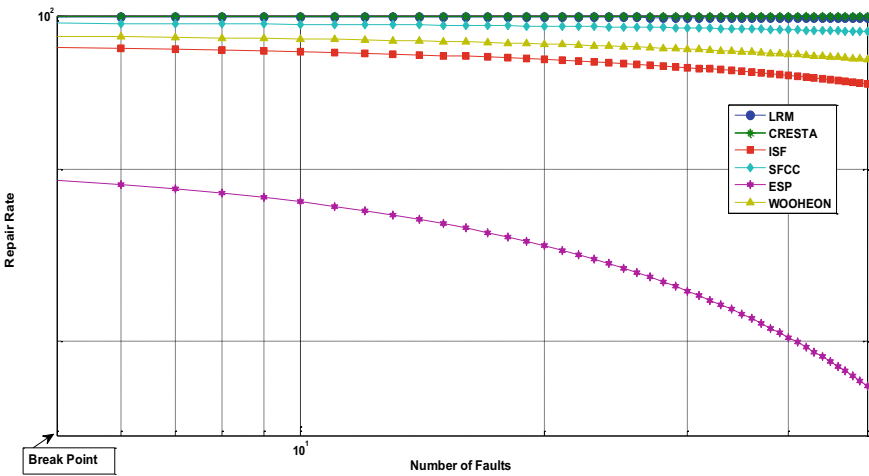


Fig. 9 Case III repair rate and numbers of faults

Table 6 shows the testing and repairing of MUT using MATLAB. Here March C, March C- and March LR Algorithms are applied on MUT. Results show that the testing time required by March LR is less as compared to others. Figure 11 shows the testing time comparison between these algorithms.

Fig. 10 Flow chart of co-design of MBIST and MBISR

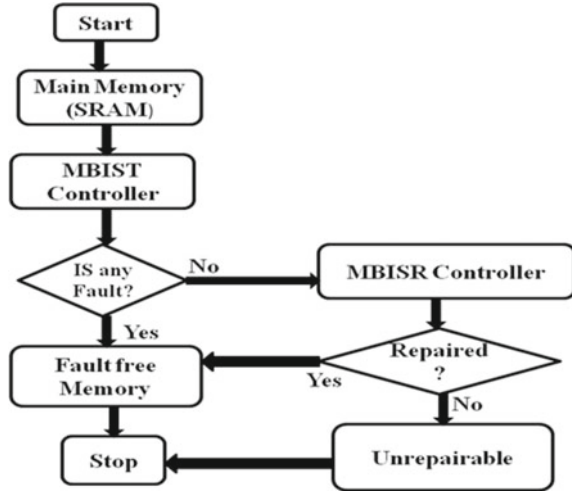
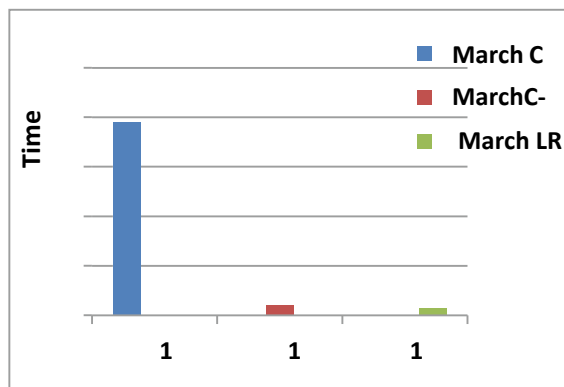


Table 6 Co-design MBIST and MBISR of Memories

S. no	Memory size	Algorithm	Spare row/column	Tool used	Testing time
1	6*6*1(10N)	MARCH C	Rw1/Cl 2	MATLAB	3.9s
2	6*6*1(10N)	MARCH C-	Rw1/Cl 2		0.21s
3	6*6*1(14N)	MARCH LR	Rw1/Cl 2		0.14s

Fig. 11 Comparison between march algorithms for co-design



8 Conclusion

This paper critically reviews the concept of memory testing and memory repair using different RA (Redundancy Analysis) algorithms in detail. In this paper, several Methodology and algorithms related to Memory built-in self-test and Memory built-in self-repair are analyzed on the bases of key parameters including area overhead

for spare register, memory row/column size, local bits, main memory sizes, testing time penalties, and repair rate are simulated and discussed. A trade-off performance of different memory sizes is an analysis using March C, March C- and March LR. The results show that the March LR shows better fault coverage and requires less testing time and for repairing CRESTA shows the optimal repair rate as compared to other repair algorithms. A co-design of MBIST and MBISR is also proposed in this paper which reduces the area overhead requirement penalty.

References

1. Manasa RV, Koppad D (2019) Implementation of BIST technology using march-LR algorithm. In: 4th international conference on recent trends on electronics, information, communication & technology (RTEICT), pp 1208–1212
2. Masnita MI, Zuha WHW, Sidek RM, Halin IA (2009) The data and read/write a controller for March-based SRAM diagnostic algorithm MBIST. In: IEEE student conference on research and development (SCORED), pp 296–299
3. Harutunyan G, Vardanian VA, Zorian Y (2007) A march-based fault location algorithm with partial and full diagnosis for all simple static faults in random access memories. In: 2007 IEEE design and diagnostics of electronic circuits and systems, pp 1–42
4. Singh B, Narang SB, Khosla A (2010) Modeling and simulation of efficient march algorithm for memory testing. *Commun Comput Inform Sci* 95(2):96–107
5. Aditya, Sharma, Prakash O (2017) CHECKERMARC: a modified novel memory testing approach for bit-oriented SRAM. *Int J Appl Eng Res* 3023–3028
6. Harutunyan G, Vardanian VA, Zorian Y (2006) Minimal march test algorithm for detection of linked static faults in random access memories. In: 24th IEEE VLSI test symposium, vol 30, pp 126–127
7. Lee M, Denq L, Wu C (2011) A memory built-in self-repair scheme based on configurable spares. *IEEE Trans Comput Aided Des Integr Circ Syst* 30(6):919–929
8. Zeli R, Silveira R, Qureshi Q (2019) SoC memory test optimization using NXP MTR solutions. In: IEEE Latin American test symposium (LATS), pp 1–5
9. Kang W, Cho H, Lee J, Kang S (2014) A BIRA for memories with an optimal repair rate using spare memories for area reduction. *IEEE Trans Very Large Scale Integr (VLSI) Syst* 12(11):2336–2349
10. Kang W, Lee C, Lim H, Kang S (2015) A 3 dimensional built-in self-repair scheme for yield improvement of 3 dimensional memories. *IEEE Trans Reliab* 64(2):586–595
11. Lee H, Cho K, Kim D, Kang S (2018) Fault group pattern matching with efficient early termination for high-speed redundancy analysis. *IEEE Trans Comput Aided Des Integr Circuits Syst* 37(7):1473–1482
12. Tekumalla R, Krishnamoorthy P (2014) Local repair signature handling for repairable memories. In: 2014 IEEE 23rd North Atlantic test workshop, pp 1–5
13. Chen TJ, Li J-F, Tseng TW (2012) Cost-efficient built-in redundancy analysis with optimal repair rate for RAMs. *IEEE Trans Comput Aided Des Integr Circ Syst* 31(6):930–940
14. Ohler P, Hellebrand S, Wunderlich H (2007) Analyzing test and repair times for 2D integrated memory built-in test and repair. *IEEE Des Diagnostics Electron Circ Syst* 1–6
15. Lu SK, Wang ZY, Tsai YM, Chen JL (2012) Efficient built-in self-repair techniques for multiple repairable embedded RAMs. *IEEE Trans Comput Des Integr Circ Syst* 31(4):620–629
16. Aditya (2019) Novel modified memory built-in self-repair (MMBISR) for SRAM using hybrid redundancy-analysis technique. *IET Circ Dev Syst* 13(6):836–842. <https://doi.org/10.1049/iet-cds.2018.5218>

17. Sasikumar M, Bhakthavatchalu R, Sreehari KN, Kumar A (2021) Scalable and rapid fault detection of memories using MBIST and signature analysis. In: *Advances in signal and data processing. Lecture notes in electrical engineering*, vol 703. Springer, Singapore, pp 351–367
18. Lv M, Sun H, Xin J, Zheng N (2021) Efficient repair analysis algorithm exploration for memory with redundancy and in-memory ECC. *IEEE Trans Comput* 70(5):775–788
19. Mayuga G, Sato Y, Inoue M (2020) Highly reliable memory architecture using adaptive combination of proactive aging-aware in-field self-repair and ECC. *IEEE Trans Comput Aided Des Integr Circ Syst* 39(8):1688–1698
20. Martínez-Peñas U, Napp D (2020) Locally repairable convolutional codes with sliding window repair. *IEEE Trans Inf Theory* 66(8):4935–4947

Rapid Protection System Using Single-End Current Data for Capacitive Compensated Power Transmission Network



Shoyab Ali , Annapurna Bhargava, and Akash Saxena 

Abstract This paper presents a new approach based on current data processing and characteristic extraction method to detect the fault in a capacitive compensated power transmission network (CCPTN). The scheme uses the transform in the level of the three-phase currents at the local bus of the CCPTN for fault detection and the WIs (wavelet indices) for phase categorization. The functioning of the scheme is extensively authenticated on the 500 kV CCPTN using MATLAB software. The simulations show that the scheme is tremendously important for the CCPTN.

Keywords Fault Detection · Power Transmission Network · Wavelet Transform

1 Introduction

The researchers face a challenge to detect and locate faults in transmission lines (TLs). In this context, this literature presents the widespread review of the latest research of the investigators. The researchers [1] have proposed progressive kurtosis-based effective fault location and detection scheme for transmission lines. The binocular vision technology (BVT) is another technique that has good application in the similar field of research. The researchers [2] have proposed a BVT-based scheme for fault location in transmission line. Wavelet is used to develop active fault detection scheme in [3]. A protection scheme for distribution lines had been presented, based on the currents and making use of the microcontroller [4]. A fault location algorithm for TCSC connected transmission line was proposed by the researchers in [5]. For detecting and locating faults in transmission lines, a distribution time domain reflectometry-based scheme is introduced in [6]. For locating different faults in VSC-HVDC transmission system, a scheme is proposed in [7]. A fault detection

S. Ali (✉) · A. Bhargava
Department of Electrical Engineering, Rajasthan Technical University, Kota, India
e-mail: ali.shoyab@gmail.com

A. Saxena
SKIT, Jaipur, Rajasthan, India

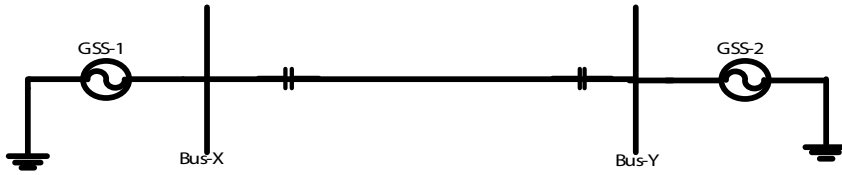


Fig. 1 Simulated system

and location scheme for transmission lines has been developed in [8] using multi-layer perceptron. An incremental current-based approach is a better alternative for LCC-HVDC transmission systems and has recently been successfully used for fault detection and classification [9]. Wavelet packet entropy and machine learning are applied for EHVTL protection in [10] and [11], respectively. PMUs are installed for fault detection and location in distribution lines [12]. Faulty phase detection using time domain current information for TCSCS has been described in [13].

This paper presents a scheme for fault detection in transmission lines connected with series capacitor units which are connected at both terminals of the transmission system.

2 Simulation Model

A double-fed and both ends capacitive compensated 50 Hz; 500 kV transmission line has been considered which has an overall length of 300 km. The simulated transmission system has been shown in Fig. 1. The transmission system has been designed in MATLAB. The current data from sending-end bus has been captured at a sampling rate of 1 kHz.

3 Relaying Algorithm

The schematic of the relaying algorithm is shown in Fig. 2.

4 Results for Fault Detection

The results of the fault detection scheme have been shown for a variety of simulating situations in the succeeding sections.

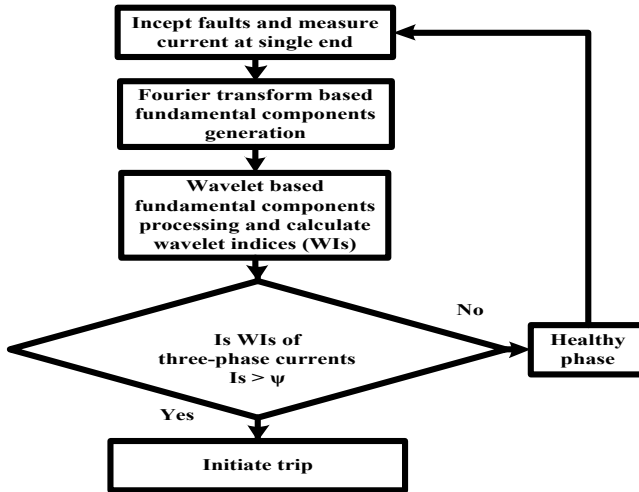


Fig. 2 Relaying algorithm

4.1 Faults Near Circuit Breaker

An LLG fault (BCG fault) has been simulated at 0.05 s near the circuit breaker. Figure 3 presents the results. It is evident from Fig. 3 that the indices of Φ_B and Φ_C cross the Ψ line just after the inception of fault. The indices of Φ_A , Φ_B , and Φ_C and the detection time for different faults are demonstrated in Table 1. The scheme is found to be insensitive for faults which occur in the neighborhood of the circuit breaker.

4.2 Faults Near Bus-Y

An LLG fault (ABG fault) has been simulated at 0.1 s near Bus-Y (second terminal) of the transmission system. Figure 4 presents the results. It is evident from Fig. 4 that the indices of Φ_A and Φ_B cross the Ψ line just after the commencement of fault. The indices of Φ_A , Φ_B , and Φ_C for different faults are given in Table 2. Table 2 also shows the detection time of different faults. The scheme is found to be not sensitive for faults which occur in the neighborhood of Bus-Y of the transmission system.

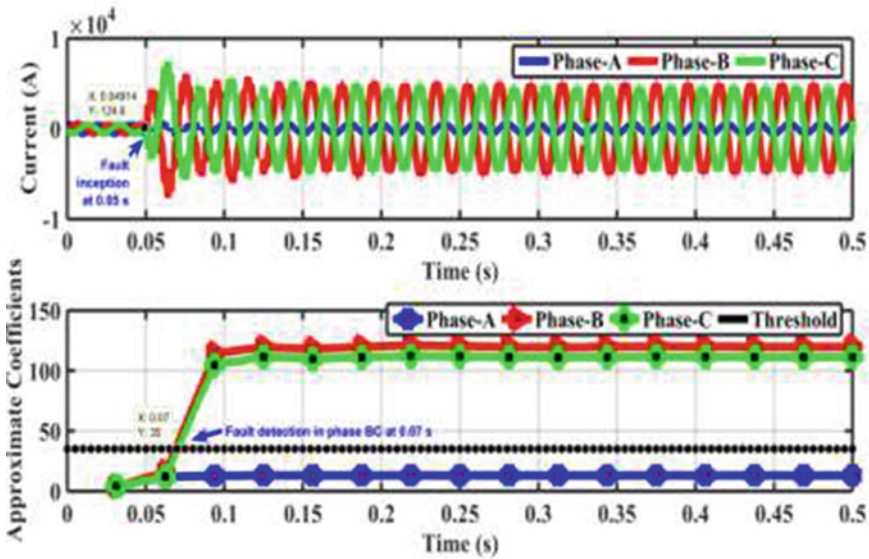


Fig. 3 Results during BCG fault at 0.05 s

Table 1 Indices for faults near circuit breaker

Fault case	FIT (s)	Indices			Fault detection time (ms)		
		ΦA	ΦB	ΦC	ΦA	ΦB	ΦC
BCG	0.05	13.0929	121.0246	112.4883	–	20	20
ABG	0.05	121.4412	112.9974	13.0916	20	20	–
AC	0.05	116.1504	11.8384	117.0760	20	–	20
AG	0.05	48.4458	12.6828	13.2716	30	–	–
ABCG	0.05	133.5495	133.3693	133.3609	20	20	20

4.3 Faults Near Generator

An LLG fault (ACG fault) has been simulated at 0.25 s in close proximity to the generator. Figure 5 presents the results. It is evident from Fig. 5 that the indices of ΦA and ΦC cross the Ψ line just after the inception of fault. The indices of ΦA , ΦB , and ΦC for different faults are presented in Table 3. Table 3 also indicates the fault detection time of various cases. The scheme is found to be insensate for faults which occur in the zone of the generator.

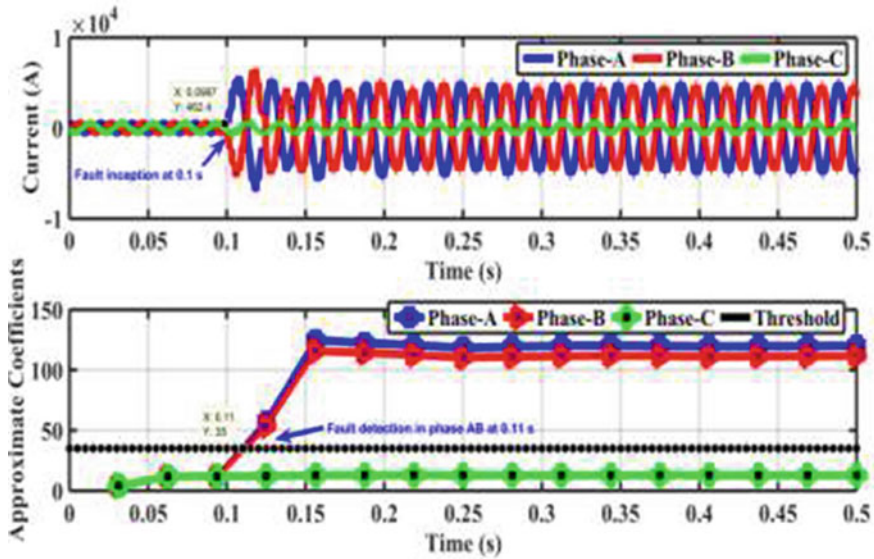


Fig. 4 Results during ABG fault at 0.1 s

Table 2 Indices for faults near Bus-2

Fault case	FIT (s)	Indices			Fault detection time (ms)		
		Φ_A	Φ_B	Φ_C	Φ_A	Φ_B	Φ_C
ABG	0.1	124.8838	115.9448	13.0900	10	10	–
ACG	0.1	120.2868	13.0905	128.3104	15	–	15
BC	0.1	11.8385	119.7920	118.6038	–	15	15
ABCG	0.1	139.7563	136.9913	139.0156	10	10	10
CG	0.1	12.6989	13.2695	47.8563	–	–	40

4.4 Effect of Fault Location

An LL fault (AB fault) has been simulated at 0.05 s at 145 km to the generator. Figure 6 presents the results. It is evident from Fig. 6 that the indices of Φ_A and Φ_B cross the Ψ line just after the inception of fault. The indices of Φ_A , Φ_B , and Φ_C for different faults as well as the fault detection time are given in Table 4. The scheme is found to be insensate for different values of fault location.

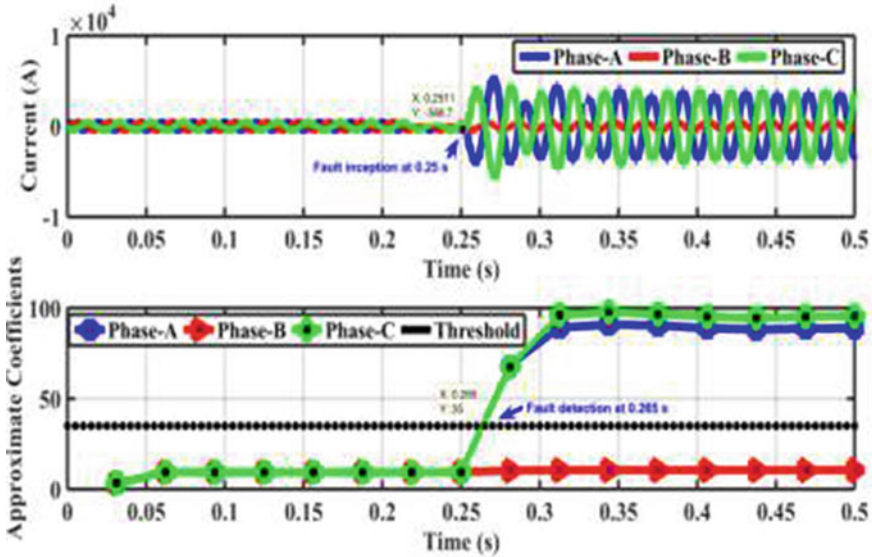


Fig. 5 Results during ACG fault at 0.25 s

Table 3 Indices for faults near generator

Fault case	FIT (s)	Indices			Fault detection time (ms)		
		Φ_A	Φ_B	Φ_C	Φ_A	Φ_B	Φ_C
ACG	0.25	90.7992	10.4619	97.7826	15	–	15
BCG	0.25	10.4712	96.7477	89.9634	–	10	10
AB	0.25	94.3649	92.9566	9.4704	10	10	–
BG	0.25	10.5443	36.0430	10.2071	–	10	–
ABCG	0.25	107.2007	106.7837	107.2984	10	10	10

4.5 Effect of Short Circuit Capacity of Generator

An LG fault (BG fault) has been simulated at 0.15 s with generator’s short circuit capacity of 80 GVA. Figure 7 presents the results. It is evident from Fig. 7 that the indices of Φ_B cross the Ψ line just after the inception of fault. The indices of Φ_A , Φ_B , and Φ_C for different faults are shown in Table 5. In Table 5 the fault detection time is also indicated for various faults. The scheme is found to be insensitive for different values of short circuit capacity of generator.

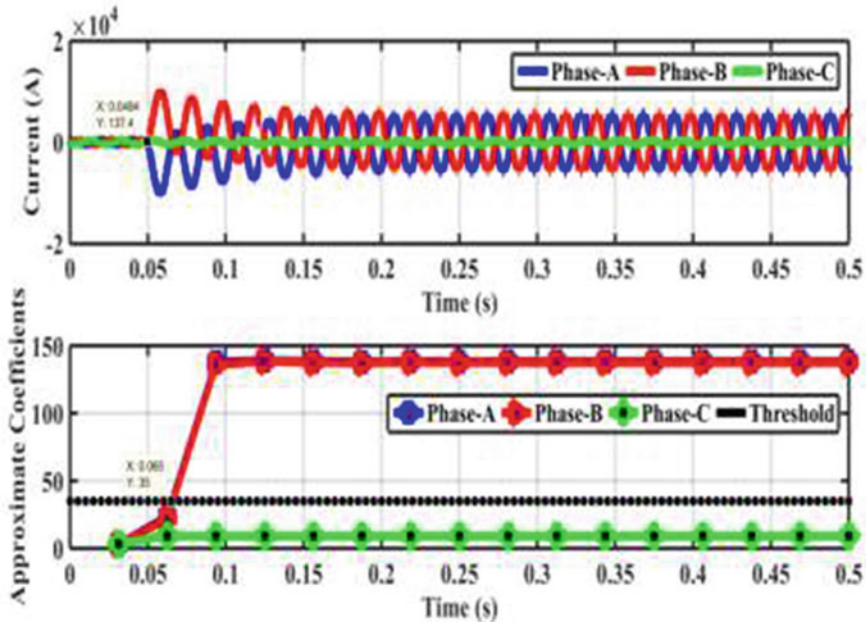


Fig. 6 Results during AB fault at 0.05 s

Table 4 Indices for faults at different locations

Fault case	FL (km)	Indices			Fault detection time (ms)		
		ΦA	ΦB	ΦC	ΦA	ΦB	ΦC
CG	135	10.296	11.077	77.042	–	–	25
AG	165	62.791	10.254	10.991	25	–	–
AB	145	139.026	138.486	9.537	15	15	–
ACG	175	113.758	10.754	123.458	20	–	20
ABCG	125	183.944	182.128	182.925	15	15	15

4.6 Effect of Fault Inception Time

An LG fault (CG fault) has been simulated at 0.2 s on power transmission network. Figure 8 presents the results. It is evident from Fig. 8 that the indices of ΦC cross the Ψ line just after the inception of fault. The indices of ΦA , ΦB , and ΦC for different faults are shown in Table 6. In Table 6 the fault detection time is also indicated for a variety of faults. The scheme is found to be insensitive for different values of fault inception time.

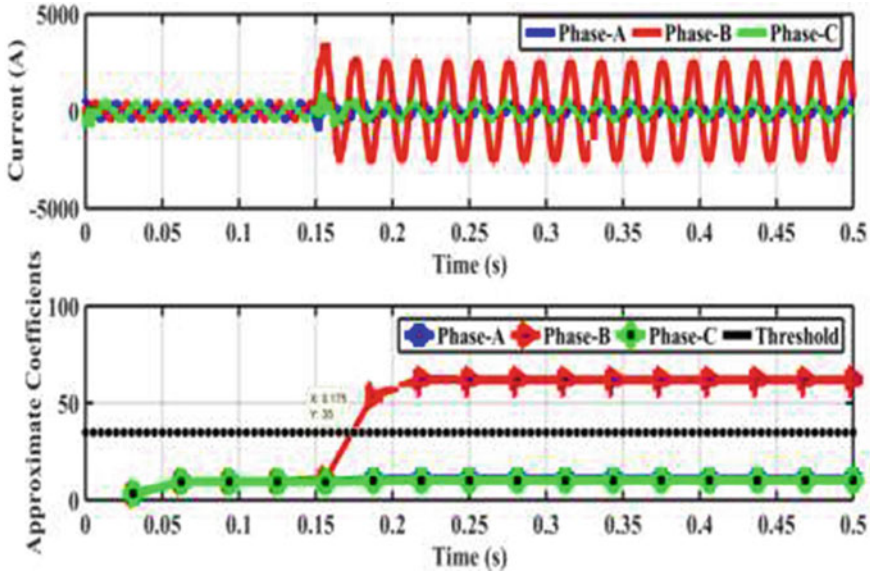


Fig. 7 Results during BG fault at 0.15 s

Table 5 Indices for faults with different generator’s SCC

Fault case	FIT (s)	SCC (GVA)	Indices			Fault detection time (ms)		
			ΦA	ΦB	ΦC	ΦB	ΦA	ΦB
ACG	0.15	50	120.4891	10.7701	130.6502	15	–	15
BC	0.15	60	9.5094	125.2793	124.7476	–	15	15
AG	0.15	70	62.2613	10.2564	10.9911	20	–	–
BG	0.15	80	10.9924	62.2480	10.2577	–	25	–
ABCG	0.15	90	148.1730	147.4966	147.0316	10	10	10

4.7 Effect of Transmission Voltage and Frequency

An LG fault (BG fault) has been simulated at 0.1 s on the power transmission network. Figure 9 presents the results. It is evident from Fig. 9 that the indices of ΦB cross the Ψ line just after the inception of fault. Table 7 shows the effect of different values of transmission voltage and frequency. The indices of ΦA , ΦB , and ΦC for different faults as well as the detection time are shown in Table 7. The scheme is found to be insensitive for different values of transmission voltage and frequency.

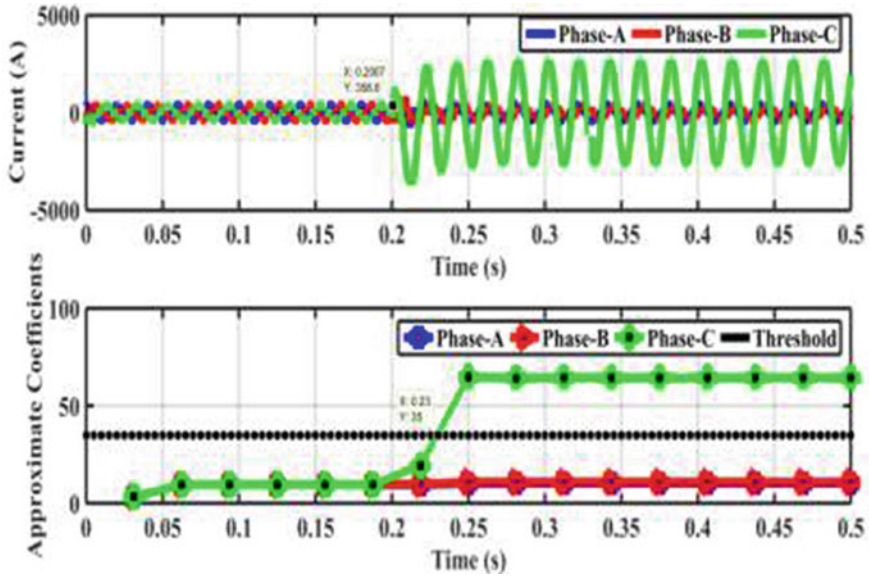


Fig. 8 Results during CG fault at 0.2 s

Table 6 Indices for faults at different FITs

Fault case	FIT (s)	FL (km)	Indices			Fault detection time (ms)			
			ΦA	ΦB	ΦA	ΦB	ΦA	ΦB	
ACG	0.05	160	123.6861	10.7924	134.1455	20	–	20	
AB	0.1	160	127.1330	126.4662	9.5385	5	5	–	
AG	0.15	160	64.7261	10.2624	11.0068	20	–	–	
CG	0.2	160	10.2628	11.0073	64.8226	–	–	30	
ABCG	0.25	160	146.0001	146.0572	146.0098	5	5	5	

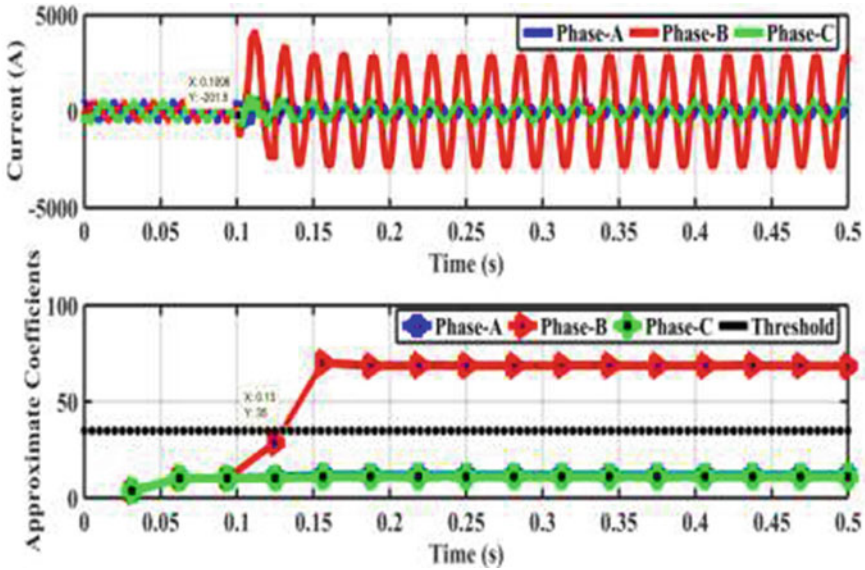


Fig. 9 Results during BG fault at 0.1 s

Table 7 Indices for faults with different TV and TF

Fault case	TF (Hz)	TV (kV)	Indices			Fault detection time (ms)		
			Φ_A	Φ_B	Φ_C	Φ_B	Φ_A	Φ_C
AG	50.20	415	72.229	10.707	11.482	20	–	–
BG	51.75	425	11.912	70.241	11.112	–	30	–
AC	49.50	450	154.458	10.665	155.176	10	–	10
ABG	52.10	390	128.476	119.366	10.769	10	15	–
ABCG	50.95	395	148.970	148.164	149.853	5	10	5

5 Conclusion

A new fault identification and phase classification scheme is presented in this paper for protecting the CCPTN. The presented scheme uses the transform in the magnitude of three-phase currents at the local bus of the CCPTN for fault identification. The scheme is tested for 500 kV CCPTN. The scheme can be realized in the FACTS compensated power transmission network as per the acquired simulation results.

References

1. Yan S, Xu J, Ju X, Wu Z, Fan H, Cao P (2022) A novel fault location method for transmission lines based on progressive kurtosis in ± 800 kV Kunbei Converter Station. In: 2022 5th international conference on energy, electrical and power engineering (CEEPE), pp 437–441. <https://doi.org/10.1109/CEEPE55110.2022.9783294>
2. Li Q, Chen G (2022) Fault distance location method of transmission line based on binocular vision technology. In: 2022 7th international conference on intelligent computing and signal processing (ICSP), pp 1807–1811. <https://doi.org/10.1109/ICSP54964.2022.9778749>
3. Sailakshmi, Navyasri GS, Deepa K, Sailaja V (2022) Fault analysis in three phase transmission lines using wavelet method. In: 2022 6th international conference on trends in electronics and informatics (ICOEI), pp 248–254. <https://doi.org/10.1109/ICOEI53556.2022.9776716>
4. Joy UB, Chakraborty S, Murad TK, Tasnim A, Barua B, Das J (2022) Microcontroller based feeder protection system from various fault conditions in distribution line. In: 2022 international conference on innovations in science, engineering and technology (ICISSET), pp 89–94. <https://doi.org/10.1109/ICISSET54810.2022.9775914>
5. Nasab MA, Zand M, Hatami A, Nikoukar F, Padmanaban S, Kimiai AH (2022) A hybrid scheme for fault locating for transmission lines with TCSC. In: 2022 international conference on protection and automation of power systems (IPAPS), pp 1–10. <https://doi.org/10.1109/IPAPS55380.2022.9763217>
6. Haddad D, Kallel AY, Amara NEB, Kanoun O (2022) Multiple faults detection and location in bus-shaped cable networks by distributed time-domain reflectometry. *IEEE Sens Lett* 6(5):1–4. <https://doi.org/10.1109/LSSENS.2022.3170645>
7. Elgamasy MM, Izzularab MA, Zhang X-P (2022) Single-end based fault location method for VSC-HVDC transmission systems. *IEEE Access* 10:43129–43142. <https://doi.org/10.1109/ACCESS.2022.3169777>
8. Yang H (2022) Transmission line fault detection based on multi-layer perceptron. In: 2022 international conference on big data, information and computer network (BDICN), pp 778–781. <https://doi.org/10.1109/BDICN55575.2022.00151>
9. Deb S, Verma HK (2022) Incremental current based fault detection and classification in LCC-HVDC transmission system. In: 2022 IEEE Delhi section conference (DELCON), pp 1–9. <https://doi.org/10.1109/DELCON54057.2022.9753565>
10. Shi Z et al (2022) Transient protection of EHV AC line based on wavelet packet entropy. In: 2022 international conference on power energy systems and applications (ICoPESA), pp 206–212. <https://doi.org/10.1109/ICoPESA54515.2022.9754400>
11. Janarthanam K, Kamalesh P, Basil TV, Kovilpillai J (2022) Electrical faults-detection and classification using machine learning. In: 2022 international conference on electronics and renewable systems (ICEARS), pp 1289–1295. <https://doi.org/10.1109/ICEARS53579.2022.9751897>
12. Conte F, D'Agostino F, Gabriele B, Schiapparelli GP, Silvestro F (2022) Fault detection and localization in active distribution networks using optimally placed phasor measurements units. *IEEE Trans Power Syst.* <https://doi.org/10.1109/TPWRS.2022.3165685>
13. Prasad CD, Biswal M (2022) Time-domain current information based faulty phase detection in thyristor controlled series compensated transmission system. In: 2020 international conference on power, instrumentation, control and computing (PICC), pp 1–5. <https://doi.org/10.1109/PICC51425.2020.9362498>

Enhancement of Breakdown Voltage Using Trench Edge Termination Technique in SiC-Based Power Device



Ankit Panchal, Ekta Sharma, Vamshi Krishna Dasarraj, and Suman

Abstract The development of technologies with high voltage and high frequency somewhat affects how comfortable modern society is. Wide bandgap semiconductors have taken the place of silicon-based devices because of their mature performance. However, edge effects are to blame for the premature collapse of wide bandgap semiconductor devices. The current work illustrates breakdown voltage increase in a Schottky diode based on SiC by adopting trench edge termination. In the structure's trench, SiO₂ was placed. The device structure has been replicated using the atlas module of the Silvaco TCAD program. There have been many models used for ionization, recombination, impact ionization, and mobility. It has been observed that the breakdown voltage rises to 100 V as a result of the electric field becoming stronger near the device's edges. Using the trench termination, the edge electric field crowding has been found spreading away from the edges of the device and in the SiO₂ layer. As a consequence, the trench edge-terminated device possesses a reverse breakdown voltage, which was increased to 500 V.

Keywords Schottky diode · Dielectric · Trench termination · Breakdown voltage · Field plate

1 Introduction

In the industrial, transportation, and medical fields of modern life, there is an increasing demand for high frequency and voltage devices. In the aforementioned applications, silicon-based devices now in use have realized their full potential. Wide

A. Panchal · E. Sharma (✉)
Chaudhary Ranbir Singh University, Jind 126102, India
e-mail: ektasharma9797@gmail.com

V. K. Dasarraj
Northern Illinois University, Dekalb, IL 60115, USA

Suman
Department of Physics, Government College for Women, Rohtak 124001, India

band gap semiconductors as SiC, Ga₂O₃, GaN, diamond, etc. enter the picture as a result [2, 4, 33]. For use in the aforementioned applications, their performances are significantly better than their silicon counterparts. The goal going ahead is to improve wide band gap semiconductors' performance and reliability [6, 9, 10, 12–15, 17, 19, 20, 24, 34]. SiC is less common than other materials on the market, but because of its excellent crystal quality, it is a promising choice for use in high-power and high-frequency devices [31, 35]. Carbon (C) and silicon (Si) atoms combine to form the crystalline material known as SiC. SiC has several important properties that explain why it is used in the production of many devices, including thermal conductivity (3–5 W/cm °C), band gap (~3.3 eV), high saturation electron velocity (2.7×10^7 cm/s), breakdown electric field ($2\text{--}6 \times 10^6$ V/cm), and high stability [5, 7, 8, 19]. Additionally, because of its powerful breakdown electric field SiC may be used to create devices with high power accompanying thin, heavily doped drift layers [10, 12]. Utilizing these thin drift layers decreases the minority charge carrier storage and raises the switching frequency of SiC-based bipolar devices. Strong temperature (i.e., up to 350 °C) and power efficient operational devices have increased as a result of SiC's characteristics like wider band gap and high thermal conductivity. SiC materials can therefore be employed to create lightweight, affordable, and compact electronics [7, 8]. A Schottky diode (SD) is the most developed power technology currently in use [35]. These devices are ideally suited for quick switching action because they don't have small carrier storage concerns [1, 23, 25]. The underside of the vertical Schottky diodes has a complete ohmic contact, allowing for higher current capability than the previous ones' lateral designs did [37]. However, the congested electric field at the SD boundaries causes a reliability problem. The lower portion on the border of the SDs has a higher electric field than the remainder of the device, which is brought on by the electric field being crowded there. In addition, devices with edge electric fields break down more quickly on the reverse bias and at lower applied fields. The most typical region of interest is close to the device's edge because there, the electric field is stronger than it is below the junction. Edge termination is the process of reducing such strong electric fields at the junction's edge. The breakdown in the device is around 20% of the optimum value without edge termination. To reduce edge terminations in the devices, a number of techniques have been implemented [28]. To reduce the fields around the margins of the devices made of SiC and GaN, various approaches have been devised, including ion implantation, field plates, guard rings, and selective swift heavy ion irradiation [13, 17, 19, 20, 24, 28, 34]. However, there are numerous issues with the existing SiC approaches. For instance, it is simple to produce the guard ring without the use of any additional photolithography steps. Despite this, this method can nevertheless achieve reduced blocking voltage efficiency, a greater surface electric field, and an intensified edge width. Although the junction termination extension technique (JTE) can be used, the process window is severely constrained by the requirement for a step known as dopant activation. Additionally, the devices' edge effect was reduced by using a field limiting ring produced by ion implantation [5, 22, 26, 27, 30]. However, the requirement for several ion implantation beams, the development of an ion shielding mask, and other procedures, such as the activation of ions at high temperature, contribute to

the complexity of the FLR manufacturing process. To achieve a surface that is thoroughly cleaned and impurity-free, a particular thermal treatment is first required. Numerous study groups have suggested trench and bevel JTE as alternatives to edge-effect mitigating techniques. However, for these procedures, a relatively wider edge width is needed. In summary, simple and affordable technology is what is required right now to produce high-power devices [2, 3, 21, 38]. In addition, the device's interface has a crucial role in determining the breakdown characteristics. Furthermore, the interface of the device is the key factor in influencing the characteristics of breakdown. Researchers are putting efforts toward improvement in the interface of the SiC-based devices [11, 16]. Additionally, low-cost, highly space-efficient gadgets are needed to develop present technologies. According to reports, the most effective and space-efficient structure for edge termination is trench termination. In order to achieve the highest breakdown voltage, our effort adjusted the trench characteristics of the SiC-based SDs. Silvaco TCAD software was used to simulate the device. The trench was created near the edge of the device being discussed. A dielectric material was poured into the trench to approximate a maximum breakdown voltage. Additionally, the terminated devices and unterminated devices were simulated and contrasted.

2 Device Structure

Devices that cannot be predicted in real time can be studied using simulation. The SILVACO TCAD software's atlas module makes it easier to build the device and simulate it to obtain electrical characteristics, which provides additional insight into the physical behavior of the device while it is in use. Modeling different devices with crystalline to amorphous materials, DC and AC properties, etc. is possible with this software. This tool uses a variety of semiconductor equations to model different device phenomena. Any gadget can be accurately modeled using the aforementioned tools. Additionally, the accuracy of the results is reliant on the accuracy of the parameter inputs. The SiC band gap, its inherent carrier concentration, electron and hole mobility, electron affinity, permittivity, substrate doping, device dimensions, diffusion lengths, and other factors are the primary factors in the current study. In the existing work, the simulated structure is schematically represented in Fig. 1.

The structure has a substrate with a height of 20 μm and doping of $1 \times 10^{19} \text{ cm}^{-3}$, which is chosen to be n + SiC in the current work. An epitaxial layer, drift layer, or top layer that is 8 μm thick and $7 \times 10^{16} \text{ cm}^{-3}$ doped is present on the substrate. In the current work, a metal with a work function of 4.5 eV was selected as the Schottky metal. The trench's dimensions are 40 μm wide and 500 nm high. The dielectric used to fill the trench was SiO₂. Permittivity and thickness are the principal dielectric factors because they have a significant impact on reverse breakdown voltage. The contact on the backside was created as an ohmic contact. Temperature $T = 300 \text{ K}$, band gap = 3.2 eV, Schottky metal work function = 4.5 eV, electron affinity = 4.12 eV, conduction band density of states = $1 \times 10^{19} \text{ cm}^{-3}$, permittivity = 9.6, and

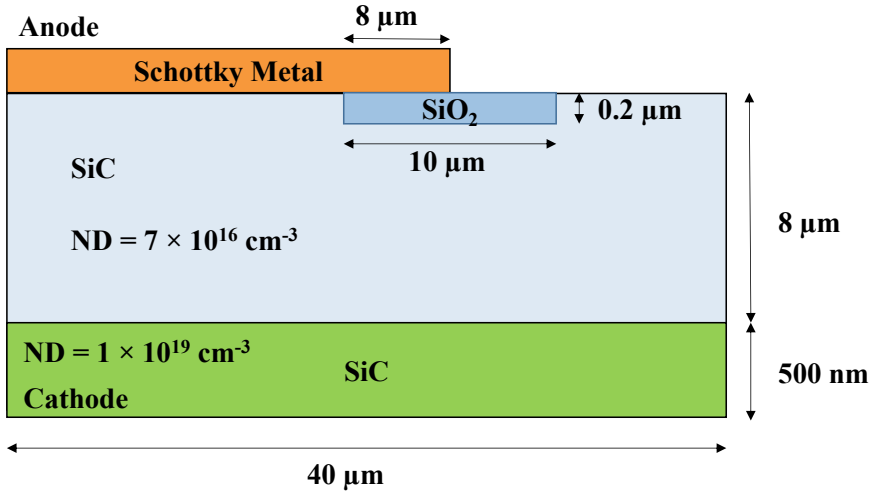


Fig. 1 A schematic representation of the simulated structure

valence band density of states = $1.2 \times 10^{19} \text{ cm}^{-3}$ have all been employed for SiC. There are many models that have been utilized, including FD statistics, SRH and Auger recombination, Selberherr impact ionization, parallel and concentration field-dependent mobility, etc. Additionally, the device's meshing was carefully chosen to avoid producing inaccurate findings. To reduce the device's problem with solution convergence, the mesh spacing was also set as a smooth variation [18].

3 Results and Discussion

Figure 1 depicts the trench termination approach that was used to minimize the device's edge electric field congestion. According to earlier research, the trench's dielectric material should be selected so that the electric field doesn't surpass its breakdown strength. As a result, the breakdown of a few dielectric materials has been demonstrated with varied permittivity as reported in the literature [21, 29, 32, 36]. Due to the development of its deposition and processing technologies in the manufacturing sector, SiO₂ is utilized in the current work. The gadget will have a greater reverse breakdown voltage because the metal employed as the field plate will deflect the edges of the high electric field away from it.

Figure 2 shows the potential profile for the unterminated device. Figure 2 demonstrates that the potential is severe at point A, which is the device's edge. Due to this large potential, the electric field will likewise be quite strong there, as depicted graphically in Fig. 2. An increase in impact ionization was induced by the free charge carriers being given energy by such an intense electric field. As a result, the device has avalanche breakdown and will fail at lower reverse voltages. It must be noted that

in actual devices, additional elements like as material flaws may also contribute to early device failure. The breakdown brought on by the edge effect still rules, though. The breakdown voltage for unterminated devices was determined to be 100 V as shown in Fig. 3b.

Figure 3a demonstrates how the potential at corner “A” of the terminated structure has been reduced relative to the unterminated structure and moved to point “B” inside the dielectric material, SiO₂. As a result, the device has a higher reverse breakdown voltage and the structure has a low electric field at its corners. The reverse breakdown

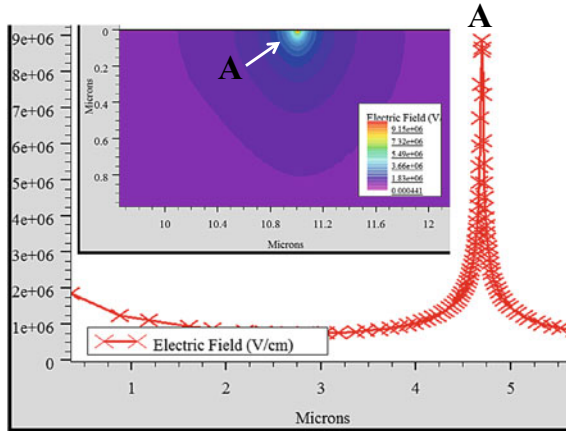


Fig. 2 The unterminated device has a potential distribution with the highest value at point A at the edge. The inset contains the corresponding electric field (EF)

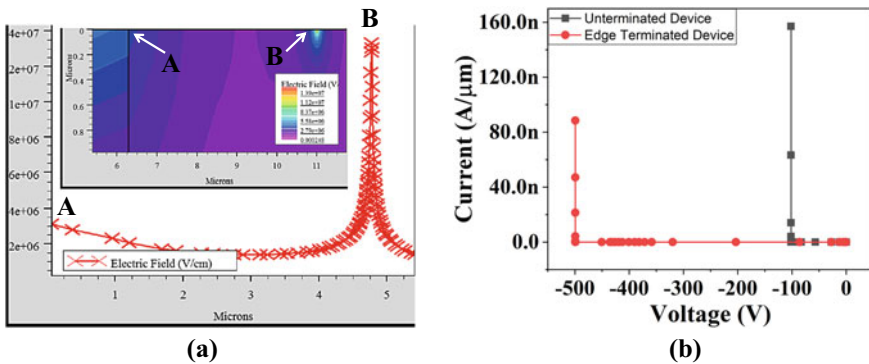


Fig. 3 (a) The edge-terminated device has a potential distribution with the highest value at point A at the edge. The inset contains the corresponding electric field (EF). It can be seen that EF, which was at point B previously, has been shifted to point A after edge termination. (b) Graph of breakdown voltage in the device

in the device was estimated by the simulation used in this work to be 500 V as depicted in Fig. 3b.

4 Conclusion

Finally, it has been investigated how trench-driven edge termination in SiC-based SDs occurs. With the aid of Silvaco TCAD simulation software, the SiC-based SD has been modeled both with and without edge termination. The edges of the unterminated device structures exhibit the largest electric field, which causes the device to quickly fail at 100 V. The breakdown voltage of the dielectric layer in the simulation was predicted using the critical field strength of the dielectric material. The electric field is weaker near the border of the SiO₂ filled trench structures, though. As the corner radius increases, it is observed that the maximum field strength in the dielectric layer decreases, increasing the breakdown voltage of the Schottky diode. The breakdown voltages of the SiC drift area and the dielectric layer are used to calculate the breakdown voltages of the SiC trench SBD. The breakdown voltage of the structure is discovered to be increased to 500 V. These results suggest that the use of trench termination structures may help reduce the size of structures by reducing the breadth of their edges.

References

1. Bahat-Treidel E et al (2012) Fast-switching GaN-based lateral power Schottky barrier diodes with low onset voltage and strong reverse blocking. *IEEE Electron Device Lett* 33(3):357–359. <https://doi.org/10.1109/LED.2011.2179281>
2. Baliga BJ (2006) Silicon carbide power devices. World Sci. <https://doi.org/10.1142/5986>
3. Brunt EV et al (2014) 22 kV, 1 cm², 4H-SiC n-IGBTs with improved conductivity modulation. In: 2014 IEEE 26th international symposium on power semiconductor devices & IC's (ISPSD). IEEE, pp 358–361. <https://doi.org/10.1109/ISPSD.2014.6856050>
4. DiMarino CM et al (2015) High-temperature silicon carbide: characterization of state-of-the-art silicon carbide power transistors. *IEEE Ind Electron Mag* 9(3):19–30. <https://doi.org/10.1109/MIE.2014.2360350>
5. Hiyoshi T et al (2008) Simulation and experimental study on the junction termination structure for high-voltage 4H-SiC PiN diodes. *IEEE Trans Electron Dev* 55(8):1841–1846. <https://doi.org/10.1109/TED.2008.926643>
6. Jones EA et al (2016) Review of commercial GaN power devices and GaN-based converter design challenges. *IEEE J Emerg Sel Top Power Electron* 4(3):707–719. <https://doi.org/10.1109/JESTPE.2016.2582685>
7. Kimoto T, Cooper JA (2014) Fundamentals of silicon carbide technology: growth, characterization, devices and applications. John Wiley & Sons Singapore Pte. Ltd, Singapore. <https://doi.org/10.1002/9781118313534>
8. Kranzer D et al (2019) Applications of SiC devices. In: Wide bandgap semiconductor power devices. Elsevier, pp 345–371. <https://doi.org/10.1016/B978-0-08-102306-8.00010-1>

9. Kumar V et al (2014) Barrier height inhomogeneities induced anomaly in thermal sensitivity of Ni/4H-SiC Schottky diode temperature sensor. *J Vac Sci Technol B Nanotechnol Microelectron Mater Process Meas Phenom* 32(4):041203. <https://doi.org/10.1116/1.4884756>
10. Kumar V et al (2016) Capacitance roll-off and frequency-dispersion capacitance-conductance phenomena in field plate and guard ring edge-terminated Ni/SiO₂/4H-nSiC Schottky barrier diodes. *Phys Status Solid* 213(1):193–202. <https://doi.org/10.1002/pssa.201532454>
11. Kumar V et al (2022) Defect levels in high energy heavy ion implanted 4H-SiC. *Mater Lett* 308:131150. <https://doi.org/10.1016/J.MATLET.2021.131150>
12. Kumar V et al (2015) Diameter dependent thermal sensitivity variation trend in Ni/4H-SiC Schottky diode temperature sensors. *J Vac Sci Technol B, Nanotechnol Microelectron Mater Process Meas Phenom* 33(5):052207. <https://doi.org/10.1116/1.4929890>
13. Kumar V et al (2020) Electronic transport in epitaxial 4H-SiC based Schottky diodes modified selectively by swift heavy ions. *Mater Sci Semicond Process* 115:105108. <https://doi.org/10.1016/j.mssp.2020.105108>
14. Kumar V et al (2020) Epitaxial 4H-SiC based Schottky diode temperature sensors in ultra-low current range. *Vacuum* 182:109590. <https://doi.org/10.1016/j.vacuum.2020.109590>
15. Kumar V et al (2020) Interface improvement of epitaxial 4H-SiC based Schottky diodes by selective heavy ion irradiation. *Appl Nanosci*. <https://doi.org/10.1007/s13204-020-01608-3>
16. Kumar V et al (2021) Interfacial and structural analysis of MeV heavy ion irradiated SiC. *Appl Nanosci*. <https://doi.org/10.1007/s13204-021-01921-5>
17. Kumar V et al (2013) Selective SHI irradiation for mesa type edge termination in semiconductor planar junction. *J Phys Conf Ser* 423:012057. <https://doi.org/10.1088/1742-6596/423/1/012057>
18. Kumar V et al (2012) Simulation based analysis of temperature effect on breakdown voltage of ion implanted Co/n-Si Schottky diode. *J Nano-Electron Phys* 4(4):04009. <http://essuir.sumdu.edu.ua/handle/123456789/30266>
19. Kumar V et al (2018) Tailoring surface and electrical properties of Ni/4H-nSiC Schottky barrier diodes via selective swift heavy ion irradiation. *Phys Status Solid* 215(5):1700555. <https://doi.org/10.1002/pssa.201700555>
20. Kumar V, Maan AS (2018) Improvement in reverse bias leakage current of Ni/4H-nSiC Schottky barrier diodes via MeV selective ion irradiation. *IOP Conf Ser Mater Sci Eng* 331:012016. <https://doi.org/10.1088/1757-899X/331/1/012016>
21. Liu Y et al (2019) Design and characterization of the deep-trench, U-shaped field-plate edge termination for 1200-V-class SiC devices. *IEEE Trans Electron Dev* 66(10):4251–4257. <https://doi.org/10.1109/TED.2019.2931638>
22. Mahajan A, Skromme BJ (2005) Design and optimization of junction termination extension (JTE) for 4H-SiC high voltage Schottky diodes. *Solid State Electron* 49(6):945–955. <https://doi.org/10.1016/j.sse.2005.03.020>
23. Millan J et al (2014) A survey of wide bandgap power semiconductor devices. *IEEE Trans Power Electron* 29(5):2155–2163. <https://doi.org/10.1109/TPEL.2013.2268900>
24. Mishra UK et al (2008) GaN-based RF power devices and amplifiers. *Proc IEEE* 96(2):287–305. <https://doi.org/10.1109/JPROC.2007.911060>
25. Oh S et al (2017) Electrical characteristics of vertical Ni/ β -Ga₂O₃ Schottky barrier diodes at high temperatures. *ECS J Solid State Sci Technol* 6(2):Q3022–Q3025. <https://doi.org/10.1149/2.0041702jss>
26. Onose H et al (2000) Over 2000 V FLR termination technologies for SiC high voltage devices. In: *IEEE international symposium on power semiconductor devices and ICs (ISPSD)*. IEEE, pp 245–248. <https://doi.org/10.1109/ispsd.2000.856817>
27. Pérez R et al (2005) Planar edge termination design and technology considerations for 1.7-kV 4H-SiC PiN diodes. *IEEE Trans Electron Dev* 52(10):2309–2316. <https://doi.org/10.1109/TED.2005.856805>
28. Rodr REZ (2005) Planar edge terminations and related manufacturing process technology for high power 4H-SiC diodes. *Process Technol*
29. Sasaki K et al (2017) First demonstration of Ga₂O₃ trench MOS-type Schottky barrier diodes. *IEEE Electron Dev Lett* 38(6):783–785. <https://doi.org/10.1109/LED.2017.2696986>

30. Sheridan DC et al (2000) Design and fabrication of planar guard ring termination for high-voltage SiC diodes. *Solid State Electron* 44(8):1367–1372. [https://doi.org/10.1016/S0038-1101\(00\)00081-2](https://doi.org/10.1016/S0038-1101(00)00081-2)
31. Singh R (2006) Reliability and performance limitations in SiC power devices. *Microelectron Reliab* 46(5–6):713–730. <https://doi.org/10.1016/j.microrel.2005.10.013>
32. Théolier L et al (2009) A new junction termination using a deep trench filled with BenzoCycloButene. *IEEE Electron Device Lett* 30(6):687–689. <https://doi.org/10.1109/LED.2009.2020348>
33. Tsao JY et al (2018) Ultrawide-bandgap semiconductors: research opportunities and challenges. *Adv Electron Mater* 4(1):1600501. <https://doi.org/10.1002/aelm.201600501>
34. Ueda T (2019) GaN power devices: current status and future challenges. *Jpn J Appl Phys* 58:SC0804. <https://doi.org/10.7567/1347-4065/AB12C9>
35. Verma J et al (2022) Trench termination in Ga₂O₃-based power device: a simulation-based study. *Appl Nanosci*. <https://doi.org/10.1007/s13204-021-02219-2>
36. Wang H et al (2018) Trench termination with SiO₂-encapsulated dielectric for near-ideal breakdown voltage in 4H-SiC devices. *IEEE Electron Device Lett* 39(12):1900–1903. <https://doi.org/10.1109/LED.2018.2874471>
37. Yang J et al (2017) High breakdown voltage (-201) β-Ga₂O₃ schottky rectifiers. *IEEE Electron Dev Lett* 38(7):906–909. <https://doi.org/10.1109/LED.2017.2703609>
38. Zhao JH et al (2003) Demonstration of the first 10-kV 4H-SiC Schottky barrier diodes. *IEEE Electron Device Lett* 24(6):402–404. <https://doi.org/10.1109/LED.2003.813370>

A Brief Review on the Barriers of Electric Vehicle Adoption and Present Scenario in India



Satyaki Biswas, Sadasiva Behera, and Nalin B. Dev Choudhury

Abstract Transportation is one of the most energy-intensive businesses in any nation. Because of carbon emissions, fossil fuel use, and other difficulties, the transportation industry is transitioning from IC engine-powered cars to electric vehicles (EV). EVs are eco-friendly and renewable energy technology that may provide an efficient transportation system without a catastrophic impact on natural resources. Despite government incentives, client demand isn't rising. This suggests impediments to EV adoption. The review discusses an overview of electric cars, varieties of EVs, charging methods, challenges to mainstream EV adoption, the EV sector in India, and the future potential of EVs in Indian markets.

Keywords Electric and hybrid vehicles · Renewable and sustainable energy · Policies · Power management

1 Introduction

Global warming, climate change, and the energy crisis are the greatest threats to humanity and the planet. CO₂ emissions are one of the key causes of catastrophic climate change, which threatens species' survival. This crisis must be mitigated [1]. Minimal fossil fuel usage for electricity generation, lowering energy consumption, and conserving carbon sequestration. According to the International Energy Agency (IEA), transportation will account for 50% or more of global greenhouse gas (GHG) emissions by 2030. To reduce GHG, the UN council voted in 2015 to establish

S. Biswas (✉) · S. Behera · N. B. D. Choudhury
Department of Electrical Engineering, National Institute of Technology Silchar, Silchar,
Assam 788010, India
e-mail: biswassatyaki9@gmail.com

S. Behera
e-mail: mail2sadasiv@gmail.com

N. B. D. Choudhury
e-mail: nalin@ee.nits.ac.in

“sustainable development objectives” by 2030. Transportation and energy usage are expanding globally. EVs are the only sustainable transportation choice. Only China, Europe, and the U.S. exhibit substantial EV sales increases. EVs are accessible, yet most people purchase and drive fossil fuel-powered cars. India produced 3202 million metric tons of CO₂ equivalent, 6.55% of world greenhouse emissions [2]. India ranked 3rd for CO₂ emissions in 2018 [3]. The rapidly developing vehicle market in India opens a major potential for the EV sector and ensures energy security, minimizes GHG emissions, and reduces import dependence. Despite the Indian government’s efforts to encourage EVs, popular acceptance is minimal. According to India’s energy projection, just 4,000 electric automobiles were sold in 2019, which is low; nevertheless, E-rickshaw sales have surged in recent years [4–7]. This data shows that it is urgent to identify the barriers to the prosperity of the electric vehicle market in India.

The Objectives of this study are as follows:

- Identifying the barriers to mainstream EV adoption.
- Discussing Indian policies and the present scenario of the EV market in India and the future directions.

Furthermore, the present paper has been arranged as follows. Generally, Sect. 2 illustrates a brief overview of electrical vehicles. In Sect. 3, types of electric vehicles have been discussed. In Sect. 5, the different methods of charging electric vehicles are illustrated briefly. Then, in Sect. 6, types of barriers to mainstream EV adoption are discussed. Finally, Sect. 7 illustrates the present electric vehicle scenario in India, and Sect. 8 concludes our findings.

2 A Brief Overview of Electrical Vehicles

Electric motors are more energy-efficient than Internal-combustion engines (ICEs). Electric motors use 90–95% of input energy to power the engine of the vehicle. Electric vehicles are dependent on batteries to store energy for powering the motors. EVs are primarily an eco-friendly option over conventional vehicles (CVs), because of the recharging system and less emission. The main key parts of an electric vehicle are—the battery, charging port, charger, DC/DC converter, drive system, regenerative braking, and power-electronics controller. Despite being expensive; usually, lithium-ion batteries are used in EVs, because of their better efficiency and lightweight. The main role of the charger is to receive an AC power supply through the charging port and convert it into DC for charging the lithium-ion battery. This charger device maintains the voltage, current, and temperature during the charging. The main purpose of the drive system is to transfer the mechanical energy to the wheel to move the vehicle. There are some differences between models according to design. For example, some designs assign small multiple motors for supplying power to each wheel individually, while some models are assigned a larger electric motor. Usually, EVs are assembled of simpler components, compared to conventional ICE vehicles [8]. The function of

the DC/DC converter is to convert the high voltage DC to low voltage DC to run the accessories of the car. The speed of the EVs is controlled by the power-electronics controllers by controlling the energy supply to the motors. Regenerative braking is a very efficient energy-saving technique in EVs. When the brakes are pressed or the car is decelerating, the kinetic energy converts into electrical energy and is sent back to the battery. Regenerative braking is widely adopted now for all kinds of EVs, because of its energy savings efficiency. Though it is unable to recharge the EV battery fully, it saves almost 15% of energy. Despite being noiseless, and eco-friendly; EVs would not run much faster than gasoline-powered vehicles run [9].

3 Types of Electric Vehicles

The market for electric vehicles is growing all over the world. There are three types of electric vehicles, based on the energy source of the engine, namely,

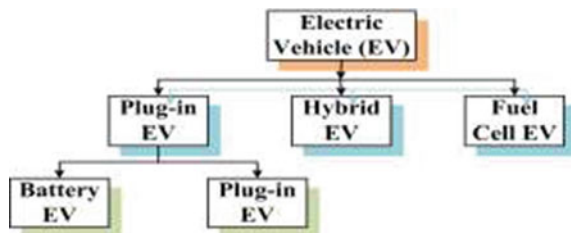
- (a) Plug-in electric vehicles (PEVs).
- (b) Hybrid electric vehicles (HEVs).
- (c) Fuel cell electric vehicles (FCEVs).

HEVs are a combination of an electric propulsion system with an internal combustion engine, which provides better drive range, better fuel economy, and low emissions than conventional ICE vehicles. There are no charging ports in HEVs. Therefore HEVs cannot be recharged from the outside of the system. Batteries of HEVs only can be charged from the IC engine or the speed of the wheel [7–9].

Fuel cell electric vehicles are usually operated on the electric propulsion system, but instead of the battery, the systems are powered by fuel cells or a combination of battery and supercapacitors.

The plug-in electric vehicles are of two types, namely: Battery electric vehicles (BEVs), and plug-in hybrid electric vehicles (PHEVs). BEVs are fully dependent on rechargeable batteries, while PHEVs are primarily running on rechargeable batteries, but can be run on IC engines for long-distance drives when the batteries get discharged. Figure 1 shows the classification of the types of EVs.

Fig. 1 Electric vehicle types



4 Types of Charging Methods of Electric Vehicles

There are mainly 3 types of charging methods: battery exchange, wireless charging, and conductive charging. Conductive charging is of two types: pantograph charging and overnight charging. Figure 2 shows the different types of electric vehicle charging methods.

4.1 Battery Exchange or Battery Swap Station

The consumer has to pay rent to the Battery Swap Station (BSS) owner for the batteries. Usually, BSS infrastructure provides slow charging methods, which will lead to a long life cycle of the battery [10]. This kind of battery swap station is ideally powered by renewable energy sources, like local solar or wind power generating units [11] however the batteries kept in stations can be utilized for Vehicle to Grid (V2G) technology [12].

Generally, the owner of the BSS owns the battery and can charge a high rate of rent for the battery, which can be very costlier in the long run for EV owners. But due to this system, the consumer can avoid huge initial investments in expensive batteries. This system requires a massive initial investment because of several batteries requirement, as well as a real estate area in an appropriate venue that is near high traffic area or city area. This system may require many models of batteries because the consumers would have different battery models [13, 14].

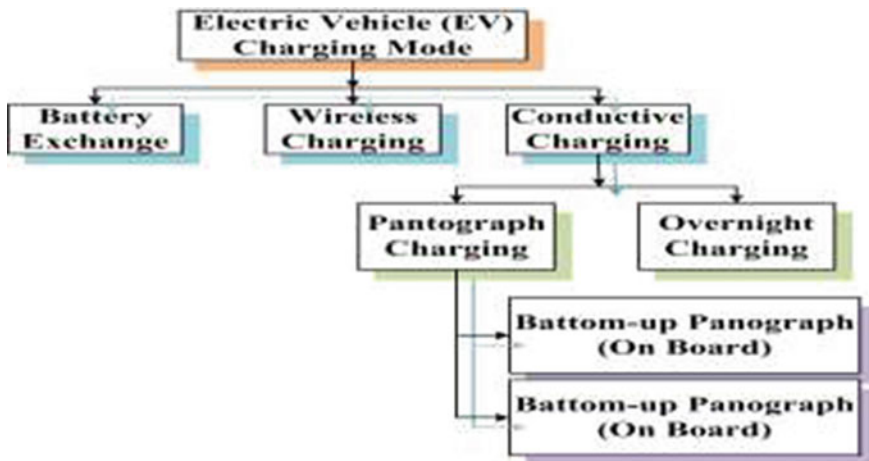


Fig. 2 Types of charging methods for electric vehicles

4.2 Wireless Battery Charging

Wireless charging is based on wireless power transfer. Electromagnetic induction between two coils is the fundamental theory of this technology. Primary coils are placed on the surface of the road and the secondary coils are placed inside the vehicle. But the distance between two coils must be between 20 and 100 cm for efficient power transfer. Though this system does not require a standard connector, they require a standard coupling technology. Though wireless power transmission (WPT) is generally weak and has high chances of eddy current loss, still, this technology is getting attention to implement in EVs, due to its convenience [15, 16].

4.3 Conductive Charging

Several levels 1, 2, and 3 conductive charging are common. Public charging stations use levels 2 and 3. Section V's topic. Voltage variation, dependability difficulties, and power loss can result from level 3 charging [17].

1. **Overnight Depot Charging:** These facilities are designed for overnight charging. Overnight charging facilities are preferable for slow charging, which will have less impact on the distribution grid [18].
2. **Pantograph Charging:** Pantograph charging is faster for larger batteries. This charging method is good for swiftly charging batteries in electric buses and trucks. This strategy minimizes the bus's initial cost by requiring less battery investment. Creating a pantograph charging infrastructure is expensive [19, 20]. Pantograph charging is of two types; a) top-down pantograph and b) bottom-up pantograph.
 - (a) **Top-Down Pantograph:** In this technique, a charging setup is put on the car's roof, and the pantograph charges the battery from above. This is a top-down off-board pantograph.
 - (b) **Bottom-Up Pantograph:** This method has the charging equipment inside the car. A pantograph connects the vehicle's roof to an overhead contact line. On-board bottom-up pantograph [21].

5 Charging and Discharging of Batteries

Battery life depends on how often it's charged and discharged. To increase a battery's lifespan, it shouldn't be overcharged. Renewable energy is uncertain. With a renewable energy producing system, the question is when and how to charge the battery for maximum vitality and longevity. Excess electricity should charge the battery, and vice versa. Choosing between charging and draining the battery is difficult. In the results and analysis portion of this model, a fuzzy control method is used to

tackle this issue. The smooth functioning of bidirectional power (load power and additional power injected into the grid), PI parameters, and fuzzy logic technique are set depending on battery SOC to improve energy management.

6 Types of Barriers to Influence of EV Adoption

Barriers to EV adoption in India can be addressed from a range of viewpoints, including technical issues, policy issues, and a lack of infrastructure. These are discussed as followed.

6.1 Codes and Standardization

Standardization and norms in charging technology hinder quality serviceability, component manufacture, and consociate technologies. This raises problems regarding robustness, performance, and safety. Some industrialized nations have charging infrastructure standards, such as Combined Charging System (CCS) in Europe, the USA, and Korea, Guobiao in China, and CHAdeMO in Japan. India has its own standard, “Bharat,” but it’s not deployed yet [22–24].

6.2 Recharge Time

Usually, batteries of EVs need a long time duration for charging; and they cover less distance compared to conventional ICE vehicles. They can’t be recharged en route because of a lack of recharging stations, especially in India, till now. Those factors are making a barrier to the mainstream adoption of EVs [25–28]. In India, the government trying to grow the EV Conductive infrastructure. There are 3 kinds of conductive charging facilities [29], which details demonstrations are shown in Table 1.

Table 1 Types of charging methods, ratings, and uses

Types of charging	Ac/dc, voltage	Takes time for a single charge (min)	Can run with a single full charge (km)	For places
Level 1	120 v AC	480	120–130	Home/workplace
Level 2	240 v AC	240	120–130	Public places
DC fast	Convert AC into DC then charges batteries	30	145	Public places/ charging stations

6.3 Battery Range

Battery range is directly related to recharging time duration. Lithium-ion batteries are now dominating the EV market over lead-acid and nickel-metal batteries because of their efficiency difference. Consumers will not be interested in the battery range is only 100–200 km per single charge. Nowadays much higher battery range EVs are available, with a range of 250–400 km per single charge. Furthermore, HEVs and PHEVs are preferable over BEVs, for long trips, because of their fuel flexibility [28, 29].

6.4 Charging Infrastructure

Charging infrastructure is one of the most crucial parts of the mainstream adoption of EVs, in any place, especially in urban areas [30, 31]. Insufficient public charging stations or few charging stations far from consumers' houses, those factors decrease the interest of consumers in EVs [32]. Adequate public charging stations to charge batteries during off-peak hours when the tariff is comparatively lower is very required for the massive adoption of EVs, especially near highways, which is still not so adequate or in a nascent stage in India [33, 34].

6.5 Safety

EVs depend on battery energy, which raises safety concerns about overheating or overcharging. Modern EV batteries like lithium-ion store more energy, which increases the danger of explosion or fire due to electrical flow [35–40]. With age, lithium particles form dendrites on the battery's carbon anode. This raises the risk of overheating, shorting out, or failing. Several researchers are concerned about the safety of EVs since battery cells and control systems are closely tied to battery pack capacity and size [39, 40].

6.6 Lack of Awareness

Less awareness, and uncertainty about the merits of EVs over conventional vehicles, less expertise and familiarity with new technology, and less awareness of long-term financial benefits [41]. In the mainstream market, EV user experience and reviews are crucial [42]. Therefore, marketing, mass communication, personal communication, and education must include the newest technical knowledge for existing and future customers [43, 44].

6.7 High Cost

EVs cost substantially more than regular conventional vehicles (CVs). Even with incentives and subsidies, the cost of EVs is still much greater than CVS in many countries [45]. The initial investment is more important than fuel/running cost reductions for a new automobile buyer [46]. Studies demonstrate that purchasers choose high operating expenses over high EV purchase prices or premiums [47].

6.8 Limited Acceptance

India is a multi-cultural country with 1.4 billion people from different socio-economic backgrounds. Few customers know about environmental advantages [48]. High gasoline costs and incentives will motivate people to embrace EVs [49]. Few firms in India manufacture EVs. After ordering, buyers must wait weeks to 4 months [50]. Overall EV acceptance is poor owing to limited exposure, model and interior/exterior design alternatives, and other issues.

6.9 Sustainability of Fuel Sources

High demand and use of EVs will raise power consumption, and if the energy sources aren't renewable or sustainable, it may harm the environment. Coal-generated power for EVs is more environmentally harmful than gasoline or diesel [51]. Few researchers are worried about battery pollution [52]. Uncertainty over EV technology and batteries further hinders the EV industry.

6.9.1 Limitation of Resources

The basic ingredients for li-ion batteries (lithium, cobalt, and nickel) are not widely accessible. 70% of the world's cobalt is produced in the DRC [53]. Lithium deposition has been projected worldwide [54]. India has little lithium reserves. The mining and extractive industries have a negative reputation for breaching human rights and environmental safety [55]. These reasons will hinder replacing most automobiles by 2030 with EVs.

6.9.2 Electric Grid

India is expanding its public charging infrastructure. India lacks fast home charging. Massive EV adoption will increase power consumption and stress the grid [47, 55].

Charging challenges will exist until a charging infrastructure is built with power quality, stable energy, and suitable load distribution.

6.9.3 Re-Sale Anxiety

Customers are not still so certain about the future value of the EV industry. Due to the lack of secondary market buyers are always having resale anxiety. Literature shows that buyers are not interested to pay high premiums, despite knowing the future savings by savings in fuel expenses, because of resale anxiety, purchasing cost, and battery charging-range problems [33–47, 50, 56].

6.9.4 Government Policies

India launches two innovative policies for replacing ICE engine-based vehicles. There are one under the National Electric Mobility Mission Plan (NEMMP) 2020 and “Faster Adoption and Manufacturing of (Hybrid &) Electric Vehicles Phase-II” (FAME II) on 1 April 2019. The outcomes of these policies [37] have enacted various rules, customer interest and acceptance remain low, which is reflected in sales [54, 56] with less or no GST on LI-ion batteries and incentives.

7 Present Electric Vehicle Scenario in India

India’s quick development and expanding demand make it a potential EV market. Indian EV sales are small. India sold 2,000 EVs per year from 2019 to 2020 [54]. 100% EV sales by 2030 [55]. Indians are limited. 2001’s “Reva” was made by Mahindra Electric Mobility Limited. 2010 saw Toyota’s Prius debut. 2013 Toyota “Camry” India offers these upgraded automobiles. Electricity powers today’s buses. India’s central and state governments promote electric autos and public transportation. The Delhi government wanted to convert 25% of cars to EVs in 2018 by offering incentives and creating charging stations. This initiative sought to build a charging station every 3 km by 2023 and exempt EVs from road tax, parking fees, and registration fees. New Delhi’s government launched a 2020 electric vehicle strategy. New Delhi’s 131 eV charging stations. Telangana has eliminated EV road tax. Telangana has a 10-year plan to promote EVs and attract \$4 billion in investment. Telangana announced INR 6 per kWh for charging EVs (TSERC). Hyderabad is switching from diesel to electric buses. Hyderabad Metro Rail and Power Grid Corporation of India Limited partner to install EV charging stations [56]. Magenta Power installs EV charging stations on Navi-Mumbai and Mumbai-Pune. BMT has electric buses. Electric buses serve Kolkata. 5000 electric buses will be in West Bengal by 2030. Saving 782,560 tons of carbon annually [57].

8 Conclusion

As per the proper review, we found that EVs provide eco-friendly mobility but are more expensive than ICE vehicles. EVs may reduce conventional oil use and boost production, which will benefit purchasers and society long-term. This article provides a full summary of the literature, various kinds of EVs, charging techniques, and the key challenges to EV adoption in India. So this article examines the present EV industry, initiatives, and subsidies offered by national and state governments in India. Which can offer methods and suggestions for EV manufacturers, legislators, and other stakeholders.

References

1. Doucette RT, McCulloch MD (2011) Modeling the prospects of plug-in hybrid electric vehicles to reduce CO₂ emissions. *Appl Energy* 88(7):2315–2323
2. Greenhouse gas emissions factsheet: India. Climatelinks.org. [Online]. Available: <https://www.climatelinks.org/resources/greenhouse-gas-emissions-factsheet-india>
3. Environment I, Shalender K, Sharma N (2021) Using extended theory of planned behaviour (TPB) to predict adoption intention of electric vehicles in. *Develop Sustain* 23(1):665–681
4. Gautam AK, Tariq M, Pandey JP, Verma KS (2022) Optimal power management strategy by using fuzzy logic controller for BLDC motor-driven E-rickshaw. *J Intell Fuzzy Syst* 42(2):1089–1098
5. Das PK, Bhat MY (2022) Global electric vehicle adoption: implementation and policy implications for India. *Environ Sci Pollut Res Int* 29(27):40612–40622
6. Axsen J, Kurani KS (2010) Anticipating plug-in hybrid vehicle energy impacts in California: constructing consumer-informed recharge profiles. *Transp Res D Transp Environ* 15(4):212–219
7. Goel S, Sharma R, Rathore AK (2021) A review on barrier and challenges of electric vehicle in India and vehicle to grid optimisation. *Transp Eng* 4(100057):100057
8. Ahmad A, Khan ZA, Saad Alam M, Khateeb S (2018) A review of the electric vehicle charging techniques, standards, progression and evolution of EV technologies in Germany. *Smart Sci* 6(1):36–53
9. Gschwendtner C, Sinsel SR, Stephan A (2021) Vehicle-to-X (V2X) implementation: an overview of predominate trial configurations and technical, social and regulatory challenges. *Renew Sustain Energy Rev* 145:110977
10. Brenna M, Foiadelli F, Zaninelli D, Graditi G, Di Somma M (2021) The integration of electric vehicles in smart distribution grids with other distributed resources. In: *Distributed energy resources in local integrated energy systems*. Elsevier, pp 315–345
11. Erdinc O, Tascikaraoglu A, Paterakis NG, Dursun I, Sinim MC, Catalao JPS (2018) Comprehensive optimization model for sizing and siting of DG units, EV charging stations, and energy storage systems. *IEEE Trans Smart Grid* 9(4):3871–3882
12. Sanguesa JA, Torres-Sanz V, Garrido P, Martinez FJ, Marquez-Barja JM (2021) A review on electric vehicles: technologies and challenges. *Smart Cities* 4(1):372–404
13. Chowdhury SR (2021) A three-phase overlapping winding based wireless charging system for transportation applications. Doctoral dissertation
14. Patil D, McDonough MK, Miller JM, Fahimi B, Balsara PT (2018) Wireless power transfer for vehicular applications: overview and challenges. *IEEE Trans Transp Electr* 4(1):3–37
15. Arif SM, Lie TT, Seet BC, Ahsan SM, Khan HA (2020) Plug-in electric bus depot charging with PV and ESS and their impact on LV feeder. *Energies* 13(9):2139

16. Arif SM, Lie TT, Seet BC, Ayyadi S (2021) A novel and cost-efficient energy management system for plug-in electric bus charging depot owners. *Electric Power Syst Res* 199:107413
17. Meishner F, Satvat B, Sauer DU (2017) Battery electric buses in European cities: economic comparison of different technological concepts based on actual demonstrations. In: 2017 IEEE vehicle power and propulsion conference (VPPC)
18. Carrilero I, González M, Anseán D, Viera JC, Chacón J, Pereirinha PG (2018) Redesigning European public transport: impact of new battery technologies in the design of electric bus fleets. *Transp Res Procedia* 33:195–202
19. Tarei PK, Chand P, Gupta H (2021) Barriers to the adoption of electric vehicles: evidence from India. *J Clean Prod* 291:125847
20. Haddadian G, Khodayar M, Shahidehpour M (2015) Accelerating the global adoption of electric vehicles: barriers and drivers. *Electr J* 28(10):53–68
21. Kim M-K, Park J-H, Kim K, Park B (2020) Identifying factors influencing the slow market diffusion of electric vehicles in Korea. *Transportation (Amst)* 47(2):663–688
22. Egbue O, Long S (2012) Barriers to widespread adoption of electric vehicles: an analysis of consumer attitudes and perceptions. *Energy Policy* 48:717–729
23. Alkhalisi AF (2020) Creating a qualitative typology of electric vehicle driving: EV journey-making mapped in a chronological framework. *Transp Res Part F Traffic Psychol Behav* 69:159–186
24. Javid RJ, Nejat A (2017) A comprehensive model of regional electric vehicle adoption and penetration. *Transp Policy (Oxf)* 54:30–42
25. Bullis K (2013) How improved batteries will make electric vehicles competitive. *Technol Rev* 116(1):19–20
26. She Z-Y, Sun Q, Ma J-J, Xie B-C (2017) What are the barriers to widespread adoption of battery electric vehicles? A survey of public perception in Tianjin, China. *Transp Policy (Oxf)* 56:29–40
27. Nocera S, Cavallaro F (2016) The competitiveness of alternative transport fuels for CO₂ emissions. *Transp Policy (Oxf)* 50:1–14
28. Haider SW, Zhuang G, Ali S (2019) Identifying and bridging the attitude-behavior gap in sustainable transportation adoption. *J Ambient Intell Humaniz Comput* 10(9):3723–3738
29. Aayog N (2021) Mobilising finance for EVs in India: a toolkit of solutions to mitigate risks and address market barriers. <https://rmi.org/people/niti-aayog/>
30. Ramboll D (2016) Clean transport-support to the member states for the implementation of the directive on the deployment of alternative fuels infrastructure: good practice examples. European Commission
31. Kalhammer FR, Kopf BM, Swan DH, Roan VP, Walsh MP (2007) Status and prospects for zero emissions vehicle technology. Report ARB Independent Expert Panel 1(1):12–36
32. Rezvanianiani SM, Liu Z, Chen Y, Lee J (2014) Review and recent advances in battery health monitoring and prognostics technologies for electric vehicle (EV) safety and mobility. *J Power Sources* 256:110–124
33. Goel P, Sharma N, Mathiyazhagan K, Vimal KEK (2021) Government is trying but consumers are not buying: a barrier analysis for electric vehicle sales in India. *Sustain Prod Consum* 28:71–90
34. Wikström M, Hansson L, Alvfors P (2016) Investigating barriers for plug-in electric vehicle deployment in fleets. *Transp Res D Transp Environ* 49:59–67
35. Sun P, Bisschop R, Niu H, Huang X (2020) A review of battery fires in electric vehicles. *Fire Technol* 56(4):1361–1410
36. Wang B, Dehghanian P, Wang S, Mitolo M (2019) Electrical safety considerations in large-scale electric vehicle charging stations. *IEEE Trans Ind Appl* 55(6):6603–6612
37. Jin L, Slowik P (2017) Literature review of electric vehicle consumer awareness and outreach. ICCT, Washington, DC
38. Berkeley N, Bailey D, Jones A, Jarvis D (2017) Assessing the transition towards battery electric vehicles: a multi-level perspective on drivers of, and barriers to, take up. *Transp Res Part A Policy Pract* 106:320–332

39. Menon A, Yang Z, Bandivadekar A (2019) Electric vehicle guidebook for Indian states
40. https://theicct.org/sites/default/files/publications/India_EV_State_Guidebook. The international council on clean transportation
41. Larson PD, Viáfara J, Parsons RV, Elias A (2014) Consumer attitudes about electric cars: pricing analysis and policy implications. *Transp Res Part A Policy Pract* 69:299–314
42. Roche MY, Mourato S, Fischedick M, Pietzner K, Viebahn P (2010) Public attitudes towards and demand for hydrogen and fuel cell vehicles: a review of the evidence and methodological implications. *Energy Policy* 38(10):5301–5310
43. Spurlock CA et al (2019) Describing the users: understanding adoption of and interest in shared, electrified, and automated transportation in the San Francisco Bay Area. *Transp Res D Transp Environ* 71:283–301
44. Matthews L, Lynes J, Riemer M, Del Matto T, Cloet N (2017) Do we have a car for you? Encouraging the uptake of electric vehicles at point of sale. *Energy Policy* 100:79–88
45. Nimesh V, Sharma D, Reddy VM, Goswami AK (2020) Implication viability assessment of shift to electric vehicles for present power generation scenario of India. *Energy (Oxf)* 195:116976
46. Cusenza MA, Bobba S, Ardente F, Cellura M, Di Persio F (2019) Energy and environmental assessment of a traction lithium-ion battery pack for plug-in hybrid electric vehicles. *J Clean Prod* 215:634–649
47. Democratic Republic of Congo (2016) ‘This is what we die for’: human rights abuses in the Democratic Republic of the Congo power the global trade in cobalt. Amnesty International, 19 Jan 2016. [Online]. Available: <http://www.amnesty.org/en/documents/afr62/3183/2016/en>
48. Electric vehicle batteries. Union of Concerned Scientists. [Online]. Available: <https://www.ucsusa.org/resources/ev-battery-recycling>
49. Vassileva I, Campillo J (2017) Adoption barriers for electric vehicles: experiences from early adopters in Sweden. *Energy (Oxf)* 120:632–641
50. Finn P, Fitzpatrick C, Connolly D (2012) Demand side management of electric car charging: benefits for consumer and grid. *Energy (Oxf)* 42(1):358–363
51. Movesummit.in. [Online]. Available: http://movesummit.in/files/EV_report.pdf. Accessed: 2018
52. Davidov S, Pantoš M (2017) Planning of electric vehicle infrastructure based on charging reliability and quality of service. *Energy (Oxf)* 118:1156–1167
53. Kumar RR, Alok K (2020) Adoption of electric vehicle: a literature review and prospects for sustainability. *J Clean Prod* 253:119911
54. Lim MK, Mak H-Y, Rong Y (2015) Toward mass adoption of electric vehicles: impact of the range and resale anxieties. *Manuf Serv Oper Manag* 17(1):101–119
55. Bjerkan KY, Nørbech TE, Nordtømme ME (2016) Incentives for promoting Battery Electric Vehicle (BEV) adoption in Norway. *Transp Res D Transp Environ* 43:169–180
56. Sahoo D, Harichandan S, Kar SK, Sreejesh SK (2022) An empirical study on consumer motives and attitude towards adoption of electric vehicles in India: policy implications for stakeholders. *Energy Policy* 165:112941
57. Abdel-Majeed MS et al (2022) A three-phase non-isolated pseudo six-phase-based integrated onboard battery charger for electric vehicles. *IEEE Trans Transp Electrification*. <https://doi.org/10.1109/TTE.2022.3191250>

Simulation of Battery Management System for Protection in Electric Vehicle Against the Battery Failures



Sachin Paliwal , Amandeep Gill, and Manjeet Singh

Abstract The developed industries are heading toward the success path, where every industry researches and develops new gadgets to make day-to-day life more reliable and accessible. It can also be said that changes and developments in life bring positive merits with some negative merits too. Similarly, observing the automotive industry, it can be easily noticed how hard these industries have worked for a long time. Bringing the internal combustion engine to market and efficiently using available fuel was a good achievement. However, due to the increase in air and noise pollution rate from internal combustion engine vehicles, hybrid electric vehicles were developed by using both conventional fuel and electricity, which has drastically decreased air and noise pollution but could not reduce it to zero. So, after hybrid electric vehicles, electric vehicles are developed which are working on batteries. The main merits points of electric vehicles are that it doesn't cause any harm to the environment, have less maintenance cost, and have high reliability. The de-merits are chances of battery failure or cells used, which leads to fire hazards. As it's not easy to handle batteries if it fails, and the results can be dangerous. This paper will define the basic idea of what a battery is, the types of batteries, how batteries fail, the consequences of the battery failure, and the battery management system and thermal protection method. The battery management system is simulated in MATLAB to take care of the battery for complete protection as it will protect the battery from overvoltage, undervoltage, and temperature rise.

Keywords Battery management system · Battery · Battery failure · Battery protection

S. Paliwal · A. Gill (✉) · M. Singh
Vivekananda Global University, Jaipur, Rajasthan 303012, India
e-mail: aamangill.87@gmail.com

1 Introduction

Energy generation was generally dependent on fossil fuels and various renewable energy sources. The energy demand is increasing daily due to population and industrial development, and providing energy instantly and efficiently after the generation from grids was difficult [1]. Many problems and challenges have arisen for the operators in the smart grids, such as the increase in the frequency variation, reduction in the transient voltage, reliability, and decrease in power quality due to the high penetration of unreliable and unbalanced Renewable Energy sources [2]. These issues were a significant concern, and the solution was to separate energy generation from energy demand. This was possible when the Energy Storage System (ESS) approach was adopted with auxiliary facilities. In ESS, the vital role was played by the battery energy storage system. The invention of the battery was in 1859 by Gaston Planté of France [3]. The battery was the device that had several advantages, which are as follows:

- Long-life cycle.
- High abilities to charge and discharge rates.
- Storage size.
- Rate of discharging.
- A small amount of conditions maintenance.
- Quick response.

Due to these advantages, the need for a battery is increasing, which adds one more merit point to it, i.e., the cost of batteries is cheaper [4].

Like the energy generating industry, the automotive industry is now using batteries. Earlier, the batteries used in the vehicle were to provide energy to the small component installed in the vehicle, for example, the lights, media player, etc. With such good reliability, it has been used in electric vehicles as a good source [5]. Installing the batteries in a vehicle reduces air and noise pollution increases the vehicle's efficiency with techniques like regenerative braking, and reduces the dependency on non-renewable fuels like petrol, diesel, and CNG [6]. Such a development has made a significant impact on industries. Then there are still some loopholes where batteries are lagging, have issues to resolve, and need to focus on development. This paper explains the battery, type of batteries, battery and cell failure reasons, and consequences of a battery failure. To all these concerns, the solution is provided by proposing two different types of BMS methods for the battery's protection. BMS is simulated in MATLAB to take care of the battery for complete protection as it will protect it from overvoltage, Undervoltage, and temperature rise.

2 Battery

Cells are the smallest electrochemical unit and deliver a voltage that depends on cell chemistry. There are two types of cells: primary (single use) and secondary (rechargeable). Batteries and battery packs are made up of a group of cells. When cells are wired either in series or in parallel or both forms a battery pack. For example, automotive 12 V lead-acid batteries comprise six 2 V cells in series. Sometimes connections can be external as per need. There are types of batteries according to efficiency, life cycle, voltage, charging, and discharging. The different battery types are differentiated. Still, the research is going on batteries for three more reliability, but these are types of batteries listed below, which are commonly used in an electric vehicle for energy purposes. Some examples are Lead-acid batteries, Lithium polymer, Lithium Phosphate, and Nickel Metal Hydride (NiMH) [7].

3 Reasons for Batteries Fail

There are several reasons listed below for which failure of batteries can be seen.

3.1 Cell Fault

When various cells are connected to form a battery package, and during that time, if a connection is not made correctly, then the chance of a short circuit getting maximum further explosion can happen. This generally happens during the installation process in vehicles.

3.2 Manufacturing Processes Out of Control

Suppose manufacturing companies do not follow the standard process and resulting in the making of cheaper quality of the battery. For example, the separator which is installed in between the electrodes works to isolate the positive and negative electrodes to avoid short circuits and self-discharge. So, during the making, if the used separator has defaulted, this could lead to battery failure.

3.3 Aging

During manufacturing, age limits are already defined. When a battery is regularly used, an electrode is due to continuous charging and discharging the reaction, so negative and positive electrodes get neutralized, and further, no reaction can occur. This generally occurs in public transport vehicles where vehicles continuously get charged and discharged with overworking.

3.4 Uncontrolled Operating Conditions

This includes overcharging and undercharging conditions. The operators already publish voltage limits on the battery. The damage from overcharging and undercharging can lead to a re or explosion. Example: if a PbA battery is not maintained at a high state of charge, lead sulfate deposits on both electrodes will begin to form hard crystals, which cannot be reconverted by a standard fixed voltage (13.6 V) battery charger [8].

3.5 Abuse

This includes battery handling. For example, if a battery while transport is not properly handled or stored, it is misplaced similarly to other components like overweighting and temperature, leading to overheating of battery cells and decreasing the battery's efficiency.

3.6 External Factors

This includes external source disturbances and load disturbances. If the battery is continuously having a disturbance in the discharging and charging process, that could affect electrode plates and lead to a breakdown of plates, and no other chemical reaction could take place and, as a result, battery failure.

3.7 Thermal Management

A battery always needs a specific temperature to be stored. For example, if a battery is used at high-temperature conditions, then the battery temperature cooling system should be used immediately. That system is known as a battery management system

(BMS), as every rated battery temperature rating may differ, and if it is not maintained correctly, the battery fails [9].

4 Reasons for Cell Failure

The reasons for cell failure are listed below.

4.1 Active Chemicals Exhausted

In a cell, chemical energy is converted into electrical energy. So, if an active chemical gets exhausted, it leads to cell failure.

4.2 Change in the Physical Structure of the Electrodes

When proper venting of cells is not done, it causes gassing (gas formation due to chemical reaction) in the cells and causes a reduction in capacity, leading to cell failure.

4.3 Breakdown of the Electrolyte

With normal chemical reactions, the electrolyte gets weaker, and no further reaction can occur, leading to cell failure.

4.4 Electrode Plating

In a lead-acid battery, the chance of electrode plates having corrosion is high, so if electrode plating is not done, no further reaction could occur, leading to cell failure.

4.5 Reduced Capacity

As already said, active chemicals get exhausted, and at one time, the capacity of cells also becomes reduced up to zero.

4.6 Increased Self-Discharge

After the decrease in capacity and increase in internal impedance, the cell starts losing its properties. Due to overcharging, one cell stops getting charged, and if it got charged, then gets discharged by itself.

4.7 Pressure Build-Up

Due to aging effects, the chemicals will exhaust, and pressure is created by the chemicals, i.e., excitation of an electron in the cell, and because of this, the cell will fail [10].

4.8 Overheating

While extended charging of battery the temperature rise is avoided, then that rise will affect the life of cell as well as plates of cell and will result in cell failure.

4.9 Undervoltages

When the batteries are not charged for a long time, the cell's voltage gets affected and will not give the proper, efficient voltage resulting in battery failure.

4.10 Overvoltage

When overvoltage is provided to cells, it affects their life cycle, and due to this, overheating issues can also occur, leading to cell failure [11].

5 Consequences of Cell Failure

If the battery and cells are a failure, then further various consequences can happen, and are listed below.

5.1 Open Circuit

In open-circuit conditions, the voltage expected to get can never be obtained.

5.2 Short Circuit

During connection, wires should be appropriately and tightly wired. If not, then the chance of a short circuit occurring are high.

5.3 Hard Short

Due to the electrode's corrosion, a permanent connection will exist.

5.4 Soft Short or Micro Short

Instead of a permanent connection, many small particles will form and get connected when in charging conditions.

5.5 Explosion or Fire

Storage thermal issues include a temperature rise, the chemical particle getting excited, and because of the explosion of the excited particle or re could happen [12].

6 Results

When considering battery protection, a device should consider the various protection features of the battery, which are as follows:

- Excessive current during charging or discharging.
- High ambient temperature
- Overvoltage—overcharging
- Abuse
- Undervoltage—exceeding preset depth of discharge (DOD) limits
- High ambient temperature

- Overheating—exceeding the cell temperature limit
- Pressure build-up inside the cell
- Polarity
- Short circuit
- System isolation in case of an accident

So, for the protection of the battery, the methods are.

6.1 Thermal Protection

When the battery is installed, it is impossible to sense the change in temperature or any damage because of temperature in cells without sensors, so for battery protection, different sensors are used, which are listed below.

Thermal Fuse

It is a physical material in the battery; whenever the temperature rises, the thermal fuse will break down so that no other process can occur.

Thermistor Fuse or Resettable Fuse

Working of both the component is the same, which is to detect the change in temperature in battery and breakdown, but the difference in both components is that in the thermal fuse while temperature changes it will get break down and will have to be replaced by a new whereas resettable fuse will get automatically recover once the normal temperature has occurred.

Temperature Sensor

When batteries are charged without checking voltage, and the battery is getting charged from overvoltage or undervoltage, the battery can get heated up, so to check that rise and protect the battery from rising temperature, a temperature sensor is used to protect it.

6.2 Simulation of Electronic Protection (Battery Management System)

This includes the protection of the battery through power electronic controllers, which is part of the Battery Management System. So, let's see how battery management protects charging and discharging. The below charging and discharging model is simulated using MATLAB Simulink. This model will help the user charge the battery automatically and also help know when the battery is low. The steps followed for the simulation of the BMS system are as follows:

NAME	VALUE
Modeling option	Uninstrumented No thermal port
▼ Main	
▼ Nominal voltage, Vnom	24 V
Configurability	Compile-time
Current directionality	Disabled
▼ Internal resistance	2 Ohm
Configurability	Compile-time
Battery charge capacity	Infinite

Fig. 1 Battery parameter

- In this model, a battery is taken whose nominal voltage is 24 V, internal resistance 2 Ω . Then taking the resistor as a load and parameter resistance value is $24/2 \Omega$, as shown in Fig. 1.
- Now the circuit is enabled, then take the MOSFET; there are two types of MOSFET. One is N-channel MOSFET, and the other is P-channel MOSFET. In the model, P-channel MOSFET is used for proper output.
- When connections are made, MOSFET will act as a relay and load and add resistor at the minimum value, i.e., resistance is 0.5 Ω . This connection is made because the circuit should be protected when reversed battery terminals.
- To check wheatear the connection is proper or not, add a voltage sensor at both at source and load.
- Similarly, for MOSFET polarity check voltage sensor is added to measure the voltage across the device.
- Now add the current sensor in between the load and source.
- Take PS-Simulink converter to connect the scope to voltage and the current sensor for the output graph.
- Before running the model, add the solver configuration because it's a simscape block model and the electrical reference ground to the model, as shown in Fig. 2.
- wo scopes are added; one will give the source voltage and MOSFET voltage graph, whereas the other Scope will provide the load voltage and load current with the Source voltage graph. So these two graphs are for comparison.

Case I When Battery is Connected with the Proper Terminals of a Battery

When the source (battery) positive is added and connected to the drain, then the current flow in a positive direction; this is due to P-channel MOSFET, and the drain will connect to the source(S) of MOSFET, and the circuit will act as a closed circuit by which load will receive the current.

When the model is run in MATLAB, there is two Scope connected to get the output graph where Scope 1 shows the Source voltage and MOSFET voltages graph, and Scope 2 shows the load current, load voltage, and source voltage. Figure 3 shows the Scope 1 output.

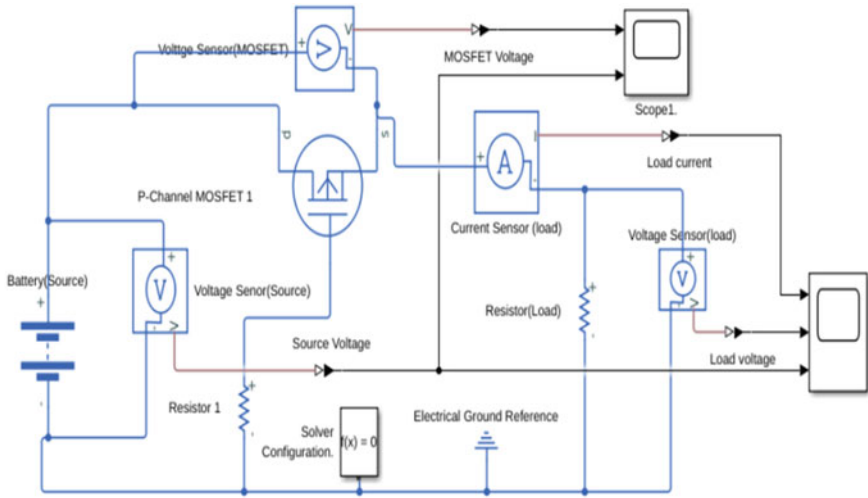


Fig. 2 Simulink model of battery management system

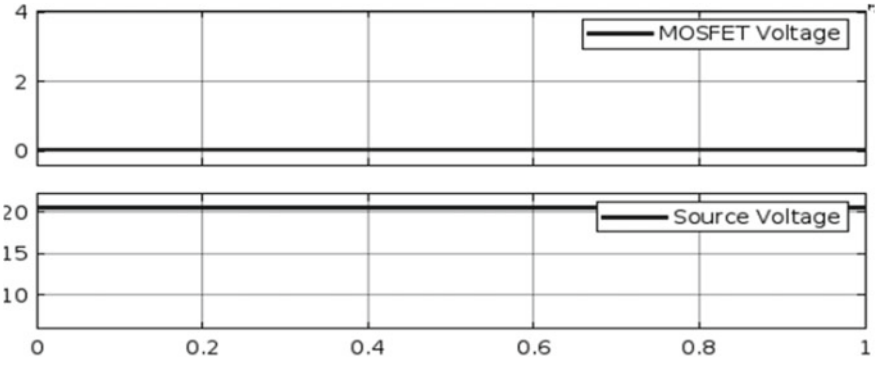


Fig. 3 Scope 1 output graph

In Fig. 4, Scope 2, it can be seen that the load receives the current where input voltage and output voltage both have the same value, which means the model is working and connected with proper terminals.

Case II When the Battery is Connected with Reverse Terminals of a Battery

When battery connections are reversed, as shown in Fig. 5, then the direction of flow of current will be in a reverse direction, and that current will flow from resistor 1 to the gate terminal of MOSFET, then drain (d terminal) will act as an open switch due to negative polarity the circuit will be open-circuit, and that leads to no flow of current to load.

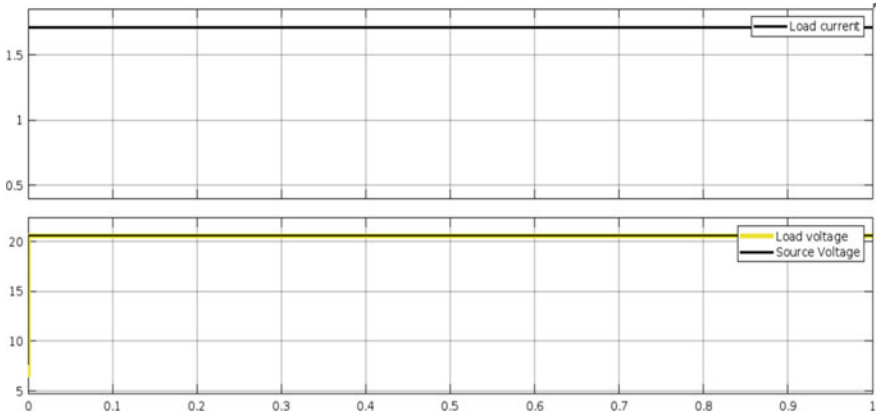


Fig. 4 Scope 2 output graph

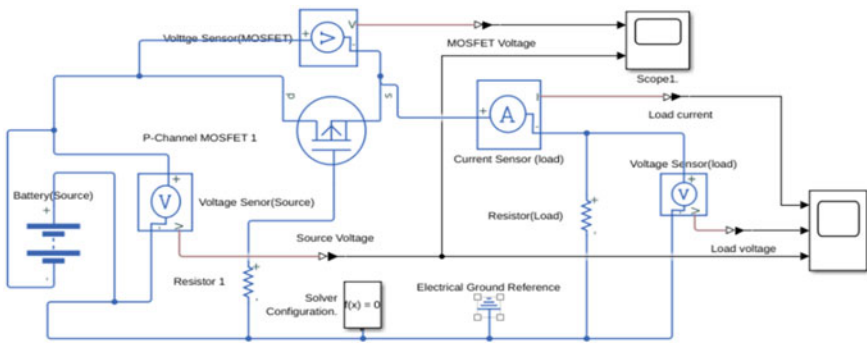


Fig. 5 Simulink model of battery management system with reverse connection

In this condition, the input voltage output has a value, whereas potential voltage across MOSFET can be seen in Fig. 6.

In Fig. 7, it is seen that the Source voltage and MOSFET voltage have a value negative which represents the reverse battery connection, whereas when Fig. 7 is seen then, it could be concluded that the circuit is an open-circuit as input voltage as the value where the output voltage is zero and also load does not receive current.

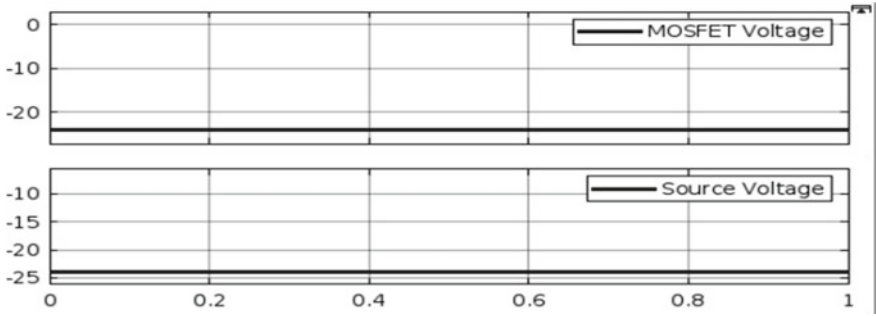


Fig. 6 Scope 1 output graph in case II

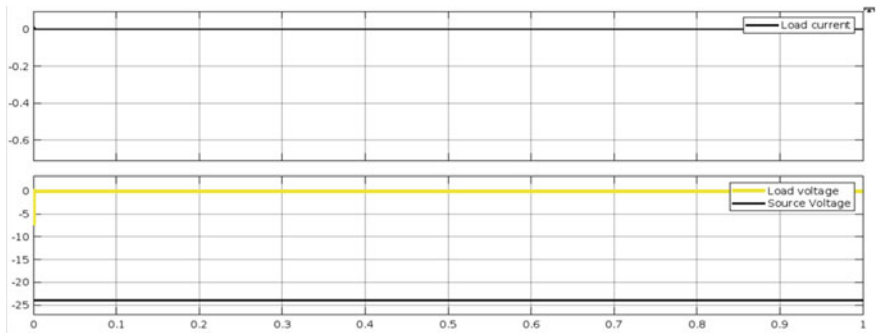


Fig. 7 Scope 2 output graph in case II

7 Conclusion

If the battery is handled with all the manual guidance, then the chance of the battery getting damaged becomes less. By following the rules in the manual, the battery life cycle and healthy backup of the battery are always longer. The proposed battery management system should be more so that it could take care of the battery with complete protection as it protects the battery from overvoltage to undervoltage, and by the rise in temperature also maintains the temperature of the battery between 25 and 27°.

References

1. Babatunde OM, Munda JL, Hamam Y (2019) A comprehensive state-of-the-art survey on power generation expansion planning with intermittent renewable energy source and energy storage. *Int J Energy Resour* 43(12):6078–6107
2. Yuwono YCH, Dewangga BR, Cahyadi AI, Herdjunto S (2018) Fault detection on the battery SOC-OCV by using observer. In: 4th international conference on science and technology (ICST), pp 1–4. <https://doi.org/10.1109/ICSTC.2018.8528607>
3. Khan N, Ullah FUM, Afran A, Ullah M, Lee Y, Baik SW (2021) Batteries state of health estimation via efficient neural networks with multiple channel charging profiles. *IEEE Access* 9:7797–7813. <https://doi.org/10.1109/ACCESS.2020.3047732>
4. Agrawal H, Talwariya A, Gill A, Singh A, Alyami H, Alosaimi W, Ortega-Mansilla A (2022) A fuzzy-genetic-based integration of renewable energy sources and e-vehicles. *Energie* 15(9):3300. <https://doi.org/10.3390/en15093300>
5. Gill A, Choudhary A, Bali H (2021) Renewable distributed generations optimal penetration in the distribution network for clean and green energy. *Asian J Water Environ Pollut* 18(2):37–43
6. Schweighofer B, Raab K, Bresseur G (2003) Modeling of high power automotive batteries by the use of an automated test system. *IEEE Trans Instrum Meas* 52(4):1087–1091. <https://doi.org/10.1109/TIM.2003.814827>
7. Kailong L, Kang L, Qiao P, Cheng Z (2018) A brief review on key technologies in the battery management system of electric vehicles. *Front Mech Eng* 14:47–64. <https://doi.org/10.1007/s11465-018-0516-8>
8. Orecchini F, Santiangeli A (2010) Automakers' powertrain options for hybrid and electric vehicles. *Electric Hybrid Veh* 22:579–636. <https://doi.org/10.1016/B978-0-444-53565-8.00022-1>
9. Nieuwenhuis P, Cipcigan L, Sonder HB (2020) The electric vehicle revolution. *Future Energy* 3:227–243. <https://doi.org/10.1016/B978-0-08-102886-5.00011-6>
10. Daniel DF (2010) Management of batteries for electric traction vehicles. *Electric Hybrid Veh* 19:493–515. <https://doi.org/10.1016/B978-0-444-53565-8.00019-1>
11. Tong S, Joseph HL, Park JW (2016) Battery state of charge estimation using a load-classifying neural network. *J Energy Storage* 7:236–243. <https://doi.org/10.1016/j.est.2016.07.002>
12. Kutkut NH, Wiegman HL, Divan DM, Novotny DW (1999) Design considerations for charge equalization of an electric vehicle battery system. *IEEE Trans Ind Appl* 35(1):28–35. <https://doi.org/10.1109/28.740842>

A Comparative Study of Deep Learning Methods for Short-Term Solar Radiation Forecasting



Praveen Kumar Singh, Amit Saraswat, Yogesh Gupta, Sunil Kumar Goyal, and Yeshpal Gupta

Abstract Energy and climate challenges have led to significant growth in solar power generation, and because of this, smart grids are increasingly utilizing solar power. The solar power is intermittent because solar energy is mainly dependent on radiation and other atmospheric factors. To ensure the reliable economic operation of micro grids and smart grids, precise forecasting of solar radiation is crucial. Deep learning techniques are proposed in this study to model the solar radiation production. Four artificial intelligence and deep learning-based forecasting models, the fully connected artificial neural network (ANN), the convolutional neural network (CNN), the long short-term memory network (LSTM), and the bidirectional neural network (Bi-LSTM) were examined for this study. To compare the prediction accuracy of all models, three performance evaluation metrics RSME, MAE, and R2 are used. The results obtained indicate that all four methods produce reasonable estimates of solar radiation generation. As a result of RMSE, MSE, and R2, the Bi-LSTM forecasting model offers the best estimate of forecasting accuracy.

Keywords Solar power · Solar radiation · Long short-term memory · Convolutional neural network · Fully connected Artificial Neural Network · Bi-Directional Neural Network

P. K. Singh

Department of Computer Applications, Manipal University Jaipur, Jaipur, Rajasthan, India

A. Saraswat (✉) · S. K. Goyal

Department of Electrical Engineering, Manipal University Jaipur, Jaipur, Rajasthan, India

e-mail: amit.saraswat@jaipur.manipal.edu

Y. Gupta

Department of Computer Science, BML Munjal University, Gurugram, India

Y. Gupta

Lincus Inc., Tempe, AZ, USA

1 Introduction

There has been a rapid increase in energy demand in recent decades, and because of this, a major threat to our future is global warming, since it affects the natural world in harmful ways. Energy demand is one of the major players in world trade, and it is a major factor in global warming because of its dependence on fossil fuels [1]. The alternative solution to this problem is renewable energy sources, which are highly dependent on metrological conditions and, for this reason, are dynamic in nature. Several forms of renewable energy can be used to meet energy demand, including nuclear power, geothermal hydropower, wind power, and solar power. In recent years, solar power has been attracting the attention of researchers due to its abundant, renewable, and sustainable nature [2]. In addition, solar power is mainly dependent on solar radiation, temperature, humidity, and other meteorological factors. Solar power systems face new challenges as a result of these characteristics, including complexity and difficulty [3].

Accurate estimation of solar radiation is strongly associated with effective planning, management, and implementation of solar power systems. The term “solar radiation” is used to refer to “horizontal global solar radiation”. A number of studies use solar radiation to forecast solar power [4, 5]. Although other literature proposes direct solar power generation forecasting using historical values of solar power [6].

According to number of literatures, there are four types of solar power forecasting methods, namely physical, statistical, machine learning, and deep learning. Methods based on deep learning and machine learning gain advantages due to non-linearity, logical thinking like human brain and strong computer simulation [7].

A horizon for forecasting is a period of time into the future over which the forecast is desired. In order to design a forecasting model, it is necessary to select a suitable time horizon. In turn, it will help to maintain the accuracy of forecasts of solar power output at a satisfactory level. The forecasting horizon for solar power output includes very short term by one minute to 60 min, short term by 60 min to 24 h, medium term by one day to one year; and the long term by one year to five years or more [8, 9]. The purpose of every forecasting horizon is mentioned in Table 1.

Our major contributors include a literature review of solar power and solar radiation forecasting using deep learning, implementation of all four proposed deep learning methods in Python, and a comparative performance analysis based on evaluation metrics. Because of this, the paper is arranged as follows: Sect. 2 discusses

Table 1 Types of forecasting horizons

Forecasting horizon	Applications
Very short-term	Monitoring electricity dispatch and pricing
Short-term	Power scheduling and operations
Medium term	Planning, maintenance and scheduling
Long-term	Planning for electricity generation

different literature on solar power and irradiance forecasting using deep learning. A detailed discussion of the framework for the proposed models is provided in Sect. 3, and the experimental results are presented in Sect. 4. Finally, conclusive remarks are provided in Sect. 5.

2 Related Work

The increase in demand for renewable energy and its incorporation into the power grid creates a viable and sustainable future. The nature of renewable energy like solar is volatile and, because of this, it creates significant challenges to the secure and reliable operation of renewable energy integrated power grid [10, 11]. A machine learning model can extract and map nonlinear, complex features efficiently. To take advantage of this, machine learning-based predictions are among the most commonly used methods for making predictions [12–14]. In the research, an artificial neural network-based model was developed using meteorological data including humidity, temperature, pressure, and wind speed as inputs. Estimation of solar irradiation is directly related to solar power and in [15] for predicting solar irradiance, the author proposes a model based on artificial neural network and the proposed method performs better than the other prediction models.

The deep neural networks perform better in extracting features than simple neural networks, and they can solve the gradient disappearance problem more significantly than neural networks [16]. With convolutional neural networks (CNN), hidden features are extracted from data through hidden layers, and regression is performed with the final fully connected layer. With solar data measured at photovoltaic plants as input, Wang et al. developed a new hybrid prediction model based on a conventional neural network and a long short-term memory neural network [17]. A hybrid model was proposed by Zeng et al. and Ray et al. to obtain better short-term forecasting accuracy for solar power by using frequency subseries that were decomposed into different frequencies by variational mode decomposition and a convolutional neural network with long short-term memory [18, 19].

Solar irradiance is directly related to solar power generation. A time series-based forecast for short-term solar power generation is proposed by Sharadga et al. using a Long Short-Term Memory model with solar irradiance as a key input parameter [20]. Mishra et al. proposed a model for short-term solar power forecast using a long short-term memory neural network at different time horizons using metrological factors with similar characteristics as input parameters [8]. Gao et. al. used weather time series classification data as input to LSTM for short-term solar power forecasting [21]. Day ahead solar irradiation prediction is required for reliable electrical grid operation and for this historical weather data as input in the LSTM network for forecasting [22].

The LSTM and Bi-LSTM are among the best deep learning models for time series prediction, since they can handle correlations in time series better than other models. For time series analysis, the Bi-LSTM provides better accuracy and a faster

learning rate due to utilizing bidirectional learning capabilities. Zhen et al. developed a prediction model using the framework of Bi-LSTM for short-term solar power output that takes solar power output time series as an input [23]. Using bidirectional LSTM, Solar power prediction is always an important part of grid scheduling and, for this, Sharadga et al. developed a model that outperforms traditional neural network models and statistical models for predicting solar power output at large scales [20].

3 Methodology

3.1 Fully Connected Neural Network

As an artificial intelligence subset, neural networks are based on the biological structure of human neurons. Neurons are simple processing elements that make up each neural network, which are organized according to a particular type of neural network. The neural networks can be trained properly to identify trends and models relating to datasets. Artificial neural networks work in two steps: learning and recalling. The weights and bias of artificial neural networks are adjusted recursively in training steps to reduce the error associated with generating output. Neural networks have input and output layers that are related, as shown in Eq. 1 [24].

$$Z = \sum_{r=1}^{N_{i-1}} X_r^{i-1} W_{r,i} - \varnothing_r \quad (1)$$

where W is the weight, X is input for the neuron at layer I and Bias is \varnothing_r .

3.2 Convolutional Neural Network

Convolutional neural network is one type of deep learning neural network and have been implemented in many fields to achieve successful performance. It is an effective technology for extracting features automatically. In addition, they also exhibit a high degree of potential for dealing with time series, for example, automatic speech recognition and wind speed forecasting. Layers in convolutional neural networks include pooling, convolutional, and fully connected layers. The following is the summary of tasks performed by each layer.

Convolutional Layer: In a Convolutional neural network, the convolutional layer is used to generate new feature maps using convolutional kernels. As kernel weights in convolution are shared among all input maps, this operation is useful for local feature extraction.

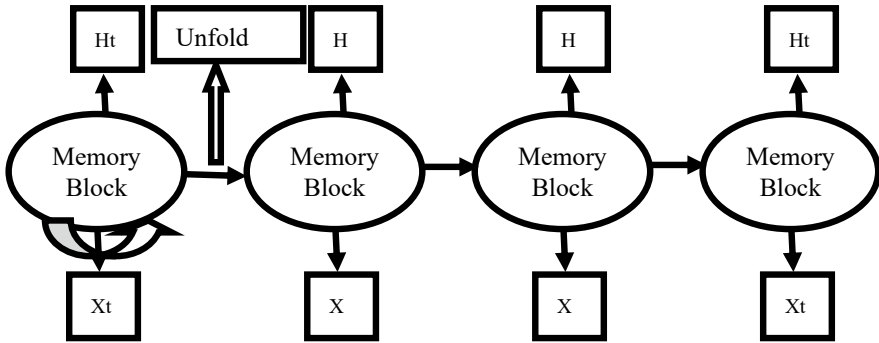


Fig. 1 LSTM neural network structure

Pooling Layer: The pooling layer reduces the dimensionality of input maps in-plane, thereby reducing the number of parameters that can be learned and reducing the probability of overfitting. Pooling can take different forms, such as average and maximum pooling.

Excitation Layer: As the final layer of the convolutional neural network, the fully connected layer functions as a “classifier.” Every neuron between two layers is connected [17].

3.3 Long Short-Term Memory Neural Network

Hochreiter and Schmidhuber analyzed and the solved vanishing gradient problem for prediction using time series data [25]. An LSTM is an upgraded version of recurrent neural network that solves the problem of long-term dependency of past information and gradient vanishing. As shown in Fig. 1. LSTM has forward propagation memory blocks for information.

Memory cell, input, forget, and output gates are the core elements of the long short-term memory network. As in Fig. 1 the input gates are (X_1, \dots, X_t) , and the output gates are (H_1, \dots, H_t) [26].

3.4 Bi-Directional Long Short-Term Memory

In Bi-directional Long Short-Term Memory (Bi-LSTM), the network is not only connected to previous generations, but to potential future generations as well. Bi-directional long short-term memory (Bi-LSTM) is characterized by two time directions. In comparison to LSTM, Bi-LSTM has more learning capabilities. Previous and future information uses as inputs in Bi-LSTM. The backward and forward layers

in Bi-LSTM are used to input information to every hidden layers. The α activation function is used to calculate the output of the Bi-LSTM network [27].

3.5 Performance Measures

Three accuracy performance indices, Mean Squared Error (MSE), Root Mean Square Error (RMSE), and coefficient of determination (R^2), were utilized to assess the effectiveness of the suggested model for the short-term forecast [28]. The following are brief descriptions of these indices.

The RMSE is a measure of the variance of prediction errors in a sample. The difference in values indicates how far apart errors are, i.e., a higher value indicates a wider error spread. To calculate the RMSE value, use the following Eq. 2

$$RMSE = \sqrt{\frac{1}{N} \sum_{i=1}^N (t_i - f_i)^2} \quad (2)$$

Mean squared error (MSE) is used to measure the error distribution. For forecast f and target t using N steps use the following Eq. 3.

$$MSE = \frac{1}{N} \sum_{i=1}^N (t_i - f_i)^2 \quad (3)$$

R^2 is a measurement that gives the information about the accuracy of a model with training and testing data.

$$R^2 = 1 - \frac{\sum (y_i - \hat{y}_i)^2}{\sum (y_i - \bar{y})^2} \quad (4)$$

4 Experimental Analysis

The required metrological data for research is downloaded from [29]. The time series dataset contains 11 variables with a resolution of 5 min, including pressure, temperature, radiation, wind speed, direction, and humidity. A total of 327,000 measurements were selected in the four months from September to December 2016 as part of the experiment.

As part of the data preprocessing step, it is always important to select input parameters for proposed models. A correlation coefficient was first used to find correlation indexes for parameters associated with solar radiation. The correlation coefficient index values are computed using the Pearson correlation coefficient. Table 2 shows the influential promoters. Based on Table 2, wind speed, pressure, and temperature are the most influential parameters.

The datasets must then be prepared for training and testing. As part of the standardization process, the dataset is prepared so that it fits better and the deviations are kept as low as possible. By removing the mean from the data and scaling it to unit variance, the standard scaler can be used to achieve this task. 80% of the data is used for training and the remaining 20% is used for testing.

Based on simulations, the effectiveness of deep learning models in this study, including fully connected neural networks, CNN, LSTM, and Bi-LSTM, was evaluated. We determine the error parameters of the proposed deep learning models based

Table 2 Correlation matrix

	Radiation	Temperature	Pressure	Humidity	Wind direction	Speed	Day of year	Day length (s)
Radiation	1.000	0.735	0.119	0.226	0.230	0.074	0.081	0.073
Temperature	0.735	1.000	0.311	0.285	0.259	0.031	0.371	0.356
Pressure	0.119	0.311	1.000	0.224	0.229	0.084	0.333	0.279
Humidity	0.226	0.285	0.224	1.000	0.002	0.212	0.064	0.087
Wind Direction (Degrees)	0.230	0.259	0.229	0.002	1.000	0.073	0.153	0.129
Speed	0.074	0.031	0.084	0.212	0.073	1.000	0.174	0.175
Day of year	0.081	0.371	0.333	0.064	0.153	0.174	1.000	0.979
Day length (s)	0.073	0.356	0.279	0.087	0.129	0.175	0.979	1.000

Table 3 Parameters settings for deep learning models

CNN	LSTM	Bi-LSTM	Fully connected neural network
Filters = 64	Units = 30,625	Dropout = 0.1	Dropout = 0.1
kernel_size = 2	Dropout = 0.1	Activation = relu	Activation = relu
Dropout = 0.1	Activation = relu	Optimizer = Adam	Optimizer = Adam
Activation = relu	Optimizer = Adam		
Optimizer = Adam			

Table 4 Comparative analysis of models

	RMSE	MSE	R2
CNN	0.28077	0.07883	0.91975
LSTM	0.26650	0.07102	0.92770
Fully connected NN	0.25359	0.06431	0.93449
Bi-LSTM	0.22630	0.05121	0.947865

on trial and error. Table 3 depicts the parameters of various deep learning models. The epoch for training and validation is 100 for each deep learning model for this paper.

The values of RMSE, MSE, and R2 are determined for each model and are shown in Table 4. Our findings show that the Bi-LSTM forecasting model performs better than other techniques for forecasting short-term solar power. In all forecasting models, the Bi-LSTM model demonstrates a lower value of RMSE, MSE, and higher value of R2 than the other models. Accordingly, the MSE of the Bi-LSTM model is 0.05121, which is best among CNN, LSTM, and Fully Connected Neural Network respectively, at 0.07883, 0.07102, 0.06431, and 39,744.4. Additionally, the Bi-LSTM model's RMSE is lower than that of other forecasting models. According to the forecasting results, Bi-LSTM outperforms the other models even if all of them have acceptable forecasting abilities.

Figure 2 shows a comparison between observed solar radiation and predicted solar radiation for CNN, LSTM, Bi-LSTM, and fully connected neural network.

As per Fig. 1 it shows that the convolutional neural network gives some negative results when it comes to predicting the output. By comparison, the fully connected neural network predicts different outcomes from what is expected. It is almost identical between the expected and predicted output values for LSTM and Bi-LSSTM, but in Bi-LSTM it is more similar than LSTM.

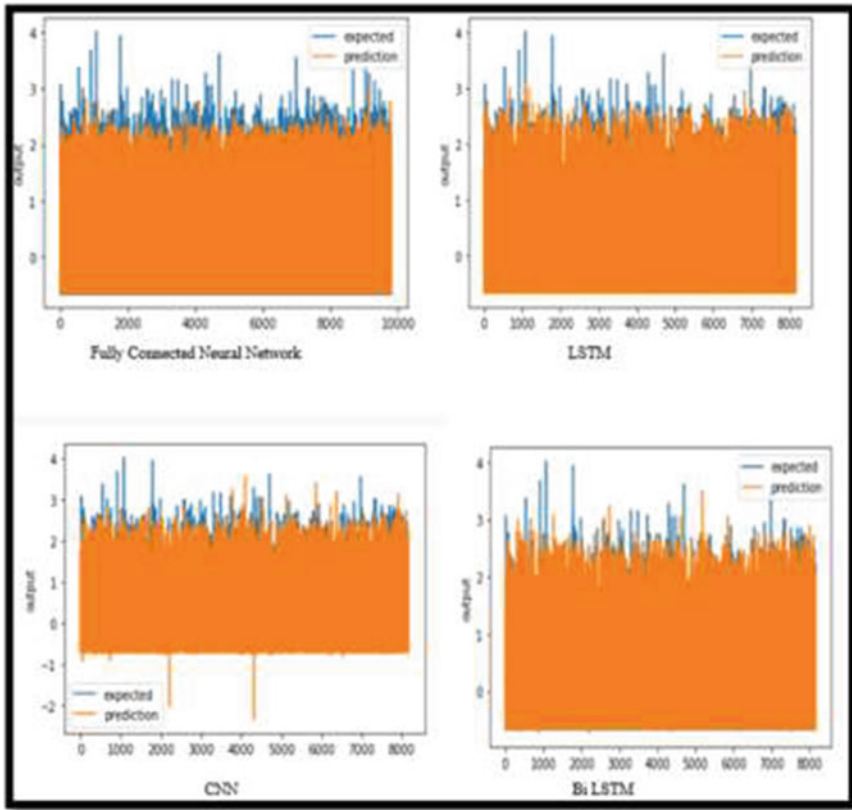


Fig. 2 Forecasting performance of different models

5 Conclusion

Future prospects for sustainable solar power are very promising. When constructing a model for forecasting, accuracy, and stability should be taken into account. Therefore, it is necessary to create an accurate and precise short-term solar energy forecasting technique. A comparison of deep learning-based forecasting approaches is presented in this paper, using RMSE, MSE, and R2 error metrics to assess their forecasting performance. By using RMSE, MSE, and R2 values, the deep learning model Bi-LSTM produces fewer statistical performance errors. In light of the numerical experimental results and analysis, the BI-LSTM model has a good degree of accuracy and precision. In this study, deep learning models were used to forecast solar radiation output. This domain will therefore be subject to further study in the future.

References

1. Poudyal R, Loskot P, Nepal R, Parajuli R, Khadka SK (2019) Mitigating the current energy crisis in Nepal with renewable energy sources. *Renew Sustain Energy Rev* 116:109388
2. Sobri S, Koohi-Kamali S, Rahim N (2018) A Solar photovoltaic generation forecasting methods: a review. *Energy Convers Manage* 156:459–497
3. Li J, Ward J, Tong J, Collins L, Platt G (2016) Machine learning for solar irradiance forecasting of photovoltaic system. *Renew Energy* 90:542–553
4. Dong Z, Yang D, Reindl T, Walsh WM (2014) Satellite image analysis and a hybrid ESSS/ANN model to forecast solar irradiance in the tropics. *Energy Convers Manage* 79:66–73
5. Gao B, Huang X, Shi J, Tai Y, Zhang J (2020) Hourly forecasting of solar irradiance based on CEEMDAN and multi-strategy CNN-LSTM neural networks. *Renew Energy* 162:1665–1683
6. Lin KP, Pai PF (2016) Solar power output forecasting using evolutionary seasonal decomposition least-square support vector regression. *J Clean Prod* 134:456–462
7. Voyant C, Notton G, Kalogirou S, Nivet M, Paoli C, Foulloy F (2017) Machine learning methods for solar radiation forecasting: a review. *Renew Energy* 105:569–582
8. Mishra M, Dash PB, Nayak J, Naik B, Swain SK (2020) Deep learning and wavelet transform integrated approach for short-term solar PV power prediction. *Measurement* 166:108250
9. Jordehi A (2018) How to deal with uncertainties in electric power systems? A review. *Renew Sustain Energy Rev* 96:145–155
10. Pan M, Li C, Gao R, Huang Y, You H, Gu T, Qin F (2020) Photovoltaic power forecasting based on a support vector machine with improved ant colony optimization. *J Clean Prod* 277:123948
11. VanDeventer W, Jamei E, Thirunavukkarasu GS, Seyedmahmoudian M, Soon TK, Horan B, Mekhilef S, Stojcevski A (2019) Short-term PV power forecasting using hybrid GASVM technique. *Renew Energy* 140:367–379
12. Yaglı GM, Yang D, Srinivasan D (2019) Automatic hourly solar forecasting using machine learning models. *Renew Sustain Energy Rev* 105:487–498
13. Mellit A, Sağlam S, Kalogirou SA (2013) Artificial neural network-based model for estimating the produced power of a photovoltaic module. *Renew Energy* 60:71–78
14. Chen C, Duan S, Cai T, Liu B (2011) Online 24-h solar power forecasting based on weather type classification using artificial neural network. *Sol Energy* 85(11):2856–2870
15. Yadav AK, Malik H, Chandel SS (2015) Application of rapid miner in ANN based prediction of solar radiation for assessment of solar energy resource potential of 76 sites in Northwestern India. *Renew Sustain Energy Rev* 52:1093–1106
16. Shi C, Pun CM (2018) Superpixel-based 3D deep neural networks for hyperspectral image classification. *Pattern Recogn* 74:600–616
17. Wang K, Qi X, Liu H (2019) A comparison of day-ahead photovoltaic power forecasting models based on deep learning neural network. *Appl Energy* 251:113315
18. Zang H, Cheng L, Ding T, Cheung KW, Wei Z, Sun G (2020) Day-ahead photovoltaic power forecasting approach based on deep convolutional neural networks and meta learning. *Int J Electr Power Energy Syst* 118:105790
19. Ray B, Shah R, Islam MR, Islam S (2020) A new data driven long-term solar yield analysis model of photovoltaic power plants. *IEEE Access* 8:136223–136233
20. Sharadga H, Hajimirza S, Balog RS (2020) Time series forecasting of solar power generation for large-scale photovoltaic plants. *Renew Energy* 150:797–807
21. Gao M, Li J, Hong F, Long D (2019) Day-ahead power forecasting in a large-scale photovoltaic plant based on weather classification using LSTM. *Energy* 187:115838
22. Qing X, Niu Y (2018) Hourly day-ahead solar irradiance prediction using weather forecasts by LSTM. *Energy* 148:461–468
23. Zhen H, Niu D, Wang K, Shi Y, Ji Z, Xu X (2021) Photovoltaic power forecasting based on GA improved Bi-LSTM in microgrid without meteorological information. *Energy* 231:120908
24. Gupta Y, Saraswat A (2021) Machine learning techniques for short-term forecasting of wind power generation. In: Hassanien A, Bhatnagar R, Darwish A (eds) *Advanced machine learning technologies and applications. AMLTA 2020. Advances in intelligent systems and computing*, vol 1141. Springer, Singapore

25. Hochreiter S, Schmidhuber J (1997) Long short-term memory. *Neural Comput* 9(8):1735–1780
26. Peng T, Zhang C, Zhou J, Nazir MS (2021) An integrated framework of Bi-directional long-short term memory (BiLSTM) based on sine cosine algorithm for hourly solar radiation forecasting. *Energy* 221:119887
27. Singla P, Duhan M, Saroha S (2021) An ensemble method to forecast 24-h ahead solar irradiance using wavelet decomposition and BiLSTM deep learning network. *Earth Sci Inf* 15(1):291–306
28. Luo X, Zhang D (2022) An adaptive deep learning framework for day-ahead forecasting of photovoltaic power generation. *Sustain Energy Technol Assess* 52:102326
29. Munawar U, Wang Z (2020) A framework of using machine learning approaches for short-term solar power forecasting. *J Electr Eng Technol* 15(2):561–569

Electric Two-Wheeler BLDC Hub Motor Design, Modeling, and Performance in Real-Time Use



Manikanta Akella, Sanjay Patil, and Kiran Wani

Abstract The push on electric mobility given by the government of India gained a lot of importance in the recent years with a subsequent growth in the electric vehicles especially two-wheeler focused. This brings an urgent need for the improvement of performance criteria in electric vehicles. Although electric vehicles are more efficient than conventional vehicles, the parameters like the efficiency of the electric motor, torque measurement, back emf, and speed of the electric vehicle and motor are to be continuously evaluated to hold the electric vehicles place at the top. In this paper, a deep research was done on the performance of a BLDC hub motor in both simulation and real-time application usage. As the stator and rotor of a brushless direct current motor play a vital role in deciding the performance, they were designed and later the modeling was done for the same using MATLAB and Simulink and the results are then compared to the experimental setup made for the torque measurement at corresponding speed, currents, and voltages.

Keywords BLDC Hub motor · Electric vehicle · Motor Torque · Performance

1 Introduction

The expansion of mid-range horsepower engines in the markets exceeds that of smaller fractional horsepower motors. The heating and cooling equipment industries are driving this demand, along with electric vehicles, which will provide the best growth opportunities. Demand is seen in all systems, from automotive, avionics, military, and space to increase performance and reduce weight. Along these lines, a

M. Akella (✉)
Tata Technologies Ltd, Pune, India
e-mail: manikanta.akella@tatatechnologies.com

S. Patil · K. Wani
ARAI Academy, Pune, India

M. Akella
Veltech University, Chennai, India

directive to increase motor performance has been released by the European markets. The military and avionics markets worldwide are also powered by decreases in size and increases in operational and ownership costs. More stable and effective engines and control techniques must be considered to accomplish these objectives. As this market continues to expand, on the basis of its reliability, performance, and scale, the brushless DC motor is the most sensible option.

In terms of other engine types, the BLDC motor offers strong advantages in terms of performance and size optimization in challenging motor applications. BLDC engines do not have brushes and need less downtime for maintenance and the system. Yet these engines require electronic controllers ranging from basic to complicated. Usually, the engines are over 80% powerful and the controls are in the 95% range [1]. Thus, the enabling technology is the BLDC motor controller's ever-improving evolution. Pulse Width Modulation (PWM) sampling is used by the most powerful controllers to drive a DC power motor [2]. There are also other criteria for power conditioning that range from rectification of an AC signal to filtering for electromagnetic interference (EMI) that is required in most applications.

A review was conducted on the performance where the controller strategy had the highest relative importance among other requirements. Motor performance came second in the importance list which plays a vital role among the powertrain components in the vehicle design [3]. The amount of power needed for the bike should be determined considering the environmental conditions [4]. A simulation environment was built and the target system was modeled in order to analyze the driving performance [5]. Research on improving motor efficiency is done intensively [6].

2 Methodology

In this paper, in order to find the performance characteristics of a bldc hub motor in simulation and real-time use, various tests were conducted to satisfy the problem statement. They include the speed control of bldc hub motor, torque measurement, and efficiency of the motor. The experiment was not limited to a single bldc hub motor, instead it was performed with multiple motors to validate the actual performance test bed of the motor. To perform these activities, first the stator and rotor of a bldc hub motor with 1000-W capacity were designed in JMAG designer providing all the required input data as per the existing 1000-W motor which can operate at 48 V (Figs. 1 and 2).

3 Torque Measurement

Although, the torque of a motor can be measured by using a torque sensor, in this article the torque estimation and measurement experiment was performed by the physical experimental setup using a brake test. This reduces the overall cost of the

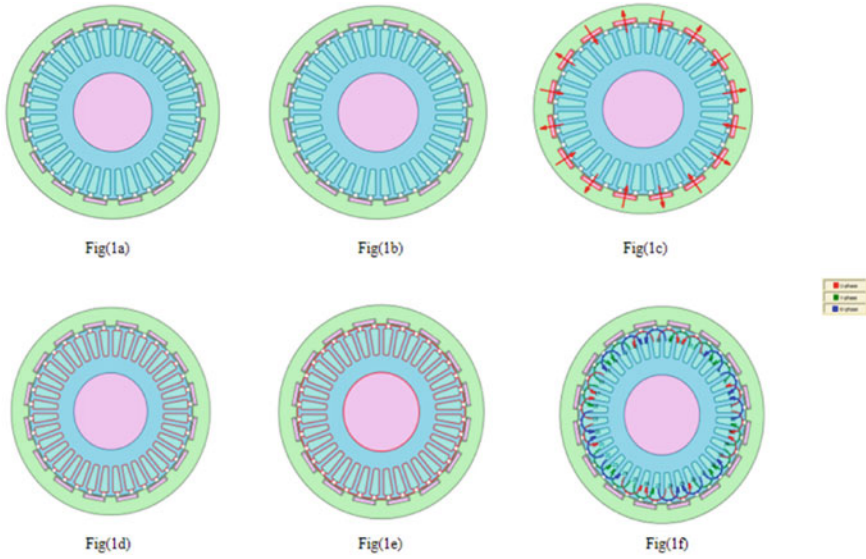


Fig. 1 a Motor diagram. b Rotor core. c Rotor magnet. d Stator coil. e Stator core. f Winding

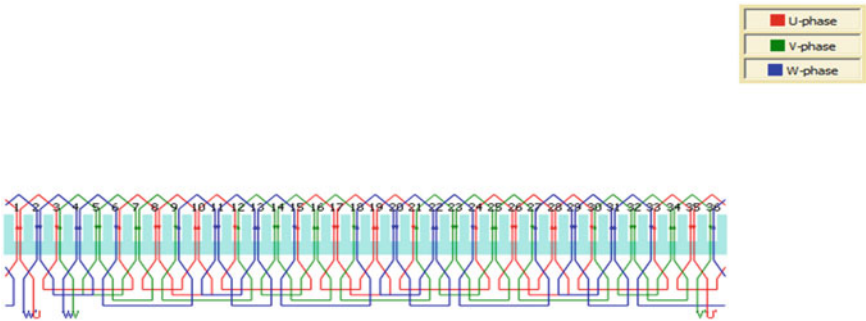
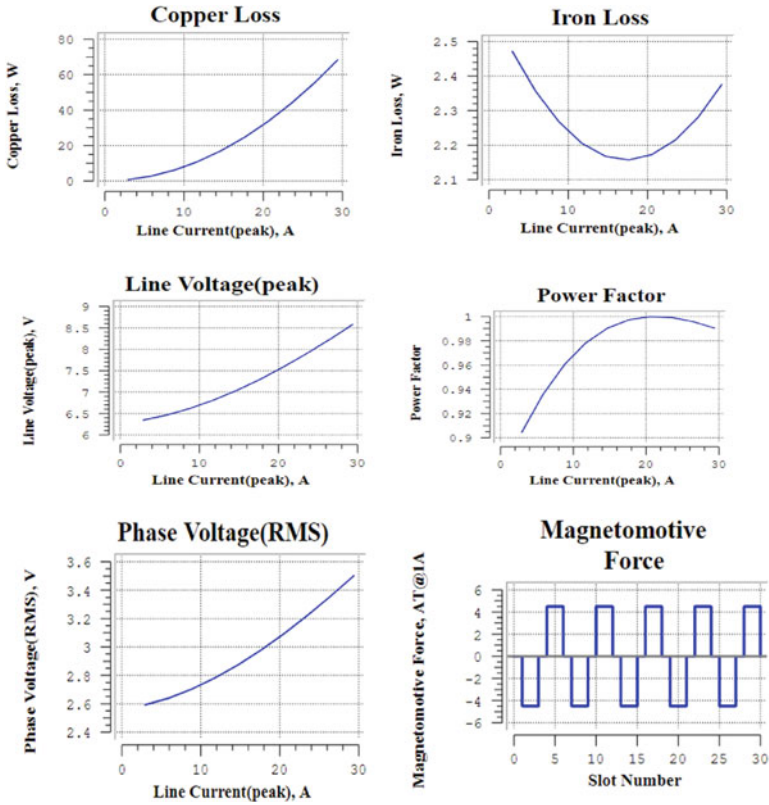


Fig. 2 Slot diagram

project with a minimal error in the output. The motor torque was measured by a spring balance and load in the rope test. The rope test was carried by varying loads such that the weights which act like a load are considered according to the load on the motorbike. The load on the bike was considered as a single rider with an average weight of 60 kg, and also with a ride pillion. The weight of the rider and pillion was considered to be 120 kg. In this test, the load was varied between 60 and 120 kg so that there will not be any discrepancy when the weight of the rider or pillion got changed.

4 Results and Discussion

4.1 Design Results



4.2 Simulation Results

The proposed comparison can be obtained by comparing the actual results obtained in the real-life use to the simulation results. While modeling this, not only the torque of the motor but also parameters like back emf, speed, and current were also simulated, and the corresponding torque for a particular speed, current, and back emf was observed. This provides the additional information to the reader about the requirements of all the parameters at a particular instant of torque (Fig. 3).

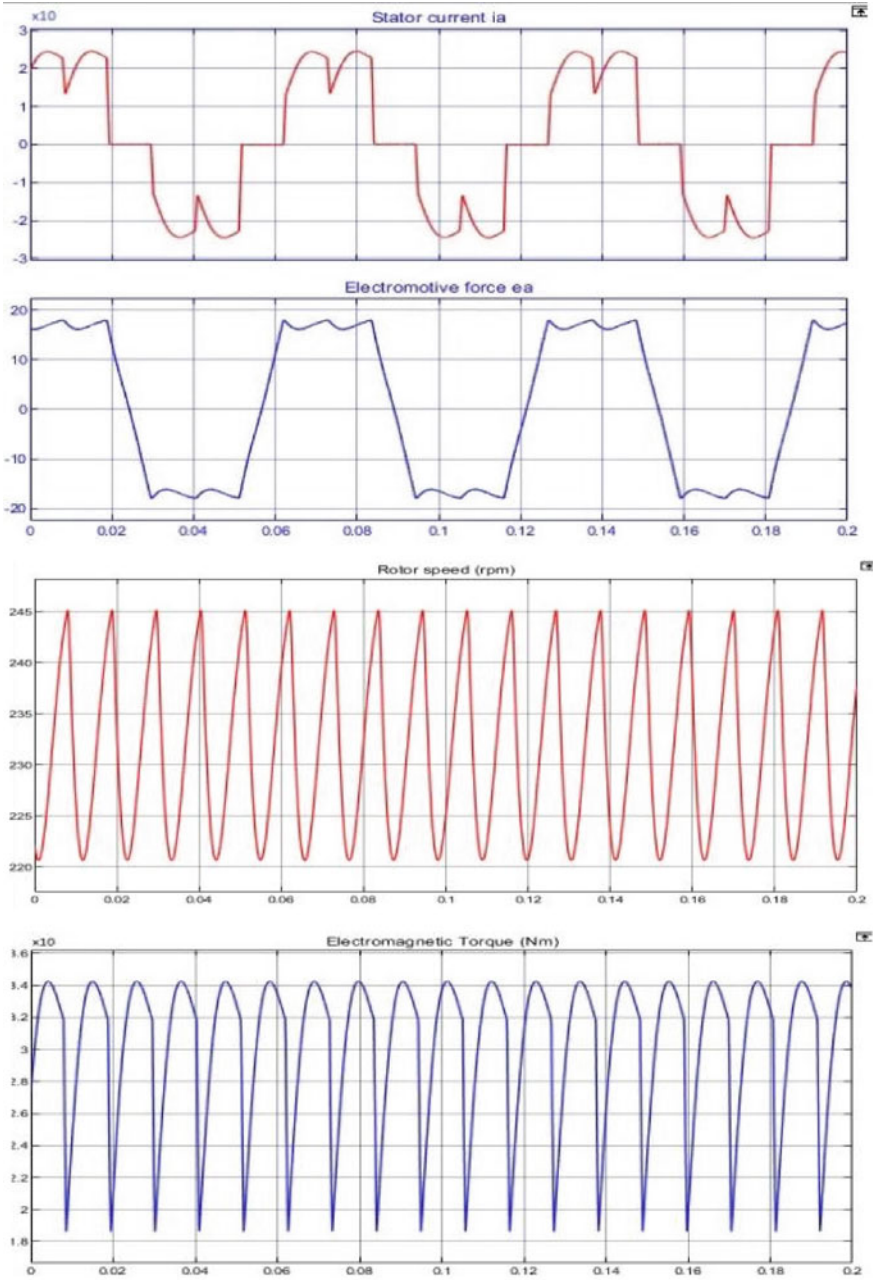


Fig. 3 Simulation results of Simulink model

Since mechanical power is the product of torque and RPM, no power is generated when there is no torque or rotation. Also, the output power of the motor is less than the input power due to heat losses.

4.3 Power Flow

Figure 4 below shows the power flow of a dc motor in which a major amount of power is being wasted in terms of various losses. So, to minimize these losses, a proper design of the motor comes into play.

The above results are used to find out the efficiency of the motor considering the obtained losses and plotted (Fig. 5).

$$K_c = 0.8;$$

$$K_i = 0.1;$$

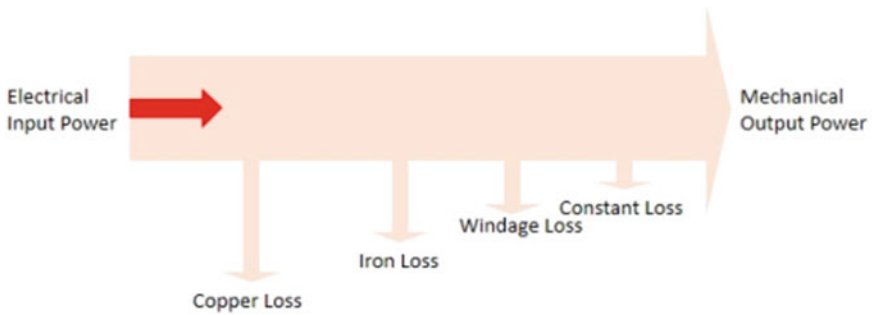
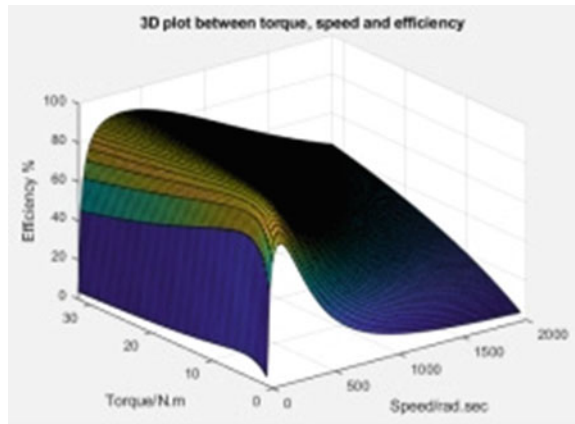


Fig. 4 Power flow

Fig. 5 Efficiency plot wrt Torque and speed



```

Kw = 0.00001;
Cl = 20;
x = linspace(1,2000);
y = linspace(1,32);
[X,Y] = meshgrid(x,y);
Po = (X.*Y);
C = (Y.^2)*Kc;
I = X*Ki;
W = (X.^3)*Kw;
Pi = Po + C + I + W + Cl;
n = (Po./Pi).*100;
surf(X,Y,n);
xlabel('Speed/rad.sec');
ylabel('Torque/N.m');
zlabel('Efficiency %');
title('3D plot between torque, speed and efficiency');
    
```

4.4 Validation Model

To validate the real-time performance of the electric motor, a vehicle model and a controller are required so that the motor can be incorporated into it at various environmental conditions with a road profile (Fig. 6). The model was run at wide open throttle running for 30 s in which the throttle gets cut off after 20 s. Later, the road profile was changed using ECE Extra urban driving cycle, and the below results were obtained (Figs. 7, 8, 9).

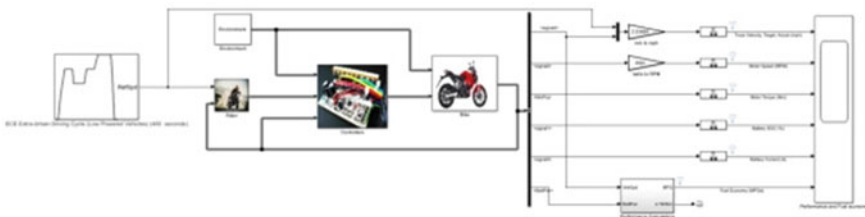


Fig. 6 Two-wheeler Vehicle model for validation

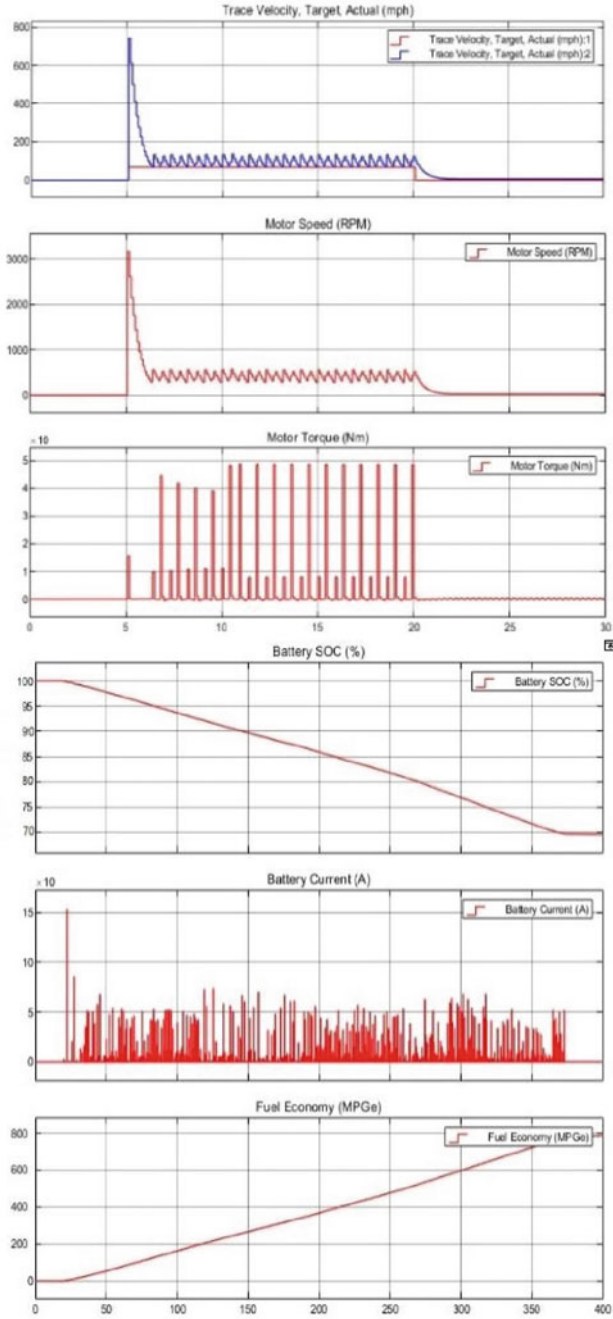


Fig. 7 WOT as road profile

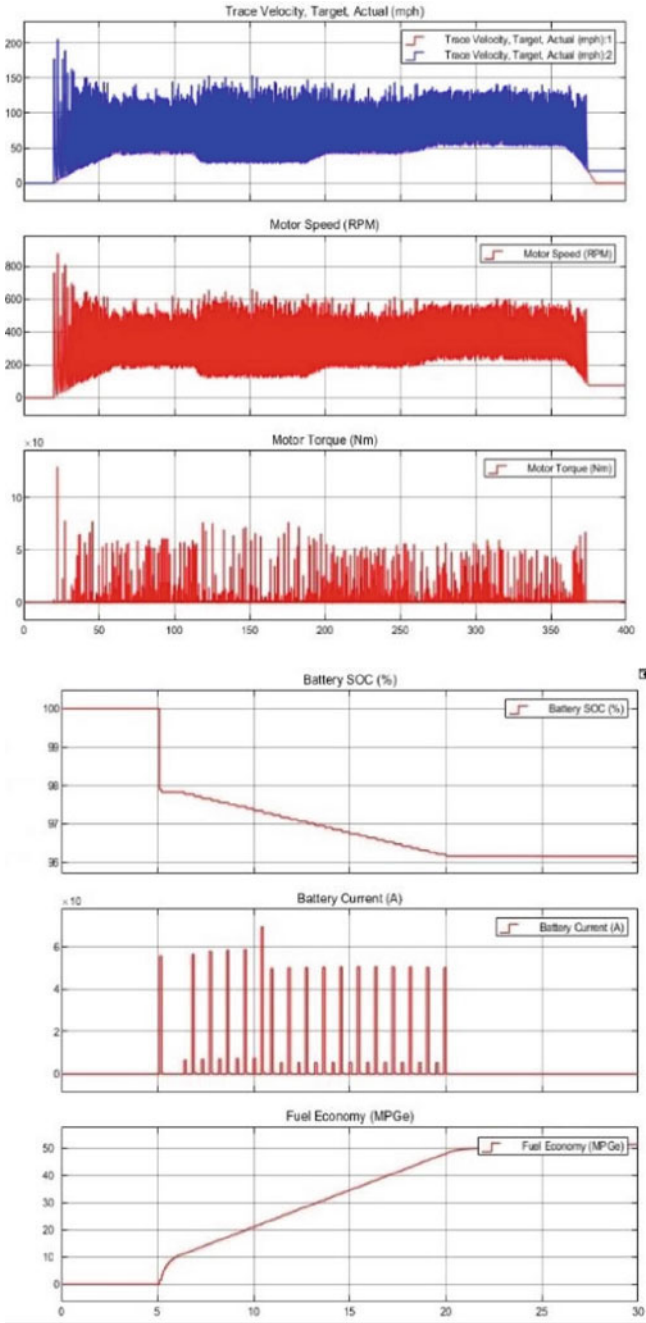
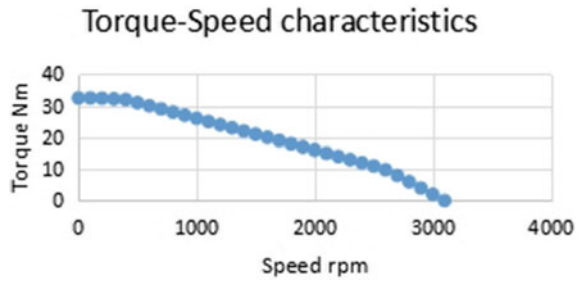


Fig. 8 ECE urban driving cycle as road profile

Fig. 9 Torque-speed result from simulation



5 Conclusion

The motor design gave the possibility to get the efficiency of the motor by detailing the losses encountered during a run. The mathematical model of motor provided the stator current, electromagnetic torque, electromotive force, and rotor speed. The validation model generated the torque speed characteristics and the torque obtained in this model is nearly equal to the torque generated by the motor in the real run at the same environmental and supply conditions.

In this research, we have studied the performance of a bldc hub motor used in electric two-wheeler and observed its performance at simulation level and experiment level. It was found that the result obtained in both the cases were all most similar and are as follows.

Obtained Torque = 32 Nm in simulation and 29 Nm in experimentation.

efficiency of the motor = 86% in simulation and 87% as specified by the manufacturer.

References

1. de la Guerra A, Alvarez-Icaza L, Torres L (2018) Brushless DC motor control with unknown and variable torque load. *IFAC-PapersOnLine* 51:644–649. <https://doi.org/10.1016/j.ifacol.2018.07.353>
2. Dahbi M, Doubabi S, Rachid A, Oulad-Abbou D (2020) Performance evaluation of electric vehicle brushless direct current motor with a novel high-performance control strategy with experimental implementation. *Proc Inst Mech Eng Part I J Syst Control Eng* 234:358–369. <https://doi.org/10.1177/0959651819854562>
3. Stilo L, Segura-Velandia D, Lugo H et al (2021) Electric bicycles, next generation low carbon transport systems: a survey. *Transp Res Interdiscip Perspect* 10:100347. <https://doi.org/10.1016/j.trip.2021.100347>
4. Uyar O, Çunkaş M, Karaca H (2022) Enhanced intelligent control with adaptive system for electrically assisted bicycle. *Eng Sci Technol an Int J*. <https://doi.org/10.1016/j.jestch.2021.08.004>

5. Park J, Jeong H, Jang IG, Hwang SH (2015) Torque distribution algorithm for an independently driven electric vehicle using a fuzzy control method. *Energies* 8:8537–8561. <https://doi.org/10.3390/en8088537>
6. Kaleb S, Hapid A, Kurnia MR (2015) Electric vehicle conversion based on distance, speed and cost requirements. *Energy Procedia* 68:446–454. <https://doi.org/10.1016/j.egypro.2015.03.276>

A Comprehensive Review of Wireless Electric Vehicle Charger



Sandesh Patel , Shekhar Yadav , and Nitesh Tiwari 

Abstract The increasing number of inner flaming engine vehicles and these vehicles are released more harmful gases due to acid rain, effects on human health, air pollution, and global warming take place. These grave issues are reduced by promoting safer, cleaner, and copious efficient vehicles which are known as electric vehicles (EVs). This article represents a spacious contemporary review of the wireless power transfer methods, topology for EV wireless chargers, and future trends in wireless power chargers. First, Wireless power transfer methods are classified into magnetic gear wireless power transfer, capacitive wireless power transfer, inductive power transfer, and resonant inductive power transfer. Then, the generally used topology for EV wireless chargers is discussed in detail. In the end, future trends in wireless power chargers are also discussed.

Keywords Wireless Charging System · Electric Vehicles (EVs) · Magnetic Gear Wireless Power Transfer · Static Wireless Charger · Dynamic Wireless Charger · Wireless V2V · Wireless V2G

1 Introduction

Nowadays fossil fuel insufficiency and due to global warming-related problems many people are shifting toward electric vehicles (EVs). The battery of electric vehicles is charged by wired and wireless charger methods. The wireless charger is a static and dynamic type [1]. Transfer of power wirelessly by a magnetic or time-varying

S. Patel (✉) · S. Yadav · N. Tiwari
Department of Electrical Engineering, Madan Mohan Malaviya University of Technology,
Gorakhpur, UP, India
e-mail: sandeshbbdniit@gmail.com

S. Yadav
e-mail: syee@mmmut.ac.in

N. Tiwari
e-mail: niteshwr1994@gmail.com

electric field. The transmission medium is used to transfer electrical power or energy. Inductor stored energy in magnetic field and capacitor in the time-varying electric field. The weight of the system is not increased by using cross ferrite bars, Cross ferrite bars are used such as core at the time of wireless power transfer. The volume of the core has very small [2]. However, the efficiency of a wireless charger for electric vehicles is less compared to a wired charger because every component of a wireless charger releases losses. The efficiency can be increased in the acting range by adjusting the active power sources like voltage and phase angle [3]. The principle of magnetic induction work between two coils. In this, the primary coil is stationary or fixed in-ground and the secondary coil is fixed into an electric vehicle for receiving power from the primary side. Transmitting of power from the primary to secondary side is based on resonance frequency [4]. Also, power transfer from vehicle-to-Grid-to-Home (V2G2H) by using proper DC-link so we running the grid, EVs, and nonlinear household loads [5]. The growth of electric vehicles is possible by solving the problem of charger points or new wireless vehicles-to-vehicles charger methods [6]. Dynamic wireless charging (DWC) is a rising technology by this technology batteries of electric vehicles are charged automatically when the vehicles are in running condition. DWC is the best option to reduce anxiety such as charging range and it is increasing the battery life cycle, and reducing the size and weight of the battery [7]. Inductive power transfer, (IPT) the system is exploited with zero-current- switching (ZCS) or Zero-voltage-switching (ZVS) methods so it is known as high-frequency power converter processing. This processing is based on a power electronic converter and efficiency is cognizable at 91.26% with resistive and battery loads [8]. The measurement system is used to measure the on-site performance and efficiency of the charging station and converters, measurement systems are more used in the inductive power transfer (IPT) vehicle charging station because it depends on a high-frequency resonant coupling circuit [9]. In wireless chargers or wireless power transport systems are used series or parallel capacitors and it is known as the compensation operation of the capacitor. These operations are used to improve system performance [10]. Wireless charging system which is also based on wind/PV system. Wind/PV system is a renewable source of energy and free from pollution, low cost easily available everywhere Wireless charging technology for electric vehicles is evolved by electromagnetic inductive coupling (EMIC) [11]. The driving range of electric vehicles can be a dynamic wireless charging system.

Here, one problem is charging pads on the road and it is more costly. The energy efficiency of wireless chargers is 86% and extended up to 90% [12]. The leading institutes and companies are researching both technologies such as wired and wireless [13]. The charging station is the most important factor for electric vehicles because it slackens air pollution. Electric vehicles supply equipment is the second name for the electric charging station. A wind/PV system will be most useful to charge the battery of electric vehicles at the charging station. Primary (transmitting) coil with secondary (receiving) coil are connected in a wireless medium then DC is flowed to charge the battery. The battery charging process is fully automatic [14]. A full or half-bridge inverter is produced an AC signal for the wireless charging system, and maximum power is obtained when minimizing the inverter harmonic

[15]. Mutual inductance is a crucial factor for wireless charging systems because it is affecting output power [16]. The size of a battery pack is reduced by the dynamic wireless charger system. Nowadays, lithium-ion batteries are more powerful so it is more preferable in electric vehicles. DC/DC converter is used for improving performance and it is used on receiving side which increased the efficiency and output voltage of the system. Movable wireless charger system, the coupling coefficient is changed due to the motion of the vehicle on track so remove this problem by using a passivity-based-proportional integral controller. This controller is used with DC/DC converter [17]. Unity power factor and good efficiency can be received along a maximum sliding distance is 10 cm and an air gap is 15 cm at a universal input voltage is 90v AC to 264v AC [18]. For a wireless charger system, the size of the transmitting and receiving twist is the most important factor so it is optimized by optimization technique [19]. The protection strategy is to protect the electric vehicles in abnormal conditions such as variation of inverter current and phase angle [20]. A smart charger for electric vehicles is required for sensors, when an electric vehicle is parked at a charging spot then sensors are detected immediately and flow wireless power [21]. The coil misalignment and charging performance are monitored by tunneling magneto-resistive (TMR) sensors matrix. This TMR technology is used in both dynamic and stationary wireless charging systems [22]. A wireless charger can improve the market of EVs because it can transferral of power by taking any type of precautions in opposite environment situations [23]. The operational temperature of the coupler is cheque after every 30 min [24]. A wireless charging system (WCS) consists of a rectifier, inverter (DC/AC), and converter (DC/DC) [25, 26].

2 Wireless Power Transfer Methods

Wireless power transfer methods are divided into four parts magnetic gear, capacitive, Inductive, and resonant inductive. In these methods, the magnetic gear power transference method is completely different from capacitive, inductive, and resonant inductive methods because the magnetic gear system used two permanent magnetic: primary and secondary magnetic. The wireless power transference system (see Fig. 1).

2.1 *Capacitive Wireless Power Transfer*

The capacitive coupler is made with the help of metal plates. It consists of four metal plates. The primary side is used two plates for power transmitting and the secondary side is also used two plates for power receiving. This power flow loop is completed with the help of two capacitive couplers. The coupling capacitance is inversely related to the distance between the plates and directly proportional to the dielectric material and plate area. The following attributes of a capacitive wireless power transfer system

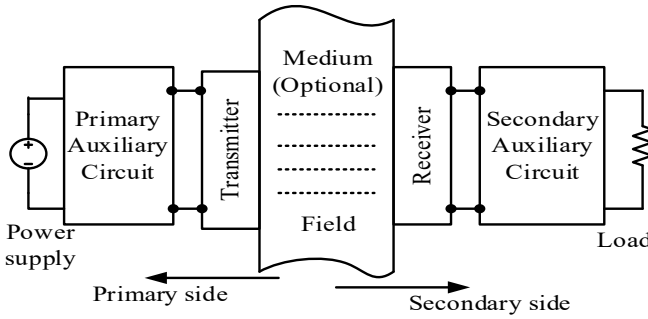


Fig. 1 The wireless power transfer system

are minimal eddy current loss, light weight, and low price. The capacitive wireless power transfer system (see Fig. 2). In pursuance of recent analysis, it is used with low power and short-distance applications like LED lighting, biomedical devices, integrated circuits, mobile charger, and USB. The coupling coefficient for capacitive wireless power transfer is given by Eq. (1).

Equations (1) and (2) are used to compute the resulting coefficient of the sending and receiving sides, which are C_1 and C_2 , respectively.

$$C_1 = C_{in1} + C_{ex1} \tag{1}$$

$$C_2 = C_{in2} + C_{ex2} \tag{2}$$

The coupling coefficient K_C is obtained by putting Eqs. (1) and (2) in (3). The coupling coefficient K_C is given by

$$K_C = \frac{C_M}{\sqrt{C_1 C_2}} \tag{3}$$

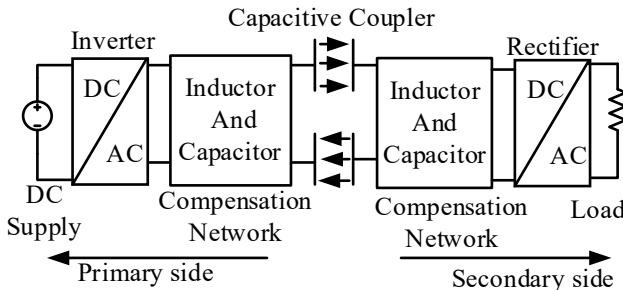


Fig. 2 The capacitive wireless power transfer system

C_{ex1} and C_{ex2} are external capacitances; C_{in1} and C_{in2} are internal capacitances.

2.2 Magnetic Gear Wireless Power Transfer

It is also known as a magnetic wireless charger for electric vehicles (EVs). The magnetic gear wireless power transmission system is completely different from the inductive methodology because it is used two permanent magnets and these permanent magnets are known as synchronized permanent magnets (PMs). One permanent magnet works as receiver winding (RW) and the other magnet works as transmitter winding (TW). The current source is connected to the transmitter which produces power into transmitter winding (TW) as well as also produced torque into the transmitter magnet and it is rotated. Due to magnetic interplay induced torque into transmitter permanent magnet (TPM) and both permanent magnets are rotated synchronically. In this system, the receiver is working in generator mode and which supplies power for battery charging. In the end, this system does not use in the movable wireless charger system.

2.3 Inductive Power Transfer

In power transfer system is generally used because it is transfer high power. The inductive power transmission uses Ampere’s and Faraday’s laws (see Fig. 3). Alternating current causes the first coil’s magnetic field to be established, which generates voltage into the secondary coil. Inductive power transfer systems are of two types. One is a loosely coupled system or contact type and the other is a closely coupled system or non-contact type. Figure 4 shows a block diagram of the inductive power transfer system. The primary and secondary side dependent voltage sources V_{12} and V_{21} are given by Eqs. (4), and (5). The coupling coefficient for inductors L_1 and L_2 is given in Eq. (6).

Primary side dependent voltage sources, V_{12} is given by

Fig. 3 Block diagram of the inductive power transfer system

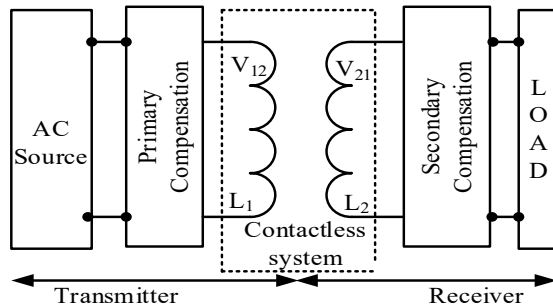
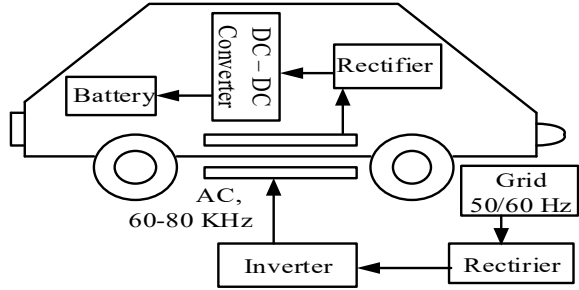


Fig. 4 Block diagram for static wireless charger



$$V_{12} = -j \omega M I_2 \tag{4}$$

Secondary side dependent voltage sources, V_{21} is given by

$$V_{21} = j \omega M I_1 \tag{5}$$

The coupling coefficient for Inductor L_1 and L_2 is given by K such as

$$K = \frac{M}{\sqrt{L_1 L_2}} \tag{6}$$

where M stands for mutual inductance. For a weakly linked inductive power transmission system, the coupling index is less than 1. I_1 and I_2 are transmitter and receiver side currents. An inductive power transmission system requires a lot of times frequency for the produced magnetic field; a high frequency is 10 K–10 MHz so high frequency is achieved by using a power amplifier. Although there are many distinct types of amplifiers, including class AB, class D, class C, class A, and class E, class D, and E amplifiers are frequently employed in power amplifiers because they offer decent efficiency at high frequency.

2.4 Resonant Inductive Power Transfer

Because of its inferior efficiency, the inductive power transmission system is not as popular and widespread. Because it increases power transfer capacity and reduces the current and voltage rating of the power supply source, resonant inductive power transmission systems are utilized in primary and secondary coils for power transmission. The grid is connected to the power supply, increasing the frequency at which it feeds the primary compensation circuitry (230 V, 50 Hz). The principal compensation circuit is coupled with the primary winding. The secondary coil or side is received power from the transmitter coil which is injected into the second compensation circuit which is rectified into DC then a battery of the electric vehicle is charged.

3 Topology for EV Wireless Charger

The topology for electric vehicle wireless chargers is two types. First is a static wireless charger it is also known as Park and charge. Secondly is a dynamic wireless charger and it is known as move and charge.

3.1 Static Wireless Charger

The primary coil sometimes referred to as the transmitting coil, is mounted to the surface. In an electric vehicle, the secondary coil sometimes referred to as the receiving coil, is injected. The electric vehicle is parked upon the transmitter coil then power is transmitted and received by the receiver coil. To charge the battery, the primary coil is linked directly to the grid. Static wireless chargers are included in the following stages such as grid 50/60 Hz, rectifier, inverter, coupling system, and power conversion system for charging the battery. The block diagram for the static wireless charger is shown in Fig. 4.

3.2 Dynamic Wireless Charger

In this charger's primary coil or transmitter, the coil is fixed to track. When electric vehicles are moving on this track then power is received by a secondary coil which is fixed into the electric vehicle. By using conversion circuits, the battery is charged. The dynamic wireless charger is shown in Fig. 5.

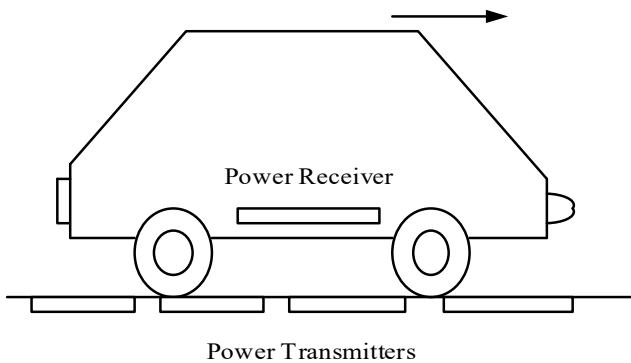


Fig. 5 Block diagram for dynamic wireless charger

4 Future Trends in Wireless Power Charger

In the future, two types of wireless power chargers are trending. One is wireless V2G and the other is wireless V2V because these chargers solved the problem of charging stations. Both wireless power chargers are used an inductive power transfer system, which are discussed.

4.1 Wireless V2G

The primary and secondary side converter is a composite of a tuned LCL circuit and reversible rectifier. In this process, power is taken by a battery of electric vehicles and converted into AC with the help of an IPT pick-up converter. This power is given to a mutual coupler and then again converted into DC by IPT primary converter after this converter one capacitor is connected for removed noise from DC and this DC is injected into the grid with the help of an inverter. L_{pt} track winding inductor and L_{st} pick-up winding inductor. M is denoted by mutual inductance between L_{st} and L_{pt} . This mutual inductance is given in Eq. (7).

$$M = k \sqrt{L_{st} L_{pt}} \quad (7)$$

The coupling factor between L_{st} and L_{pt} in this instance is k . A DC voltage source called V_{out} receives output from a pick-up converter. The tracking frequency (f_T) is used to tune both LCL circuits. The tracking frequency is produced by primary reversible rectifiers and the tracking frequency is in order of 10–50 kHz. The output power is the flow between the load and the DC bus by an inductive power transfer system. This output power is directly proportional to the square of the output voltage across the load and inversely proportional to the impedance of the load.

4.2 Wireless V2V

Based on a single-phase-matrix-converter (SPMC) comprising four bidirectional switches, this wireless V2V system may conduct or block current in both directions. SPMC works as a bidirectional converter that converts DC to AC. In a wireless V2V system power transfers in two stages, one is DC to AC and the other is AC to DC. SPMC of vehicle 1 transfers DC to AC power at a high frequency, which is injected into the transmitter coil and this power is received by the receiver coil. Then SPMC of vehicle 2, which converted again from AC to DC for charging the battery of EV. This wireless V2V system is based on a single-phase-matrix-converter (SPMC) with four bidirectional switches so it blocks or conducts the current in both directions. SPMC works as a bidirectional converter that converts DC to AC. In a wireless V2V

system power transfers in two stages; one is DC to AC and the other is AC to DC. SPMC of vehicle 1 transfers DC to AC power at a high frequency, which is injected into the transmitter coil and this power is received by the receiver coil. Then SPMC of vehicle 2, which converted again from AC to DC for charging the battery of EV. By using this process for wireless power transfer to V2V.

5 Conclusion

To increase automobiles such as buses, cars, motorcycles, trucks, all automobiles are consumed fossil fuels and generated harmful gases, e.g., CO, SO₂, NO_x, etc. so to reduce this type of environmental issue the best option is electric vehicles (EVs).

The market revenue of electric vehicles is increased year by year, it was 260.63 billion, US, dollars in 2021 and increased continuously will be reached 1,046.8 billion, US, dollars in 2026. When the number of electric vehicles is increased the required to charge these electric vehicles by wired or wireless charging technology in compression both types of charging technology wireless charging is more convenient and safe. As a result, several wireless power transmission methods were covered in this paper. Resonant inductive wireless power transmission methods were chosen because of their superior performance. The topology of the EV wireless charger system is static and dynamic type. In the future, dynamic wireless charging systems are used because it reduces the weight of electric vehicles and the size of batteries and their future applications are V2V and V2G.

References

1. Mude KN (2018) Battery charging method for electric vehicles: From wired to on-road wireless charging. *Journal* 4(4):1–15
2. Badwey MA, Abbasy NH, Eldallal GM (2022) An efficient design of LC-compensated hybrid wireless power transfer system for electric vehicle charging applications. *Journal* 61(8):6565–6580
3. Shi B, Yang F, Wang S, Ouyang M (2019) Efficiency improvement of wireless charging system based on active power source in receiver. *IEEE Acc* 7:98136–98143
4. Jitson T, Cheapanich S (2021) Study of dynamic charging for electric vehicles using stationary wireless power transfer charging. In: 2021 9th international electrical engineering congress, pp 17–20
5. Wang L, Madawala UK, Wong MC (2020) A wireless vehicle-to-grid-to-home power interface with an adaptive DC link. *IEEE J* 9(2):2373–2383
6. Mou X, Zhao R, Gladwin DT (2018) Vehicle to vehicle charging (V2V) bases on wireless power transfer technology. In: IECON 2018–44th annual conference of the IEEE industrial electronics society, pp 4862–4867
7. Jeong S, Jang YJ, Kum D, Lee MS (2018) Charging automation for electric vehicles: is a smaller battery good for the wireless charging electric vehicles? *IEEE Trans* 16(1):486–497
8. Nama JK, Verma AK, Srivastava M, Tomar PS (2020) An efficient inductive power transfer topology for electric vehicle battery charging. *IEEE Trans* 56(6):6925–6936

9. Zucca M, Squillari P, Pogliano U (2020) A measurement system for the characterization of wireless charging stations for electric vehicles. In: 2020 conference on precision electromagnetic measurements, vol 70, pp 1–2
10. Yan XY, Yang SC, He H, Tang TQ (2018) An optimization model for wireless power transfer system based on circuit simulation. *Phys A: Stat Mech App* 509:873–880
11. Yin X, Lu S, Wang Y, Du Z (2022) Wireless charging structure and efficiency analysis based on wind-solar hybrid power supply system. *Energy Rep* 8(4):746–755
12. Tavakoli R, Pantic Z (2017) Analysis, design, and demonstration of a 25-kW dynamic wireless charging system for roadway electric vehicles. *IEEE J* 6(3):1378–1393
13. Mohammed SAQ, Jung JW (2021) A comprehensive state-of-the-art review of wired/wireless charging technologies for battery electric vehicles: classification/common topologies/future research issues. *IEEE Access* 9:19572–19585
14. Kandasamy V, Keerthika K, Mathankumar M (2021) Solar based wireless on the road charging station for electric vehicles. *Mater Today: Proc* 45(5):8059–8063
15. Sis SA, Akça H (2020) Maximizing the efficiency of wireless power transfer systems with an optimal duty cycle operation. *Int J Elect Comm* 116:153081
16. Song B, Cui S, Li Y, Zhu C (2020) A fast and general method to calculate mutual inductance for EV dynamic wireless charging system. *IEEE Trans* 36(3):2696–2709
17. Liu J, Liu Z, Su H (2021) Passivity-based PI control for receiver side of the dynamic wireless charging system in electric vehicles. *IEEE Trans* 69(1):783–794
18. Hsieh YC, Lin ZR, Chen MC, Hsieh HC, Liu YC, Chiu HJ (2016) High-efficiency wireless power transfer system for electric vehicle applications. *IEEE Trans* 64(8):942–946
19. Mohamed N, Aymen F, Alqarni M, Turkey RA, Alamri B, Ali ZM, Aleem SHA (2022) A new wireless charging system for electric vehicles using two receiver coils. *Eng J* 13(2):101569
20. Zhou H, Zhu A, Deng Q, Chen J, Yang F, Hu W (2020) Protection strategy for wireless charging electrical vehicles. *IEEE Trans* 69(11):13510–13520
21. Rozman M, Ikpehai A, Adebisi B, Rabie KM, Gacanin H, Ji H, Fernando M (2019) Smart wireless power transmission system for autonomous EV charging. *IEEE Access* 7:112240–112248
22. Liu X, Liu C, Han W, Pong PW (2018) Design and implementation of a multi-purpose TMR sensor matrix for wireless electric vehicle charging. *IEEE Sens J* 19(5):1683–1692
23. Baroi S, Islam MS, Baroi S (2017) Design and simulation of a wireless charging system for electric vehicles. In: 2017 2nd international conference on electrical & electronic engineering, pp 1–4
24. Liang C, Yang G, Yuan F, Huang X, Sun Y, Li J, Song K (2020) Modeling and analysis of thermal characteristics of the magnetic coupler for wireless electric vehicle charging system. *IEEE Access* 8:173177–173185
25. Frechter Y, Kuperman A (2020) Analysis and design of inductive wireless power transfer link for feedback-less power delivery to enclosed compartment. *Appl Energy* 278:115743
26. Tiwari N, Yadav S, Arya SR (2022) Battery and super capacitor powered energy management scheme for EV/HEV using fuzzy logic controller and PID controller. *Int J Power Electron* 15(3–4):309–333

Investigation of Control Algorithm for PMSM-Based Electric Vehicle Using Vehicle Dynamics



Bharat Singh, Ankur Chowdhury, Vishal Mishra, and Ankur Jain

Abstract Concerns about the finite supply of fossil fuels have sparked a frenzy of effort in the hunt for alternate road transportation propulsion solutions. Furthermore, legislative efforts to minimize urban pollution, CO₂ emissions, and city noise have made plug-in electric vehicles an appealing option to internal combustion engines. The driving of a permanent magnet synchronous motor (PMSM) is investigated and in order to produce continuous torque, sinusoidal stator currents are required for PMSM. This paper presents a mathematical analysis of the motor's operation using the dq axis model. Because of its amazing accuracy, rapid dynamic response, and small footprint, PMSM has now become popular in industrial applications. The speed of a Permanent Magnet Synchronous Motor can be controlled in a number of ways. The vector control approach was employed to regulate the speed of the PMSM motor drive in this research. To construct the PMSM drive for speed control, the vector control approach uses a PMSM motor, inverter, speed regulator, and coordinate transformation. The design of Proportional Integral (PI) and Proportional Integral Derivative (PID) is used to regulate the speed of the PMSM.

Keywords Electric vehicles · EV motor · PMSM

1 Introduction

PMSMs are widely used in contrast to other types of machines because of their qualities such as enhanced dynamic performance, better efficiency, compact size, and ease of maintenance. PMSMs are now widely employed in household appliances, as well as other industries such as industrial robots, air conditioning, wind-generation systems, electric cars, national defense, agriculture, washing machines, and everyday life [1]. Because of its nonlinearity, controlling PMSM is challenging. Many methods for manipulating the torque, current, and speed of synchronous motors (such as PMSM) are now available, allowing them to be used more in industries. There are

B. Singh · A. Chowdhury · V. Mishra (✉) · A. Jain
EEE, BVCOE, New Delhi, India
e-mail: vishalbathard@gmail.com

© The Author(s), under exclusive license to Springer Nature Singapore Pte Ltd. 2024
S. K. Goyal et al. (eds.), *Flexible Electronics for Electric Vehicles*, Lecture Notes
in Electrical Engineering 1065, https://doi.org/10.1007/978-981-99-4795-9_56

599

various techniques, such as vector and scalar control, that have been presented and verified for PMSM, which are similar to dc and induction motors and have features that are extremely desirable for control. The performance of PMSM has a significant impact on parameter fluctuations over time. As a result, a high-performance controller must be included in the PMSM design, which employs algorithms that are simple to implement, have high precision, provide immediate responses, and also robust in contrast to motor parameters and load torque variations. Vector and scalar control techniques are used in the drive system to adjust torque, speed, and current based on the mathematical modeling of PMSM. Vector control is concerned with the vector quantities that will be used in this method [2]. PM machines are machines that produce air-gap magnetic flux using magnets rather than field coils, as in DC commutator machines, or the magnetizing component of stator current, as in induction machines.

Using PMs for field excitation in AC machines has a number of advantages. The PMs enable loss-free excitation in a compact manner, without the hassles and complexities of external stationary electric circuit connections. This is especially true for smaller machines, because delivering the rotor field via electrical circuits always incurs an excitation penalty. Because the losses in the exciter circuit, known as the excitation penalty, are minimal in comparison to the exorbitant cost of magnets, big synchronous machines use rotor conductors to deliver the excitation [3]. The mmf required for smaller machines is mild, and the resistive effects frequently become equivalent and dominant, leading in reduced efficiency. The resistive loss effect is exacerbated by the reduced cross-sectional area of the windings in compact power machines. Furthermore, when the motor size decreases, the cross-sectional area accessible for winding diminishes. The loss-free excitation of PM in smaller machines with a miniature configuration is a distinct advantage, with the sole disadvantage being high price of the PMs. Nonetheless, despite their increased size, PM machines are a formidable challenger for electric and hybrid vehicle drives. The traction motor of every production passenger hybrid vehicle is a PM machine. The brilliant performance and high-power density achieved by PM machine drives are the elements driving the trend.

2 Vehicle Dynamics

2.1 Longitudinal Vehicle Model

In practical terms, a vehicle travels not just on a level road, but also up and down the slope of a highway, as well as through bends, curves, and corners. To mimic this motion, a straight roadway with two-dimensional movement can be used to simplify the description of the roadway. This two-dimensional model will concentrate on vehicle performance, such as speed, acceleration, and gradeability, as well as braking [4]. The link between vehicle acceleration and forces acting on the vehicle

body can be expressed using fundamental concepts and principles of mechanical systems as follows:

$$ma = F_t - F_w - F_g - F_r$$

2.2 Aerodynamic Drag

Normal pressure and shear stress are created on the vehicle's body when air passes over it. Shape drag and skin friction are the two elements that make up exterior aerodynamic resistance. As the vehicle drives itself through the air, it creates high-pressure zones in front of it and low-pressure zones behind it, causing shape drag. These zones, the high-pressure zones, and low-pressure zones work against the vehicle's motion, whereas the skin friction is caused by shear stress in the boundary layer on the vehicle's body's surface. Shape drag, on the other hand, is substantially larger in magnitude than skin friction, accounting for more than 90% of a vehicle's total external aerodynamic drag. Aerodynamic drag is determined by the aerodynamic drag coefficient, C_d , and the effective vehicle frontal area, A , both of which are heavily reliant on vehicle body design:

$$F_w = \frac{1}{2} \rho A C_d (V + V_w)^2$$

where V is the vehicle's longitudinal speed, V_w is the wind speed, ρ is the air density.

2.3 Grading Resistance

Gravity acting on a vehicle as it drives up or down an incline provides a force that is always directed downward. During climbing, this force opposes forward motion and assists forward motion during descending. Only uphill operation is considered in most vehicle performance models since it opposes the whole tractive force [5]. This force's equation is based on the road angle θ , vehicle mass m , and gravitational acceleration g :

$$F_g = mg \sin(\theta)$$

For a relatively small angle of θ , $\sin \theta = \tan \theta$. The grade resistance may be estimated using this approximation by $mg \tan \theta$, or mgG , where G is the grade slope.

2.4 Rolling Resistance

The hysteresis of the wheel at the contact patch as it rolls down the road causes rolling resistance force [6]. The rolling resistance force is the force owing to the moment that resists the wheel's motion and always aids in the braking or stunting of the vehicle's motion.

$$F_r = F_z f_r \cos(\theta)$$

For this force the equation is essentially a function of the rolling resistance coefficient f_r and the F_z which denotes normal load.

2.5 Gradeability

The highest gradient on which a vehicle may begin ascending from a standstill with all four wheels on the gradient at the time of commencement is referred to as the vehicle's grade ability [7].

2.6 Braking Force

The principal braking force F_b is generated by the brake system, which is formed at the contact between the road and the wheel [8]. When the braking force is less than the tire-road adhesion limit, the braking force is calculated as follows:

$$F_b = \frac{T_b - \sum I \alpha_{an}}{r}$$

where applied braking torque is represented by T_b , I denote the rotational inertia associated with the decelerated wheel, α_{an} is the corresponding angular deceleration, and r is the wheel's rolling radius [9]. The braking force can't grow any further once it hits the limit of tire-road adhesion. The rolling resistance of wheels, resistance of slope, aerodynamic resistance, and powertrain resistance all influence vehicle's motion upon braking, in conjunction to the braking force [10].

3 Mathematical Modelling of PMSM

The model of PMSM without damper winding has been developed on rotor reference frame using the following assumptions:

1. Saturation is neglected.
2. The induced EMF is sinusoidal.
3. Eddy currents and hysteresis losses are negligible.
4. There are no field current dynamics.

Voltage equations are given by

$$v_q = R_s \dot{i}_q + \omega_r \lambda_d + \rho \lambda_q \quad (1)$$

$$v_d = R_s i_d - \omega_r \lambda_q + \rho \lambda_d \quad (2)$$

Flux linkages are given by

$$\lambda_q = l_q i_q \quad (3)$$

$$\lambda_d = L_d i_d + \lambda_f \quad (4)$$

Arranging equation in matrix form

$$\begin{bmatrix} v_q \\ v_d \end{bmatrix} = \begin{bmatrix} R_s + \rho l_q & \omega_r L_d \\ -\omega_r L_q & R_s + \rho L_d \end{bmatrix} \begin{bmatrix} i_q \\ i_d \end{bmatrix} + \begin{bmatrix} \omega_r \lambda_f \\ \rho \lambda_f \end{bmatrix} \quad (5)$$

The developed torque motor is being given by

$$T_e = 3/2 * p/2(\lambda_d \lambda_q - \lambda_q \lambda_d) \quad (6)$$

The mechanical Torque equation is

$$T_e = T_L + B\omega_m + j\left(\frac{d\omega_m}{dt}\right) \quad (7)$$

Solving for the rotor mechanical speed from equation

$$\omega_m = \int (T_e - T_L - B\omega_m/dt) dt \quad (8)$$

Park Transformation Converting the phase voltages variables V_{abc} to V_{dqo} Variables in rotor reference frame the following equations are obtained

$$\begin{bmatrix} V_q \\ V_d \\ V_o \end{bmatrix} = \frac{2}{3} \begin{bmatrix} \cos\theta_r & \cos(\theta_r - 120) & \cos(\theta_r + 120) \\ \sin\theta_r & \sin(\theta_r - 120) & \sin(\theta_r + 120) \\ 1/2 & 1/2 & 1/2 \end{bmatrix} \begin{bmatrix} V_a \\ V_b \\ V_c \end{bmatrix} \quad (9)$$

Convert V_{dqo} to V_{abc}

$$\begin{bmatrix} V_a \\ V_b \\ V_c \end{bmatrix} = \begin{bmatrix} \cos\theta_r & \sin\theta_r & 1 \\ \cos(\theta_r - 120) & \sin(\theta_r - 120) & 1 \\ \cos(\theta_r + 120) & \sin(\theta_r + 120) & 1 \end{bmatrix} \begin{bmatrix} V_q \\ V_d \\ V_o \end{bmatrix} \quad (10)$$

Considering the currents as inputs, the three currents are

$$i_a = I_m \sin(\omega_r t + \alpha) \quad (11)$$

$$i_b = I_m \sin(\omega_r t + \alpha - \frac{2\pi}{3}) \quad (12)$$

$$i_c = I_m \sin(\omega_r t + \alpha + \frac{2\pi}{3}) \quad (13)$$

Writing equation in the matrix form

$$\begin{bmatrix} i_a \\ i_b \\ i_c \end{bmatrix} = \begin{bmatrix} \cos(\omega_r t + \alpha) \\ \cos(\omega_r t + \alpha - \frac{2\pi}{3}) \\ \cos(\omega_r t + \alpha + \frac{2\pi}{3}) \end{bmatrix} [I_m] \quad (14)$$

- (1) Measuring rotor position and speed ω_r from a sensor which is set in motor rotation axis.
- (2) The motor at the flux weakening region with a speed loop T_e is obtained from the PI controller.
- (3) Calculate I_q using equation

$$i_q = \frac{T_e}{(\frac{3}{2})(\frac{P}{2})\lambda_f} \quad (15)$$

- (4) Calculate I_d using equation

$$i_d = \frac{(\lambda_d - \lambda_f)}{L_d} \quad (16)$$

- (5) Calculate α using equation

$$\alpha = \tan^{-1}\left(\frac{i_q}{i_d}\right) \quad (17)$$

- (6) Using α and rotor position the controller will generate the reference currents as per equation

$$\begin{bmatrix} i_a \\ i_b \\ i_c \end{bmatrix} = \begin{bmatrix} \cos(\omega_r t + \alpha) \\ \cos(\omega_r t + \alpha - \frac{2\pi}{3}) \\ \cos(\omega_r t + \alpha + \frac{2\pi}{3}) \end{bmatrix} [I_m] \quad (18)$$

- (7) Then the current controller makes use of the reference signals to control the inverter for the desired output currents.
- (8) The load torque is adjusted to the maximum available torque for the reference speed

$$T_L = T_{e(rated)} \frac{\omega_{rated}}{\omega_r} \quad (19)$$

4 Simulink Model

In this work input is given in terms of km/hr and that speed is compared with the actual speed. To give the torque we are simulating the vehicle dynamics in terms of body load. So, this block is the total road load of the vehicle's body which is used to simulate the body functions of the vehicle. This consists of Mass, Rolling resistance, Aerodynamic drag, and Initial velocity. Giving the velocity of the vehicle as input "x_{dot}" and "x_{ddot}" is the acceleration of the vehicle, and the Grade can also be applied if the vehicle is running on the slope. So, here given input is in terms of km/hr, so it should be converted into RPM first for the motor to understand.

The battery connected to the motor is Li-ion battery. Here in the closed-loop subsystem of the motor, a reference speed is given at the input, and inside this we have a PID controller. These blocks are used to cut at the reference speed when speed is zero, then the controller will not calculate the error unnecessarily. Here gain blocks are used to convert a reference input value to voltage magnitude and frequency, and this is the block which is used to generate sine PWM. To generate the sine wave PWM we have to give amplitude of the voltage and frequency, when sine wave is generated, it is applied to PWM generator. Then pulsed output will be applied to the gates of the inverter switch. Here we have motor ON/OFF command which is connected to brake pedal, in this zero corresponds to no braking and 0.95 corresponds to heavy braking. Once the value of brake pedal is more than zero, motor will turn off. When speed reaches zero in T_L block, there shouldn't be any torque applied to the motor. Once speed reaches zero then there will be no braking (Figs. 1, 2, 3 and 4) (Table 1).

The battery block consists of the following parameters and ratings.

Nominal Voltage (V) = 300 V.

Rated Capacity = 50 Ah.

State of Charge (SOC) = 50%.

Response Time = 30 secs.

Table 1 Values of vehicle body total road load and PMSM motor simulink block

Parameters	Values
Rolling resistance coefficient	0.1
Rolling and driveline resistance coefficient	0.002232
Aerodynamic drag coefficient	0.00389
Gravitational constant	9.81
Number of phases	3
Back EMF waveform	Sinusoidal
Rotor type	Round
Armature inductance (H)	0.000395
Stator phase resistance (Rs)	0.0485

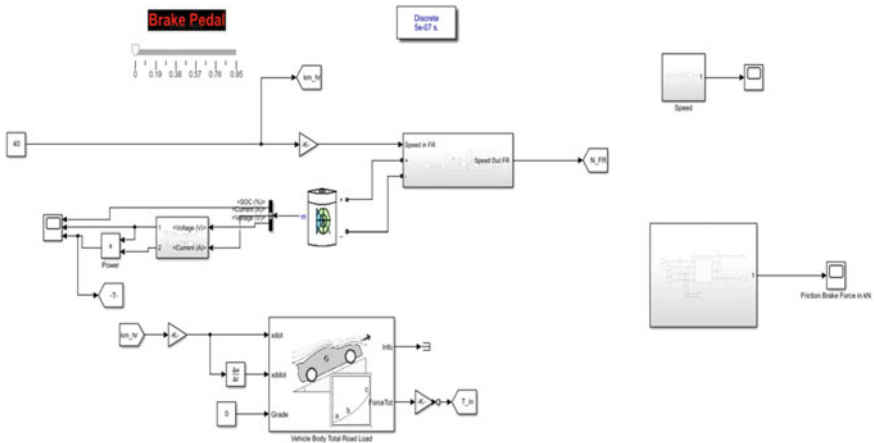


Fig. 1 Simulink model employing PMSM motor

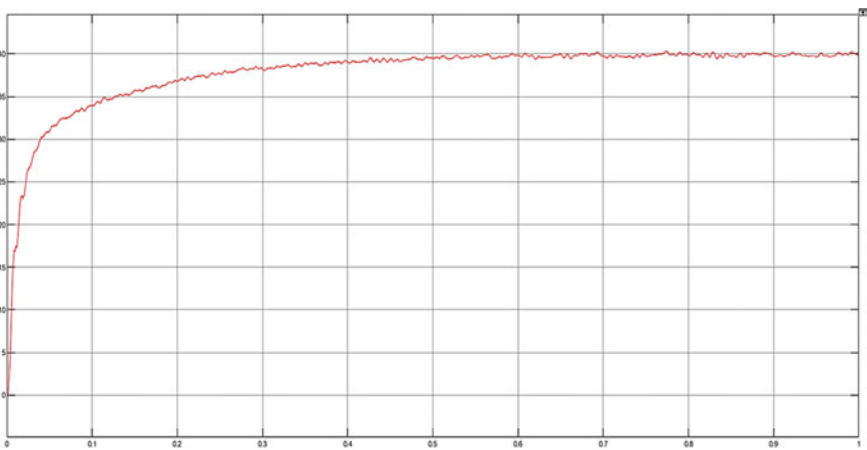


Fig. 2 Speed response without braking

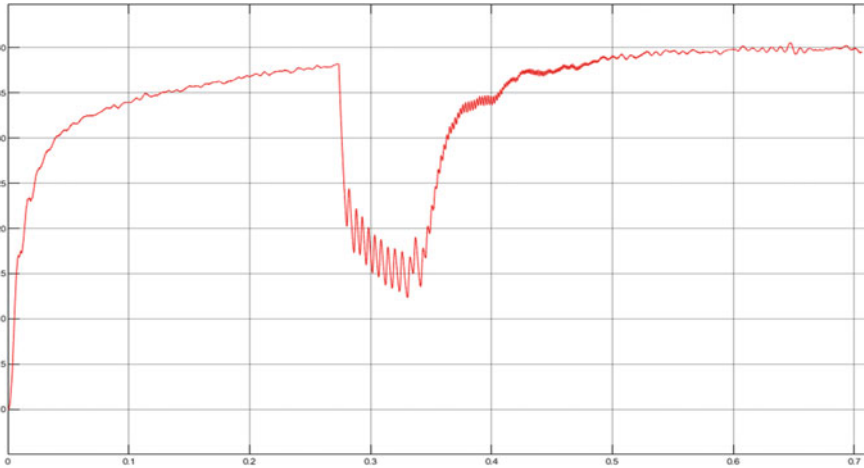


Fig. 3 Speed response with braking

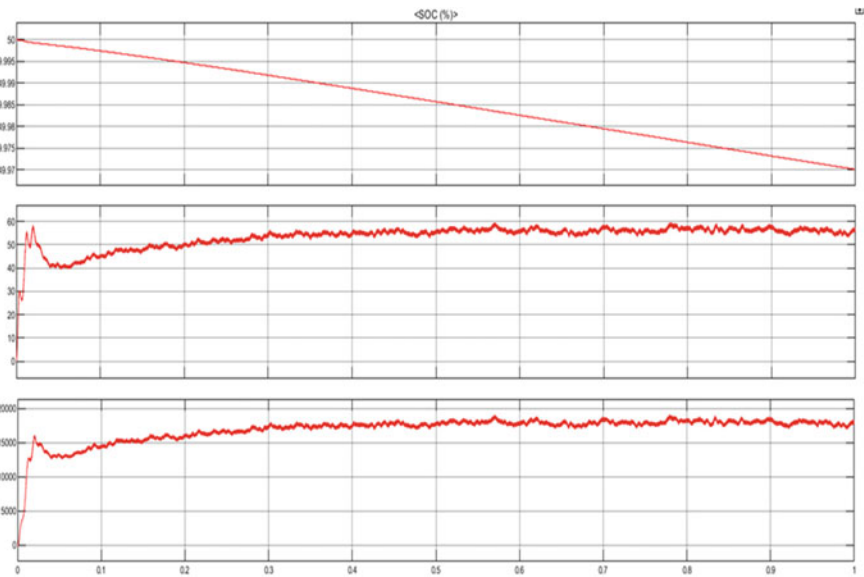


Fig. 4 Battery parameters

5 Conclusion

In this work we designed the Simulink model of friction disc braking in an electric vehicle with vehicle dynamics employing PMSM Motor and we have also discussed results with and without braking. Basic theory and mathematical modeling of the

machine are also discussed in this work with various conventions of fundamental vehicles. As we can see in the model reference input is given initially and it will be compared with the actual value with the help of the feedback system and PID Controller. The total body road load block is used to produce torque for various values of vehicle dynamics and applied at motor input by which required torque and speed is obtained for the vehicle. And achieved speed, torque, and brake applied at the input of wheels of vehicles, this Simulink model helps us in analyzing how PMSM machine works smoothly in the electric vehicle with and without a braking system. This work can also be further extended by adding regenerative braking with PMSM Machine.

References

1. Singh B, Chowdhury A, Dixit AK, Mishra V, Jain A, Kumar N (2022) Investigation on electric vehicle motor challenges, solutions and control strategies. *J Inf Optim Sci* 43(1):185–191. <https://doi.org/10.1080/02522667.2022.2039466>
2. Fan YV, Perry S, Klemeš JJ, Lee CT (2018) A review on air emissions assessment: transportation. *J Cleaner Prod* 194:673–684
3. Stranges N, Findlay RD (2000) Methods for predicting rotational iron losses in three-phase induction motor stators. *IEEE Trans Magn* 5:3112–3114
4. Lin R, Haavisto A, Arkkio A (2010) Analysis of eddy-current loss in end shield and frame of a large induction machine. *IEEE Trans Magn* 3:942–948
5. Singh S, Alam M, Singh B (2020) Orthogonal moment feature extraction and classification of melanoma images. *J Inf Optim Sci* 41(1):195–203
6. Singh B, Urooj S, Singh S (2020) Analysis of autopilot system, integrated with modelling and comparison of different controllers with the system. *J Discret Math Sci Cryptogr* 23(5):1059–1068
7. Kumar L, Jain S (2014) Electric propulsion system for electric vehicular technology: a review. *Renew Sustain Energy Rev* 29:924–940
8. Karamuk M (2013) A survey on electric vehicle powertrain systems. *Int Aegean Conf Electr Mach Power Electron, ACEMP 2011 Electromotion 2011 Jt Conf* 315–324
9. Rajashekara K (2013) Present status and future trends in electric vehicle propulsion technologies. *IEEE J Emerg Sel Top Power Electron* 1(1):3–10
10. Frieske B, Kloetzke M, Mauser F (2013) Trends in vehicle concept and key technology development for hybrid and battery electric vehicles. *2013 World Electr Veh Symp Exhib* 1–12